Appendix A: Literature Review and Survey

CONTENTS

1 Literature Review

1.1 Fresh SCC Properties

1.1.1 *Rheological Properties*

1.1.1.1 Models of Rheological Properties

The fresh cementitious materials are viscoelastic materials. When shear stress is applied to the viscoelastic cementitious material, the mixture will start to flow at a certain shear stress known as yield stress, τ_0. After the mixture starts to flow, various equations/models can be used to assess the flowing ability based on the relationship between the shear strain and shear stress. For different fluids, the relations between strain rate and shear stress are different. The simplest flow model is the Newtonian liquid, which is characterized by a direct proportionality between the shear stress (τ) and shear rate (γ). The constant ratio of the stress and strain is called viscosity (μ_p), and the straight line passes through the origin for Newtonian liquid. However, the relation between stress and strain of concrete is not as simple as this. For a mixture with a yield stress, the relation between shear stress and strain should be in the form of $\tau = \tau_0 + f(\gamma)$. The simplest form of this equation is $\tau = \tau_0 + \mu_p\gamma$ and μ_p is a constant defined as plastic viscosity. The model named the Bingham Model is often used to describe the flow characteristics of concrete (Tattersall and Banfill, 1983). The Bingham Model is an ideal model but the real shear stress-shear rate relationship is not linear especially at the beginning of the curve. For cementitious materials, with the increase of shear rate, the viscosity decreases/increases in a phenomenon known as shear thinning/thickening. To better exhibit the shear thinning property of concrete at a low shear rate, other models have been proposed, such as the Herschel-Bulkley model, the Vom Berg model, the Eyring model, the Ostwald de Waele model and the Robertson-Stiff model (Ferraris, 1996). These models relate the shear stress (τ) to the strain rate (γ) in various power laws. The most popular one of this kind is the Herschel-Bulkley model, the mathematical representation of which is expressed as: $\tau = \tau_0 + \mu_p\gamma^n$. The n in the equation represents the consistency, and it is able to capture more of the low strain rate behavior. For both the Bingham and Herschel - Bulkley models, the shear stress axis intercept represents the yield stress (τ_0). For the Bingham model, the slope of the curve represents the plastic viscosity. For the Hershel-Bulkley model, the slope represents the apparent viscosity, which changes with the shear strain rate. The yield stress and plastic viscosity are two critical parameters that govern the flowability and segregation resistance of cement and concrete and these two parameters are always used to evaluate the corresponding features of SCC (Tregger et al., 2008; Schwartzentruber et al., 2006).

1.1.1.2 Thixotropy Effects on SCC

Another critical feature of cementitious materials is that chemical hydration proceeds through the whole process, which will bring new particle interactions and consequently the rheological property of material changes with time. This behavior strongly influences a property known as thixotropy, which, in concrete, is considered as the increase in viscosity for a mixture at rest, and a decrease in viscosity for a mixture that is subjected to shear stress; this happens due to the breakdown and buildup of the material structure (Ferron et al., 2007). Thixotropy is usually quantified by measuring the area between the up and down flow curves (shear stress-rotation speed curve), known as breakdown area, using a rheometer. These curves might be induced by

applying a growing rotational speed up to concrete/mortar at a certain rate and then gradually unloading up to stopping (Assaad et al., 2003b). A smaller breakdown area means a more flowable and less cohesive mixture (i.e., low thixotropy). The buildup of the material structure during and/or after mixing, transportation, and placing is vital for segregation resistance (the greater the thixotropy, the lower the potential for segregation), pumpability (the quicker the buildup of the material structure, the poorer the pumpability), formwork pressure reduction (the greater the thixotropy, the faster the formwork pressure decay) and shape-holding ability (the quicker the buildup of the concrete structure, the easier for SCC to hold its original shape).

1.1.1.3 Rheology Test Methods

To measure the rheological parameters of cementitious materials, various types of rheometers are used. There are three main types of rheometer geometries that are typically used: the coaxial cylinder rheometer, the vane configuration rheometer and the parallel plate rheometer. The shape of the vane/cylinder varies with the rheometer. All rheometers measure the resistance to flow of concrete at varying shear rate conditions. A torque is applied to the material while the rotational speed required to maintain the force is measured, or vice versa. To determine the yield stress of a cement mixture, different strain rates or stress protocols are used depending on the type of rheometer, mixture composition and what properties are sought after. For the vane configuration rheometer, a common technique is to use a very low, constant rotational speed **(**Barnes and Nguyen, 2001**)**. For the coaxial cylinder rheometer, the most common protocol involves a decreasing, step-wise process. For this protocol, it is important to vary the strain rate within a range that is comparable to the range experienced during the application for which concrete is used. Saak et al. (2001) reported that one major advantage of the vane configuration rheometer is that the vane ensures that shear occurs within the material, rather than in wall slip, which can be a major issue for coaxial geometries. Wall slip occurs when the material begins to shear against the wall of the cylinder and not within the material itself. This can result in a yield stress that is lower than the actual, and that found by a vane rheometer. To remedy this situation, grooves can be cut into the cylinders to prevent slipping, or the sides can be roughened with sand paper. The gap between the cylinders should be as small as possible to ensure uniform flow and satisfy the assumption that the stress profile in the gap between the cylinders remains linear (Shaughnessy and Clark, 1988). Therefore, absolute values of rheological parameters vary from one rheometer to another.

1.1.2 ***Workability Properties and Test Methods***

Self-consolidating concrete (SCC) is a kind of highly flowable concrete that can pass through reinforcing bars and fill the formwork corners that normal concrete could not achieve without mechanical consolidation. For a high quality SCC, three basic properties are required: high deformability, high passing ability, and high resistance against segregation (Khayat, 1999). These properties are very sensitive and depend on several parameters, including the placement and transportation methods, the complexity and shape of the formwork, the degree of congestion of the structural member, labor skills, as well as quality assurance measures (Khayat, 2005).

The two most contradicting characteristics of SCC are its high flowability and segregation resistance. To get high flowability, an increase in water-cementitious materials ratio is a normal choice, which, however, increases the probability of the loss of cohesiveness of the paste and mortar. Added water will reduce shear stress and viscosity, thus, the segregation resistance

feature will be sacrificed. Therefore, a balance is required to enhance flowability without a substantial reduction in cohesiveness. To fulfill that, the use of high-range water reducing admixture (HRWRA) is a must in SCC. The presence of HRWRA in a mixture will reduce shear stress while not affecting viscosity significantly. Meanwhile, an increase of paste, either an increase of portland cement amount or partial replacement of supplementary material, is another option.

Segregation is defined as the failure of the mixture to maintain a homogeneous distribution of its various constituents during all the processes. Bridge structures are often heavily reinforced, thus, the passing and filling ability of SCC is critical. The unique flowability helps SCC to be useful in this case; however, there is a need to improve segregation resistance. A surface settlement test and the penetration test are methods used to evaluate this property; however, they address the static segregation only. There is no universal test method for evaluating the dynamic segregation of SCC (Shah et al., 2009). Moreover, the theoretical background of these methods is still unclear and their precision is unknown. Another method is the conventional slump flow test together with time elapsed for the mix flow to reach a diameter of 50 cm (20 in.) (T_{50}), which is used to evaluate the rheological properties of a mix. However, mixes having almost the same T_{50} may vary considerably in their yield stress and viscosity. Numerous efforts have been explored for testing methods for SCC in the past decade. In this section, the test methods for assessing the fresh-state properties of SCC mixtures are reviewed.

1.1.2.1 Filling Ability (Flowability)

To evaluate the flowability of SCC, the conventional concrete cone is mostly used in the laboratory and on site. A sample of freshly mixed concrete is placed in a slump cone in one lift without tamping or vibration. The cone, shown in Figure A-1, can be either in the upright or inverted position (the slump flow will be the same (Khayat, 2005)). The mold is raised, and the concrete is allowed to spread. After spreading ceases, the spread diameters are measured in two directions and Eq. A.1 is used to calculate the slump flow.

$$\text{Slump flow} = (D_1+D_2)/2 \qquad \text{(A.1)}$$

D_1 = the largest diameter of the circular spread of the concrete, and

D_2 = the circular spread of the concrete at an angle approximately perpendicular to D_1

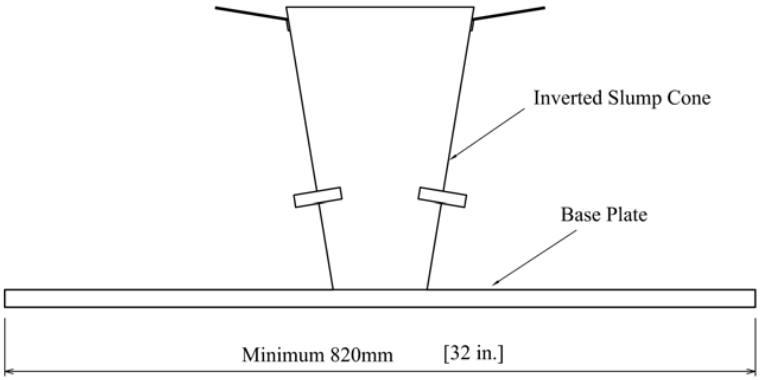

Figure A-1. Diagram of slump flow test setup (AASHTO T 347-13) and its application

The flowing ability of SCC can not only be reflected by how far it flows, but also by how fast it can flow. When performing the slump flow test, the time it takes for the outer edge of the concrete mass to reach a diameter of 50 cm (20 in.) (T_{50}) from the time the mold is first raised, provides such information.

1.1.2.2 Passing Ability

SCC is frequently used in heavily reinforced elements. To reach every corner of the forms, SCC mixtures should have a good passing ability. Methods used to evaluate the passing ability of SCC usually use an apparatus that contains reinforcement bars. Example test methods are shown below.

1.1.2.2.1 J-Ring Test:

AASHTO T 345-12 describes a procedure for using a slump-flow cone and J-Ring to simulate concrete passing through steel bars. This apparatus is simple and portable and is used for acceptance in Europe (Bartos, 2005). A sample of freshly mixed concrete is placed in the conventional cone, which is placed concentric within the J-Ring as shown in Figure A-2. Concrete is placed in one lift without tamping or vibration. When the mold is raised, the concrete is allowed to spread through the J-Ring as shown in Figure A-2. Similar to the slump-flow measurement, the J-Ring flow is measured and the difference between the slump flow and J-Ring flow is an indicator of the passing ability of the concrete. Table A-1 is used to assess the passing ability of SCC, in a semi-quantitative manner.

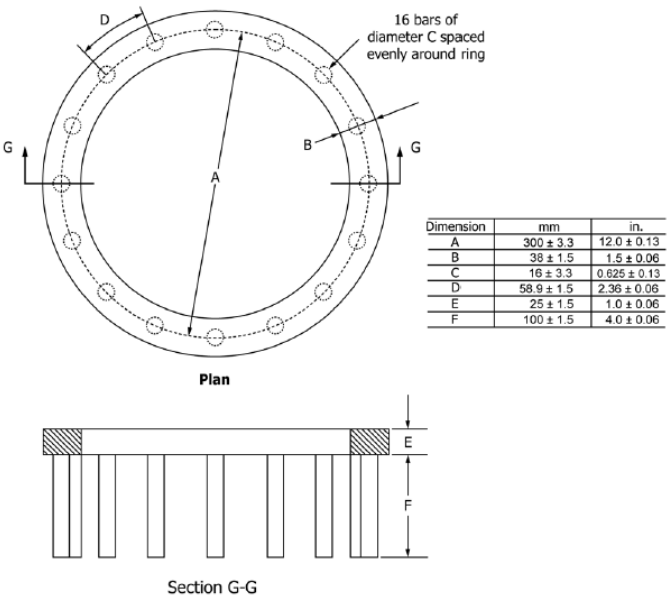

Dimension	mm	in.
A	300 ± 3.3	12.0 ± 0.13
B	38 ± 1.5	1.5 ± 0.06
C	16 ± 3.3	0.625 ± 0.13
D	58.9 ± 1.5	2.36 ± 0.06
E	25 ± 1.5	1.0 ± 0.06
F	100 ± 1.5	4.0 ± 0.06

Figure A-2. J-Ring dimensions (ASTM C1621-14) and its application

Eq. A.2 is used to calculate J-Ring flow:

$$\text{J-Ring flow} = (j_1 + j_2)/2 \qquad \text{(A.2)}$$

where:

j_1 = the largest diameter of the circular spread of the concrete from the J-Ring test, and

j_2 = the circular spread of the concrete at an angle approximately perpendicular to j_1.

Table A-1. Blocking Assessment (ASTM C1621-14)

Flow difference between slump flow and J-Ring flow (ΔD)	Blocking assessment
0 -1 in. (0 – 25 mm)	No visible blocking
1 – 2 in. (25 – 50 mm)	Minimal to noticeable blocking

> 2 in. (> 50 mm)	Noticeable to extreme blocking

Another measurement of the J–Ring test is the height difference of mix inside and outside of the J-Ring, as shown in Figure A-3. When SCC stops flowing, the difference between the sample height inside and outside the four support rods is measured. The greater the difference of the height inside and outside of the J–ring, the poorer the passing ability of the SCC.

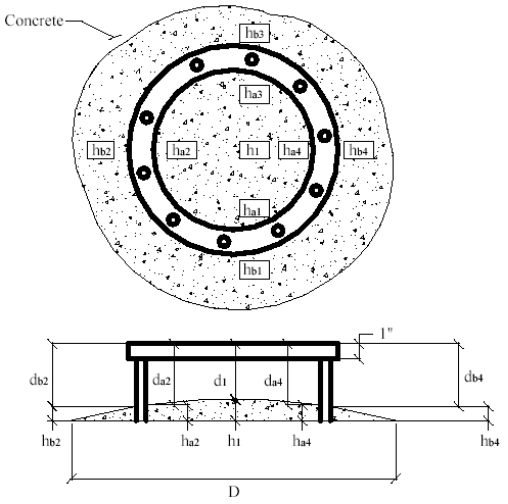

Figure A-3. J-Ring height measurements (PCI, 2003)

To evaluate the passing ability of SCC, the following calculation steps are taken:

a. Measure the value d_1 in the center of the J-Ring and also 4 values d_a and d_b just inside and just outside the ring (measurements in mm);
b. Calculate $h_1 = 125 – d_1$ and all h values $h_{a/b\ x} = 125 – d_{a/b\ x}$ (x = 1 to 4);
c. Calculate mean height h_{am};
d. Calculate mean height h_{bm};
e. Calculate the difference of mean heights $h_{ab} = h_{am} – h_{bm}$
f. Calculate $2(h_{ab}) – (h_1 – h_{am})$. This is the J-Ring Δh test value.

The satisfactory passing ability without blockage is attained when the Δh value is less than 0.6 in. (15 mm) (AASHTO T 345-12).

This apparatus is simple and portable, and is used for acceptance in Europe (Bartos, 2005). Khayat and Mitchell (2009) recommended acceptance values of J-Ring ΔD of 0 - 3.0 in. for precast, prestressed applications. They also classified the passing ability of all mixtures for three relative performance levels depending on the difference between the slump flow and J-Ring flow as shown in Table A-2.

Table A-2. Relative performance of SCC mixtures for precast, prestressed applications regarding passing ability (Khayat and Mitchell, 2009)

	High	Medium	Low
Slump flow – J-Ring flow (ΔD)	≤ 2 in. (50 mm)	2.0 – 3.0 in. (50 - 75 mm)	3.0 – 4.0 in. (75-100 mm)

1.1.2.2.2 The Caisson Test (Filling Vessel Test)

This method can simulate the flowing of SCC passing through reinforcing bars or prestressing strands. The apparatus consists of a transparent acrylic container and 35 obstacles made of copper tube with a diameter of 0.60 in. (16 mm) and a distance center to center of 2 in. (50 mm) as shown in Figure A-4. The container is filled with concrete through the top and the area occupied by the concrete is used as a measure of the filling capacity (FC) of SCC. According to AASHTO T 349-13, the percent of filling capacity (FC%) is calculated as shown in Eq. A-3.

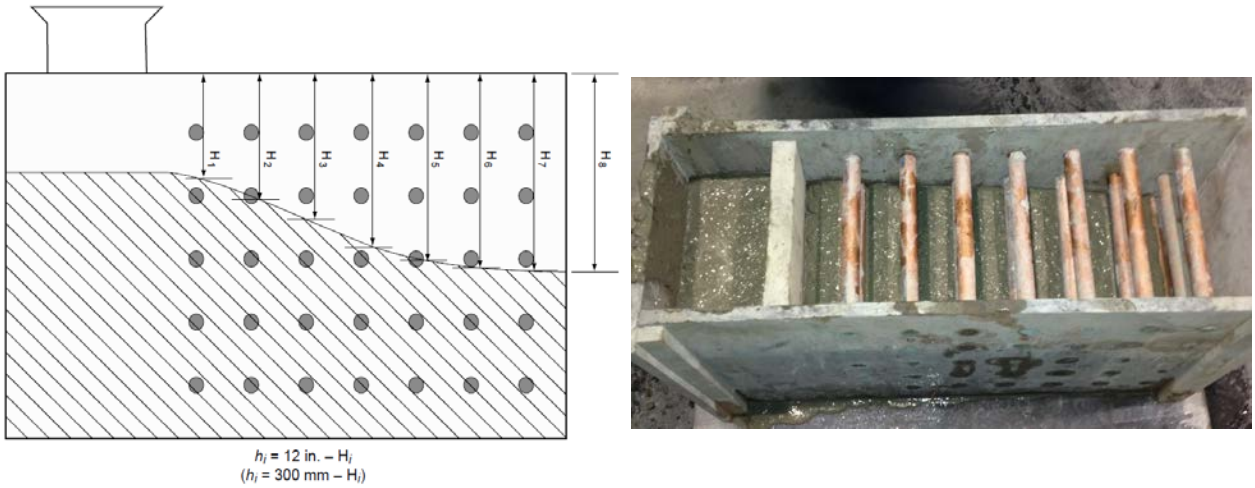

Figure A-4. Filling capacity caisson measurements (AASHTO T 349-13) and its application

$$FC\% = \left(\frac{\sum_{i=1}^{7} \left(h_i + h_{i+1} \right)}{h_1 \times 14} \right) \times 100 \qquad \text{(A-3)}$$

A minimum filling capacity value of 80% is considered a lower limit to achieve proper passing of highly congested or restricted sections (Khayat, 1999). A lower limit of 70% can be tolerated for relatively simple elements (Khayat and Mitchell, 2009).

1.1.2.3 Static Stability

Due to its high flowability, SCC is especially prone to segregation/sedimentation under static and dynamic conditions. Poor segregation resistance can induce blocking around reinforcement, induce high drying shrinkage, and cause non-uniformity when the concrete hardens (Brinks, 2005). Concrete can segregate in both vertical and horizontal directions. Vertical segregation normally occurs when fresh concrete is at rest (static), and is thus called static segregation. Horizontal segregation occurs during flowing and is thus called dynamic segregation.

The viscosity and yield stress of the mixture, the binder density, aggregate size, aggregate density, as well as the content of fines were studied to assess their effects on segregation. Within common ranges of SCC mixtures and densities of aggregate, it was argued that the most important factor that governs the rate of sedimentation is the aggregate size (Bonen and Shah, 2005). Greater fines content increases mix stability either because it increases the viscosity or increases the density of the matrix. Silica fume can be used as a viscosity modifier, and slag and limestone are also examples of density modifiers. Fly ash is used to modify the rheological properties of SCC (Kim et al., 2010a). More recently, mineral additives are used to modify the yield and viscosity properties of concrete mixes (Tregger et al., 2010; Pekmezci et al., 2007).

To evaluate the static segregation potential of a mixture, various methods are proposed. Below are examples of the standard methods.

1.1.2.3.1 Penetration Test

A penetration apparatus was introduced as a rapid assessment method to quantitatively evaluate the static segregation of SCC (Bui et al., 2002). The penetration apparatus is placed above the surface of SCC, as shown in Figure A-5, and the hollow cylinder is released after 80±5 sec. to stabilize the concrete. The penetration depth is measured after 30±2 sec. to indicate the resistance to segregation. ASTM C1712-14 describes the degree of static segregation resistance based on the penetration depth as listed in Table A-3.

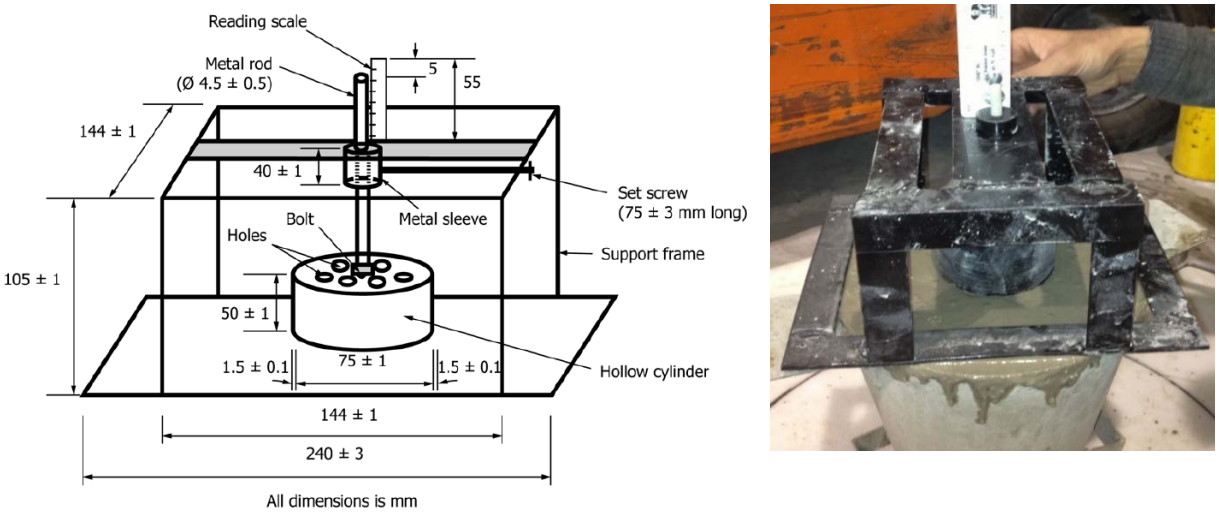

Figure A-5. Dimensions of penetration apparatus (ASTM C1712-14) and its application

Table A-3. Degree of Static Segregation Resistance (ASTM C1712-14)

Penetration depth (P_d)	Degree of static segregation resistance
$P_d \leq 3/8$ in. (10 mm)	Resistant
3/8 in. (10 mm) < P_d < 1.0 in. (25 mm)	Moderately resistant
$P_d \geq 1.0$ in. (25 mm)	Not resistant

1.1.2.3.2 Visual Stability Index

The simplest way of investigating segregation in SCC is by the appearance of the mix, however this is a qualitative measurement that depends on the evaluator. There are two kinds of visual assessment methods used to evaluate the segregation of SCC. One is based on the fresh state (AASHTO T 351-14) and the other is measured in hardened samples (AASHTO PP 58-12).

1.1.2.3.2.1 Fresh Visual Stability Index (VSI)

AASHTO T 351-14 presents a method to evaluate the stability of a mix after the slump flow test has been conducted. After the concrete has stopped spreading, the stability is determined by visually inspecting the distribution of the coarse aggregate within the concrete mass, the distribution of the mortar fraction particularly along the perimeter, and the bleeding characteristics. Table A-4 contains VSI values with corresponding criteria.

Table A-4. Visual Stability Index Values (AASHTO T 351-14)

Rating	**0 (Highly Stable)**	**1 (Stable)**	**2 (Unstable)**	**3 (Highly Unstable)**
Image	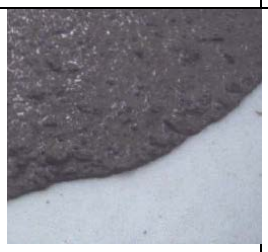			
Description	No evidence of segregation or bleeding.	No evidence of segregation and slight bleeding observed as a sheen on the concrete mass.	A slight mortar halo ≤ 3/8 in. (10 mm) and/or aggregate pile in the concrete mass.	Clearly segregating by evidence of a large mortar halo > 3/8 in. (10 mm) and/or a large aggregate pile in the center of the concrete mass.

1.1.2.3.2.2 Hardened Visual Stability Index (HVSI)

Another visual method is based on observing a hardened cylinder of the SCC sample. The test parameter, known as HVSI, is based on the top-to-bottom distribution of coarse aggregate in a cut cylinder and the thickness of top mortar layer (AASHTO PP 58-12). The ratings shown in Table A-5 are assigned on the basis of visual observation.

Table A-5. Hardened Visual Stability Index (HVSI) values (AASHTO PP 58-12)

Rating	**0 (Highly Stable)**	**1 (Stable)**	**2 (Unstable)**	**3 (Highly Unstable)**
Image	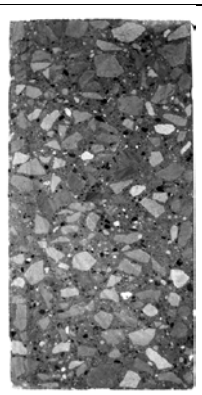	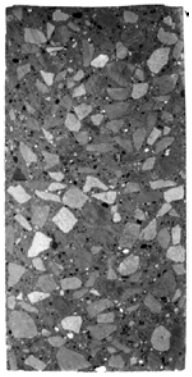	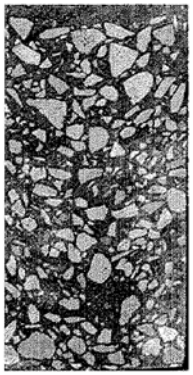	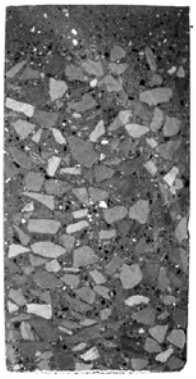
Description	No top mortar layer or variance in aggregate distribution.	Top mortar layer is ≤ ¼ in. (6 mm) thick and slight variance in aggregate distribution.	Top mortar layer is ≤ 1 in. (25 mm) thick and distinct variance in aggregate distribution.	Top mortar layer is > 1 in. (25 mm) thick and considerable variance in aggregate distribution.

1.1.2.3.3 Column Technique

A sample of freshly mixed SCC is placed in a tall cylindrical mold without tamping or vibration. The mold is separated into three sections representing different levels of the specimen (Figure A-6). After casting, concrete is left undisturbed for 14-16 min. Concrete from the top and bottom sections are then washed on a 3/16 in. (4.75 mm) sieve. The mass of coarse aggregate in the top and the bottom sections is determined and the percent static segregation (S) is calculated.

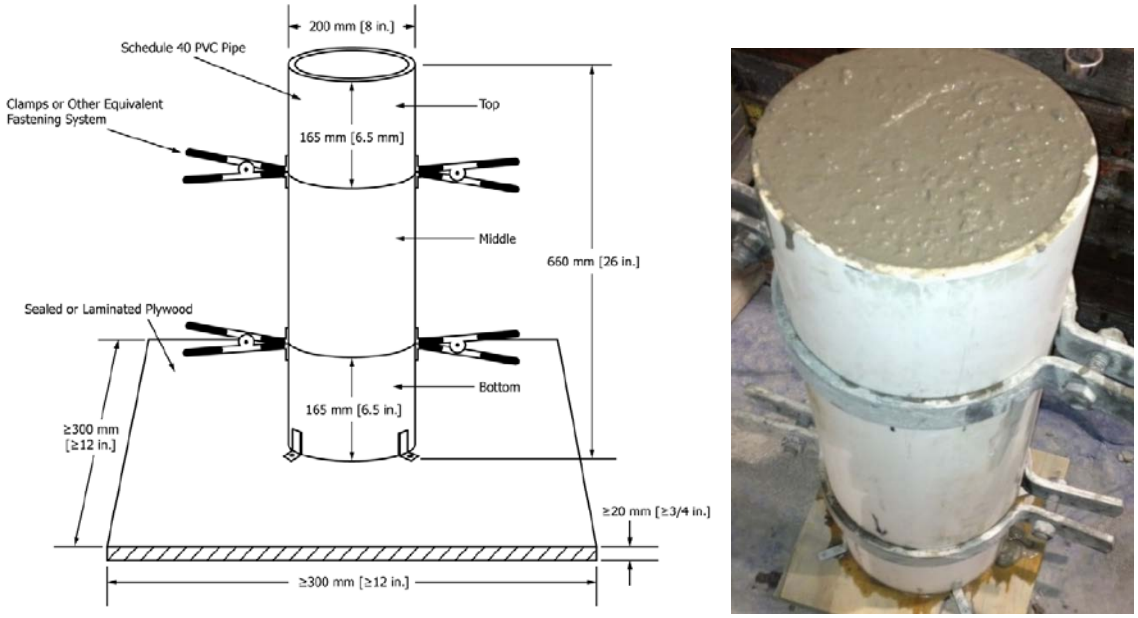

Figure A-6. Schematic of column mold (ASTM C1610-14) and its application

Eq. A.4 is used to calculate the percent static segregation according to ASTM C1610-14:

$$S = 2\left[\frac{(CA_B - CA_T)}{(CA_B + CA_T)}\right] * 100, \quad if\ CA_B > CA_T \qquad (A.4)$$

$$S = 0, \quad if\ CA_B \leq CA_T$$

Where:

S = static segregation, percent

CAT = mass of coarse aggregate in the top section of the column

CAB = mass of coarse aggregate in the bottom section of the column

The column segregation test is useful for determining the distribution of coarse aggregate concentration shortly after casting (Assaad et al., 2004). (Khayat and Mitchell, 2009) recommended S value of less than 15% to secure homogenous in-situ properties of SCC.

1.1.2.4 Dynamic Stability

When SCC flows for some distance, the segregation mechanism becomes different from that in the static state. A static segregation test cannot predict the dynamic segregation which happens during the casting period and becomes more difficult to assess. There is no standard measurement method at the present for dynamic segregation. A laboratory method for dynamic segregation was developed at UIUC (Lange et al., 2008b). In their research, considering a long flow distance is needed when investigating the dynamic segregation; a long trough was designed as shown below. The trough is made of wood with internal dimensions of 6 × 6 × 72 in. (150 × 150 × 1800 mm). An inclined angle of 7° (9-in. (230-mm) height difference between the two ends) is set up as shown in Figure A-7.

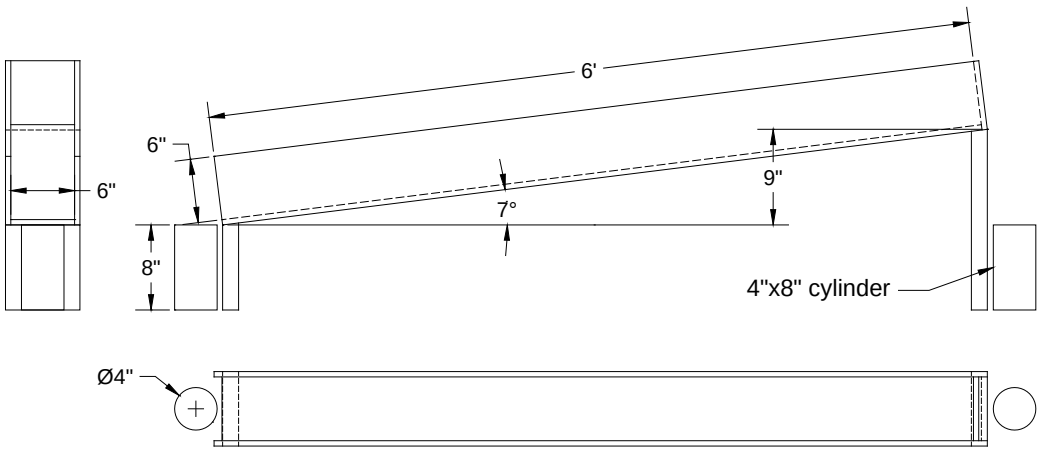

Figure A-7. Flow trough for dynamic segregation

Concrete is poured at the top end, and a sample is collected at the bottom of the trough. The change in density between the top and bottom samples is measured and used as an indicator of the dynamic segregation property. Eq. A.5 is used to calculate the Dynamic Segregation Index.

$$DSI = (CA_1 - CA_2)/CA_1 \quad (A.5)$$

where CA_1 is weight of coarse aggregate from the sample of original SCC and CA_2 is weight of coarse aggregate from the sample collected at the bottom of the trough. A 3/16 in. (4.75 mm)-sieve is used to determine the aggregate amount. Due to the length of the trough, the flowability can also be obtained from this device. However, because of the length of the apparatus, the trough is not very suitable for on-site use.

1.1.2.5 Workability Retention

It is critical that SCC exhibit proper workability at the time of placement. Workability retention is the ability of a concrete mixture to maintain its workability properties over time. Workability retention and setting time are different properties and should be evaluated separately. Workability retention depends on the HRWRA type and dosage, retarder type and dosage, mixture proportions, concrete temperature, weather conditions, and degree of agitation. The extent of workability retention should be tailored to the application because excessive workability retention is unnecessary and may increase formwork pressure and susceptibility to segregation (Koehler and Fowler, 2007).

The effects of production and transport on the workability properties of SCC must therefore be taken into account when testing time dependent properties of SCC. SCC used in a precast element plant, for example, is normally placed about 10 to 30 minutes after mixing, but with ready-mixed concrete this time span can be up to 120 minutes.

It may be necessary to provide a number of different mixtures to be able to provide consistent workability properties under the diverse conditions occurring on the typical bridge site. Factors that affect workability include fluctuating weather conditions (temperature, rate of water evaporation) and aggregate moisture states. Therefore, attention must be paid to obtain consistent long term workability from batch to batch (Felekoğlu and Sarıkahya, 2008). Khayat and Mitchell

(2009) reported that SCC is often proportioned with polycarboxylate-based or copolymer HRWRA that can develop better fluidity retention than naphthalene- or melamine-based HRWRA. Better slump flow retention can be obtained with SCC made with low w/cm given the higher HRWRA demand to achieve 26.0 to 27.5 in. (660 to 700 mm) slump flow. Additionally, the binder type had a significant effect on the slump flow retention. SCC containing 20% class F fly ash developed high fluidity retention. They also classified the fluidity retention of all mixtures for three relative performance levels depending on the difference between the slump flow at 10 mins and 40 mins as shown in Table A-6.

Table A-6. Relative performance of SCC mixtures for precast, prestressed applications regarding fluidity retention (Khayat and Mitchell, 2009)

	High	Medium	Low
Slump flow at 10 mins – slump flow at 40 mins	< 1.0 in (25.0 mm)	1.0 – 2.5 in (25.0 - 62.5 mm)	>2.5 in (62.5 mm)

Zhang et al. (2010) studied the effects of different superplasticizers on the workability retention and setting time of SCC. Water-to-cement ratios of 0.26 and 0.32 were used with different types and dosages of superplasticizers in pastes with a yield stress < 6 Pa at 30 min. The following conclusions were drawn:

1. The lignosulphonate (PLS), polycarboxylate (PCE), and polynaphthalene (PNS) based superplasticizers investigated retarded cement hydration. The PLS admixture had a much stronger retarding effect than the PCE and PNS admixtures.
2. The yield stress and effective viscosity of PCE and PNS admixtures increased more rapidly with time compared with the PLS admixture. This indicated that the paste with the PLS admixture had a longer workable time than that with the PCE and PNS admixtures.
3. Although the pastes with PLS admixture had longer workable time, the longer setting time has to be taken into consideration in practice whenever early strength development is essential.
4. The initial setting was monitored by heat development, change of rheological parameters with time, and penetration depth in cement pastes. Since the initial setting time indicates the loss of workability to such an extent that the paste is no longer workable, the initial setting time determined by the change of yield stress provides more precise information than the penetration depth test of the cement pastes. The heat development curves may provide useful information for estimating initial setting time of cement pastes incorporating superplasticizers with retarding effects at a given w/c.

1.2 Early-Age SCC Properties

1.2.1 *Formwork Pressure*

To support the newly cast SCC, stronger formwork is required, and as a consequence, the cost of formwork may exceed the cost of concrete and steel materials combined (ACI committee 347, 2014). For a liquid, the lateral pressure of a certain height is computed as the unit weight times the height and the lateral pressure is equal to the vertical pressure. Though concrete is very different from a liquid, a current guideline recommends that an SCC formwork should resist the lateral pressure equal to full water head of concrete (ACI committee 347, 2014). The instant after SCC is placed, it behaves as a fluid. As time passes, however, concrete progressively evolves into a solid, building up an internal structure capable of self-support.

Tests performed by Vanhove and Djelal (2002) showed a maximum of 64% of maximum hydrostatic pressure for a wall placed at 25 m/h from above, and a maximum of 68% of maximum hydrostatic pressure for a wall placed at 19.5m/h by pumping from the bottom of the wall. In their study, the maximum pressure was not found at the bottom of the wall but at a height of 1.5 m. Many other researchers (Khayat and Omran, 2010; Billberg et al., 2005; Tejeda-Dominguez et al., 2005; Khayat et al., 2005; and Assaad and Khayat, 2006) have shown similar results.

1.2.1.1 Factors Affecting Formwork Pressure

The formwork pressure is a function of the physical/chemical properties of a concrete mixture (Assaad and Khayat, 2004). Thus, factors affecting the physical/chemical properties of SCC, such as particle interlocking/friction, concrete-formwork friction, binding component types and content, gelation process of SCC and chemical agent types and content, as well as external and internal temperatures, will have effects on the formwork pressure development of SCC. These factors can be classified into two categories: intrinsic factors related only to the material itself and extrinsic factors related to external environment and the formwork conditions. The major intrinsic and extrinsic factors are listed as the following.

1.2.1.1.1 Intrinsic Factors

- **Cementitious material type and content**

From a microstructural development point of view, the reduction in lateral pressure exerted on the formwork by SCC is due to the stiffening/gelation of the cementitious material. For a given binder content, the initial lateral pressure and its rate of drop with time are significantly affected by the binder type (Assaad and Khayat, 2004). Concrete made with Type I cement and no supplementary cementitious material exhibited the highest initial pressure and the lowest rate of pressure drop with time. Mixtures made with ternary cement or Type III cement exhibited lower initial pressures and higher rates of pressure drop. Partial replacement of cement with a supplementary cementitious material with lower specific gravity will increase solids content of the paste for a given w/cm. This may result in an increase in particle interlocking, leading to greater thixotropy and reduced formwork pressure (Gregori et al., 2008). Kim et al. (2010a) studied the effect of various mineral additives on formwork pressure. The mineral additives decrease the lateral pressure developed immediately after vertical pressure is applied (instantaneous response), but their effect does not significantly decrease the lateral pressure when vertical pressure is maintained. Their most interesting finding is that a small amount of

processed clay, Metakaolin and wet-processed attapulgite clay (a kind of magnesium alumino-silicate), effectively enhances the shear resistance, leading to reduced formwork pressure.

- **Coarse aggregate**

One explanation for the reduction of formwork pressure with the increase of binder is the reduction of aggregate ratio in the mixture. It has been shown that lateral pressure is significantly influenced by the sand/aggregate value (Assaad and Khayat, 2005). Right after casting, mixtures with sand/aggregate values of 1.0 and 0.75 developed initial lateral pressures of 99 and 96% of hydrostatic pressure, respectively. With the increase in coarse aggregate concentration (sand/aggregate of 0.50 to 0.30), the initial relative lateral pressure decreased to 92 and 77%, respectively, and the rate of drop in pressure was more pronounced. This can be related to the increased coarse aggregate volume that reduces the mobility of the mixture and results in lower lateral pressure. Aggregate bridging is one mechanism that has been identified that occurs soon after the mixture is at rest. It is thought that as the material fills the form, the aggregate particles will contact each other to form a skeleton in the fresh concrete. As the gelation and hydration processes occur, this bridging will get stronger and will reduce formwork pressure.

- **Viscosity-modifying admixtures**

A great deal of research has gone into studying the influence of thixotropic properties of SCC mixtures on formwork pressure. Two methods are used to modify the thixotropic properties of SCC. One is by altering the binder type and content, and the other is by adding a Viscosity Modifying Agent (VMA). Mixtures that develop cohesion at faster rates will exhibit lower maximum lateral pressures for similar casting rates. The incorporation of a set-accelerating agent resulted in an increase in the rate of pressure drop. Conversely, the use of a set-retarding agent resulted in a delay in cement hydration that led to a slower rate of drop in lateral pressure. Assaad and Khayat (2006) investigated the incorporation of VMA with polycarboxylate-based HRWRA. The results showed that SCC made with a relatively low dosage of VMA (polysaccharide based) at 0.40 w/cm exhibits sharper rates of pressure drop compared to similar mixtures made without VMA and w/cm of 0.36. Incorporation of cellulose-based VMA along with polycarboxylate-based HRWRA could increase the degree of thixotropy of SCC compared to mixtures containing powder or liquid polysaccharide-based VMA and naphthalene-based HRWRA. The SCC containing cellulose-based VMA, however, exhibits a lower rate of increase in thixotropy with time because of the polycarboxylate-based HRWRA that enhances fluidity retention. Increased VMA content led to higher lateral pressure development, which is due to the greater HRWRA demand.

1.2.1.1.2 Extrinsic Factors

- **Casting rate**

It is easy to know that the faster the material is poured, the greater the maximum formwork pressure will be. Measurements and modeling were conducted to investigate the effect of casting rate on later formwork pressure. Gregori et al. (2008) reported that casting rate reduction from 14m/h to 7m/h will result in a peak lateral formwork pressure reduction from 280 kPa to 250 kPa. Birch (2007) also compared the formwork pressure for three different casting rates (4, 8, and 16 ft/hr). The slowest casting rate limited the pressure to under 5 psi while the rapid casting rate reached 20 psi. Given that a typical industrial formwork is rated at about 7 psi, construction at the slowest rate could proceed with no problems, while construction at the 16 ft/hr could overload the formwork and lead to form failure.

- **Casting temperature**

The influence of intrinsic/extrinsic temperature of SCC on formwork pressure is due to its effect on the rate of gelation of concrete mixture. Lateral formwork pressure of SCC will drop more quickly at high temperatures due to accelerated hydration. Tejeda-Dominguez et al. (2005) has shown that the increase of casting temperature from 10^{o}C to 40^{o}C, could reduce the time it takes to drop the lateral pressure to zero by 3 hours.

- **Wall friction**

Wall friction exerted on SCC by formwork can be a factor in reducing lateral formwork pressure. Using different column formworks with various cross-sections, Kwon et al. (2011) investigated the effects of formwork wall friction on the formwork pressure. It revealed that a wider cross-section formwork induces greater friction stress that decreases the extent and retention time of formwork pressure.

1.2.1.2 Formwork Pressure Modeling

It has been acknowledged that the lateral formwork pressure of SCC is lower than the hydrostatic head. A lack of a lateral formwork pressure prediction method leads to potentially over-conservative formwork design. In considering formwork pressure, two main parameters should be considered to ensure a safe yet cost effective formwork system. The first is the initial maximum lateral pressure exerted by the freshly placed SCC. This value is critical because it directly affects the design of the formwork system. A design value smaller than the maximum will result in failure. The second parameter is the rate of the pressure decay, which is directly related to the speed of placement of concrete. The rate of reduction of formwork lateral pressure is also important for better scheduling of formwork usage. Research work has been done to predict the magnitude of formwork pressure as discussed below.

1.2.1.2.1 Sherbrooke University SCC Formwork Pressure Model

This model for formwork pressure prediction is related to rheological parameters of SCC (Assaad et al., 2003a). The idea behind the model is that the reduction of formwork pressure is controlled by friction and cohesion between particles. A column apparatus with pressure measurement sensors was used to measure the pressure exerted by various mixtures. To model the effect of higher pressure values, a portable pressure column was developed in which air pressure is gradually applied to simulate pressure increase due to concrete placement at a given rate up to 13 m head. The rheological properties of SCC were measured using a coaxial rheometer, where torque was recorded at various rotation rates. Thixotropy was quantified by measuring the breakdown area. It was found that breakdown area and lateral pressure were nearly linearly related. This resulted in a model that used the initial breakdown area, determined during the first 30 minutes after mixing, to predict lateral pressure as a function of hydrostatic pressure and time (Assaad et al., 2003b).

UIUC Formwork Pressure Model

The formwork pressure prediction model developed at the University of Illinois at Urbana-Champaign (UIUC) is also based on the characteristics of pressure measurement curve (Lange et al., 2008a). The primary devices used are a mounting apparatus and pressure sensor. A model to predict the formwork pressure was developed using the characteristic pressure decay curve measured on a three feet tall column (Lange et al., 2008a). The principle of the model is that

SCC exhibits a pressure decay that can be detected a few minutes after the SCC is at rest in a form. A hyperbolic function is used to cure-fit the decay signature:

$$C(t)_{\text{modeled}}=C_0 / (at^2+1)^{\alpha} \quad \text{(A.5)}$$

Where C_0 is the initial pressure just after placing the concrete in the column, t is the time since casting, and a and α are coefficients used for fitting the curve and are specific to the time units used in the analysis. Then the predicted pressure is obtained by multiplying the $C(t)_{\text{modeled}}$ function by unit weight and filling height over time, which is a function of time.

$$P(t)_{\text{predicted}}= C(t)_{\text{modeled}}*h(t)*\gamma \quad \text{(A.6)}$$

Where $h(t)$ is the casting rate and γ is the unit weight of concrete. As stated by the author, though the formwork prediction model is a relatively easy, straightforward approach, there might be various irregularities on a jobsite that may affect formwork pressure.

1.2.2 ***Heat of Hydration***

Cement hydration is an exothermic process: heat is released when portland cement compounds react with water. Any action that promotes the hydration process would increase the heat liberation, and vice versa. For instance, increasing the portland cement quantity in the mix or using finer cements will increase the amount of heat released.

The heat of hydration can be determined by various means. Traditionally, it has been determined in accordance with ASTM C186, where the heat of solution of the dry cement and the heat of solution of a separate portion of the cement that has been partially hydrated for 7 and for 28 days are determined. The difference between these values is the heat of hydration for the respective hydrating period. More recently, calorimetry tests are increasingly used for monitoring heat of hydration in cement based materials with time. From a purely theoretical standpoint, there are two major types of calorimetry tests, isothermal and adiabatic. In isothermal calorimetry, the heat of hydration is measured by monitoring the heat flow from the specimen while both the specimen and the surrounding environment are maintained at approximately the same temperature. In an adiabatic calorimetry test, the heat of hydration is measured by monitoring the heat flow from the specimen while the specimen is under an insulated condition and has no or very little heat loss. The isothermal calorimetry test is often used for determining the rate and amount of heat of generation (ASTM C1702) as well as for studying hydration kinetics of cementitious materials (ASTM C1679). In mass concrete, such as concrete in dams, large bridge foundations, and pavements, the adiabatic calorimetry test is often used to monitor the temperature rise in the concrete since it is a major concern for thermal cracking. Since a "perfect" isothermal or adiabatic calorimetry test is nearly impossible to conduct without delicate (and thus expensive) equipment, a hybrid termed semi-adiabatic calorimetry test is more frequently employed (Wang et al. 2006).

Schindler and Folliard (2005) have proposed a general hydration model based on heat released during hydration, and stated that the heat of hydration is influenced by the cement chemical composition, cement fineness, use of supplementary cementitious materials (SCMs) and the concrete mixture proportions. The effect of these parameters (i.e., the contribution of each parameter to the overall hydration process) was obtained. The degree of hydration is characterized by the start of the acceleration phase, rate of hydration, and ultimate value. The effect of each parameter is given qualitatively (i.e., insignificant represented by dash, small,

medium and large). It was observed that using Class C fly ash delays the start of the acceleration phase.

Bouzoubaa and Lachemi (2001) studied the temperature rise in SCC mixtures. All mixtures were maintained to have a constant content of the cementitious materials of 400 kg/m^3 (672 lb/yd^3). These mixtures had a cement replacement of 40%, 50%, and 60% by Class F fly ash. They observed that the temperature rise of the mixtures with higher percentage of replacement was lower than that of the control mixture. They also reported that higher percentage of replacement is associated with lower peak of temperature rise.

Troli et al. (2003) studied a special SCC in a mass concrete application. The temperature rises of two SCC concrete mixes were compared. The core temperature changes were kept below 20^{o}C, which was the target. The fly ash mixture displayed a lower total heat output. Collepardi et al. (2005) obtained similar results with a slag cement SCC mix.

Poppe and Schutter (2005a) studied the effect of limestone filler on the heat of hydration of SCC. They compared the effects of limestone and quartzite fillers. Addition of limestone filler causes the induction period to be shortened and an extra heat production peak occurs. These cannot be seen when a quartzite filler is used. Furthermore, they found a linear dependency of the maximum heat production rate on the cement-limestone powder ratio. Ye et al. (2007) found that the cumulative heat release and the rate of release in self-consolidating cement paste are higher compared to traditional cement paste and high performance cement paste. They also concluded that the limestone powder influences the hydration; it does not participate in the chemical reaction but provides initiation points for hydration that accelerates energy release.

Some studies involving portland limestone cement reported that limestone powder not only accelerates the initial hydration reaction but also influences the hydration products. Limestone leads to the formation of carbo-aluminates at the expense of mono-sulfate (Lothenbach et al., 2008; Weerdt et al., 2011).

1.2.3 *Time of Initial Setting*

Initial time of setting is the elapsed time after initial contact of cement and water required for sieved mortar to reach a penetration resistance of 3.5 MPa (500 psi). (AASHTO T 197). It is needed to control the schedule of construction activities in addition to indicating the pressure decay on the formwork. Bouzoubaa and Lachemi (2001) reported that the initial setting time of SCC with Class F fly ash SCM ranged from 4.8 to 7.75 hr. It was higher than that of CVC and was attributed to the high dosage of superplasticizer and the low cement content used in this study. Khayat and Mitchell (2009) reported that SCC normally incorporates a greater dosage of HRWRA than CVC, which typically results in some retarding effect of setting time. SCC has a prolonged setting time of 1-2 hours when compared to normal concrete of similar type. In this study, the initial setting time of SCC ranged between 4 to 13 hr.

1.3 **Hardened SCC Properties**

1.3.1 ***Mechanical Properties***

1.3.1.1 Compressive Strength

Compressive strength of SCC should be relatively high since SCC is often proportioned with relatively low *w/cm* and contains supplementary cementitious materials and fillers that can serve as nucleation sites and refine the porosity of the cement paste (Khayat and Mitchell, 2009).

The ACI 209 and CEB-FIP MC90 provide two different models to predict the development of concrete strength with time. The ACI 209 model depends on the curing method and cement type. The CEB-FIP MC90 is affected by the strength class and hardening characteristics (normal or rapid) of cement. Holschemacher and Klug (2002) surveyed the development of different SCC mixtures with various fillers and supplementary cementitious materials (SCMs). They evaluated the CEB-FIP MC90 prediction model and concluded that the actual strength ratio after 28 days does not significantly differ from the predicted values. Khayat and Mitchell (2009) evaluated the ACI 209 and CEB-FIP MC90 models for SCC mixtures with different types of cement and curing methods and concluded that both of them underestimate the development of compressive strength by around 5% but the latter reflects less scatter as shown in Figure A-8.

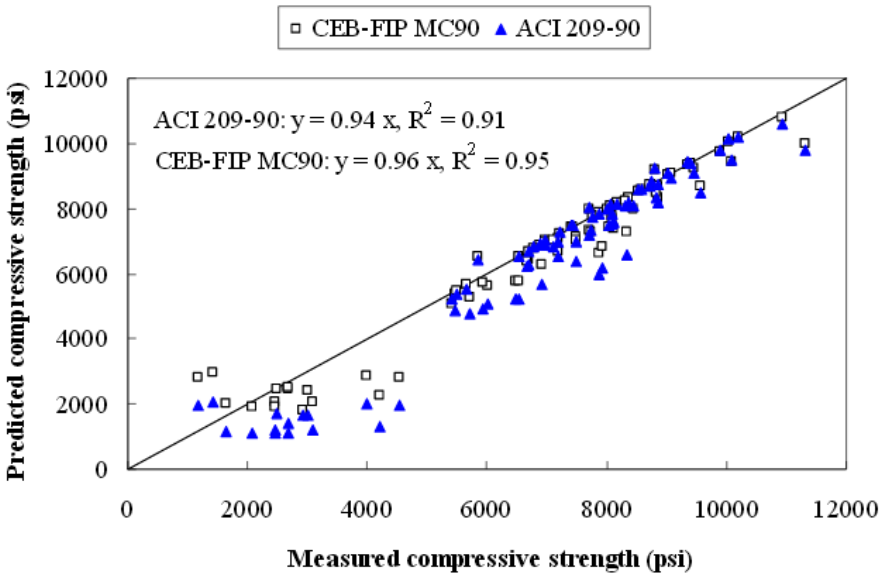

Figure A-8. Comparison of measured and predicted compressive strength (plotted data include 18-hour, 7-, 28-, and 56-day compressive strength results) (Khayat and Mitchell, 2009)

1.3.1.2 Modulus of Elasticity

The modulus of elasticity of concrete depends on the proportion of the Young's modulus of elasticity of the individual components and their percentages by volume. Thus, the modulus of elasticity of concrete increases with increasing content of aggregates of high rigidity, but it decreases with increasing paste content and increasing porosity. For this reason, lower values of modulus of elasticity can be expected for SCC because of the higher content of fines and lower content of coarse aggregates with SCC (Klug and Holschemacher, 2003). Pineaud et al. (2005)

studied the effect of paste volume in the range of 359 to 452 l/m3 and reported that increasing the paste volumes decreases the modulus of elasticity of SCC.

For similar compressive strength, gravel SCC mixtures develop lower modulus of elasticity than those for mixtures made with crushed aggregates of the same MSA under moist curing conditions at 56 days (Khayat and Mitchell, 2009). Su et al. (2002) reported that the elastic modulus of SCC was not significantly affected by sand-to-aggregate (S/A) ratio when total aggregate volume was kept constant.

The literature review showed that the modulus of elasticity of SCC is generally lower than or the same as that for CVC, mainly due to the lower coarse aggregate volume of SCC (Turcry et al., 2002; Holschemacher and Klug, 2002; Ambroise and Pèra, 2002; Vieira and Bettencourt, 2003; Dinakar et al., 2007; Georgiadis et al., 2007; Nassif et al., 2008; Sonebi et al., 2000; Parra et al., 2007; Schindler et al., 2007). However, under air-drying conditions, the elastic modulus of SCC can be higher than normal concrete in the long term due to the lower loss of water that may occur in the case of SCC (Vieira and Bettencourt, 2003).

Turcry et al. (2002) found the ratio of elastic modulus to compressive strength at 28 days to be lower in the case of SCC than for ordinary concrete. Holschemacher and Klug (2002) showed that the elastic modulus of SCC could be up to 20% lower compared with CVC of the same compressive strength made with the same aggregate type. Ambroise and Pèra (2002) reported that the modulus of SCC mixtures was lower by about 10% than the corresponding CVC. Dinakar et al. (2007) describes the results of an investigation aimed at producing and evaluating SCCs of various strength grades designed at desired fly ash percentages of 0, 10, 30, 50, 70 and 85%, and compared with five different mixtures of CVC. Fly ash SCC had 8% lower elastic modulus compared to CVC for an identical compressive strength. For compressive strength over 60 MPa, the elastic modulus of SCC was almost the same as that of CVC. Nassif et al. (2008) reported that the modulus of elasticity of SCC is 5% lower than that of CVC. Sonebi et al. (2000) reported the elastic modulus of SCC to be the same as that of reference mixtures of CVC. Parra et al. (2007) concluded that no significant differences were found between SCC and CVC regarding modulus of elasticity, although SCC tends to be slightly more deformable because of higher paste content. However, the little differences disappear when the quality of the concrete is improved. Schindler et al. (2007) found that the 18-hour modulus of elasticity of SCC was less than that of the control CVC mixture with comparable concrete strength. At 56 days, they were similar.

Several existing prediction models for CVC (i.e., AASHTO 2007, CEB-FIP 90 model, ACI 363-92, ACI 318-99, ACI 318-08, Eurocode2 (EC-2), New Zealand NZS 3101:2006, and Canadian CSA A23.3-04) have been used to evaluate the modulus of elasticity of SCC.

Khayat and Mitchell (2009) found that the AASHTO 2007 code achieved the best correlation between the predicted and measured values. As shown in Figure A-9, the CEB-FIP 90 model overestimates the elastic modulus, while ACI 363-92 and ACI 318-99 underestimate the elastic modulus for SCC with compressive strength greater than 4,350 psi (30 MPa).

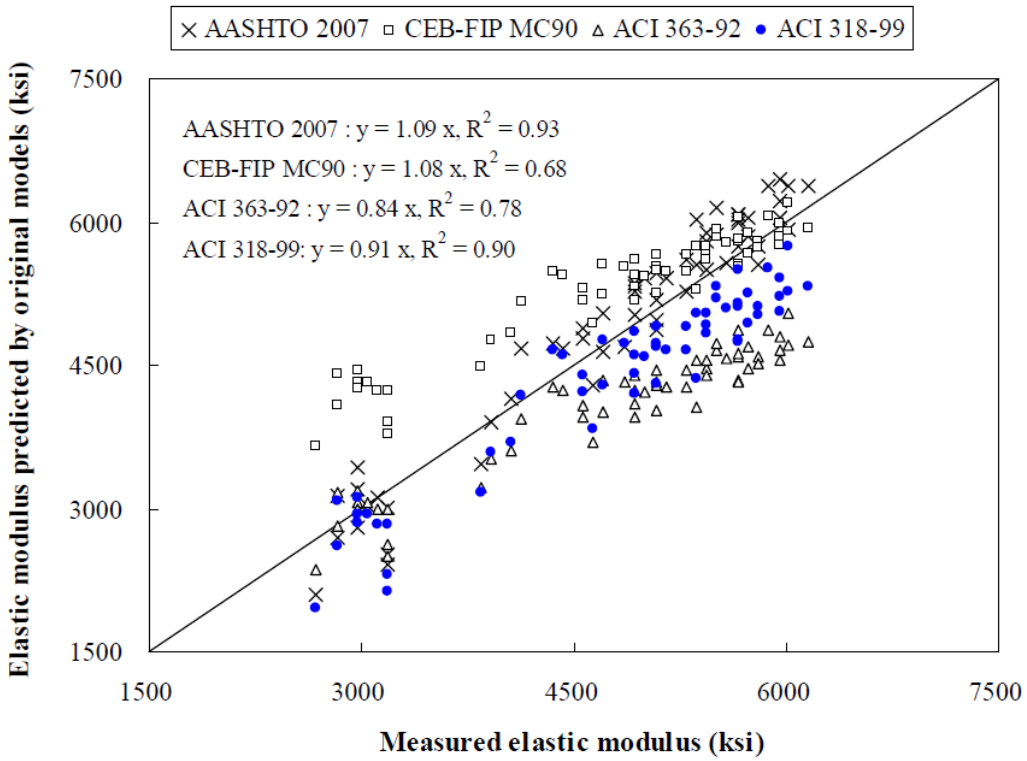

Figure A-9. Comparison of measured and predicted modulus of elasticity for SCC (Khayat and Mitchell, 2009)

A survey by Desnerck et al. (2014) of 314 results reported that EC-2 provides an adequate prediction and ACI318-08 underestimates the modulus of elasticity for SCC. Ma and Dietz (2002) reported that the measured elastic modulus values of SCC at 28 days corresponded to approximately 80% of values estimated by the CEB-FIP 90 model. Mokhtarzadeh and French (2000) found that the ACI 318-99 model overestimated the elastic modulus based on the compressive strength of concrete, while equations proposed by the ACI 363-92 model and the CEB-FIP 90 model resulted in the most reasonable predictions. Vilanova et al. (2011) evaluated modulus of elasticity by different code models. The ACI 318-08 model slightly overestimates the measured value. The EC-2 model also overestimates the measured modulus of elasticity. The NZS 3101:2006 and the CSA A23.3-04 underestimate the modulus of elasticity.

1.3.1.3 Splitting Tensile Strength

Tensile strength of the concrete may be determined in three ways: (1) direct tensile test, (2) splitting tensile strength test and (3) flexural tensile strength test (modulus of rupture). Due to the difficulties of conducting the direct tensile test, splitting and flexural tensile strength are the most common methods to indicate the tensile strength of concrete. Desnerck et al. (2014) analyzed the results of 6 SCC mixtures from one study by Itterbeeck et al. (2010). This study indicated that the ratio between splitting tensile strength and direct tensile strength is 0.84±0.04 and the ratio between flexural tensile strength and direct tensile strength is 0.59 ± 0.10.

Parra et al. (2007) reported the tensile strength of SCC is about 18% less than that of CVC. However, Klug and Holschemacher (2003) conducted a literature review of tensile strength of SCC and reported that higher tensile strength values are obtained with SCC than with CVC. Turcry et al. (2002) showed the 28-day tensile to compressive strength ratio for SCC mixtures to be higher than that for CVC, i.e., between 0.087 and 0.1 compared to 0.075 in the case of CVC. Bosiljkov (2003) reported that the splitting tensile strength to compressive strength ratio of SCC could range between 0.08 and 0.09 for mixtures made with limestone filler and low *w/b* of 0.22 to 0.25. Sonebi et al. (2000) reported the ratios of splitting tensile strength to compressive strength of SCC made with 0.36 *w/b* containing 38% slag replacement to be 0.059 at 28 days and 0.062 at 180 days.

Holschemacher (2004) illustrated that the majority of measured splitting tensile strength data lie within the range of valid regulations by CEB-FIB 90 provisions. In about 30% of the data, a higher splitting tensile strength was obtained. He found an increase in tensile strength when fly ash and silica fume are used. Mokhtarzadeh and French (2000) reported that the splitting tensile strength of both heat-cured and moist-cured SCC cylinders was more closely predicted by the ACI318 model than the ACI363 model. Desnerck et al. (2014) reported a survey for 256 data results from 27 studies and concluded that EC2 provides adequate prediction limits for tensile splitting strength for SCC mixtures with limestone or gravel aggregate but underestimates for mixtures with granite aggregate.

1.3.1.4 Flexural Tensile Strength

The values reported by various investigators for the modulus of rupture of both lightweight and normal weight high-strength concretes fall in the range of $0.24\sqrt{f'_c}\ to\ 0.38\sqrt{f'_c}$ where both the modulus of rupture and the compressive strength are expressed in ksi (ACI 363). Mokhtarzadeh and French (2000) reported that flexural tensile strength of moist-cured SCC specimens were closely predicted by the ACI 363 model and the flexural tensile strength of heat-cured SCC specimens lie between the two models, with ACI 318 ($f_r = 0.24\sqrt{f'_c}$) as the lower limit and ACI 363($f_r = 0.37\sqrt{f'_c}$) as the upper limit. Desnerck et al. (2014) presented a survey of 27 data results for the 4-point loading test and 78 data results for the 3-point loading test of flexural tensile strength. This survey compared the measured data with two different code provisions: EC2 and the Model Code 2010 (MC2010). It reported that the data of the 3-point test lie above the upper range of the predicted values by both models. Both models provided an adequate prediction of flexural strength of SCC measured by the 4-point test.

Khayat and Mitchell (2009) evaluated the AASHTO 2007, ACI 363-84 and Khayat et al. models (Khayat et al., 1995) for flexural strength. As presented in Figure A-10 (a), the AASHTO 2007 and ACI 363-84 models overestimated the flexural strength results of SCC for mixtures having compressive strengths lower than 6,530 psi (45 MPa). Thereafter, the two models yielded better estimates of the measured values. On the other hand, the model proposed by Khayat et al. (1995) provided better prediction of flexural strength for concrete with compressive strength lower than 6,530 psi (45 MPa).

Relevant changes to the constants of the three models were proposed to provide better fit to the measured data. The results are the modified models plotted in Figure A-10 (b). The suggested changes in the prediction models are summarized in Table A-7. The three modified models offered a similar degree of prediction of flexural strength of SCC.

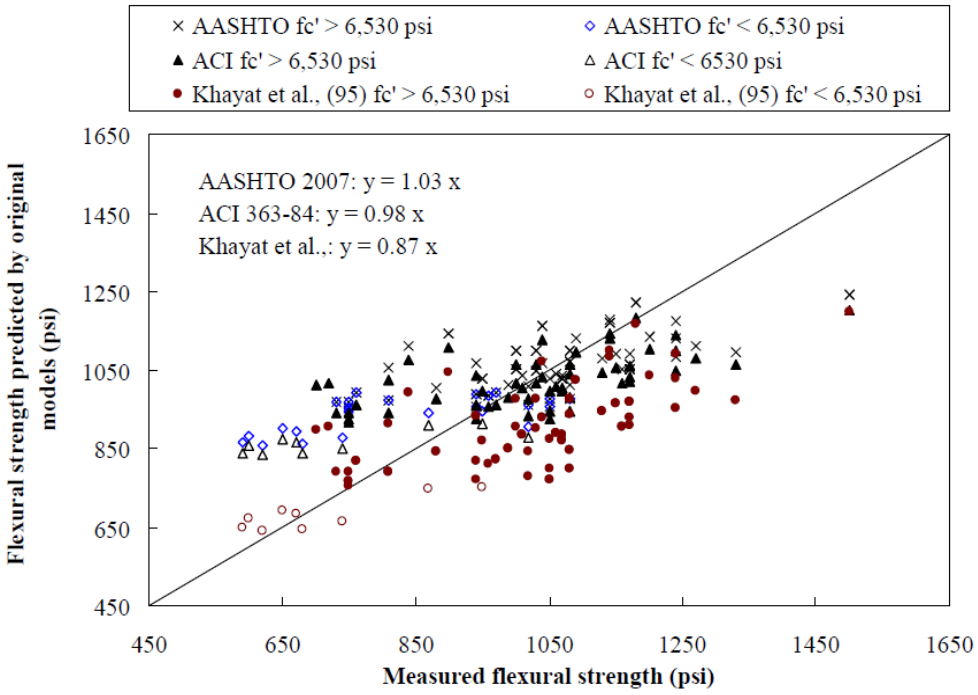

(a) Existing models

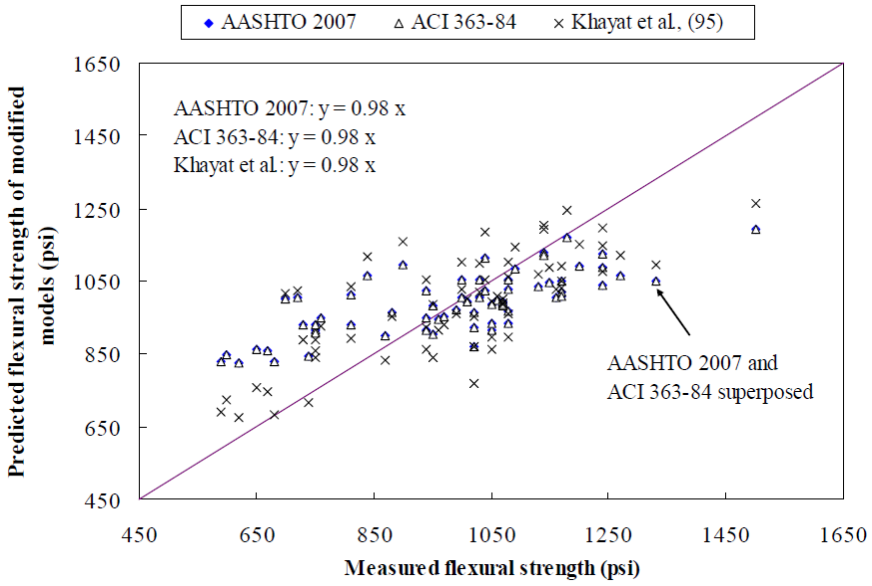

(b) Modified models

Figure A-10. Comparison of measured and predicted flexural strengths (Khayat and Mitchell, 2009)

Table A-7. Modified Flexural Strength Prediction Models (Khayat and Mitchell, 2009)

	Original model equations	Modified equations
AASHTO 2007	Compressive strength up to 15230 psi (105 MPa)	
	$f_r = 0.97\sqrt{f_c'}$	$f_r = 0.93\sqrt{f_c'}$
ACI 363-84	f'_c in MPa	
	$f_r = 0.94\sqrt{f_c'}$	$f_r = 0.93\sqrt{f_c'}$
Khayat et al. (1995)	Compressive strength with 6,525-15,955 psi (45-110 MPa)	
	$f_r = 0.23 + 0.12 f_c' - 2.18\times10^{-4}(f_c')^2$	$f_r = -3.2 + 0.26 f_c' - 1.43\times10^{-3}(f_c')$

1.3.1.5 Bond Strength

Bond stress is the shear stress transferred from the concrete to the reinforcing bar. Initially bond stress is derived from a weak chemical bond between the steel and the hardened hydrated cement paste of concrete. Once slip occurs, friction contributes to the bond and the bond resistance is derived principally from the bearing, or mechanical interlock of the ribs on the surface of the deformed bar with the concrete (Hassan et al., 2010). Bleeding, segregation, and surface settlement are the major factors that affect bond.

Beam and pull out tests are used to evaluate the bond strength of SCC in the literature (Almeida et al., 2008). Pull out failure of embedded bars without cracking or spalling of concrete cover is attributed to the confinement effects of the adequate concrete cover and presence of heavy reinforcement around the embedded bars (Morita and Kaku, 1979). Otherwise, concrete, more typically, shows a splitting failure when unreinforced small specimens are used (Cattaneo and Rosati, 2009).

König et al. (2001 and 2003) and Almeida et al. (2005) found that CVC performed better in bond tests and might achieve 15 to 20% greater bond strength than that of SCC. Almeida et al. (2008) evaluated the bond behavior of SCC by varying compressive strength and steel bar diameter in pull out and beam tests. The comparison between test results and code equations showed that the same equations adopted for CVC can be used for SCC, which means that bond properties of SCC are similar to those of CVC. Hassan et al. (2010) reported that the normalized bond stress was slightly higher in SCC than that in CVC at 3, 7, 14 and 28 days in pull out tests. Aslani and Nejadi (2012) reported that the bond strength of SCC is as high as the bond strength for CVC when large bar diameters are studied. For smaller bar diameters, the bond strength of SCC is slightly higher, with the largest difference occurring for the smallest bar diameters.

Valcuende and Parra (2009) conducted pull out tests to examine the bond strength between reinforcement steel and concrete. They reported that relative steel-concrete slip of pull out tests should be limited without exceeding the perfect bond stress hypothesis on which the capacity of reinforced concrete sections is calculated. Thus, they calculated the mean bond strength from the arithmetic mean of the stresses recorded for slips of 0.01 mm, 0.1 mm and 1 mm. It was found that the mean bond stress was about 30% greater in SCC than in CVC in 30 MPa concrete, but

these differences decrease to less than 10% in 60 MPa concrete. However, the differences tend to disappear for ultimate bond stress.

The enhanced cohesiveness of SCC ensures better suspension of solid particles in the fresh state and this, therefore, produces good deformability and filling capability. Bleeding, segregation and surface settlement as a result of high water-to-cement ratio (w/c) or excessive vibration is generally not a factor when SCC is used. Hence, the application of SCC is expected to increase the strength of the concrete and the bond between steel and concrete even in deep concrete members (Hassan et al., 2010).

According to Gibbs and Zhu (1999), the differences recorded between the bond strength for the two types of concrete were less than 4%, whereas Wang and Zheng (2005) reported 9%, and Daoud et al. (2003) reported 5% higher bond strength for SCC. Sonebi and Bartos (1999) reported 16–40% while Collepardi et al. (2005) reported as much as 70% higher bond strength for SCC than that of CVC.

Zhu et al. (2004) reported that the normalized bond strengths of the SCC mixes were found to be about 10-40% higher than those of CVC mixes with the same strength, while the maximum bond strength decreased when the diameter of the steel bar increased from 12 to 20 mm. Cattaneo and Rosati (2009) found SCC exhibits higher bond strength and, compared to CVC, requires larger concrete cover to attain pullout failure. Desnerck et al. (2009) conducted beam tests to evaluate the bond of reinforcement in SCC and CVC and found for the same compressive strength the bond strength of SCC is as high as that of CVC for large bar diameters, or slightly higher than that of CVC for smaller bar diameters. The bar diameters ranged from 12 mm to 40 mm.

Greater amounts of bleeding, segregation, and surface settlement occur as the depth of the beam increases (Hoshino M., 1989). Therefore, the top bars in a beam more than 12 in. (300 mm) deep, generally show poor bond characteristics compared to the bottom bars. The ACI 318 and Canadian (CSA, 2005) codes take this into account by requiring 30% excess development length for top-cast deformed bars.

Most researchers agreed that SCC still shows the top-bar effect but the extent is less than or similar to CVC, and for concretes of more than 50 MPa, the differences between SCC and CVC are not significant. Khayat (1998) found VMA helped reduce surface settlement related to bleeding and segregating and significantly reduced the top-bar effect. Attiogbe et al. (2002) concluded that highly stable SCC mixtures have a level of top-bar effect for deformed bars that is similar to that of 4 to 6-in. slump concrete. Chan et al. (2003) conjectured that the plastic settlement during hardening of SCC may still cause top-bar effect, and reported that less top-bar effects were found for SCC in the pull out tests than for CVC. Castel et al. (2006) concluded that bond strength of SCC is not affected by the orientation of the bars. For the top casting surface, the maximum ultimate bond strengths obtained were approximately 20% higher for SCC than for CVC, regardless of the concrete strength. Hassan et al. (2010) reported that the bond stress-slip curve showed similar trends of variation for both SCC and CVC pull out specimens in the bottom bars. Higher bond stress and stiffness in the top and middle bars were observed in SCC compared to CVC. Trezos et al. (2010) found the top-bar effect seems to be less intense in SCC when the stress corresponds to slip of 0.25 mm; bond stress is selected as the bond strength.

Valcuende and Parra (2009) found SCC behaved more homogeneously than CVC in vertically cast pieces and exhibited less top-bar effect than CVC. The variation of mean bond stress with height for SCC and CVC were compared and indicated that the loss of bond strength between the

upper and lower zones of the columns varies between 40% and 61% in SCC and between 79% and 86% in CVC. The current standards usually put the factor at 1.4, which takes into account the top-bar effect for CVC for calculating the anchorage length of reinforcements in columns, but 1.25 was proposed for the special case of high viscosity powder-type SCC. Khayat et al. (1997) reported that the top-bar factor for reinforcing bars positioned approximately at 1.4 m from the bottom of a wall varied between approximately 1.3 and 1.6 for the SCC compared to 2.0 for the conventional concrete.

Esfahani et al. (2008) studied the effect of bar position on the bond strengths of reinforcing bars using pull out tests with top, middle and bottom bars. It was found that the local bond strength of bottom cast bars was almost the same for CVC and SCC, but for the top cast bars, the local bond strength for SCC was about 20% less than that for CVC. Valcuende et al. (2008) found that these results were not representative due to the small concrete cover-bar diameter ratio used. In tests carried out by Chan et al. (2003), Khayat et al. (1997), and Castel et al. (2006), where the concrete cover-to-bar diameter ratio was much greater, the results obtained opposed those obtained by Esfahani et al. (2008).

The orientation of the rebar has a significant effect on the bond strength. The horizontal rebars, which are parallel to the direction of casting, have a lower bond strength than vertical rebars. This is attributed to the accumulative bleeding water under the rebar, which leads to a decrease in the interfacial bond strength. The static instability of concrete leads to surface settlement that reduces the bond strength of horizontal rebars more than the vertical rebars (CEB-fib, 2000).

As a summary, the following conclusions can be made:

- Beam and pull out tests have been used to evaluate the bond strength of SCC in the literature. The types of failures included pull out failure without cracks or spalling or splitting failure.
- A few researchers reported higher bond strength for CVC than SCC and no significant difference between them. Conversely, most of the researchers come to the conclusion that the bond strength of SCC with reinforcement is higher than that of CVC, and the bond strength decreases when the bar diameter increases.
- VMAs help to reduce surface settlement related to bleeding and segregating and significantly reduced the top-bar effect of SCC.
- Most researchers agreed that SCC exhibits the top-bar effect but it is less pronounced than that in CVC, and for concretes of more than 50 MPa, the differences between SCC and CVC are not significant.

1.3.1.6 Shear Strength

Shear forces in reinforced concrete members are resisted by the reinforcement and shear capacity of concrete. In cracked sections, the shear capacity of concrete is provided by the dowel action of reinforcing bars and aggregate interlock, which resists the shear displacement.

1.3.1.6.1 Nominal Shear Resistance

Ebrahimi and Beygi (2009) conducted an experiment on nine rectangular beams, 1.4 m long, 18 cm wide, and 20 cm deep, to investigate the shear behavior of reinforced concrete beams made of SCC and CVC. Three beams were made of 40 MPa CVC, three beams were made of 60 MPa SCC, and three beams were made of 80 MPa SCC. Three different stirrup spacings were used in each group. The nine beams were tested using four-point loading and were heavily reinforced in

flexure to experience shear failure. Testing results indicated that the ultimate shear strength was dependent on the concrete strength and stirrup spacing and not on the type of concrete. In all cases, the ultimate shear strength of CVC and SCC was found to be higher than predicted using the ACI code and the cracking patterns of CVC and SCC beams were similar.

Lachemi et al. (2005) tested nine 8 m long rectangular beams to study the shear failure mechanism of SCC versus that of CVC. Three concrete mixtures (two SCC "S" and one CVC "N") were used to cast three different cross sections (150, 200, and 300 mm high), 100 mm wide, and using two aggregate sizes (12 mm and 19 mm). Test results indicated that the increase in the maximum aggregate size from 12 mm to 19 mm in SCC decreases the shear capacity at the first shear crack and increases the ultimate shear resistance. Overall, SCC with the same maximum aggregate size and type as CVC has almost the same shear capacity of CVC despite the lower volume of coarse aggregate in SCC.

Hegger et al. (2007) investigated the shear carrying capacity of nine prestressed beams made of two different types of SCC mixtures and variable shear reinforcement ratio. Comparing test results with a database of more than 250 shear tests on CVC indicated that there is no significant difference in the shear capacity of SCC and CVC. Also, calculated shear capacity agreed well with test results.

Choulli et al. (2008) tested four full-scale precast/prestressed I-beam specimens made with high strength SCC (90 MPa). Another two I-beam specimens were made of CVC and were tested for comparison. The beams had different levels of shear reinforcement including no shear reinforcement and different levels of prestressing. Beams were tested twice (one test at each end). Test results indicated that SCC had lower shear capacity than CVC in the range of 12-18%. The cracking patterns and failure mechanisms of SCC and CVC beams were almost the same. Also, code predictions of ultimate shear strength were conservative for all specimens.

1.3.1.6.2 Interface Shear

Whenever two elements of a concrete member are cast at separate times, adequate bond along the interface of the two elements is essential to act as a fully composite member. Interface shear resistance is the ability to transfer shear stresses across an interface between the two elements. Factors contributing to the transfer of shear stresses and resistance against shear displacements (slip) along the interface are cohesion, interlock, and shear friction developed by the force in the reinforcement crossing the plane of the interface.

In the design of this interface shear reinforcement, the structural designer should take into account not only the total amount of steel crossing the interface, but also the surface condition of the interface prior to casting of the second element. Both the AASHTO LRFD and ACI 318 design codes distinguish between a surface roughened to a ¼-in. amplitude and a not-roughened surface for strength calculations. This surface roughness is typically achieved by raking the top surface of the girder after casting.

Desnerck et al. (2009) conducted several push off tests on SCC and CVC specimens with reinforcement ratio ranging from 0.45 to 2.68%. The results of shear capacity for the specimens made of SCC and CVC with different reinforcement ratios indicated that the ultimate shear strength of SCC is approximately 15% to 20% higher than that of CVC. It also indicated that the reinforcement ratio is the predominant factor in determining the ultimate shear strength and not the size or content of coarse aggregate.

Kim et al. (2010b) evaluated the effect of coarse aggregate volume and type on the shear capacity of SCC and CVC. This investigation was performed on 48 push off specimens made of four mixtures of SCC and CVC containing river gravel and limestone as coarse aggregate. Test results indicated that the SCC has a lower fracture reduction factor (c) than CVC, and mixtures with limestone aggregate have a lower friction coefficient (μ) than those with river gravel aggregate. Concrete mixtures, both SCC and CVC, containing river gravel exhibit more aggregate interlock than those containing limestone. Also, the results indicated that maximum shear strength is dependent on the amount of coarse aggregate crossing the failure plane, which results in lower shear capacity for SCC mixtures than CVC. This conclusion is in line with those found by Khayat and Mitchell (2009), where lower shear capacity was observed in precast/prestressed concrete girders made of SCC versus those made of CVC.

Boehm (2008) tested twelve I-girders in flexure, six of them experienced a separation and horizontal displacement, or "slip," of the cast-in-place (CIP) deck relative to the girder. This separation and slip were only observed in SCC girders and can be attributed to inadequate shear transfer between the girder and the CIP deck. More specifically, it is believed that the failure to achieve proper interface surface roughness on the finished top surface of the SCC girders was a significant factor. As a result, for I-girders used as composite members with a cast-in-place deck, special precautions should be taken in order to ensure that proper surface roughness is achieved. Raking of the girder top surface should be postponed until the concrete has begun to set. The finished surface condition for the SCC girders should be inspected carefully. This will eliminate the tendency of the SCC to reconsolidate.

Maguire et al. (2009) has conducted an experimental investigation to evaluate interface shear transfer between a high strength (15 ksi) SCC double tee girder and 4 ksi conventional concrete deck when surface roughening is eliminated. Test results and failure mode had indicated that interface shear in members with wide flange, such as double tee, is highly dependent on the finished surface condition, which consequently affects the flexural capacity of the composite section. Unless adequate roughening is achieved, lower cohesion/friction coefficients than those provided by AASHTO Section 5.8.4.3 should be used to estimate the interface shear capacity.

In summary the factors that affect the nominal shear strength of SCC are similar to those that affect the shear strength of CVC, which include maximum aggregate size, coarse aggregate type and volume, shear reinforcement ratio and spacing. For interface shear capacity, roughening amplitude and reinforcement ratio are the influencing factors.

1.3.2 *Visco-Elastic Properties and Test Methods*

1.3.2.1 Shrinkage

Shrinkage is a change in the volume of concrete due to various reasons. For convenience, the magnitude of volume changes is generally stated in linear rather than volumetric units (Kosmatka 2002). In practice, total shrinkage of concrete can be evaluated by autogenous and drying shrinkage. Autogenous shrinkage occurs in the absence of moisture exchange due to the hydration reactions taking place inside the cement matrix, while drying shrinkage occurs in a specimen that is exposed to the environment and allowed to lose moisture (ACI Committee 209, 1997). High autogenous shrinkage occurs in concrete mixtures containing high binder content and low w/cm. Autogenous shrinkage increases with the fineness of cement, and amount of supplementary cementitious materials. An increase in binder content also increases drying

shrinkage because there is more paste. The volume of paste includes cement, fly ash, limestone powder, water, superplasticizers and shrinkage reducing admixture. The effect of HRWRA and VMA on shrinkage of SCC is reported to be beneficial. Indeed, the use of HRWRA reduces the surface tension of the water, thus decreasing the capillary tension of pore water. However, the air content may increase when using polycarboxylate-based HRWRA, which could lead to greater shrinkage (Khayat and Mitchell, 2009). As autogenous shrinkage is usually significantly lower than drying shrinkage in normal strength SCC, total shrinkage is dominated by drying shrinkage (Rozière et al. 2007). Therefore, drying shrinkage can be used for comparing the influence of mix design parameters (Leeman and Lura 2014). Most cast-in-place concrete components experience shrinkage while they are restrained, which results in tensile stresses that cause cracking.

1.3.2.1.1 Autogenous shrinkage

Embedded vibrating wire gages can be used to evaluate autogenous shrinkage of SCC (Khayat and Long, 2010). Autogenous shrinkage was measured on 3 × 3 × 11.8 in. (75 × 75 × 285 mm) prisms. The prisms were sealed immediately after removal from the molds at 18 hours of age and kept at 73 ± 4°F (23 ± 2°C) until the end of testing. Autogenous shrinkage was monitored using embedded vibrating wire strain gages until stabilization, which occurred after approximately 3 weeks of age. The autogenous shrinkage was obtained by subtracting the total shrinkage from thermal deformation. A linear thermal expansion coefficient of 6.4 μin./in./°F (11.5 μm/m/°C) was assumed for adjusting vibrating wire gage readings. The thermal expansion coefficient of the concrete was determined from the slope of the total deformation versus temperature curve of concrete prisms subjected to controlled temperature changes. Two prisms were initially immersed in water at the approximate temperature of 122°F (50°C). Once the temperature of the specimens was stabilized, the water was allowed to cool down to approximately 68°F (20°C). The resulting deformations were used to estimate the coefficient of thermal expansion/ contraction of the concrete. They reported that autogenous shrinkage is highly affected by w/cm and binder content. Rozière et al. (2007) reported that increasing the paste volume of SCC increases the autogenous shrinkage at constant W/P ratio. Increasing the amount of replacement of cement by limestone powder decreases the autogenous shrinkage at constant W/P ratio (Poppe and Schutter 2005b). Craeye et al. (2010) reported that using finer limestone filler increases the autogenous shrinkage in the first day. Esping (2008) presented a study on the use of limestone fillers with different specific surface area and their effect on the fresh and hardened properties of SCC. The results showed that fillers with a large surface area resulted in increased autogenous shrinkage, decreased evaporation, lower plastic cracking tendency, and a higher compressive strength.

1.3.2.1.2 Drying (Free) Shrinkage

1.3.2.1.3 Factors Affecting Drying Shrinkage

AASHTO T 160 (2009) and ASTM C157 (2003) can be used to measure drying shrinkage (Olive and Cramer, 2008). Bonen and Shah (2004) re-analyzed the data from Bui and Montgomery (1999) and found the shrinkage is proportional to the calculated plain portland cement paste volume rather the total binder volume. Loser and Leemann (2009) indicated that shrinkage increased with the increase of the volume of paste. Ma et al. (2009) reported that the increase of water to binder ratio (0.3-0.4) causes an increase in drying shrinkage. An increase of volume of coarse aggregate can reduce drying shrinkage significantly and the change of sand volume ratio has little effect on drying shrinkage of SCC with medium strength. Schindler et al. (2007) also

reported that a change in S/A from 0.38 to 0.46 had no significant effect on the 112-day drying shrinkage strain of SCC.

Supplementary cementitious materials (SCMs) (such as fly ash (FA), ground granulated blast furnace slag (GGBFS), silica fume (SF), and metakaolin (MK),) are indispensable ingredients in the production of SCC. In addition to SCMs, other powder materials such as limestone dust and clay additives are often employed in SCC. It was found that different SCMs had diverse effects on the shrinkage (including plastic, chemical, autogenous as well as drying shrinkage) of SCC.

Higher shrinkage is expected due to the denser matrix of the system leading to small capillary voids, which allow faster removal of water than large voids (Mokarem 2002). However, Güneyisi et al. (2010) researched the use of ternary and quaternary cementitious blends of mineral admixtures in the production of SCCs. The control mixture included only portland cement (PC) as the binder while the remaining mixtures incorporated binary, ternary, and quaternary cementitious blends of PC, fly ash (FA), GGBFS, and silica fume (SF). It was found that using of FA and GGBFS reduced the free shrinkage of the SCCs while the SF increased the drying shrinkage when used in binary blends. However, combined use of the mineral admixtures greatly diminished the adverse effect of the SF.

The influence of class F Fly Ash (FA) on the properties of SCC was investigated by Khatib (2008). In this study, portland cement (PC) was partially replaced with 0–80% FA; the water-to-binder ratio (w/p) was maintained at 0.36 for all mixes. The results indicate that 40% FA replacement for PC can produce high strength (≥65 N/mm^2 at 56 days) SCC. There is a systematic reduction in shrinkage as the FA content increases. At 80% FA content, the shrinkage at 56 days reduced by two-thirds compared with the control mixture. Nassif et al. (2008) found fly ash was the best overall pozzolan for controlling the drying shrinkage of SCC with a 10% reduction over normal SCC. Bonen and Shah (2004) concluded that the shrinkage can be reduced by incorporation of fillers, especially non-pozzolanic ones. Higher replacement of cement by limestone powder at constant W/P by volume, lower total shrinkage (Poppe and Schutter 2005b). Hwang and Khayat (2008) reported SCC made with a high concentration of SRA (and no fibers) developed 40% lower drying shrinkage after 56 days of drying compared with similar concrete prepared without SRA.

1.3.2.1.4 Comparisons Between SCC and CVC

Bonen and Shah (2004) concluded that a strict comparison of the reported values of shrinkage in the literature was problematic because of differences in formulations, experimental procedures, specimens' size, and the ambient humidity that the specimens were exposed to. A controversy exists regarding the shrinkage of SCC compared to CVC. Most researchers have reported larger shrinkage values of SCC mixtures than CVC (Kim and Han, 1997; Rols et al., 1999; Heirman and Vanderwalle, 2003; Song et al., 2001; Hammer, 2003; Turcry and Loukili, 2003; Klug and Holschemacher, 2003; Turcry et al., 2002; Holschemacher, 2004; Loser and Leemann, 2009; Wu et al., 2010; Khayat and Wu, 2010; Nassif et al., 2008).

Kim and Han (1997) prepared concretes made with fly ash in which the paste fraction varied from 0.243 to 0.287 and the reported shrinkage was about 30-50% greater than the corresponding conventional concrete. Rols et al. (1999) reported that for SCC made with paste volume fraction of 0.312 and composed of cement and limestone at 90 days, the drying shrinkage was about 50% higher than that of ordinary concrete, which contained about the same amount of cement. Holschemacher (2004) found, in the majority of the evaluated data, the shrinkage of SCC is 10-

50% higher than that of CVC, and there is a steeper rise of deformation particularly for young concrete aged up to 28 days. Nassif et al. (2008) reported that the drying shrinkage of SCC was approximately 30% higher than that of CVC and approximately 40% higher than that of HPC. Loser and Leemann (2009) found that at the age of 91 days SCC at constant relative humidity of 70% had 10-40% higher shrinkage than that of CVC. It might be attributed to the higher volume of paste in SCC than in CVC. Wu et al. (2010) tested four full-scale girders and concluded that both HPC and SCC mixtures developed similar autogenous shrinkage for the mixtures made with similar *w/cm*. The SCC mixtures developed about 20% greater drying shrinkage than the HPC mixture after 112 days of drying. Khayat and Wu (2010) found SCC exhibits 5% to 30% higher drying shrinkage at 300 days than HPC made with similar w/cm but with similar autogenous shrinkage.

Some researchers reported that shrinkage of SCC is similar to or less than that of CVC. For a given compressive strength, shrinkage of SCC was reported to be similar to that observed with normal concrete (Persson, 1999 and 2001a; Vieira and Bettencourt, 2003; Pons et al., 2003; Assié et al., 2003; Attiogbe et al., 2002; Bouzoubaa and Lachemi, 2001; Holt and Schodet, 2002; Sonebi and Bartos, 1999; Schindler et al., 2007). Sonebi and Bartos (1999) reported that shrinkage values for SCC made with cement and limestone powder were lower than that of the CVC reference concrete by about 30% due to the significantly higher W/P ratio of CVC mixtures. Schindler et al. (2007) reported that 112-day drying shrinkage strains for SCC were of the same order or less than those of CVC reference mixtures with 9.0 in slump and a higher W/P ratio than SCC.

1.3.2.1.5 Prediction Models

The existing prediction models for shrinkage of CVC (i.e., AASHTO 2007 or 2014, AASHTO 2004, ACI 209, CEB-FIP 1990, and GL 2000 [Gardner and Lockman, 2001]) have been tested to evaluate their ability to predict shrinkage of SCC (Khayat and Mitchell, 2009; Schindler et al., 2007; Landsberger and Fernandez-Gomez, 2007; Heirman et al., 2008).

Khayat and Mitchell (2009) measured drying shrinkage values between 1 and 252 days of 16 SCC and two HPC mixtures, which were compared to shrinkage strains predicted by the AASHTO 2007, AASHTO 2004, ACI 209, CEB-FIP 1990, and GL 2000 models. The AASHTO 2007 model underestimates shrinkage and results in large scattering compared to the AASHTO 2004 model, as shown in Figure A-11 (a). The CEB-FIP 90 model provided the best fit of measured data for SCC with maximum shrinkage of 600 μstrain after 9 months while other models underestimated shrinkage above 600 μstrain, as shown in Figure A-11 (a)-(b). They attributed this to the fact that the CEB-FIP 90 model takes into consideration the cement type that was varied in the tested mixtures. Thus, they proposed a coefficient for cement type (A) for the AASHTO 2004 model to provide a better prediction for the drying shrinkage. It was found that both the CEB-FIP 90 and modified AASHTO 2004 model provide an adequate prediction of shrinkage for precast, prestressed SCC, as shown in Figure A-11 (c).

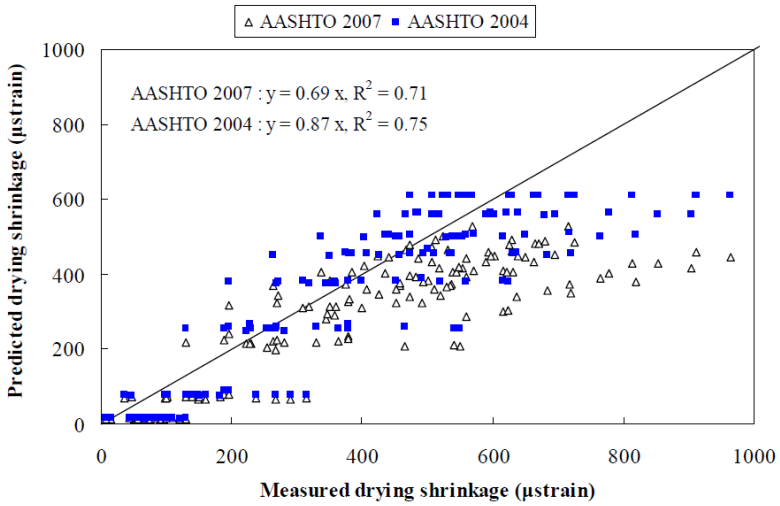

(a) AASHTO 2007 and 2004 models

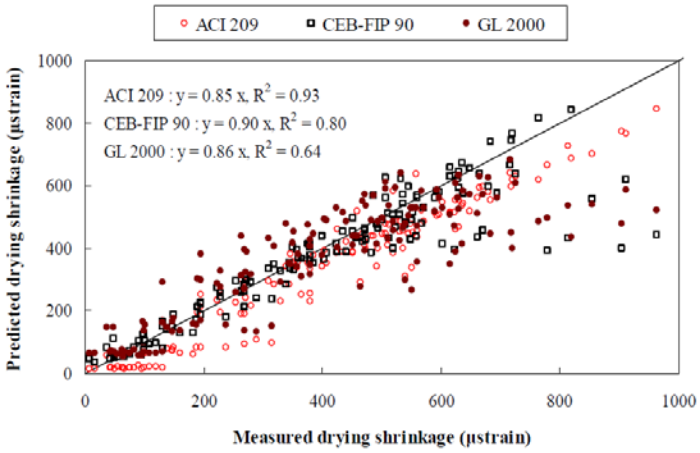

(b) ACI 209, CEB-FIP 90, and GL 2000 models

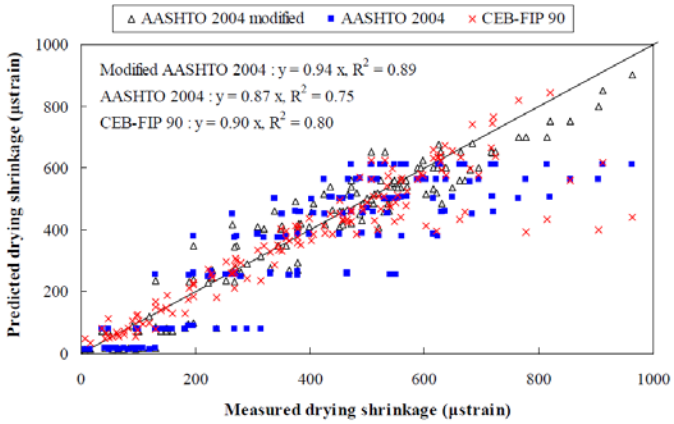

(c) Modified AASHTO 2004

Figure A-11. Comparison of measured and predicted drying shrinkage values (Khayat and Mitchell, 2009)

Schindler et al. (2007) reported that the 112-day shrinkage of SCC varied between 382-500 Microstrain. The ACI 209R procedure underestimates the drying shrinkage at 7 and 14 days for SCC. At later ages of 56 and 112 days, the shrinkage values were predicted well by the ACI 209R procedure. At 7 days, the AASHTO 2004 model underestimated the shrinkage values (0-300 μstrain), whereas it overestimated the shrinkage at later ages (56 and 112 days, 300-500 μstrain) for SCC.

Landsberger and Fernandez-Gomez (2007) reported that the ACI 209R best estimate of the shrinkage strains for SCC and the CEB-FIP 1990 model and GL2000 model substantially underestimated the shrinkage strains for SCC. Each of the models predicted the shrinkage strains with similar accuracy for SCC and CVC. Heirman et al. (2008) proposed a modification to the CEB-FIP 1990 model to properly predict the time-dependent behavior of limestone powder type SCC in terms of the total shrinkage strain prediction.

1.3.2.1.6 Restrained Shrinkage

Shrinkage reducing admixtures (SRAs) have been commonly used in CVC and other types of concrete in structures with a high surface-area-to-volume ratio, such as floors, parking lots, and bridge decks. See and Attiogbe (2005) reported the performance of the SCC mixtures compared to that of conventional concrete mixtures to assess the effect of fluidity level on resistance to restrained shrinkage cracking. In addition, the SCC mixtures were evaluated for the effects of sand-to-aggregate ratio (S/A), paste content, aggregate shape, and use of an SRA on cracking potential. The results showed that the cracking resistance of SCC was similar to that of conventional concrete, indicating that the higher fluidity of SCC was not detrimental to performance under restrained shrinkage. The cracking potential of the SCC mixtures was found to be influenced by the mixture composition.

Loser and Leemann (2009) investigated whether the risk of cracking in restrained conditions would be increased with the use of SCC. In their study, shrinkage of thirteen different SCC mixtures varying in volume of paste, water content, type of binder, grain size distribution or content of SRA was compared with shrinkage of three different CVC mixtures with a constant volume of paste but variable w/b. Furthermore, the risk of cracking of the different SCC and CVC mixtures in restrained conditions was studied under constant and varying curing conditions. Due to the higher volume of paste, SCC displayed higher shrinkage than CVC and adding an SRA was the only measure to reduce shrinkage of SCC to the values of CVC. Restrained shrinkage cracking was dependent on shrinkage rate, mechanical properties and drying velocity. For slow shrinkage stress development, cracking risk of SCC could be lower compared to CVC despite the higher shrinkage rate. Hwang and Khayat (2008) reported SCC made with a high concentration of SRA (and no fibers) developed 2.4 times longer interval before cracking, compared with similar concrete prepared without SRA. The combined use of SRA and fibers at a dosage rate of 0.25% or 0.50% was effective in producing high-performance SCC of low cracking potential.

1.3.2.2 Creep

Creep of concrete takes place under stress and is influenced by the capillary porosity of the concrete. High early-strength cement can lead to lower creep. Since the presence of aggregate restrains creep deformation in the paste, an increase in the volume and elastic modulus of the aggregate can lower creep.

Persson (1999) found that for a given compressive strength, creep of SCC could be similar to that of normal concrete. Pons et al. (2003) reported that creep in SCC and CVC made with the same coarse aggregate is comparable. Turcry et al. (2006) reported no difference in creep strain between conventionally vibrated concrete (CVC) and SCC having the same compressive strength. Kavanaugh (2008) reported that all SCC mixtures cured under elevated or standard laboratory temperature exhibited creep values similar to or less than the CVC mixture. This was attributed to low w/cm, which decreases permeability of SCC mixtures. Landsberger and Fernandez-Gomez (2007) presented a database of creep results for SCC and CVC, and concluded that the mean specific creep of CVC was higher than that of SCC and the standard deviation is equivalent.

Heirman et al. (2008) reported that the use of limestone powder as SCM increases creep strain due to the slow gain of concrete compressive strength. Song et al. (2001) conducted creep measurements on SCC mixtures at loading times of 1, 3, 7, and 28 days incorporating 40% GGBFS and found the effect of fineness of GGBFS on creep was significant at early-age (1-3 days) of loading, but becomes quite small for loading at later ages. Kim et al. (2011) reported that SCC with river gravel coarse aggregate had lower creep values compared to SCC with limestone coarse aggregate, which indicated that stiffness of aggregated aggregate may significantly influence the creep. Leemann and Lura (2014) reported that the higher the paste volume of SCC, the higher the creep strain.

Conversely, the creep potential of SCC appears to be higher than that of CVC made with the same raw materials and having the same 28-day design strength (Attiogbe et al., 2002; Kim et al., 1996; Byun et al., 1998; Zheng et al., 2009). Khayat and Mitchell (2009) reported SCC exhibited 10% to 20% higher creep after 300 days than HPC made with similar *w/cm*. Kim et al. (1996) showed that SCC mixtures presented 15-25% higher creep than normal concrete. However, it should be noted that these results were obtained on mixtures made with different binder contents, 530 kg/m^3 and 400 kg/m^3 for the SCC and normal concrete mixtures, respectively. Byun et al. (1998) reported that for similar constant compressive strength and elastic modulus values, the creep rate of SCC can be greater than that of normal concrete at early ages, up to 20 days of testing. However, after 20 days of testing, both the SCC and normal concrete showed similar creep rates. Zheng et al. (2009) conducted creep testing on 69 specimens (w/p of around 0.30) and concluded that the creep rate of SCC was greater than that of CVC at early age but decreased with age. In spite of the coarser aggregate contained in CVC, the basic creep was always greater than SCC because of the more compacting structure of SCC.

The existing prediction models for creep of CVC (i.e., AASHTO 2007, AASHTO 2004, ACI 209, CEB-FIP 1990, and GL 2000) have been tested to evaluate their ability to predict creep of SCC (Khayat and Mitchell, 2009; Kim et al., 2011; Heirman et al., 2008; Kavanaugh, 2008; Landsberger and Fernandez-Gomez, 2007).

Kim et al. (2011) found that the AASHTO 2006 model, which is as typical as the AASHTO 2007 model, predicted the creep compliance with the highest accuracy among all the models, AASHTO 2004, ACI 209, and the CEB-FIP 1990 models, which also provide fairly good predictions of the creep. Khayat and Mitchell (2009) measured creep in 16 SCC and two HPC mixtures, which were compared to creep strains predicted by the AASHTO 2007, AASHTO 2004, ACI 209, CEB-FIP 1990, and GL 2000 (Gardner and Lockman, 2001) models. The ACI 209, AASHTO 2004, and AASHTO 2007 models underestimated creep at most loading ages.

The GL 2000 model overestimated the creep strains because the maturity of concrete increased by accelerated curing is not taken into consideration in the GL 2000 model. The CEB-FIP 90 model provided a closer prediction.

Kavanaugh (2008) concluded that AASHTO 2007 underestimates the creep strain of early-age concrete and overestimates the creep strain of later-age concrete. The CEB-FIP 1990 model was the only model to predict creep well for both CVC and SCC. The GL 2000 model overestimated the creep strain of both the conventional-slump and SCC mixtures. The ACI 209 creep prediction method was unable to accurately predict the creep strain in the high-strength concrete mixtures. Heirman et al. (2008) reported that the CEB-FIP 1990 model could remain unmodified for a limestone powder type SCC application for predicting creep. Landsberger and Fernandez-Gomez (2007) found the CEB 90 method, ACI 209 model, and GL 2000 all underestimate the creep, while the ACI 209 model predicted the creep with the least dispersion and the GL 2000 model better predicted creep. Naito et al. (2006) reported that the ACI 209 model underestimates the creep coefficient for both CVC and SCC but dramatically for the latter one.

1.4 **Durability Properties and Test Methods**

1.4.1 ***Air Void System***

For both SCC and CVC, different mix designs lead to different pore microstructures in their cement matrixes as well as in the interfacial transition zones (ITZs). Consequently, the concrete mixes display different durability, including resistance to freeze-thaw (F-T) damage. The microstructure of SCC and CVC obtained using petrography analysis with fluorescent light indicated little porosity around the aggregate particles in the SCC, indicating a good interfacial transition zone (ITZ) between aggregates and the matrix of the SCC (Schutter, 2008). However, increased light intensity is seen around the aggregate particles in CVC, indicating a more porous ITZ in the conventional concrete. Similar to CVC, critically saturated SCC is susceptible to damage when exposed to repeated F-T cycles. An adequate air-void system is crucial for all kinds of concrete to resist freeze-thaw cycles, and despite the highly flowable nature of SCC, air bubbles can be entrained in a stable manner using air entraining admixtures, especially in concrete with relatively low w/cm or in SCC containing VMA (Schutter, 2008; Beauprd et al., 1999).

1.4.2 ***Penetrability***

The movement of gases, liquids and ions through concrete occurs due to differentials in air or water pressure, humidity solution concentrations, and/or temperature. Depending on the driving force of the process and the nature of the transported matter, different transport processes for deleterious substances through concrete are distinguished as absorption, permeation and diffusion. (Zhu, 2007). Diffusion tests are used to determine diffusion characteristics by measuring the transport of gas, water vapor, or ions due to a concentration gradient across concrete, and can be classified as (1) gas diffusion tests, (2) water vapor diffusion tests, and (3) ionic diffusion tests (Zhu, 2007). For instance, the rapid chloride penetrability test (RCPT) is used for determining the chloride permeability of hardened concrete (AASHTO T 277). On the other hand, the surface resistivity (SR) test (AASHTO TP 95) has been shown to have a strong correlation with the RCPT test (LADOTD, 2011; FDOT, 2011; INDOT, 2013; FHWA 2013).

The most important ion transport issue for reinforced concrete is chloride penetration. Chlorides do not directly result in any damage to concrete, but can induce corrosion of steel in concrete. There are two main sources for chlorides to penetrate into concrete structures: seawater and de-icing agents used in the winter seasons in cold climate regions. As stated by Tang and Zhu (2007), the chloride penetration of SCC varies more than that of CVC and depends on the dispersion of filler (Tang et al., 1999), the types of filler and VMA (Zhu and Bartos, 2003), binder content (Persson, 2001b), and the ratio of water to powder (Audenaert et al., 2005).

Tang et al. (1999) found that, at w/c of 0.4, the chloride diffusivity of SCC was remarkably higher than that of CVC due to poor dispersion of limestone filler. Persson (2001b) found the chloride migration coefficient was on average 60% higher for SCC than for CVC. Such a significant increase in the chloride migration coefficient for SCC mixes was thought to be due to lower coarse aggregate content and higher paste volume. Audenaert et al. (2005) reported that the chloride penetration depth in SCC by cyclic immersion was lower than that in the CVC. Decreasing water/cement or water/powder would lead to a decreasing chloride penetration depth. Boubitsas and Paulou (2000) reported that the SCC mixtures that contained blended/composite cement had a significantly lower chloride migration coefficient than that of the CVC mix, especially for SCC with slag cement. This is not surprising because it is known that slag cement will bind chlorides. Mamaghani et al. (2010) performed rapid chlorine ion penetrability tests based on ASTM C1202. The results indicated that SCC mixes exhibit comparable penetrability to that of the CVC mix.

Zhu and Bartos (2003) found the chloride diffusivity was very much affected by the type of powders used in the concrete mixes. Particularly, the concrete mixes containing fly ash showed a much lower chloride migration coefficient compared to the other mixes, especially for the lower strength grade mixes. Sonebi and Nanukuttan (2009) reported that SCC mixes for both grades of strength, made with fly ash, showed much lower diffusivity values in comparison to other mixtures, whereas the SCC mixtures with VMA showed higher diffusivity.

SCCs with binary, ternary, and quaternary cementitious blends of mineral admixtures showed low chloride permeability values as reported by Nehdi et al. (2004). Binary mixtures incorporating 50% class F fly ash decreased the rapid chloride penetrability from a high to a moderate range. In SCC made with high volume replacement ternary and quaternary cementitious blends, the 28-day rapid chloride ion penetrability was decreased from a high range for the reference 100% OPC mixture to a low range. The most efficient mixtures in decreasing the 28-day chloride ion penetrability were quaternary mixtures incorporating either 6% silica fume or 6% rice husk ash (RHA). Hwang et al. (2005) reported that SCC mixtures made with quaternary cement containing fly ash, blast furnace slag, and silica fume yielded the lowest level of rapid chloride-ion penetrability.

Sahmaran et al. (2009) presented the transport properties of SCC that contained high percentages of low-lime fly ash with a lime content of 2.21% (FA_L) and high-lime fly ash with a lime content of 10.07% (FA_H). It was found that when evaluating the durability of SCC by its transport properties, the addition of fly ash at high volumes seemed to be beneficial (especially low-lime fly ash), leading to a potentially more durable concrete. SCCs containing five different contents of high-lime and low-lime (30, 40, 50, 60 and 70 by weight of total cementitious material) were examined. For comparison, a control SCC mixture without any FA was also produced. Limestone powder (LP) was used as a fine material (5 μm average diameter) in all mixtures. For all the mixtures, the total amount of cementitious material (Portland Cement (PC)

+ FA) and the amount of chemical admixture were kept constant. The water-cementitious material ratio ranged between 0.30 and 0.35. The transport properties were determined at 28, 90, 180 and 365 days using absorption, sorptivity and rapid chloride penetrability tests. RCPT tests showed total charge passed results for SCC mixtures containing high-lime FA were always lower than that for the control concrete at the same w/cm ratio. On the other hand, increases in high-lime FA content showed no significant effect on chloride ion penetration. The chloride ion penetration of concrete with low-lime FA was also lower than the concrete mixture without FA and the reductions increased with the increasing FA content. At the end of 180 and 365 days, all total charge passed results for the high- and low-lime FA were nearly same.

2 Summary of the National Concrete Consortium (NCC) Survey

Table A-8. Summary of SCC applications in different states

No.	State	SCC Application(s)	Specifications
1	Pennsylvania (PA)	Drilled Cassions	Guidelines
2	Missouri (MO)	Drilled Shafts and Precast Prestressed	Job Special Provisions
3	Indiana (IN)	Not Approved	None
4	Iowa (IA)	Precast and Limited CIP Applications	Guidelines on Mix Design and Testing
5	Michigan (MI)	Not Approved	None
6	Wisconsin (WI)	Precast sound wall panels	None
7	Kansas (KS)	Prestressed Beams	Special Provisions to Standard Specifications
8	California (CA)	Precast Elements	Specifications
9	Ohio (OH)	Precast Elements	None
10	South Dakota (SD)	Precast and CIP Box Culverts and Prestressed Girders	Draft Special Provisions
11	Colorado (CO)	Limited CIP	Draft Project Special Provisions
12	Washington (WA)	Precast Elements	Specifications
13	Illinois (IL)	Precast and Cast-in-Place Elements	Special Provisions
14	Alabama (AL)	Drilled Shafts and Prestressed Girders	Job Special Provisions

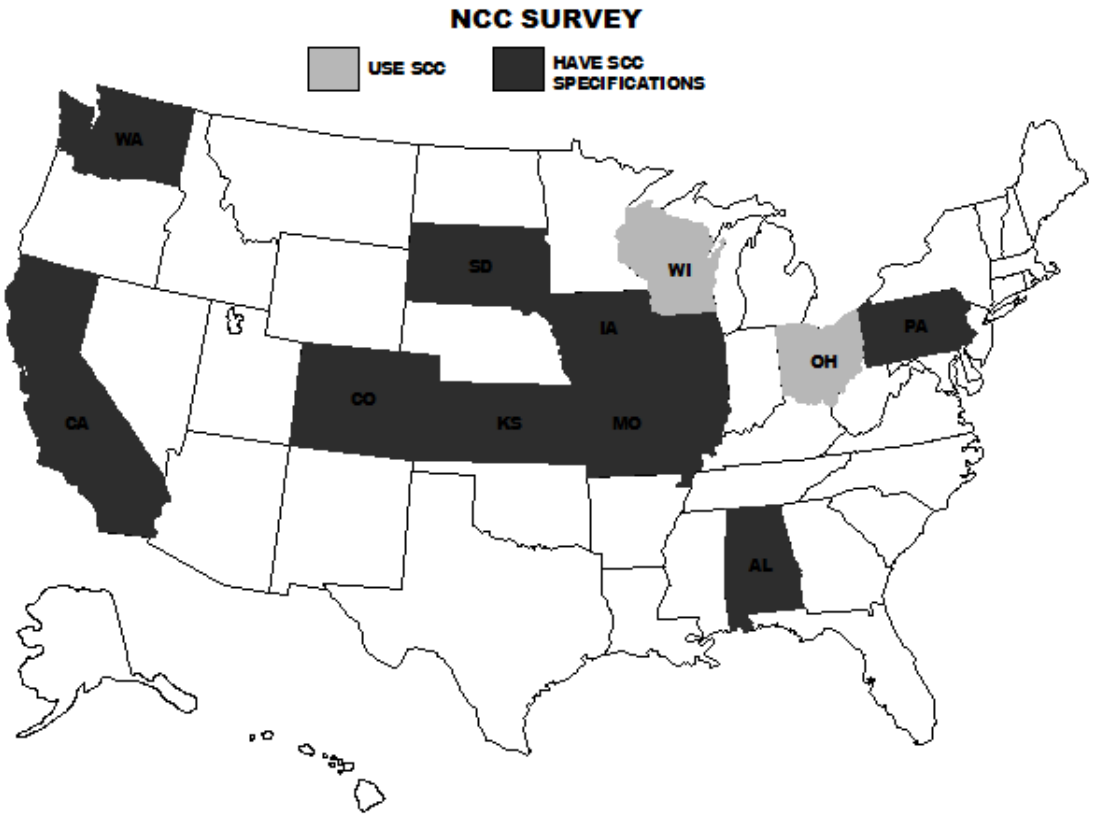

Figure A-12. States within the survey

Table A-9. Typical responses of different states according to the use of SCC

No.	State	Specifications	Application(s)	Response
1	Pennsylvania (PA)	Guidelines	Drilled shafts	"I don't think were using SCC on bridge decks, but I did find SCC used for drilled caissons"
2	Missouri (MO)	Job Special Provisions	Drilled Shafts, Precast/Prestress Concrete	"Attached is a draft job special provisions for using SCC in precast/prestress concrete. Missouri University of Science and Technology is currently conducting a SCC study for MoDOT. Results from this research will be used to confirm the JSP and adopted it for official use. The above specification was modified for the new Mississippi River Bridge in St. Louis, MO. The design team wanted to include the option of using SCC in the drilled shafts. Attached is the JSP used in the contract"
3	Indiana (IN)	None	–	"We don't approve SCC yet in Indiana, there is no spec and no special provision."
4	Iowa (IA)	Guidelines	Precast Operations, Limited CIP	"We have used SCC in mostly precast operations. We have used SCC in the field on a couple intricate shapes with lots of reinforcing steel. We don't really have any specifications other than some general guidance on mixes and testing in the Materials IM's. It would seem difficult to use on a bridge deck with any cross slope or elevation differences."
5	Michigan (MI)	None	–	"Michigan DOT does not have specifications for SCC."
6	Wisconsin (WI)	None	Precast Sound Wall Panels	"Wisconsin has not yet developed any specifications for SCC use. It seems likely that the first application that will develop here is for prestressed concrete girders."
7	Kansas (KS)	Special Provisions	Prestressed Bridge Beams	"We have only used SCC in prestressed bridge beams. We have worked with KSU on an application for post tensioned haunch slabs in the anchor areas. The specification is very much a performance specification."
8	California (CA)	Specifications	Precast Elements	"This is our spec for SCC for precast elements."

9	Ohio (OH)	None	Precast Elements	"We don't have an SCC spec."
10	South Dakota (SD)	Special Provisions	Precast and CIP Box culverts, Precast/Prestressed Girders	"I'm attaching the special provisions that SDDOT has used mostly under researching SCC applications. These are currently under review and will have some work done to them, as we are working toward using them to begin general implementation of SCC starting in 2012. SCC will be a contractor option for some structural concrete applications"
11	Colorado (CO)	Project Special Provisions	Limited CIP	"Colorado DOT has limited exposure with SCC. We tried on an experimental project a few years back and also this year. Attached is our project special specification. Please do not redistribute as this was not a final version."
12	Washington (WA)	Specifications	Precast Elements	"We do have a SCC specification but it is not in the standard spec's for prestressed girders. We have a SCC spec for precast items for drainage, etc. that is being used on a regular basis. Our CIP SCC was construction/Contractor driven change. We do not have specifications or special provisions for CIP SCC"
13	Illinois (IL)	Special Provisions	CIP and Precast Elements	"Here is the link to our specifications. One is cast-in-place and the other is for precast. We are working on a specification for prestress. We do not allow SCC for bridge decks. The thought is that constructing the crown for the roadway could be difficult because of the high slump flow."
14	Alabama (AL)	Special provisions	Drilled shafts and Prestressed Girders	"We have two research projects that involve SCC. The first has SCC for drilled shafts. The second has SCC for prestressed girders. I've attached the Special Provisions (which are job specific for the two research projects) for both."

3 Material, Proportioning, and Performance Requirements in 17 States

Table A-9. Material, proportioning, and performance requirements in AL, CA, CO, and FL

State	AL		CA	CO	FL	
Application	Drilled shafts	Prestressed girders	Precast components	Limited cast-in-place	Cast-in-place	Precast/prestressed concrete
Constituent Materials						
Cement Type	Type I or II				Types I or II	Types I or II
SCM	Class C or F fly ash: max 30% Slag: min 25%, max 50%	30% Class C/F fly ash or 50% slag or 10% micro silica or 20% Class C/F fly ash + 10% micro silica or 20% Class C/F fly ash + 20% slag		Class F fly ash: min 30%, max 40%		
Agg. type and gradation	Coarse agg. No. 67 or No.78 Fine agg. shall be natural sand	Max agg. size 3/4 in.		AASHTO M 43 size No.8 coarse agg.		
Chemical admixtures	Type D, Type F, VMA All shall be from the same manufacturer	VMA			Type F, and VMA	Type F, Type G, and VMA
Mix Proportioning						
Cementitious composition	min 600 lbs/yd^3 cementitious max 800 lbs/yd^3 cementitious	min 600 lbs/yd^3 cementitious				
Water-cementitious ratio	max 0.40	max 0.40		max 0.40	max 0.41	
Sand-aggregate ratio					Max 50% fine aggregate	Max 50% fine aggregate
Performance requirements						
Slump flow	21 ± 3 in.	min 25 in., max 29 in.	min 20 in.	26 - 30 in.	24-30 in.	Max 27 in. ± 2.5 in.
J-ring value		max 3 in.	within 2 in. of slump flow	max 2 in.	max 2 in.	max 2 in.
L-box blocking ratio						
Visual stability index	max 1.5	max 2	max 1		max 2	max 2
Column segregation		15%	max 15%	max 10%		
Flow rate - T_{50}			2 - 7 seconds		2 - 7 seconds	2 - 7 seconds
Bleeding			max 2.5%			
Air content	max 6%	Target 4.5%; max 6%		max 8%		1% - 6%
Compressive Strength	min 4000 psi at 28 days	min 5000 psi at 28 days	specified + 600 psi	min 4500 psi at 28 days		
Flexural Strength						
Temperature	min 50°F, max 95°F	min 50°F, max 95°F				
Shrinkage		max 0.04% at 7 days				max 0.04% at 28 days

(cont.) Table A-10. Material, proportioning, and performance requirements in GA, IA, ID, IL, and KS

State	GA	IA	ID	IL		KS
Application	Precast prestressed concrete bridge members	Precast products and limited cast-in-place	Precast products	Cast-in-place	Precast	Prestressed beams
Constituent Materials						
Cement Type	Types I or III				Type III	Types I, IP, I(PM), II or III
SCM	No more than three types (Fly ash, slag, micro silica or metakaolin); max 20% when using one SCM; max 40% when using two or three SCMs.		max 30% Class F fly ash; max 35% GGBFS			
Agg. type and gradation		Well graded Max agg. size of 3/4 in.				
Chemical admixtures	Type F, Type G, and VMA	HRWR, VMA				
Mix Proportioning						
Cementitious composition		700 - 1000 lbs/yd^3; 550 - 700 lbs/yd^3 (with viscosity modifying agent)		min 565 lbs/yd^3 (central mixed); min 605 lbs/yd^3 (truck mixed); max 705 lbs/yd^3	min 565 lbs/yd^3; max 705 lbs/yd^3	min 602 lbs/yd^3; max 752 lbs/yd^3
Water-cementitious ratio	max 0.35	0.25 - 0.44	max 0.45	0.32 - 0.46	0.25 - 0.44	max 0.44
Sand-aggregate ratio		40 - 50% fine aggregate		Max 50% sand	Max 50% sand	
Performance requirements						
Slump flow	26 - 28 in. ± 3 in.	max 27 in.	18 - 32 in.	min 20 in., max 28 in.	min 20 in., max 28 in.	min 25 in., max 28 in.
J-ring value		max 2 in.		max 4 in.	max 4 in.	
L-box blocking ratio	min 0.80; max 1.0			min 60%	min 60%	
Visual stability index			max 1.5	max 1	max 1	0 or 1
Column segregation						
Flow rate - T_{50}	3-8 seconds					
Bleeding						
Air content	3.5% - 6.5%		max 6.5% ± 1.5%	5.0 - 8.0%	5.0 - 8.0%	6 ± 2 %
Compressive Strength	min 5000 psi at 28 days				min 4500 psi at 28 days	min 6000 or 7000 psi at 28 days (based on the grade)
Flexural Strength				min 650 psi at 14 days		
Temperature	min 50^{o}F, max 95^{o}F					
Shrinkage						

(cont.) Table A-11. Material, proportioning, and performance requirements in KY, MO, NE, NJ, NY, and PA

State	KY	MO	NE	NJ		NY	PA
Application	Precast products	Drilled shafts and prestressed concrete	Cast-in-place	Drilled shafts	Precast concrete	Removal and replacement	Drilled caissons
Constituent Materials							
Cement Type			Types I				Type II Sulfate Resistant
SCM			25% Class F fly ash				Blending of slag/pozzolan is not allowed
Agg. type and gradation		100% of each fraction shall pass 3/4 in.	Max agg. size 1/2 in.				#8 dredged river gravel or rounded gravel. Only natural sand
Chemical admixtures		AASHTO M 194 Type F or G polycarboxylate based HRWR AASHTO M 194 viscosity-modifying agent	Type B, Type F, and VMA	Type F, and VMA	Type F, and VMA		
Mix Proportioning							
Cementitious composition	min 564 lbs/yd^3 cementitious	min 650 lbs/yd^3;	min 810 lbs/yd^3 cementitious				
Water-cementitious ratio	max 0.46	0.32 - 0.45	max 0.37				max 0.45
Sand-aggregate ratio		35 - 50% fine aggregate	75% fine aggregate	Max 50% fine aggregate	Max 50% fine aggregate		
Performance requirements							
Slump flow		min 22 in., max 30 in.	min 22 in., max 29 in.	21 ± 3 in.	24-28 in.	As specified	
J-ring value		max 2 in.					within 2 in. of slump flow
L-box blocking ratio							
Visual stability index		max 1	0 or 1	max 1	max 1	As specified	max 1.5
Column segregation							
Flow rate - T_{50}							
Bleeding							
Air content	6.0% ± 2%	5.0 %	Min 6%	6.5-7.5% ± 2.0%	3.25-3.75% ± 1.0%	As specified	2 ± 0.5 %
Compressive Strength		min 4000 psi at 28 days	min 6000 psi at 28 days			As specified	
Flexural Strength							
Temperature							
Shrinkage							

(cont.) Table A-12. Material, proportioning, and performance requirements in SD, and WA

State	SD			WA
Application	Cast-in-place box culverts	Precast box culverts	Prestressed girders	Precast units
Constituent Materials				
Cement Type	Type I/II	Type I/II	Type I/II	Type III permitted
SCM		None allowed	None allowed	
Agg. type and gradation	Quartzite or limestone Max agg. size of 3/4 in. Specified boundaries Flat and elongated particles <30 %	Quartzite or limestone Max agg. size of 1/2 in. Specified boundaries Flat and elongated particles <25 %	Quartzite or limestone Max agg. size of 1/2 in. Specified boundaries Flat and elongated particles <20 %	
Chemical admixtures	VMA and polycarboxylate	VMA	VMA	
Mix Proportioning				
Cementitious composition	min 700 lbs/yd^3 cement max 800 lbs/yd^3 cementitious	min 700 lbs/yd^3 cement	min 700 lbs/yd^3 cement	
Water-cementitious ratio	max 0.46	max 0.47	max 0.37	
Sand-aggregate ratio	min 45% coarse agg.	min 40% coarse agg.	min 40% coarse agg.	
Performance requirements				
Slump flow	22 - 28 in.	22 - 28 in.	23 - 28 in.	Specified ±2 in.
J-ring value	within 2 in. of slump flow	within 2 in. of slump flow	within 2 in. of slump flow	max 1.5 in.
L-box blocking ratio				
Visual stability index	max 1	max 1	max 1	max 1
Column segregation				10%
Flow rate - T_{50}				max 6 seconds
Bleeding				
Air content	5.0 - 7.5%	4.5 - 7.5%	4.5 - 7.5%	
Compressive Strength	min 4500 psi at 28 days	min specified at 28 days	min specified at 28 days	
Flexural Strength				
Temperature				
Shrinkage				

4 State-DOT-Sponsored Research Projects on Cast-in-Place SCC

Table A-13. Sponsored research projects by DOTs

Report Year	Research University / Institute	Principle Investigator	Sponsoring Organization	Project / Report Title	Bridge Application(s)
2011	University of New Mexico	Reda Taha, M.M.	New Mexico Department of Transportation	Examining Short & Long Term Properties of Self-Consolidating Concrete (SCC)	Highway construction and specialized transportation projects
2010	University of North Dakota	Mamaghani, I.H.P.	North Dakota Department of Transportation	Evaluation of Self-Consolidating Concrete (SCC) for Use in North Dakota Transportation Projects	Transportation projects
2010	The Bureau of Materials and Physical Research at Illinois	Stitt, S. E.	Illinois Department of Transportation	Special Provision for Self-Consolidating Concrete for Cast-In-Place Construction	Cast-in-place construction
2008	Auburn University	Dachelet, D. O.	Alabama Department of Transportation	The Effectiveness of Self-Consolidating Concrete (SCC) for Drilled Shaft Construction	Drilled shafts
2008	University of Illinois at Urbana-Champaign	Lange D. A.	Illinois Department of Transportation	Performance and Acceptance of Self-Consolidating Concrete: Final Report	Retaining wall structures
2008	Rutgers, The State University	Nassif, H.	New Jersey Department of Transportation	Self-Consolidating Concrete (Phase I & II)	Drilled shaft construction and surveyed applications in tee walls and noise walls
2007	University of Nebraska - Lincoln	Nowak, A. S.	Nebraska Department of Roads	Development of a Guide for Cast-in-Place Applications of Self-Consolidating Concrete	Cast-in-place construction and concrete barriers
2006	Auburn University	Schindler, A.K.	South Carolina Department of Transportation	Evaluation of Self-Consolidating Concrete for Drilled Shaft Applications at the Lumber River Bridge Project, South Carolina	Drilled shafts
2005	University of Michigan	Nowak, A.S.	Transportation Research Board	US Specific Self Compacting Concrete for Bridges	Cast-in-place construction
2005	South Carolina DOT; S&ME, Inc.	Holley, D.W.	Kimley-Horn and Associates, Inc.	Self Consolidating Concrete (SCC) in Drilled Shafts Research Project	Drilled shafts
2005	Auburn University	Bailey, J. D.	Federal Highway Administration	An Evaluation of the Use of Self-Consolidating Concrete (SCC) for Drilled Shaft Applications	Drilled shafts

REFERENCES

American Association of State Highway and Transportation Officials (AASHTO). 2007. AASHTO LRFD Bridge Design Specifications. 4th Edition, Washington, DC.

ACI Committee 209. 1990. *Prediction of Creep, Shrinkage and Temperature Effects in Concrete Structures*. American Concrete Institute, Farmington Hills, Michigan.

ACI Committee 318. 1999, 2008. *Building Code Requirements for Structural Concrete*. American Concrete Institute, Farmington Hills, Michigan.

ACI Committee 347. 2014. *Guide to Formwork for Concrete*. American Concrete Institute, Farmington Hills, Michigan.

ACI Committee 363. 1992. *State-of-the-Art Report on High-Strength Concrete*. American Concrete Institute, Farmington Hills, Michigan.

Almeida, F.M., El Debs, M.K., and El Debs, A.L.H.C. 2008. "Bond-Slip Behavior of Self-Compacting Concrete and Vibrated Concrete Using Pullout and Beam Tests." *Materials and Structures*, Vol. 41, No. 6, pp. 1073-1089.

Almeida, F.M., Nardin, S., and Gresce, A.L.H. 2005. "Evaluation of the bond strength of self-compacting concrete in pull-out tests." *Proceedings of Second North American Conference on the Design and Use of Self-Consolidating Concrete and Fourth International RILEM Symposium on Self-Compacting Concrete*, Chicago, Illinois, pp. 953–958.

Ambroise, J. and Pèra, J. 2002. "Design of Self-Leveling Concrete." *Proceedings of 1st North American Conference in the Design and Use of Self-Consolidating Concrete*, Chicago, Illinois, pp. 89-94.

Aslani, F. and Nejadi, S. 2012. "Bond Behavior of Reinforcement in Conventional and Self-Compacting Concrete." *Advances in Structural Engineering*, Vol. 15, No. 12, pp. 2033-2051.

Assaad, J., and Khayat, K.H. 2004. "Kinetics of Formwork Pressure Drop of Self-Consolidating Concrete Containing Various Types and Contents of Binder." *Cement and Concrete Research*, Vol. 35, No. 8, pp. 1522-1530

Assaad, J., and Khayat, K.H. 2005. "Effect of Coarse Aggregate Characteristics on Lateral Pressure Exerted by Self-Consolidating Concrete." *ACI Materials Journal*, VOL. 102, No. 3, pp.145-153.

Assaad, J., and Khayat, K.H. 2006. "Effect of Viscosity-Enhancing Admixtures on Formwork Pressure and Thixotropy of Self-Consolidating Concrete." *ACI Materials Journal*, Vol. 103, No. 4, 280-287.

Assaad, J., Khayat, K.H., and Daczko, J. 2004. "Evaluation of Static Stability of Self-Consolidating Concrete." *ACI Materials Journal*, Vol. 101, No. 3, pp. 201-215.

Assaad, J., Khayat, K.H., and Mesbah, H. 2003(a). "Variation of Formwork Pressure with Thixotropy of Self -Consolidating Concrete." *ACI Materials Journal*, Vol. 100, No. 1, pp. 29-37.

Assaad, J., Khayat, K.H., and Mesbah, H. 2003(b). "Assessment of Thixotropy of Flowable Self – Consolidating Concrete." *ACI Materials Journal*, Vol. 100, No. 2, pp. 99-107.

Assié, S., Escadeillas, G., and Marchese, G. 2003. "Durability of Self-Compacting Concrete." *Proc., 3rd International RILEM Symposium on Self-Compacting Concrete*, Reykjavik, Iceland, pp. 655-662.

Attiogbe, E.K., See, H.T., and Daczko, J.A. 2002. "Engineering Properties of Self-Consolidating Concrete." *First North American Conference on the Design and Use of Self-Consolidating Concrete*, Chicago, Illinois, pp. 331-336.

Audenaert, K., Boel, V., and Schutter, G. 2005. “Chloride Penetration in Self Compacting Concrete By Cyclic Immersion.” *1st International Symposium on Design, Performance and Use of Self-Consolidating Concrete*, China, pp. 355-362.

Barnes, H.A. and Nguyen, Q.D. 2001. “Rotating Vane Rheometry - a Review.” *Journal of Non-Newtonian Fluid Mechanics*, Vol. 98, No. 1, pp. 1-14.

Bartos, P. J. M. 2005. “Assessment of Key Characteristics of Fresh Self-Compacting Concrete: A European Approach to Standardization of Tests.” *The Second North American Conference on the Design and Use of Self-Consolidating Concrete (SCC) and the Fourth International EILEM Symposium on Self-Compacting Concrete*, pp. 807-829.

Beauprd D., Lacombe P., and Khayat K.H. 1999. “Laboratory Investigation of Rheological Properties and Scaling resistance of Air Entrained Self-Consolidating Concrete.” *Materials and Structures*, Vol. 32, pp. 235-240.

Billberg, P., Silfwerbrand, J., and Österberg, T. 2005. “Form Pressures Generated by Self-Consolidating Concrete.” *Concrete International*, Vol. 27, No. 10, pp. 35-42.

Birch, B. 2007. *Formwork Pressure of Self Consolidating Concrete*. M.Sc. thesis, University of Illinois, Urbana-Champaign.

Boehm K.M. 2008. *Structural Performance of Self-Consolidating Concrete in AASHTO Type I Prestressed Girders.* M.Sc. thesis, Auburn University, Alabama.

Bonen, D. and Shah, S.P. 2004. “The Effects of Formulation on the Properties of Self-Consolidating Concrete.” International RILEM Symposium on Concrete Science and Engineering: A Tribute to Arnon Bentur, pp. 43- 56.

Bonen, D. and Shah, S.P. 2005 “Fresh and Hardened Properties of Self-Consolidating Concrete.” *Progress in Structural Engineering Materials Journal*, Vol. 7, No. 1, pp. 14-26.

Bosiljkov, V.B. 2003. “SCC Mixes with Poorly Graded Aggregate and High Volume of Limestone Filler.” *Cement and Concrete Research*, Vol. 33, pp. 1279-1286.

Boubitsas D. and Paulou K. 2000. *Self-Compacting Concrete for Marine Environment*. Report TVBM-5048, Lund institute of Technology, Sweden.

Bouzoubaa N, and Lachemi M. 2001. “Self-Compacting Concrete Incorporating High Volumes of Class F Fly Ash: Preliminary Results.” *Cement and Concrete Research*, Vol. 31, pp. 413-420.

Brinks, A. J. 2005. *A Layered Finite Element Model for the Analysis of Segregation of Self Consolidating Concrete*. M.Sc. thesis, University of Illinois Urbana-Champaign, IL.

Bui, V.K. and Montgomery, D. 1999. “Drying Shrinkage of Self-Compacting Concrete Containing Milled Limestone.” *1st Intern. RILEM Symposium on Self-Compacting Concrete*, Stockholm, pp. 227-238.

Bui, V.K., Montgomery, D., Hinczak, I., and Turner, K. 2002. “Rapid Testing Method for Segregation Resistance of Self-Compacting Concrete.” *Cement and Concrete Research*, Vol. 32, No. 9, pp. 1489–1496

Byun, K.J., Kim, J.K., and Song, H.W. 1998. “Self-Compacting Concrete in Korea.” *Proceedings of International Workshop on Self-Compacting Concrete*, Kochi, Japan, pp. 23–33.

Castel, A, Vidal T, and Viriyametanont, K, and François, R. 2006. “Effect of Reinforcing Bar Orientation and Location on Bond with Self-Consolidating Concrete.” *ACI Structural Journal*, Vol. 103, No. 4, pp. 559-567.

Cattaneo, S. and Rosati, G. (2009). "Bond between Steel and Self-Consolidating Concrete: Experiments and Modeling." *ACI Structural Journal*, Vol. 106, No. 4, pp. 540-550.

CEB-FIP. 1990. *Model Code (MC90)*. Comité Euro-International du Béton.

Chan Y-W, Chen Y-S, and Liu Y-S. 2003. "Development of Bond Strength of Reinforcement Steel in Self-Compacting Concrete." *ACI Structural Journal*, Vol. 100, No. 4, pp. 490-498.

Choulli, Y., Mari, A.R., and Cladera, A. 2008 "Shear Behavior of Full-Scale Prestressed I-Beams Made with Self-Compacting Concrete." *Materials and Structures*, Vol. 41, pp. 131-141.

Collepardi, M., Borsoi, A., Collepardi S., and Troli, R. 2005. "Strength, Shrinkage and Creep of SCC and Flowing Concrete." *Proceedings of second North American conference on the design and use of self-consolidating concrete and fourth international RILEM symposium on self-compacting concrete*, Chicago, pp. 911–1009.

Craeye, B., De Schutter, G., Desmet, B., Vantomme, J., Heirman, G., Vandewalle, L., Cizer, Ö., Aggoun, S., and Kadri, E.H. 2010. "Effect of Mineral Filler Type on Autogenous Shrinkage of Self-Compacting Concrete." Cement and Concrete Research, Vol. 40, pp. 908–913.

CSA CAN3-A23.3. 2004. *Design of concrete structures*. Canadian Standards Association, Rexdale, Ontario, Canada.

Daoud A., Lorrain M., and Laborderie C. 2003. "Anchorage and Cracking Behaviour of Self-Compacting Concrete." *Proceedings of 3rd International RILEM Symposium on Self-Compacting Concrete, Bagneux, France*, pp. 692-702.

Desnerck P., Schutter G.D., and Taerwe L. 2009. "Bond Strength of Reinforcing Bars in Self-Compacting Concrete: Experimental Determination." *Proceedings of 3rd North American conference on the Design and Use of Self-Consolidating Concrete*, Challenges and barriers to application, Center for Advanced Cement-Based Materials (ACBM), Chicago, IL, pp. 433-438.

Desnerck, P., Boel, V., Craeye, B., and Van Itterbeeck, P. 2014. ''Mechanical Properties of SCC: Mechanical Properties" *State-of-the-Art Report of the RILEM Technical Committee TC 228-MPS*, pp. 15-71.

Dinakar, P., Babu, K.G., and Santhanam, M. 2007. "Mechanical Properties of High Volume Fly Ash Self-Compacting Concretes." *Proceedings of 5th International RILEM Symposium on Self-Compacting Concrete*, pp. 651–657.

Ebrahimi, H.R., and Beygi, M.H.A. 2009 "The investigation of shear behavior of R.C. beams made of self-compacting concrete with high strength." *Proceedings of* 2nd *International Symposium on Design*, Performance, and Use of Self-Consolidating Concrete, Beijing, China.

Esfahani, M. R., Lachemi, M., and Kianoush, M. R. 2008. "Top-Bar Effect of Steel Bars in Self-Consolidating Concrete (SCC)." *Cement & Concrete Composites*, Vol. 30, pp. 52–60.

Esping O. 2008. "Effect of Limestone Filler BET (H2O)-Area on the Fresh and Hardened Properties of Self-Compacting Concrete." *Cement and Concrete Research*, Vol. 38, No. 7, pp. 938–944.

Eurocode 2 (EC-2). 2002. *Design of Concrete Structures—Part 1: General Rules and Rules for Buildings*. European Committee of Standardization, Brussels.

Federal Highway Administration (FHWA) 2013. Surface Resistivity Test Evaluation as an Indicator of the Chloride Permeability of Concrete. Publication No. FHWA-HRT-13-024.

Felekoğlu, B. and Sarıkahya, H. 2008. "Effect of Chemical Structure of Polycarboxylate-Based Superplasticizers on Workability Retention of Self-Compacting Concrete." *Construction and Building Materials*, Vol. 22, No. 9, pp. 1972-1980.

Ferraris, C. 1996. *Measurement of Rheological Properties of High Performance Concrete: State of the Art Report*. Technical Report NISTIR 5869. National Institute of Standards and Technology, Gaithersburg, MD.

Ferron R.P., Gregori, A., Sun, Z. and Shah, S. P. (2007). "Rheological Method to Evaluate Structural Buildup in Self-Consolidating Concrete Cement Pastes." *ACI Materials Journal*, Vol. 104, No. 3, pp. 242-250,

Florida Department of Transportation (FDOT). 2011. *Results of Round-Robin Testing for the Development of Precision Statements for the Surface Resistivity of Water Saturated Concrete*. Report No. FL/DOT/SMO/11-549.

Gardner, N. J. and Lockman, M. J. 2001. "Design Provisions for Drying Shrinkage and Creep of Normal-Strength Concrete." *ACI Materials Journal*, Vol. 98, No. 2, pp.159-167.

Georgiadis, A.S., Anagnostopoulos, N.S., and Sideris, K.K. 2007. "Mechanical characteristics of self-compacting concretes produced with different filler materials." *Proceedings of 5th International RILEM Symposium on Self-Compacting Concrete*, pp. 611–618.

Gibbs, J.C., and Zhu, W. 1999. "Strength of Hardened Self-Compacting Concrete." *Proceedings of 1st International Rilem Symposium on Self-Compacting Concrete*, Stockholm, pp. 199-209.

Gregori, A., Ferron, R., Sun, Z., and Shah, S.P. 2008. "Experimental Simulation of SCC Formwork Pressure." *ACI Materials Journal*, Vol. 105, No. 1, pp. 97-104.

Güneyisi E., Gesoğlu M., Erdoğan Özbay E. 2010. "Strength and Drying Shrinkage Properties of Self-Compacting Concretes Incorporating Multi-System Blended Mineral Admixtures." *Construction and Building Materials*, Vol. 24, No. 10, pp. 1878-1887.

Hammer, T.A. 2003. "Cracking Susceptibility Due to Volume Change of Self-Compacting Concrete." *Proceedings of the 3rd International RILEM Symposium on Self-Compacting Concrete*, Reykjavik, Iceland, pp. 553-557.

Hassan, A.A.A., Hossain, K.M.A., and Lachemi, M. 2010. "Bond Strength of Deformed Bars in Large Reinforced Concrete Members Cast with Industrial Self-Consolidating Concrete Mixture." *Construction and Building Materials*, Vol. 24, pp. 520–530.

Hegger, J., Will, N., and Bulti, S. 2007. "Bond Strength and Shear Capacity of Prestressed Beams Made of SCC." *American Concrete Institute*, Vol. 247, pp. 123-138.

Heirman, G., and Vanderwalle, L. 2003. "The Influence of Fillers on the Properties of Self- Compacting Concrete in Fresh and Hardened State." *Proceedings of the 3rd International RILEM Symposium on Self-Compacting Concrete*, Reykjavik, Iceland, pp. 606-618.

Heirman, G., Vandewalle, L., Gemert, D.V., Boel, V., Audenaert, K., De Schutter, G., Desmet, B., and Vantomme, J. 2008. "Time-Dependent Deformations of Limestone Powder Type Self-Compacting Concrete." *Engineering Structures*, Vol. 30, pp. 2945–2956.

Holschemacher, K. 2004. "Hardened Material Properties of Self-Compacting Concrete." *Journal of Civil Engineering and Management*, Vol.10, No. 4, pp. 261-266.

Holschemacher, K., and Klug, Y. 2002. *A Database for the Evaluation of Hardened Properties of SCC*. Leipzig Annual Civil Engineering Report No. 7, Universität Leipzig, pp. 123-134.

Holt, E., and Schodet, O. 2002. *Self-Consolidating Concrete: Early-Age Shrinkage*. VTT Building and Transport, Internal Report, RTE40-IR-21, Finland.

Hoshino, M. 1989. "Relationships between Bleeding, Coarse Aggregate, and Specimen Height of Concrete." *ACI Materials Journal*, Vol. 86, No. 2, pp. 185–90.

Hwang, S.D. and Khayat, K.H. 2008 “Effect of Mixture Composition on Restrained Shrinkage Cracking of Self-Consolidating Concrete Used in Repair.” *ACI Materials Journal*, Vol. 105, pp.499-510.

Hwang, S.D., Khayat, K.H. and Bonneau, O. 2005. “Transport Properties of Self-Consolidating Concrete of Different Mix Design Approaches.” *Proceedings of 1st International Symposium on Design,* Performance and Use of Self-Consolidating Concrete, China, pp. 119-127.

Indiana Department of Transportation (INDOT). 2013. *Electrical Testing of Cement-Based Materials: Role of Testing Techniques, Sample Conditioning, and Accelerated Curing*. Report No. FHWA/IN/JTRP-2013/28

Kavanaugh, B.P. 2008. *Creep Behavior of Self-Consolidating Concrete*. M.Sc. thesis, Auburn University, Auburn, AL.

Khatib, J.M. 2008. “Performance of Self-Compacting Concrete Containing Fly Ash.” *Construction and Building Materials*, Vol. 22, pp. 1963-1971.

Khayat, K.H. 1998. “Use of Viscosity Modifying Admixture to Reduce Top-Bar Effect of Anchored Bars Cast with Fluid Concrete.” *ACI Structural Journal*, Vol. 95, No. 2, pp. 158-167.

Khayat, K.H. 1999. “Workability, Testing, and Performance of Self-Consolidating Concrete.”, *ACI Materials Journal*, Vol. 96, No. 3, pp. 346-353.

Khayat, K. H. 2005. *Literature Review of Factors Affecting Performance of SCC in Precast Prestressed Applications*. Interim Report NCHRP 18-12, Sherbrooke, Canada.

Khayat, K. H. and Mitchell, D. 2009. *Self-consolidating concrete for precast, prestressed concrete bridge elements*. National Corporative Highway Research Program (NCHRP), Report 628, Transportation Research Board.

Khayat, K. H. and Omran, A. 2010. *State-of-the-Art Review of Form Pressure Exerted by Self-Consolidating Concrete*. Final report to the Ready - Mixed Concrete Research and Education Foundation and the Strategic Development Council, American Concrete Constitute, Sherbrooke, Canada.

Khayat, K.H. and Wu, J.L. 2010. “Shrinkage of Precast, Prestressed Self-Consolidating concrete.” *ACI Materials Journal*, Vol. 107, No. 3, pp. 231-238.

Khayat, K.H., and Assaad, J., 2005. “Use of Rheological Properties of SCC to predict Formwork Pressure.” *Proceedings of SCC 2005, The Second North American Conference on the Design and Use of Self – Consolidating Concrete (SCC) and the Fourth International RILEM Symposium on Self – compacting Concrete*, pp. 671-677.

Khayat, K. H., Assaad, J. J., Mesbah, H., and Lessard, M. 2005. “Effect of Section Width and Casting Rate on Variations of Formwork Pressure of Self-Consolidating Concrete.”, *Materials and Structures Journal*, Vol. 38, No. 1, pp. 73-78.

Khayat, K. H., Bickley, J.A., and Hooton, R.D. 1995. “High-Strength Concrete Properties Derived from Compressive Strength Values.” Cement, Concrete and Aggregates Journal, Vol. 17, No. 2, pp.121-129.

Khayat, K.H. and Long, W.J. 2010. “Shrinkage of Precast, Prestressed Self-Consolidating Concrete.” ACI Materials Journal. Vol. 107, pp. 231–238.

Khayat, K.H., Manai, K., and Trudel, A. 1997. “In Situ Mechanical Properties of Wall Elements Cast Using Self-Consolidating Concrete.” ACI Materials Journal, Vol. 94, No. 6, pp. 491–500.

Kim, J.H., Beacraft, M., and Shah, S. P. 2010(a). “Effect Of Mineral Admixtures On Formwork Pressure Of Self-Consolidating Concrete.” *Cement and Concrete Composites*, Vol. 32, No.9, pp. 665-671.

Kim, J.K., Han, S.H., Park, Y.D., Noh, J.H., Park, C.L., Kwon, Y.H., and Lee, S.G. 1996. "Experimental Research on the Material Properties of Super Flowing Concrete." *Proceedings of International RILEM Conference on Production Methods and Workability of Concrete*, Paisely, Scotland, London, E&FN Spon, pp. 271-284.

Kim, J-K. and Han, S-H. 1997. "Mechanical properties of self-flowing concrete." *Proceedings of 3rd CANMET/ACI Intern. Conference, ACI SP-172*, High-Performance Concrete: Design and Materials and Recent Advances in Concrete Technology, pp. 637-652.

Kim, Y.H., Hueste, M.B., Trejo, D., and Cline, D.B.H. 2010(b) "Shear Characteristics and Design for High Strength Self-Consolidating Concrete." *ASCE Journal of Structural Engineering*, Vol. 136, No. 8, pp. 989-910.

Kim, Y. H., Trejo, D., Hueste, M. B. D., and Kim, J. J. 2011. "Experimental Study on Creep and Durability of High-Early-Strength Self-Consolidating Concrete for Precast Elements." *ACI Materials Journal*, V. 108, No.2, pp. 128-138.

Klug, Y., and Holschemacher, K. 2003. "Comparison of the Hardened Properties of Self- Compacting and Normal Vibrated Concrete." *Proceedings of 3rd International RILEM Symposium on Self-Compacting Concrete*, Reykjavik, Iceland, pp. 596-605.

Koehler, E.P. and Fowler, D.W. 2007. "Mixture Proportioning, Testing, and Early-Age Engineering Properties of Self-Consolidating Concrete for Precast Structural Applications," *Center for Transportation Research*, Austin, TX.

König G, Holschemacher K, Dehn F, and Weibe D. 2001. "Self-compacting concrete-time development of material properties and bond behavior." P*roceedings of second international RILEM symposium on self-compacting concrete*, Tokyo, pp. 507–516.

König G, Holschemacher K, Dehn F, and Weibe D. 2003. "Bond of reinforcement in self-compacting concrete (SCC) under monotonic and cyclic loading." *Proceedings of third international RILEM symposium on self-compacting concrete*, Reykjavik, pp. 939–947.

Kosmatka, S.H., Kerkhoff, B., and Panarese W.C. (2002). *Design and Control of Concrete Mixtures*. PCA, Skokie, Illinois

Kwon, S.H. Phung, Q.T., Park, H.Y., Kim, J.H., and Shah, S.P. 2011. "Effect of Wall Friction on Variation of Formwork Pressure over Time in Self-Consolidating Concrete." *Cement and Concrete Research*, Vol. 41, No. 1, pp. 90–101.

Lachemi, M., Hossain, K. M. A., and Lambros, V. 2005. "Shear Resistance of Self-Consolidating Concrete Beams – Experimental Investigations." *Canadian Journal of Civil Engineering*, Vol. 32, pp. 1103-1113.

Landsberger G. A. and Fernandez-Gomez J. 2007. "Evaluation of Creep Prediction Models for Self Consolidating Concrete." *Proceedings of 5th International RILEM Symposium on Self-Compacting Concrete*, Ghent, Belgium, pp. 605-610.

Lange, D. A., Birch, B., Henschen, J., Liu, Y., Tejeda-Dominguez, F., and Struble, L.J. 2008(a). "Modeling Formwork Pressure of SCC." *Proceedings of third North American Conference on the Design and Use of Self-Consolidating Concrete*, Chicago, pp. 295-300.

Lange, D. A., Struble, L. J., Dambrosia, M. D., Shen, L., Tejeda – Dominguez F, Birch, B. F., and Brinks, A. J. 2008(b). *Performance and Acceptance of Self – Consolidating Concrete: Final Report*. Report FHWA – ICT – 08 – 020, Illinois Center for Transportation, IL.

PCI, 2003. *Interim Guidelines for the Use of Self-Consolidating Concrete in Precast/Prestressed Concrete Institute Member Plants*. Precast/Prestressed Concrete Institute, Chicago, IL.

Leemann, A., and Lura, A. 2014. *Mechanical Properties of SCC: Creep and Shrinkage of SCC*. State-of-the-Art Report of the RILEM Technical Committee TC 228-MPS, pp. 73-94.

Loser, R. and Leemann, A. 2009. "Shrinkage and Restrained Shrinkage Cracking of Self-Compacting Concrete Compared to Conventionally Vibrated Concrete." *Materials and Structures*, Vol. 42, No.1, pp. 71-82.

Lothenbach, B., Le Saout, G., Galucci, E., and Scrivener, K. 2008. "Influence of Limestone on the Hydration of Portland Cements." *Cement and Concrete Research*, Vol. 38, pp. 848-860

Louisiana Department of Transportation and Development (LADOTD). 2011. *Evaluation of Surface Resistivity Measurements as an Alternative to the Rapid Chloride Permeability Test for Quality Assurance and Acceptance*. Report No. FHWA/LA.11/479.

Ma, J., and Dietz, J. 2002. *Ultra-High Performance Self Compacting Concrete*. Leipzig Annual Civil Engineering Report No. 7, Universität Leipzig, pp. 33-42.

Ma, K., Xie, Y., Long, G., and Luo, Y. 2009. "Drying shrinkage of medium strength SCC." *Proceedings of 2nd International Symposium on Design, Performance and Use of Self Consolidating Concrete*, Beijing, China, pp. 657-663.

Maguire, M., Morcous, G., Hanna, K., and Tadros, M. K., 2009. "Ultra-High-Performance Concrete in Standard Precast/Prestressed Concrete Products." *PCI National Bridge Conference*, San Antonio, TX

Mamaghani, I. H. P., Moretti, C., Sethre, D., and Dockter, B.A. 2010. *Evaluation of Self-Consolidating Concrete (SCC) for Use in North Dakota Transportation Projects*. Report to North Dakota Department of Transportation, Contract Number: 91-402-0808, University of North Dakota.

Mokarem, D. W. 2002. *Development of Concrete Shrinkage Performance specifications*. Doctor of Philosophy in Civil and Environmental Engineering, Virginia Polytechnic Institute and State University, Blacksburg, Virginia.

Mokhtarzadeh, A., and French, C. 2000. "Mechanical Properties of High-Strength Concrete with Consideration for Precast Applications." *ACI Materials Journal*, Vol. 97, No. 2, pp. 136-146.

Morita, S, and Kaku, T. 1979. "Splitting Bond Failures of Large Deformed Reinforcing Bars." ACI Journal Proceedings, Vol. 76, No. 1, pp. 93–110.

Naito, C. J., Parent, G., and Brunn, G. 2006. "Performance of Bulb-Tee Girders Made with Self-Consolidating Concrete." *PCI Journal*, Vol. 51, No. 6, pp. 72-85.

Nassif, H., Aktas, K., Najm, H., Suksawang, N., and El-Khoury, R. 2008. *Self-Consolidating Concrete (Phase I & II)*. Final report to New Jersey Department of Transportation Federal Highway Administration, Report No. FHWA NJ-2007-021, Rutgers, the State University and Florida International University.

Nehdi, M., Pardhan, M., and Koshowsky, S. 2004. "Durability of self-consolidating concrete incorporating high-volume replacement composite cements." *Cement concrete research*, Vol. 34, pp. 2103-2112.

NZS 3101 (2006). *Concrete Structures Standard*. New Zealand Standards Association, New Zealand.

Olive, M.G., and Cramer, S. 2008. *Self-Consolidating Concrete: Creep and Shrinkage Characteristics*. Report to Spancrete and County Materials, Department of Civil and Environmental Engineering, University of Wisconsin.

Parra, C., Valcuende, M., and Benlloch, J. 2007. "Mechanical properties of self-compacting concretes." *Proceedings of 5th International RILEM Symposium on Self-Compacting Concrete*, pp. 645 – 650.

Pekmezci, B.Y., Voigt, T., Wang, K. and Shah, S.P. 2007. "Low Compaction Energy Concrete for improved Slipform Casting of Concrete Pavements." *ACI Materials Journal*, Vol. 104, No. 3, pp. 251-258.

Persson, B. 1999. "Creep, Shrinkage and Elastic Modulus of Self-Compacting Concrete." *Proceedings of 1st International RILEM Symposium on Self-Compacting Concrete*, Stockholm, Sweden, pp. 239-250.

Persson, B. 2001(a). "A Comparison between Mechanical Properties of Self-Compacting Concrete and the Corresponding Properties of Normal Concrete." *Cement and Concrete Research*, Vol. 31, pp. 193-198.

Persson, B. 2001(b). *Assessment of the chloride migration coefficient, internal frost resistance, salt frost scaling and sulphate resistance of self-compacting concrete*. Report TVBM-3100, Lund Institute of Technology.

Pineaud, A., Cabrillac, R., Rémond, S., Pimienta, P., and Rivillon, P. 2005. "Mechanical Properties of Self-Compacting Concrete—Influence of Composition Parameters." *Proceedings of 4th International RILEM Symposium on Self-Compacting Concrete*, pp. 863–868.

Pons, G., Proust, E., and Assié, S. 2003. "Creep and Shrinkage of Self-Compacting Concrete: A Different Behaviour Compared with Vibrated Concrete?" *Proceedings of 3rd International RILEM Symposium on Self-Compacting Concrete*, Reykjavik, Iceland, pp. 645-654.

Poppe, A.M., Schutter, G. 2005(a). "Cement Hydration in the Presence of High Filler Contents." *Cement and Concrete Research*, Vol. 35, pp. 2290-2299.

Poppe, A.M., Schutter, G. 2005(b) "Creep and shrinkage of self-compacting concrete." In: Yu, Z., Shi, C., Khayat, K.H., Xie, Y. (eds.) *Proceedings of the 1st International RILEM Symposium on SCC* RILEM Publications S.A.R.L, Bagneux, pp. 329–336.

Rols, S., Ambroise, J. and Pèra, J. 1999. "Effects of Different Viscosity Agents on The Properties of Self-Leveling Concrete." *Cement and Concrete Research*, Vol. 29, No.2, pp. 261-266.

Rozière, E., Granger, S., Turcry, P., and Loukili, A. 2007 "Influence of Paste Volume on Shrinkage Cracking and Fracture Properties of Self-Compacting Concrete." *Cement and Concrete Composites*. Vol. 29, pp. 626–636

Saak, A., Jennings, H. and Shah, S. 2001. "The Influence of Wall Slip on Yield Stress and Viscoelastic Measurements of Cement Paste." *Cement and Concrete Research*, Vol. 31, No.2, pp. 205–212.

Sahmaran, M., Yaman, I.O., and Tokyay, M. 2009. "Transport and Mechanical Properties of Self-Consolidating Concrete with High Volume Fly Ash." *Cement and Concrete Composites*, V. 31No. 2, pp. 99–106.

Schindler, A.K., and Folliard, K.J. 2005 "Heat of Hydration Models for Cementitious Materials." *ACI Materials Journal*, Vol. 102, pp. 24-33.

Schindler, A. K., Barnes, R. W., Roberts, J. B., and Rodriguez, S. 2007. "Properties of Self-Consolidating Concrete for Prestressed Members." *ACI Materials Journal*, Vol. 104, No. 1, pp. 53-61.

Schutter, G. 2008. "Hydration, Microstructure, and Durability of Self-Compacting Concrete." *Proceedings of 1st International Conference on Microstructure Related Durability of Cementitious Composites*, Nanjing, China, pp. 13-15.

Schwartzentruber, L.D., Roy, R.L., and Cordin, J. 2006. "Rheological Behavior of Fresh Cement Pastes Formulated from a Self-Compacting Concrete (SCC)." *Cement and Concrete Research*, Vol. 36, No. 7, pp. 1203-1213.

See, H. T., and Attiogbe, E. K. 2005. “Performance of Self-Consolidating Concrete Under Restrained Shrinkage.” *International Concrete Research & Information Portal*, Vol. 227, pp. 303-316.

Shah, S.P., Ferron, R.P., Tregger, N.A., Ferrara, L. and Beacraft, M.W. 2009. “ Self-Consolidating Concrete: Now and Future.”Proc*eedings of Second International Symposium on Design, Performance and Use of Self-Consolidating Concrete SCC*, China, Beijing, pp. 3-15.

Shaughnessy, R. and Clark, P. 1988. “The Rheological Behavior of Fresh Cement Pastes.” *Cement and Concrete Research*, Vol.18, No. 3, pp. 327–341.

Sonebi, M., and Nanukuttan, S., 2009. “Transport Properties of Self-Consolidating Concrete.” *ACI Materials Journal*, Vol. 106, No.2, pp. 161-166.

Sonebi, M. and Bartos, P.J.M. 1999. “Hardened SCC and Its Bond with Reinforcement.” *Proceedings of 1st Intern. RILEM Symposium on Self-Compacting Concrete*, RILEM Publications S.A.R.L. Stockholm, pp. 275-289.

Sonebi, M., Bartos, P. J. M., Zhu, W., Gibbs, J., and Tamimi, A., 2000. *Task 4 – Properties of Hardened Concrete*. Final report of Brite EuRam Project No. BE96-3801/Contract BRPR-CT96-0366.

Song, H.-W., Cho, H.-J., Park, S.-S., Byun, K.-I, and Maekawa, K. 2001. “Early-Age Cracking Resistance Evaluation of Concrete Structures.” *Concrete Science and Engineering*, Vol. 3, pp. 62-72.

Su, J. K., Cho, S. W., Yang, C. C., and Huang, R. 2002. “Effect of Sand Ratio on the Elastic Modulus of Self-Consolidating Concrete.” *Journal of Marine Science and Technology*, V. 10, No. 1, pp.8-13.

Tang, L., and Zhu, W. 2007. *Chloride Penetration*. Durability of Self-Compacting Concrete - State-of-the-Art Report of RILEM Technical Committee 205-DSC, Edited by G. De Schutter and K. Audenaert, Chapter 4, pp. 77 – 88.

Tang, L., Andalen, A., Johansson, J.O., and Hjelm, S. 1999. “Chloride Diffusivity of Self-Compacting Concrete.” In Proceedings of 1st International RILEM Symposium on Self-Compacting Concrete, pp. 187-198.

Tattersall, G.H., and Banfill, P.F.G. 1983. *The Rheology of Fresh Concrete*. Pitman Advanced Publishing Program, Boston/London/Melbourne.

Tejeda-Dominguez, F., Lange, D.A., and D’Ambrosia, M.D. 2005. “Formwork Pressure of Self-Consolidating Concrete in Tall Wall Field Applications.” *Journal of the Transportation Research Board*, No.1914, pp. 1-7.

Tregger, N. A., Ferrara, L. and Shah, S.P. 2008. “Identifying Viscosity of Cement Paste From Mini-Slump-Flow Test.” *ACI Materials Journal*, Vol. 105, No. 6, pp. 558-566.

Tregger, N. A.., Margaret E. P., and Shah, S. P. 2010. “Influence of Clays on the Rheology of Cement Pastes.” *Cement and Concrete Research*, Vol. 40, No. 3, pp. 384-391.

Trezos, K.G., Sfikas, I.P., Palmos, M.S. and Sotiropoulou, E.K. 2010. *Top-Bar Effect in Self-Compacting Concrete Elements*. Design, Production and Placement of Self-Consolidating Concrete, RILEM Book Series, Vol. 1, pp. 355-366.

Troli K., Ogoumah, J. J. O., Monosi, S., and Collepardi, M. 2003. “Low Heat Development in Self-Compacting Concrete for Massive Structures.” *Proceedings of Seventh CANMET/ACI International Conference on Superplasticizers and Other Chemical Admixtures in Concrete*, Berlin, Germany, October, pp. 103-112

Turcry, P., and Loukili, A. 2003. “A Study of Plastic Shrinkage of Self-Compacting Concrete.” *Proceedings of 3rd International RILEM Symposium on Self-Compacting Concrete*, Reykjavik, Iceland, pp. 576-585.

Turcry, P., Loukili, A., and Haidar, K. 2002. “Mechanical Properties, Plastic Shrinkage and Free Deformations of Self-Consolidating Concrete.” Proceedings of 1st North American Conference on the Design and Use of Self-Consolidating Concrete, Chicago, Illinois, pp. 335-340.

Turcry, P., Loukili, A., and Haidar, K., Pijaudier-Cabot, G., and Belarbi, A. 2006. "Cracking Tendency of Self-Compacting Concrete Subjected to Restrained Shrinkage. Experimental Study and Modeling. *Journal of Materials in Civil Engineering*, Vol. 18, No.1, pp. 46–54.

Valcuende, M. and Parra, C. 2009. “Bond Behavior of Reinforcement in Self-Compacting Concretes.” Construction and Building Materials, 23, pp. 162–170.

Valcuende, M., Parra, C., and Balasch, S. (2008). A discussion of the paper ‘‘Top-bar effect of steel bars in self-consolidating concrete (SCC)” by M. Reza Esfahani, M. Lachemi, M. Reza Kianoush. *Cement & Concrete Composites*, Vol.30, No.10, pp.1020.

Vanhove, Y., and Djelal, C., 2002. “Formwork Pressures with Self-Compacting Concrete.” *Concrete Magazine*, Vol. 36, No. 6, pp. 22-23.

Vieira, M., and Bettencourt, A. 2003. “Deformability of Hardened SCC.” *Proceedings of 3rd International RILEM Symposium on Self-Compacting Concrete*, Reykjavik, Iceland, pp. 637-644.

Vilanova, A., and Fernandez-Gomez, J. 2011. “Evaluation of the Mechanical Properties of Self Compacting Concrete Using Current Estimating Models: Estimating the Modulus of Elasticity, Tensile Strength, and Modulus of Rupture of Self Compacting Concrete.” *Construction and Building Materials*, Vol. 25, No. 8, pp. 3417-3426.

Wang, G., and Zheng, J. 2005. “Bond Behaviors of Self-Compacting Concrete.” *Proceedings of first international symposium on design, performance and use of self-consolidating concrete*. China, Changsha, pp. 465–71.

Wang, K., Ge, Z., Grove, J., Ruiz, J.M., and Rasmussen, R. 2006. *Developing a Simple and Rapid Test for Monitoring the Heat Evolution of Concrete Mixtures for Both Laboratory and Field Applications*. FHWA DTF61-01-00042 (Project 17, Phase I).

Weerdt, K., Haha, M., Saout, G., Kjellsen, K.O., Justnes, H., Lothenbach, B. 2011. “Hydration Mechanisms of Ternary Portland Cements Containing Limestone Powder and Fly Ash.” *Cement and Concrete Research*, Vol. 41, No. 3, pp. 279-291.

Wu, J. L., Khayat, K. H., and Xing, F. 2010. “Shrinkage of Full-Scale Girders Cast with Self-Consolidating Concrete.” *Advanced Materials Research*, Vols. 129-131, pp. 381-385.

Ye, G., Liu, X., Schutter, G., Poppe, A. M., and Taerwe. 2007. “Influence of Limestone Powder Used as Filler in SCC on Hydration and Microstructure of Cement Pastes.” *Cement & Concrete Composites*, Vol. 29, pp. 94-102.

Zhang, M.H., Sisomphon, K., Ng, T. S., and Sun, D. J. 2010. “Effect of Superplasticizers on Workability Retention and Initial Setting Time of Cement Pastes.” *Construction and Building Materials*, Vol. 24, No. 9, pp.1700-1707.

Zheng, J., Chao, P., and Luo, S. 2009. “Experimental Study on Factors Influencing Creep of Self-Compacting Concrete.” *Proceedings of 2nd Int. Symposium on Design, Performance and Use of Self Consolidating Concrete*, pp. 703 – 709.

Zhu, W. 2007. *Transport Properties: Durability of Self-Compacting Concrete*. State-of-the-Art Report of RILEM Technical Committee 205-DSC, Edited by G. De Schutter and K. Audenaert, Chapter 3, pp. 41-60.

Zhu, W. and Bartos, P.M.J. 2003. “Permeation Properties of Self-Compacting Concrete.” *Cement and Concrete Research*, Vol. 33, No. 6, pp. 921-926.

Zhu, W., Sonebi, M., and Bartos, P.J.M. 2004. “Bond and interfacial properties of reinforcement in self-compacting concrete.” *Materials and Structures*, Vol. 37, pp. 442-448.

APPENDIX B: Material Properties

Contents

1. Material Sources

Table B-1. Materials used in the project and their sources

Constituent	Type	Standard (Name)	Sources
Aggregates	Natural Sand	AASHTO M6/ASTM C 33	Lyman Richey Co., Bellevue, NE
	Natural Gravel	AASHTO M80/ASTM C 33 (No. 67)	Aggregate Industries, Eagan, MN
		AASHTO M80/ASTM C 33 (No. 78)	
		AASHTO M80/ASTM C 33 (No. 8)	
	Crushed Limestone	AASHTO M80/ASTM C 33 (No. 67)	Lyman Richey Co., Bellevue, NE
		AASHTO M80/ASTM C 33 (No. 78)	
		AASHTO M80/ASTM C 33 (No. 8)	
Cement	Type I/II	AASHTO M85/ASTM C 150	Ash Grove Packaging Group, Fremont, NE
	Type IPF	AASHTO M240/ASTM C 595	Ash Grove Packaging Group, Fremont, NE
Mineral Additives	Class F Fly Ash	AASHTO M295/ASTM C 618	Ash Grove Cement Co., Louisville, NE
	Class C Fly Ash	AASHTO M295/ASTM C 618	Ash Grove Cement Co., Louisville, NE
	GGBFS	AASHTO M302/ASTM C 989	Central Plains Cement Co. (formerly Lafarge), Omaha, NE
	Limestone Powder (Coarse)	(UniCal P)	Iowa Limestone Company, Weeping Water, NE
	Limestone Powder (Fine)	(Betocarb 3-PT)	OMYA, Inc., Cinncinati, OH
Chemical Admixtures	High-Range Water Reducing Admixture (HRWRA)	ASTM C 494 (Glenium 3030 NS)	BASF, Omaha, NE
	Viscosity Modifying Admixture (VMA)	ASTM C 494 (Rheomac VMA 362)	
	Workability Retaining Admixture (WRA)	ASTM C 494 (RheoTEC Z-60)	
	Air Entraining Admixture (AEA)	AASHTO M154 (MB-AE 90)	

2. Physical Analysis of Cementitious Materials and Filler

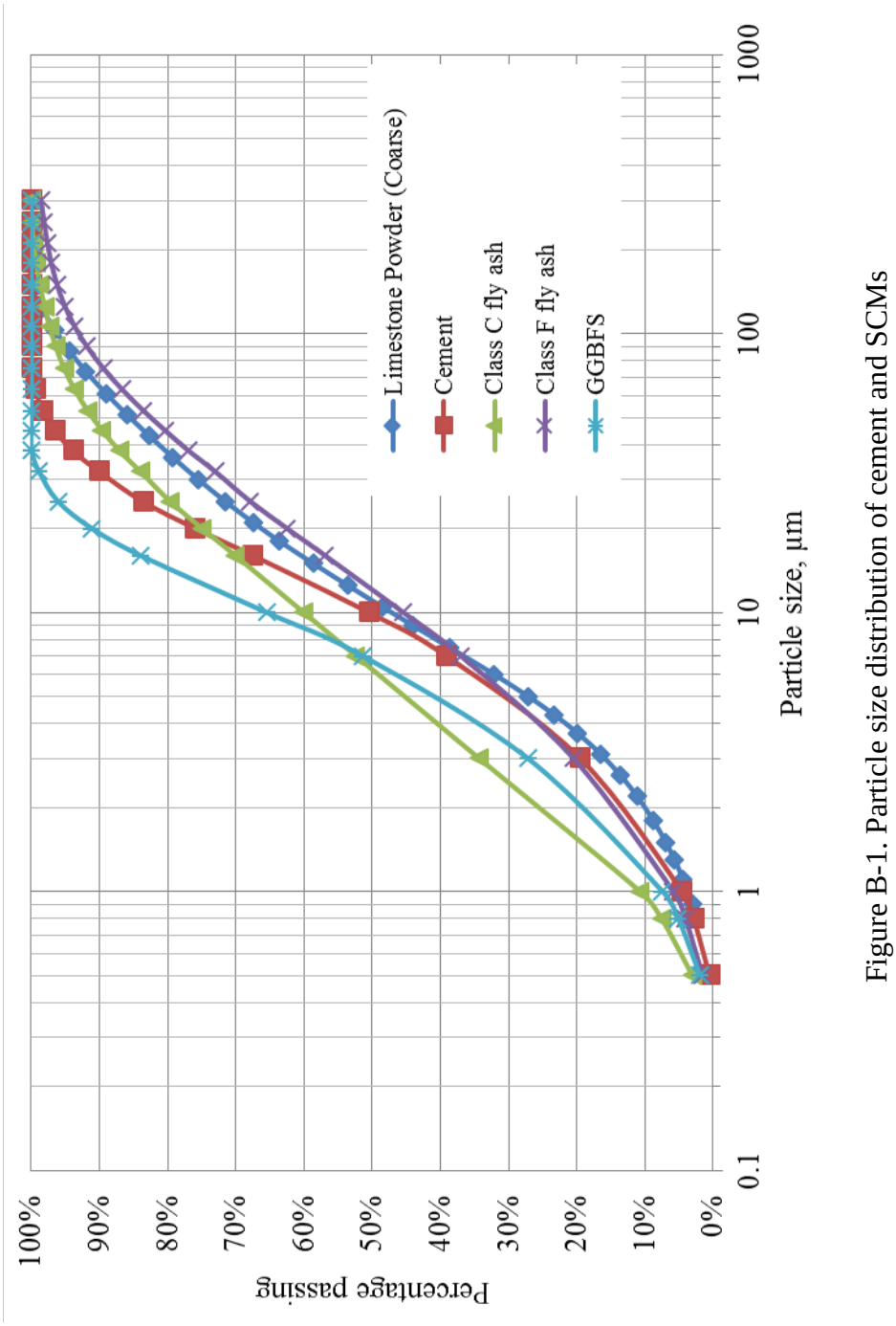

Figure B-1. Particle size distribution of cement and SCMs

Table B-2. Test results for Type I/II cement

Type I/II Cement Analysis

Brand: *Ash Grove Cement*
Type: *Type I/II*
Mill Location: *Louisville, NE*
Field I.D.: *1567 Tests*

Sampled By: *UNL*
Date Sampled:
Date Received:

Sample ID:

Chemical Test	Method	*Results*	Limit	Requirements
Air Content of Mortar	C185	7	max %, 12	Required by ASTM
Autoclave Expansion	C151	0.09	max %, 0.8	Required by ASTM
Compressive Strength at 3 Days	C109	3650	min psi, 1450	Required by ASTM
Compressive Strength at 7 Days	C109	4330	min psi, 2470	Required by ASTM
Fineness, Air Permeability	C204	440	min m^2/kg, 280	Required by ASTM
Vicat Final Set	C191	225	max 375 min.	Required by ASTM
Vicat Initial Set	C191	145	min 45 min	Required by ASTM

Pass/Fail: PASS

Chem Lab:
Date of Report:

Table B-3. Test results for Type IPF Cement

Type IPF Cement Analysis

Brand: *Ash Grove Cement*
Type: *Type 1PF*
Mill Location: *Louisville, NE*
Field I.D.: *1567 Tests*

Sampled By: *UNL*
Date Sampled:
Date Received:

Sample ID:

Chemical Test	Method	*Results*	Limit	Requirements
Air Content of Mortar	C185	4.9	max %, 12	Required by ASTM
Autoclave Expansion	C151	-0.02	max %, 0.8	Required by ASTM
Compressive Strength at 3 Days	C109	3350	min psi, 1450	Required by ASTM
Compressive Strength at 7 Days	C109	4230	min psi, 2470	Required by ASTM
Vicat Final Set	C191	230	max 375 min.	Required by ASTM
Vicat Initial Set	C191	135	min 45 min	Required by ASTM

Pass/Fail: PASS

Chem Lab:
Date of Report:

Table B-4. Test results for Class F Fly Ash

Class C Fly Ash Analysis

Brand: *Gerald Gentlemen Station #1 & #2* **Sampled By:** *UNL*
Type: *Class C Fly Ash* **Date Sampled:**
Mill Location: *Sutherland,NE* **Date Received:**
Field I.D.: *1567 Tests*

Sample ID: **2006.127.FA**

Chemical Test	Method	*Results*	Limit	Requirements
Autoclave Expansion or Contraction	C151	0.08	Max %, 0.8	Required by ASTM
Density, Max Variation from Average	C188	2.65	Max %, 5	Required by ASTM
Fineness, Wet-Sieved on No. 325	C430	18.63	Max %, 34	Required by ASTM
Strength Activity Index, 7 days	C311	102	Min %, 75	Required by ASTM
Water Requirements	C311	94	Max % 105	Required by ASTM

Pass/Fail: PASS

Chem Lab:
Date of Report:

Table B-5. Test results for GGBFS

GGBFS Analysis

Brand: *Lafarge North America*
Type: *Chicago, IL*
Mill Location: *South Chicago Plant*
Field I.D.: *1567 Tests*

Sampled By: *UNL*
Date Sampled:
Date Received:

Sample ID:

Chemical Test	Method	*Results*	Limit	Requirements
Air Content of Mortar	C185	5.7	Max %, 12	Required by ASTM
Density, Max Variation from Average	C188	3.18	Max %, 5	Required by ASTM
Fineness, Wet-Sieved on No. 325	C430	0.53	Max %, 20	Required by ASTM
Strength Activity Index, 28 days	C311	127	Min %, 110	Required by ASTM
Stength Activity Index, 7 days	C311	97	n/a	Required by ASTM
Water Requirements	C311	98	Max % 105	Required by ASTM

Pass/Fail: PASS

Chem Lab:
Date of Report:

3. Chemical Analysis of Cementitious Materials

Table B-6. Chemical compositions of the used cementitious materials and filler

Chemical Composition	Type I/II Cement	Class C fly ash	Class F fly ash	GGBFS	Limestone Powder (coarse)
SiO2	20.10	42.46	50.87	31.63	1.56
Al2O3	4.44	19.46	20.17	11.30	-
Fe2O3	3.09	5.51	5.27	0.34	0.48
SO3	3.18	1.20	0.61	3.30	1.77
CaO	62.94	21.54	15.78	41.31	52.77
MgO	2.88	4.67	3.19	10.77	0.48
Na2O	0.10	1.42	0.69	0.19	0.03
K2O	0.61	0.68	1.09	0.36	0.09
P2O5	0.06	0.84	0.44	0.02	-
TiO2	0.24	1.48	1.29	0.56	-
SrO	0.09	0.32	0.35	0.04	-
BaO	-	0.67	0.35	-	-
LOI	2.22	0.19	0.07	-	42.50
Total	**100**	**100**	**100**	**100**	**100**

Table B-7. Chemical analysis of Type I/II cement

Cement Analysis

Brand: *Ash Grove Cement*
Type: *Type I/II*
Mill Location: *Louisville, NE*
Field I.D.: *1567 Tests*

Sampled By: *UNL*
Date Sampled:
Date Received:

Sample ID
Sample 1:
Sample 2:
Sample 3:

Chemical Test	Method	Results for Each Sample			Limit	Requirements
		Sample 1	*Sample 2*	*Sample 3*		
Aluminum Oxide (Al_2O_3)	C114	4.27	4.21	4.21	max, 6%	Required by ASTM
Calcium Oxide (CaO)		61.84	61.93	61.84	n/a	Required by NDOR
Ferric Oxide (Fe_2O_3)	C114	3.02	3.02	3	max, 6%	Required by ASTM
Free Lime (CaO)		1.17	-	-	n/a	Required by NDOR
Insoluble Residue	C114	0.54	-	-	max, 0.75%	Required by ASTM
Loss on Ignition	C114	2.91	2.95	2.97	max, 3%	Required by ASTM
Magnesium Oxide (MgO)	C114	3.12	3.1	3.14	max, 6%	Required by ASTM
Potassium Oxide (K_2O)		0.58	0.58	0.59	n/a	Required by NDOR
Silicon Dioxide (SiO_2)	C114	20.37	20.27	20.29	n/a	Required by ASTM
Sodium Oxide (Na_2O)		0.12	0.12	0.12	n/a	Required by NDOR
Sulfur Trioxide (SO_3)	C114	2.86	2.86	2.86	max, 3%	Required by ASTM
Tricalcium Aluminate (C_3A)	C114	6.2	6	6.1	max, 8.5%	Required by ASTM
Equivalent Alkalies	C114	0.51	0.51	0.51	max, 0.6%	Optional for ASTM
Pass/Fail:		***Pass***	***Pass***	***Pass***		

Chem Lab:
Date of Report:

Table B-8. Chemical analysis of Type IPF Cement

Cement Analysis

Brand: *Ash Grove Cement* **Sampled By:** *UNL*
Type: *Type IPF* **Date Sampled:**
Mill Location: *Louisville, NE* **Date Received:**
Field I.D.: *1567 Tests*

Sample ID
Sample 1:
Sample 2:
Sample 3:

Chemical Test	Method	Results for Each Sample			Limit	Requirements
		Sample 1	*Sample 2*	*Sample 3*		
Aluminum Oxide (Al_2O_3)		8.32	8.33	8.29	n/a	Required by NDOR
Calcium Oxide (CaO)		51.83	51.69	51.8	n/a	Required by NDOR
Ferric Oxide (Fe_2O_3)		3.22	3.21	3.21	n/a	Required by NDOR
Free Lime (CaO)		1.15	-	-	n/a	Required by NDOR
Loss on Ignition	C114	1.14	1.24	1.25	max, 5%	Required by ASTM
Magnesium Oxide (MgO)	C114	2.79	2.85	2.83	max, 6%	Required by ASTM
Potassium Oxide (K_2O)		0.66	0.65	0.66	n/a	Required by NDOR
Silicon Dioxide (SiO_2)		28.05	28.13	27.99	n/a	Required by NDOR
Sodium Oxide (Na_2O)		0.2	0.21	0.21	n/a	Required by NDOR
Sulfur Trioxide (SO_3)	C114	3.39	3.33	3.36	max, 4%	Required by ASTM
Equivalent Alkalies	C114	0.64	0.64	0.64	n/a	Optional for NDOR
Pass/Fail:		***Pass***	***Pass***	***Pass***		

Chem Lab:
Date of Report:

Table B-9. Chemical analysis of Class C Fly Ash

Fly Ash Analysis

Brand: *Plains Pozzolanic*
Type: *Class C Fly Ash*
Mill Location: *Gerald Gentlemen Station*
Field I.D.: *1567 Tests*

Sampled By: *UNL*
Date Sampled:
Date Received:

Sample ID
Sample 1:
Sample 2:
Sample 3:

Chemical Test	Method	Results for Each Sample			Limit	Requirements
		Sample 1	*Sample 2*	*Sample 3*		
Aluminum Oxide (Al_2O_3)		18.72	18.7	-	n/a	Required by NDOR
Calcium Oxide (CaO)		28.15	28.15	-	n/a	Required by NDOR
Equivalent Alkalies		1.8	1.8		max, 1.9%	Required by NDOR
Ferric Oxide (Fe_2O_3)		5.1	5.12	-	n/a	Required by NDOR
Free Lime (CaO)		0.02	-	-	n/a	Required by NDOR
Magnesium Oxide (MgO)		4.84	4.82	-	n/a	Required by NDOR
Potassium Oxide (K_2O)		0.4	0.4	-	n/a	Required by NDOR
Silicon Dioxide (SiO_2)		33.99	34.12	-	n/a	Required by NDOR
$SiO_2 + Al_2O_3 + Fe_2O_3$	C311	57.81	57.94	-	min, 49.5%	Required by ASTM
Sodium Oxide (Na_2O)		1.54	1.54	-	n/a	Required by NDOR
Sulfur Trioxide (SO_3)	C311	1.86	1.84	-	max, 5%	Required by ASTM
Loss on Ignition	C311	0.4	0.35	-	max, 6%	Optional for ASTM
Pass/Fail:		***Pass***	***Pass***	**-**		

Chem Lab:
Date of Report:

Table B-10. Chemical analysis of GGBFS

Ground Granulated Blast Furnace Slag Analysis

Brand: *Lafarge North America*
Type: *GGBFS (Slag)*
Mill Location: *South Chicago Plant*
Field I.D.: *1567 Tests*

Sampled By: *UNL*
Date Sampled:
Date Received:

Sample ID
Sample 1:
Sample 2:
Sample 3:

Chemical Test	Method	Results for Each Sample			Limit	Requirements
		Sample 1	*Sample 2*	*Sample 3*		
Sulfide Sulfur (S)	C989	1.3	1.3	1.3	max, 2.5%	Required by ASTM
Total Sulfate ion as SO_3	C989	3.3	3.3	3.3	n/a	Required by ASTM
Aluminum Oxide (Al_2O_3)		11.25	11.31	11.31	n/a	Optional for NDOR
Calcium Oxide (CaO)		43.31	43.27	43.3	n/a	Optional for NDOR
Ferric Oxide (Fe_2O_3)		0.36	0.35	0.34	n/a	Optional for NDOR
Magnesium Oxide (MgO)		10.6	10.74	10.73	n/a	Optional for NDOR
Manganic Oxide (Mn_2O_3)		0.43	0.43	0.42	n/a	Optional for NDOR
Phosphorus Pentoxide (P_2O_5)		0.02	0.02	0.02	n/a	Optional for NDOR
Potassium Oxide (K_2O)		0.36	0.36	0.36	n/a	Optional for NDOR
Silicon Dioxide (SiO_2)		31.63	31.69	31.83	n/a	Optional for NDOR
Sodium Oxide (Na_2O)		0.19	0.19	0.19	n/a	Optional for NDOR
Strontium Oxide (SrO)		0.04	0.04	0.04	n/a	Optional for NDOR
Titanium Dioxide (TiO_2)		0.55	0.56	0.56	n/a	Optional for NDOR
Pass/Fail:		***Pass***	***Pass***	***Pass***		

Chem Lab:
Date of Report:

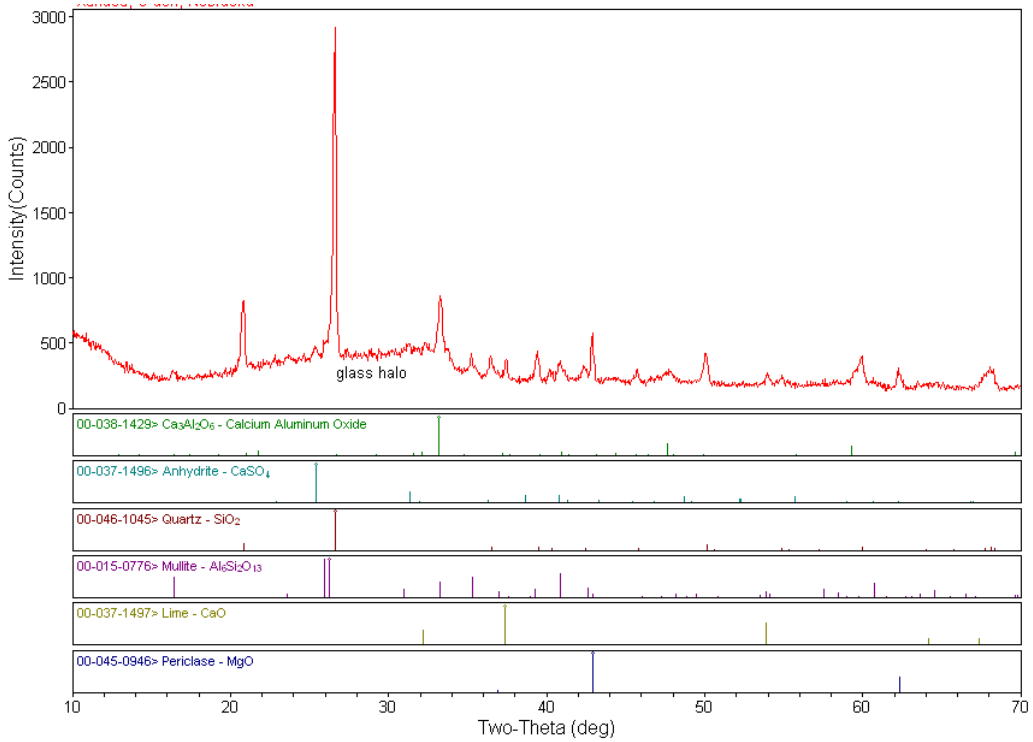

Figure B-2. Diffractogram of Class C Fly Ash

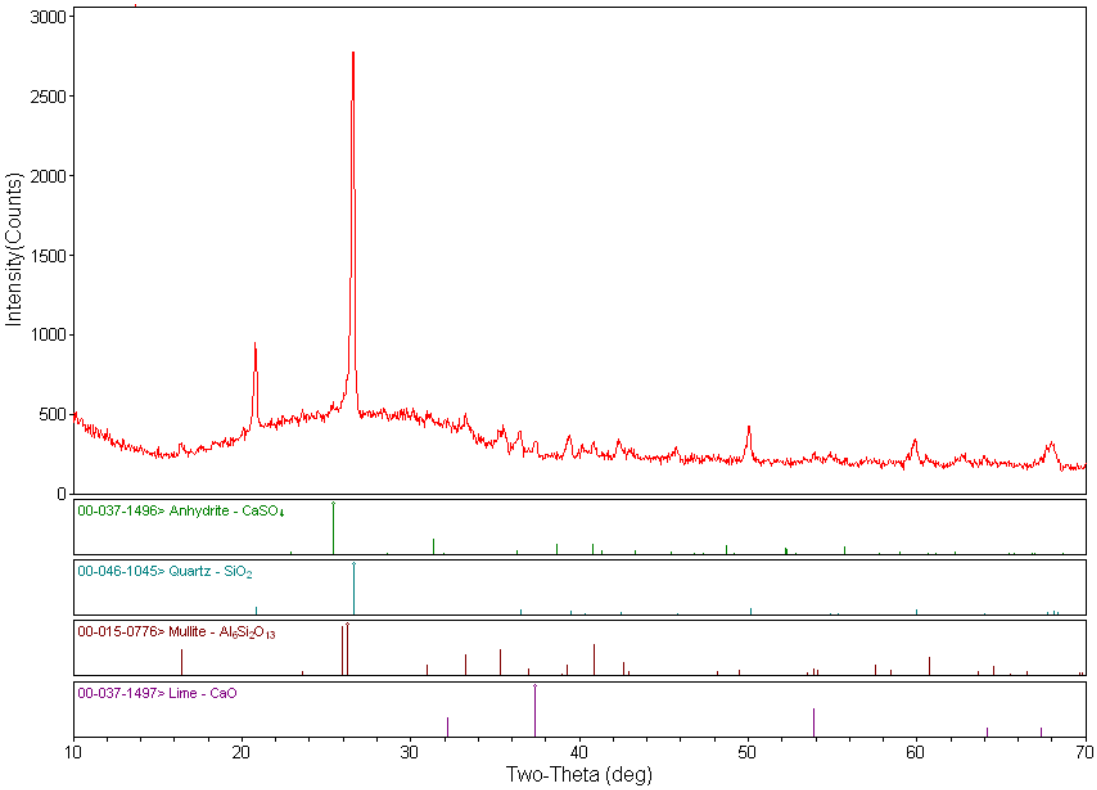

Figure B-3. Diffractogram of Class F Fly Ash

4. Physical Analysis of Aggregates

Table B-11. Physical properties of natural sand

Sieve Size		Natural Sand			AASHTO M 6 Sand	
No.	**mm**	**% Retained**	**Cumulative % Retained**	**Cumulative % Passing**	**Min.**	**Max.**
3/8"	**9.5**	0.0%	0.0%	100.0%	100%	100%
#4	**4.75**	0.3%	0.3%	99.7%	95%	100%
#8	**2.36**	3.2%	3.5%	96.5%	80%	100%
#16	**1.18**	19.9%	23.4%	76.6%	50%	85%
#30	**0.6**	30.7%	54.1%	45.9%	25%	60%
#50	**0.3**	33.4%	87.5%	12.5%	10%	30%
#100	**0.15**	11.6%	99.1%	0.9%	2%	10%
			Fineness Modulus	**2.68**	**3.38**	**2.15**

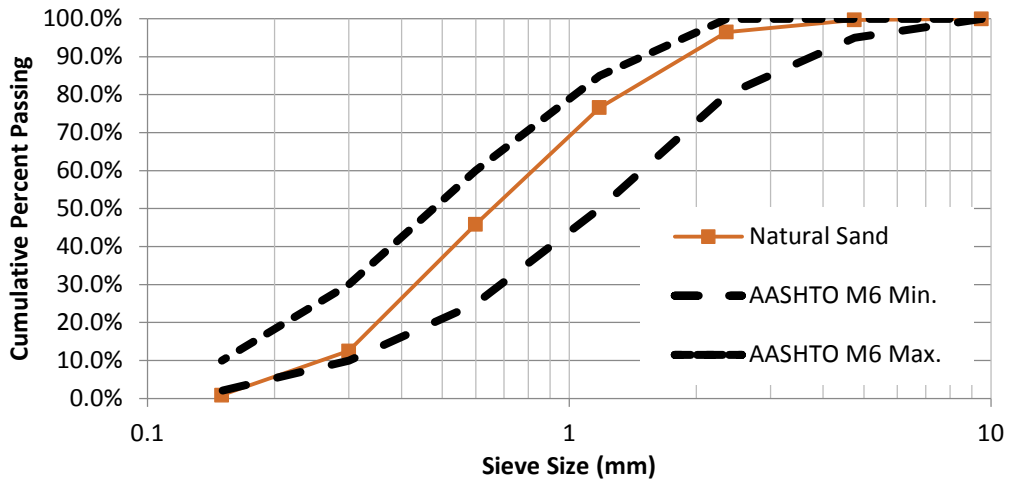

Figure B-4. Particle size distribution of natural sand

Figure B-5. Photo of natural sand

Table B-12. Physical properties of ¾ in. NMSA crushed limestone

Sieve Size		Crushed Limestone NMSA ¾ in.			AASHTO M 43 Size No. 67	
No.	**mm**	**% Retained**	**Cumulative % Retained**	**Cumulative % Passing**	**Min.**	**Max.**
1"	**25**	0.0%	0.0%	100.0%	100%	100%
3/4"	**19**	12.0%	12.0%	88.0%	90%	100%
1/2"	**12.5**	29.0%	41.0%	59.0%	55%	78%
3/8"	**9.5**	29.0%	70.0%	30.0%	20%	55%
#4	**4.75**	23.0%	93.0%	7.0%	0%	10%
#8	**2.36**	1.0%	94.0%	6.0%	0%	5%
#16	**1.18**	1.0%	95.0%	5.0%	0%	5%
#30	**0.6**	1.0%	96.0%	4.0%	0%	0%
#50	**0.3**	0.0%	96.0%	4.0%	0%	0%
#100	**0.15**	0.0%	96.0%	4.0%	0%	0%

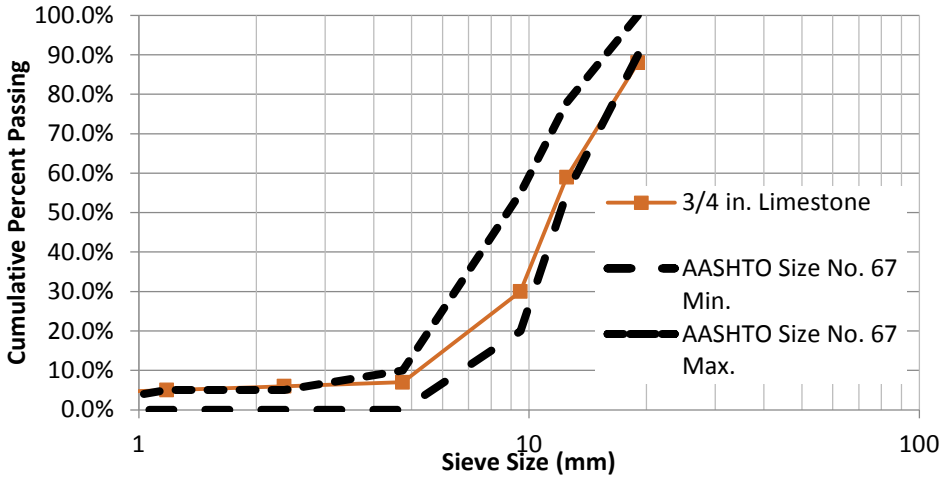

Figure B-6. Particle size distribution of ¾ in. NMSA crushed limestone

Figure B-7. Photo of ¾ in. NMSA crushed limestone

Table B-13. Physical properties of ½ in. NMSA crushed limestone

Sieve Size		Crushed Limestone NMSA ½ in.			AASHTO M 43 Size No. 78	
No.	mm	% Retained	Cumulative % Retained	Cumulative % Passing	Min.	Max.
1"	25	0.0%	0.0%	100.0%	100%	100%
3/4"	19	0.0%	0.0%	100.0%	100%	100%
1/2"	12.5	0.0%	0.0%	100.0%	90%	100%
3/8"	9.5	35.3%	35.3%	64.7%	40%	75%
#4	4.75	51.8%	87.1%	12.9%	5%	25%
#8	2.36	7.9%	95.0%	5.0%	0%	10%
#16	1.18	0.8%	95.8%	4.2%	0%	5%
#30	0.6	0.4%	96.2%	3.8%	0%	0%
#50	0.3	0.3%	96.5%	3.5%	0%	0%
#100	0.15	0.1%	96.6%	3.4%	0%	0%

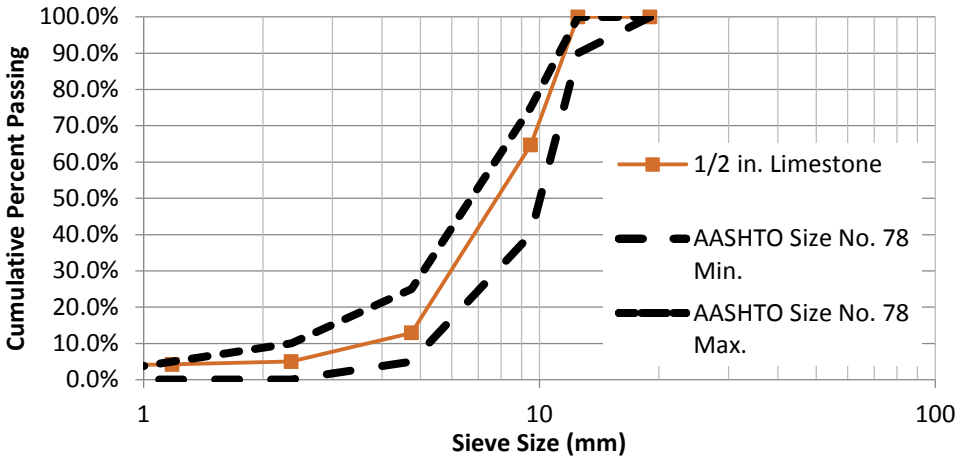

Figure B-8. Particle size distribution of ½ in. NMSA crushed limestone

Figure B-9. Photo of ½ in. NMSA crushed limestone

Table B-14. Physical properties of $^{3}/_{8}$ in. NMSA crushed limestone

Sieve Size		Crushed Limestone NMSA $^{3}/_{8}$ in.			AASHTO M 43 Size No. 8	
No.	**mm**	**% Retained**	**Cumulative % Retained**	**Cumulative % Passing**	**Min.**	**Max.**
1"	**25**	0.0%	0.0%	100.0%	100%	100%
3/4"	**19**	0.0%	0.0%	100.0%	100%	100%
1/2"	**12.5**	0.1%	0.1%	99.9%	100%	100%
3/8"	**9.5**	1.1%	1.2%	98.8%	85%	100%
#4	**4.75**	73.8%	75.0%	25.0%	10%	30%
#8	**2.36**	20.0%	95.0%	5.0%	0%	10%
#16	**1.18**	3.3%	98.3%	1.7%	0%	5%
#30	**0.6**	0.6%	98.9%	1.1%	0%	0%
#50	**0.3**	0.5%	99.4%	0.6%	0%	0%
#100	**0.15**	0.3%	99.7%	0.3%	0%	0%

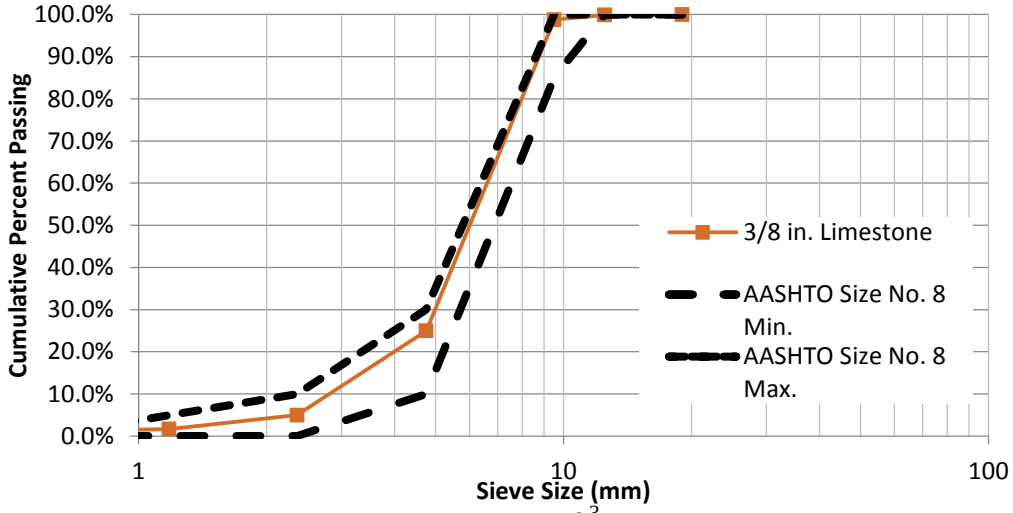

Figure B-10. Particle size distribution of $^{3}/_{8}$ in. NMSA crushed limestone

Figure B-11. Photo of $^{3}/_{8}$ in. NMSA crushed limestone

Table B-15. Physical properties of ¾ in. NMSA gravel

Sieve Size		Gravel NMSA ¾ in.			AASHTO M 43 Size No. 67	
No.	**mm**	**% Retained**	**Cumulative % Retained**	**Cumulative % Passing**	**Min.**	**Max.**
1"	**25**	0.0%	0.0%	100.0%	100%	100%
3/4"	**19**	4.0%	4.0%	96.0%	90%	100%
1/2"	**12.5**	33.0%	37.0%	63.0%	55%	78%
3/8"	**9.5**	22.0%	59.0%	41.0%	20%	55%
#4	**4.75**	34.8%	93.8%	6.2%	0%	10%
#8	**2.36**	5.4%	99.2%	0.8%	0%	5%
#16	**1.18**	0.6%	99.8%	0.2%	0%	5%
#30	**0.6**	0.0%	99.8%	0.2%	0%	0%
#50	**0.3**	0.0%	99.8%	0.2%	0%	0%
#100	**0.15**	0.0%	99.8%	0.2%	0%	0%

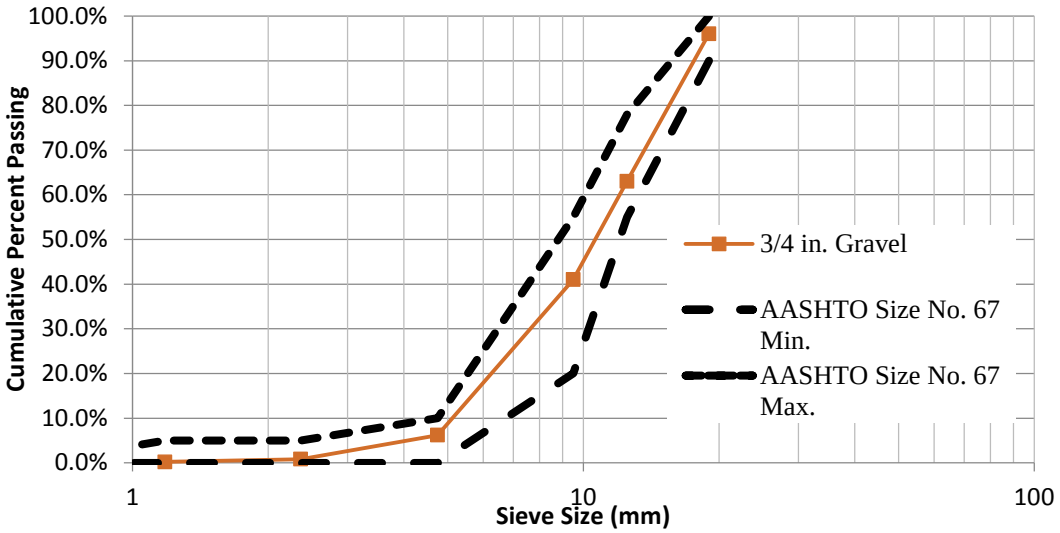

Figure B-12. Particle size distribution of ¾ in. NMSA gravel

Figure B-13. Photo of ¾ in. NMSA gravel

Table B-16. Physical properties of ½ in. NMSA gravel

Sieve Size		Gravel NMSA 1/2 in.			AASHTO M 43 Size No. 78	
No.	**mm**	**% Retained**	**Cumulative % Retained**	**Cumulative % Passing**	**Min.**	**Max.**
1"	**25**	0.0%	0.0%	100.0%	100%	100%
3/4"	**19**	0.0%	0.0%	100.0%	100%	100%
1/2"	**12.5**	8.0%	8.0%	92.0%	90%	100%
3/8"	**9.5**	25.0%	33.0%	67.0%	40%	75%
#4	**4.75**	64.1%	97.1%	2.9%	5%	25%
#8	**2.36**	2.7%	99.8%	0.2%	0%	10%
#16	**1.18**	0.0%	99.8%	0.2%	0%	5%
#30	**0.6**	0.0%	99.8%	0.2%	0%	0%
#50	**0.3**	0.0%	99.8%	0.2%	0%	0%
#100	**0.15**	0.0%	99.8%	0.2%	0%	0%

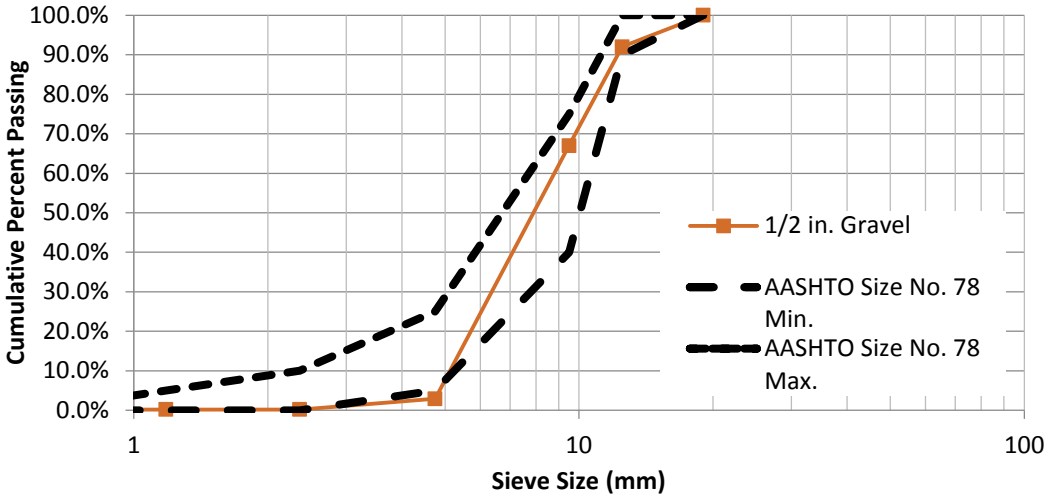

Figure B-14. Particle size distribution of ½ in. NMSA gravel

Figure B-15. Photo of ½ in. NMSA gravel

Table B-17. Physical properties of $^{3}/_{8}$ in. NMSA gravel

Sieve Size		Gravel NMSA $^{3}/_{8}$ in.			AASHTO M 43 Size No. 8	
No.	**mm**	**% Retained**	**Cumulative % Retained**	**Cumulative % Passing**	**Min.**	**Max.**
1"	**25**	0.0%	0.0%	100.0%	100%	100%
3/4"	**19**	0.0%	0.0%	100.0%	100%	100%
1/2"	**12.5**	0.2%	0.2%	99.8%	100%	100%
3/8"	**9.5**	5.8%	6.0%	94.0%	85%	100%
#4	**4.75**	72.0%	78.0%	22.0%	10%	30%
#8	**2.36**	21.0%	99.0%	1.0%	0%	10%
#16	**1.18**	0.7%	99.7%	0.3%	0%	5%
#30	**0.6**	0.1%	99.8%	0.2%	0%	0%
#50	**0.3**	0.0%	99.8%	0.2%	0%	0%
#100	**0.15**	0.0%	99.8%	0.2%	0%	0%

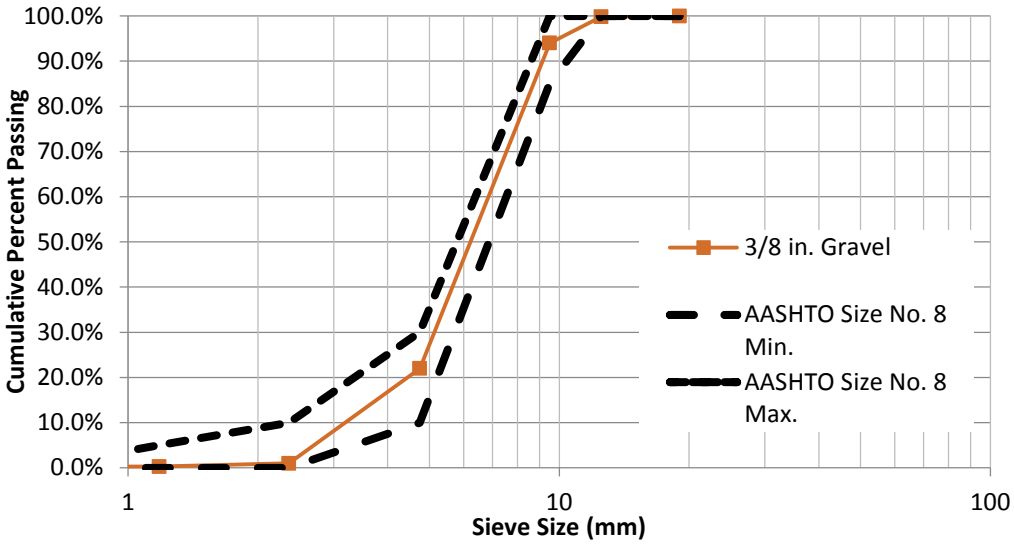

Figure B-16. Particle size distribution of $^{3}/_{8}$ in. NMSA gravel

Figure B-17. Photo of $^{3}/_{8}$ in. NMSA gravel

Table B-18. Combined aggregate grading

				Sand and Limestone			**Sand and Gravel**		
				S/A Ratio			S/A Ratio		
Sieve Size		Size (in.)	Size $^{0.45}$	0.45	0.47	0.50	0.45	0.47	0.50
No.	mm			No. 67	No. 78	No. 8	No. 67	No. 78	No. 8
1"	25.4	1.000	4.287	100.0	100.0	100.0	100.0	100.0	100.0
3/4"	19	0.748	3.762	93.4	100.0	100.0	97.8	100.0	100.0
1/2"	12.5	0.492	3.116	77.5	100.0	100.0	79.7	95.8	99.9
3/8"	9.5	0.374	2.754	61.5	81.3	99.4	67.6	82.5	97.0
#4	4.75	0.187	2.016	48.7	53.7	62.4	48.3	48.4	60.9
#8	2.36	0.093	1.472	46.7	48.0	50.8	43.9	45.4	48.8
#16	1.18	0.046	1.077	37.2	38.2	39.2	34.6	36.1	38.5
#30	0.6	0.024	0.795	22.9	23.6	23.5	20.8	21.7	23.1
#50	0.3	0.012	0.582	7.8	7.7	6.6	5.7	6.0	6.4
#100	0.15	0.006	0.426	2.6	2.2	0.6	0.5	0.5	0.5
#200	0	0	0.000	-	-	-	-	-	-

Table B-19. Physical properties of aggregate

PROPERTY	Limestone			Gravel			River Sand
	3/4"	1/2"	3/8"	3/4"	1/2"	3/8"	
Specific Gravity (SSD)	2.66	2.66	2.66	2.74	2.68	2.69	2.62
Absorption	1.3%	1.3%	1.3%	1.1%	1.4%	1.4%	0.5%
S/A Ratio	0.45	0.47	0.50	0.45	0.47	0.50	N/A
Combined DRUW (lb/cf)	117	118	118	127	124	123	N/A
Percent of Voids	29.0	28.4	28.4	23.7	25.9	27.0	N/A

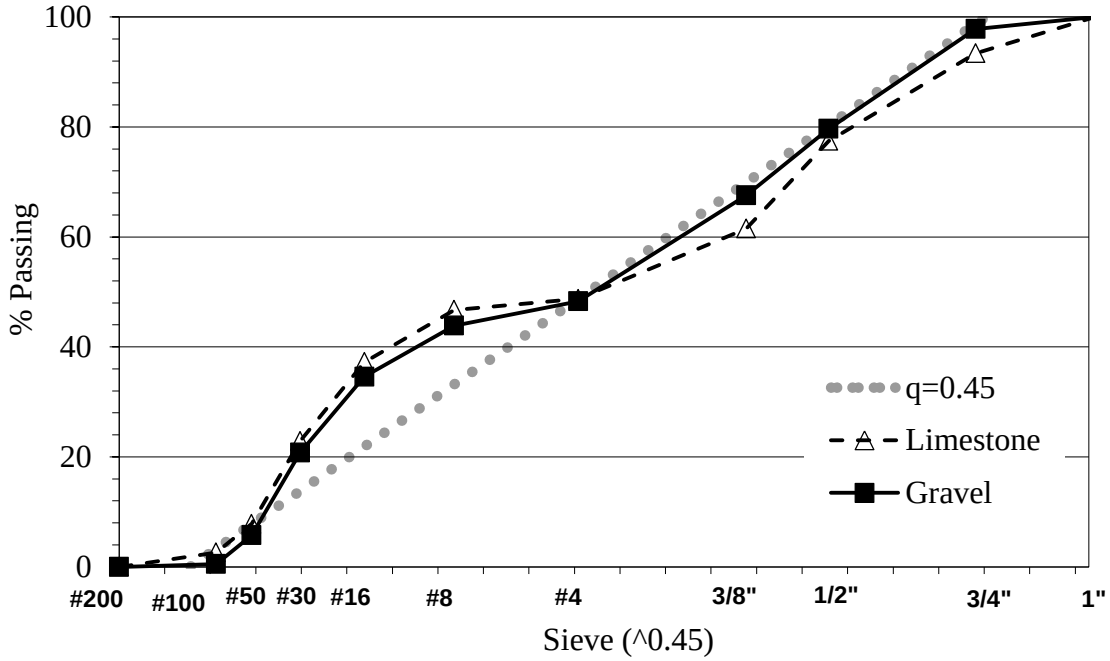

Figure B-18. Particle size distribution of combined ¾ in. coarse aggregate and sand

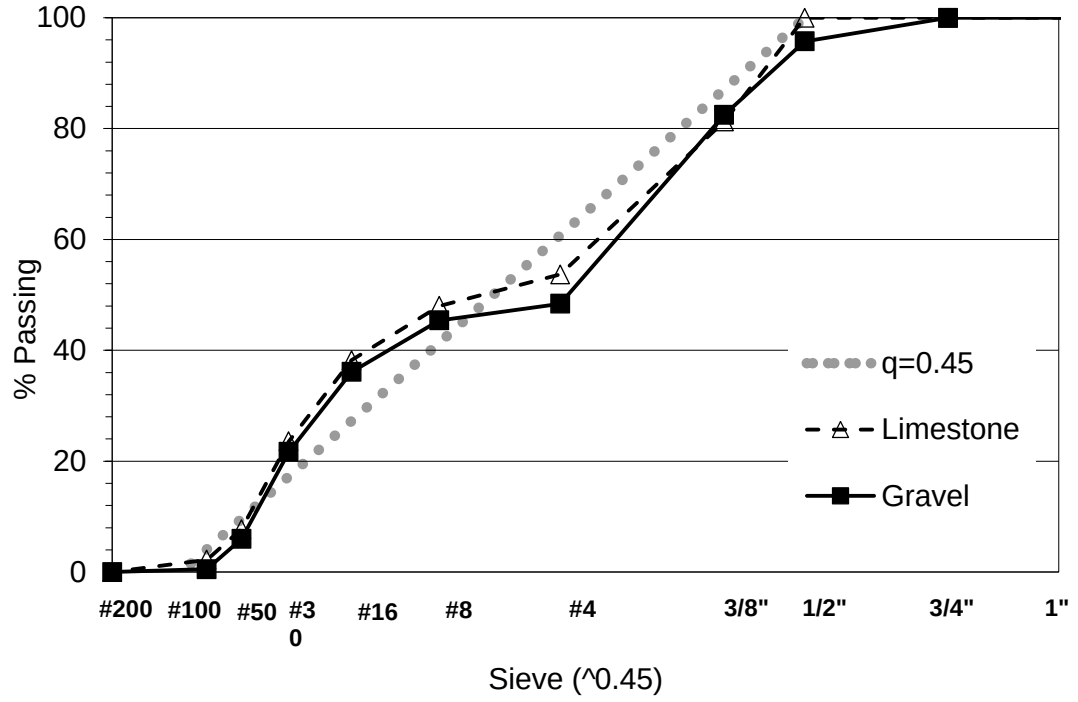

Figure B-19. Particle size distribution of combined ½ in. coarse aggregate and sand

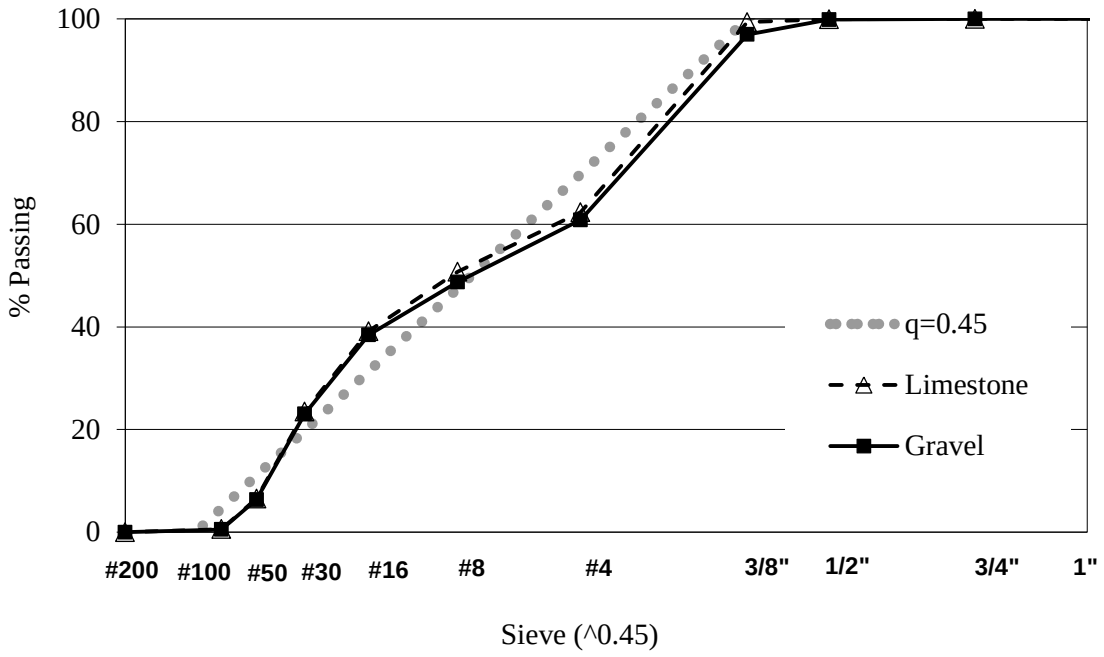

Figure B-20. Particle size distribution of combined $^{3}/_{8}$ in. coarse aggregate and sand

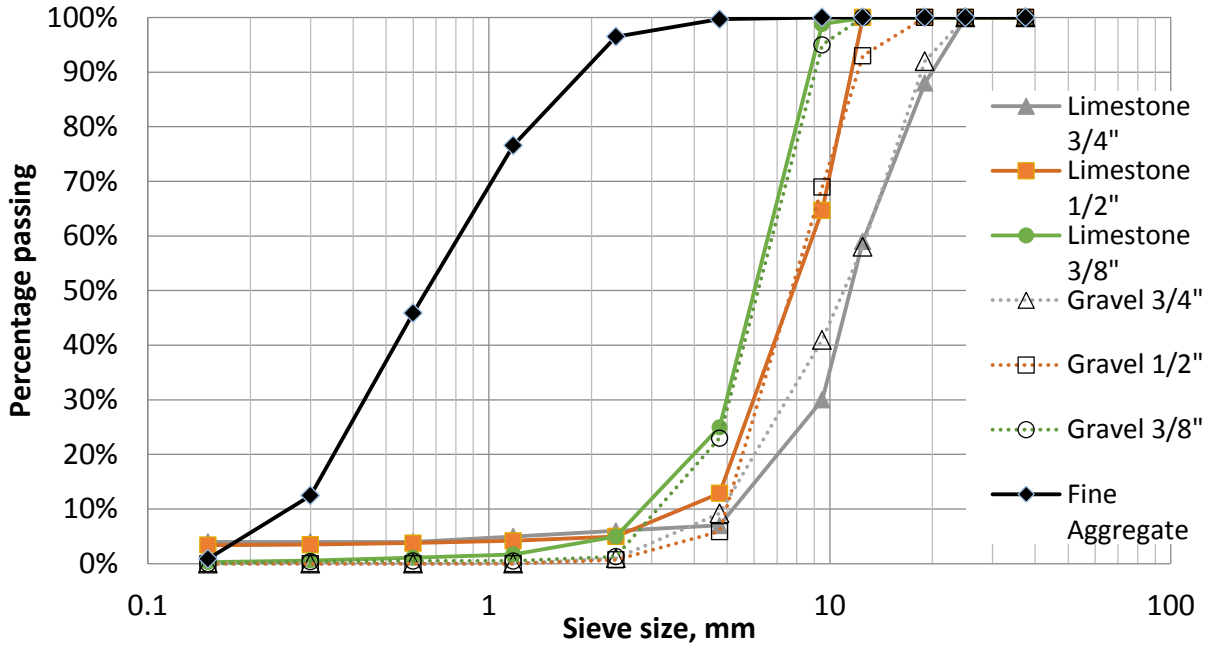

Figure B-21. Particle size distribution of all fine and coarse aggregates

5. Data Sheets of Chemical Admixtures and Fillers

Description

Glenium 3030 NS ready-to-use full-range water-reducing admixture is a patented new generation of admixture based on polycarboxylate chemistry. Glenium 3030 NS admixture is very effective in producing concretes with different levels of workability including applications that require the use of Rheodynamic® Self-Consolidating Concrete (SCC). Glenium 3030 NS admixture meets ASTM C 494/C 494M requirements for Type A, water-reducing, and Type F, high-range water-reducing, admixtures.

Applications

Recommended for use in:

- Concrete where high flowability, high-early and ultimate strengths and increased durability are needed
- Self-consolidating concrete
- Concrete where normal, mid-range, or high-range water-reduction is desired
- Concrete where normal setting times are required
- 4x4™ Concrete for fast track construction
- Pervious Concrete
- Self-consolidating grout

GLENIUM® 3030 NS

Full-Range Water-Reducing Admixture

Features

- Reduced water content for a given slump
- Dosage flexibility for normal, mid and high-range water reduction
- Produces cohesive and non-segregating concrete mixture
- Increased compressive strength and flexural strength performance at all ages
- Providing faster setting times and strength development
- Enhanced finishability and pumpability

Benefits

- Providing economic benefits to the entire construction team through higher productivity and reduced variable costs

Performance Characteristics

Mixture Data: 600 lb/yd³ of Type I cement (360 kg/m³); slump, 8.5-9.25 in. (210-235 mm); non-air-entrained concrete; dosage rate adjusted to obtain 25-30% water reduction.

Setting Time

Mixture	Initial Set (h:min)	Difference (h:min)
Plain	4:24	–
Conventional Superplasticizer	6:00	+ 1.36
Glenium 3030 NS admixture	5:00	+0.36

Compressive Strength

Mixture	1 day		7 days	
psi	psi	MPa	psi	MPa
Plain	1700	12	4040	28
Conventional Superplasticizer	3460	24	6380	44
Glenium 3030 NS admixture	4120	28	7580	52

Slump Retention - in. (mm)

Mixture	Minutes		
	15	30	45
Plain	8.5 (215)	8.5 (215)	7.5 (200)
Conventional Superplasticizer	8.5 (215)	4.25 (110)	3.5 (90)
Glenium 3030 NS admixture	9.25 (235)	9.25 (235)	8.25 (210)

Rate of Hardening: Glenium 3030 NS admixture is formulated to produce normal setting characteristics throughout its recommended dosage range. Setting time of concrete is influenced by the chemical and physical composition of the basic ingredients of the concrete, temperature of the concrete and ambient conditions. Trial mixtures should be made with actual job materials to determine the dosage required for a specified setting time and a given strength requirement.

Guidelines for Use

Dosage: Glenium 3030 NS admixture has a recommended dosage range of up to 3 fl oz/cwt (195 mL/100 kg) for Type A applications, 3-6 fl oz/cwt (195-390 mL/100 kg) for mid-range use and up to 18 fl oz/cwt (1,170 mL/100 kg) for Type F applications. The dosage range is applicable to most concrete mixtures using typical concrete ingredients. However, variations in job conditions and concrete materials, such as silica fume, may require dosages outside the recommended range. In such cases, contact your local BASF Construction Chemicals representative.

Mixing: Glenium 3030 NS admixture can be batched with the initial mixing water or as a delayed addition. However, optimum water reduction is generally obtained with a delayed addition.

Product Notes

Corrosivity – Non-Chloride, Non-Corrosive: Glenium 3030 NS admixture will neither initiate nor promote corrosion of reinforcing steel embedded in concrete, prestressed concrete or of galvanized steel floor and roof systems. Neither calcium chloride nor other chloride-based ingredients are used in the manufacture of Glenium 3030 NS admixture.

Compatibility: Glenium 3030 NS admixture is compatible with most admixtures used in the production of quality concrete, including normal, mid-range and high-range water-reducing admixtures, air-entrainers, accelerators, retarders, extended set control admixtures, corrosion inhibitors, and shrinkage reducers.

Do not use Glenium 3030 NS admixture with admixtures containing beta-napthalene-sulfonate. Erratic behaviors in slump, slump flow, and pumpability may be experienced.

For directions on the proper evaluation of Glenium 3030 NS admixture in specific applications, contact your BASF Construction Chemicals representative.

Storage and Handling

Storage Temperature: If Glenium 3030 NS admixture freezes, thaw at 45 °F (7 °C) or above and completely reconstitute by mild mechanical agitation. ***Do not use pressurized air for agitation.***

Shelf Life: Glenium 3030 NS admixture has a minimum shelf life of 12 months. Depending on storage conditions, the shelf life may be greater than stated. Please contact your BASF Construction Chemicals representative regarding suitability for use and dosage recommendations if the shelf life of Glenium 3030 NS admixture has been exceeded.

Packaging

Glenium 3030 NS admixture is supplied in 55 gal (208 L) drums, 275 gal (1040 L) totes and by bulk delivery.

Related Documents

Material Safety Data Sheets: Glenium 3030 NS admixture.

Additional Information

For additional information on Glenium 3030 NS admixture or its use in developing concrete mixes with special performance characteristics, contact your BASF Construction Chemicals representative.

The Admixture Systems business of BASF Construction Chemicals is a leading provider of innovative additives for specialty concrete used in the ready mix, precast, manufactured concrete products, underground construction and paving markets throughout the NAFTA region. The Company's respected Master Builders brand products are used to improve the placing, pumping, finishing, appearance and performance characteristics of concrete.

RheoTEC™ Z-60

Workability-Retaining Admixture

Description

RheoTEC Z-60 admixture is a revolutionary new technology based on significant advances in admixture chemistry. RheoTEC Z-60 admixture is used as part of an admixture system to provide customized admixture solutions for a wide range of concrete applications. RheoTEC Z-60 admixture is a workability-retaining admixture that provides flexible degrees of slump retention without retardation.

RheoTEC Z-60 admixture provides the concrete producer with the ability to immediately create the optimal admixture system for changing and fluctuating regional raw materials, environmental conditions and project requirements. RheoTEC Z-60 admixture gives the concrete producer the ability to consistently produce and deliver quality concrete mixtures.

RheoTEC Z-60 admixture meets the interim requirements of ASTM C 494/C 494M Type S, Specific Performance, admixtures.

Applications

Recommended for use in:

- Concrete with varying slump requirements
- Concrete mixtures utilizing supplementary cementitious materials
- Concrete where high flowability, increased stability and durability are needed
- Production of self-consolidating concrete (SCC) mixtures

Features

- Workability retention without retardation
- Flexible levels of workability retention by adjusting dosage
- Improved early- and late-age compressive strengths

Benefits

- Promotes greater consistency of concrete workability at the jobsite
- Promotes consistency in compressive strengths via minimized jobsite addition of water
- Minimizes re-dosing of high-range water-reducing admixture at the job site
- Consistent air-entrainment
- Fewer rejected loads and better customer satisfaction due to consistent quality of concrete
- Faster truck turn-around time
- Expanded concrete delivery range

Performance Characteristics

The data in the following graph represents the dramatic performance achievable through the use of RheoTEC Z-60 admixture. Represented in the graph are four mixtures. The first mixture utilized a primary water reducer without RheoTEC Z-60 admixture. The three remaining mixtures utilized the same primary water reducer with a low, medium and high dosage of the RheoTEC Z-60 admixture. These mixtures had concrete temperatures of 90 °F (32 °C) and contained 600 lb/yd³ (356 kg/m³) of cement with a w/c of 0.40.

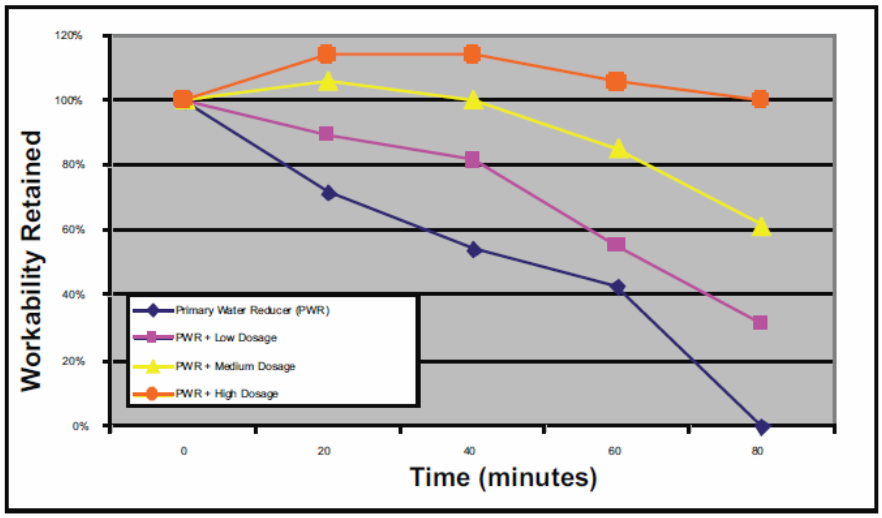

Master

Guidelines for Use

Dosage: RheoTEC Z-60 admixture has a recommended dosage range of 3-12 fl oz/cwt (195-750 mL/100 kg) of cementitious materials.

Mixing: RheoTEC Z-60 admixture can be added with the initial batch water or as a delayed addition.

Product Notes

Corrosivity – Non-Chloride, Non-Corrosive: RheoTEC Z-60 admixture will neither initiate nor promote corrosion of reinforcing steel embedded in concrete, prestressing steel or of galvanized steel floor and roof systems. Neither calcium chloride nor other chloride-based ingredients are used in the manufacture of RheoTEC Z-60.

Compatibility: RheoTEC Z-60 admixture is compatible with most admixtures used in the production of quality concrete, including normal, mid-range and high-range water-reducing admixtures, air-entrainers, accelerators, retarders, extended set control admixtures, corrosion inhibitors, and shrinkage reducers.

Do not use RheoTEC Z-60 admixture with admixtures containing beta-naphthalene sulfonate. Erratic behaviors in slump, workability retention and pumpability may be experienced.

RheoTEC Z-60 admixture has only been tested with admixtures manufactured by BASF Construction Chemicals. As a result, use of RheoTEC Z-60 admixture with non-BASF admixtures may produce unpredictable results. BASF denies any warranty expressed or implied with respect to any application using a non-BASF admixture in connection with the use of RheoTEC Z-60 admixture.

Storage and Handling

Storage Temperature: RheoTEC Z-60 admixture must be stored at temperatures above 40 °F (5 °C). If RheoTEC Z-60 admixture freezes, thaw and reconstitute by mechanical agitation. **Do not use pressurized air for agitation.**

Shelf Life: RheoTEC Z-60 admixture has a minimum shelf life of 6 months. Depending on storage conditions, the shelf life may be greater than stated.

Packaging

RheoTEC Z-60 admixture is supplied in 55 gal (208 L) drums, 275 gal (1040 L) totes and by bulk delivery.

Related Documents

Material Safety Data Sheets: RheoTEC Z-60 admixture.

Additional Information

For additional information on RheoTEC Z-60 admixture or on its use in developing concrete mixtures with special performance characteristics, contact your local sales representative.

BASF Construction Chemicals is a leading provider of innovative chemical admixtures and silica fume for specialty concrete used in the ready-mixed, precast, manufactured concrete products, underground construction and paving markets in the North American region. The Company's respected Master Builders brand products are used to improve the placing, pumping, finishing, appearance and performance characteristics of concrete.

RHEOMAC® VMA 362

Viscosity-Modifying Admixture

Description

Rheomac VMA 362 viscosity-modifying admixture (VMA) is a ready-to-use, liquid admixture that is specially developed for producing concrete with enhanced viscosity and controlled rheological properties. Concrete containing Rheomac VMA 362 admixture exhibits superior stability, thus increasing resistance to segregation and facilitating placement and consolidation. Rheomac VMA 362 admixture meets ASTM C 494/C 494M requirements for Type S, Specific Performance, admixtures.

Applications

Recommended for use in:

- Concrete containing "gap-graded" aggregates
- Lean concrete mixtures
- Concrete containing manufactured sand
- Concrete as a pumping aid
- Concrete as a finishing aid
- Concrete mixtures requiring "more body"
- Rheodynamic® Self-Consolidating Concrete (SCC)
- Liquid Sand™ program
- Pervious Concrete
- Self-Consolidating Grout

Features

- Modifies viscosity of concrete
- Thixotropic properties

Benefits

- Controls bleeding
- Provides flexibility in mixture proportioning and batching
- Provides concrete stability during transport and placement
- Reduces segregation, even with highly fluid concrete mixtures
- Enhances pumping and finishing
- Enhances surface appearance
- Provides superior and predictable in-place concrete properties
- Facilitates production of highly fluid concrete mixtures such as Rheodynamic Self-Consolidating Concrete (SCC)

Performance Characteristics

Setting Time: Rheomac VMA 362 admixture has little to no impact on concrete setting time within the recommended dosage range of 2-14 fl oz/cwt (130-920 mL/100 kg) of cementitious materials.

Compressive Strength: Rheomac VMA 362 admixture does not affect the compressive strength of concrete.

Viscosity: Concrete containing Rheomac VMA 362 admixture will exhibit an increase in viscosity with increasing dosage of the admixture. This desirable characteristic facilitates concrete placement, consolidation and finishing and provides stability to very fluid concrete mixtures.

Workability: Because of its thixotropic properties, concrete containing Rheomac VMA 362 admixture can increase in viscosity if left in a mixing vessel without agitation. Workability can be restored by simply remixing the concrete mixture.

Air Content: Rheomac VMA 362 admixture does not affect the air content in either air-entrained or non-air-entrained concrete. Typical dosages of air-entraining admixtures may be used to achieve the desired air content.

Guidelines for Use

Dosage: The recommended dosage range for Rheomac VMA 362 admixture is 2-14 fl oz/cwt (130-910 mL/100 kg) of cementitious materials. A dosage of 2-6 fl oz/cwt (130-390 mL/100 kg) is recommended for typical concrete mixtures requiring "more body" to facilitate pumping and finishing procedures. A dosage of up to 14 fl oz/cwt (910 mL/100 kg) is recommended to provide stability in self-consolidating concrete mixtures. Because of variations in concrete materials, job site conditions and/or applications, dosages outside of the suggested range may be required.

Mixing: Rheomac VMA 362 admixture is typically added with the initial mix water. Alternately, Rheomac VMA 362 admixture may be added after all other concreting ingredients have been batched and thoroughly mixed, either at the batch plant or at the jobsite.

Product Notes

Compatibility: Rheomac VMA 362 admixture is compatible with most admixtures used in the production of quality concrete including normal, mid-range and high-range water-reducing admixtures and air entrainers. Rheomac VMA 362 admixture is also compatible with typical accelerators, retarders, extended set-control admixtures, corrosion inhibitors, and shrinkage reducers. However, a field trial mixture is recommended to ensure appropriate performance.

Storage and Handling

Storage Temperature: Rheomac VMA 362 admixture must be stored at temperatures above 32 °F (0 °C) and below 130 °F (54 °C). Protect Rheomac VMA 362 admixture from freezing because it cannot be reconstituted after thawing.

Shelf Life: A product stability evaluation has shown that Rheomac VMA 362 admixture has a shelf life of 8 months. Please contact your local sales representative regarding suitability for use and dosage recommendations if the stated minimum shelf life of Rheomac VMA 362 admixture has been exceeded.

Dispensing: Rheomac VMA 362 admixture should be dispensed using direct-feed dispensing systems. It is recommended that fail-safe features must be included in this dispenser application for potential meter malfunctions. Consult your local sales representative for the proper dispensing equipment for Rheomac VMA 362 admixture.

Packaging

Rheomac VMA 362 admixture is supplied in 55 gal (208 L) drums, 275 gal (1040 L) totes, and by bulk delivery.

Related Documents

Material Safety Data Sheets: Rheomac VMA 362 admixture.

Additional Information

For additional information on Rheomac VMA 362 admixture or its use in developing concrete mixtures with special performance characteristics, contact your local sales representative.

The Admixture Systems business of BASF Construction Chemicals is a leading provider of innovative admixtures for specialty concrete used in the ready mix, precast, manufactured concrete products, underground construction and paving markets throughout the North American region. The Company's respected Master Builders brand products are used to improve the placing, pumping, finishing, appearance and performance characteristics of concrete.

Description

MB-AE 90 air-entraining admixture is for use in concrete mixtures. It meets the requirements of ASTM C 260, AASHTO M 154 and CRD-C 13.

Applications

Recommended for use in:

- Concrete exposed to cyclic freezing and thawing
- Production of high-quality normal or lightweight concrete (heavyweight concrete normally does not contain entrained air)
- All paving-related concrete exposed to freezing and thawing cycles

MB-AE™ 90

Air-Entraining Admixture

Features

- Ready-to-use in the proper concentration for rapid, accurate dispensing

Benefits

- Improved resistance to damage from cyclic freezing and thawing
- Improved resistance to scaling from deicing salts
- Improved plasticity and workability
- Reduced permeability – increased watertightness
- Reduced segregation and bleeding

Performance Characteristics

Concrete durability research has established that the best protection for concrete from the adverse effects of freezing and thawing cycles and deicing salts results from: proper air content in the hardened concrete, a suitable air-void system in terms of bubble size and spacing, and adequate concrete strength, assuming the use of sound aggregates and proper mixing, transporting, placing, consolidation, finishing and curing techniques. MB-AE 90 admixture can be used to obtain adequate freeze-thaw durability in a properly proportioned concrete mixture, if standard industry practices are followed.

Air Content Determination: The total air content of normal weight concrete should be measured in strict accordance with ASTM C 231, "Standard Test Method for Air Content of Freshly Mixed Concrete by the Pressure Method" or ASTM C 173/C 173M, "Standard Test Method for Air Content of Freshly Mixed Concrete by the Volumetric Method." The air content of lightweight concrete should only be determined using the Volumetric Method. The air content should be verified by calculating the gravimetric air content in accordance with ASTM C 138/C 138M, "Standard Test Method for Density (Unit Weight), Yield, and Air Content (Gravimetric) of Concrete." If the total air content, as measured by the Pressure Method or Volumetric Method and as verified by the Gravimetric Method, deviates by more than 1-1/2%, the cause should be determined and corrected through equipment calibration or by whatever process is deemed necessary.

Guidelines for Use

Dosage: There is no standard dosage for MB-AE 90 admixture. The exact quantity of air-entraining admixture needed for a given air content of concrete varies because of differences in concrete-making materials and ambient conditions. Typical factors that might influence the amount of air entrained include: temperature, cementitious materials, sand gradation, sand-aggregate ratio, mixture proportions, slump, means of conveying and placement, consolidation and finishing technique.The amount of MB-AE 90 admixture used will depend upon the amount of entrained air required under actual job conditions. In a trial mixture, use 1/4 to 4 fl oz/cwt (16-260 mL/100 kg) of cementitious material. Measure the air content of the trial mixture, and, if needed, either increase or decrease the quantity of MB-AE 90 admixture to obtain the desired air content.

In mixtures containing water-reducing or set-control admixtures, the amount of MB-AE 90 admixture needed may be somewhat less than the amount required in plain concrete.

Due to possible changes in the factors that can affect the dosage of MB-AE 90 admixture, frequent air content checks should be made during the course of the work. Adjustments to the dosage should be based on the amount of entrained air required in the mixture at the point of placement.

If an unusually high or low dosage of MB-AE 90 admixture is required to obtain the desired air content, consult your Local sales representative. In such cases, it may be necessary to determine that, in addition to a proper air content in the fresh concrete, a suitable air-void system is achieved in the hardened concrete.

Dispensing and Mixing: Add MB-AE 90 admixture to the concrete mixture using a dispenser designed for air-entraining admixtures, or add manually using a suitable measuring device that ensures accuracy within plus or minus 3% of the required amount.

For optimum, consistent performance, the air-entraining admixture should be dispensed on damp, fine aggregate. If the concrete mixture contains fine lightweight aggregate, field evaluations should be conducted to determine the best method to dispense the air-entraining admixture.

Precaution

In a 2005 publication from the Portland Cement Association (PCA R&D Serial No. 2789), it was reported that problematic air-void clustering that can potentially lead to above normal decreases in strength was found to coincide with late additions of water to air-entrained concretes. Late additions of water include the conventional practice of holding back water during batching for addition at the jobsite. Therefore, caution should be exercised with delayed additions of water to air-entrained concrete. Furthermore, an air content check should be performed after any post-batching addition to an air-entrained concrete mixture.

Product Notes

Corrosivity – Non-Chloride, Non-Corrosive: MB-AE 90 admixture will neither initiate nor promote corrosion of reinforcing and prestressing steel embedded in concrete, or of galvanized floor and roof systems. No calcium chloride or other chloride-based ingredients are used in the manufacture of this admixture.

Compatibility: MB-AE 90 admixture may be used in combination with any BASF admixture, unless stated otherwise on the data sheet for the other product. When used in conjunction with other admixtures, each admixture must be dispensed separately
into the concrete mixture.

Storage and Handling

Storage Temperature: MB-AE 90 admixture should be stored and dispensed at 31 °F (-0.5 °C) or higher. Although freezing does not harm this product, precautions should be taken to protect it from freezing. If MB-AE 90 admixture freezes, thaw at 35 °F (2 °C) or above and completely reconstitute by mild mechanical agitation. ***Do not use pressurized air for agitation.***

Shelf Life: MB-AE 90 admixture has a minimum shelf life of 18 months. Depending on storage conditions, the shelf life may be greater than stated. Please contact your Local sales representative regarding suitability for use and dosage recommendations if the shelf life of MB-AE 90 admixture has been exceeded.

Safety: Chemical goggles and gloves are recommended when transferring or handling this material.

Packaging

MB-AE 90 admixture is supplied in 55 gal (208 L) drums, 275 gal (1040 L) totes and by bulk delivery.

Related Documents

Material Safety Data Sheets: MB-AE 90 admixture.

Additional Information

For additional information on MB-AE 90 admixture, or its use in developing a concrete mixture with special peformance characteristics, contact your Local sales representative.

The Admixture Systems business of BASF's Construction Chemicals division is a leading provider of innovative admixtures for specialty concrete used in the ready-mixed, precast, manufactured concrete products, underground construction and paving markets throughout the North American region. The Company's respected Master Builders brand products are used to improve the placing, pumping, finishing, appearance and performance characteristics of concrete.

Unical-P

Weeping Water, NE
Plant #1

Unical-P is a powdered ground limestone product processed in Weeping Water, NE from mined high calcium limestone with minimum calcium content of 33%

% Ca	37.69
$\%CaC0_3$	94.23

Typical Analyses		
Magnesium (Mg)	0.287	%
Silicon (Si)	0.730	%
Silica (SiO_2)	1.560	%
Iron (Fe)	0.168	%
Sodium (Na)	0.012	%
Potassium (K)	0.039	%
Sulfur (S)	0.709	%
Manganese (Mn)	0.022	%
Phosphorus (P)	< 0.0005	%
Chloride (Cl)	< 0.056	%
Chromium (Cr)	6	ppm
Aluminum (Al)	883	ppm
Boron (B)	15	ppm
Barium (Ba)	37.000	ppm
Lead (Pb)	< 5	ppm
Nickel (Ni)	7.000	ppm
Cobalt (Co)	< 5	ppm
Copper (Cu)	< 5	ppm
Zinc (Zn)	130.000	ppm
Cadmium (Cd)	3.500	ppm
Iodine (I)	< 5	ppm
Arsenic (As)	< 5	ppm
Beryllium (Be)	< 5	ppm
Selenium (Se)	1.160	ppm
Mercury (Hg)	< 0.050	ppm
Vanadium (V)	2.090	ppm
Molybdenum (Mo)	< 5	ppm
Fluorine (F)	1.120	ppm
Bismuth (Bi)	< 5	ppm
Antimony (Sb)	< 5	ppm

% Acid Solubility	
Average	79.32
Maximum	82.45
Minimum	75.55
H_20	< 0.05%
Bulk Density	(lbs./cu.ft.)
Loose:	63
Packed:	73

Particle Size Measurement -- Laser Diffraction

Average Particle Size = 11.07 microns

Ave particle size: half of the particles are above and half are below this point on the "S" shaped cumulative distribution graph.

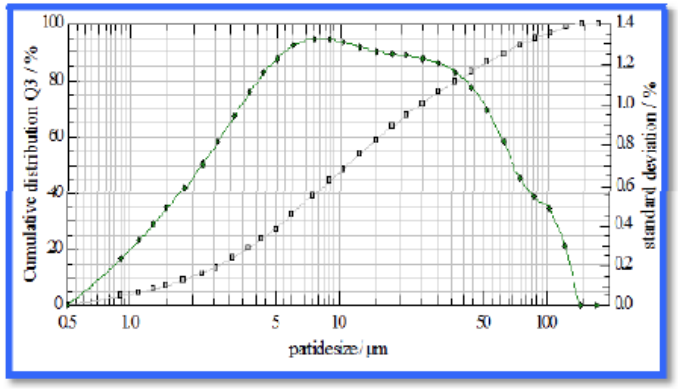

µm = micron (1/1000 of a millimeter)

Particle Distribution--U.S.Screen Comparison			
Minus 200 mesh product			
Micron Size	U.S.Screen	% Retained	% Passing
300	**50**	0.0	100.0
212	**70**	0.0	100.0
180	**80**	0.0	100.0
150	**100**	0.0	100.0
75	**200**	7.7	92.3
45	**325**	8.8	83.5
38	**400**	3.3	80.3
25	**500**	8.7	71.6
13	**1000**	17.0	54.6
6	**2300**	22.5	32.1
2.5	**Pan**	32.1	
		100.0	

cumulative distribution *(laser diffraction)*			
Microns	% Passing	Microns	% Passing
175	100	10.5	48.59
147	100	9	44.10
123	98.43	7.5	38.70
103	96.52	6	32.14
87	94.48	5	27.12
73	91.98	4.3	23.32
61	89.07	3.7	19.93
51	85.91	3.1	16.47
43	82.73	2.6	13.56
36	79.26	2.2	11.20
30	75.53	1.8	8.80
25	71.55	1.5	6.95
21	67.46	1.3	5.68
18	63.59	1.1	4.37
15	58.69	0.9	3.01
12.5	53.58		

Omya Inc.

9987 Carver Road, Suite 300
Cincinnati, OH 45242
Tel: (800) 451-6110 Fax: (888) 322-7952
www.omya-na.com

Product Data Sheet

Betocarb® 3 - PT

Production Plant	Perth, ON/Canada		
Short Description of Product	A dry ground calcium carbonate with excellent fineness and dispersion characteristics.		
Chemical Analysis of Raw Material	Calcium Carbonate, percent		96
	Magnesium Carbonate, percent		2
Typical Properties	Retained on 325 mesh, percent		0.003
	Moisture Loss at 110°C, percent		0.08
	Specific Gravity		2.71
	Apparent Bulk Density, Loose	0.6 g/cc	37 lbs./ft.³
	Apparent Bulk Density, Packed	1.1 g/cc	69 lbs./ft.³
General Product Data	Blaine, m²/kg		1100

Applications

An ideal mineral filler for ready-mix, self-compacting, and pre-cast concrete, pavers, bricks, and mortars.

Benefits

In concrete and cement applications, reduces cementitious content: cement, fly ash, and GBFS. Improves hydration, green strength, and surface finish with no loss in compression resistance.

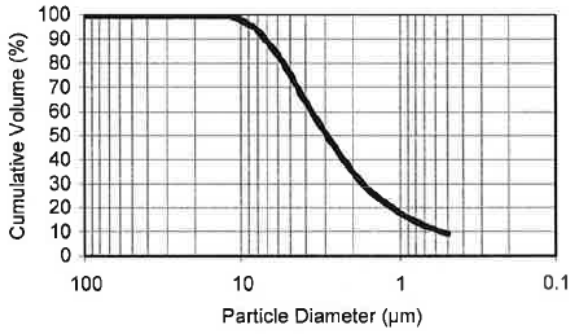

APPENDIX C: Fresh Concrete Properties

Contents

Labelling of SCC Mixtures

Coarse Aggregate	Workability Target ID	SCM/Filler Type
LS = Limestone	111	C = class C fly ash
G = Gravel	112	F = class F fly ash
	121	S = GGBFS
	221	FLP = class f fly ash + limestone powder
	222	

Labelling of CVC Mixtures

Coarse Aggregate	NMSA	Concrete Type
LS = Limestone	0.75	CVC
G = Gravel	0.5	
	0.375	

1. Rheology

1.1. Flow curves of CVC and SCC mortars

Figure C-1. Brookfield mortar rheometer

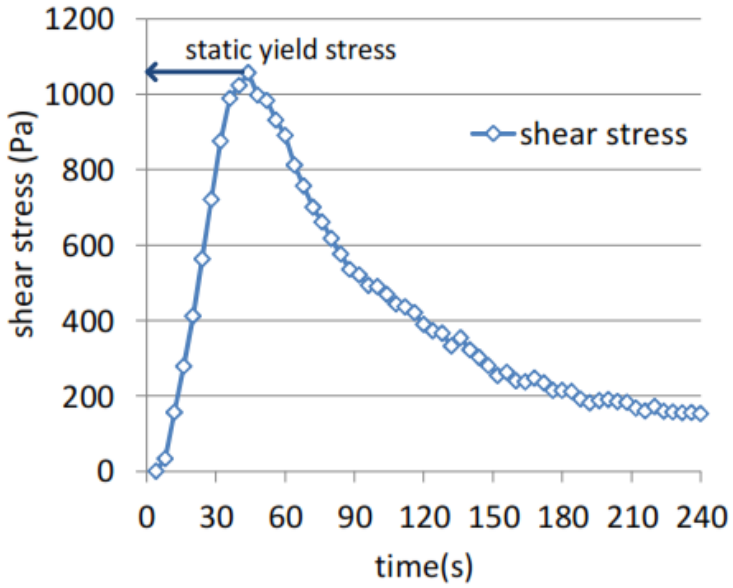

Figure C- 2. Typical flow curve by mortar rheometer

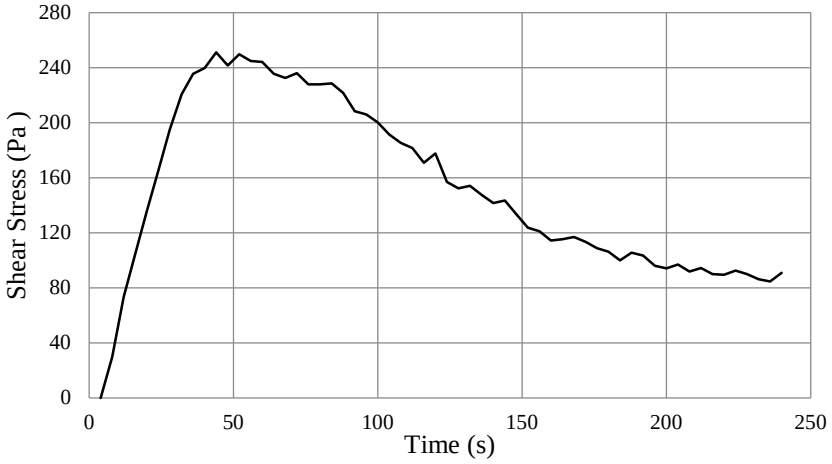

(1) LS0.75 CVC

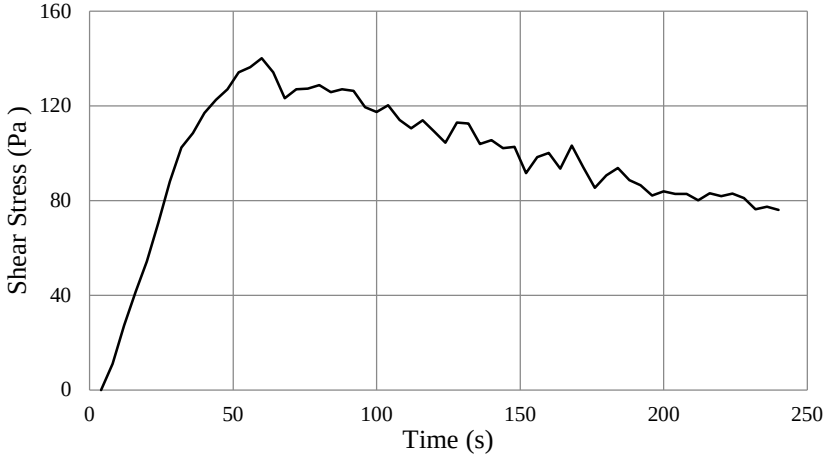

(2) LS111C

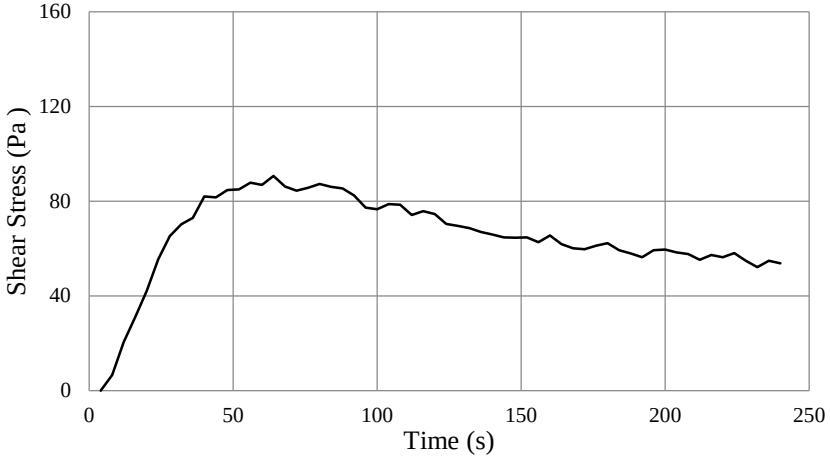

(3) LS111F

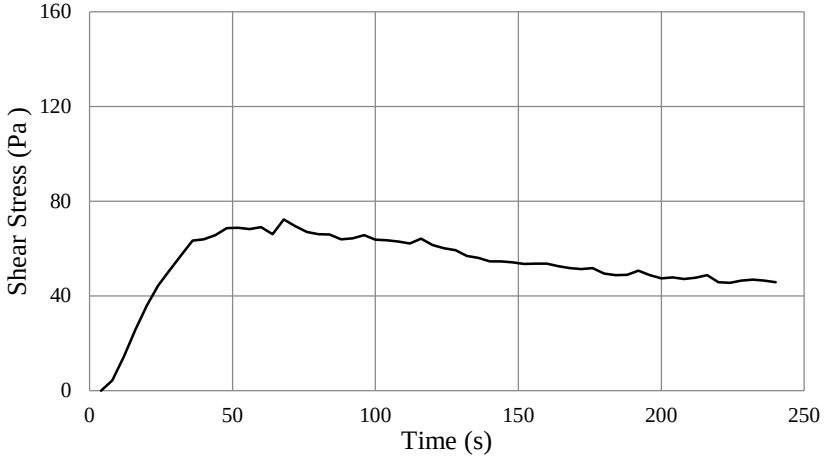

(4) LS111S

Figure C-3. Flow curves of CVC and SCC mortars

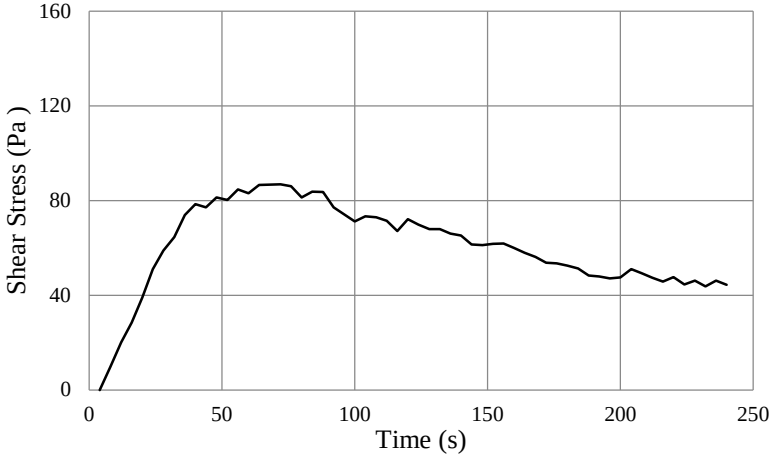

(5) LS111FLP

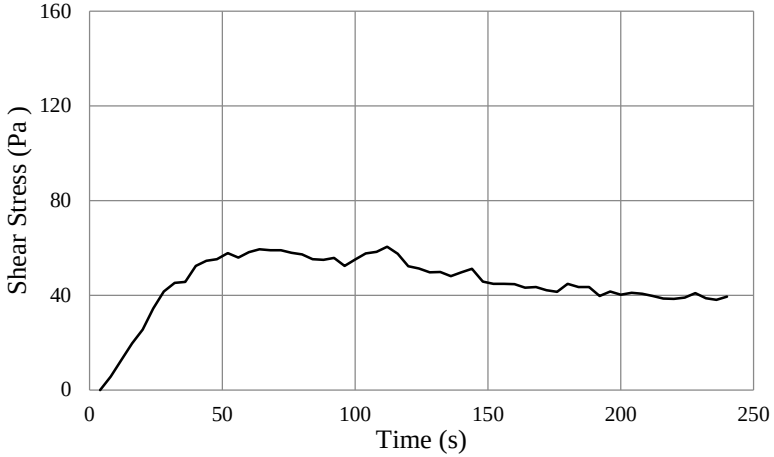

(6) LS211C

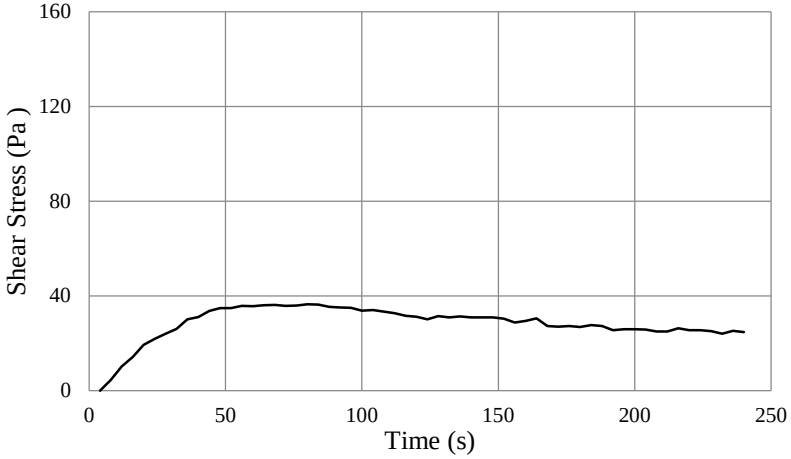

(7) LS211F

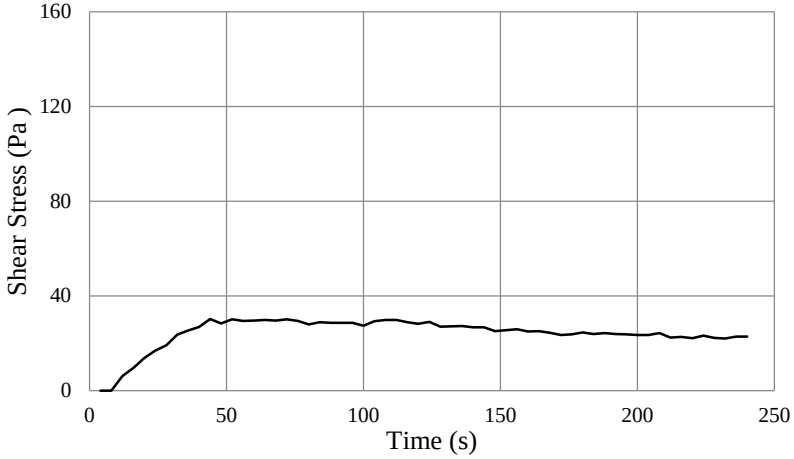

(8) LS211S

(Cont.) Figure C-3. Flow curves of CVC and SCC mortars

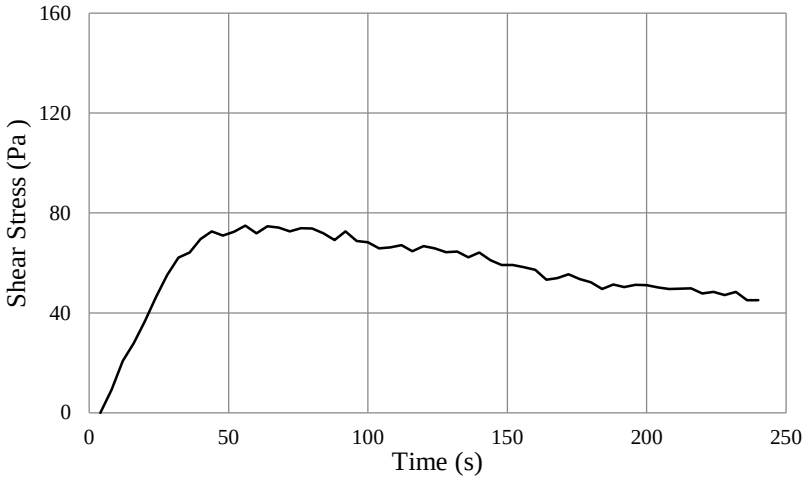

(9) LS211FLP

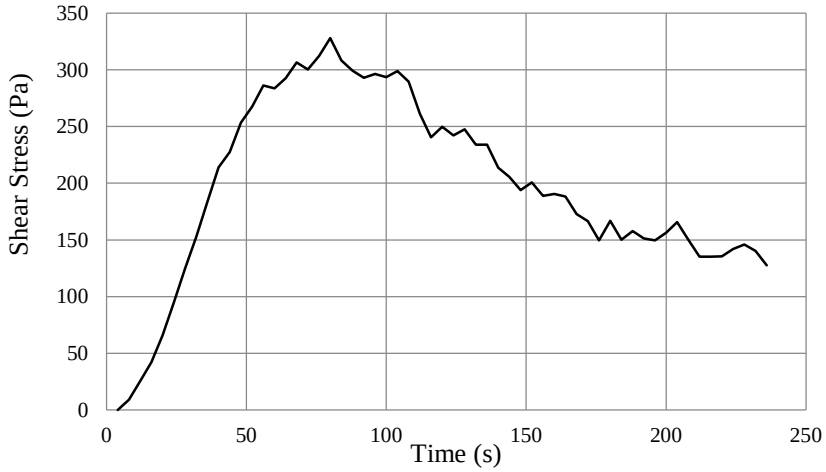

(10) LS0.50 CVC

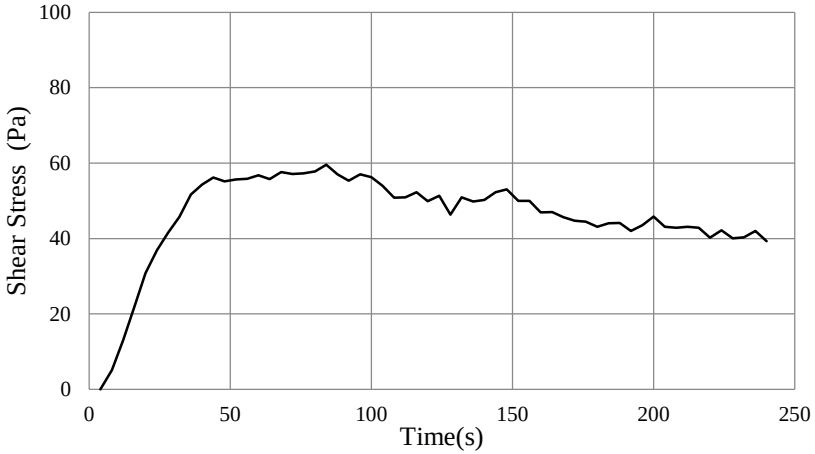

(11) LS121C

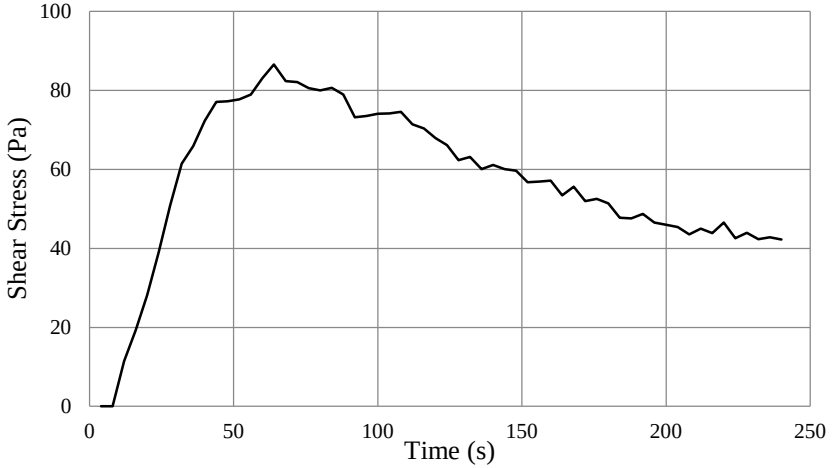

(12) LS121F

(Cont.) Figure C-3. Flow curves of CVC and SCC mortars

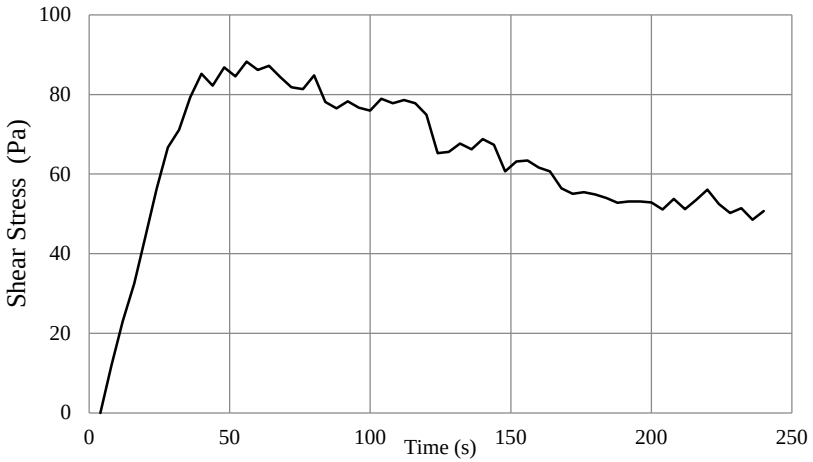

(13) LS121S

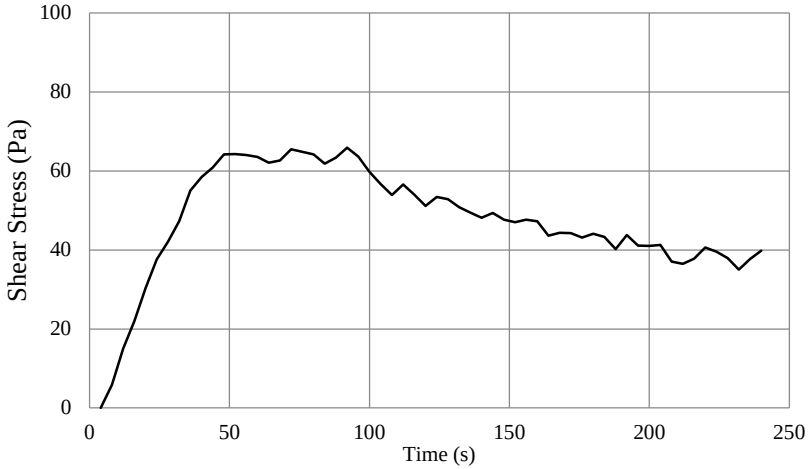

(14) LS121FLP

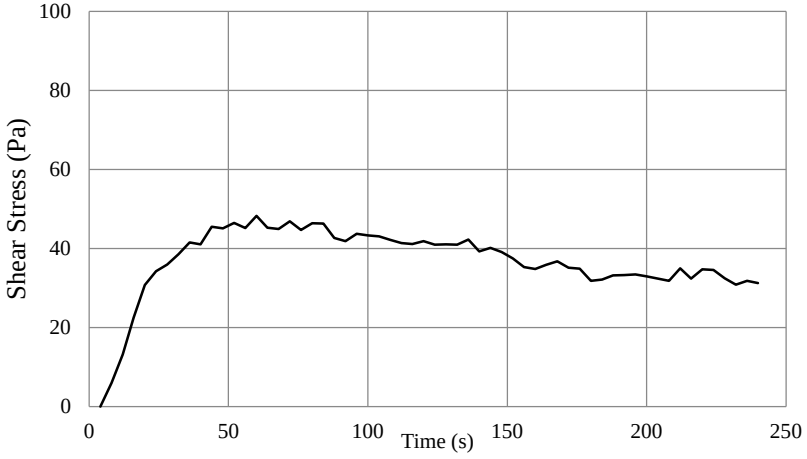

(15) LS221C

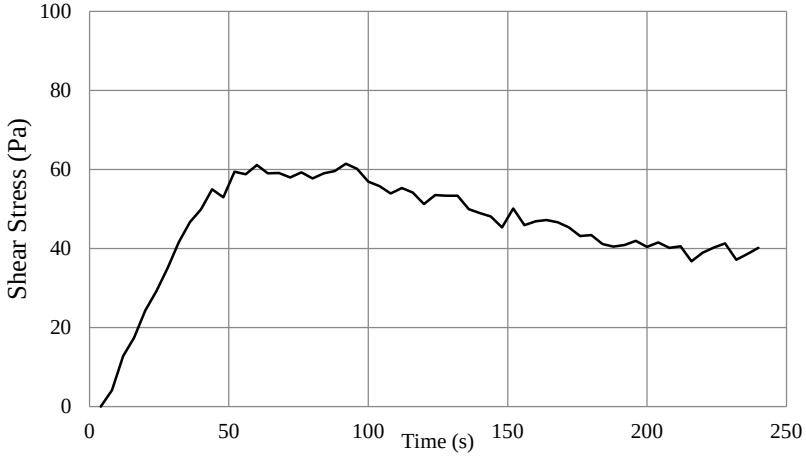

(16) LS221F

(Cont.) Figure C-3. Flow curves of CVC and SCC mortars

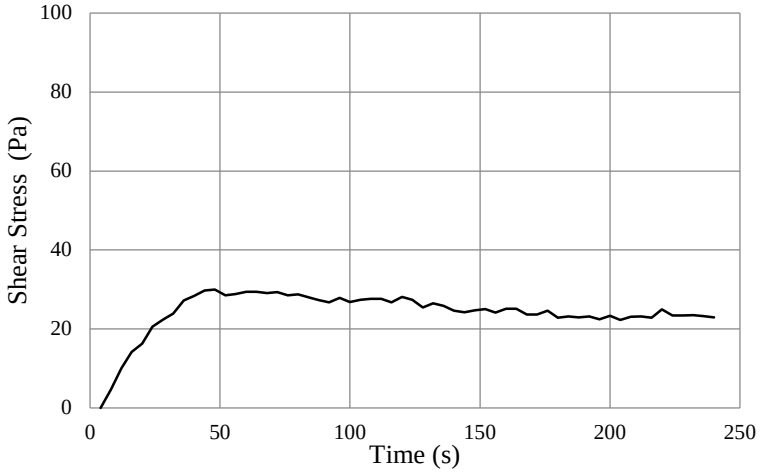

(17) LS221S

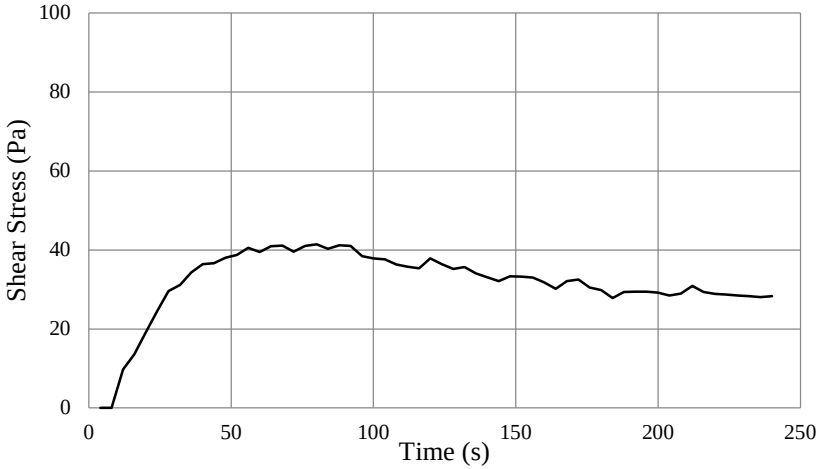

(18) LS221FLP

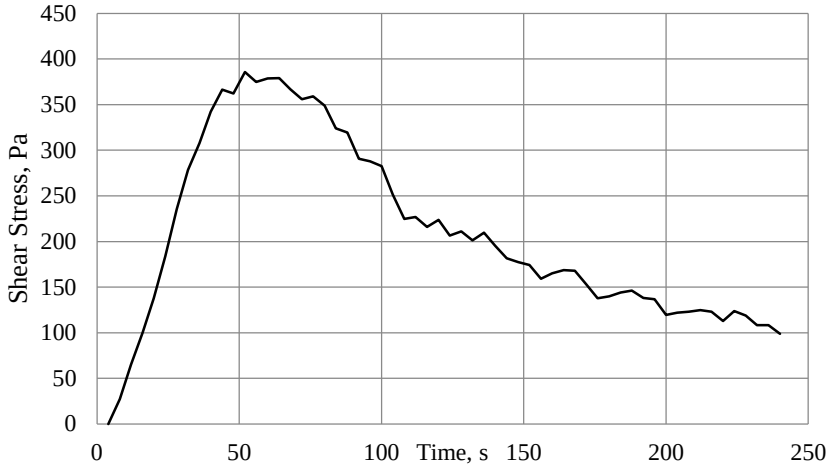

(19) LS0.375 CVC

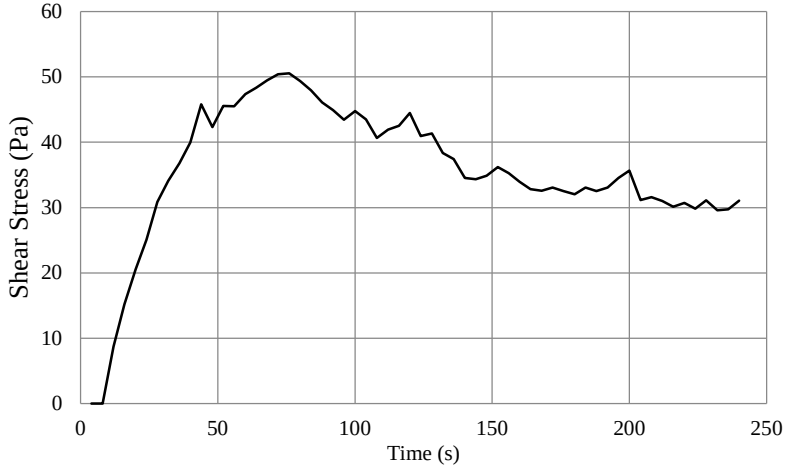

(20) LS222C

(Cont.) Figure C-3. Flow curves of CVC and SCC mortars

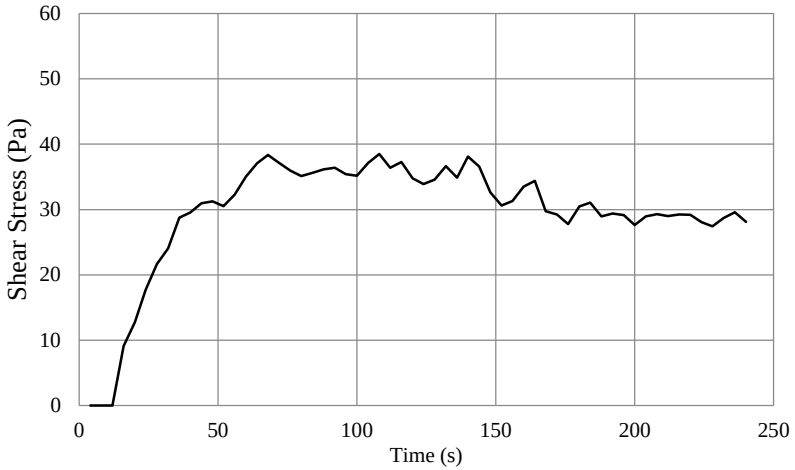

(21) LS222F

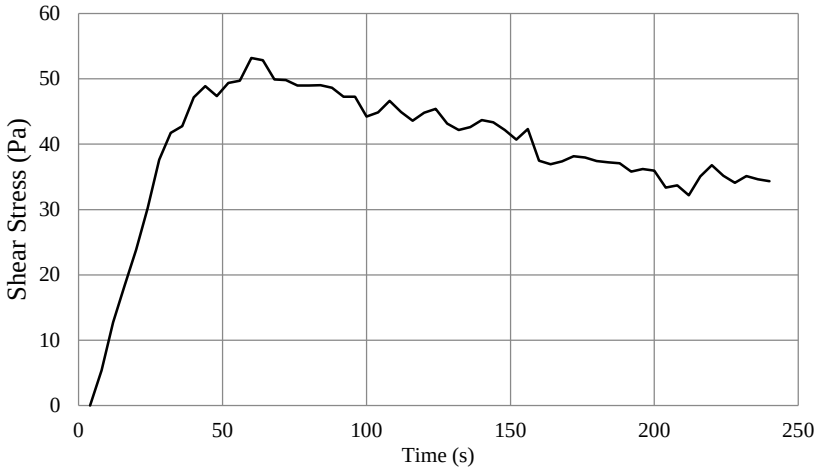

(22) LS222S

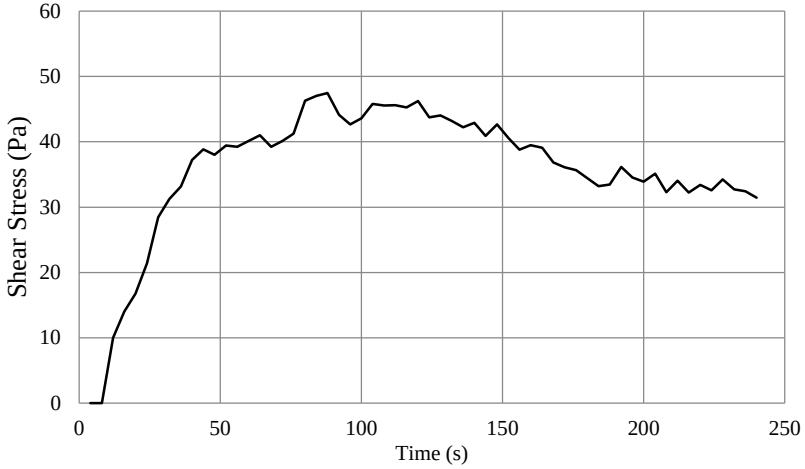

(23) LS222FLP

(Cont.) Figure C-3. Flow curves of CVC and SCC mortars

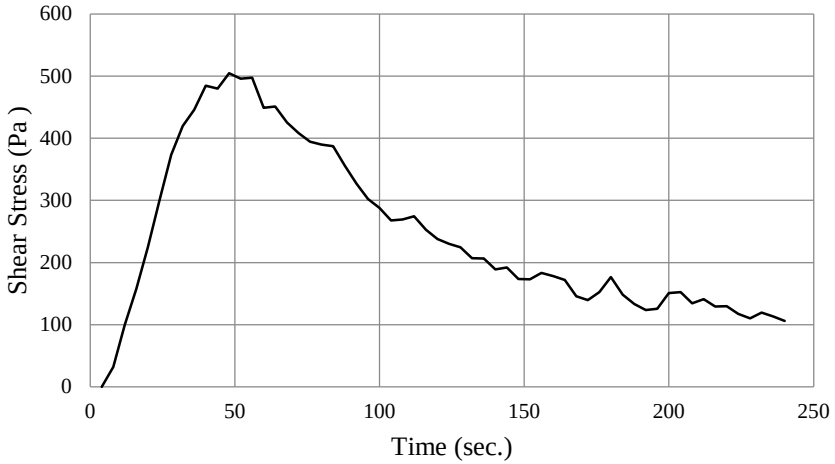

(24) G0.75 CVC

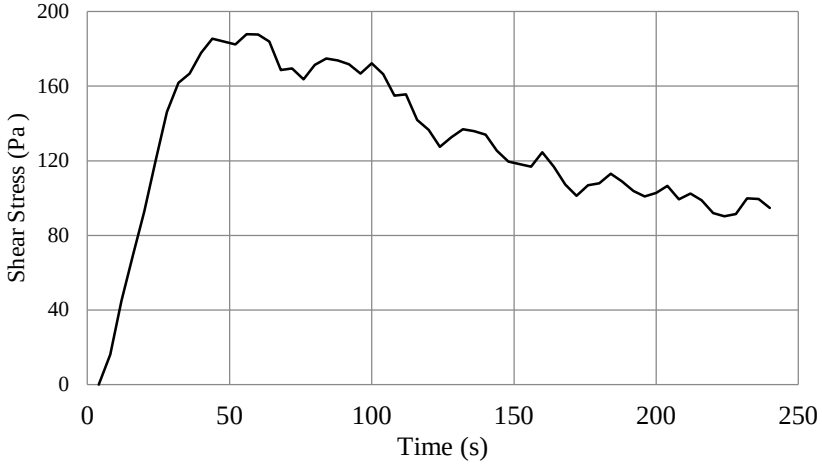

(25) G111C

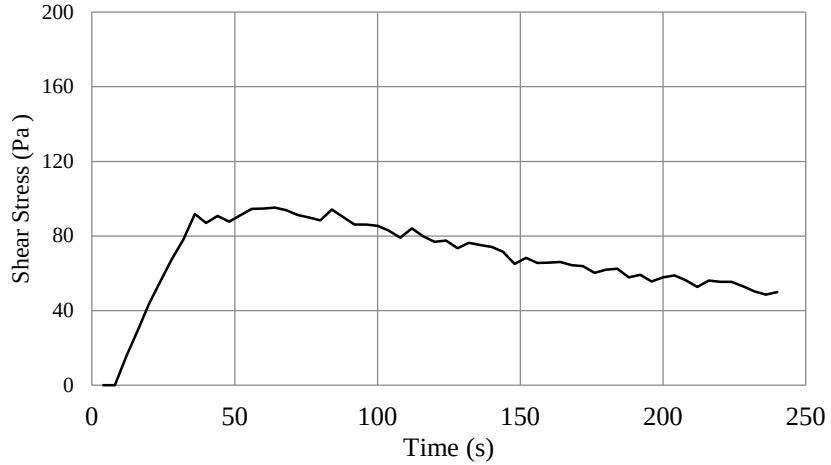

(26) G111F

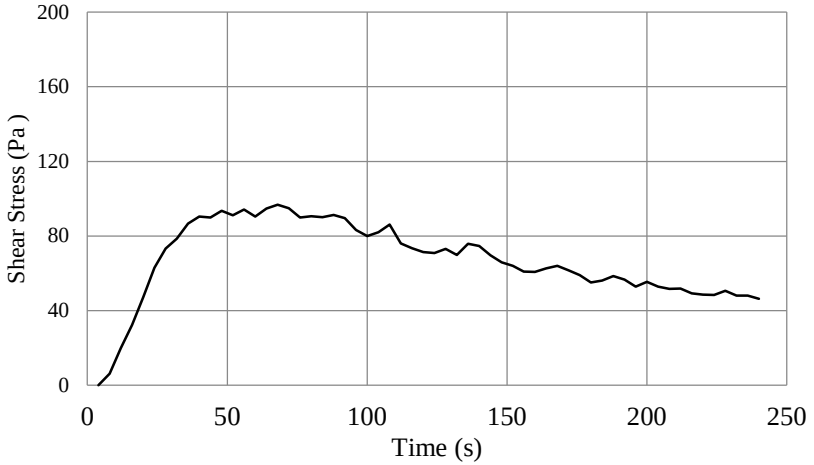

(27) G111S

(Cont.) Figure C-3. Flow curves of CVC and SCC mortars

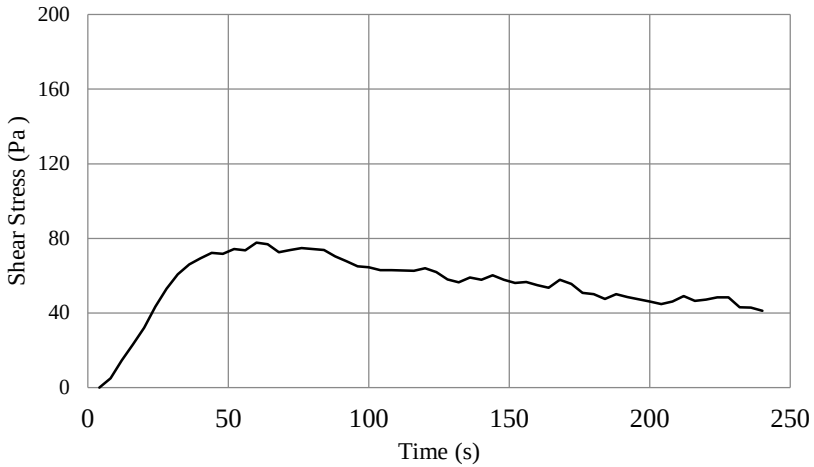

(28) G111FLP

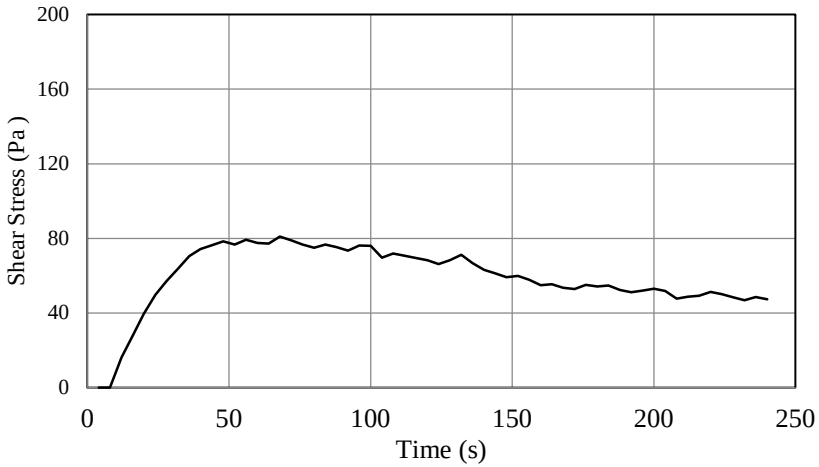

(29) G211C

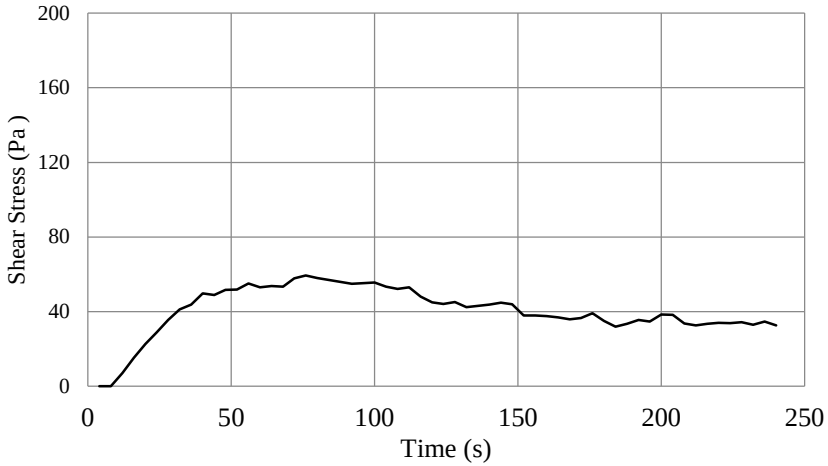

(30) G211F

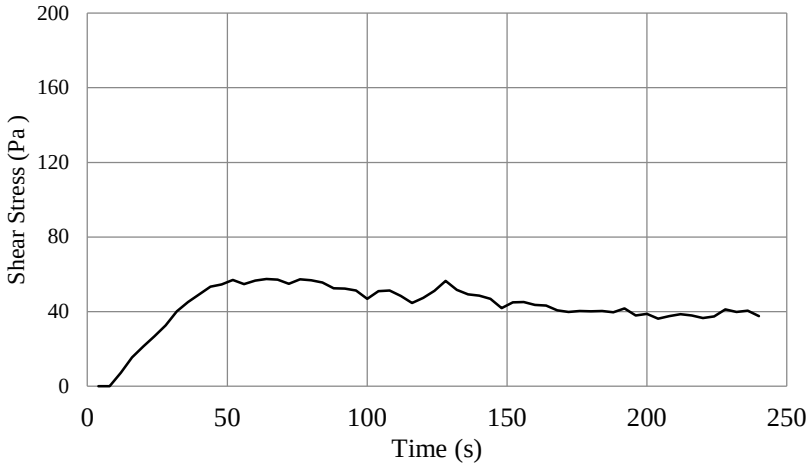

(31) G211S

(Cont.) Figure C-3. Flow curves of CVC and SCC mortars

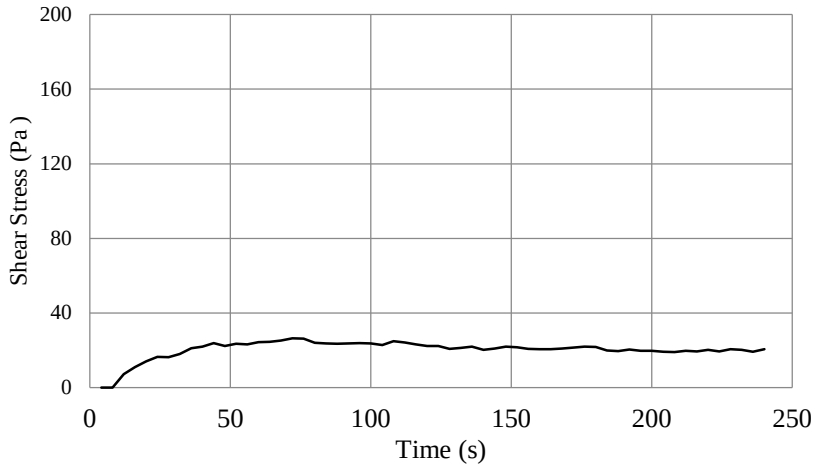

(32) G211FLP

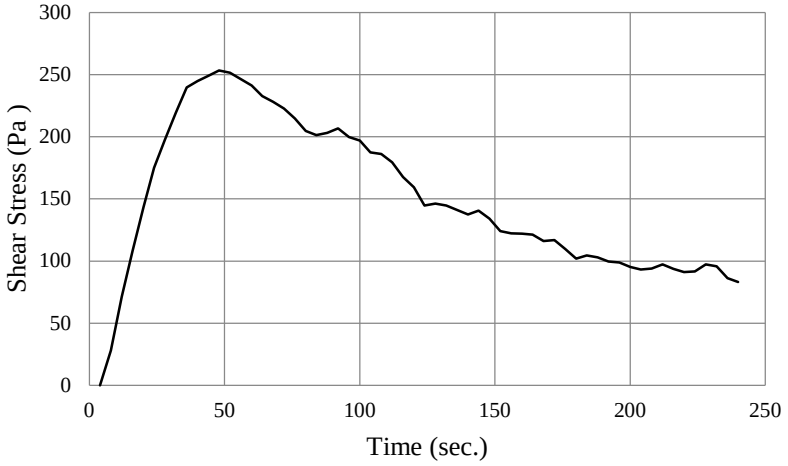

(33) G0.50 CVC

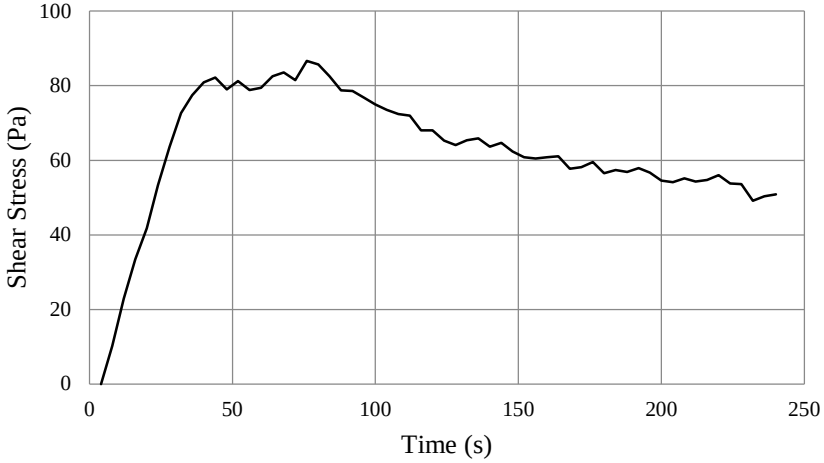

(34) G121C

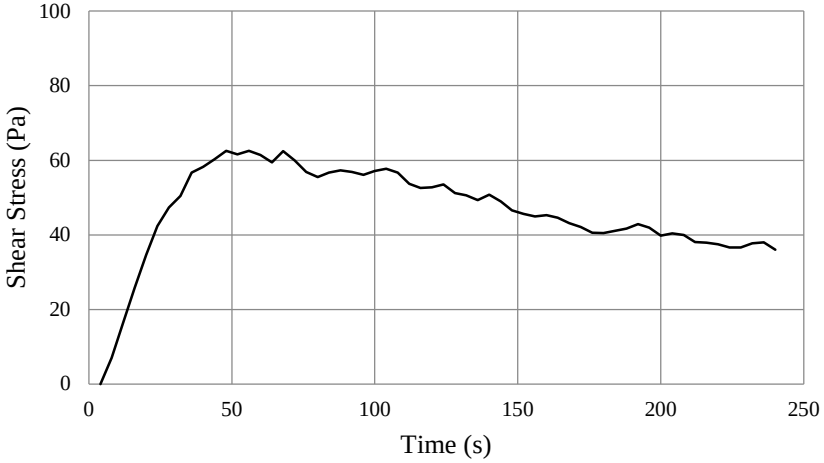

(35) G121F

(Cont.) Figure C-3. Flow curves of CVC and SCC mortars

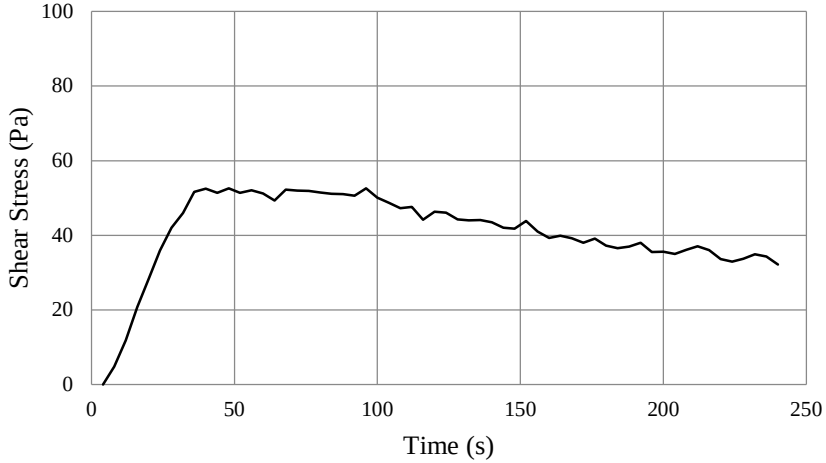

(36) G121S

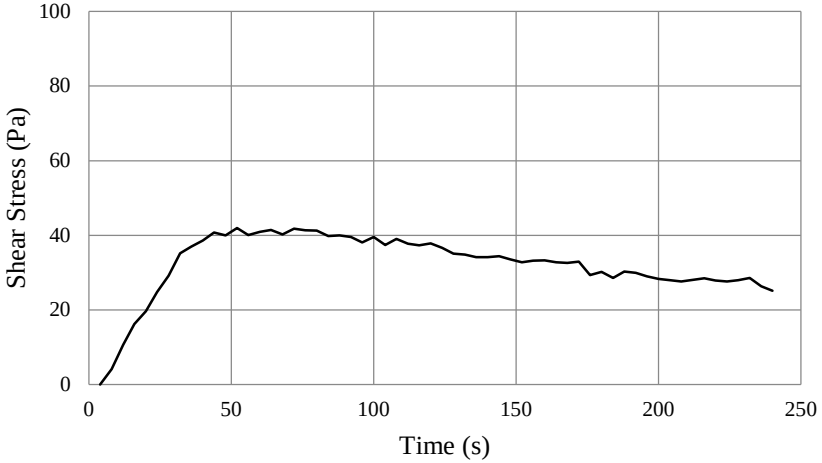

(37) G121FLP

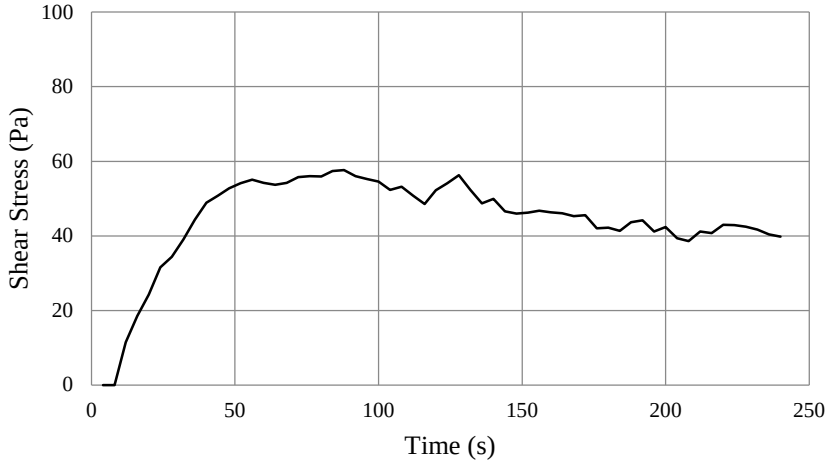

(38) G221C

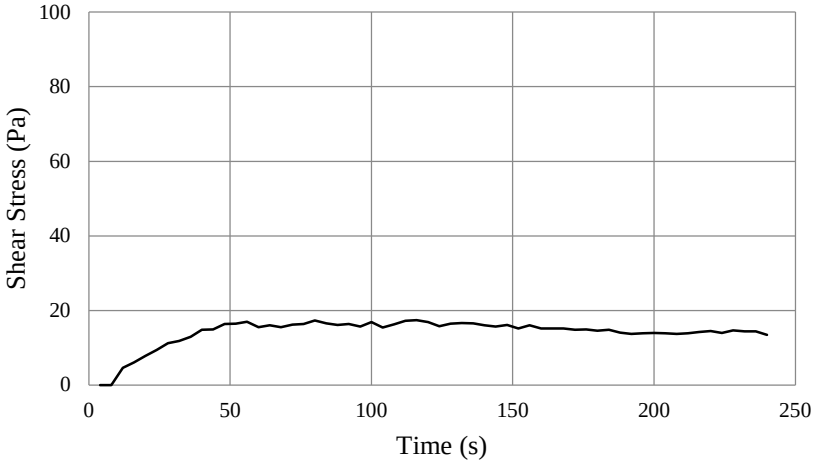

(39) G221F

(Cont.) Figure C-3. Flow curves of CVC and SCC mortars

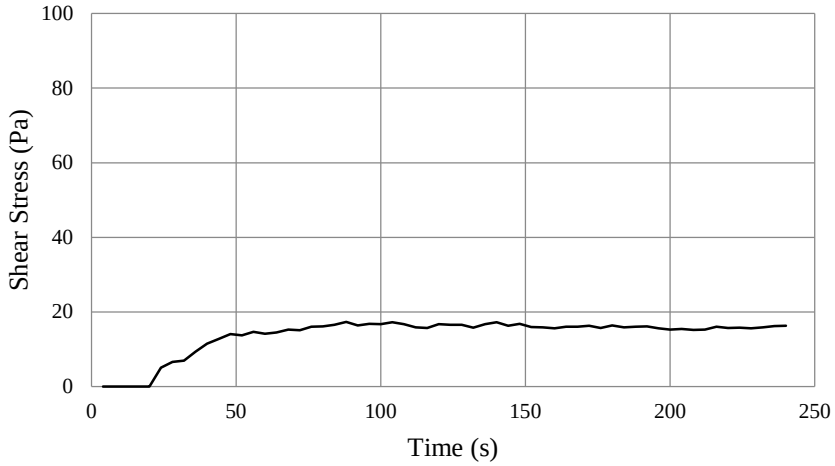

(40) G221S

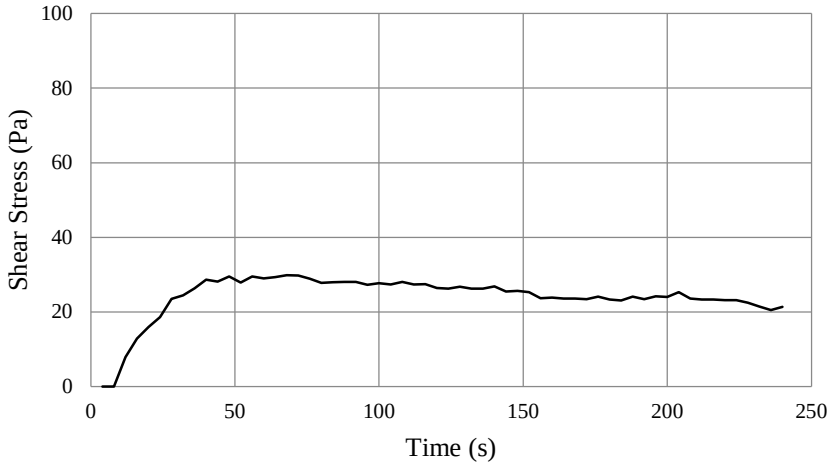

(41) G221FLP

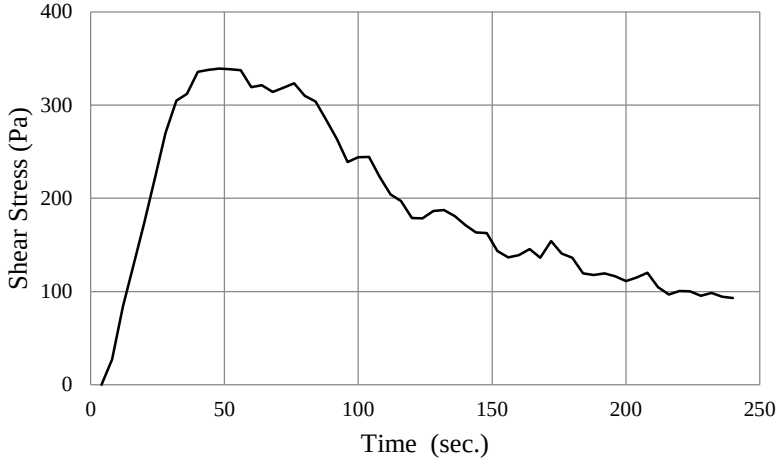

(42) G0.375 CVC

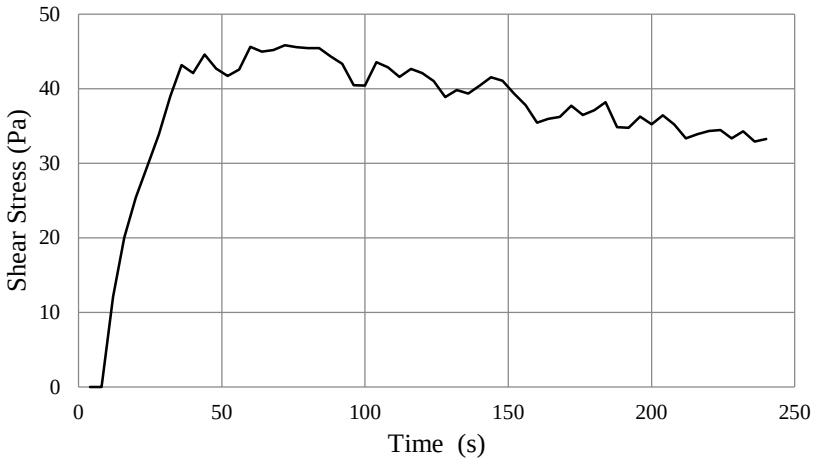

(43) G222C

(Cont.) Figure C-3. Flow curves of CVC and SCC mortars

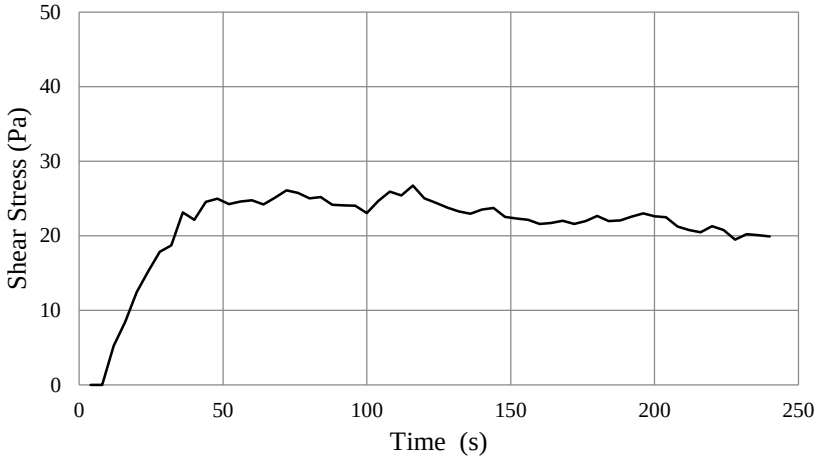

(44) G222F

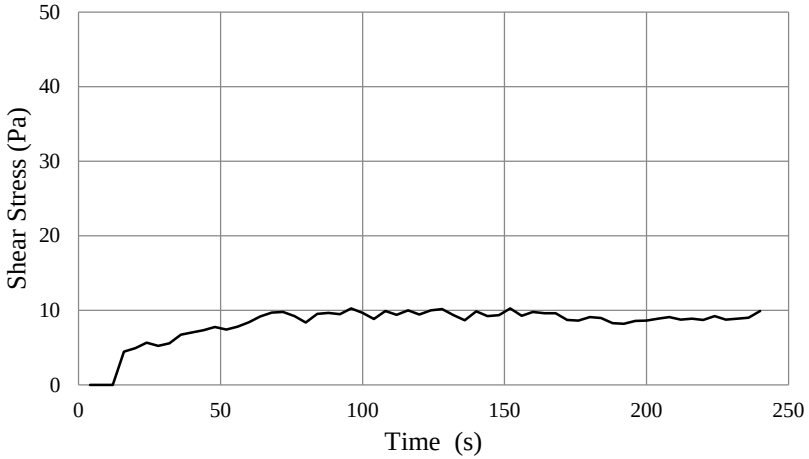

(45) G222S

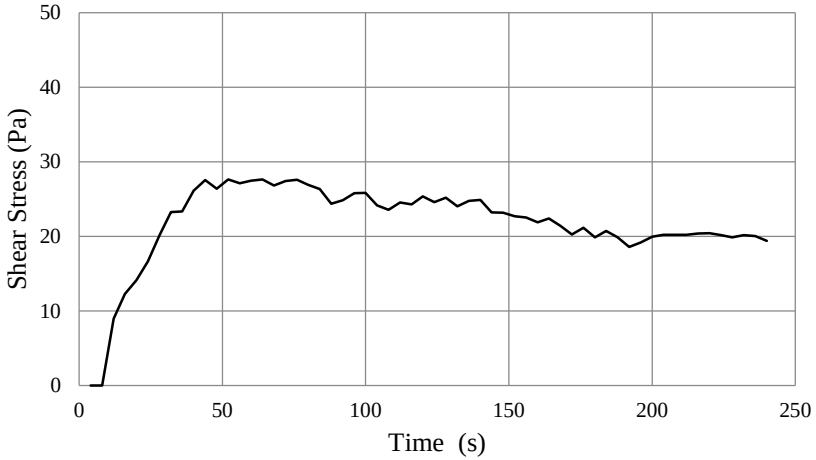

(46) G222FLP

(Cont.) Figure C-3. Flow curves of CVC and SCC mortars

1.2. Breakdown area curves of CVC and SCC mortars

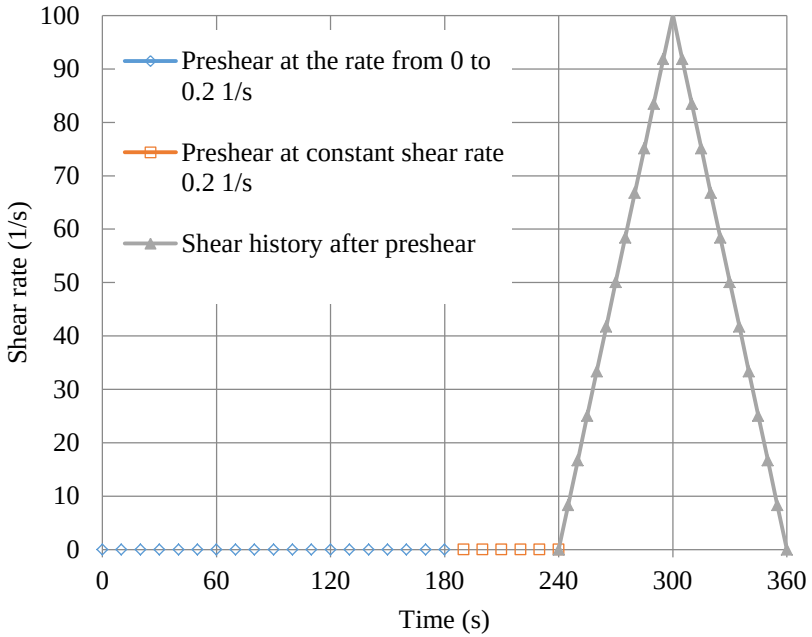

Figure C-4. Loading history

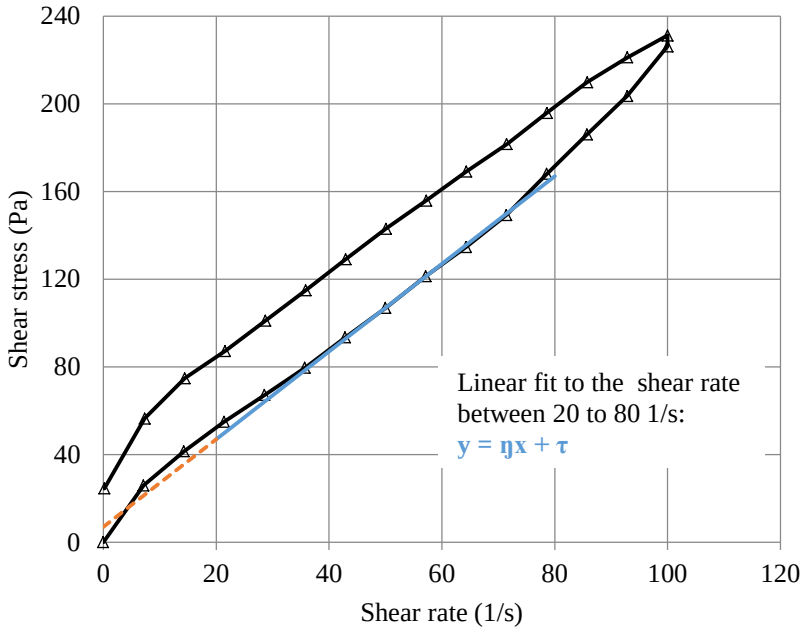

Figure C-5. Flow curve of a typical mortar mixture

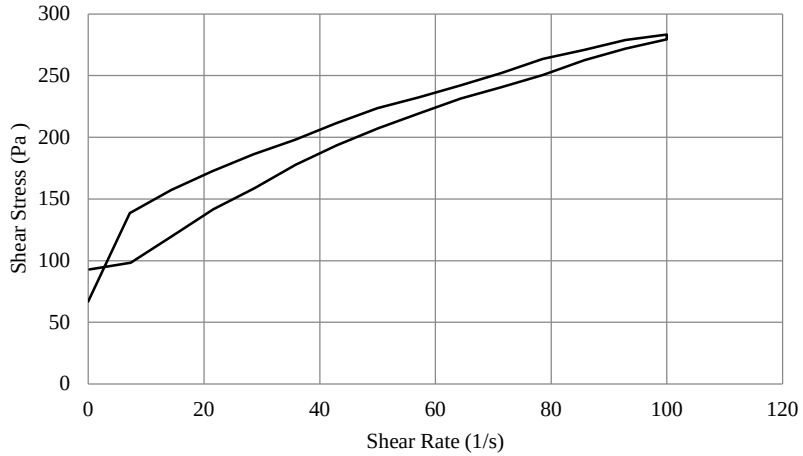

(1) LS0.75 CVC

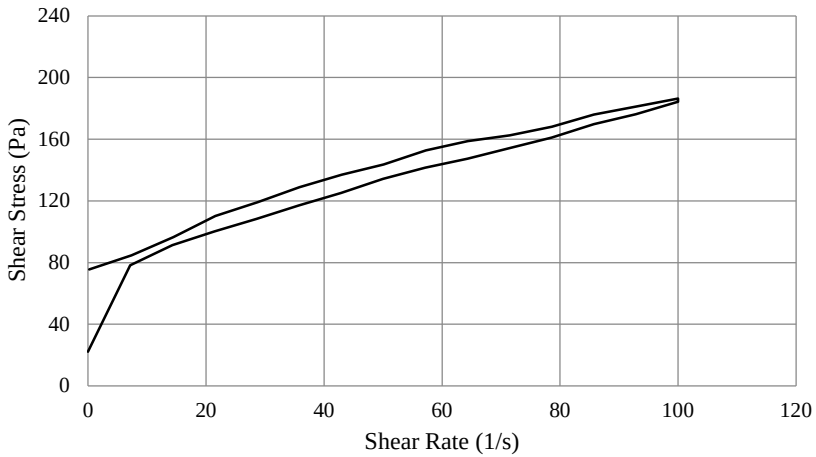

(2) LS111C

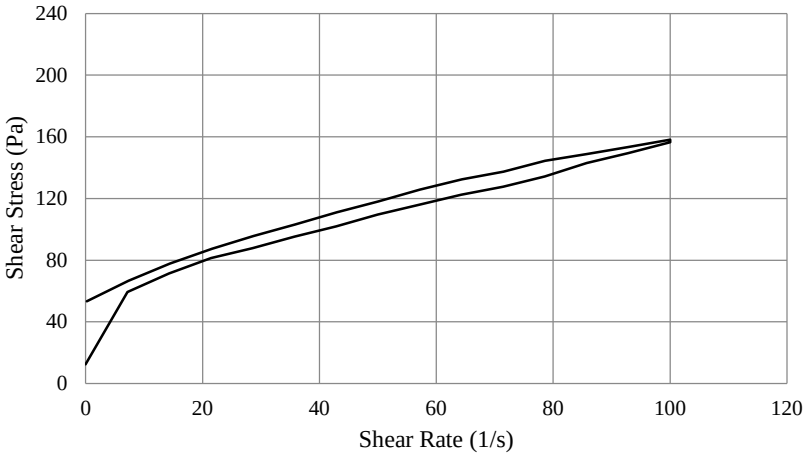

(3) LS111F

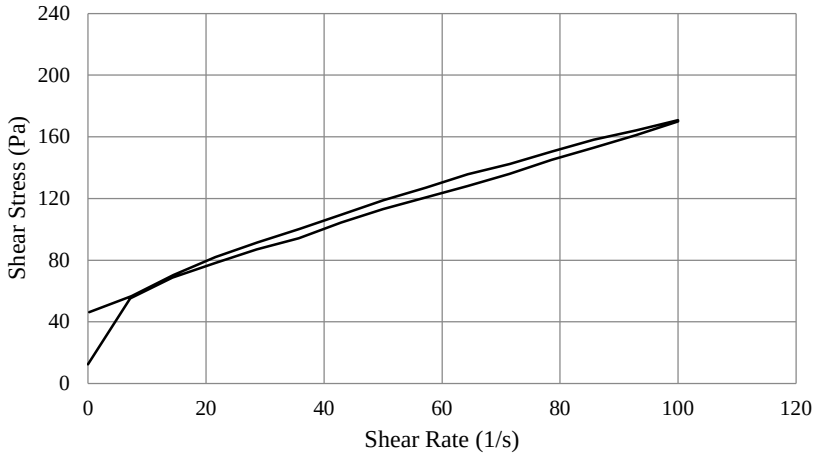

(4) LS111S

Figure C-6. Breakdown area curves of CVC and SCC mortars

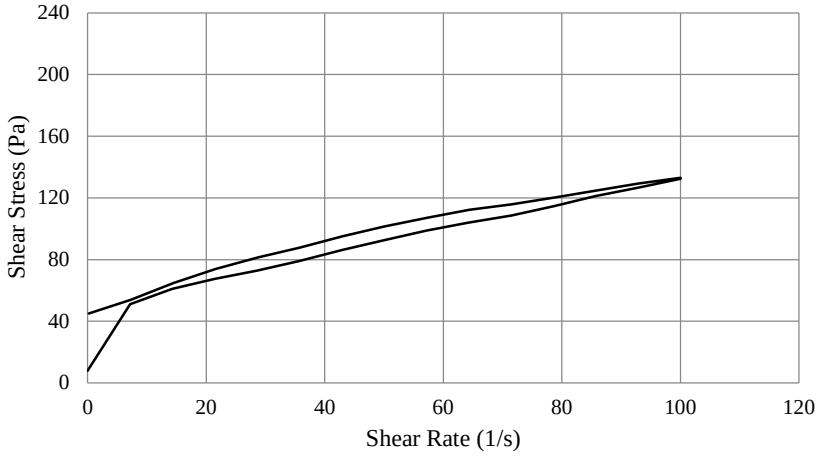

(5) LS111FLP

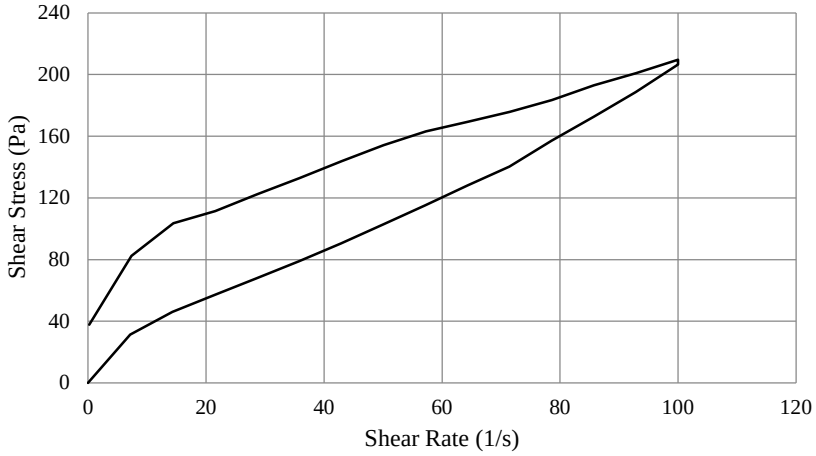

(6) LS211C

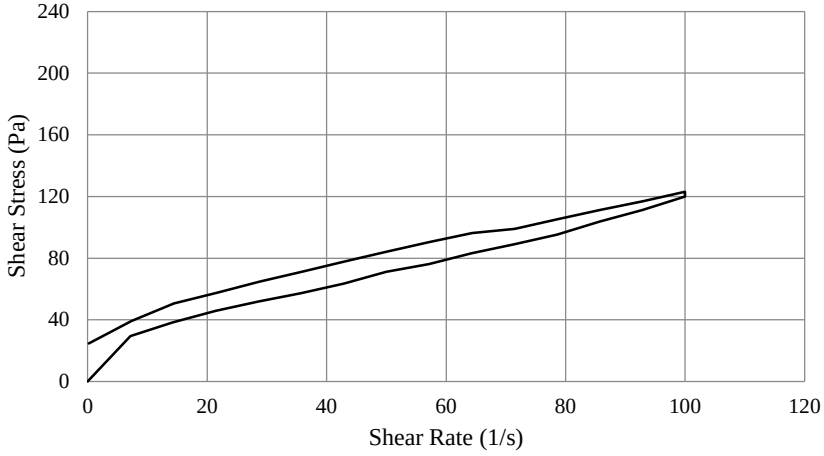

(7) LS211F

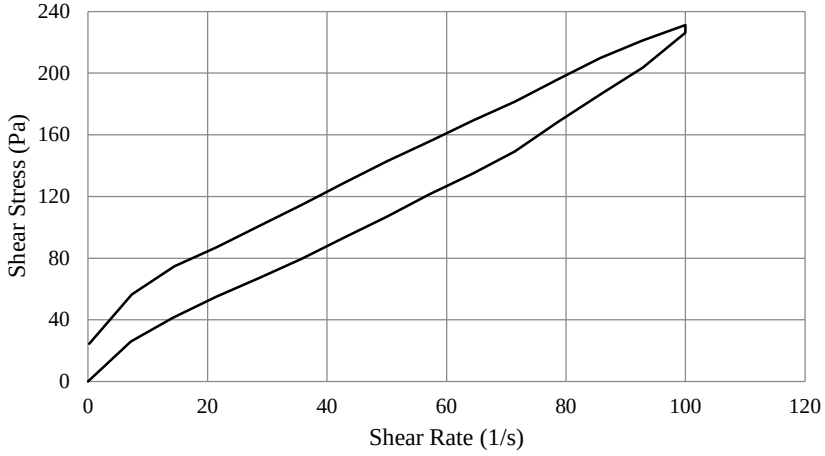

(8) LS211S

(cont.) Figure C-6. Breakdown area curves of CVC and SCC mortars

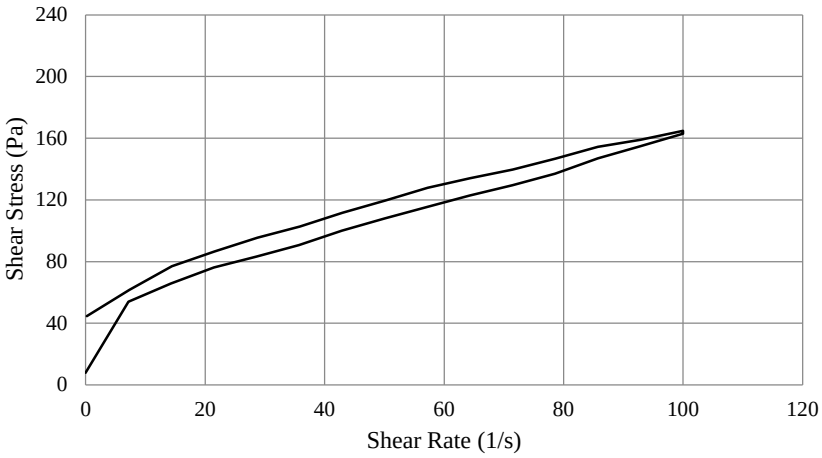

(9) LS211FLP

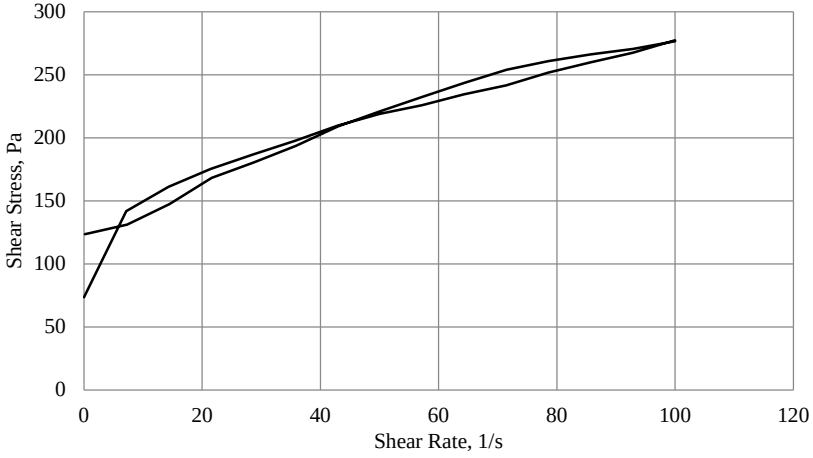

(10) LS0.50 CVC

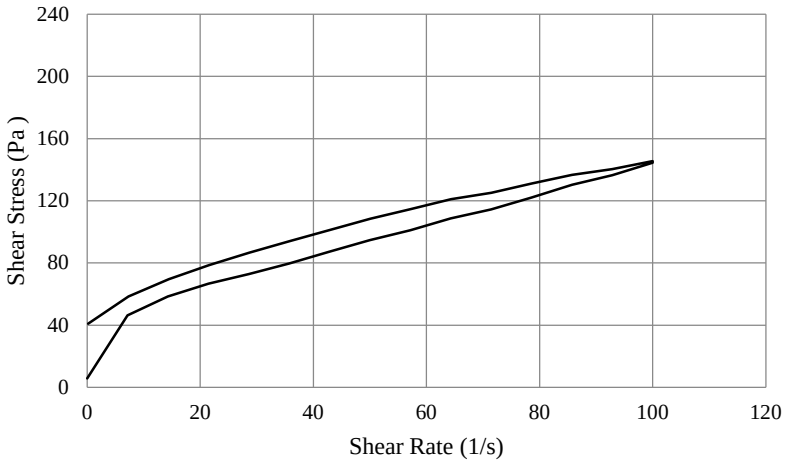

(11) LS121C

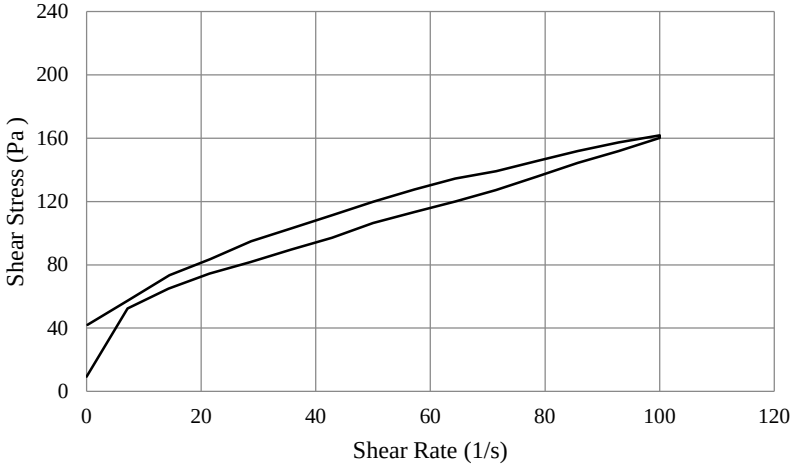

(12) LS121F

(cont.) Figure C-6. Breakdown area curves of CVC and SCC mortars

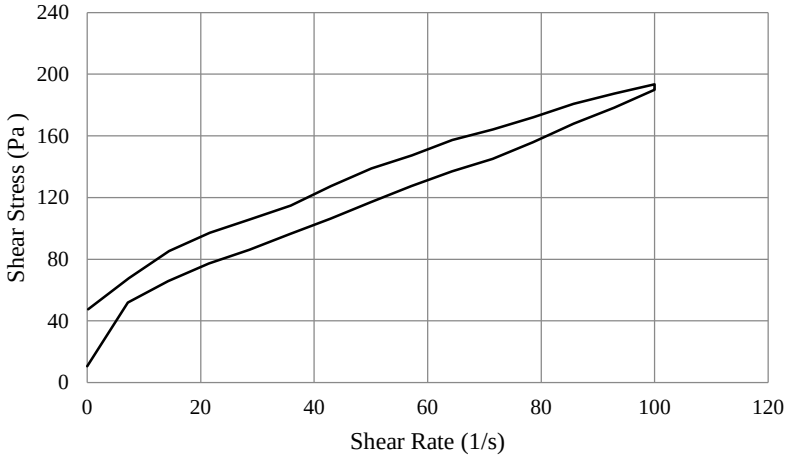

(13) LS121S

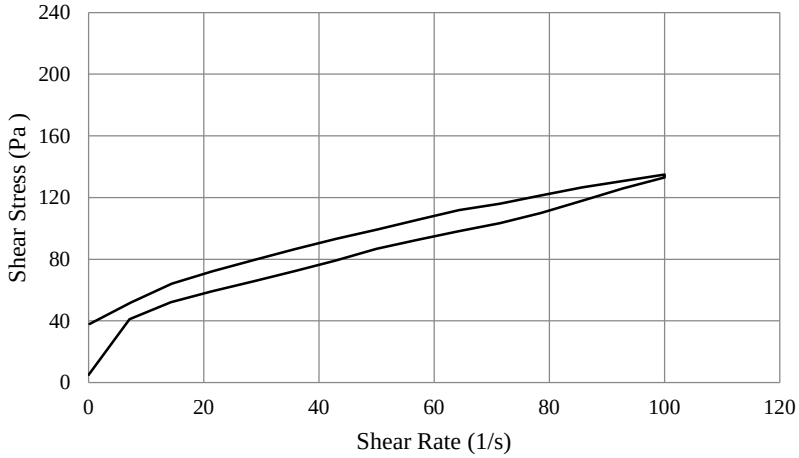

(14) LS121FLP

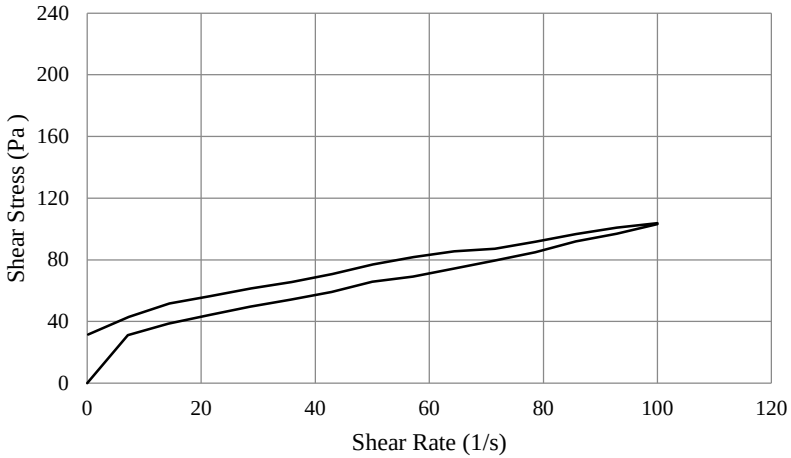

(15) LS221C

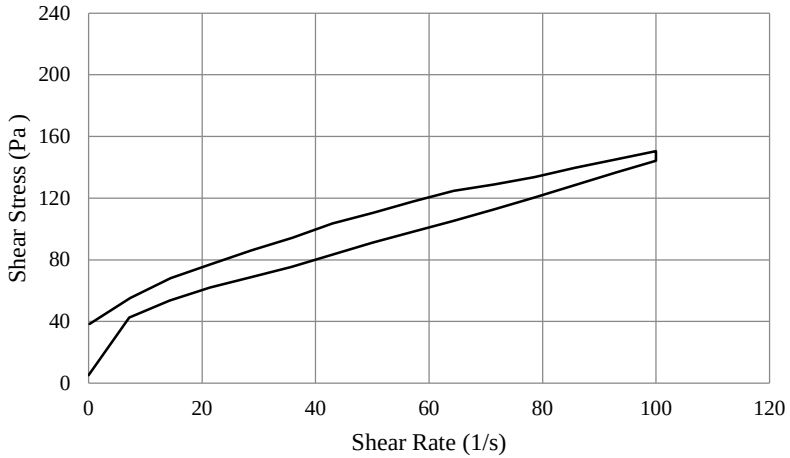

(16) LS221F

(cont.) Figure C-6. Breakdown area curves of CVC and SCC mortars

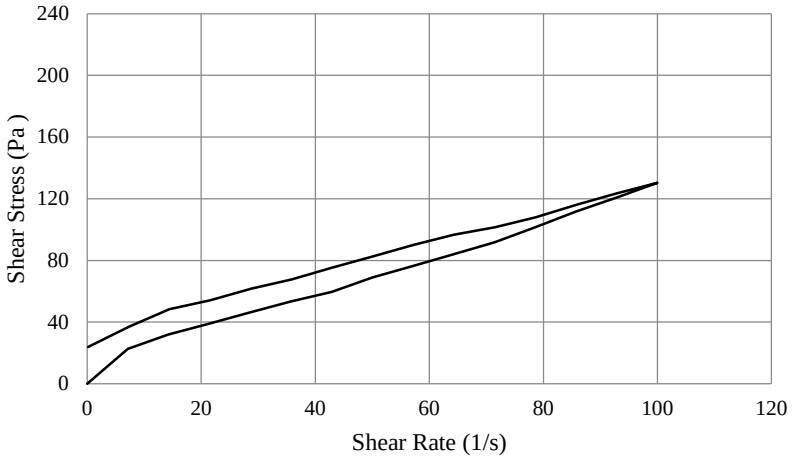

(17) LS221S

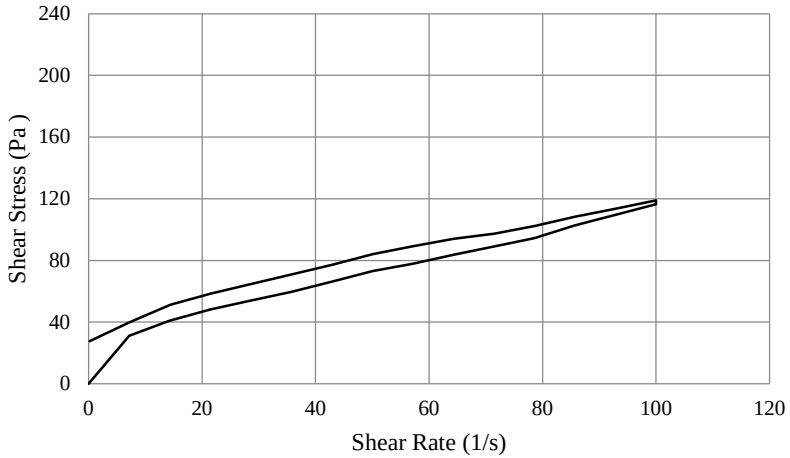

(18) LS221FLP

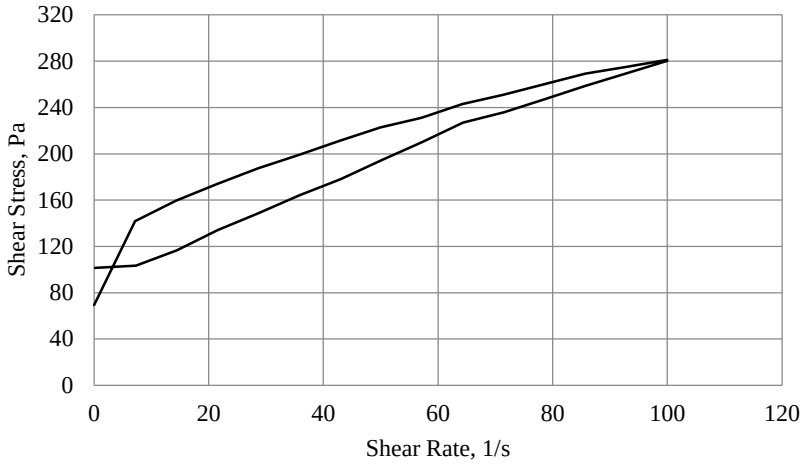

(19) LS0.375 CVC

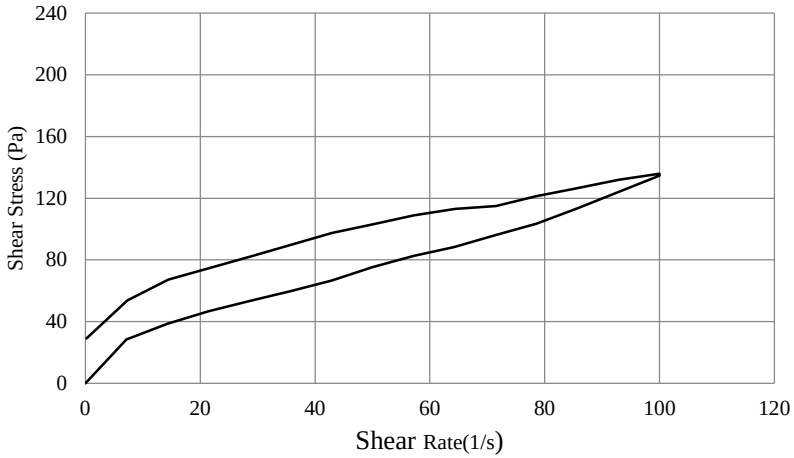

(20) LS222C

(cont.) Figure C-6. Breakdown area curves of CVC and SCC mortars

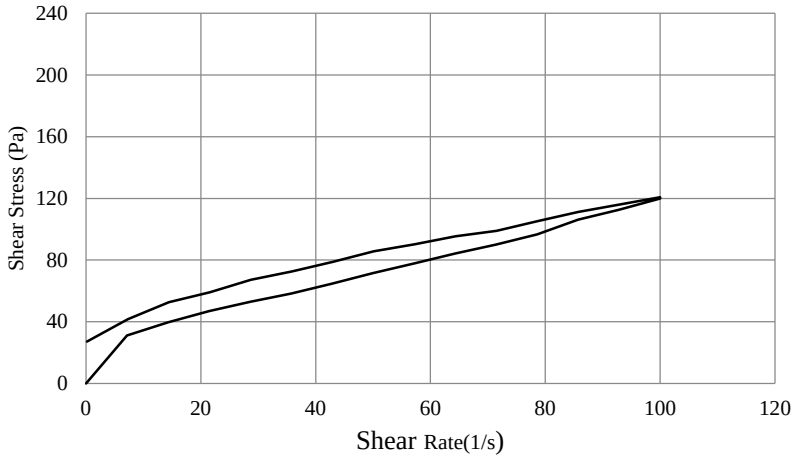

(21) LS222F

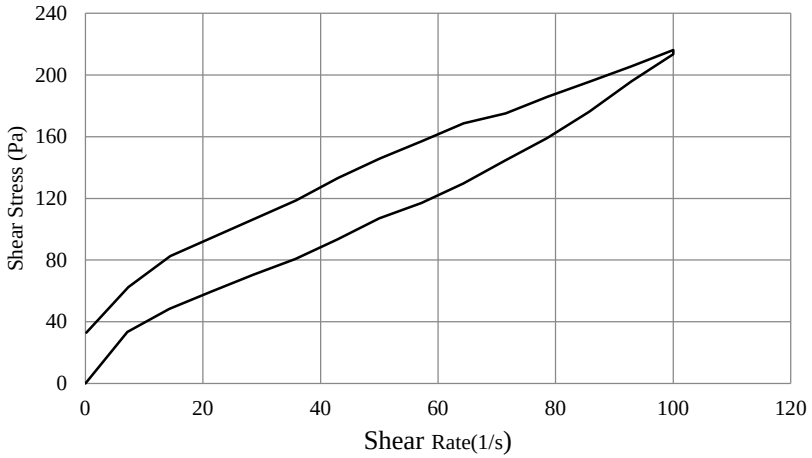

(22) LS222S

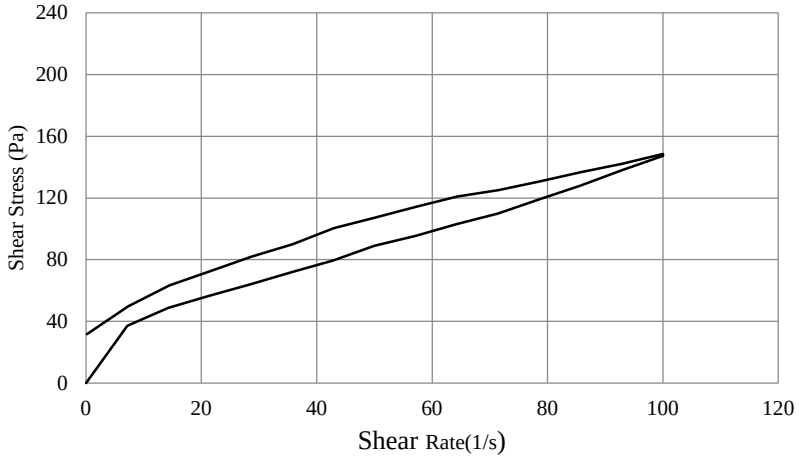

(23) LS222FLP

(cont.) Figure C-6. Breakdown area curves of CVC and SCC mortars

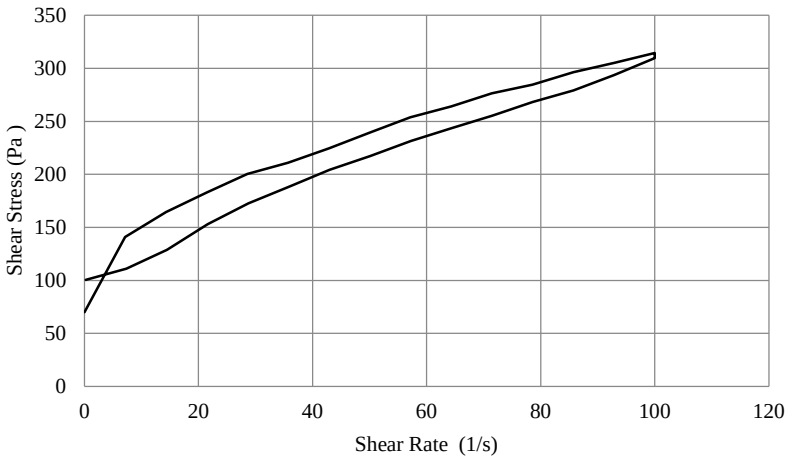

(24) G0.75 CVC

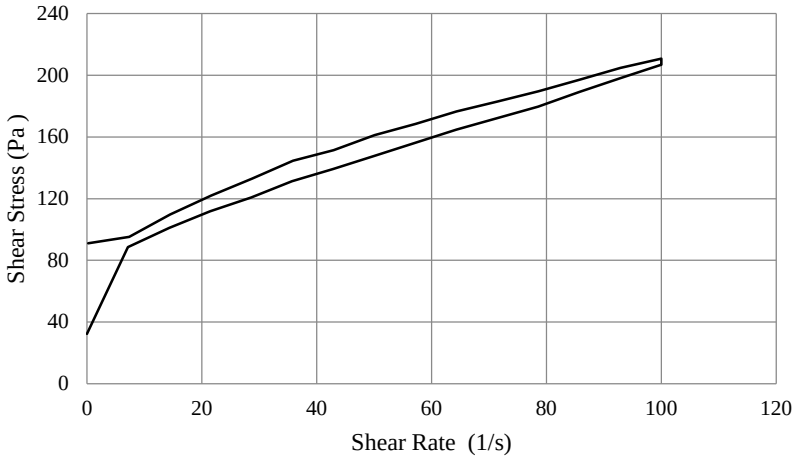

(25) G111C

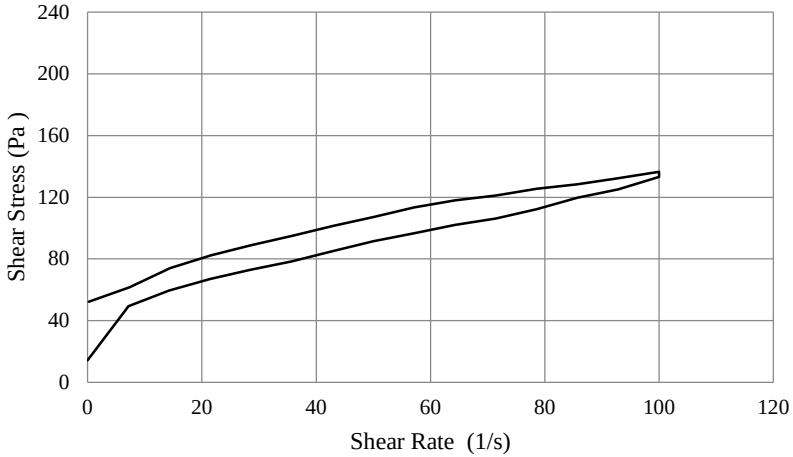

(26) G111F

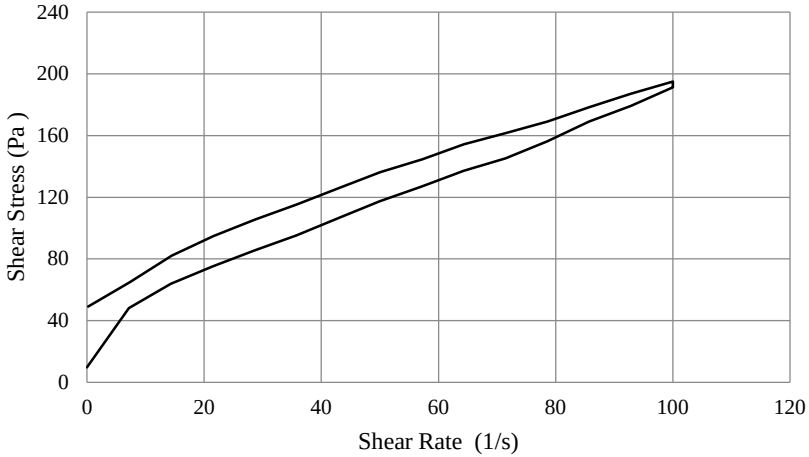

(27) G111S

(cont.) Figure C-6. Breakdown area curves of CVC and SCC mortars

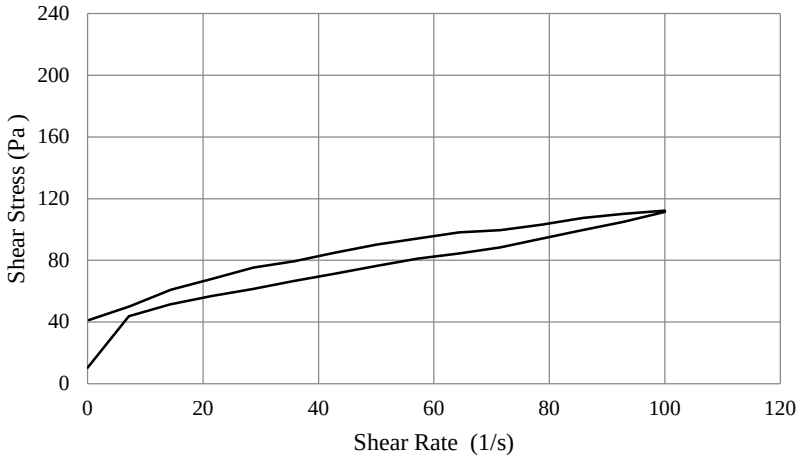

(28) G111FLP

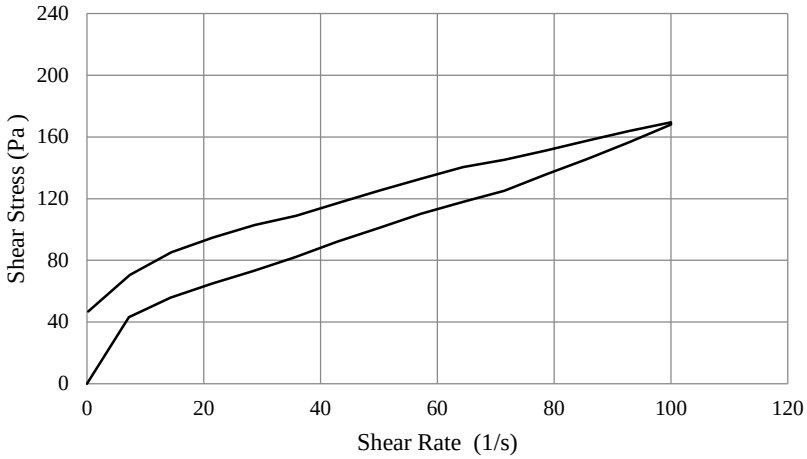

(29) G211C

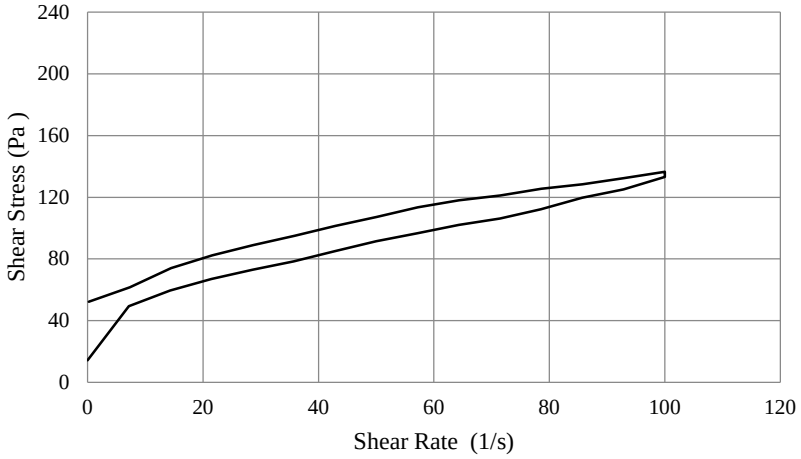

(30) G211F

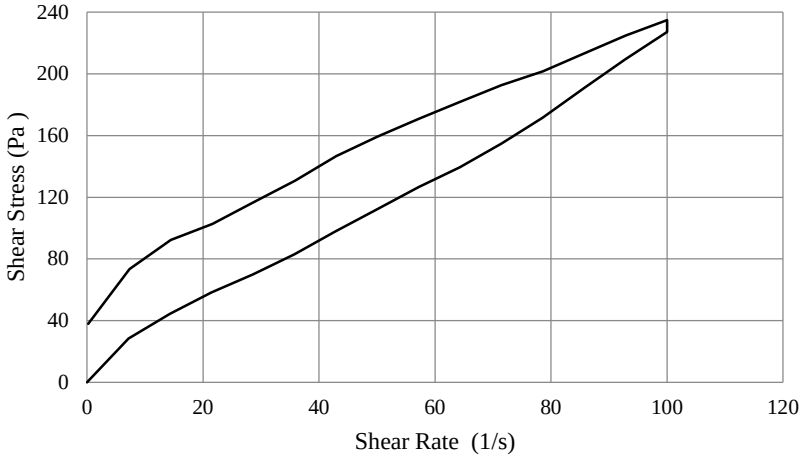

(31) G211S

(cont.) Figure C-6. Breakdown area curves of CVC and SCC mortars

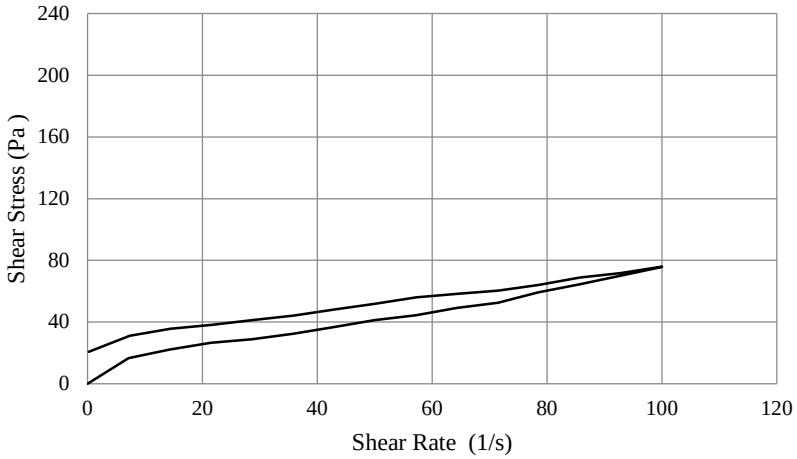

(32) G211FLP

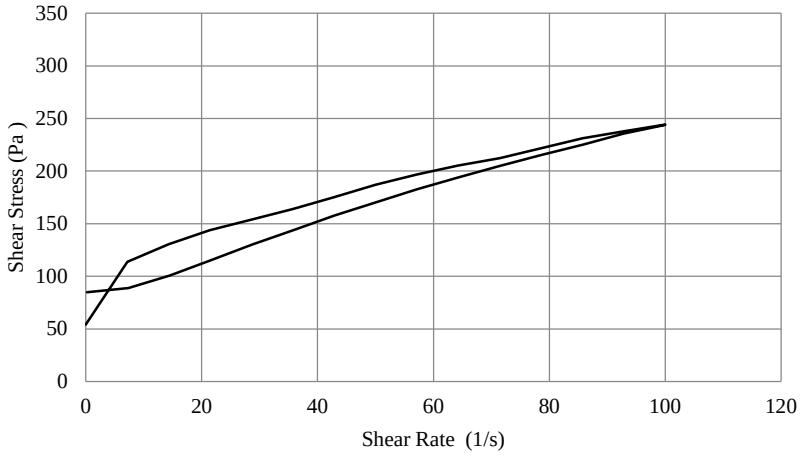

(33) G0.50 CVC

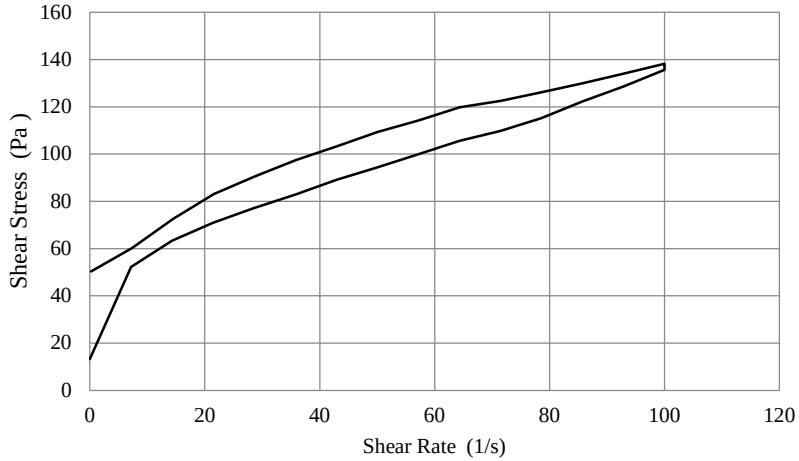

(34) G121C

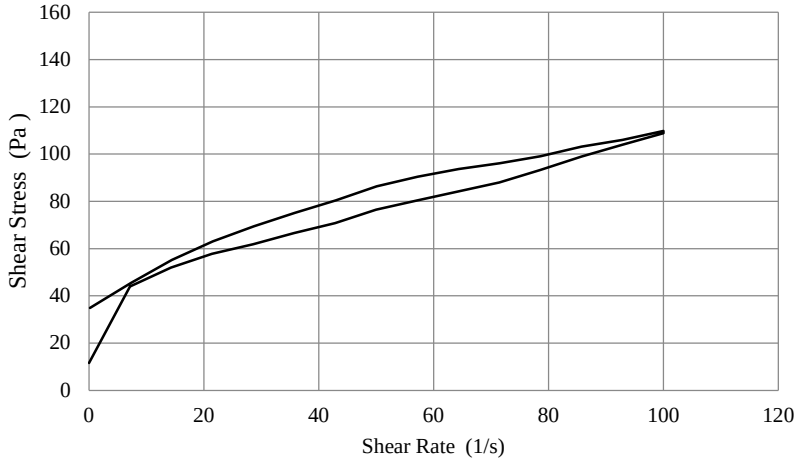

(35) G121F

(cont.) Figure C-6. Breakdown area curves of CVC and SCC mortars

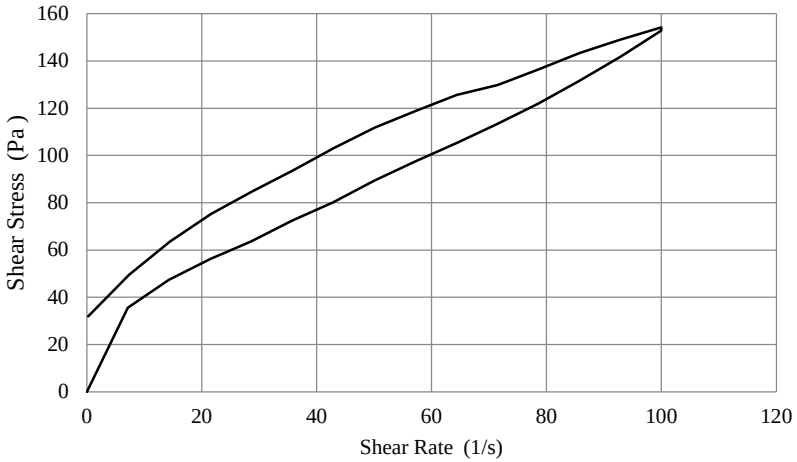

(36) G121S

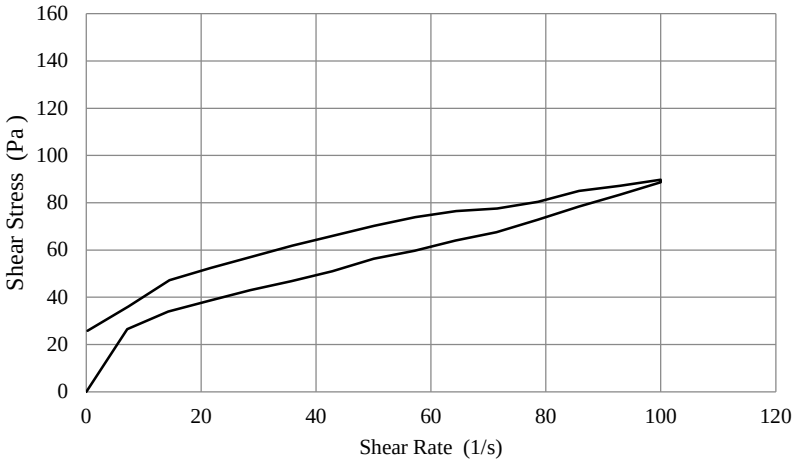

(37) G121FLP

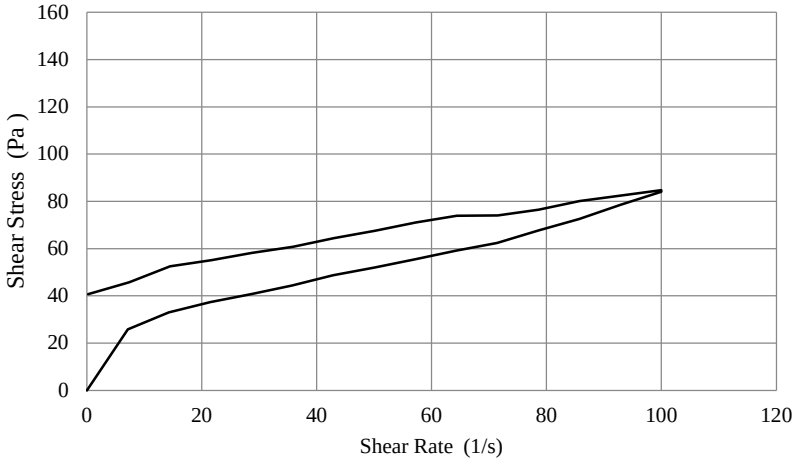

(38) G221C

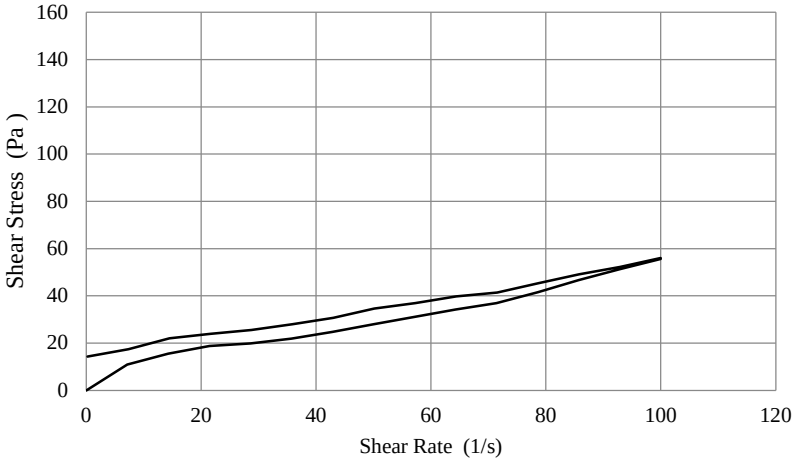

(39) G221F

(cont.) Figure C-6. Breakdown area curves of CVC and SCC mortars

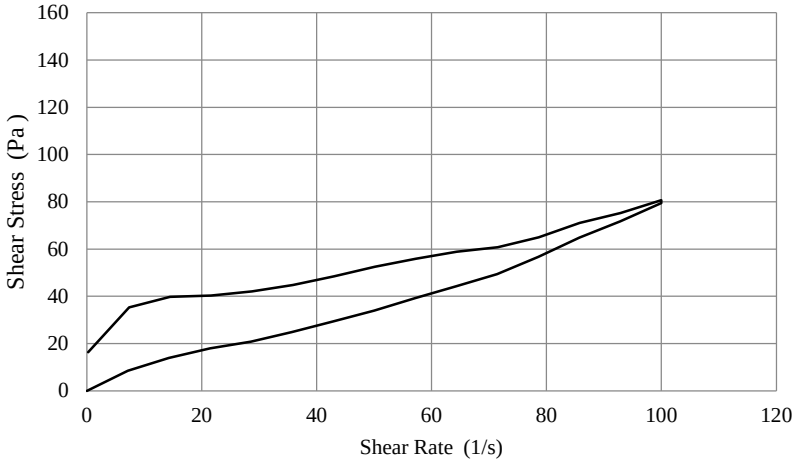

(40) G221S

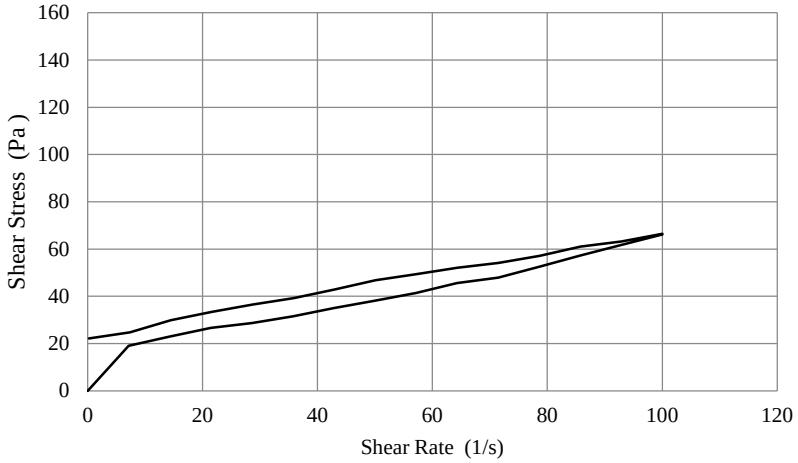

(41) G221FLP

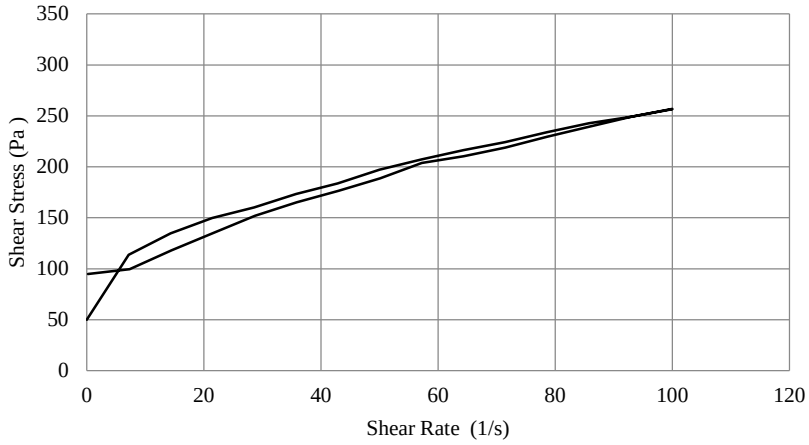

(42) G0.375 CVC

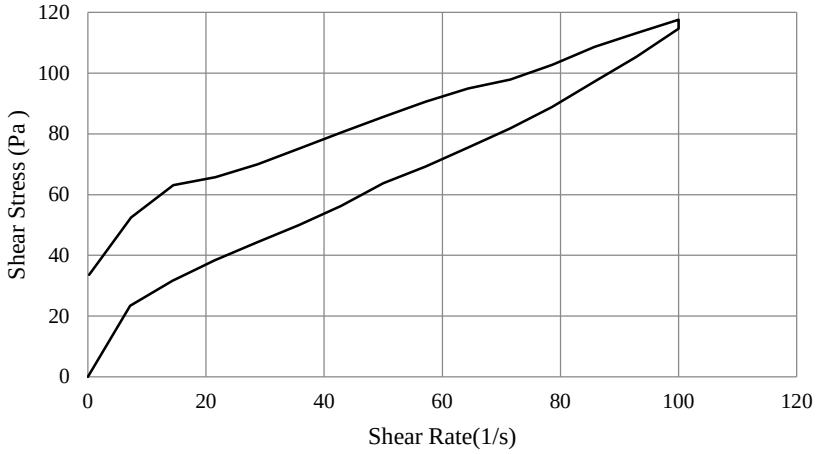

(43) G222C

(cont.) Figure C-6. Breakdown area curves of CVC and SCC mortars

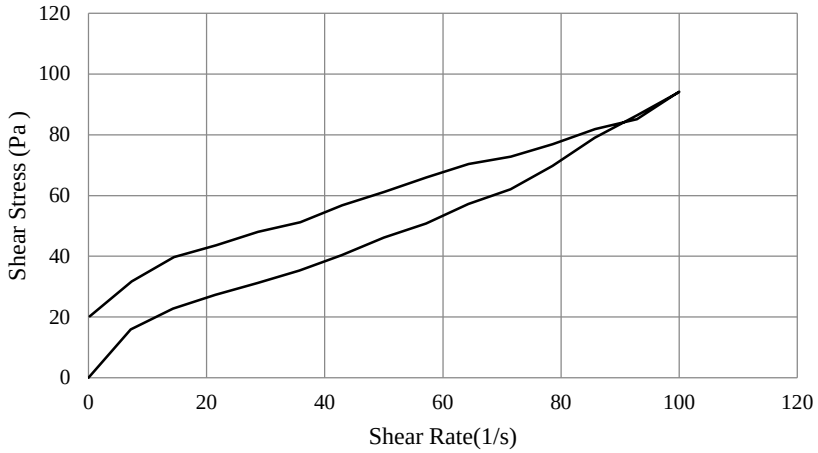

(44) G222F

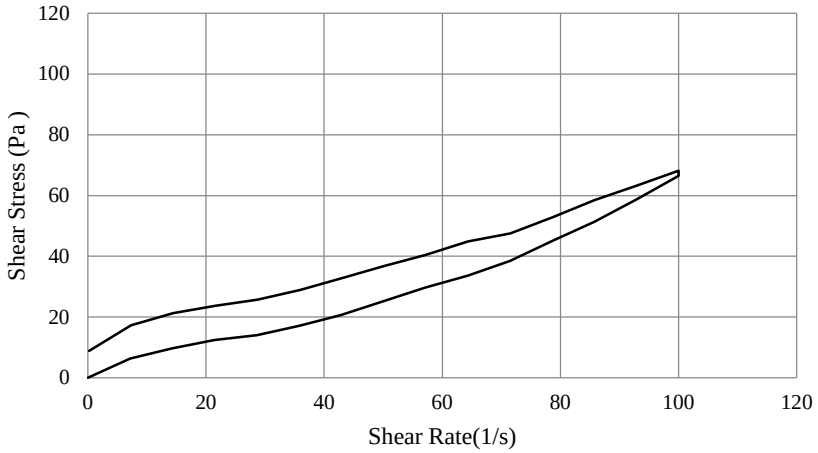

(45) G222S

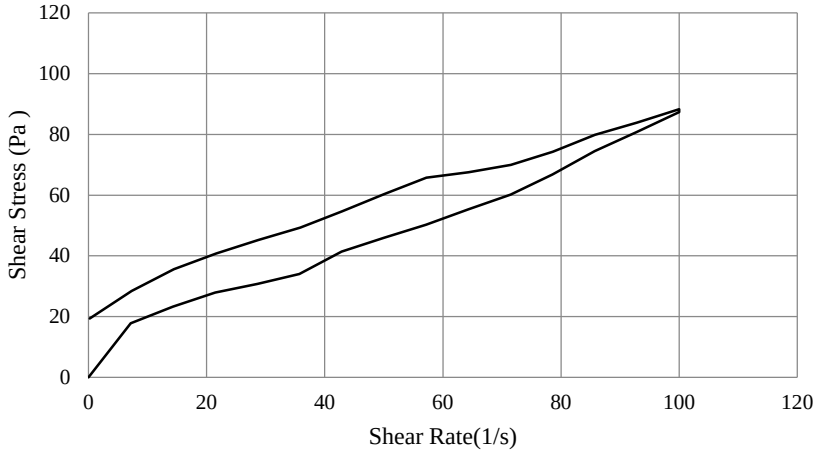

(46) G222FLP

(cont.) Figure C-6. Breakdown area curves of CVC and SCC mortars

1.3. Concrete rheology test results of CVC and SCC mixtures

Figure C-7. IBB concrete rheometer

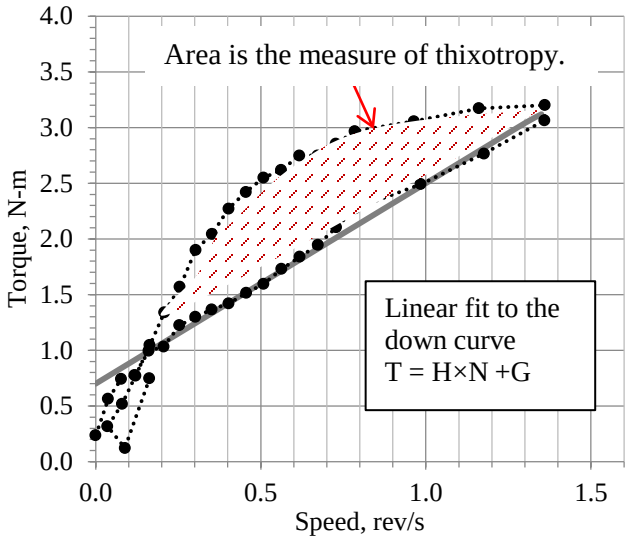

Figure C-8. Flow curve of a typical concrete mixture

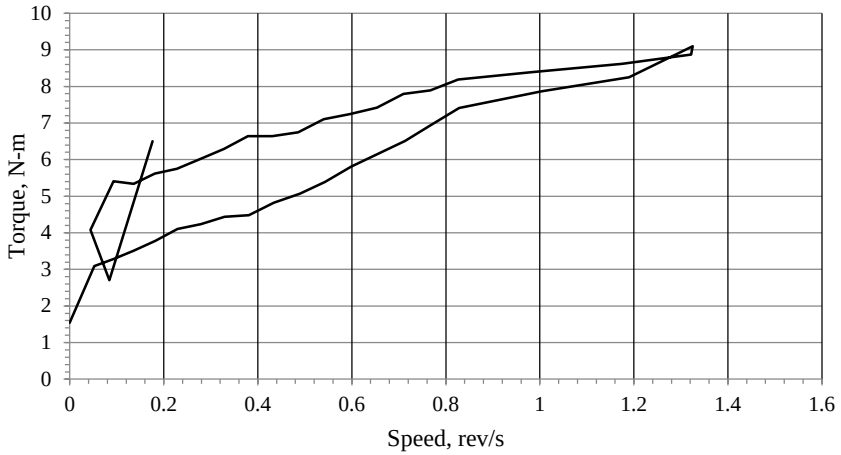

(1) LS0.75 CVC

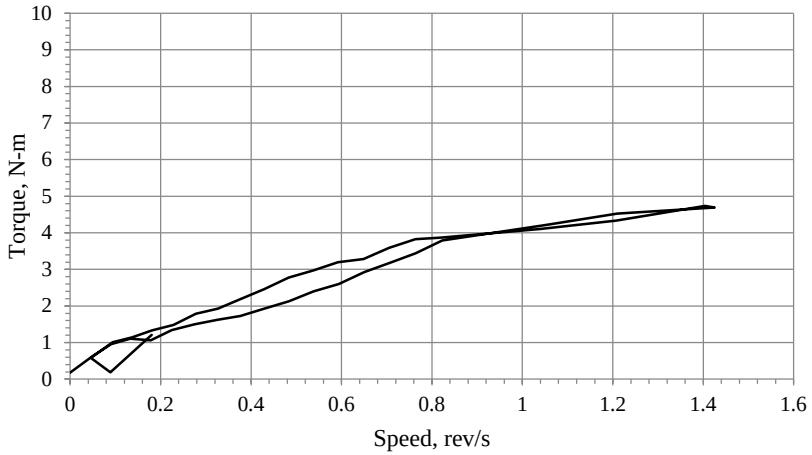

(2) LS111C

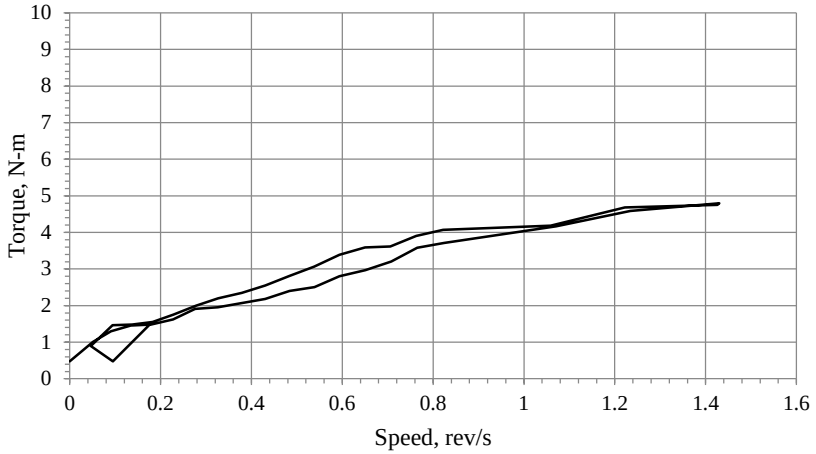

(3) LS111F

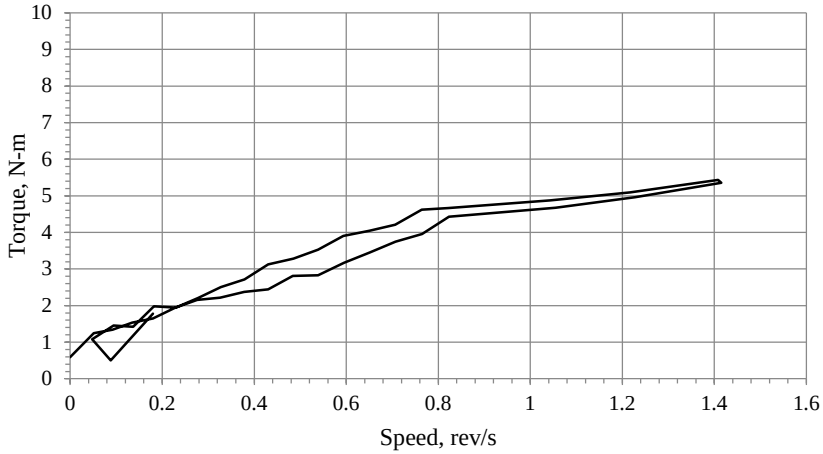

(4) LS111S

Figure C-9. Flow curve of CVC and SCC mixtures

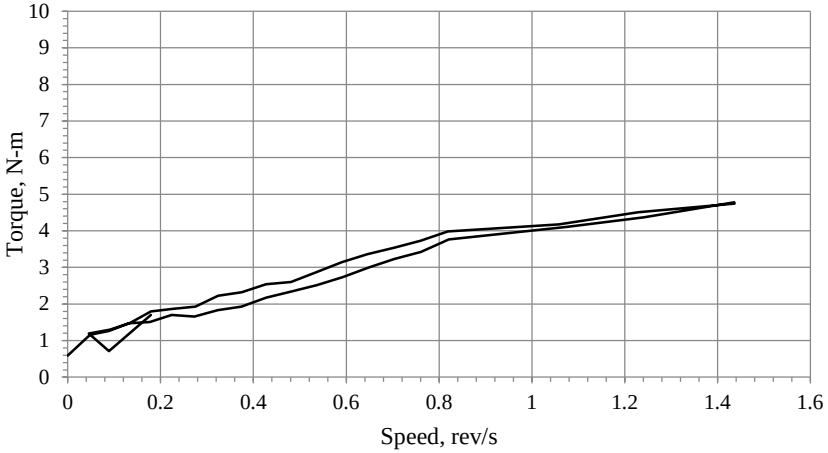

(5) LS111FLP

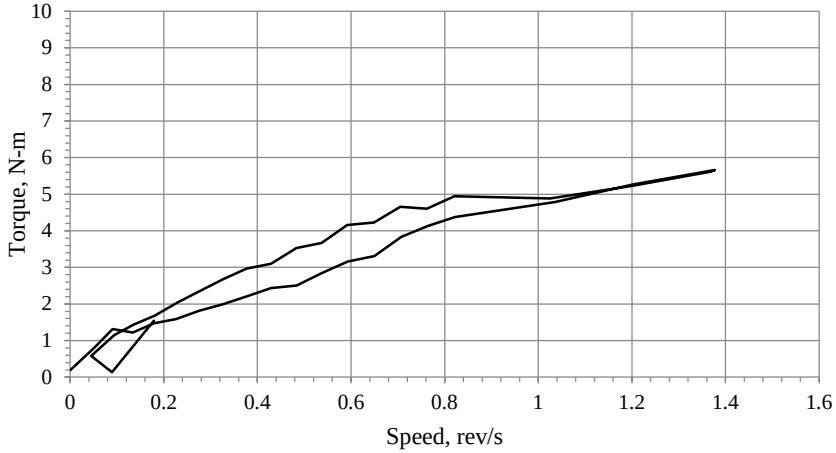

(6) LS211C

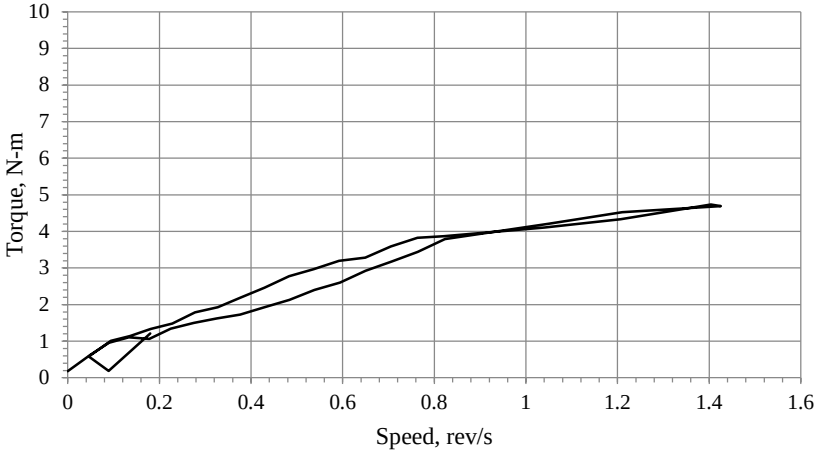

(7) LS211F

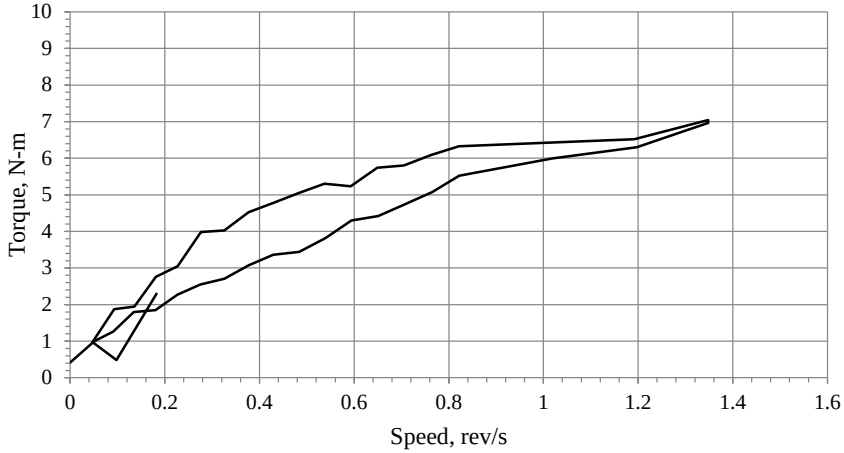

(8) LS211S

(Cont.) Figure C-9. Flow curve of CVC and SCC mixtures

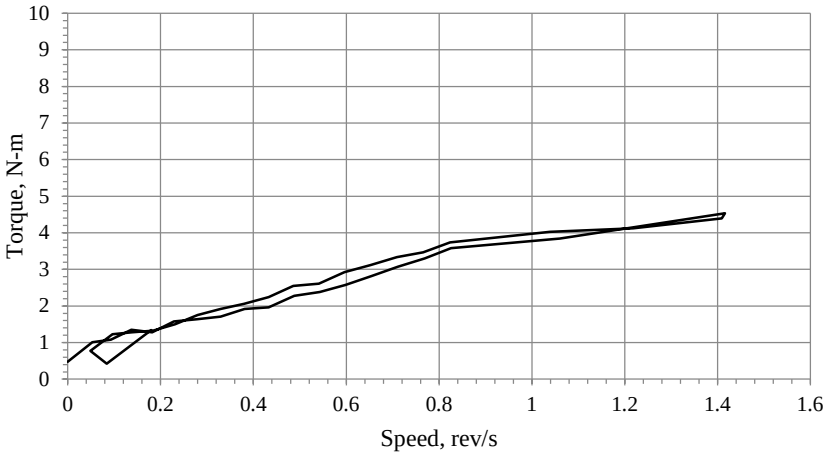

(9) LS211FLP

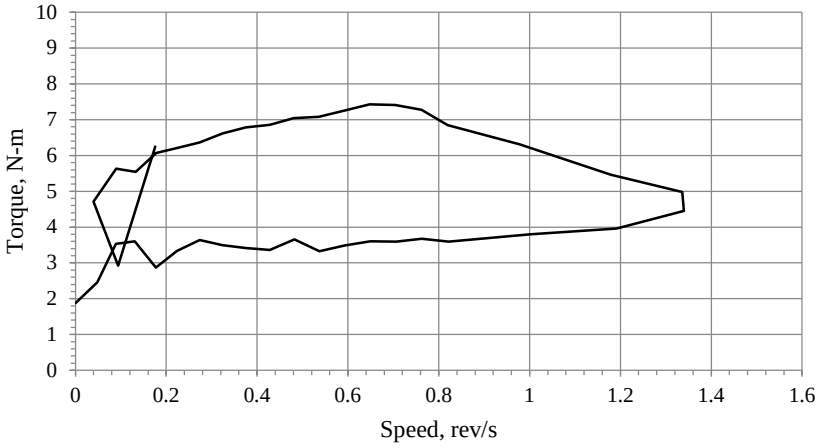

(10) LS0.50 CVC

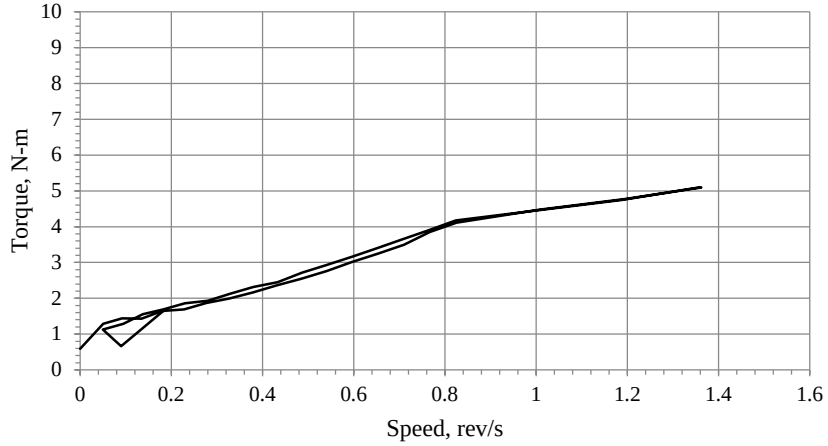

(11) LS121C

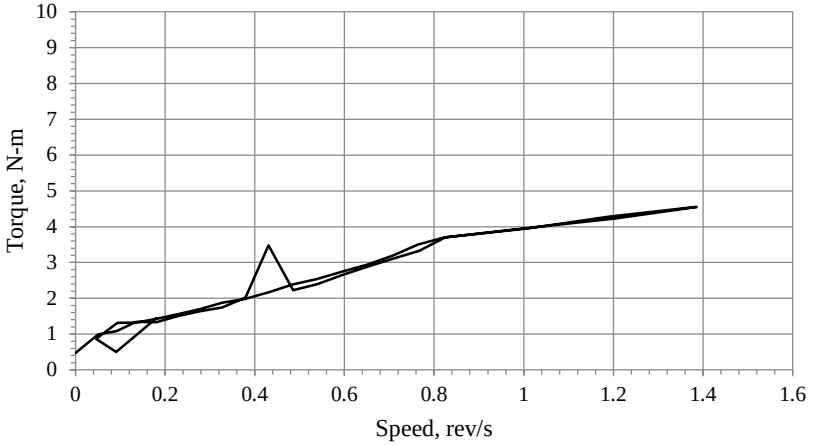

(12) LS121F

(Cont.) Figure C-9. Flow curve of CVC and SCC mixtures

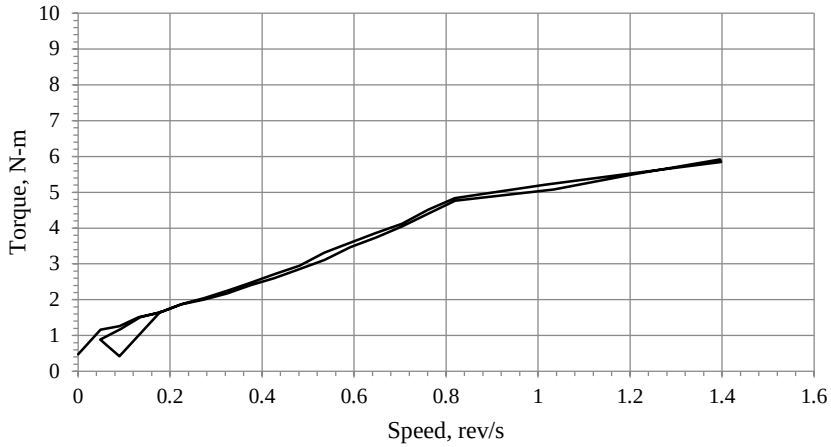

(13) LS121S

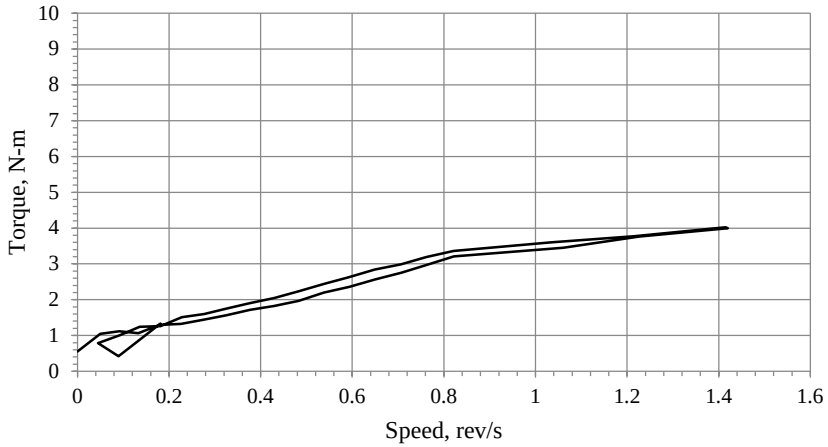

(14) LS121FLP

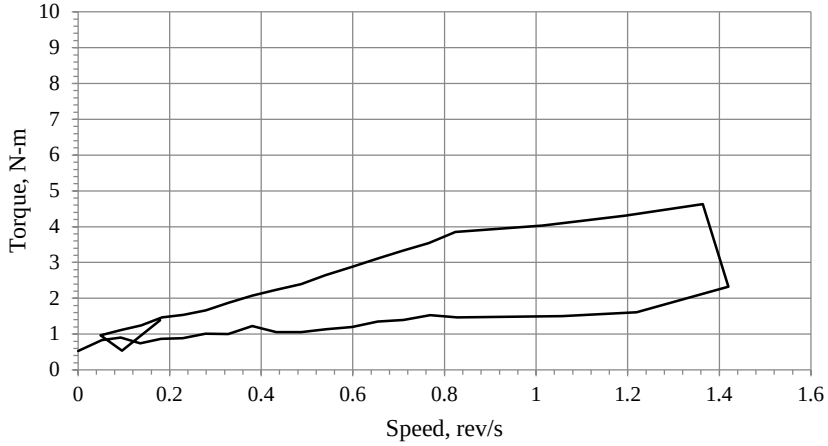

(15) LS221C

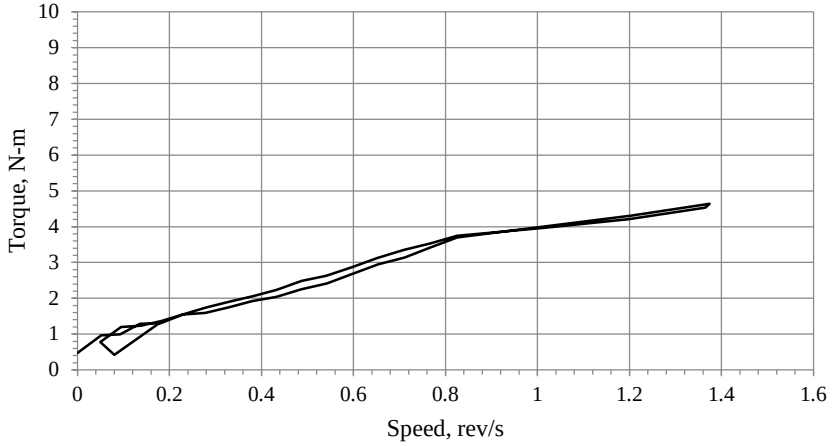

(16) LS221F

(Cont.) Figure C-9. Flow curve of CVC and SCC mixtures

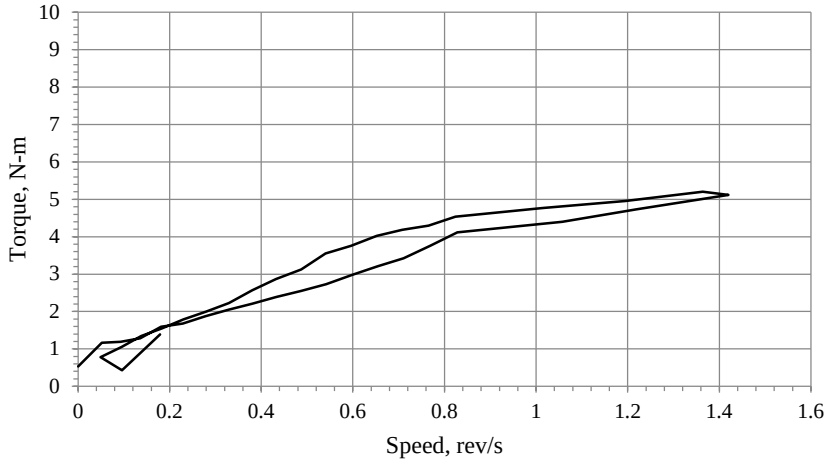

(17) LS221S

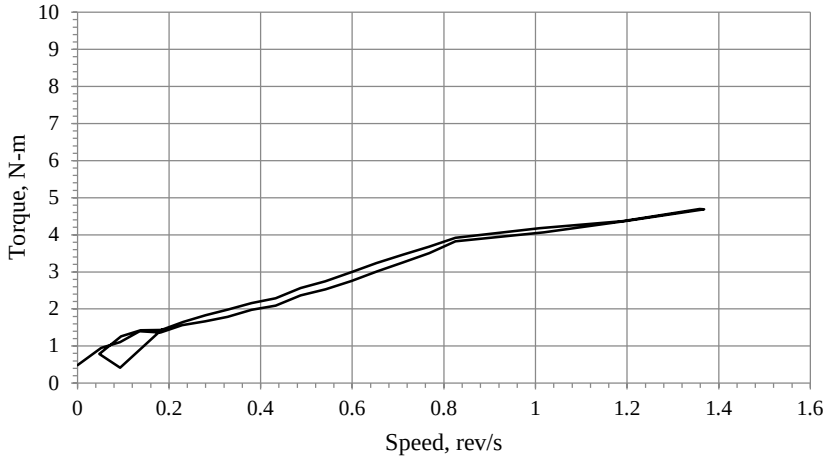

(18) LS221FLP

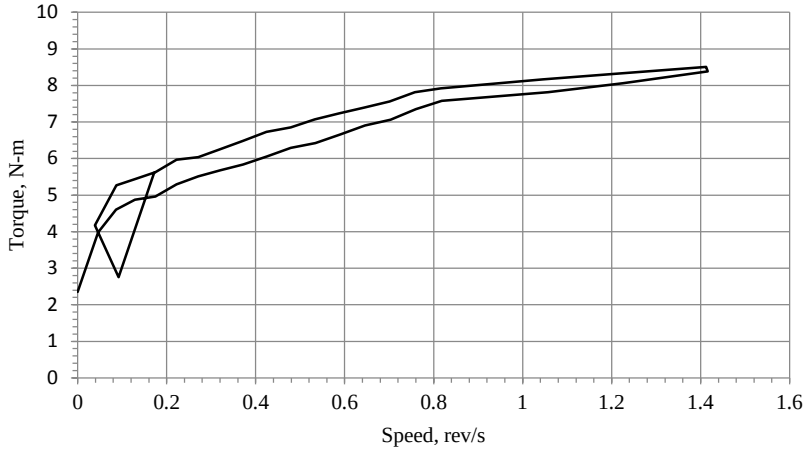

(19) LS0.375 CVC

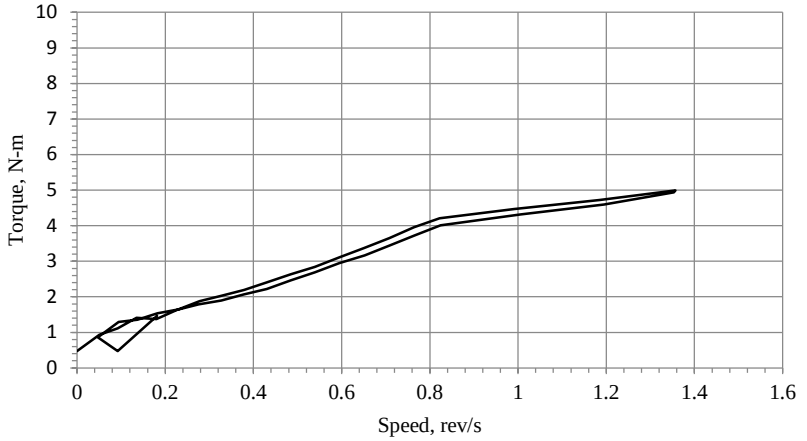

(20) LS222C

(Cont.) Figure C-9. Flow curve of CVC and SCC mixtures

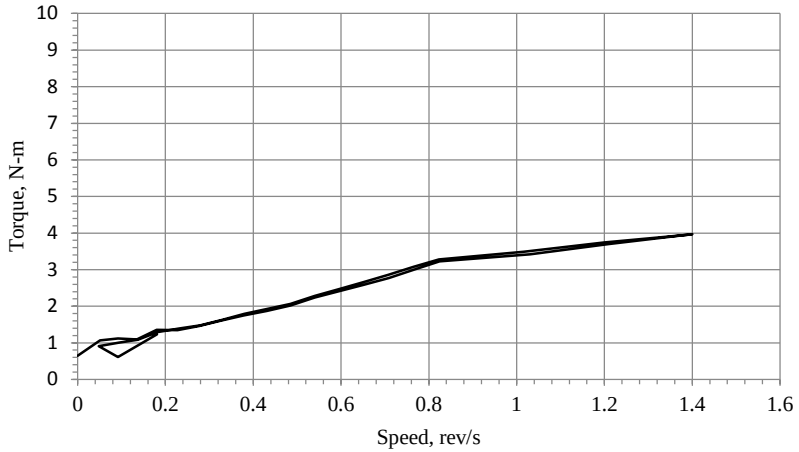

(21) LS222F

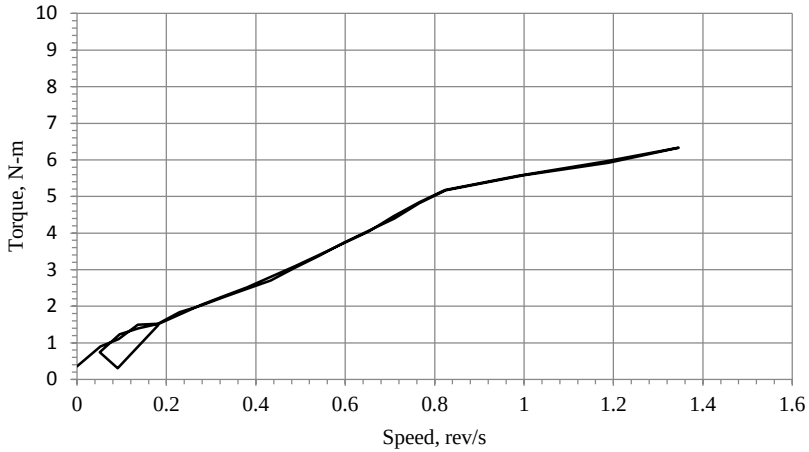

(22) LS222S

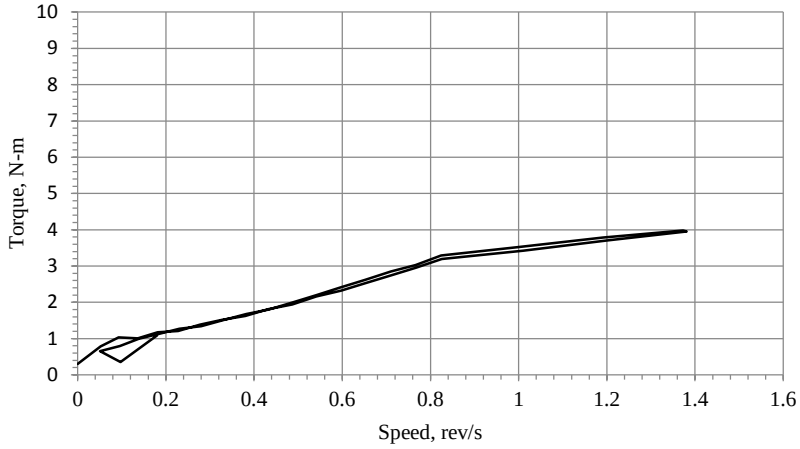

(23) LS222FLP

(Cont.) Figure C-9. Flow curve of CVC and SCC mixtures

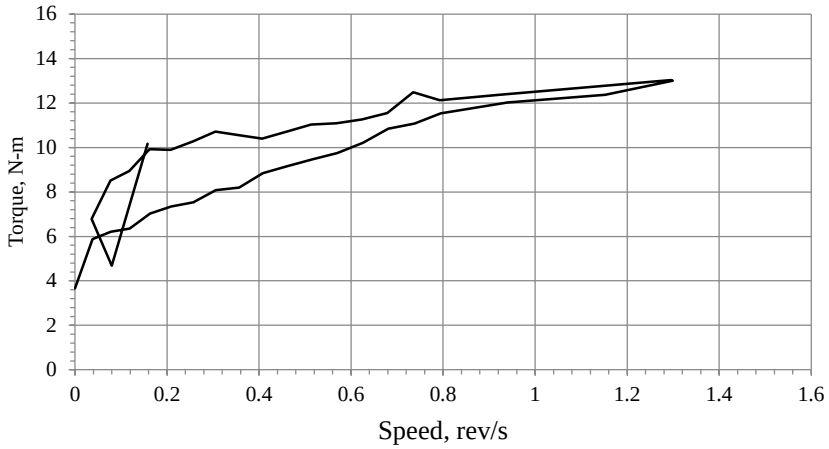

(24) G0.75 CVC

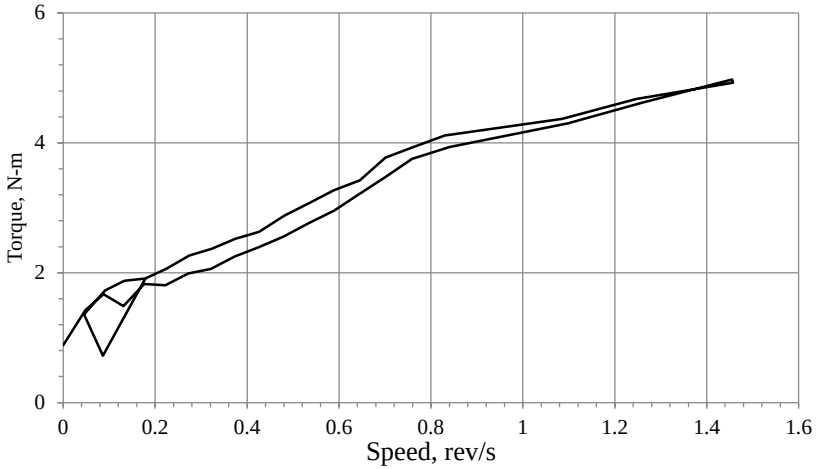

(25) G111C

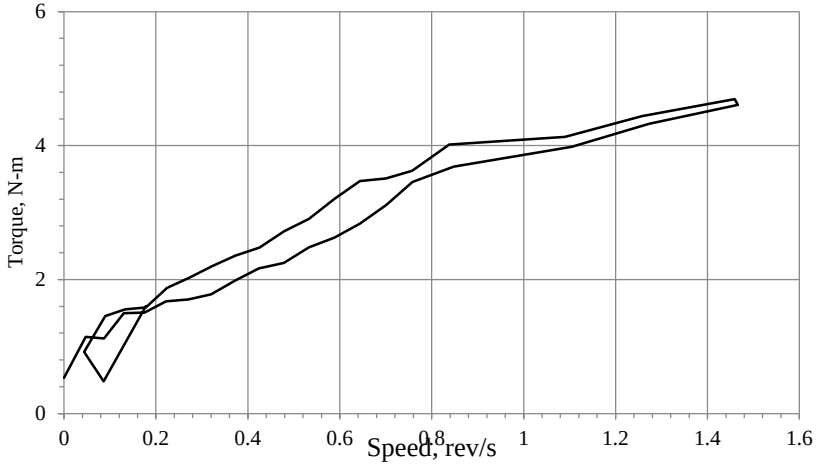

(26) G111F

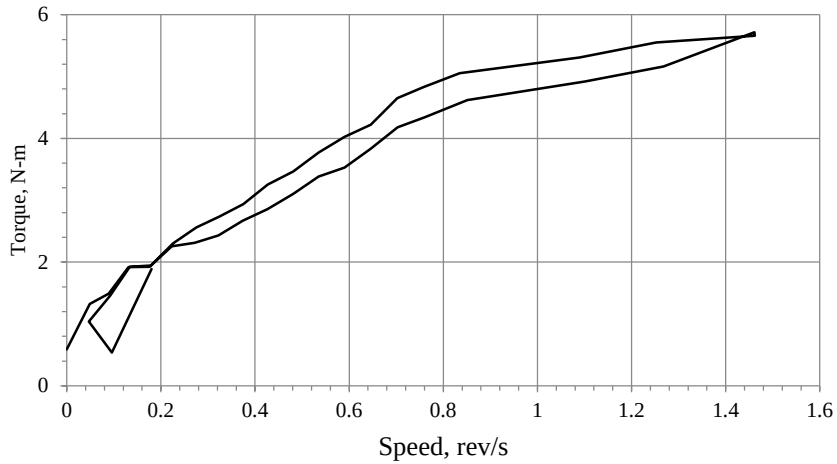

(27) G111S

(Cont.) Figure C-9. Flow curve of CVC and SCC mixtures

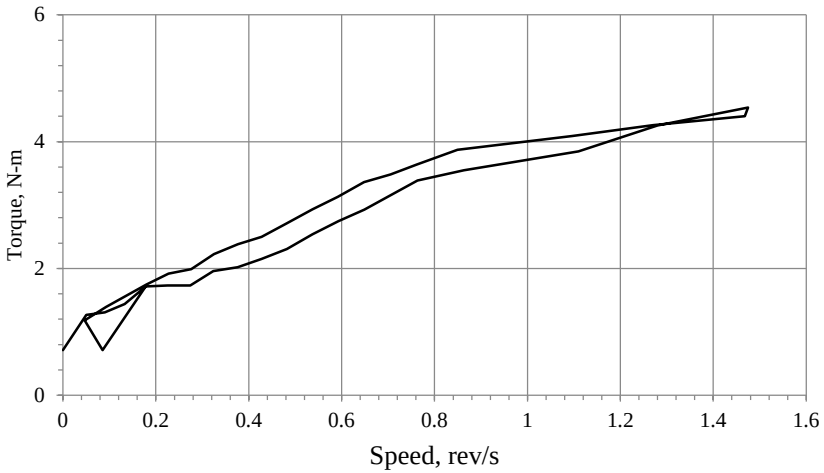

(28) G111FLP

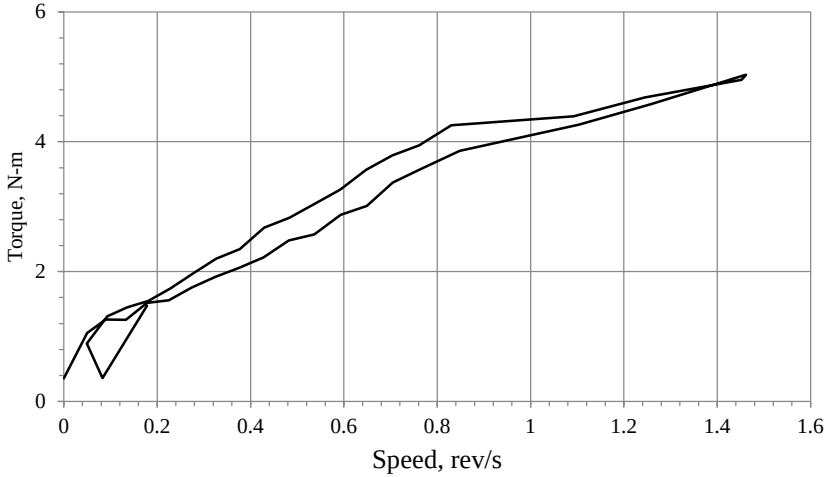

(29) G211C

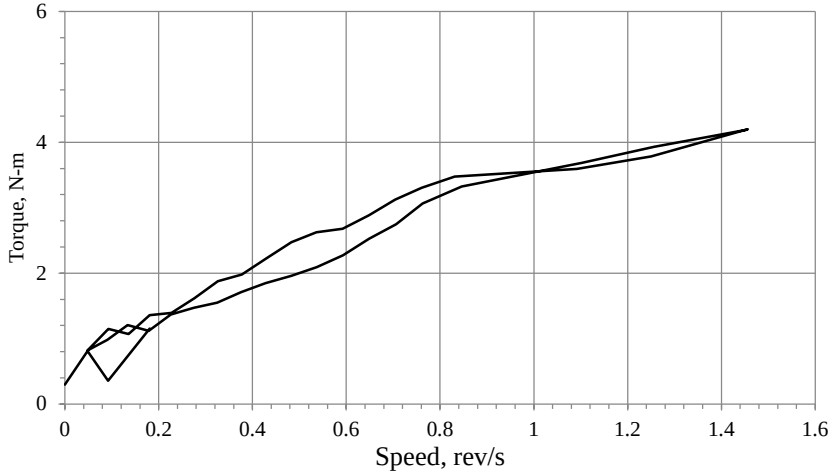

(30) G211F

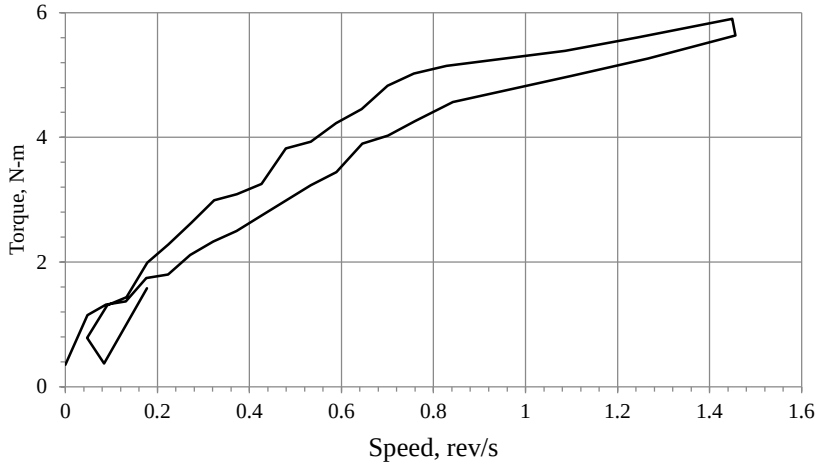

(31) G211S

(Cont.) Figure C-9. Flow curve of CVC and SCC mixtures

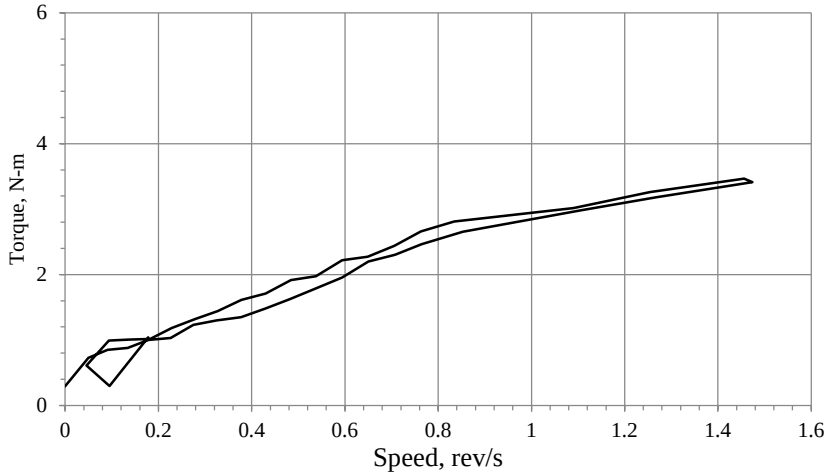

(32) G211FLP

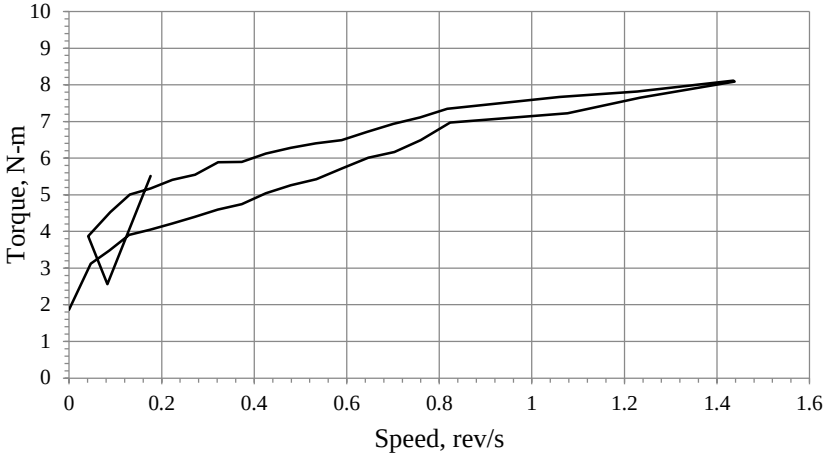

(33) G0.50 CVC

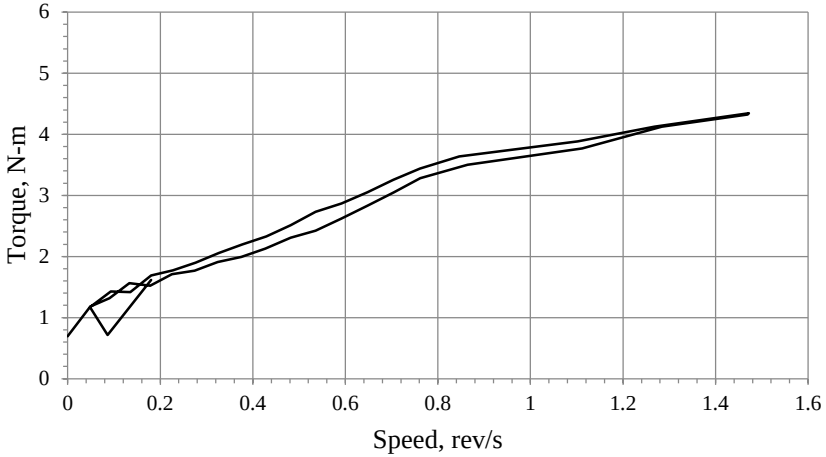

(34) G121C

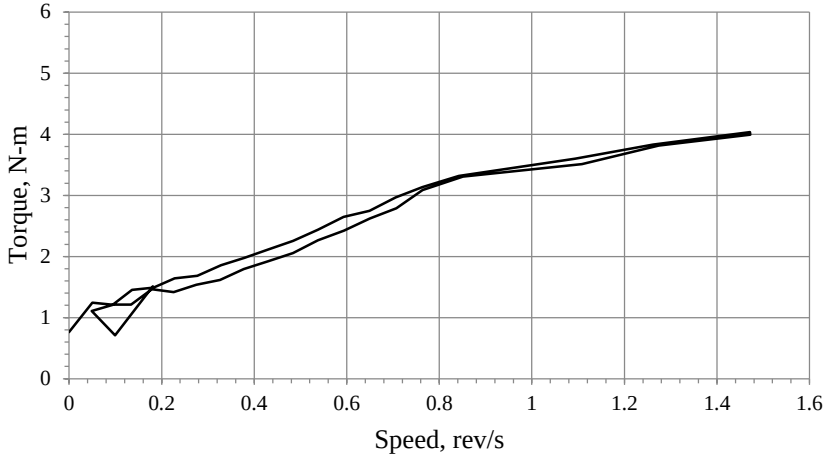

(35) G121F

(Cont.) Figure C-9. Flow curve of CVC and SCC mixtures

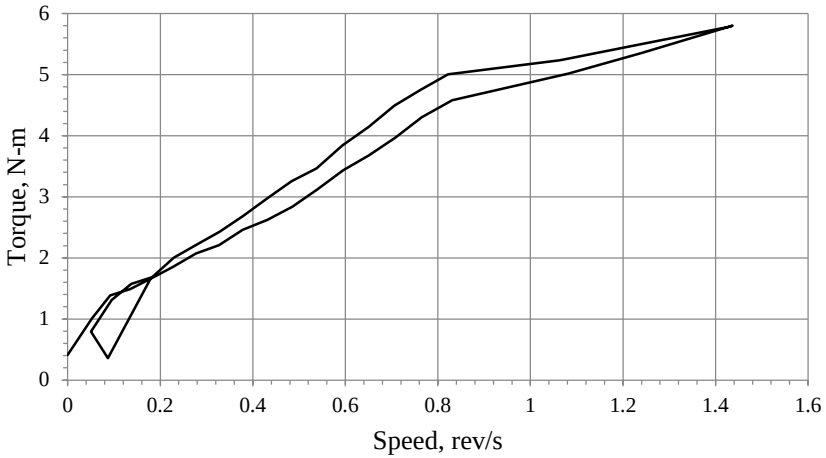

(36) G121S

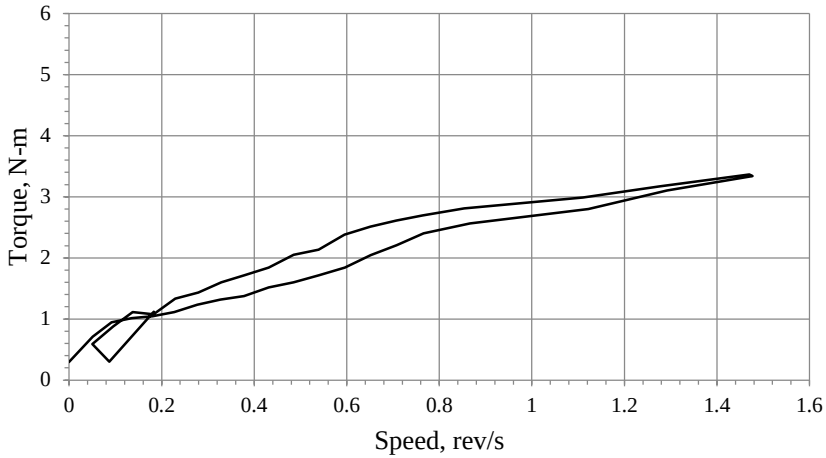

(37) G121FLP

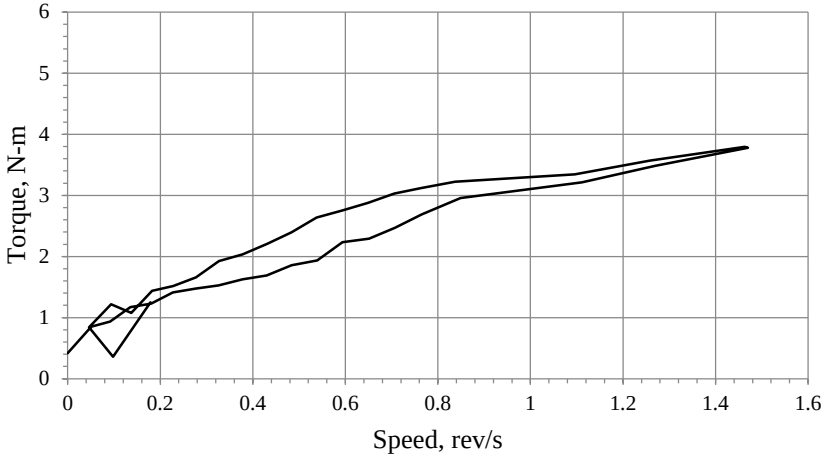

(38) G221C

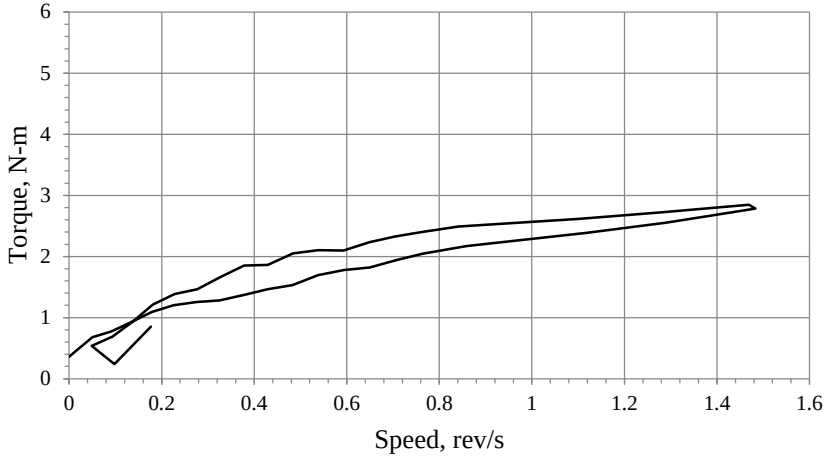

(39) G221F

(Cont.) Figure C-9. Flow curve of CVC and SCC mixtures

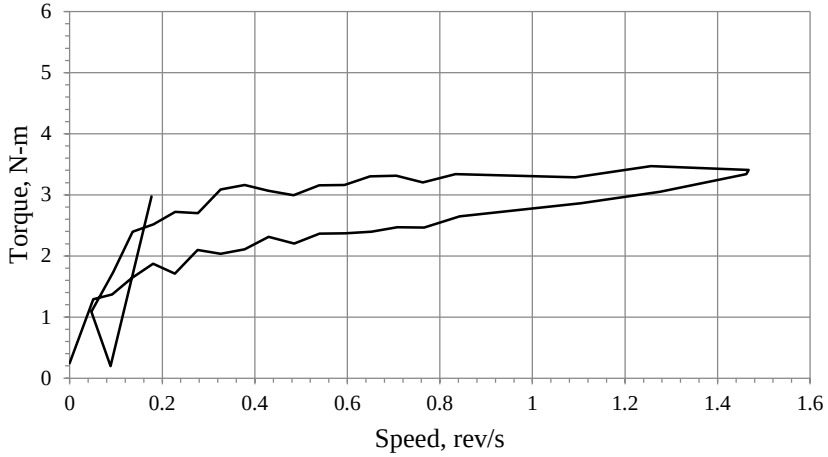

(40) G221S

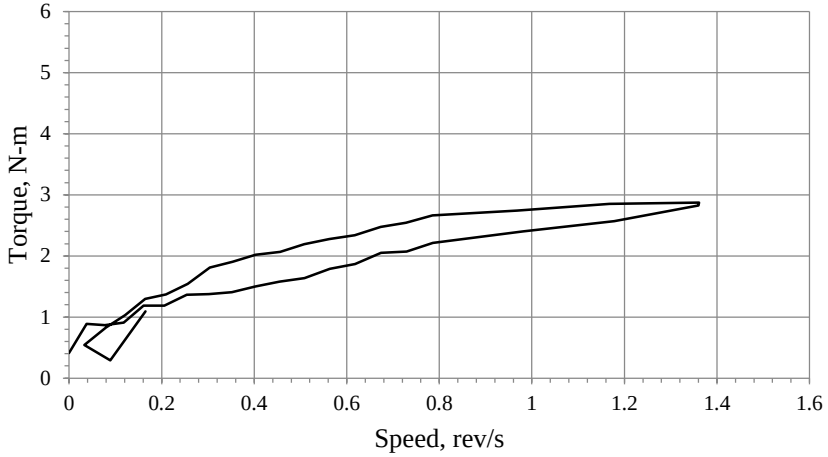

(41) G221FLP

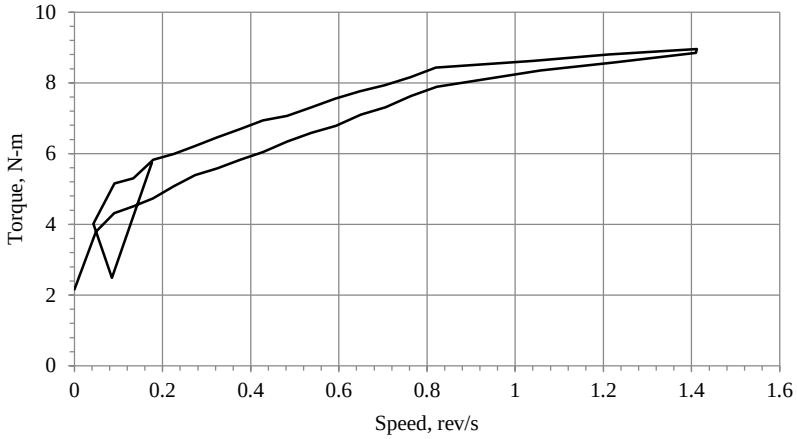

(42) G0.375 CVC

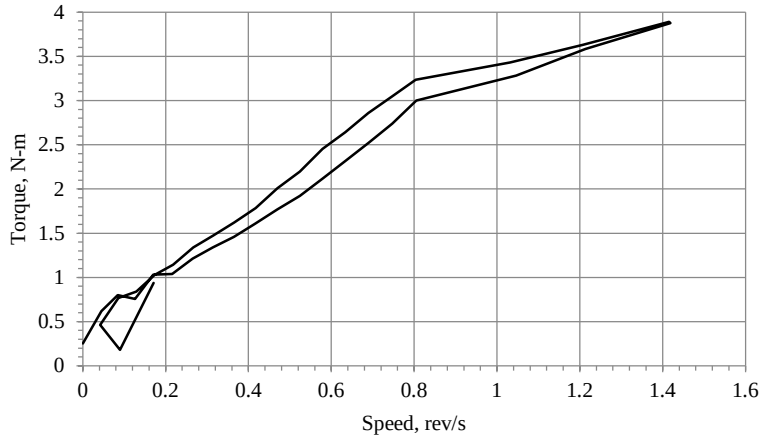

(43) G222C

(Cont.) Figure C-9. Flow curve of CVC and SCC mixtures

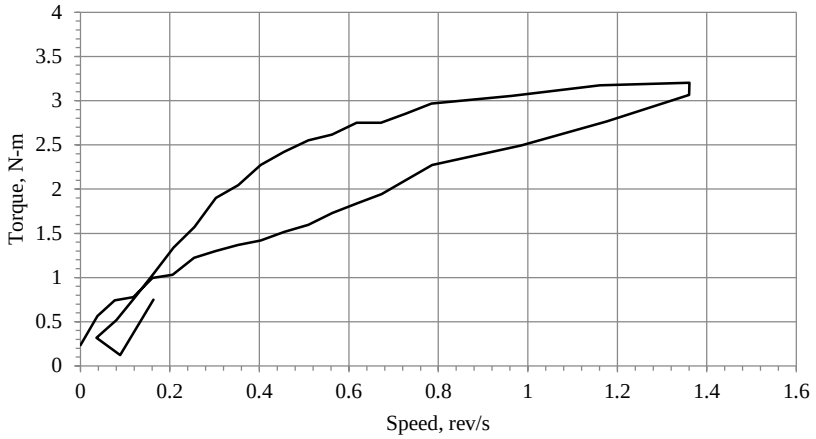

(44) G222F

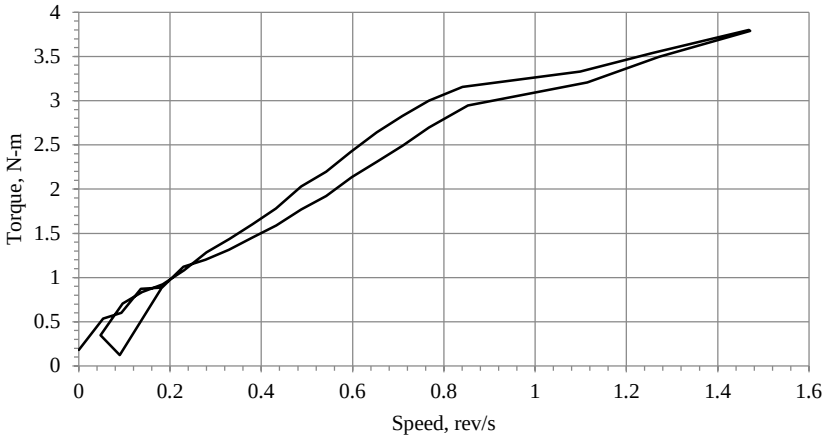

(45) G222S

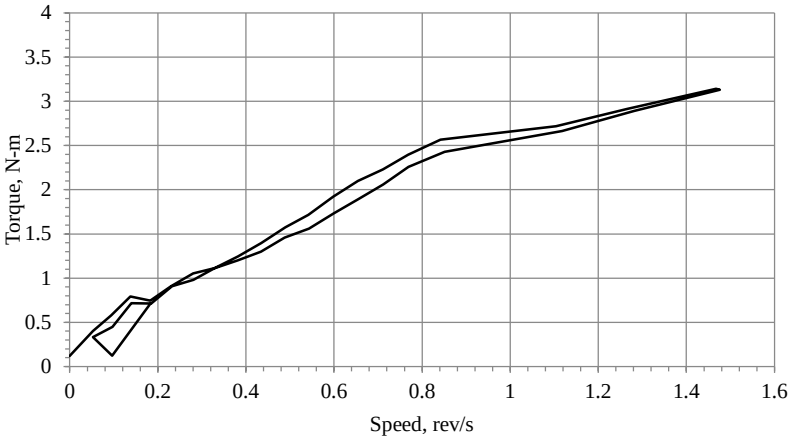

(46) G222FLP

(Cont.) Figure C-9. Flow curve of CVC and SCC mixtures

Table C-1. Summary of rheological properties for limestone mixtures

Mixture ID	Bingham Model Parameters for Mortar Rheology				Parameters for Concrete Rheology	
	Static yield stress	Dynamic yield stress	Plastic viscosity	Thixotropy	Yield torque	Slope
	Pa	Pa	Pa-s	Pa/s	N-m	N-m-s
LS0.75 CVC	251.03	142.05	1.56	1774.30	2.84	4.91
LS0.5 CVC	328.17	150.40	1.31	174.60	2.93	1.15
LS0.375 CVC	385.66	144.89	1.50	2335.60	4.60	3.12
LS111C	140.13	78.70	1.07	987.89	1.11	2.95
LS111F	90.71	61.95	0.93	859.30	1.01	2.94
LS111S	72.30	53.54	1.17	549.00	1.14	3.34
LS111FLP	86.91	49.87	0.83	714.32	1.02	2.87
LS211C	60.58	37.87	1.73	4114.00	0.78	3.89
LS211F	36.42	26.80	0.87	1593.25	0.61	3.32
LS211S	30.25	10.73	1.95	2989.50	0.54	4.78
LS2111FLP	74.88	53.11	1.08	1059.10	0.88	2.83
LS121C	59.55	45.44	0.97	2160.40	1.03	3.29
LS121F	86.54	51.56	1.07	1107.30	0.84	3.13
LS121S	88.23	47.08	1.39	1787.60	1.00	3.96
LS121FLP	65.93	40.73	0.89	1210.98	0.84	2.48
LS221C	48.28	29.29	0.71	1029.37	0.65	1.03
LS221F	61.45	39.50	1.03	1140.80	0.80	3.08
LS221S	29.99	14.77	1.08	1177.66	0.68	3.30
LS221FLP	41.44	30.88	0.82	958.30	0.86	3.11
LS222C	50.57	24.61	1.00	3291.00	0.87	3.35
LS222F	38.49	27.60	0.88	2097.50	0.87	2.47
LS222S	53.21	20.29	1.73	3078.00	0.78	4.69
LS222FLP	47.48	33.30	1.09	1485.70	0.70	2.64

Table C-2. Summary of rheological properties for gravel mixtures

Mixture ID	Bingham Model Parameters for Mortar Rheology				Parameters for Concrete Rheology	
	Static yield stress	Dynamic yield stress	Plastic viscosity	Thixotropy	Yield torque	Slope
	Pa	Pa	Pa-s	Pa/s	N-m	N-m-s
G0.75 CVC	504.53	147.56	1.80	2070.90	6.151	6.08
G0.5 CVC	253.30	115.50	1.38	1420.90	3.601	3.47
G0.375 CVC	339.03	119.61	1.49	587.12	3.875	4.28
G111C	187.81	87.63	1.89	1168.00	3.792	1.282
G111F	95.19	50.72	0.79	1440.80	2.705	1.038
G111S	96.83	45.16	1.42	1659.80	3.238	1.496
G1111FLP	77.69	43.50	0.64	1104.93	2.506	1.168
G211C	80.99	38.63	1.23	2239.83	3.014	0.984
G211F	59.32	18.58	0.82	1849.74	2.628	0.756
G211S	57.39	13.50	1.98	3851.90	2.145	1.191
G211FLP	20.84	12.83	0.57	960.00	2.106	0.645
G121C	86.63	55.20	0.77	1209.90	2.681	1.178
G121F	62.52	44.47	0.62	681.34	2.317	0.994
G121S	52.60	31.10	1.15	1735.87	2.716	1.058
G121FLP	41.94	25.92	0.59	1151.50	1.914	0.716
G221C	57.68	25.98	0.52	1454.50	2.171	0.841
G221F	17.44	8.36	0.40	512.90	1.486	0.791
G221S	17.33	1.39	0.68	1584.53	1.381	1.478
G221FLP	29.82	15.77	0.46	659.90	1.555	0.871
G222C	45.81	18.93	0.88	2080.75	2.605	0.561
G222F	26.75	9.75	0.74	1211.30	1.436	0.682
G222S	10.26	0.00	0.53	970.30	1.492	0.525
G222FLP	27.64	11.36	0.69	1108.30	2.031	0.453

2. Workability Properties

Figure C-10. Slump flow test

Figure C-11. J-ring test

Figure C-12. Caisson Test

Figure C-13. Column segregation test

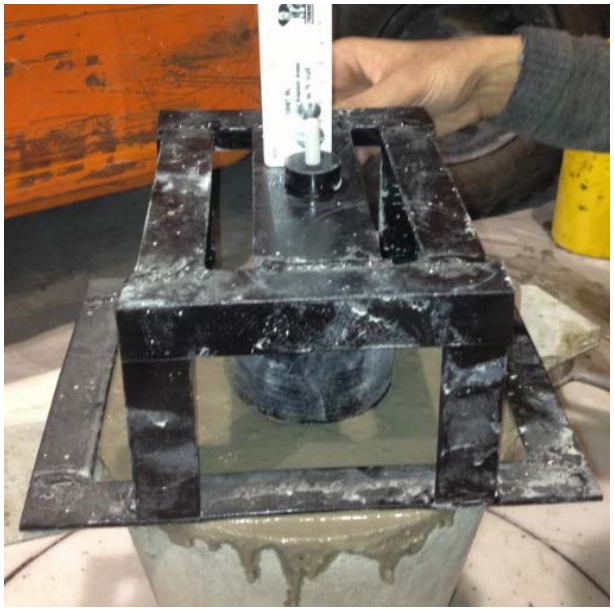

Figure C-14. Rapid penetration test

Figure C-15. Modified long trough test

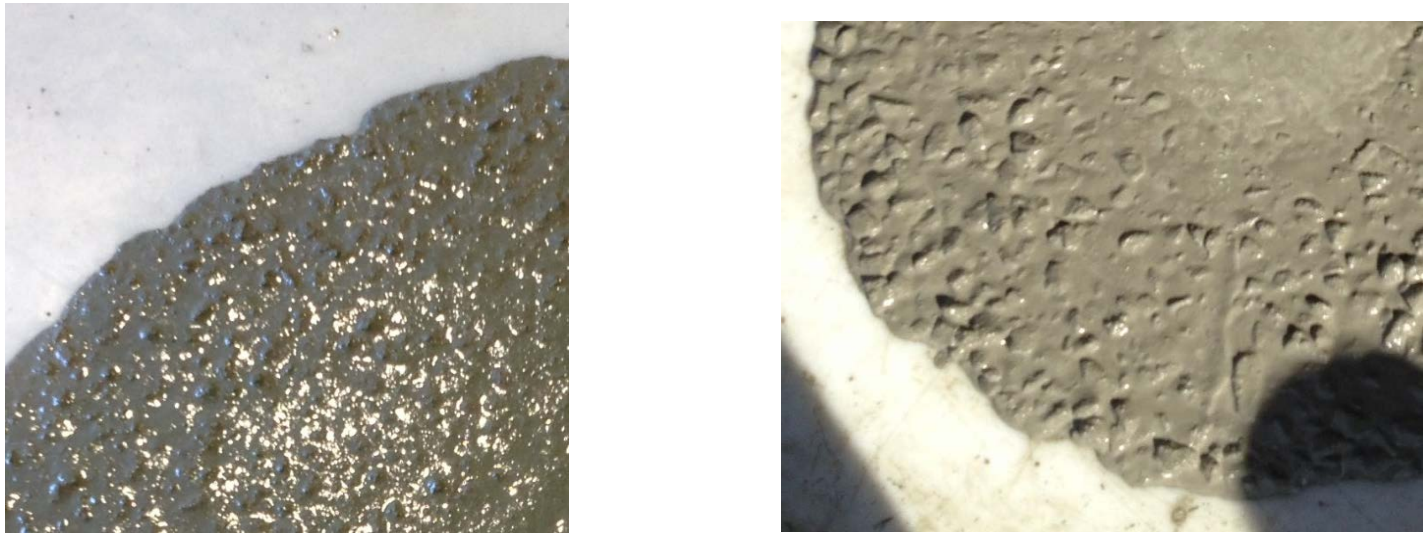

Figure C-16. Examples of visual stability index (VSI) of 0 (left) and 1 (right)

Figure C-17. Examples of hardened visual stability index (HVSI) of 0 (left) and 1 (right)

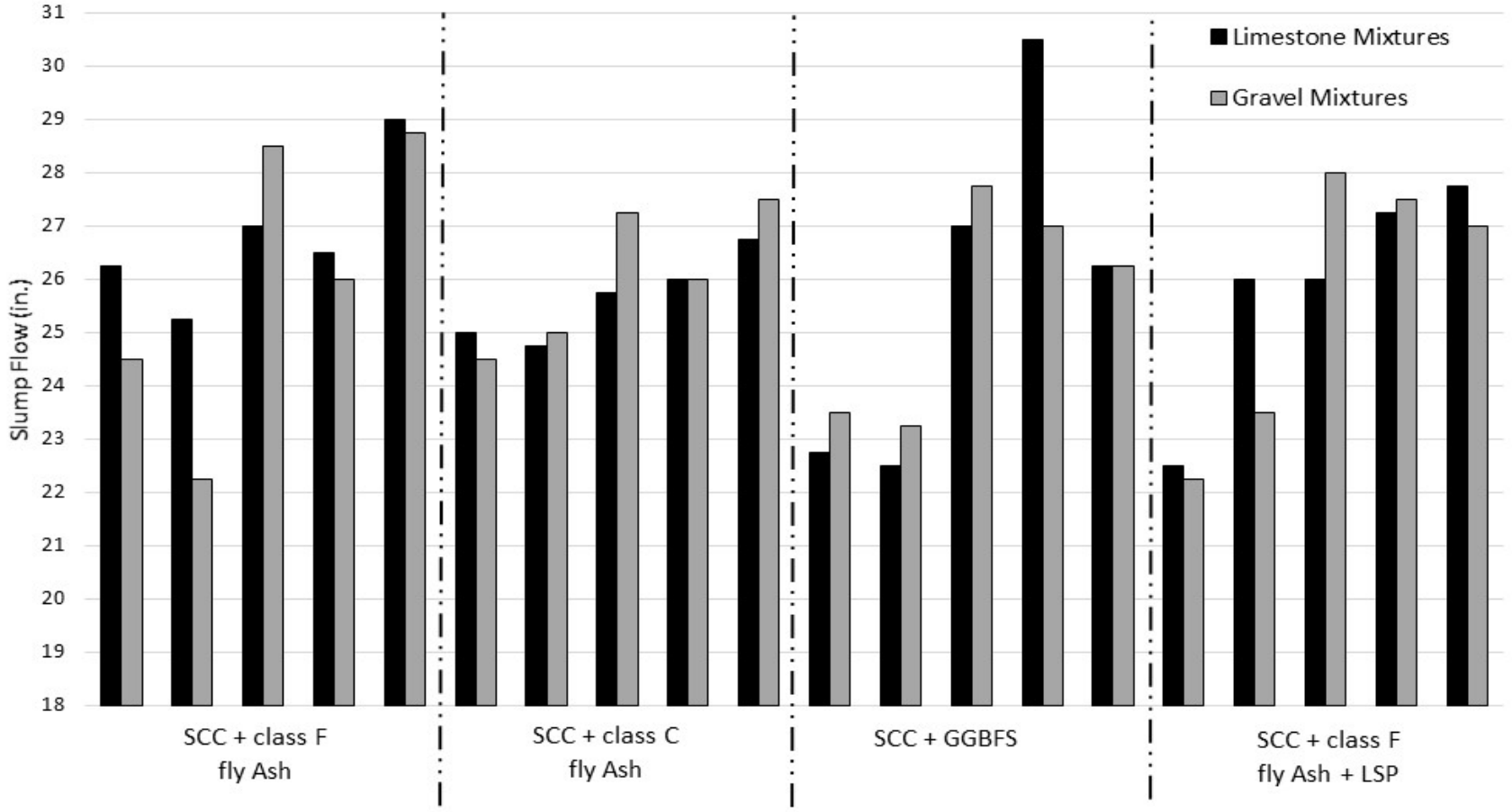

Figure C-18. Average slump flow for SCC and CVC mixtures with limestone and gravel aggregates

Table C-3. Summary of workability properties for limestone mixtures

Coarse Aggregate Type	NMSA	ID	Slump Flow			J-Ring		Caisson	Penetration	Column Technique	Long trough	Static Stability
			D_{av} (in.)	T_{50}	VSI	ΔD (in.)	ΔH (in.)	FC (%)	P_d (in.)	Seg. Static (%)	Seg. Dynamic (%)	HVSI
Limestone	3/4 in.	LS111C	25.75	1.90	0	4.00	0.56	75.5%	0.16	5.2%	7.23%	1
	3/4 in.	LS111F	26.25	1.20	1	4.50	0.56	79.0%	0.08	13.2%	N/A	0
	3/4 in.	LS111FLP	22.50	1.90	0	1.50	0.63	70.2%	0.13	2.1%	N/A	0
	3/4 in.	LS111S	22.75	1.70	0	3.25	0.63	80.6%	0.25	4.2%	N/A	1
	3/4 in.	LS211C	25.00	< 2.0	0	0.75	0.25	75.5%	0.12	0.4%	31.96%	1
	3/4 in.	LS211F	27.00	1.20	1	2.50	0.56	86.1%	0.25	3.9%	35.70%	1
	3/4 in.	LS211FLP	26.00	<2	1	0.75	0.44	81.4%	0.25	13.9%	24.33%	1
	3/4 in.	LS211S	27.00	2.00	1	0.50	0.50	78.3%	0.38	10.8%	10.17%	0
	½ in.	LS121C	24.75	< 2.0	1	1.25	0.19	80.8%	0.13	2.0%	N/A	0
	½ in.	LS121F	25.25	< 2.0	0	0.88	0.15	91.5%	0.24	10.1%	N/A	0
	½ in.	LS121FLP	26.00	< 2.0	1	0.25	0.38	91.2%	0.25	4.9%	N/A	0
	½ in.	LS121S	22.50	< 2.0	0	0.50	0.56	81.7%	0.25	0.0%	N/A	1
	½ in.	LS221C	26.00	2.00	0	0.25	0.13	71.4%	0.16	2.1%	5.21%	1
	½ in.	LS221F	26.50	< 2.0	0	1.50	0.44	79.6%	0.20	5.2%	39.86%	1
	½ in.	LS221FLP	27.25	< 2.0	1	0.25	0.13	94.2%	0.50	8.1%	23.43%	1
	½ in.	LS221S	30.50	< 2.0	0	1.00	0	95.8%	0.13	5.50%	35.60%	1
	3/8 in.	LS222C	26.75	< 2.0	0	0.50	0.50	83.3%	0.16	3.4%	25.48%	0
	3/8 in.	LS222F	29.00	< 2.0	1	0.50	0.25	91.4%	0.08	0.0%	11.90%	1
	3/8 in.	LS222FLP	27.75	1.70	0	0.25	N/A	93.7%	0.25	3.8%	N/A	0
	3/8 in.	LS222S	26.25	2.70	0	0.00	0.31	89.5%	0.55	3.0%	18.26%	0

Table C-4. Summary of workability properties for gravel mixtures

Coarse Aggregate Type	NMSA	ID	Slump Flow			J-Ring		Caisson	Penetration	Column Technique	Long trough	Static Stability
			D_{av} (in.)	T_{50}	VSI	ΔD (in.)	ΔH (in.)	FC (%)	P_d (in.)	Seg. (%)	Seg. (%)	HVSI
Gravel	3/4 in.	G111C	24.50	1.60	1	2.00	0.50	86.2%	0.13	12.7%	N/A	1
	3/4 in.	G111F	24.50	1.20	1	1.25	0.25	90.2%	0.25	9.5%	N/A	1
	3/4 in.	G111FLP	22.25	1.44	0	0.25	0.75	73.2%	0.00	17.4%	N/A	1
	3/4 in.	G111S	23.50	1.87	0	0.75	0.63	82.8%	0.13	9.8%	N/A	0
	3/4 in.	G211C	27.25	1.29	1	0.75	0.25	91.8%	0.50	3.7%	19.3%	1
	3/4 in.	G211F	28.50	1.20	1	0.50	0.00	96.2%	0.75	18.9%	45.0%	1
	3/4 in.	G211FLP	28.00	1.60	1	1.25	0.25	94.1%	0.63	19.3%	37.6%	1
	3/4 in.	G211S	27.75	2.30	1	0.75	0.25	95.1%	1.00	18.4%	45.5%	1
	½ in.	G121C	25.00	1.04	0	1.00	0.13	87.6%	0.25	1.0%	N/A	1
	½ in.	G121F	22.25	1.40	0	2.75	0.75	71.2%	0.00	4.8%	N/A	0
	½ in.	G121FLP	23.50	1.03	0	1.25	0.25	89.6%	0.13	5.1%	N/A	0
	½ in.	G121S	23.25	1.80	0	0.00	0.50	82.3%	0.25	2.7%	6.9%	1
	½ in.	G221C	26.00	1.50	0	1.00	0.25	94.4%	0.50	4.1%	25.5%	0
	½ in.	G221F	26.00	1.10	0	0.50	0.25	88.4%	0.25	1.4%	4.3%	0
	½ in.	G221FLP	27.50	0.90	1	0.50	0.25	93.9%	0.50	9.0%	20.9%	1
	½ in.	G221S	27.00	2.30	0	0.00	0.50	92.4%	0.25	12.7%	16.8%	0
	3/8 in.	G222C	27.50	1.39	0	1.50	0.25	93.9%	0.63	5.1%	15.6%	0
	3/8 in.	G222F	28.75	1.28	1	0.75	0.25	93.5%	1.00	11.4%	15.8%	0
	3/8 in.	G222FLP	27.00	1.13	0	0.75	0.00	95.2%	0.63	12.4%	2.4%	0
	3/8 in.	G222S	26.25	1.80	1	0.50	0.25	89.5%	0.25	18.1%	5.0%	0

2. Workability Retention

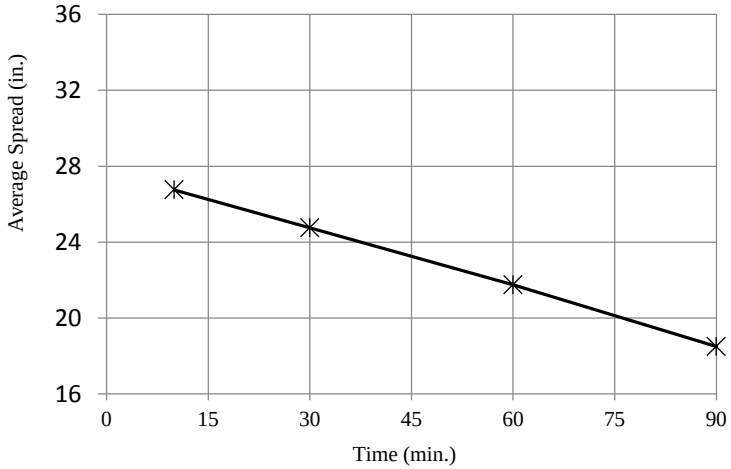

(1) LS121C

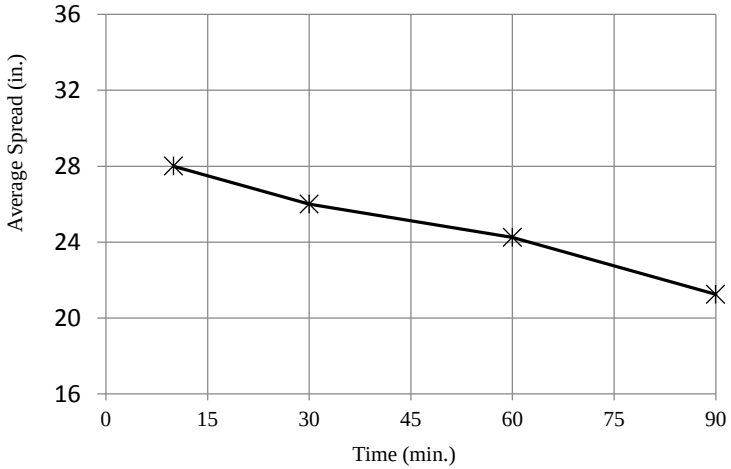

(2) LS221C

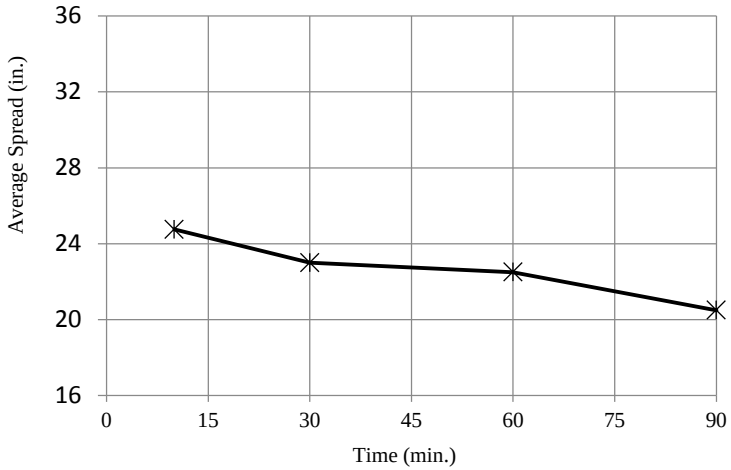

(3) LS121F

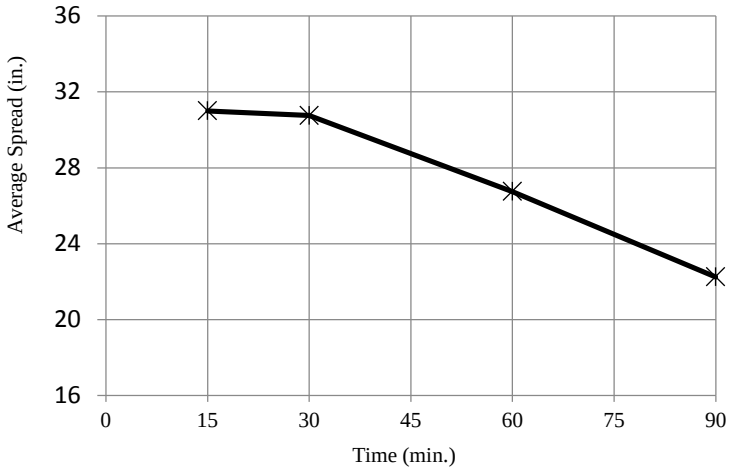

(4) LS221F

Figure C-19. Losing flowability with time for SCC mixtures

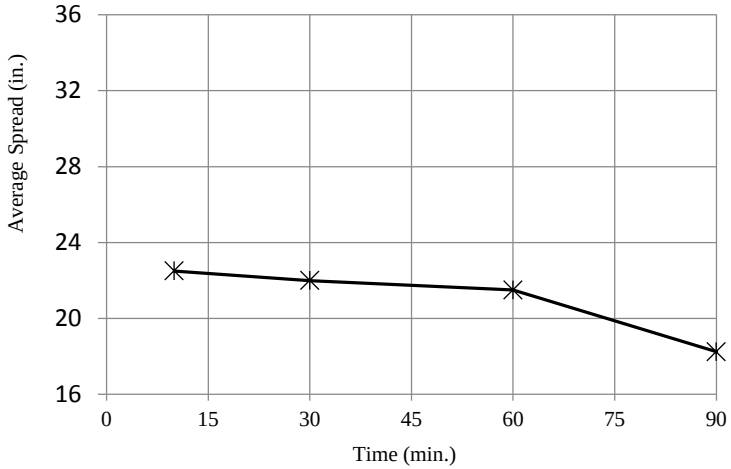

(5) LS121S

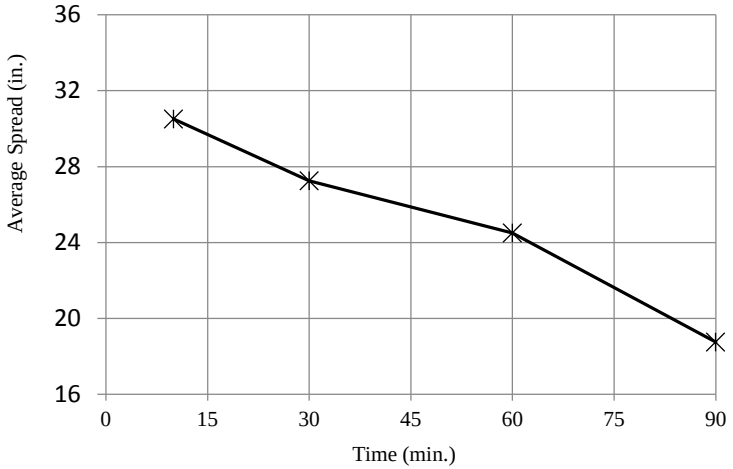

(6) LS221S

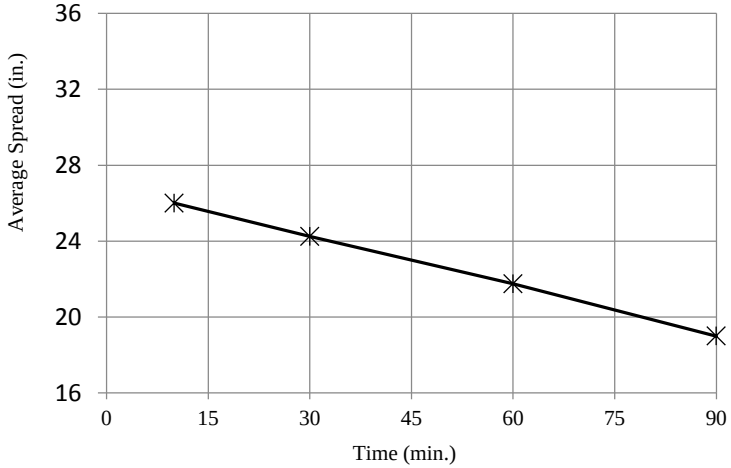

(7) LS121FLP

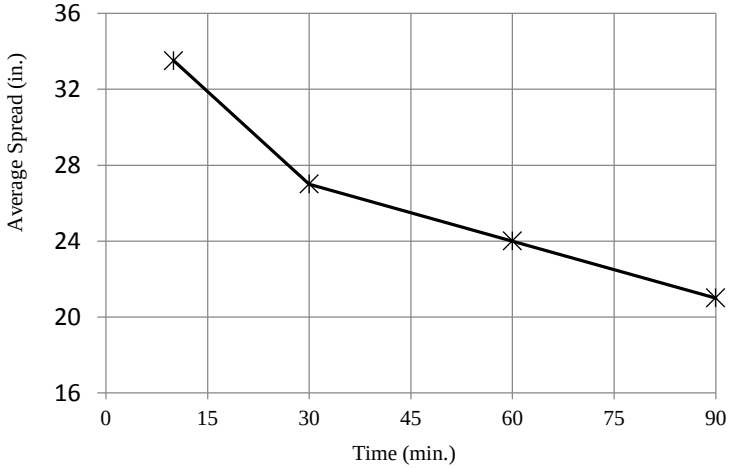

(8) LS221FLP

(cont.) Figure C-19. Losing flowability with time for SCC mixtures

APPENDIX D: Early-Age Concrete Properties

Contents

1. Formwork pressure

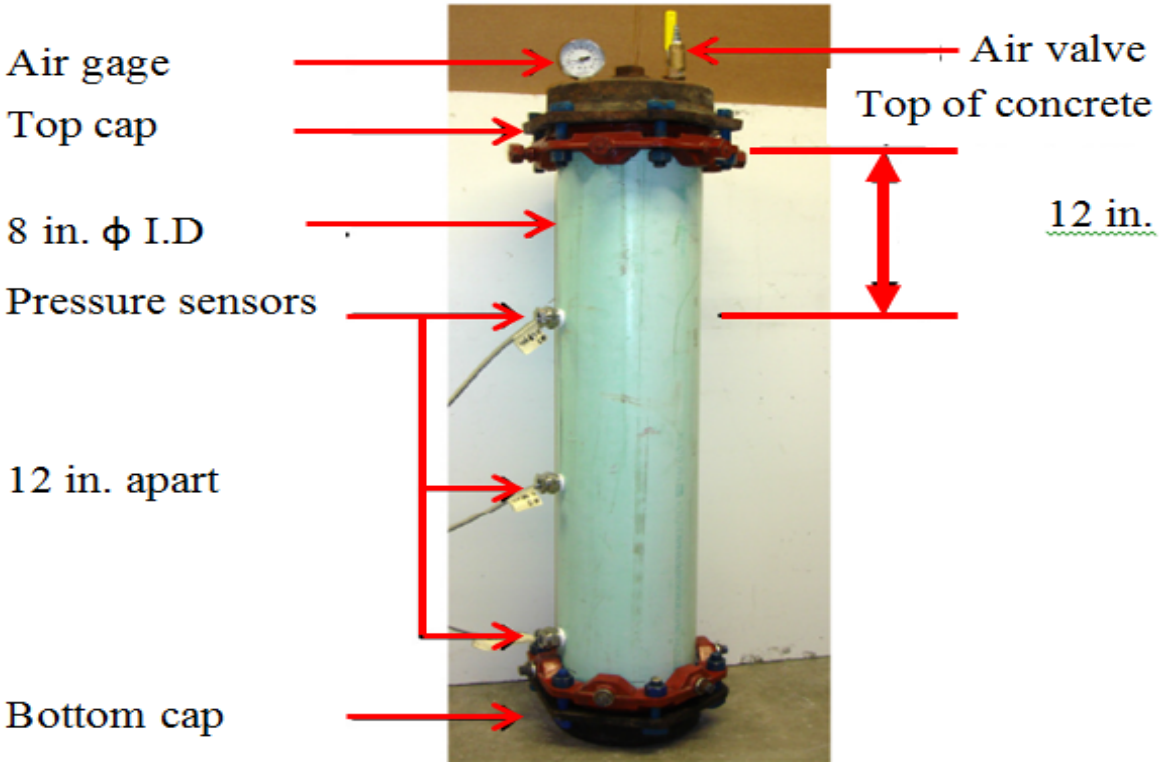

Figure D-1. Form pressure device setup

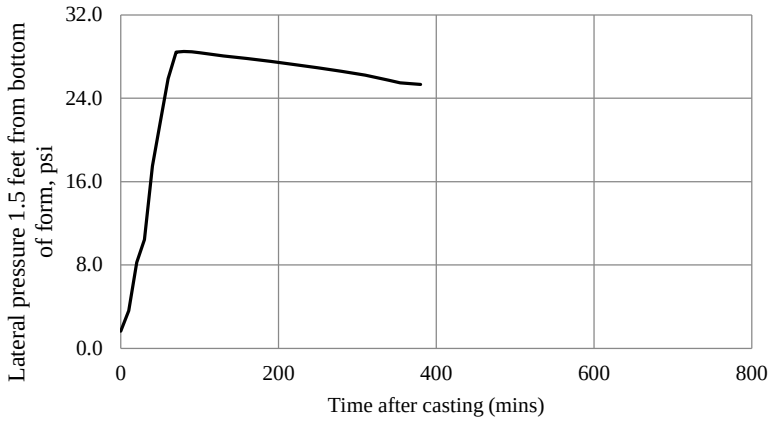

(1) LS0.75 CVC

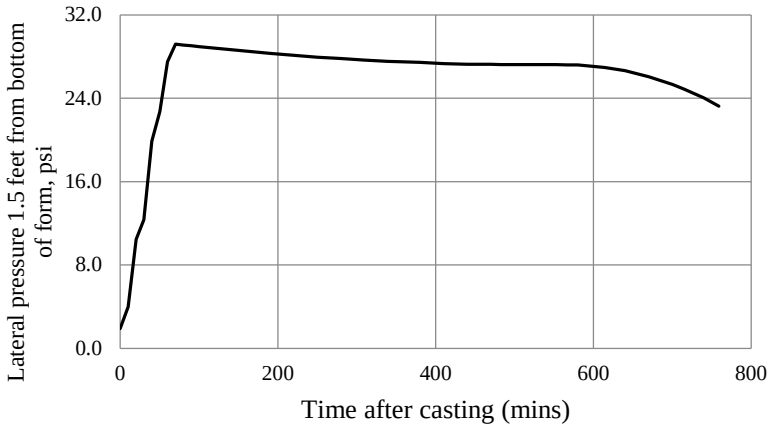

(2) LS211C

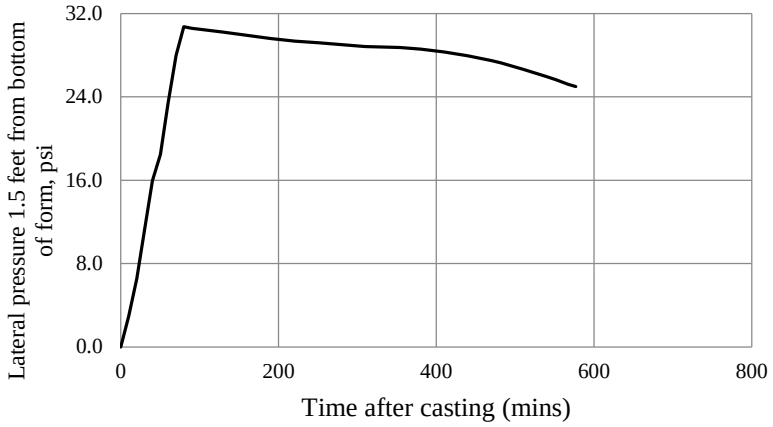

(3) LS211F

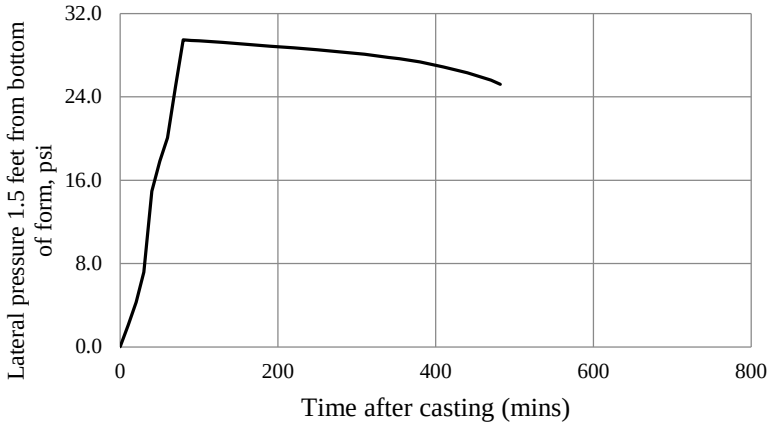

(4) LS211S

Figure D-2 Relation between time after casting and lateral pressure at 1.5 feet from the bottom of form

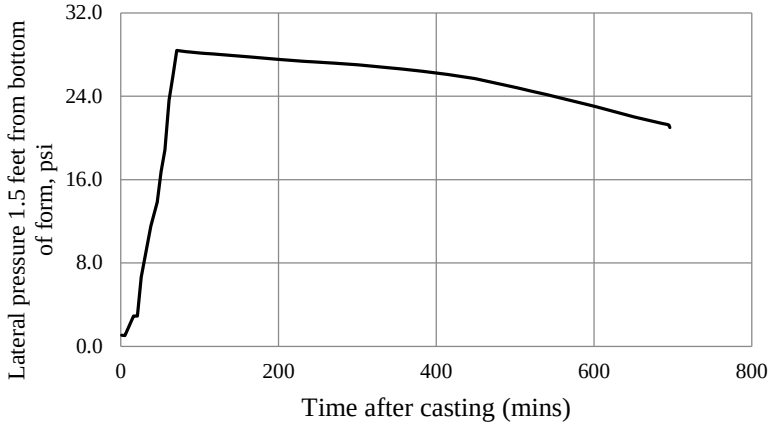

(5) LS211FLP

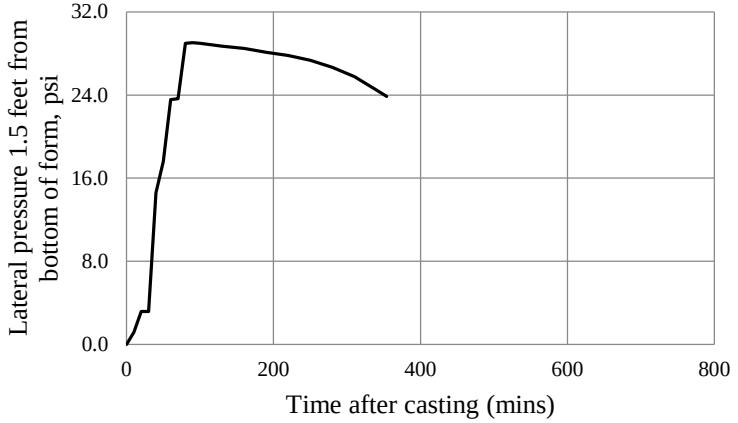

(6) LS0.50 CVC

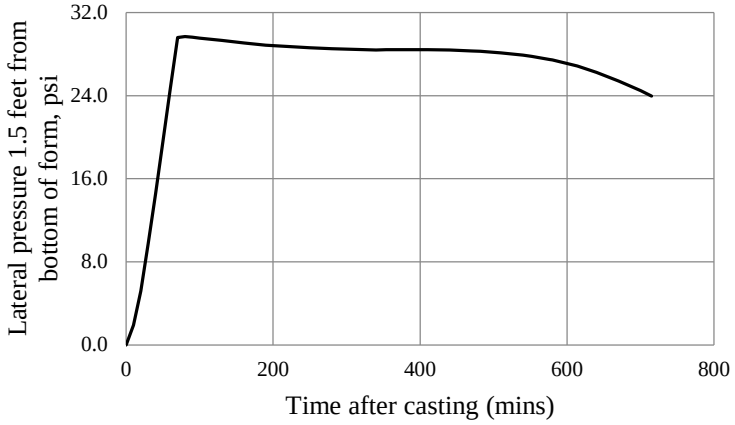

(7) LS121C

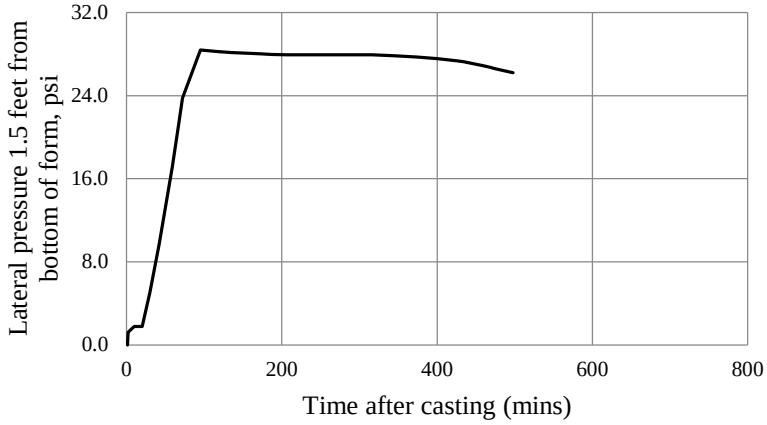

(8) LS121F

(cont.) Figure D-2 Relation between time after casting and lateral pressure at 1.5 feet from the bottom of form

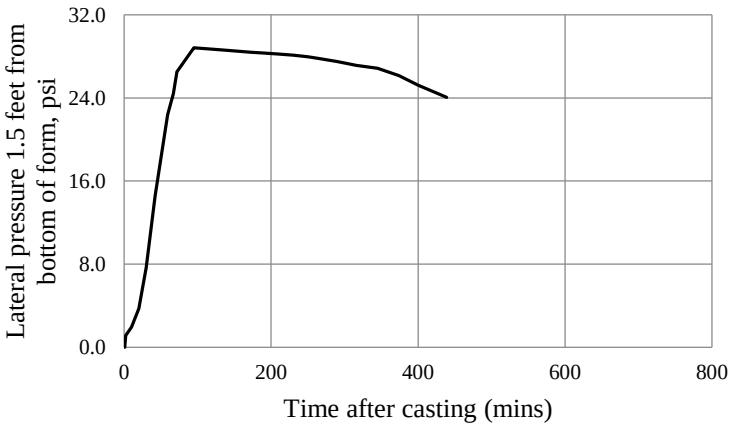

(9) LS121S

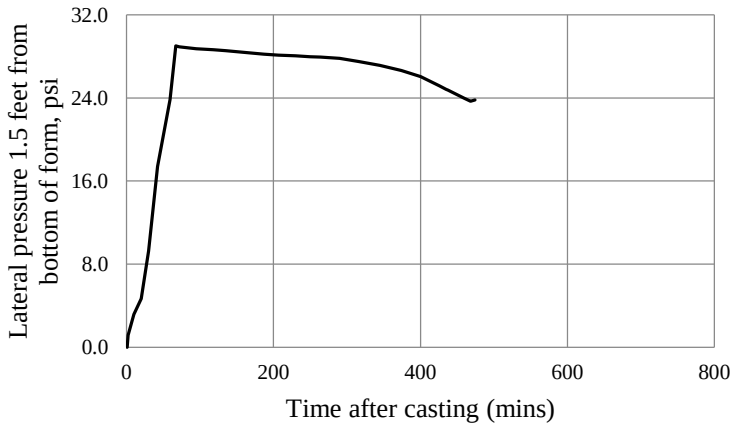

(10) LS121FLP

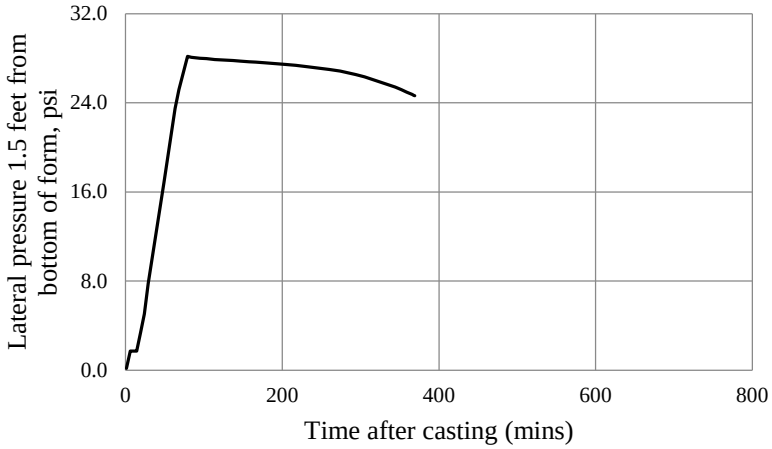

(11) LS0.375 CVC

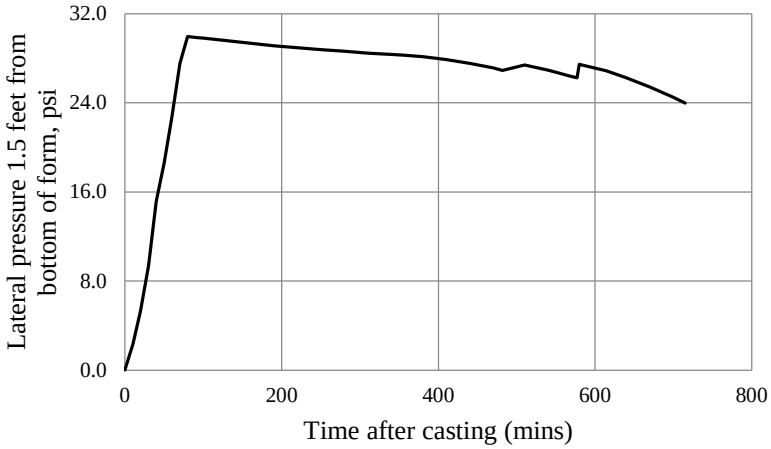

(12) LS222C

(cont.) Figure D-2 Relation between time after casting and lateral pressure at 1.5 feet from the bottom of form

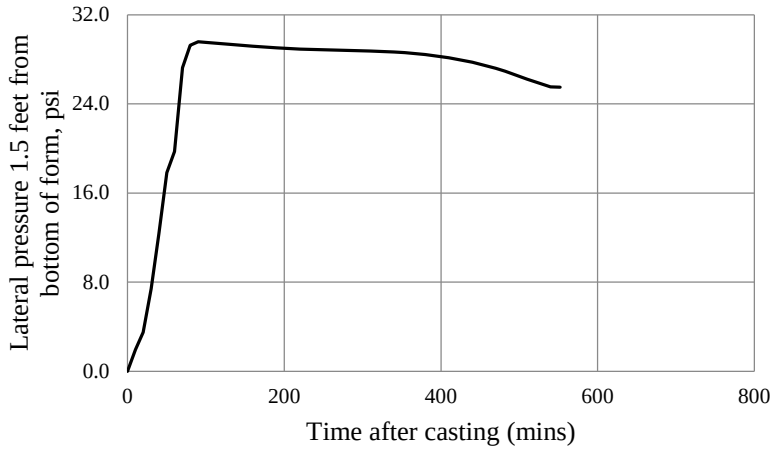

(13) LS222F

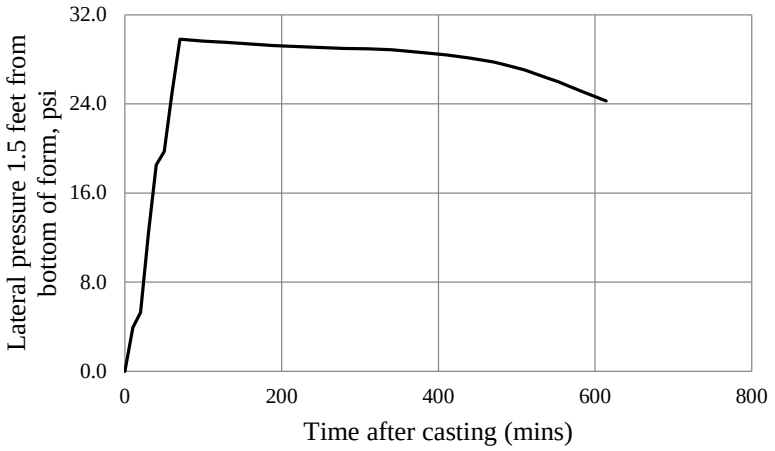

(14) LS222S

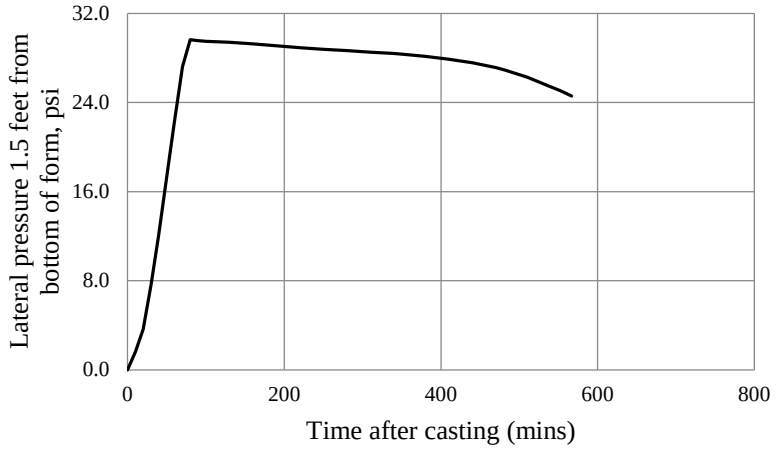

(15) LS222FLP

(cont.) Figure D-2 Relation between time after casting and lateral pressure at 1.5 feet from the bottom of form

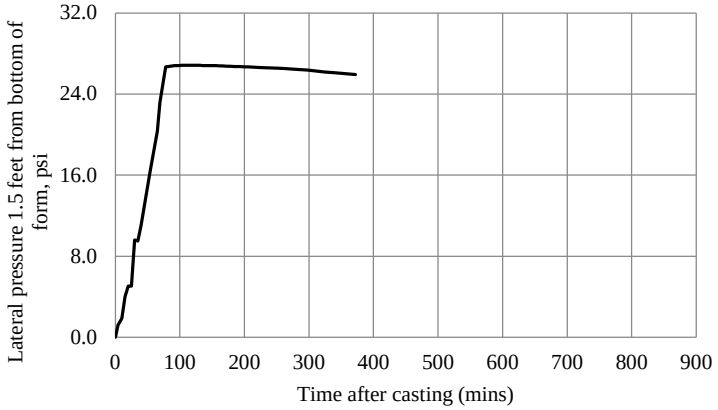

(16) G0.75 CVC

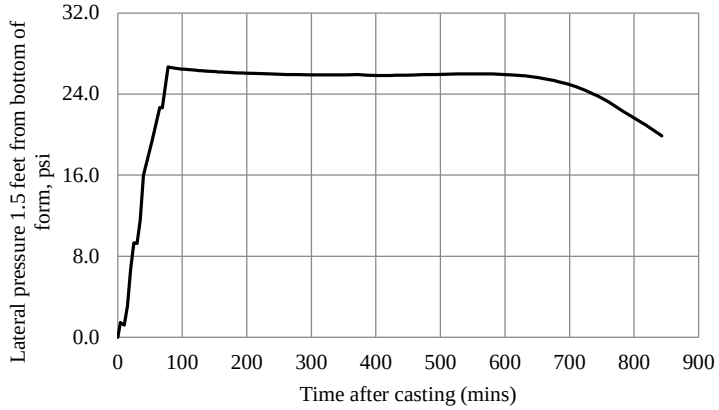

(17) G211C

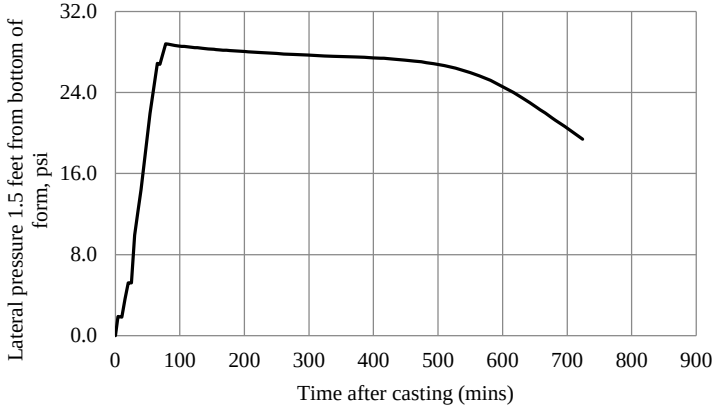

(18) G211F

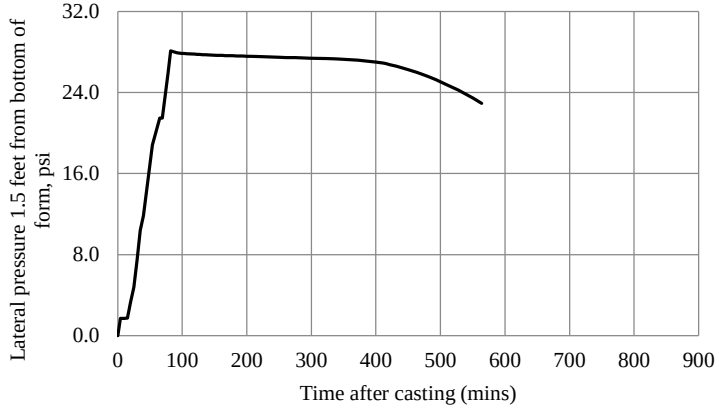

(19) G211S

(cont.) Figure D-2 Relation between time after casting and lateral pressure at 1.5 feet from the bottom of form

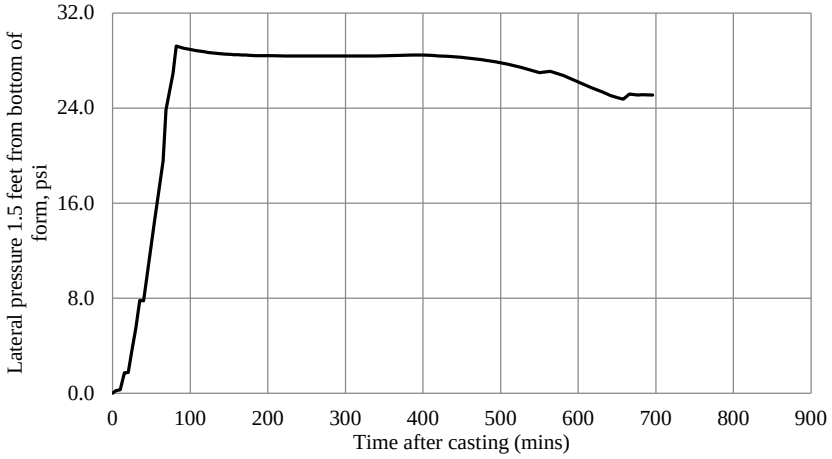

(20) G211FLP

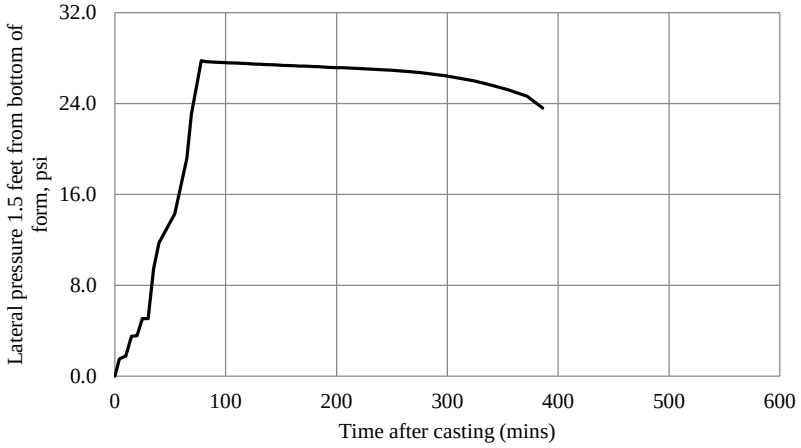

(21) G0.50 CVC

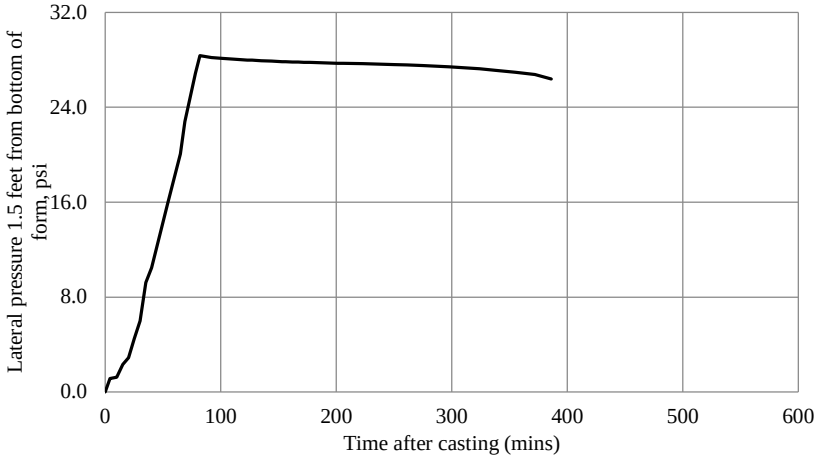

(22) G121C

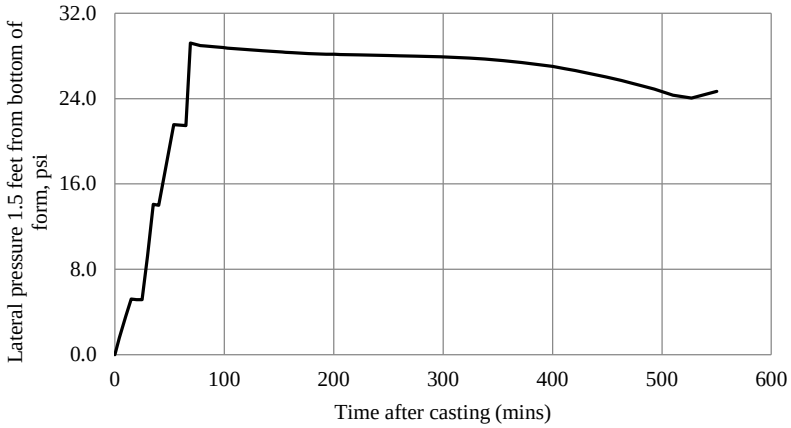

(23) G121F

(cont.) Figure D-2 Relation between time after casting and lateral pressure at 1.5 feet from the bottom of form

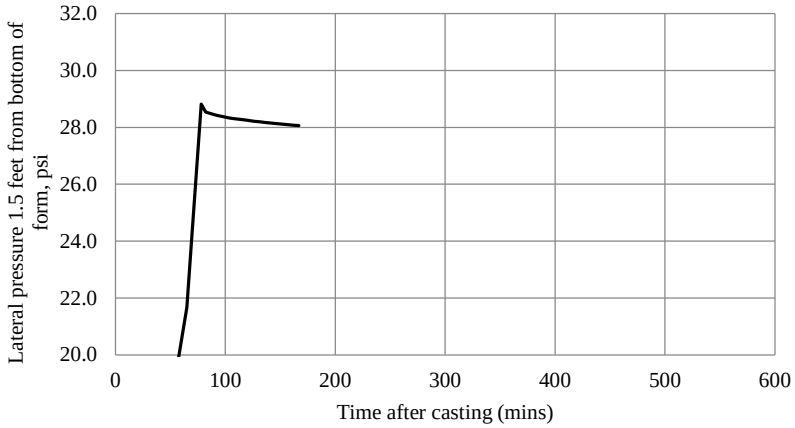

(24) G121S

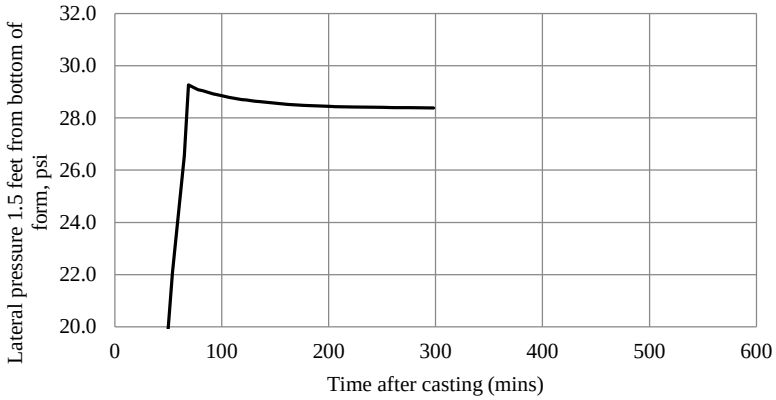

(25) G121FLP

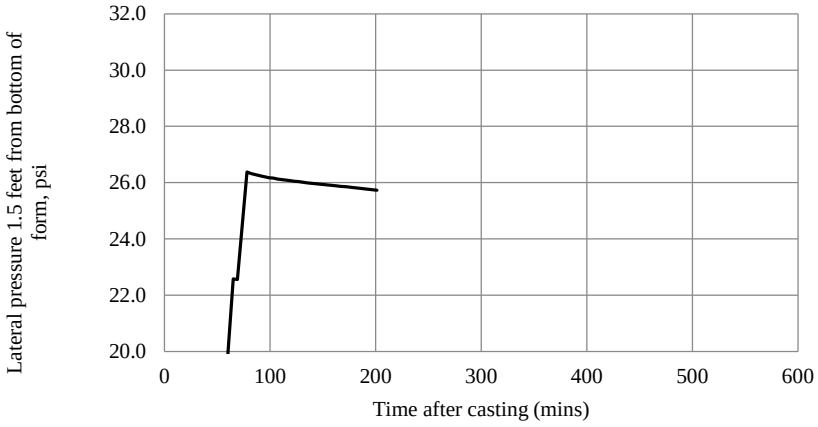

(26) G0.375 CVC

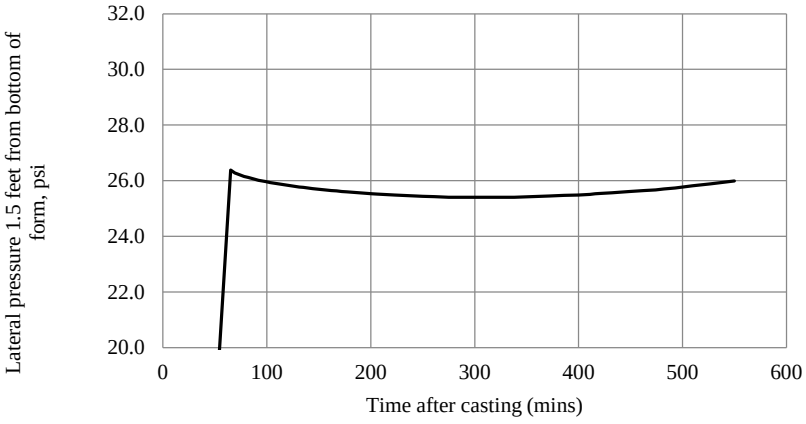

(27) G222C

(cont.) Figure D-2 Relation between time after casting and lateral pressure at 1.5 feet from the bottom of form

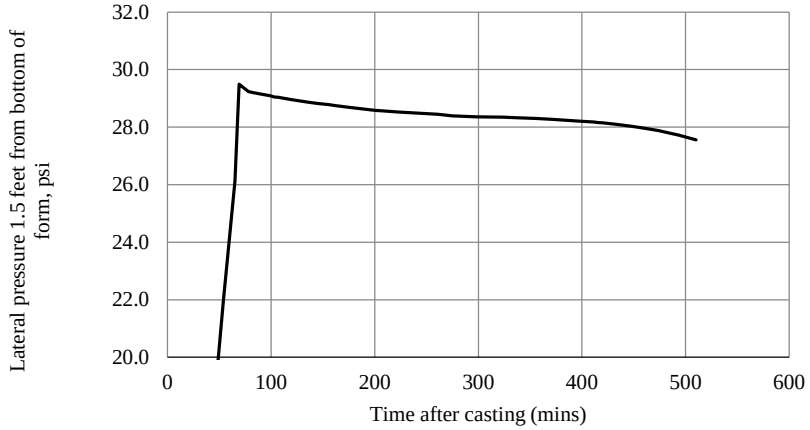

(28) G222F

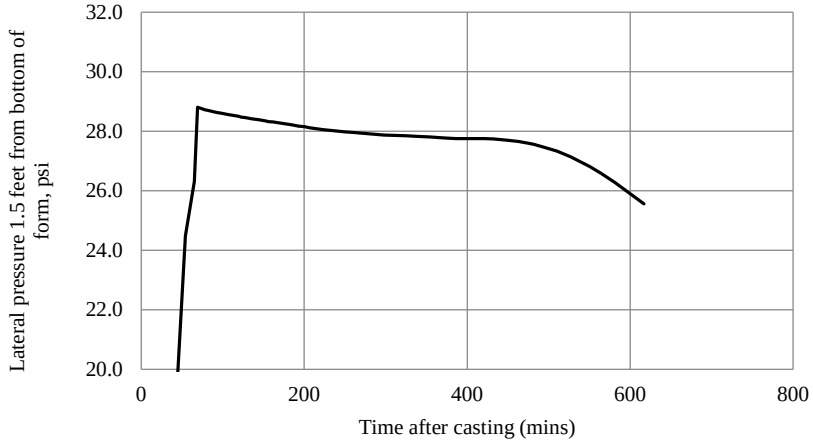

(29) G222S

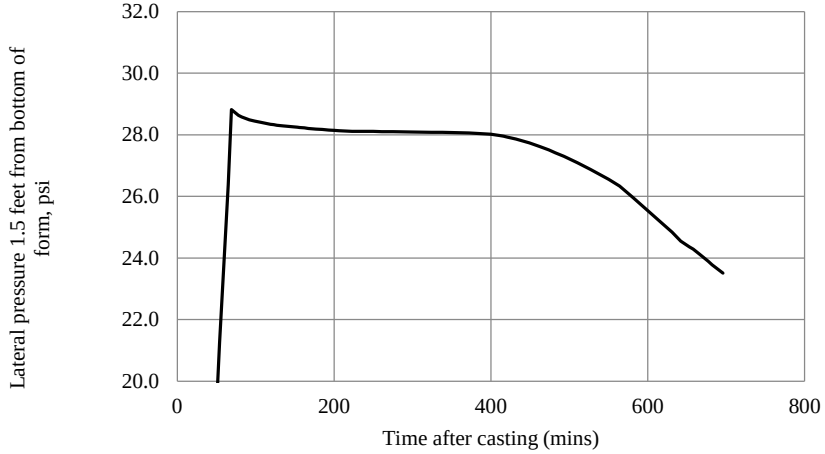

(30) G222FLP

(cont.) Figure D-2 Relation between time after casting and lateral pressure at 1.5 feet from the bottom of form

2. Heat of Hydration

Figure D-3. Semi-adiabatic calorimeter for measuring heat of hydration

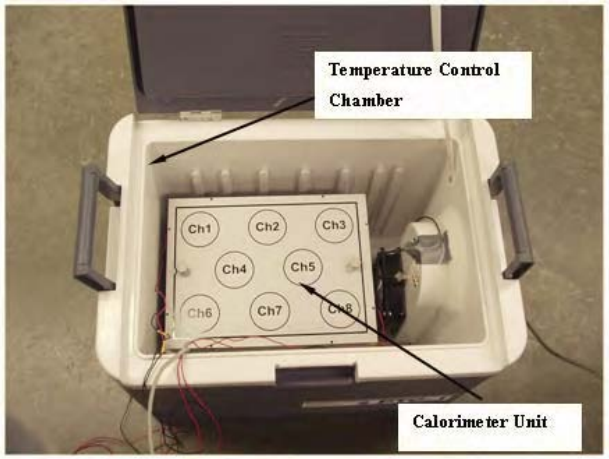

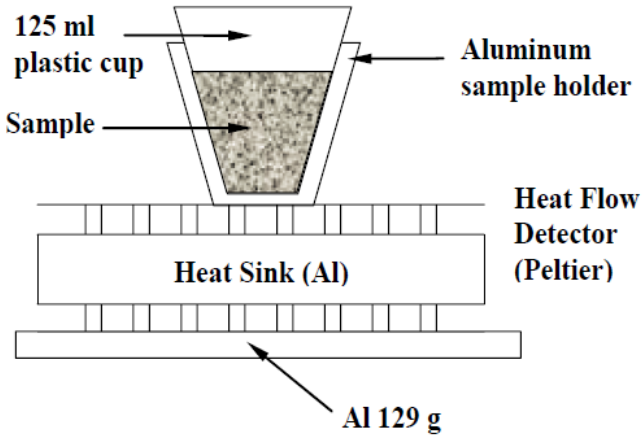

Figure D-4 Isothermal calorimeter unit and test configuration

2.1 Semi-adiabatic calorimetry test results

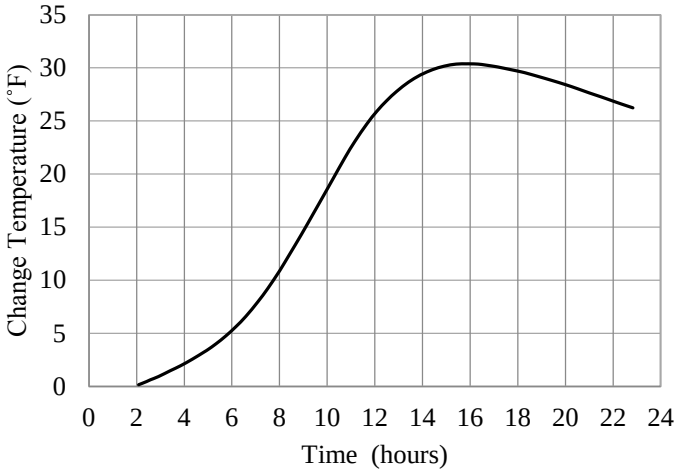

(1) LS0.75 CVC

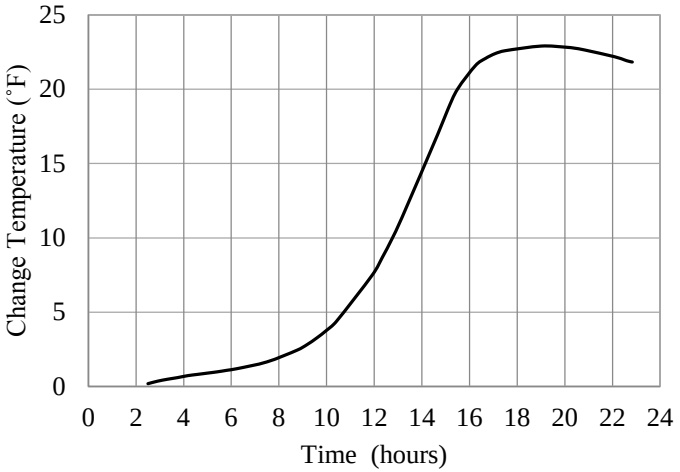

(2) LS111C

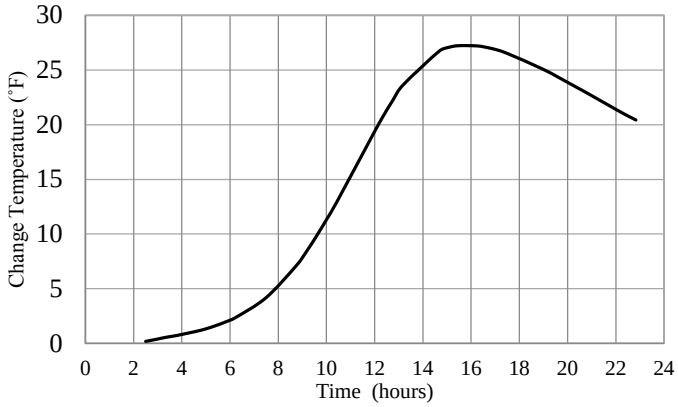

(3) LS111F

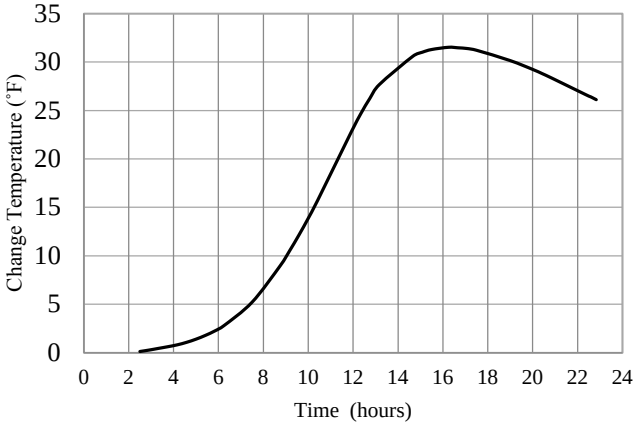

(4) LS111S

Figure D-5. Relation between time and change of temperature

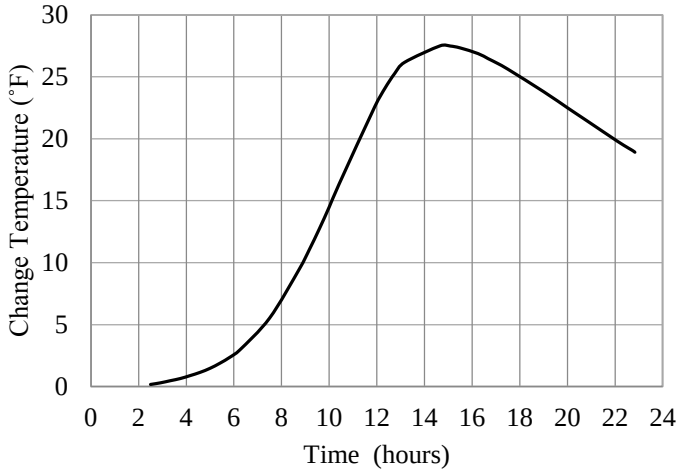

(5) LS111FLP

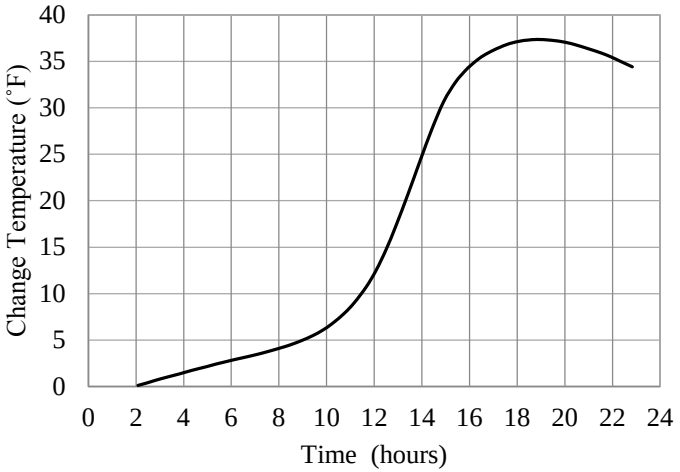

(6) LS211C

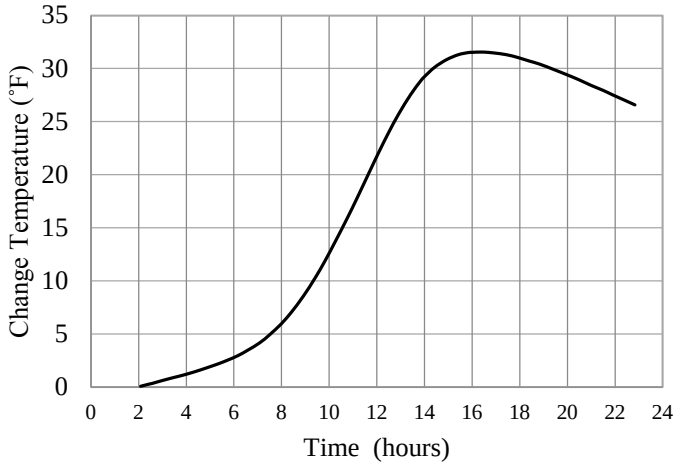

(7) LS211F

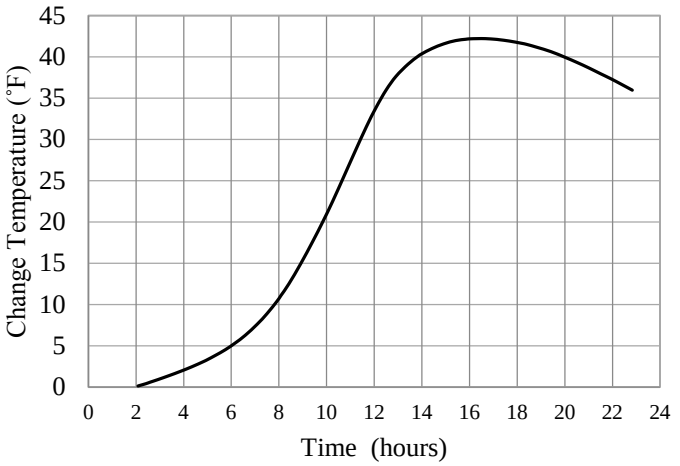

(8) LS211S

(Cont.) Figure D-5. Relation between time and change of temperature

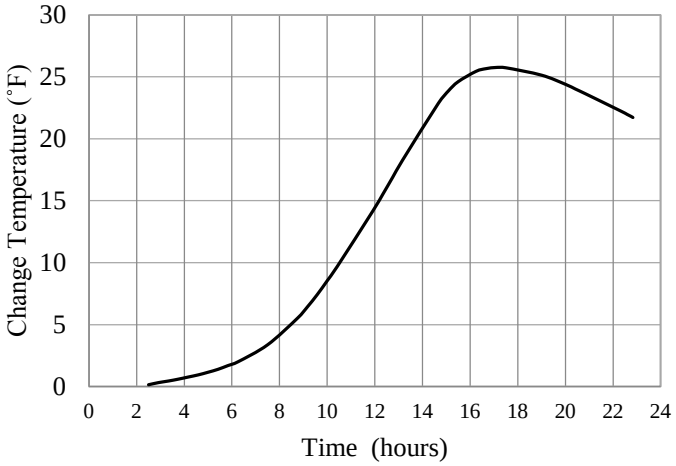

(9) LS211FLP

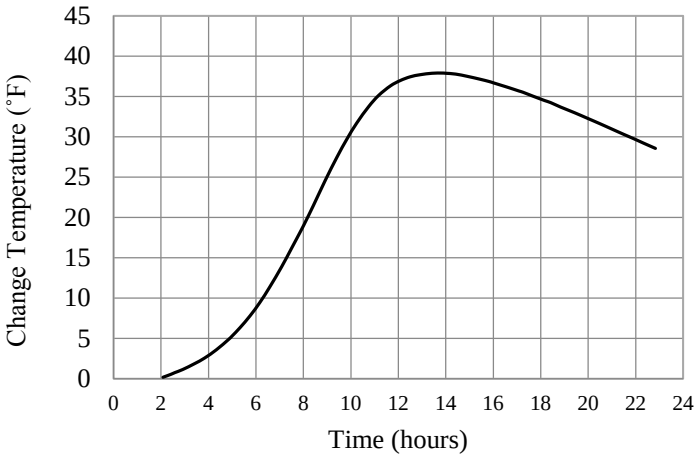

(10) LS0.50 CVC

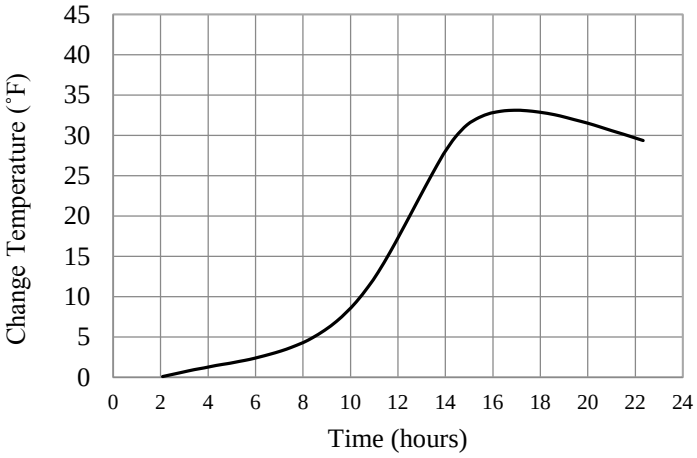

(11) LS121C

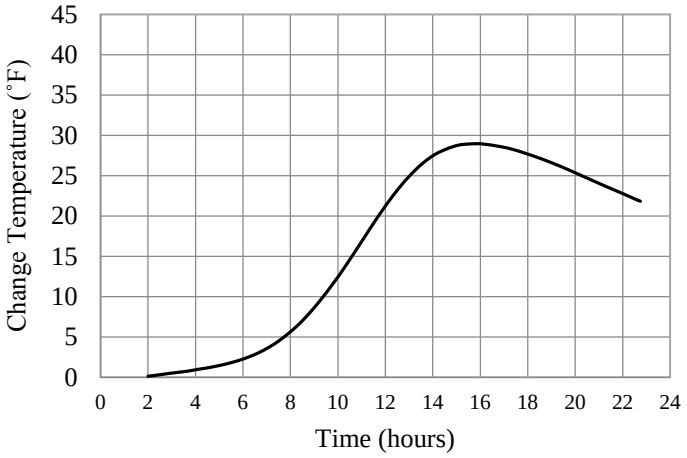

(12) LS121F

(Cont.) Figure D-5. Relation between time and change of temperature

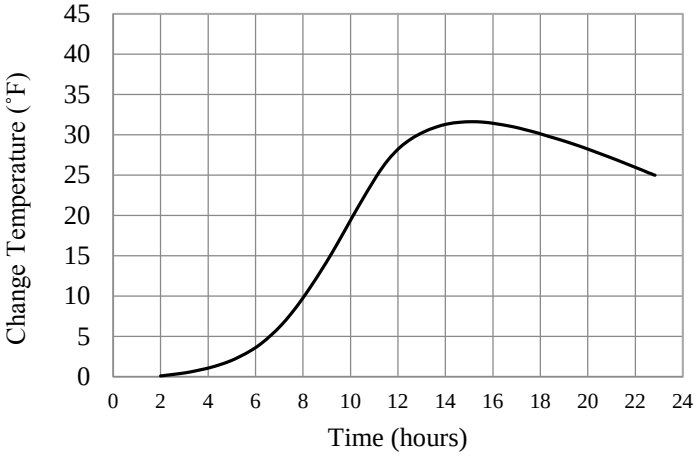

(13) LS121S

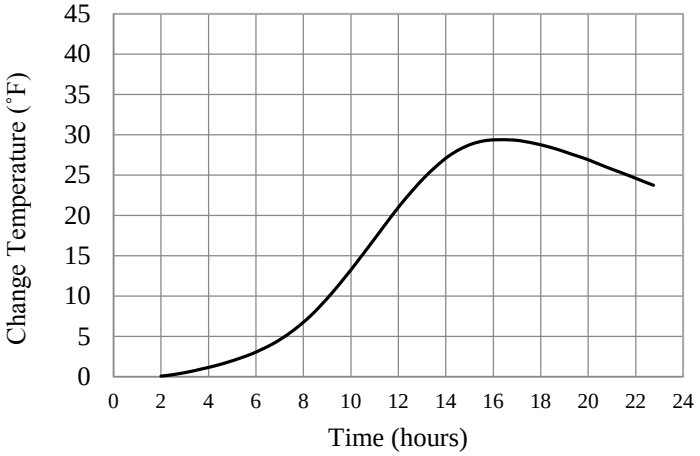

(14) LS121FLP

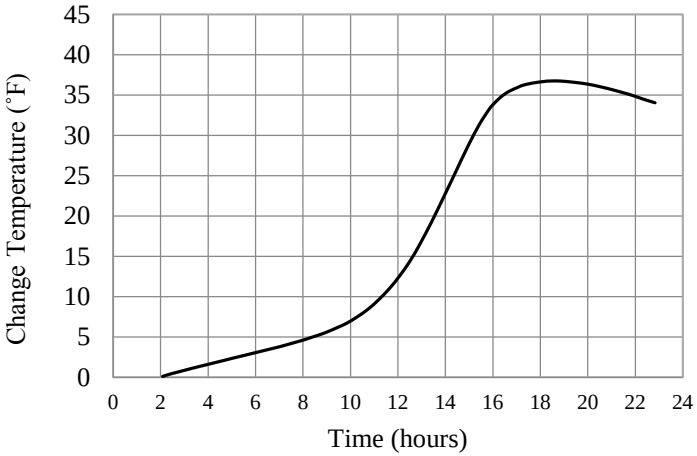

(15) LS221C

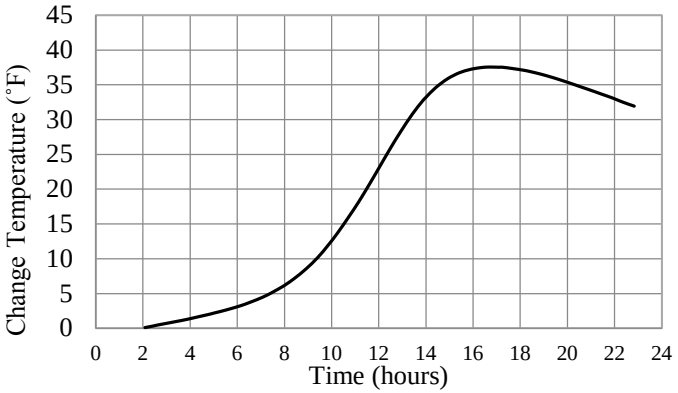

(16) LS221F

(Cont.) Figure D-5. Relation between time and change of temperature

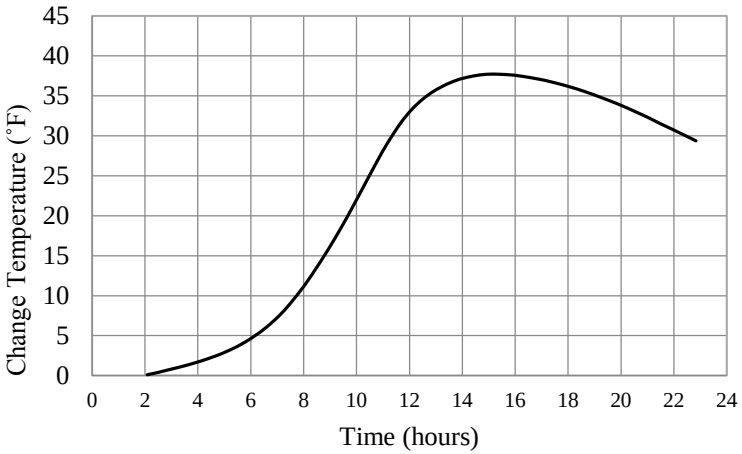

(17) LS221S

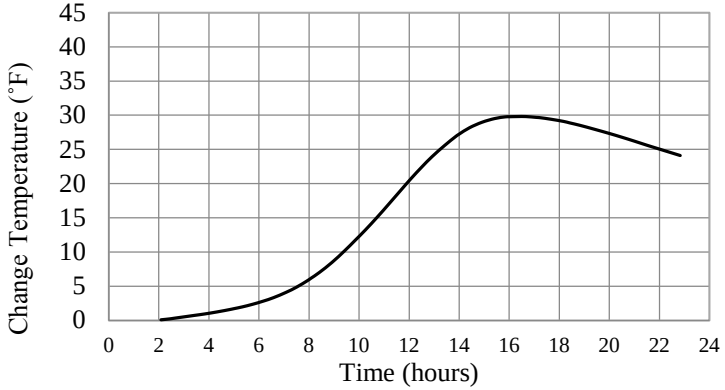

(18) LS221FLP

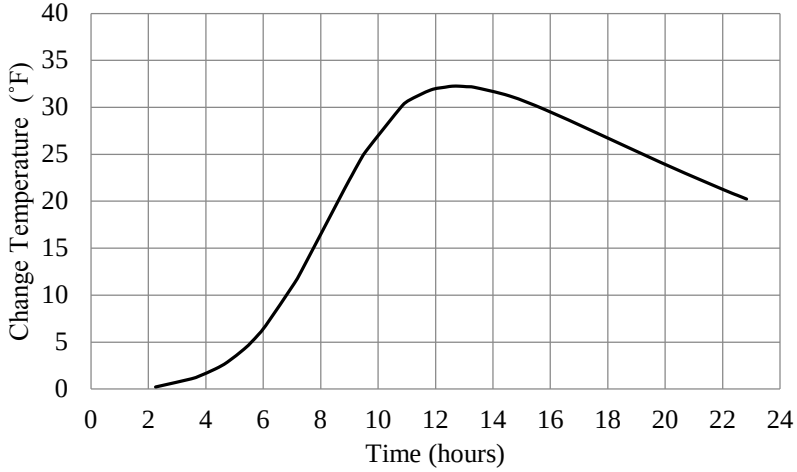

(19) LS0.375 CVC

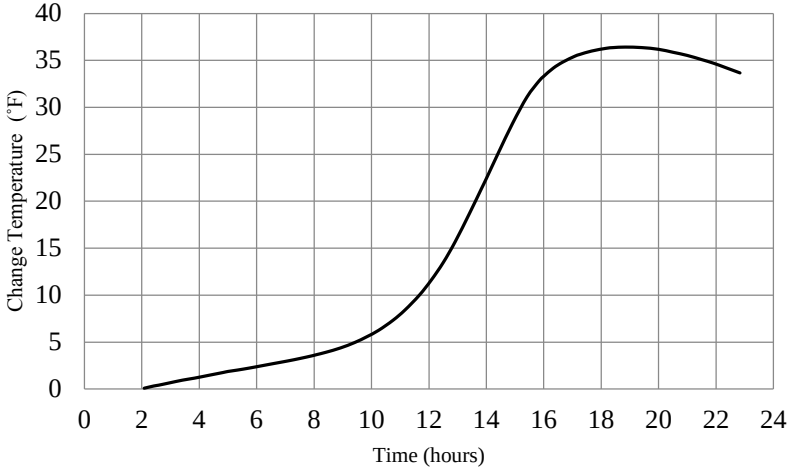

(20) LS222C

(Cont.) Figure D-5. Relation between time and change of temperature

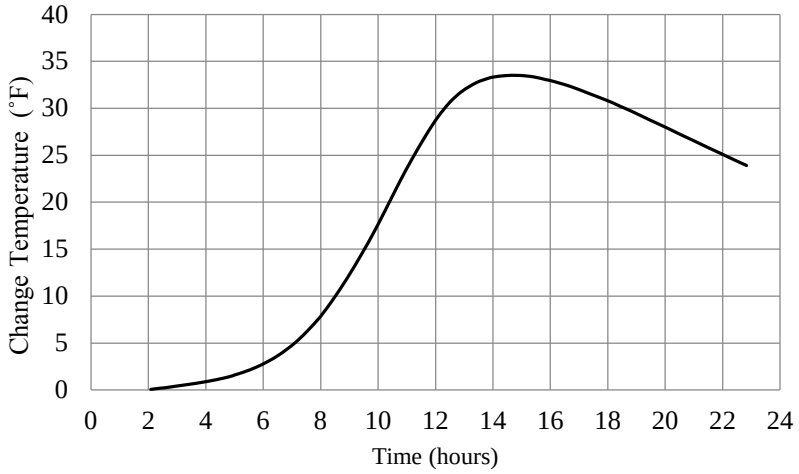

(21) LS222F

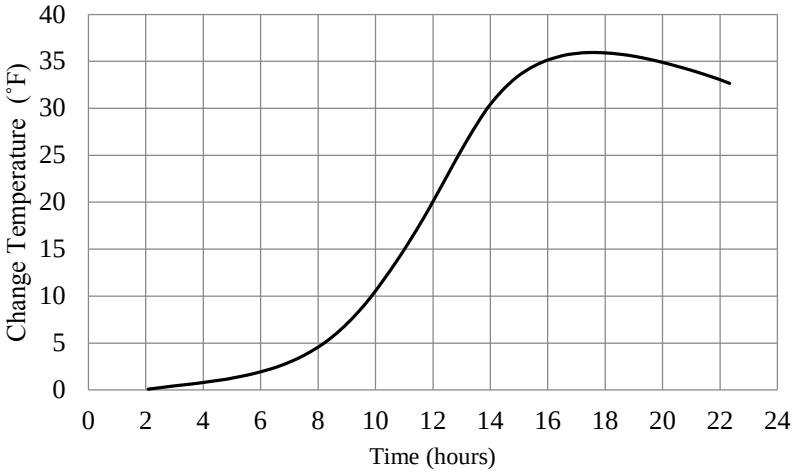

(22) LS222S

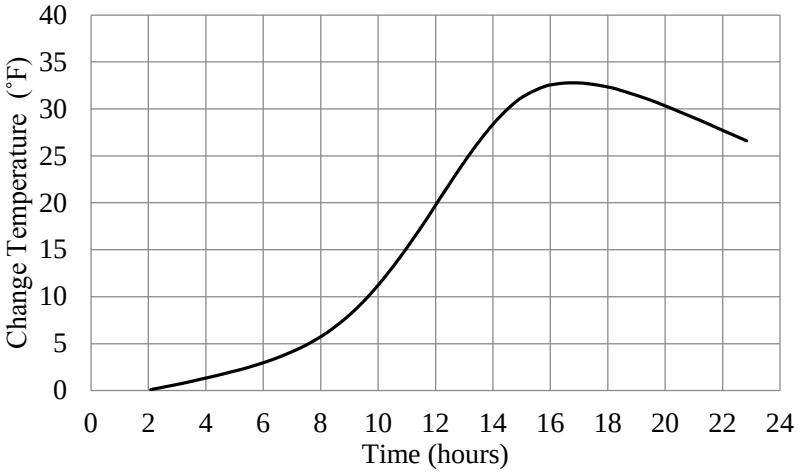

(23) LS222FLP

(Cont.) Figure D-5. Relation between time and change of temperature

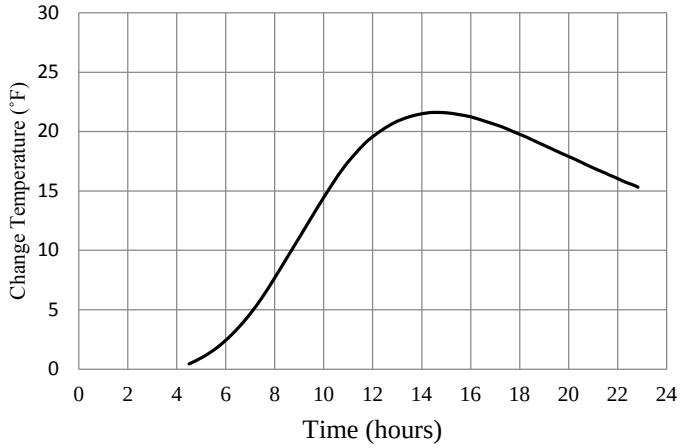

(24) G0.75 CVC

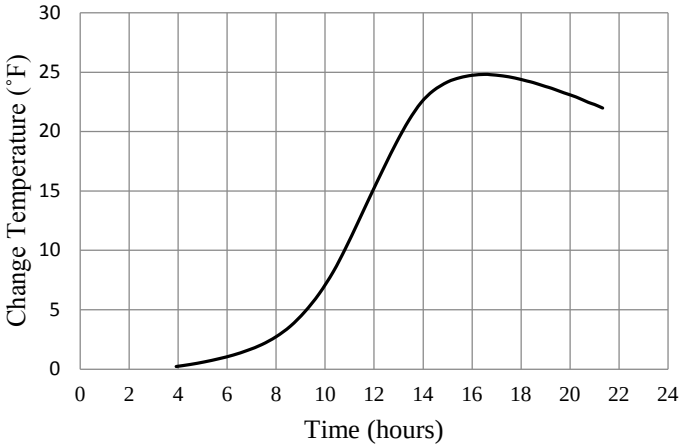

(25) G111C

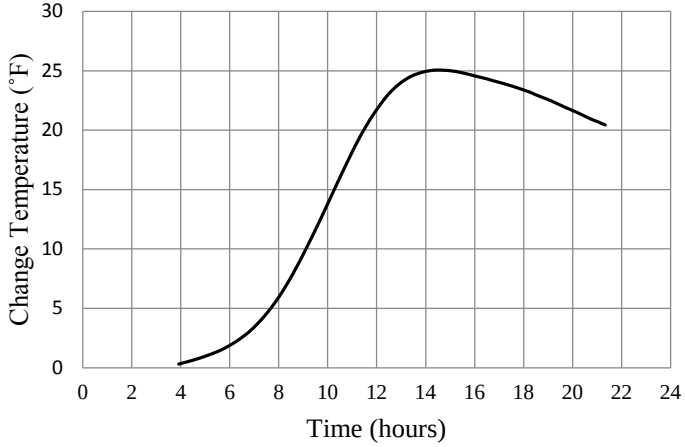

(26) G111F

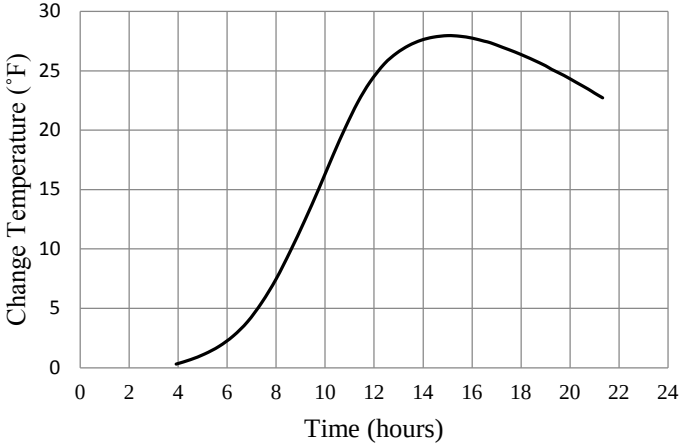

(27) G111S

(Cont.) Figure D-5. Relation between time and change of temperature

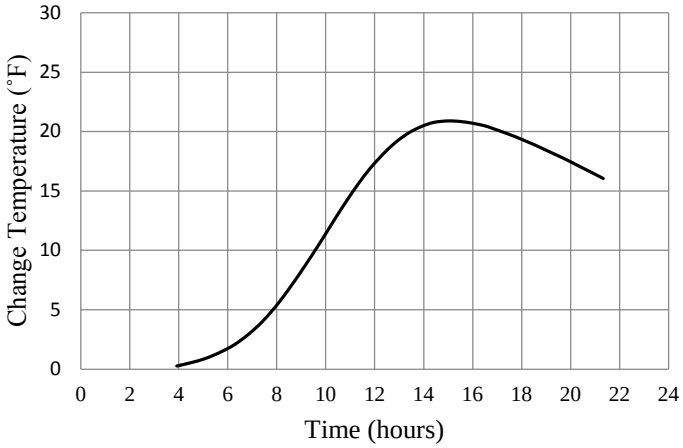

(28) G111FLP

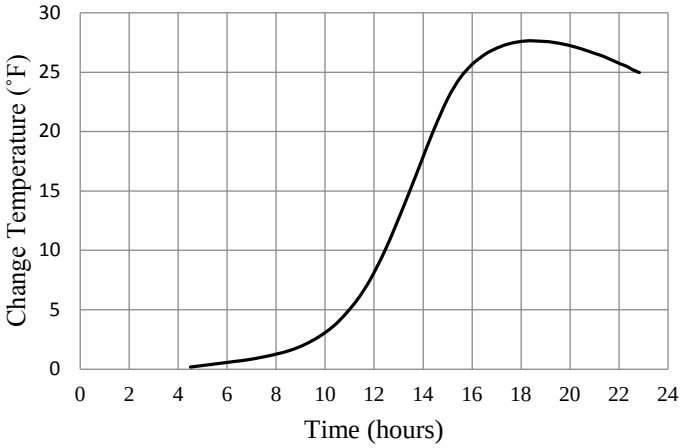

(29) G211C

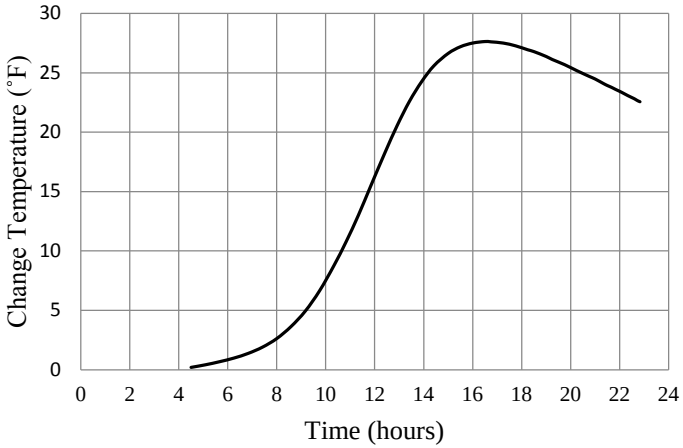

(30) G211F

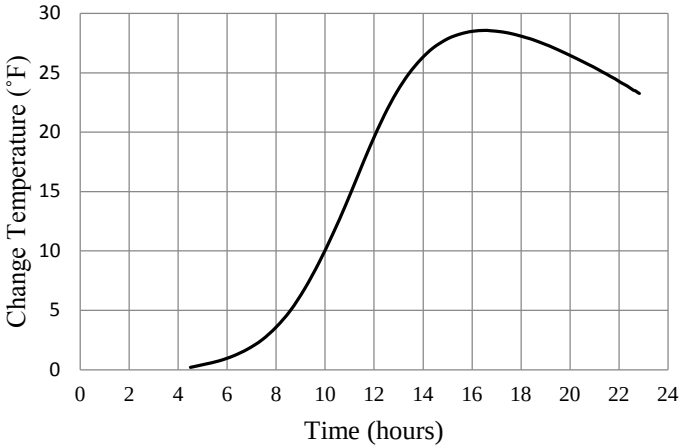

(31) G211S

(Cont.) Figure D-5. Relation between time and change of temperature

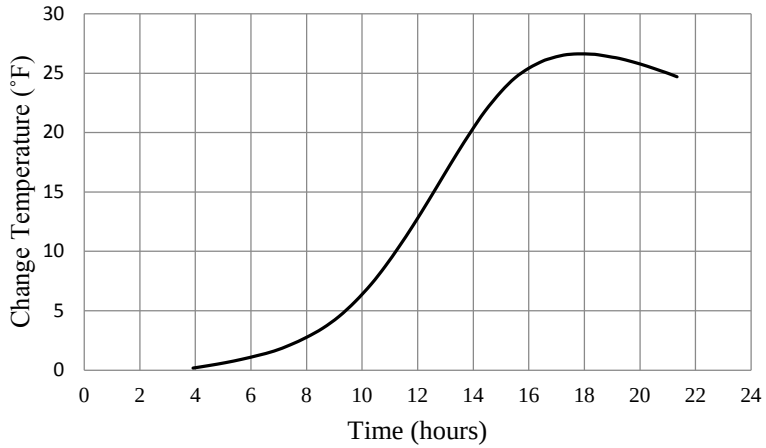

(32) G211FLP

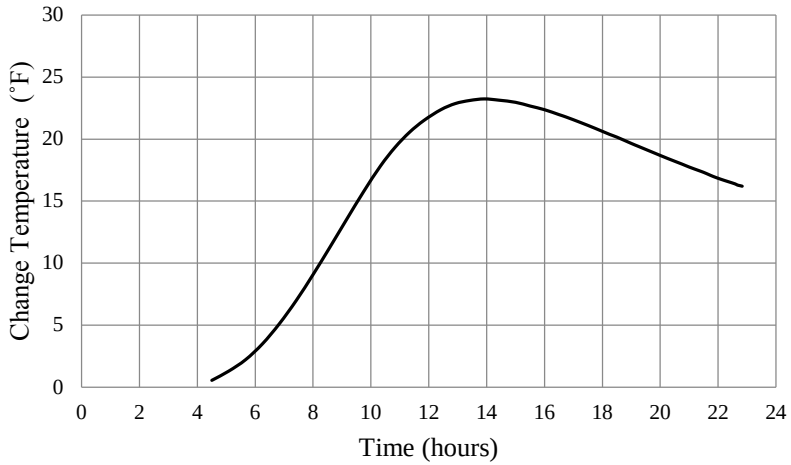

(33) G0.50 CVC

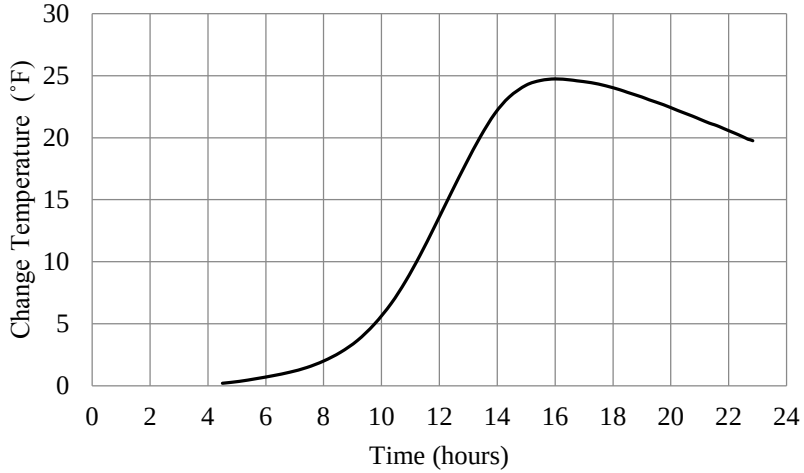

(34) G121C

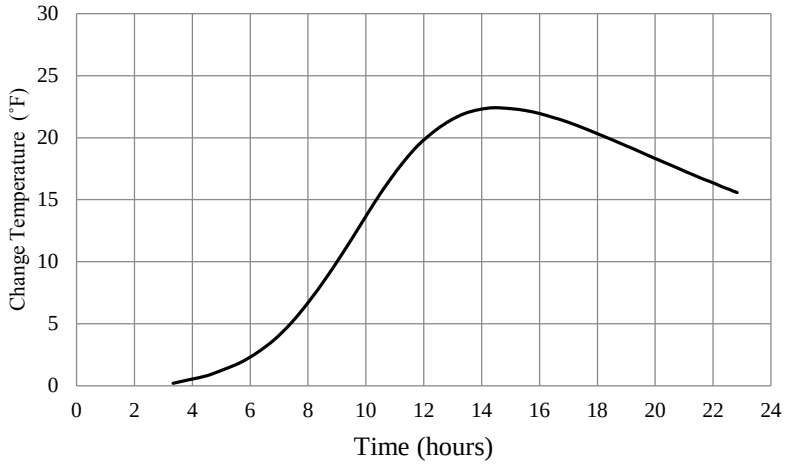

(35) G121F

(Cont.) Figure D-5. Relation between time and change of temperature

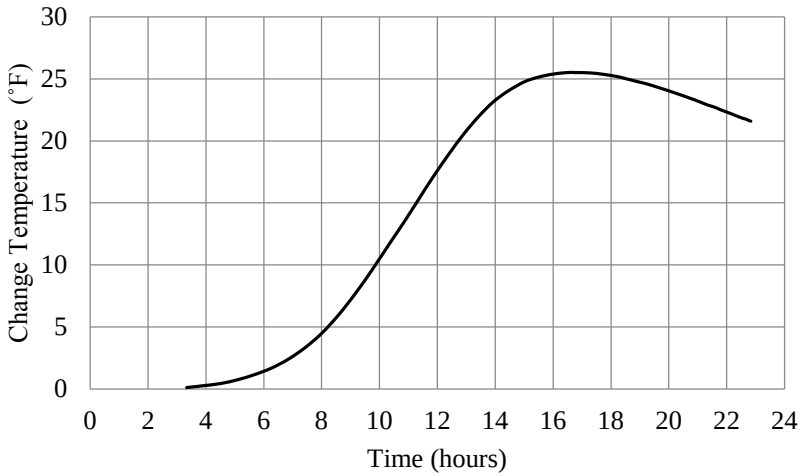

(36) G121S

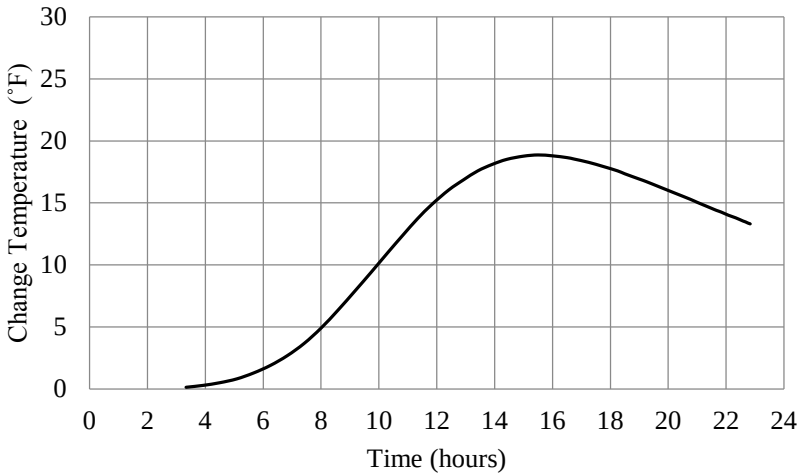

(37) G121FLP

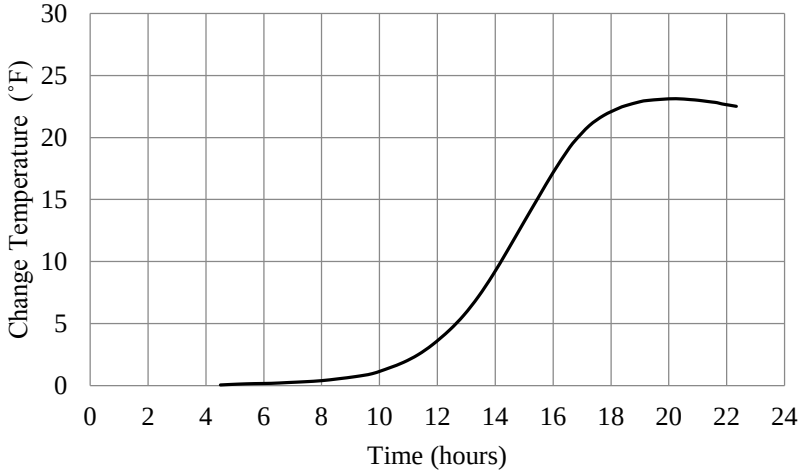

(38) G221C

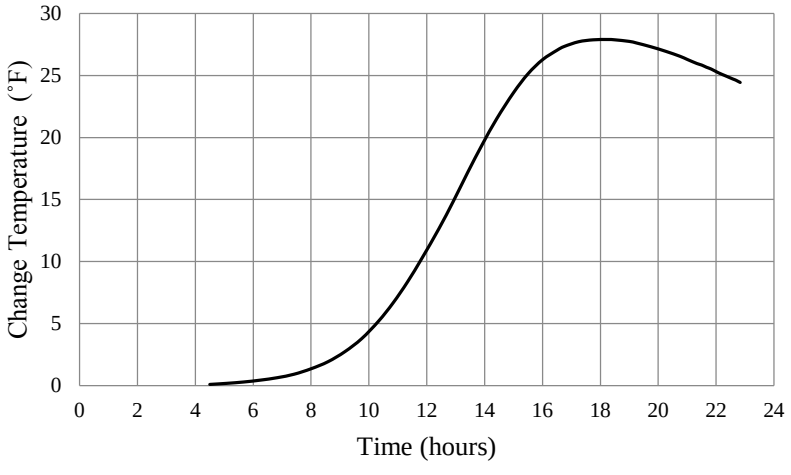

(39) G221F

(Cont.) Figure D-5. Relation between time and change of temperature

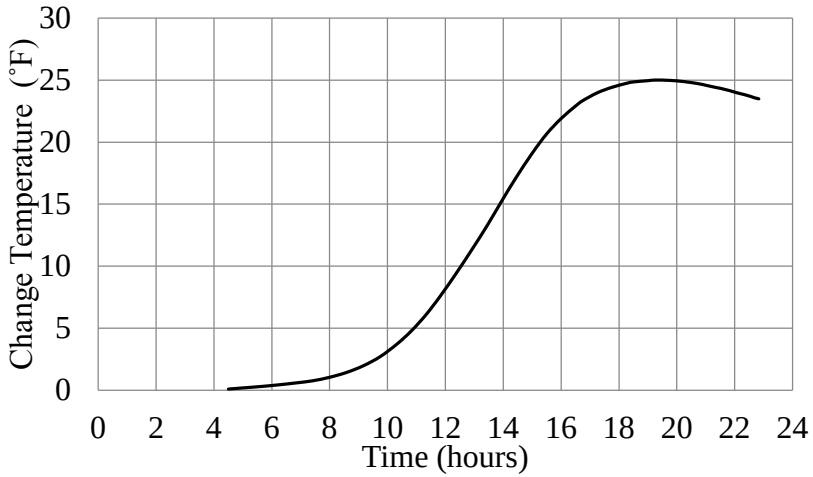

(40) G221S

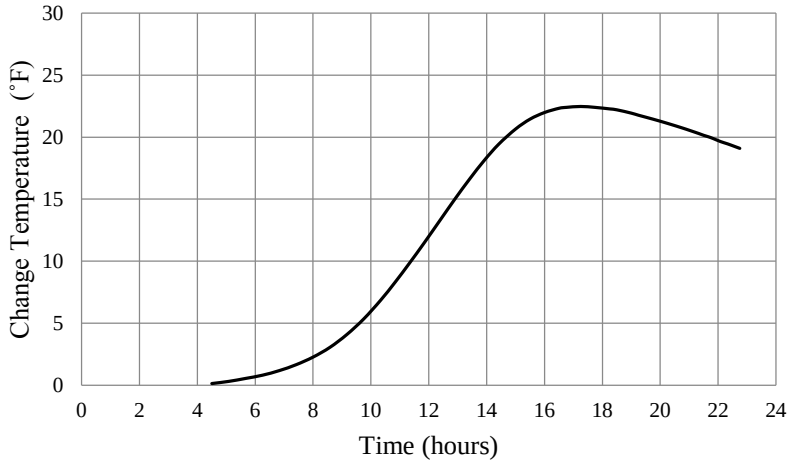

(41) G221FLP

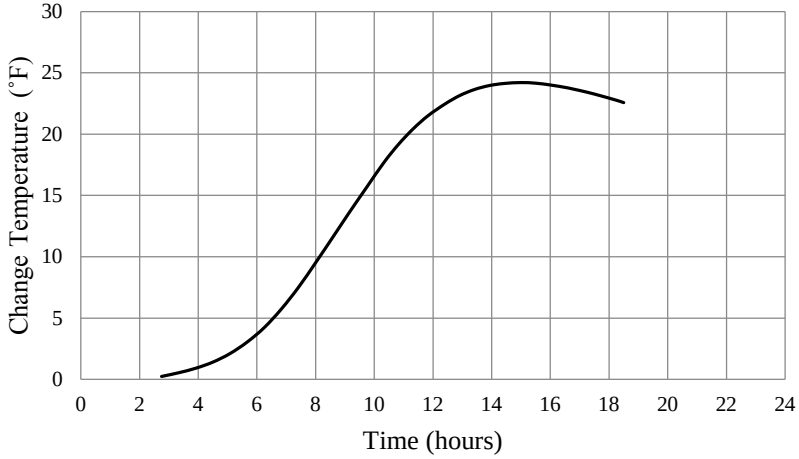

(42) G0.375 CVC

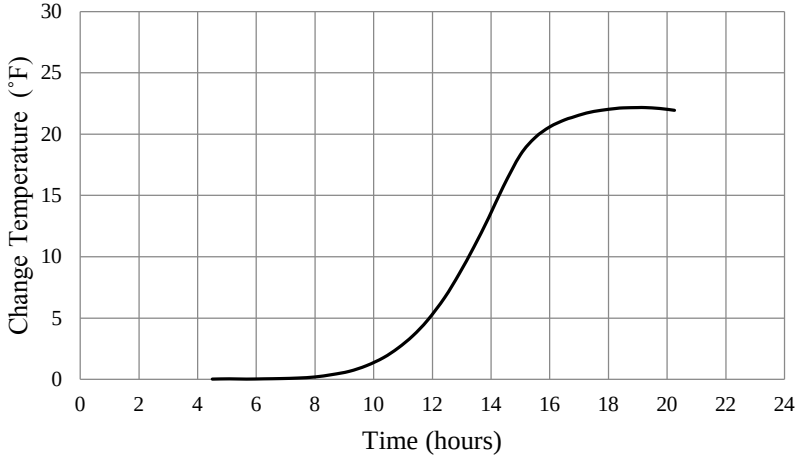

(43) G222C

(Cont.) Figure D-5. Relation between time and change of temperature

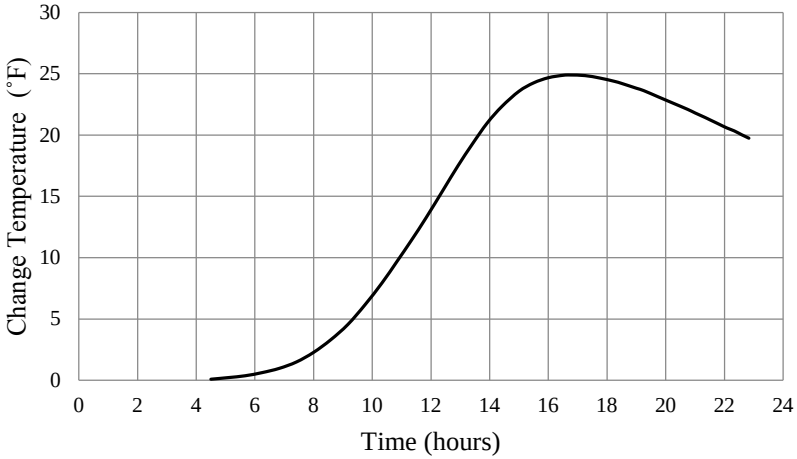

(44) G222F

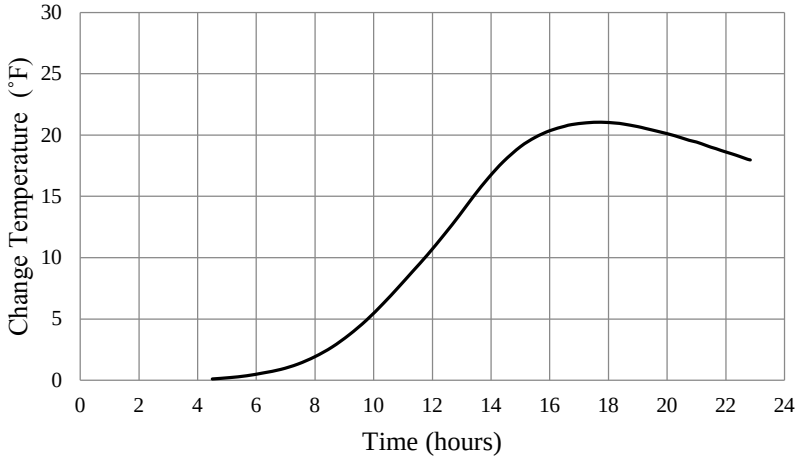

(45) G222S

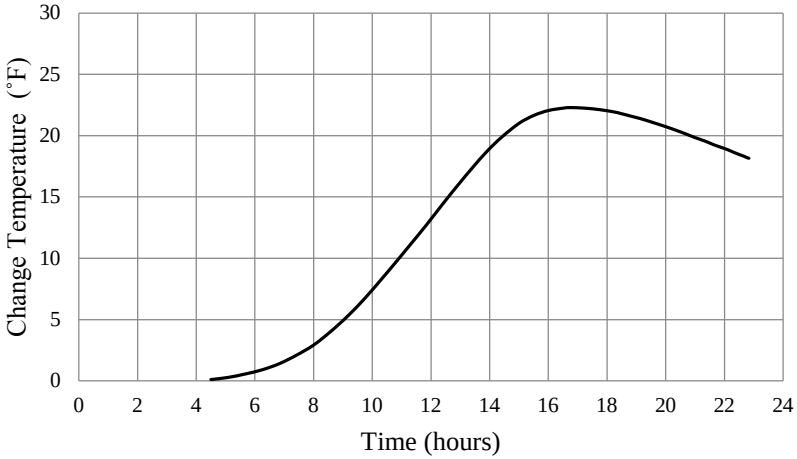

(46) G222FLP

(Cont.) Figure D-5. Relation between time and change of temperature

2.2 Isothermal calorimetry test results

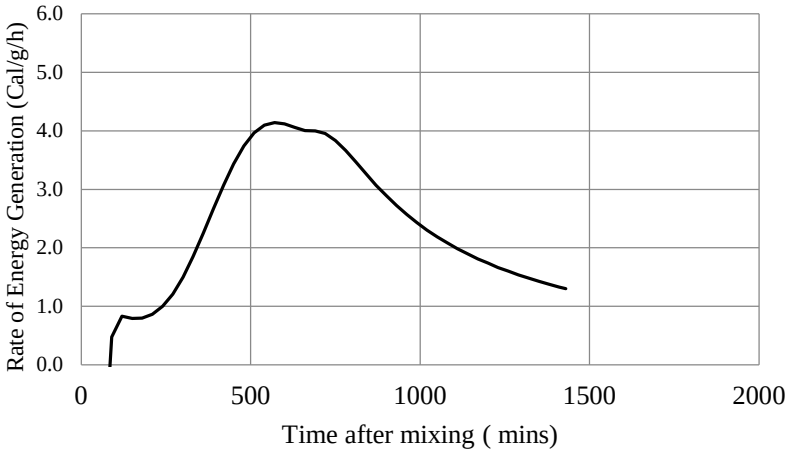

(1) LS0.75 CVC

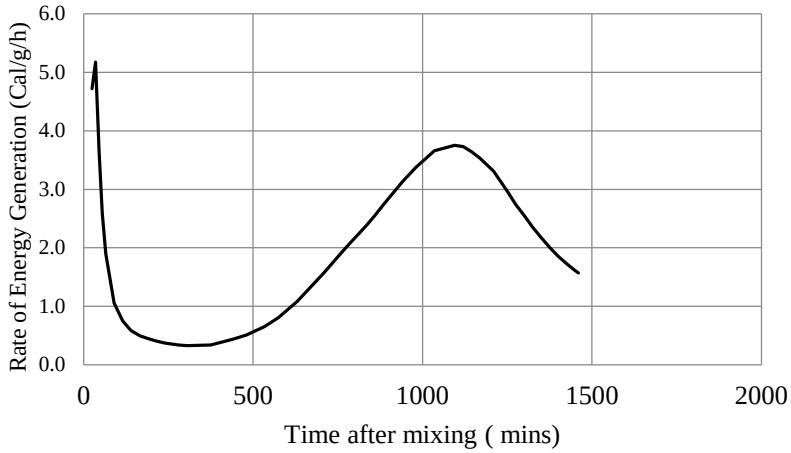

(2) LS111C

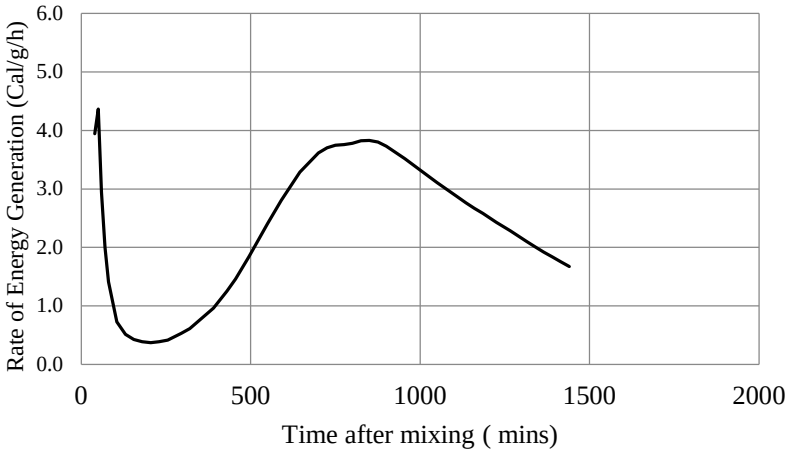

(3) LS111F

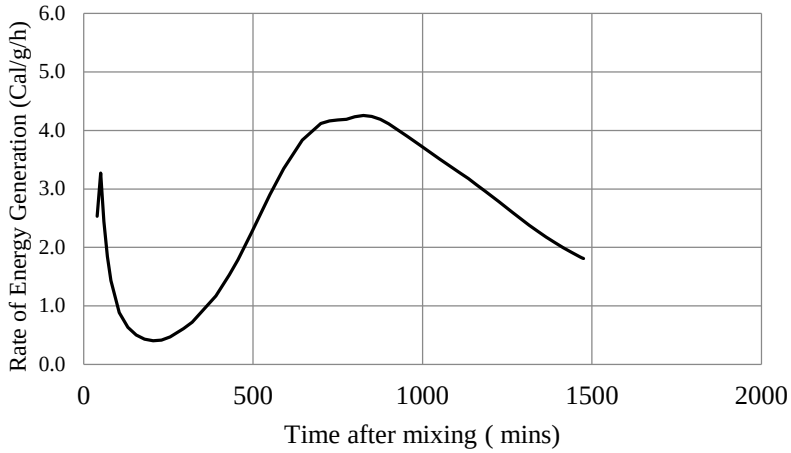

(4) LS111S

Figure D-6. Relation between time after mixing and rate of energy generation

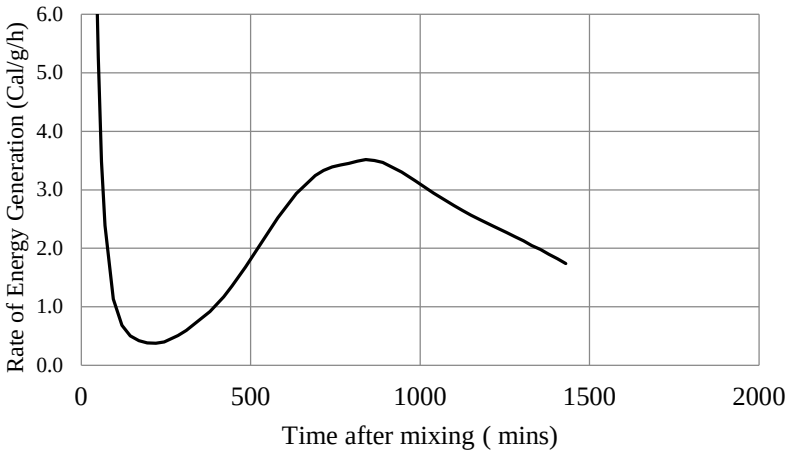

(5) LS111FLP

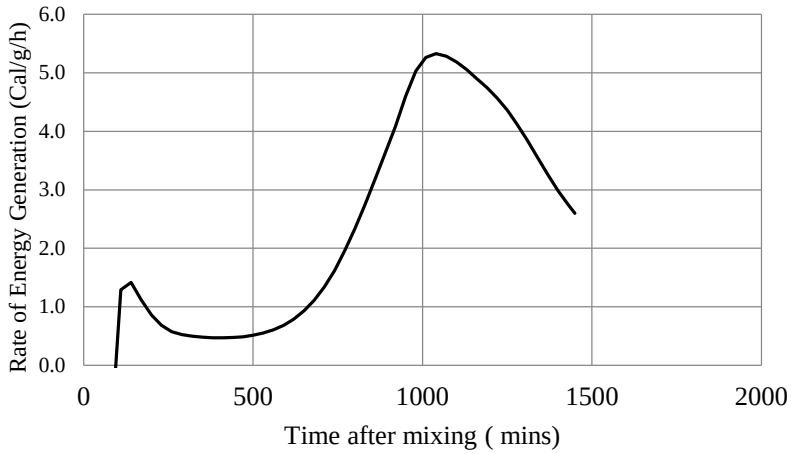

(6) LS211C

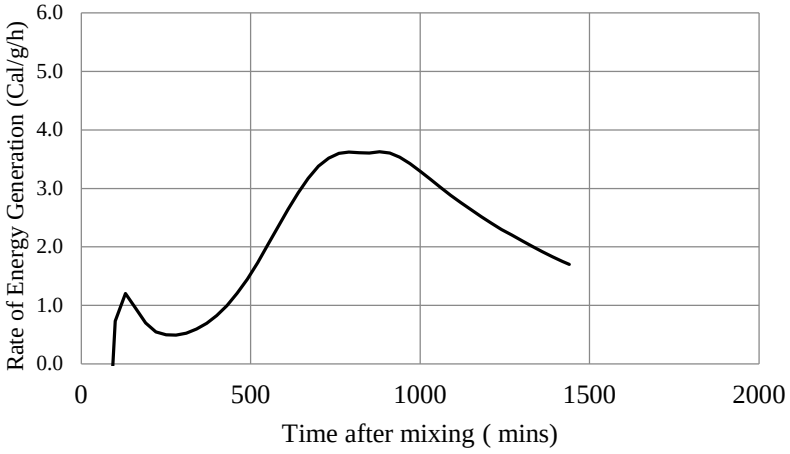

(7) LS211F

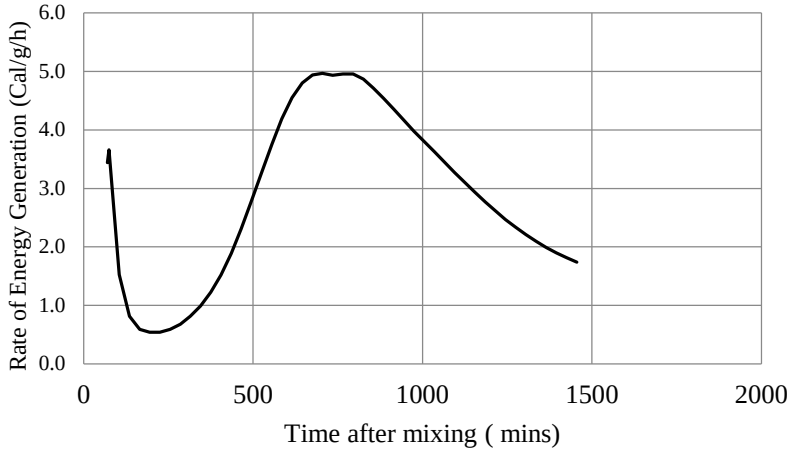

(8) LS211S

(Cont.) Figure D-6. Relation between time after mixing and rate of energy generation

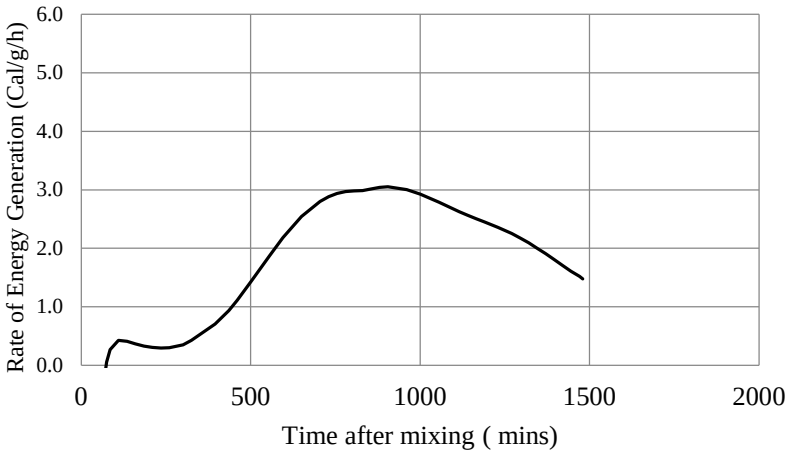

(9) LS211FLP

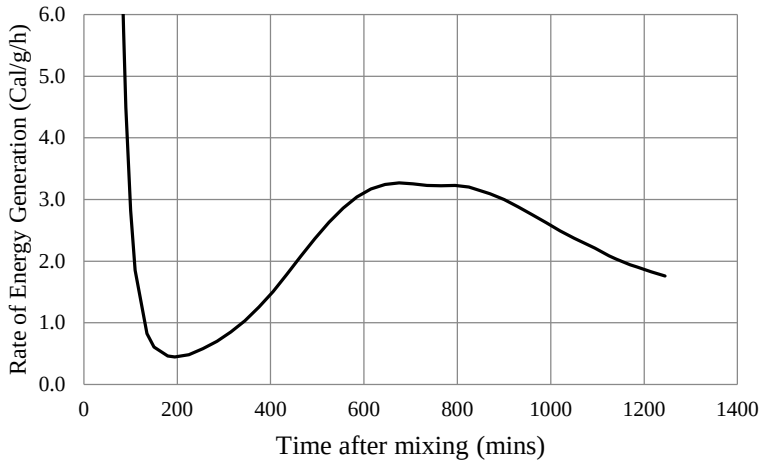

(10) LS0.50 CVC

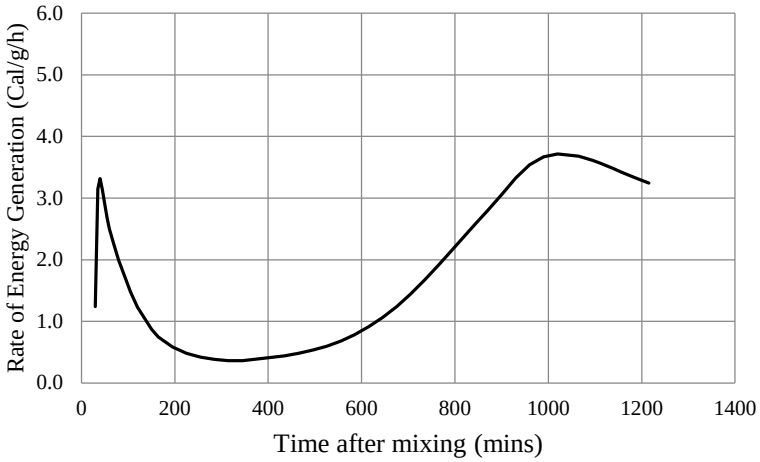

(11) LS121C

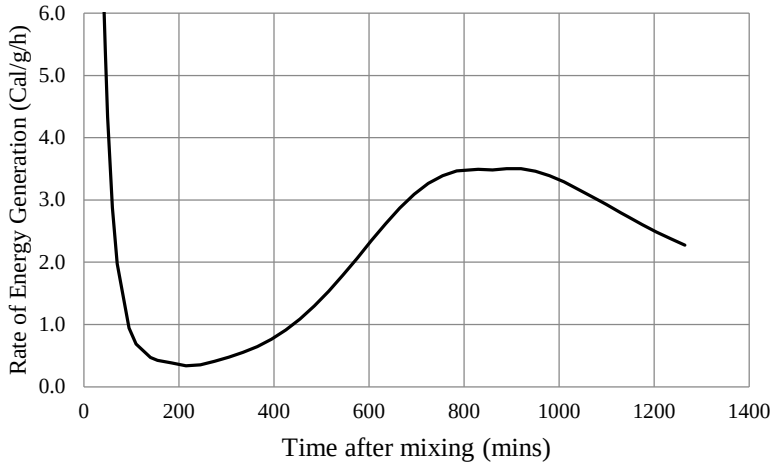

(12) LS121F

(Cont.) Figure D-6. Relation between time after mixing and rate of energy generation

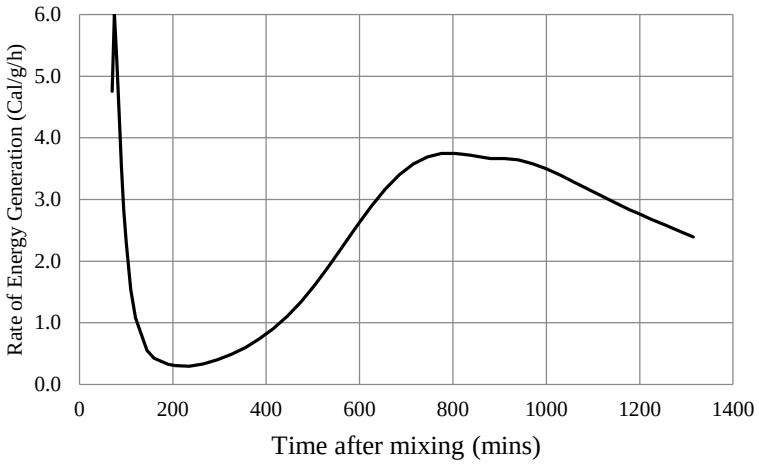

(13) LS121S

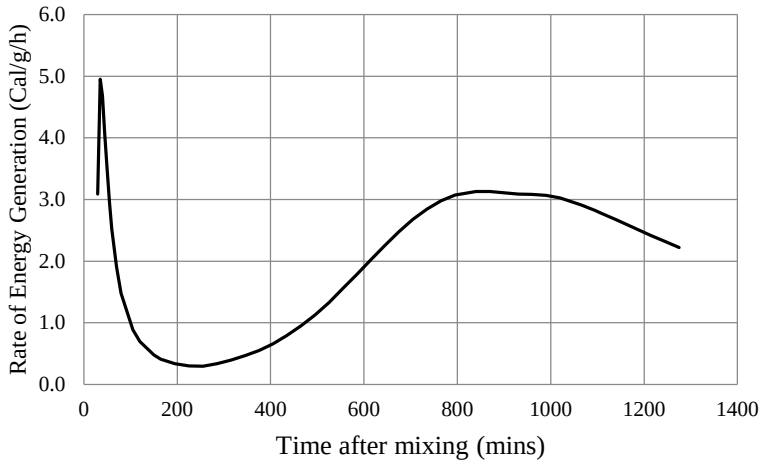

(14) LS121FLP

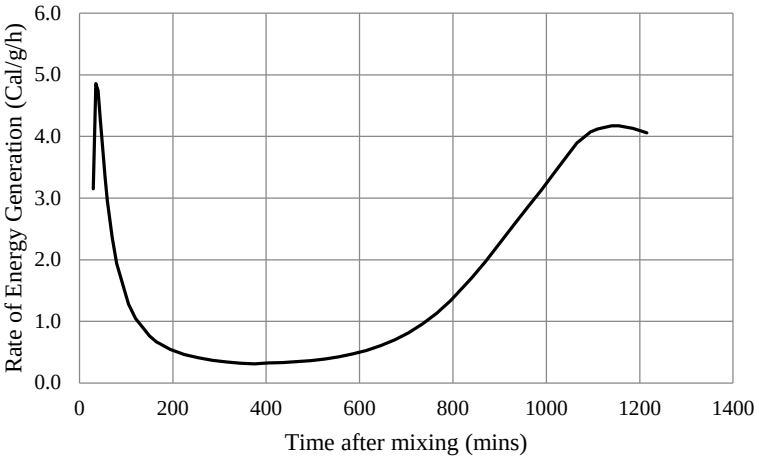

(15) LS221C

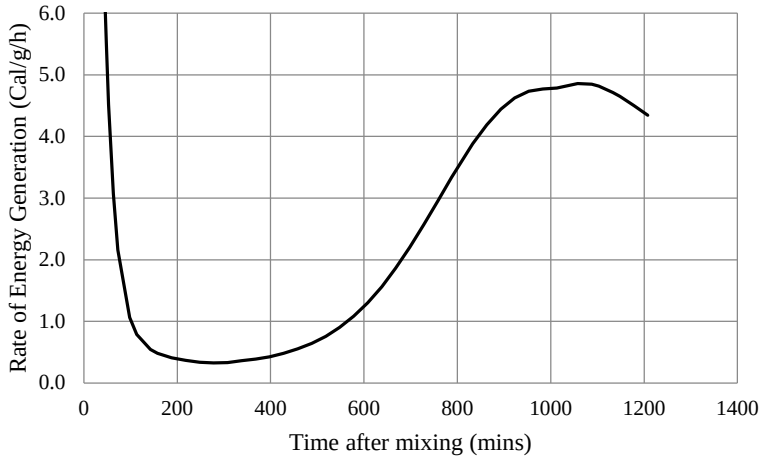

(16) LS221F

(Cont.) Figure D-6. Relation between time after mixing and rate of energy generation

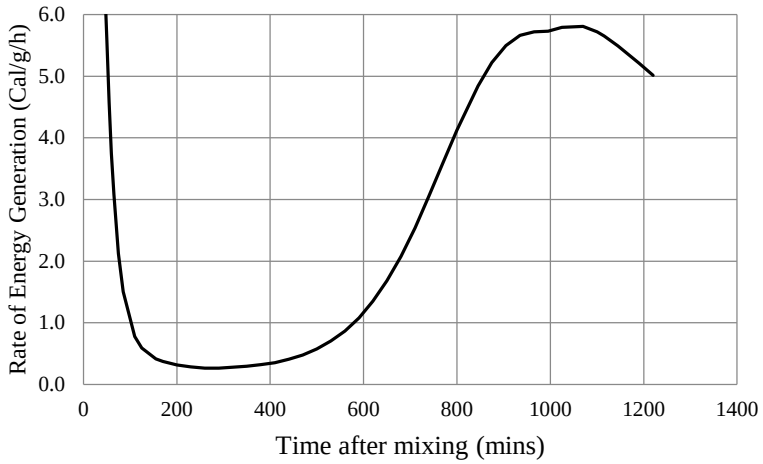

(17) LS221S

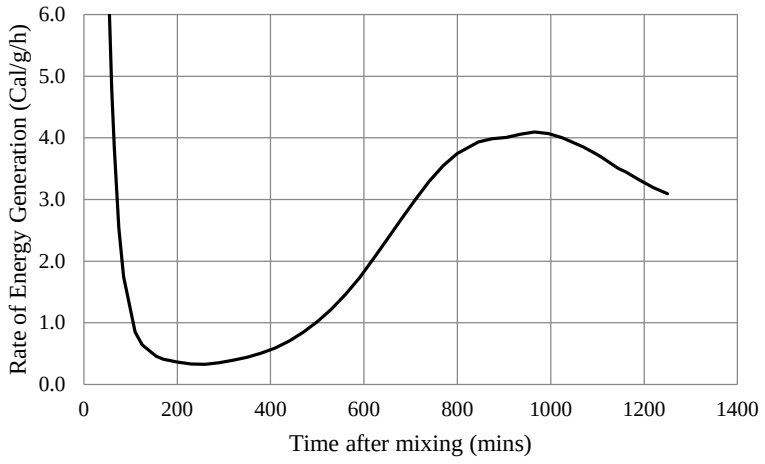

(18) LS221FLP

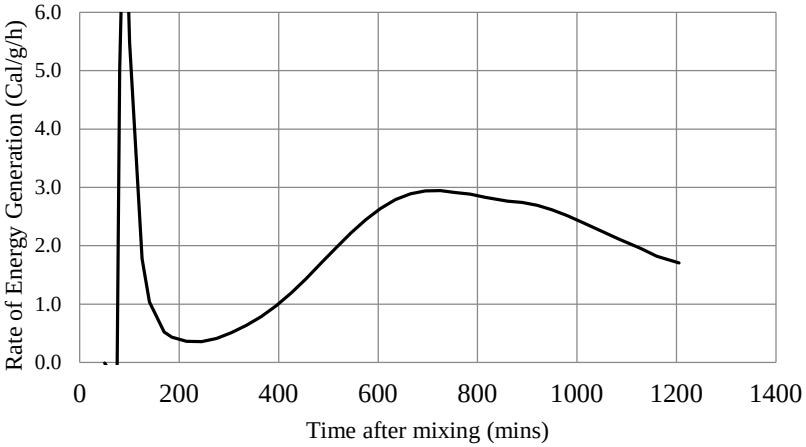

(19) LS0.375 CVC

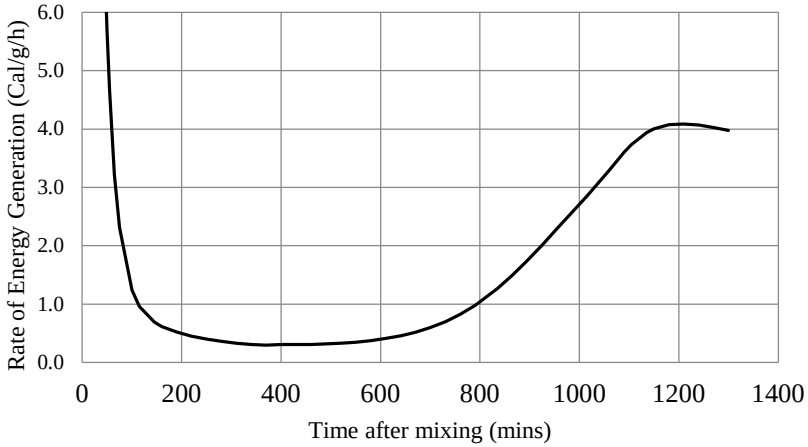

(20) LS222C

(Cont.) Figure D-6. Relation between time after mixing and rate of energy generation

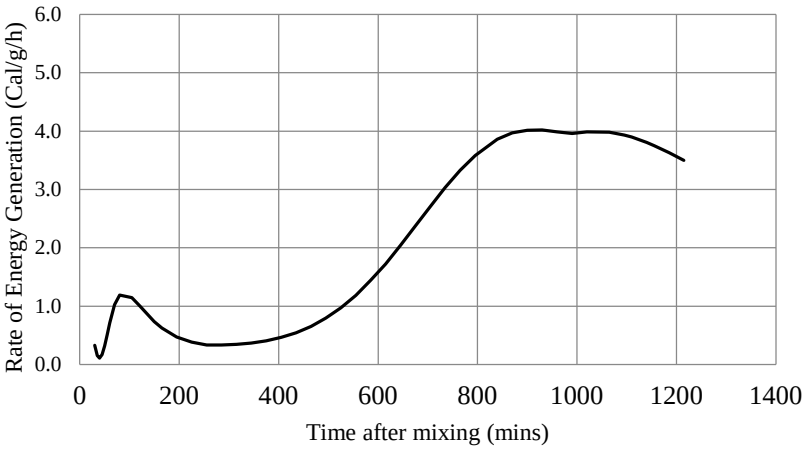

(21) LS222F

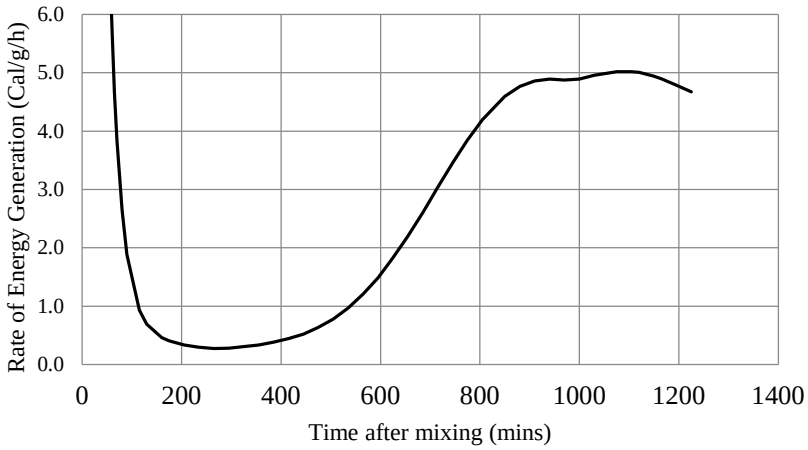

(22) LS222S

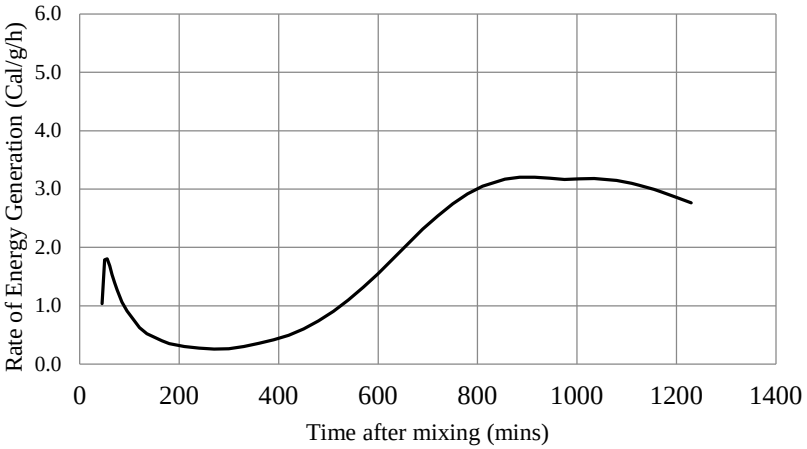

(23) LS222FLP

(Cont.) Figure D-6. Relation between time after mixing and rate of energy generation

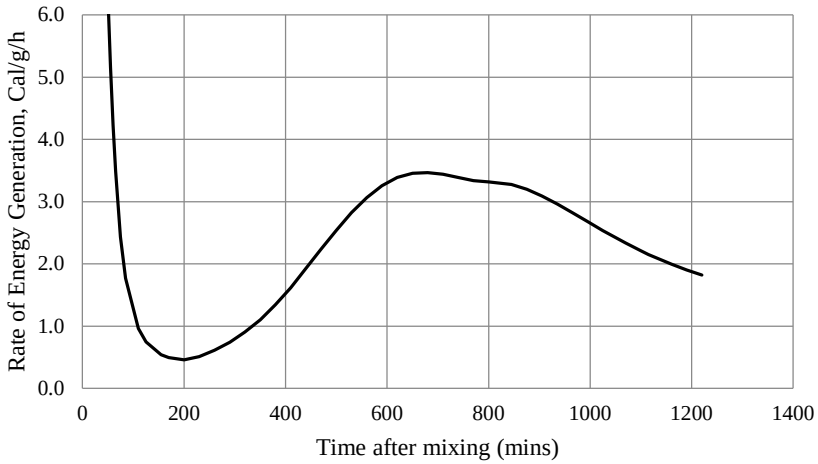

(24) G0.75 CVC

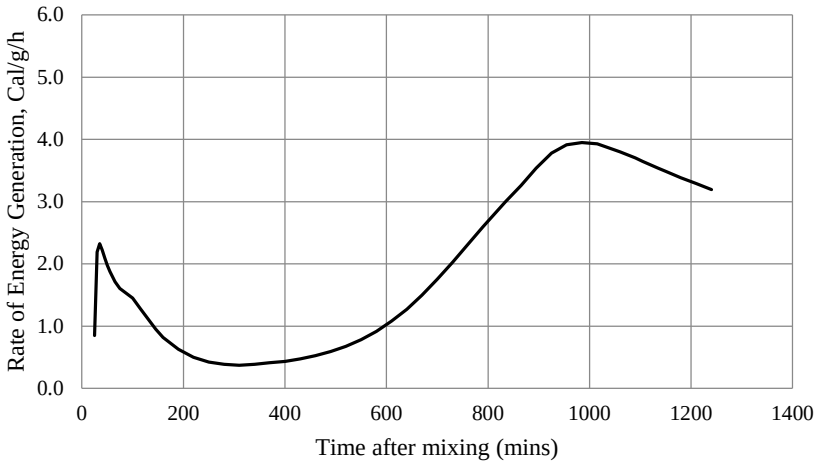

(25) G111C

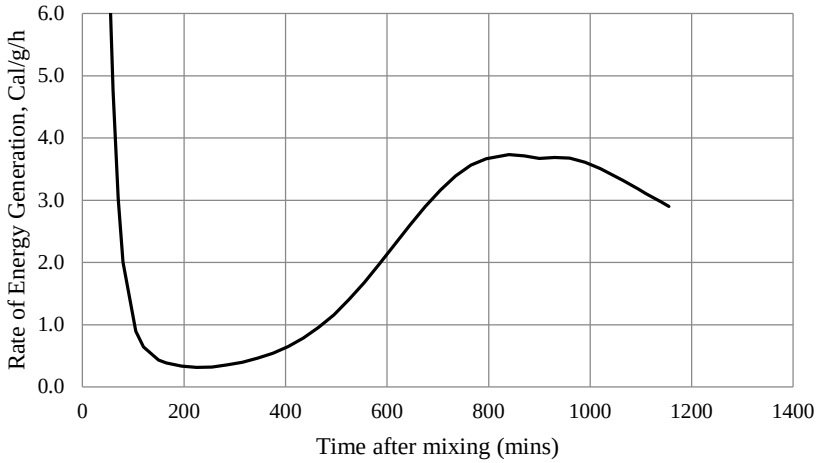

(26) G111F

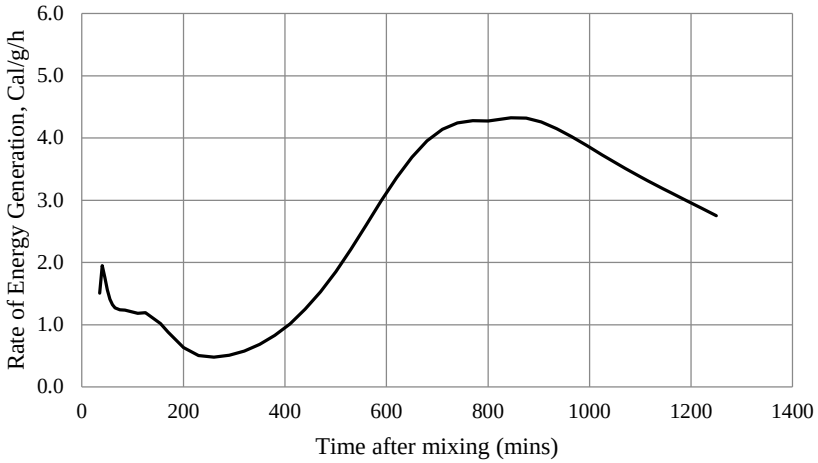

(27) G111S

(Cont.) Figure D-6. Relation between time after mixing and rate of energy generation

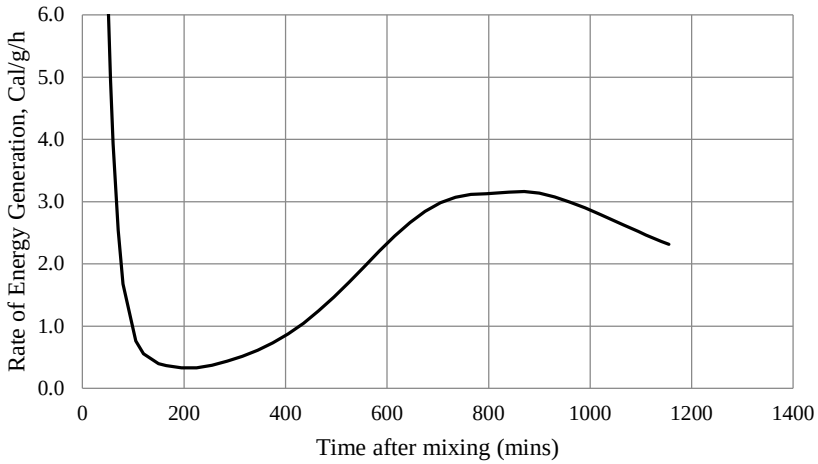

(28) G111FLP

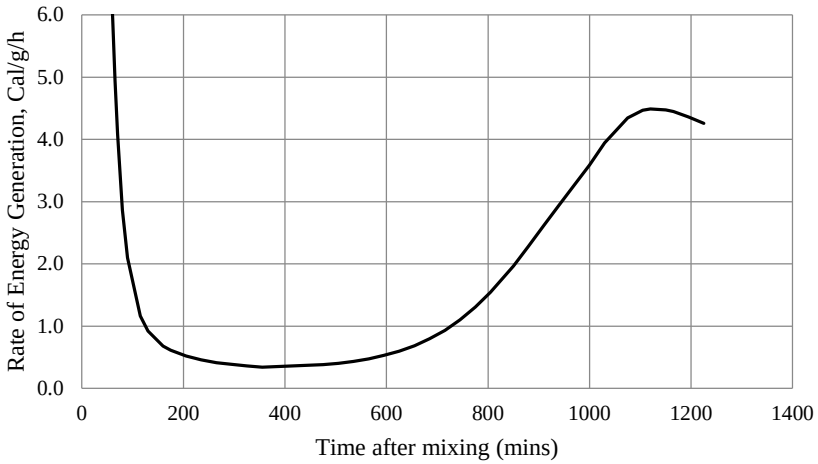

(29) G211C

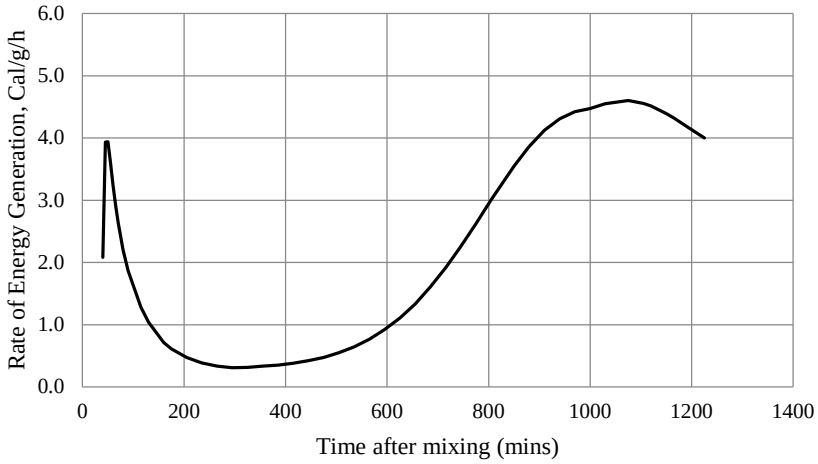

(30) G211F

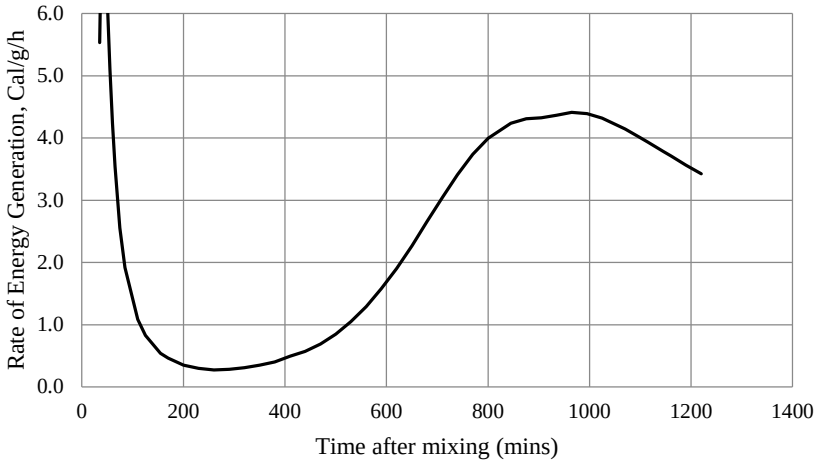

(31) G211S

(Cont.) Figure D-6. Relation between time after mixing and rate of energy generation

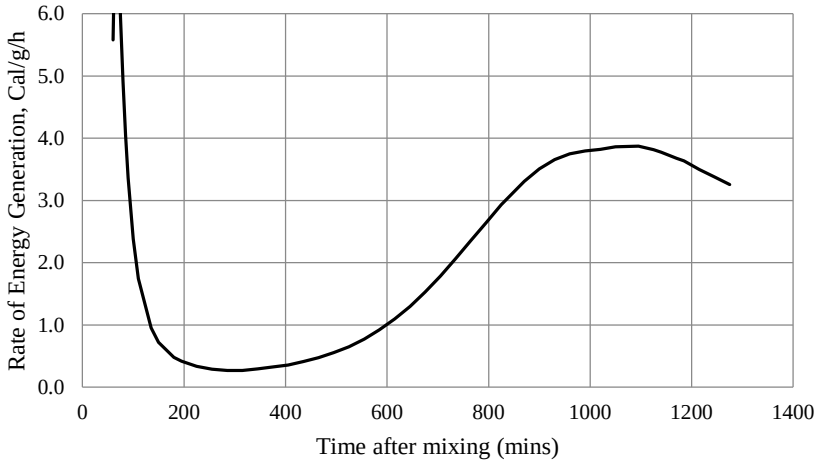

(32) G211FLP

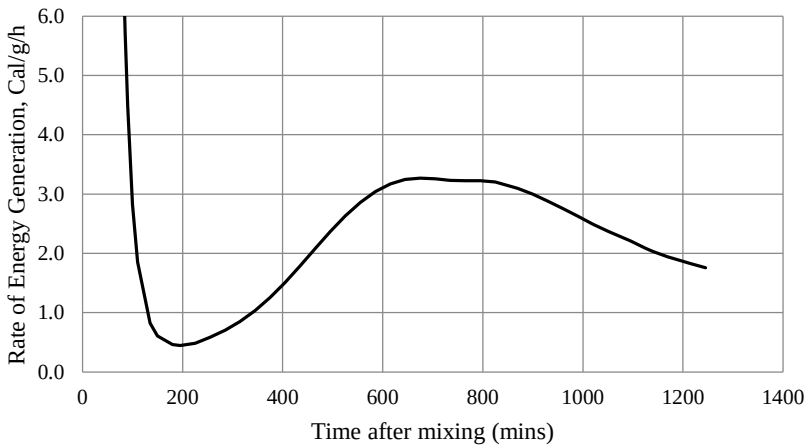

(33) G0.50 CVC

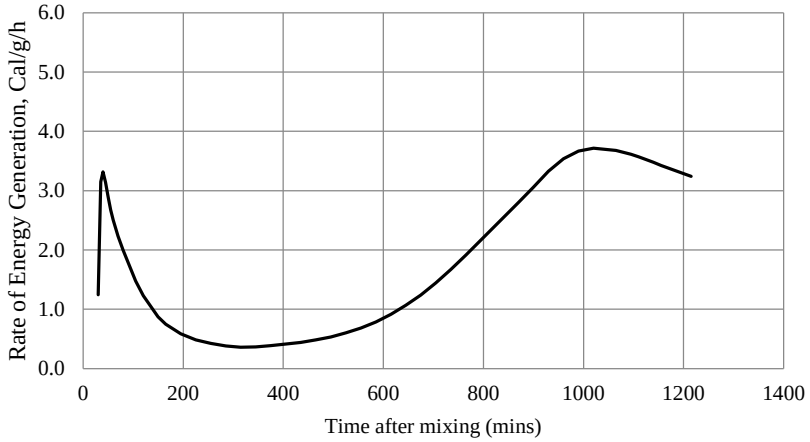

(34) G121C

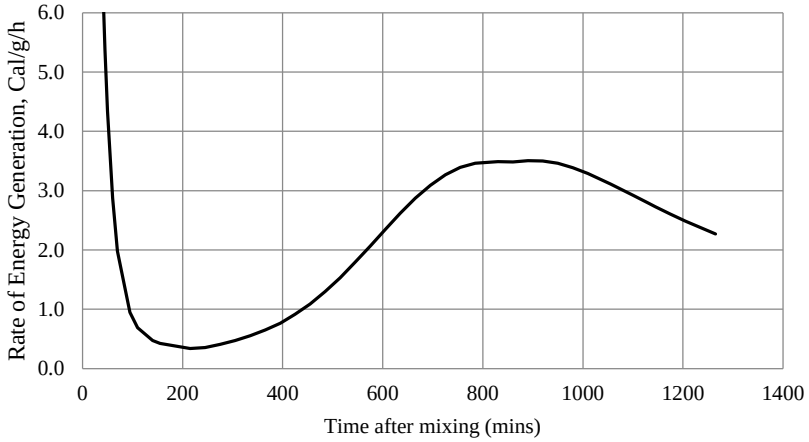

(35) G121F

(Cont.) Figure D-6. Relation between time after mixing and rate of energy generation

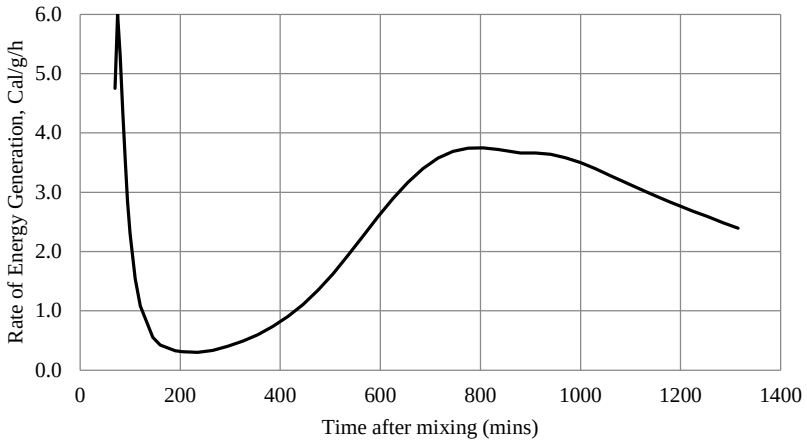

(36) G121S

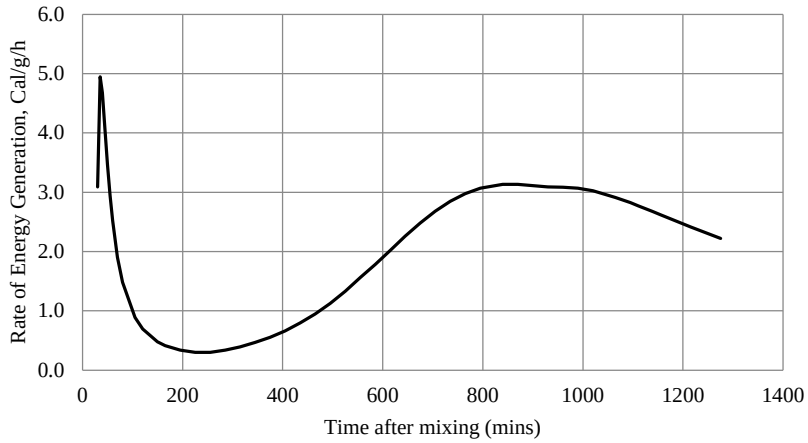

(37) G121FLP

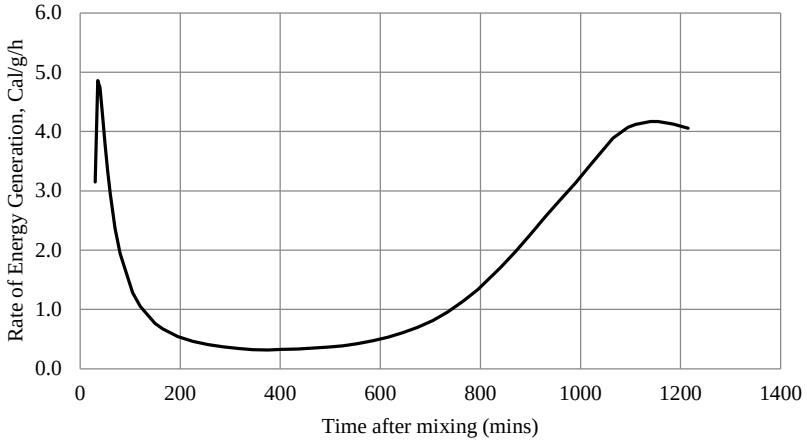

(38) G221C

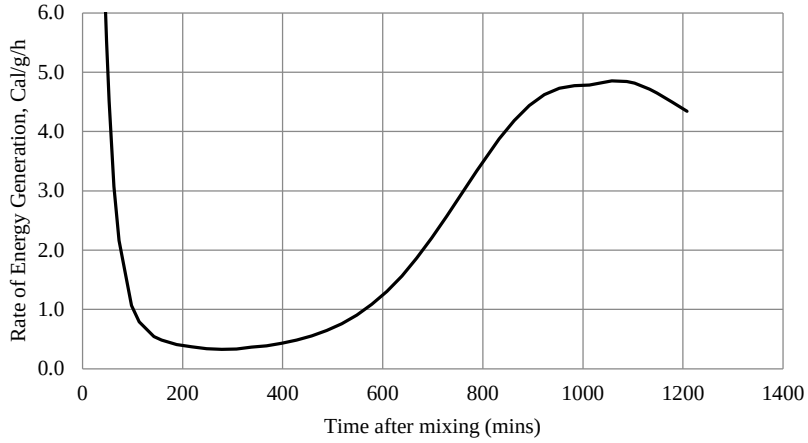

(39) G221F

(Cont.) Figure D-6. Relation between time after mixing and rate of energy generation

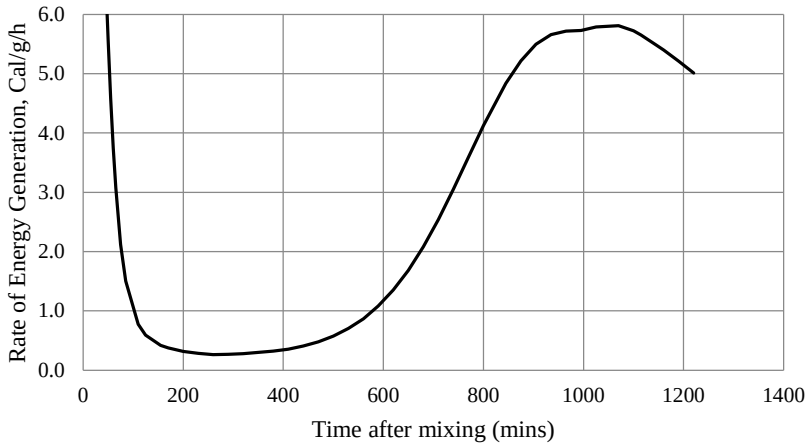

(40) G221S

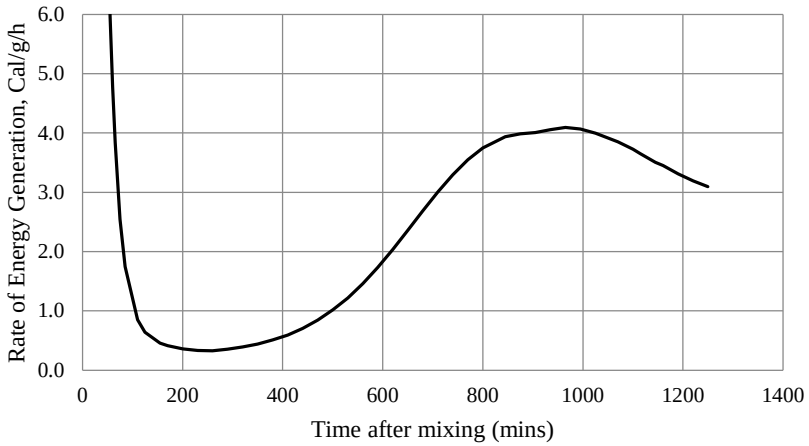

(41) G221FLP

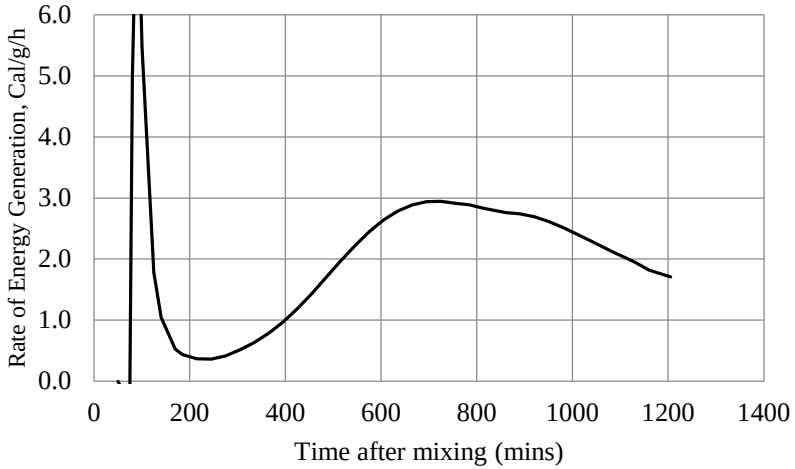

(42) G0.375 CVC

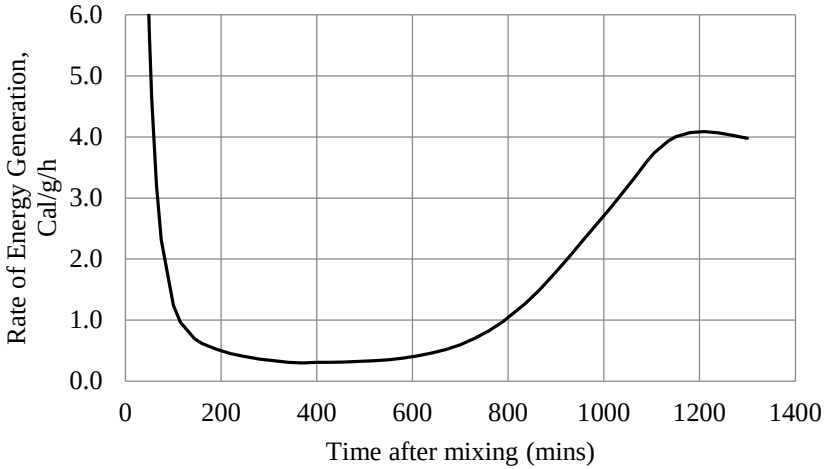

(43) G222C

(Cont.) Figure D-6. Relation between time after mixing and rate of energy generation

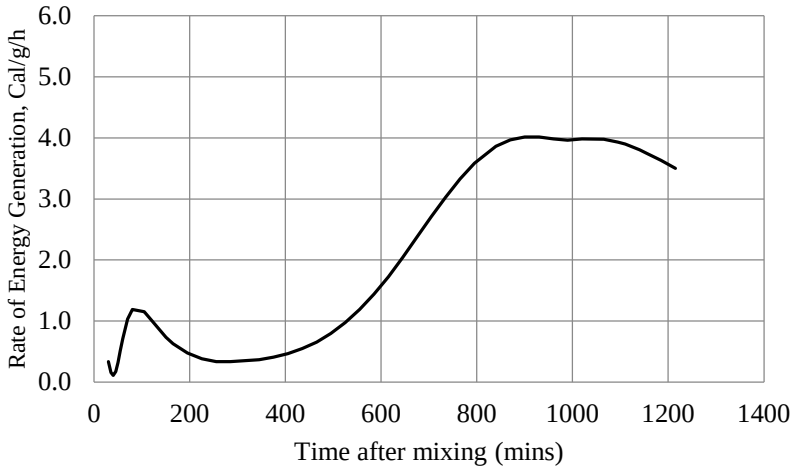

(44) G222F

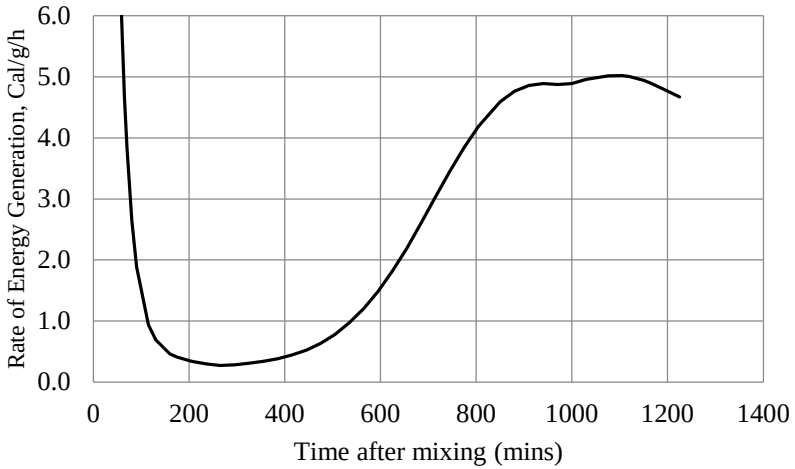

(45) G222S

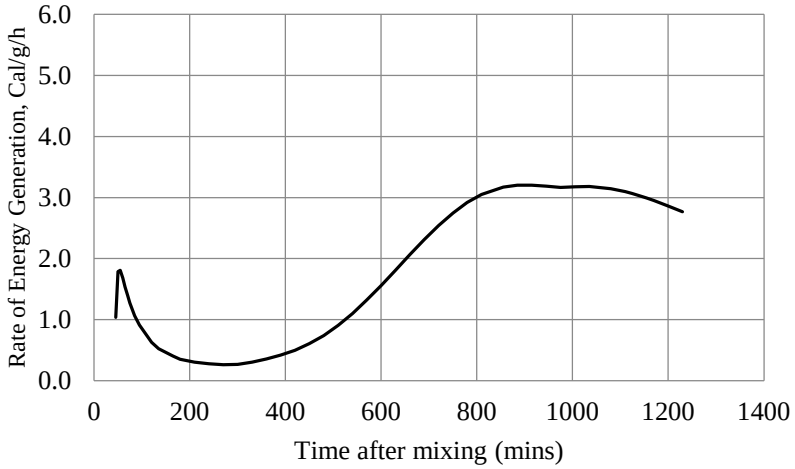

(46) G222FLP

(Cont.) Figure D-6. Relation between time after mixing and rate of energy generation

3. Time of Setting

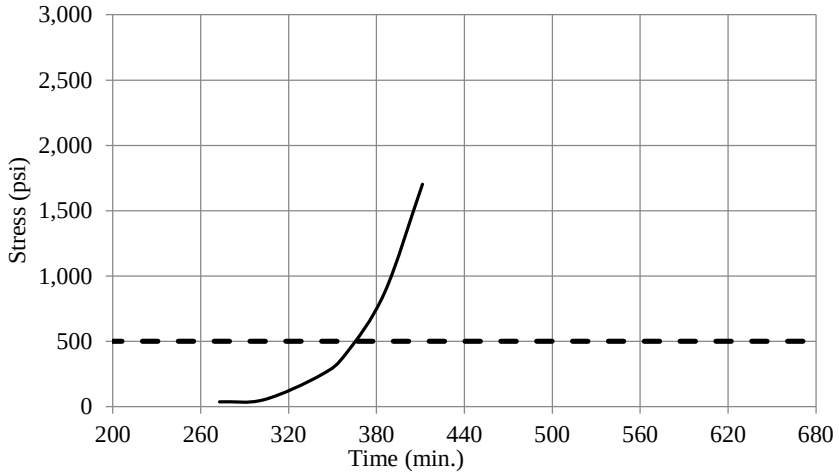

(1) LS0.50 CVC

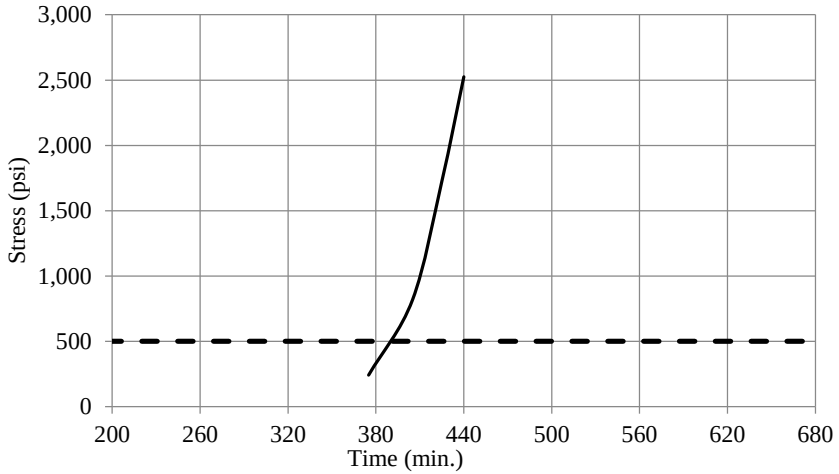

(2) LS121C

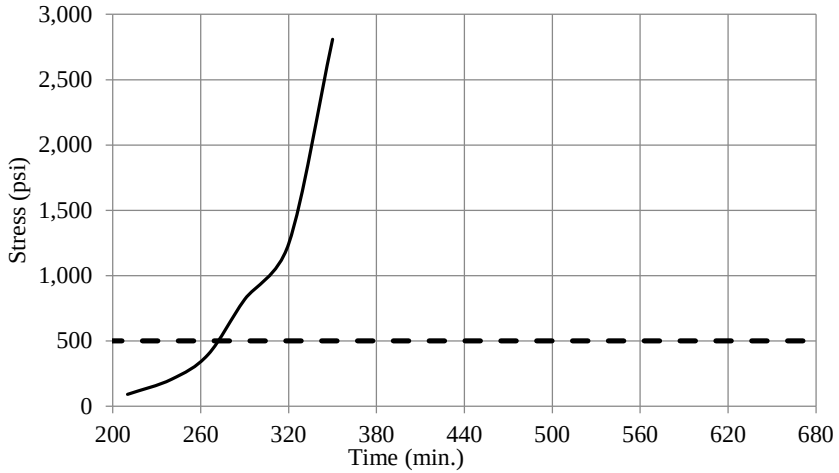

(3) LS121F

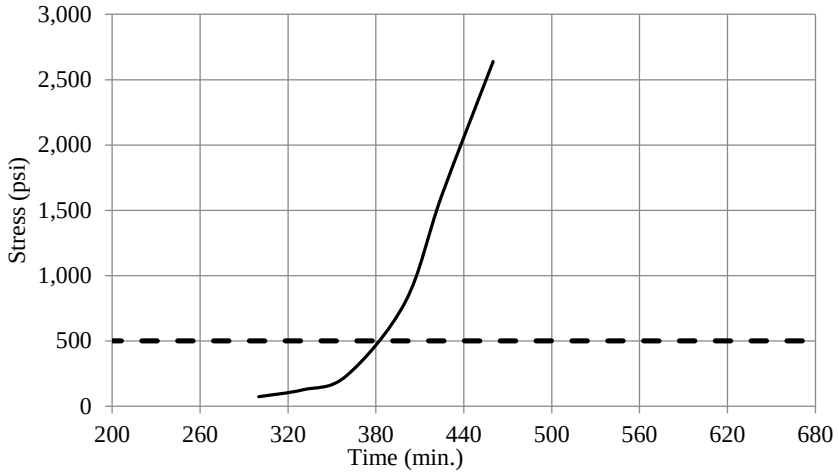

(4) LS121S

Figure D-7. Time of setting penetration stress results for SCC and CVC mixtures

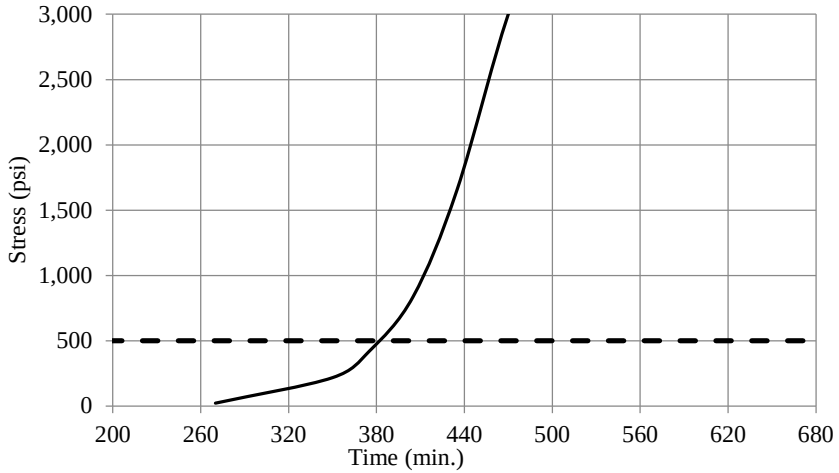

(5) LS121FLP

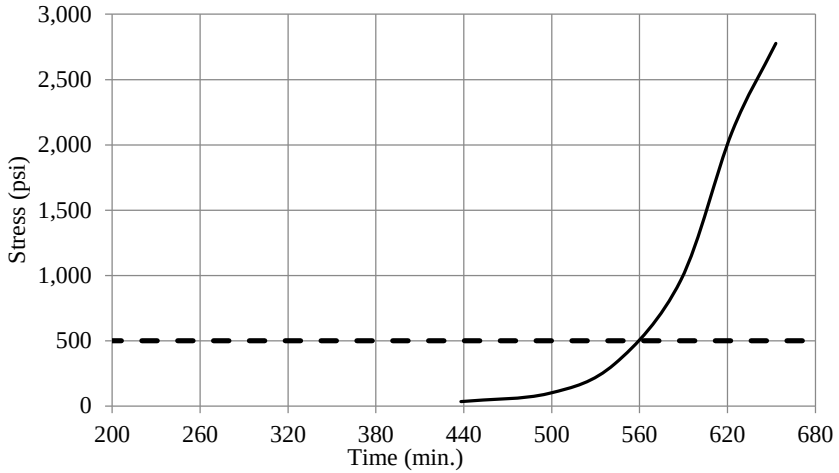

(6) LS221C

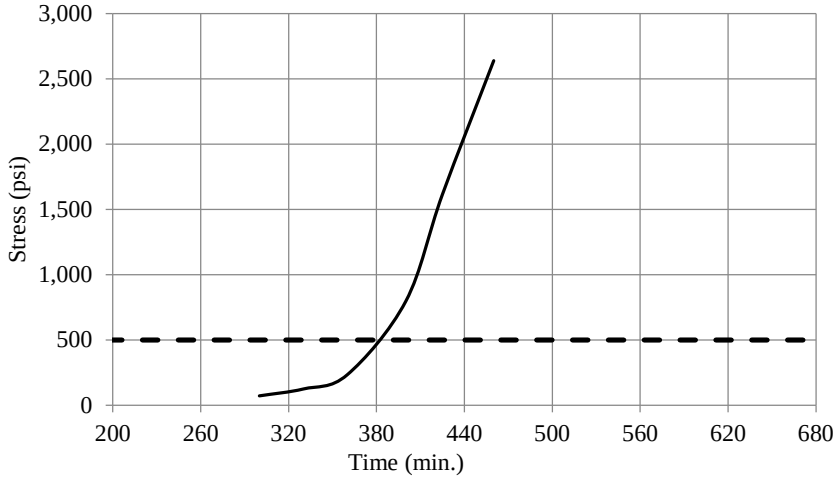

(7) LS221F

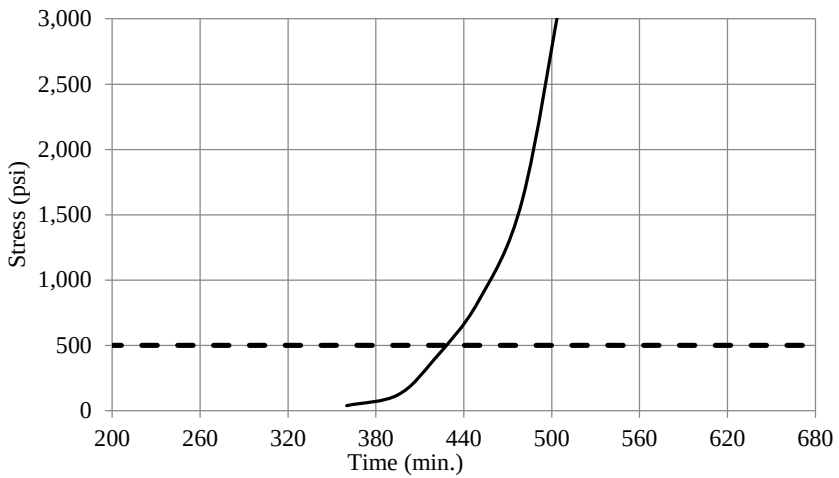

(8) LS221S

(Cont.) Figure D-7. Time of setting penetration stress results for SCC and CVC mixtures

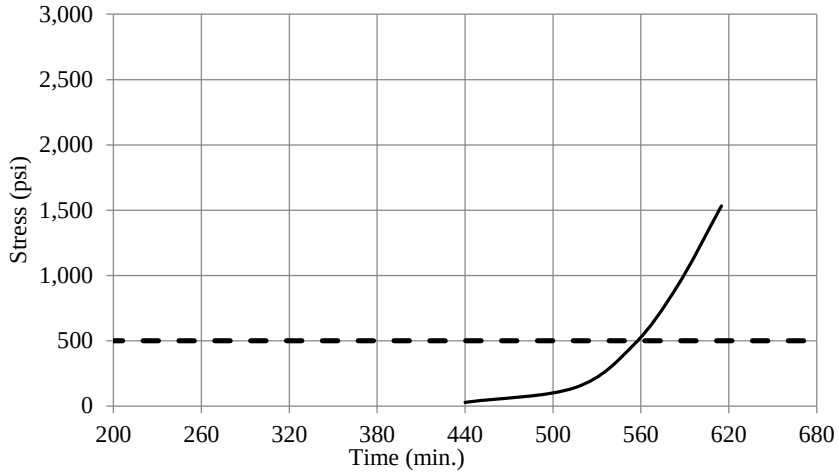

(9) LS221FLP

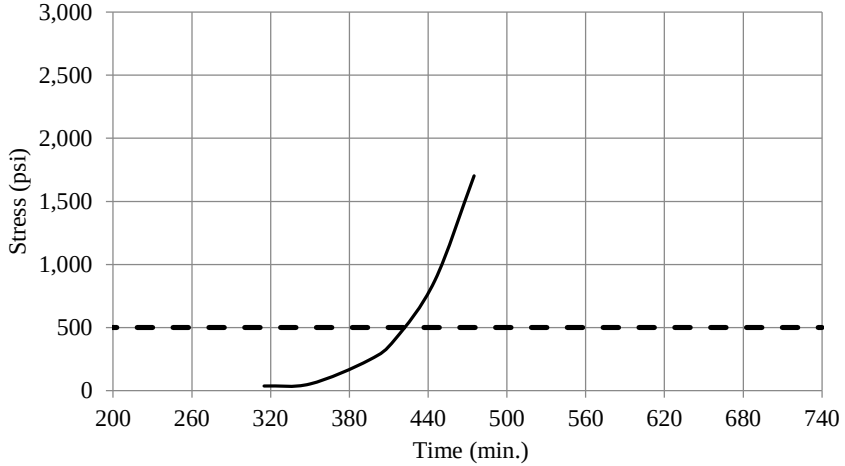

(10) G0.50 CVC

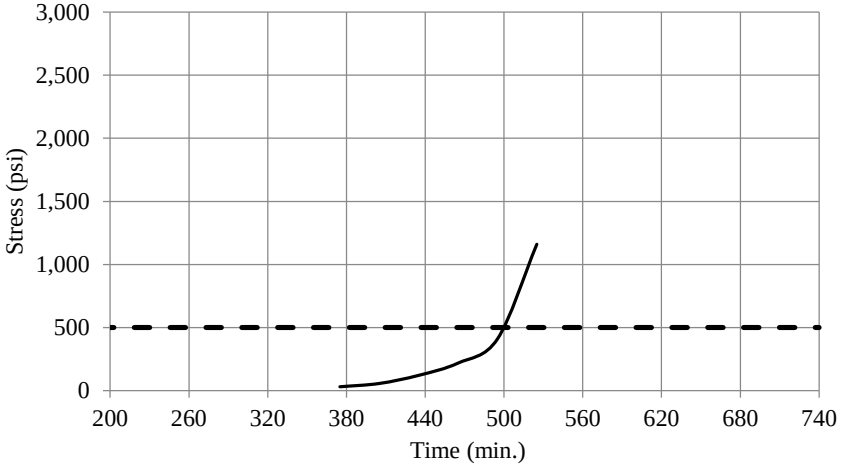

(11) G121C

(Cont.) Figure D-7. Time of setting penetration stress results for SCC and CVC mixtures

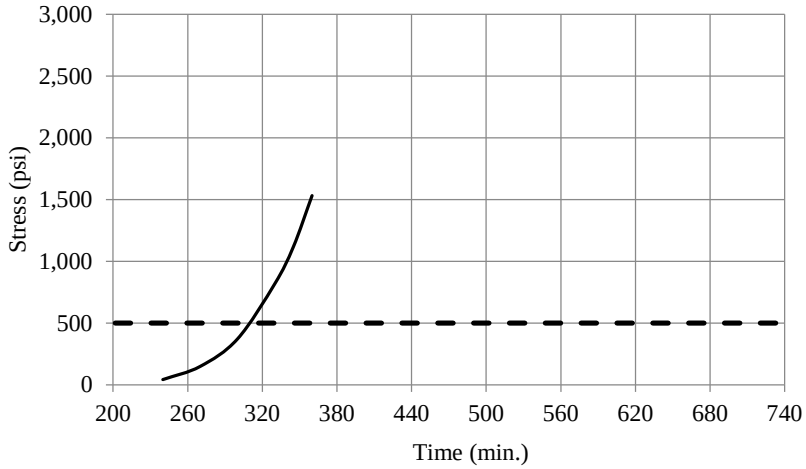

(12) G121F

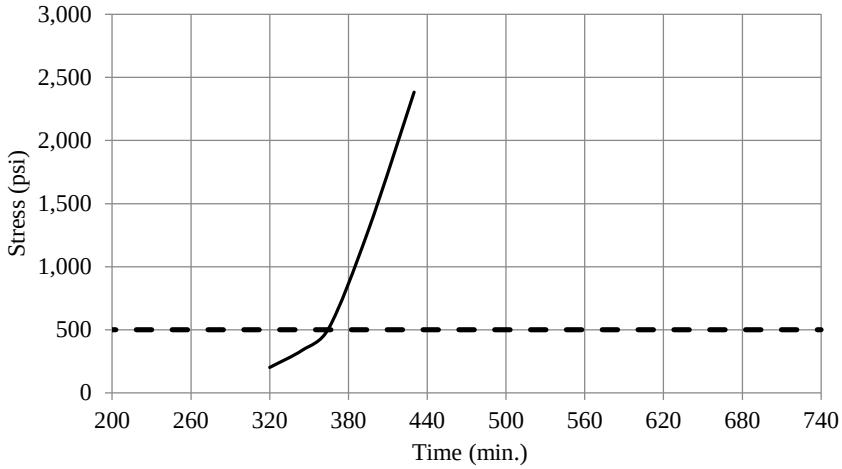

(13) G121S

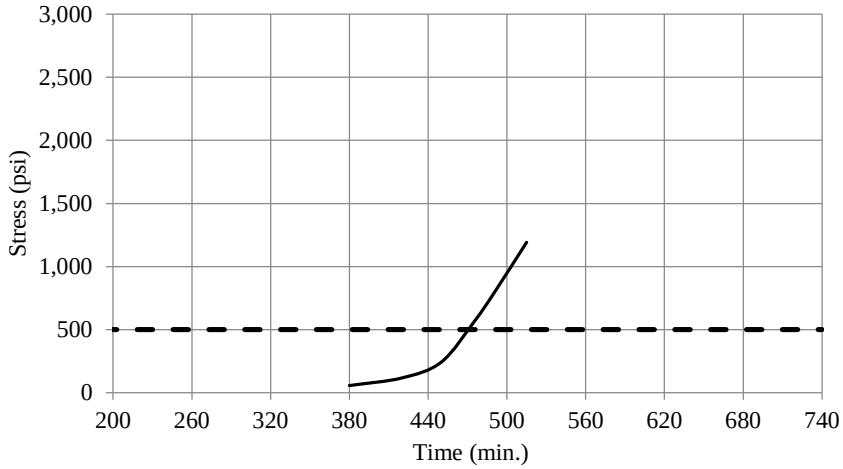

(14) G121FLP

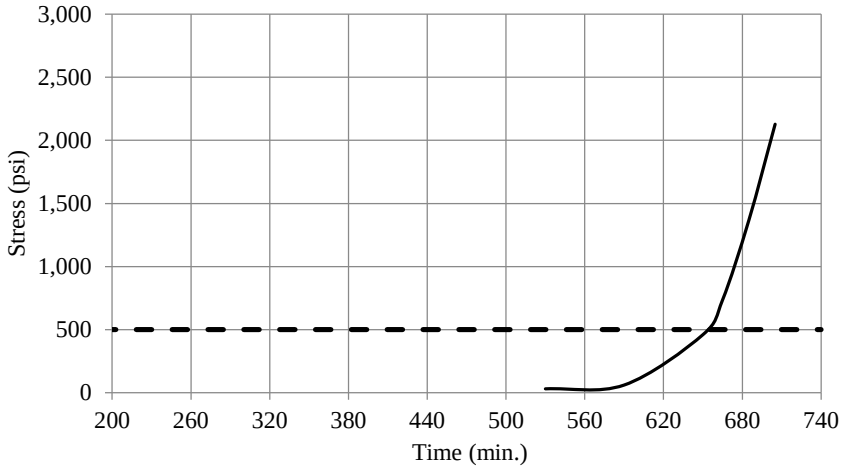

(15) G221C

(Cont.) Figure D-7. Time of setting penetration stress results for SCC and CVC mixtures

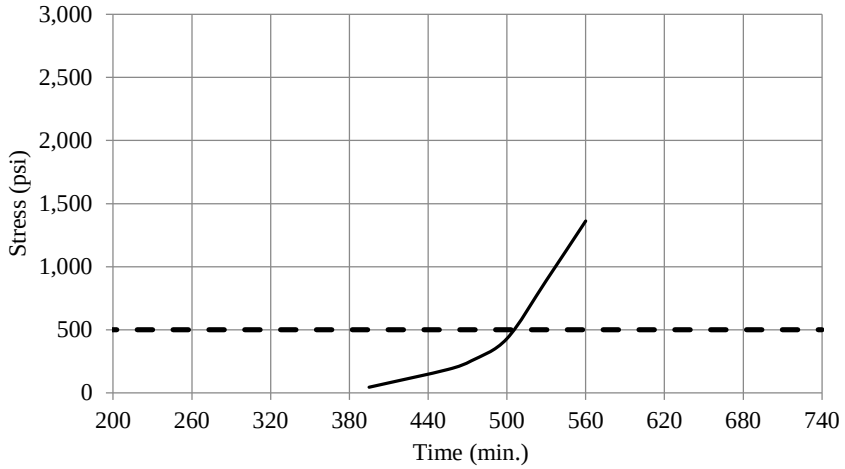

(16) G221F

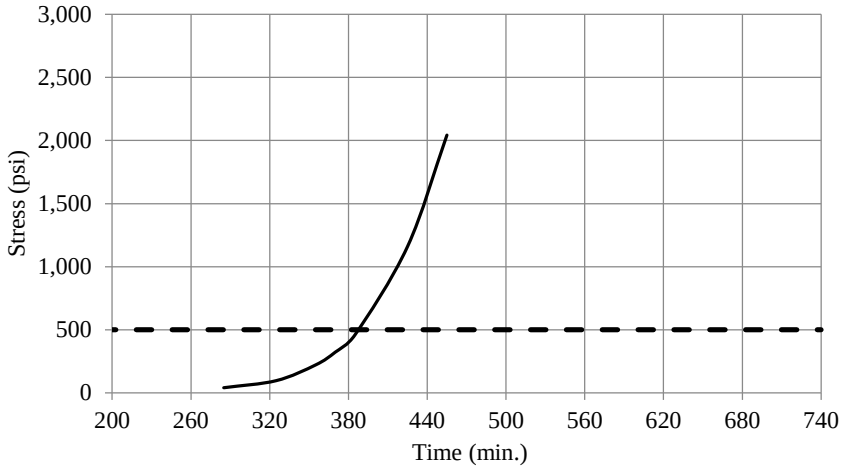

(17) G221S

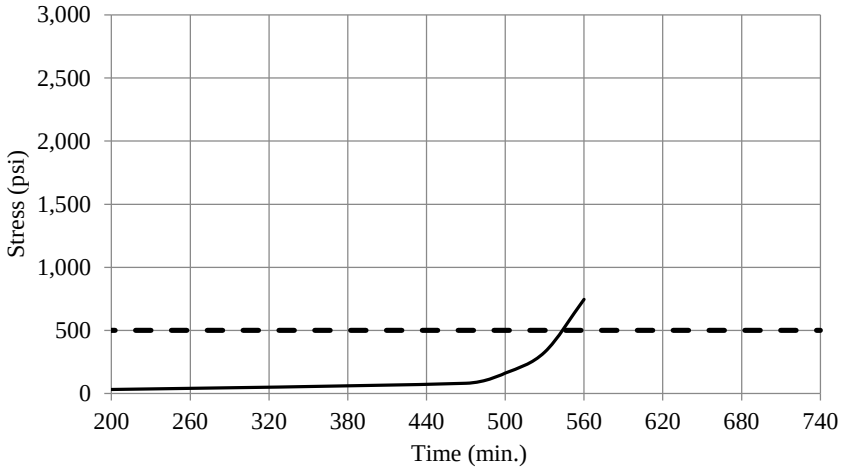

(18) G221FLP

(Cont.) Figure D-7. Time of setting penetration stress results for SCC and CVC mixtures

APPENDIX E: Hardened Concrete Properties

Contents

1. Compressive Strength

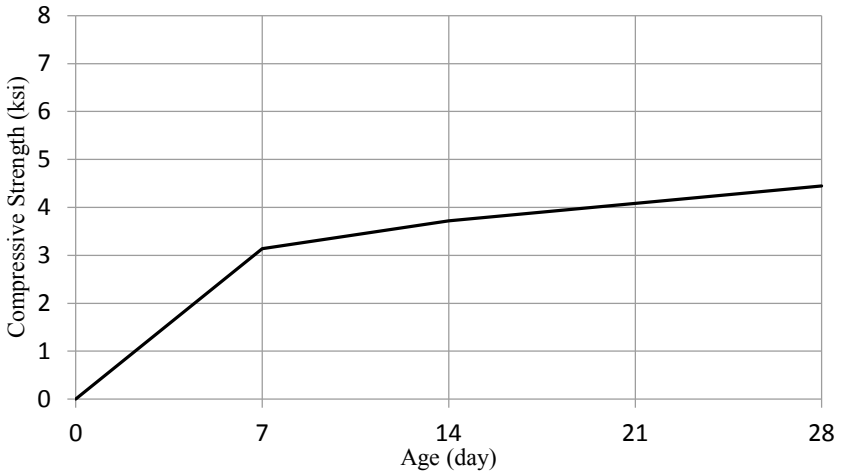

(1) LS0.75 CVC

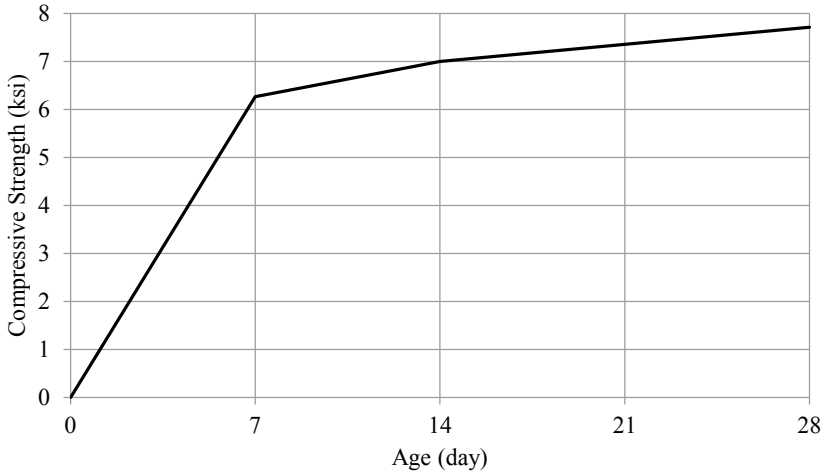

(2) LS111C

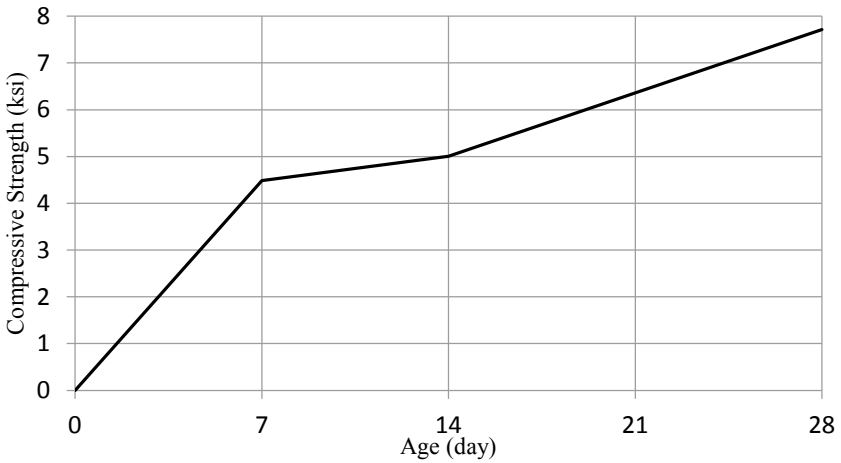

(3) LS111F

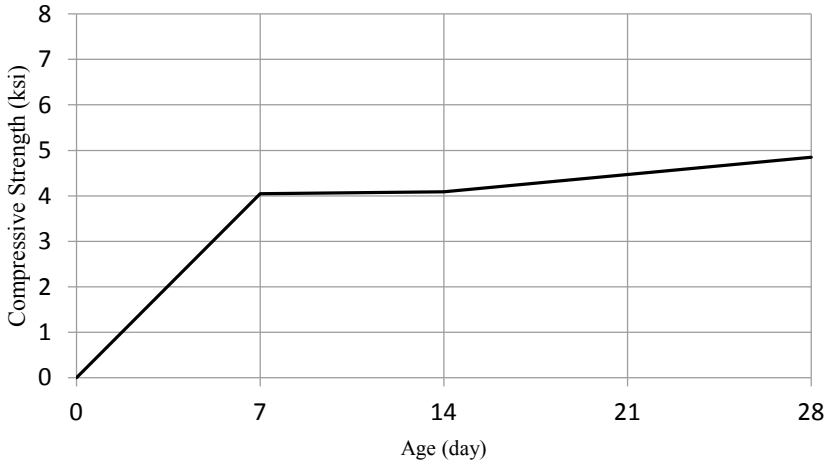

(4) LS111S

Figure E-1. Relationship between compressive strength of hardened concrete and age after casting

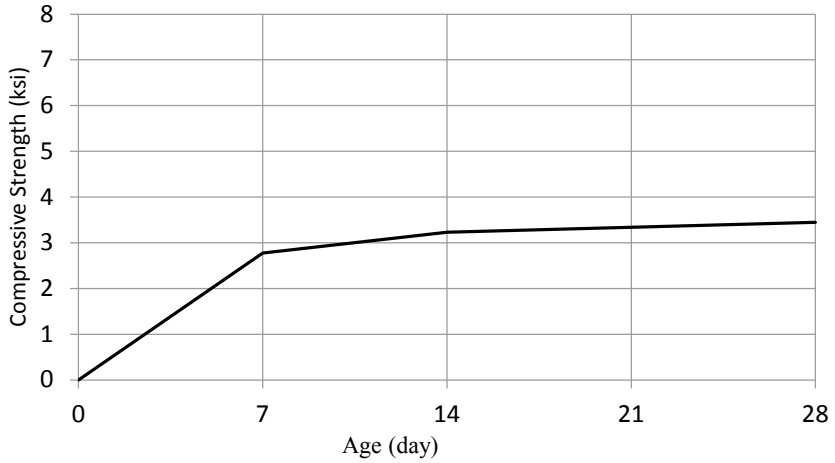

(5) LS111FLP

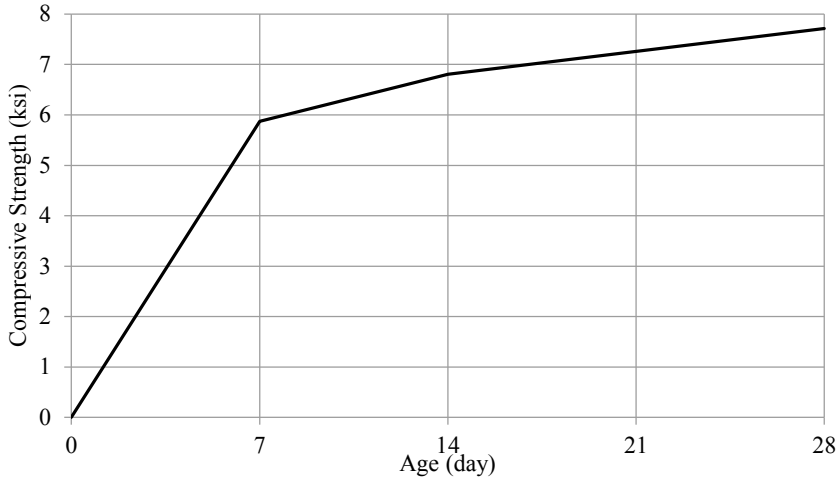

(6) LS211C

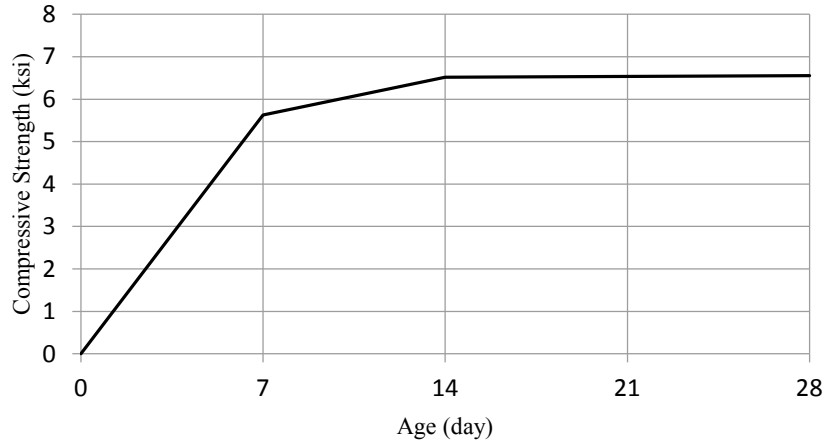

(7) LS211F

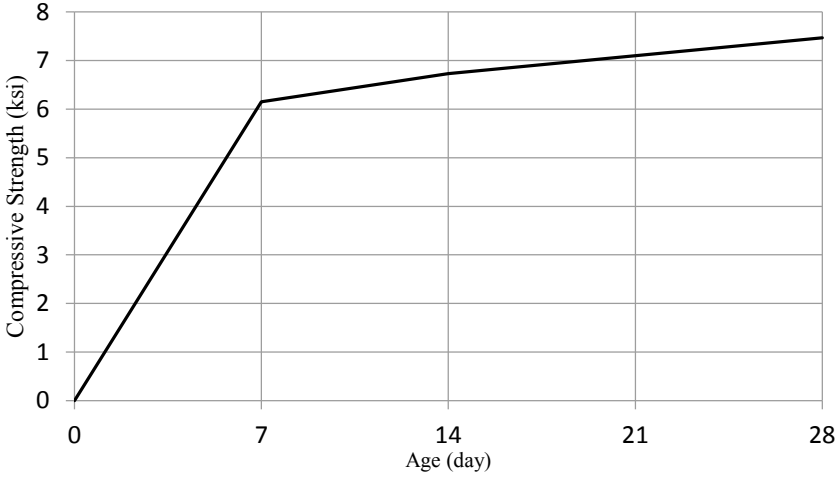

(8) LS211S

(Cont.) Figure E-1. Relationship between compressive strength of hardened concrete and age after casting

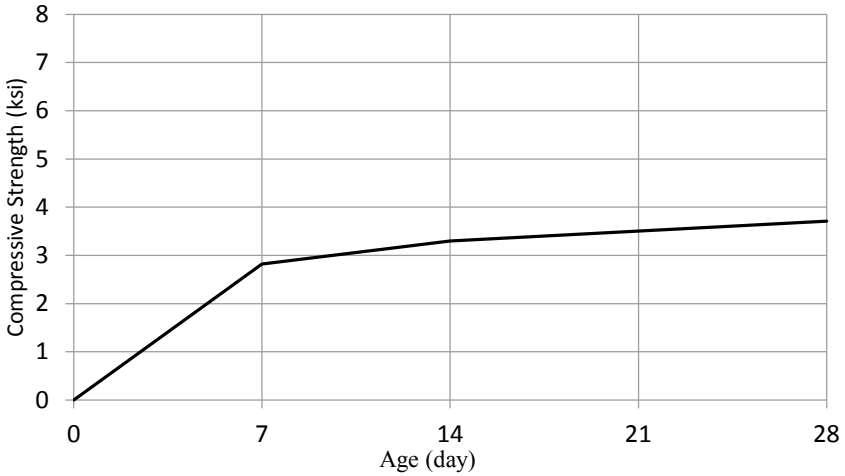

(9) LS211FLP

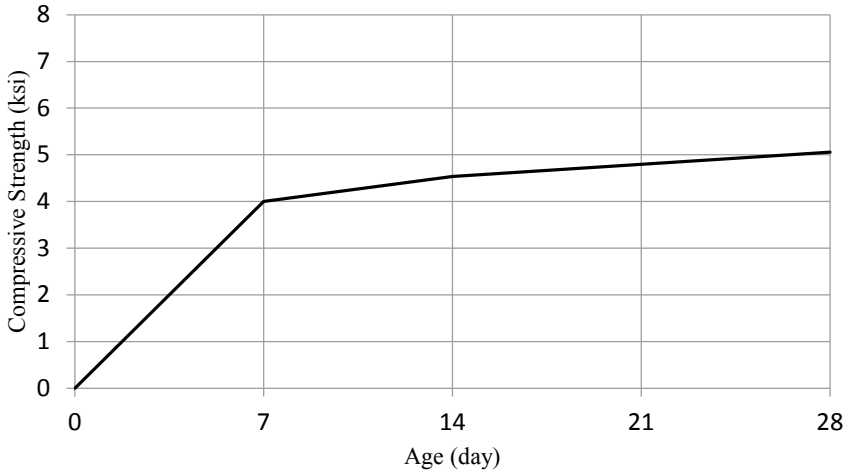

(10) LS0.50 CVC

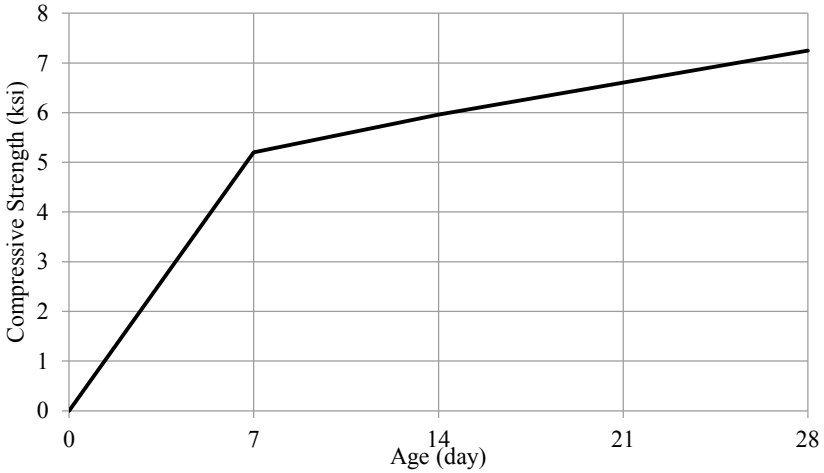

(11) LS121C

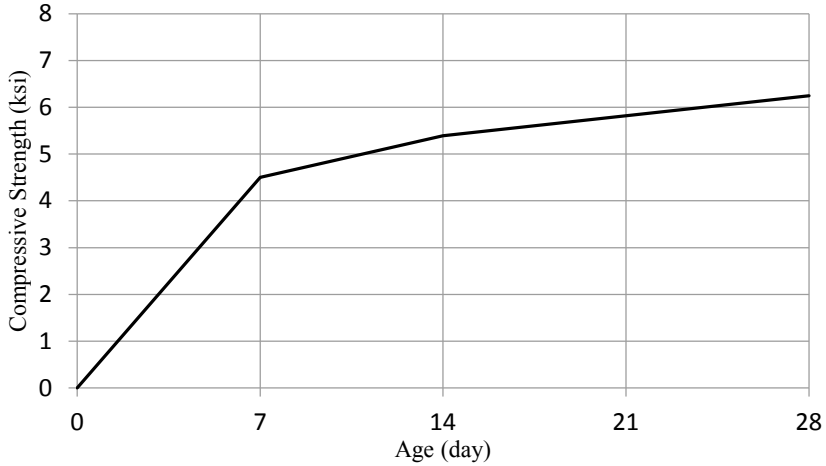

(12) LS121F

(Cont.) Figure E-1. Relationship between compressive strength of hardened concrete and age after casting

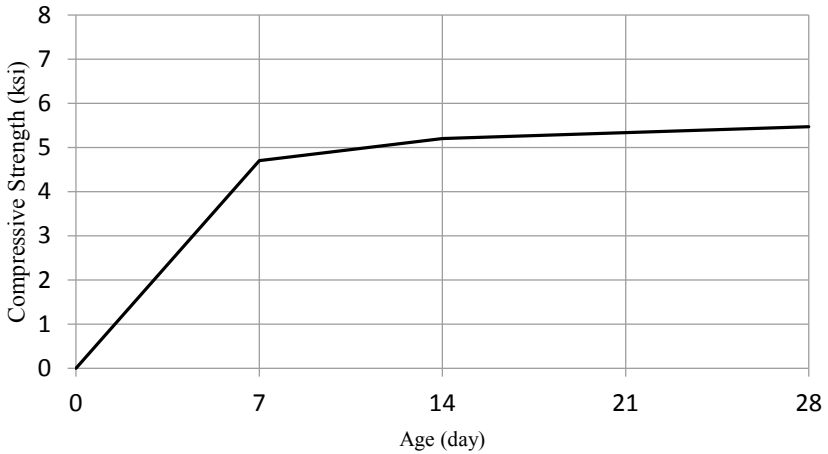

(13) LS121S

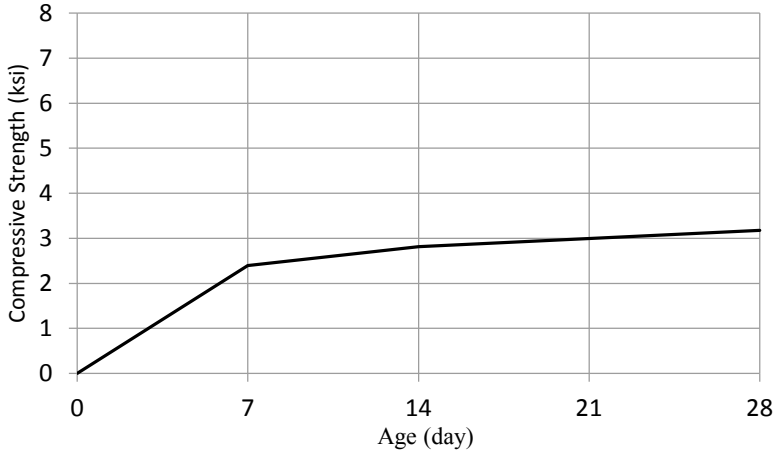

(14) LS121FLP

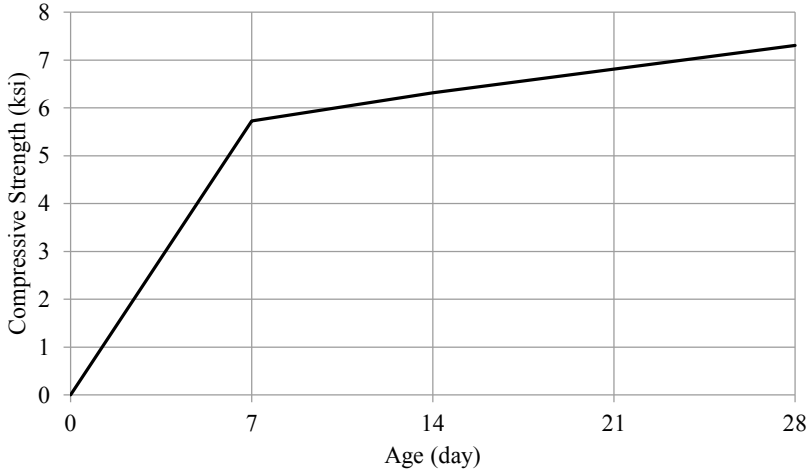

(15) LS221C

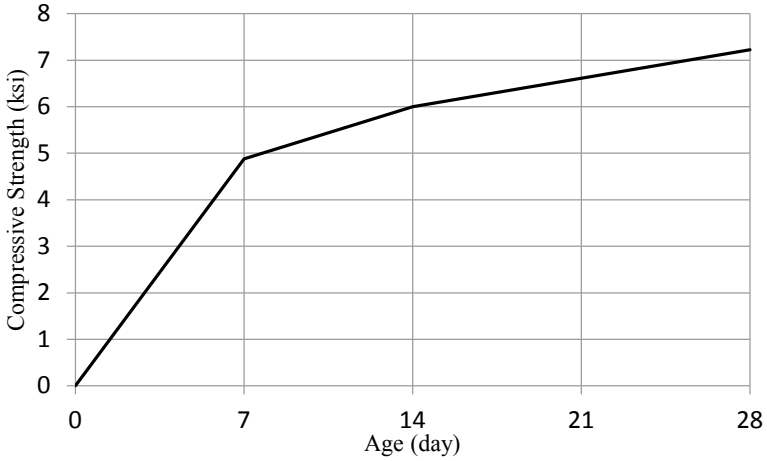

(16) LS221F

(Cont.) Figure E-1. Relationship between compressive strength of hardened concrete and age after casting

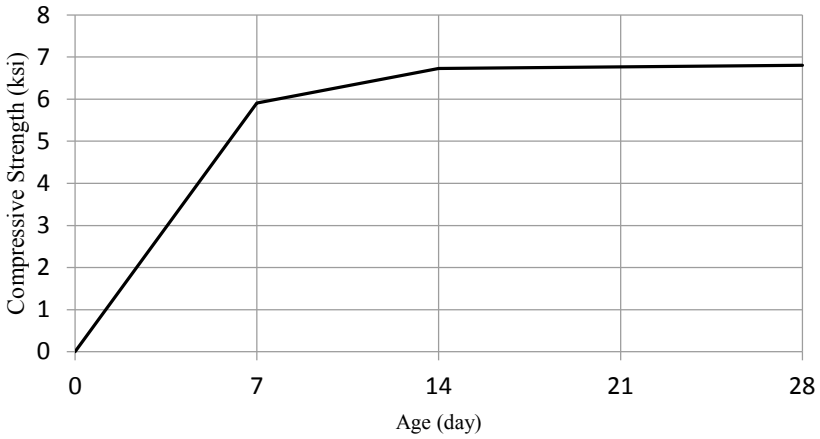

(17) LS221S

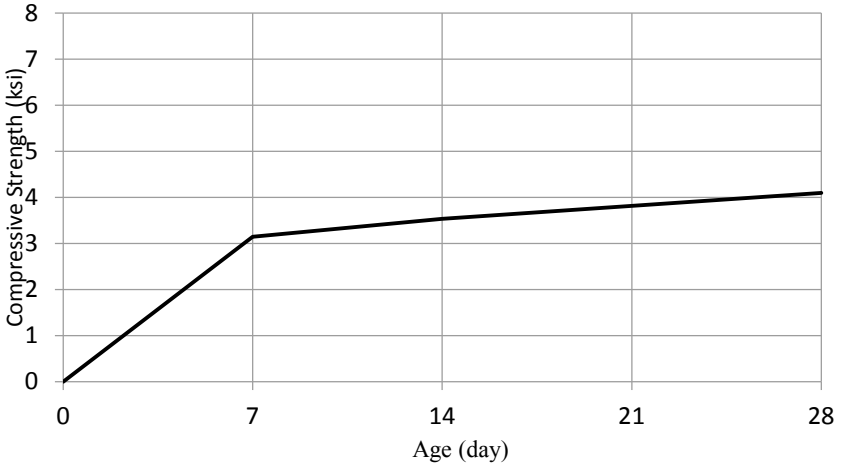

(18) LS221FLP

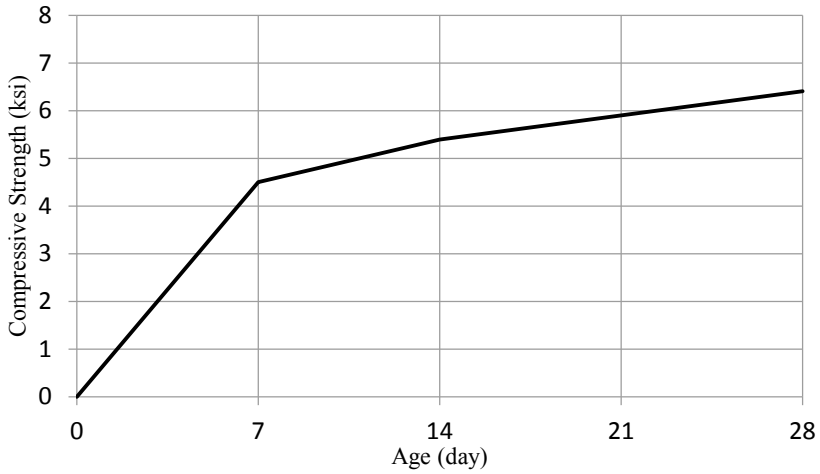

(19) LS0.375 CVC

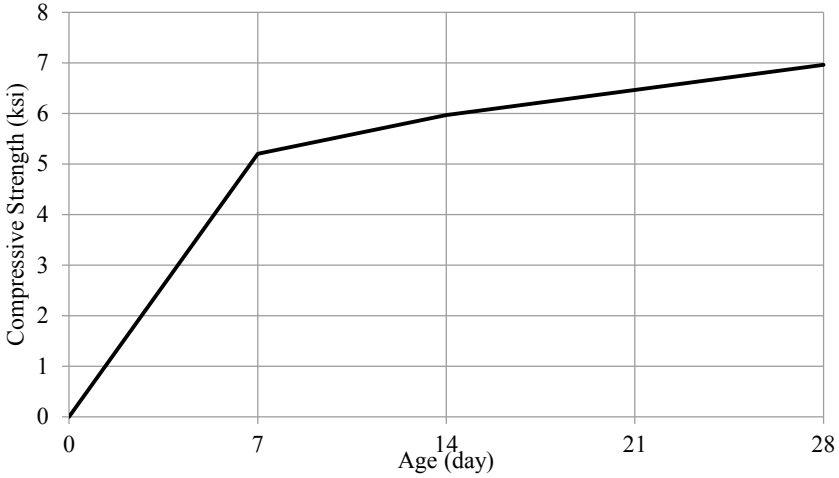

(20) LS222C

(Cont.) Figure E-1. Relationship between compressive strength of hardened concrete and age after casting

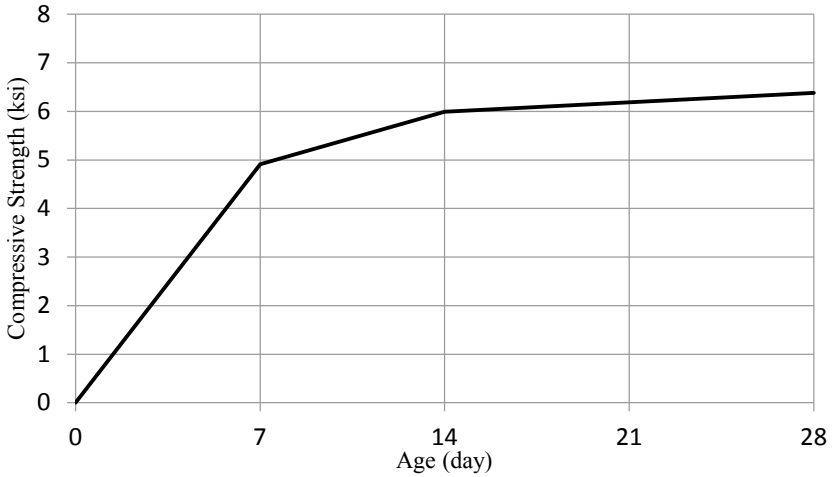

(21) LS222F

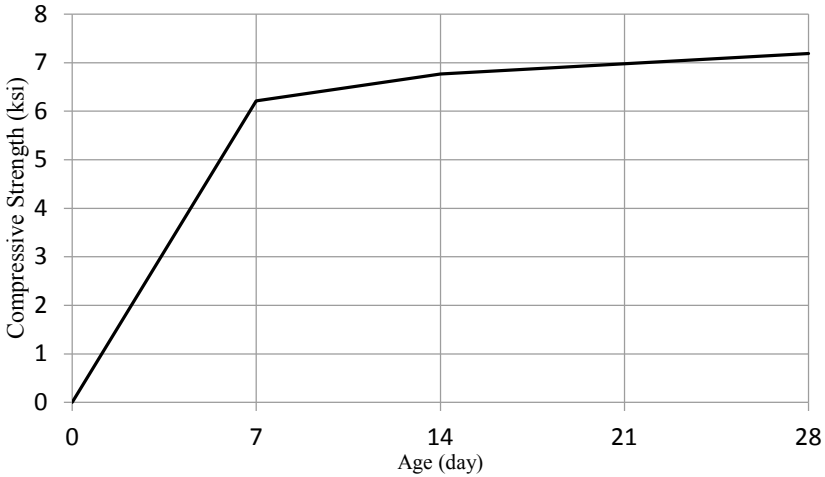

(22) LS222S

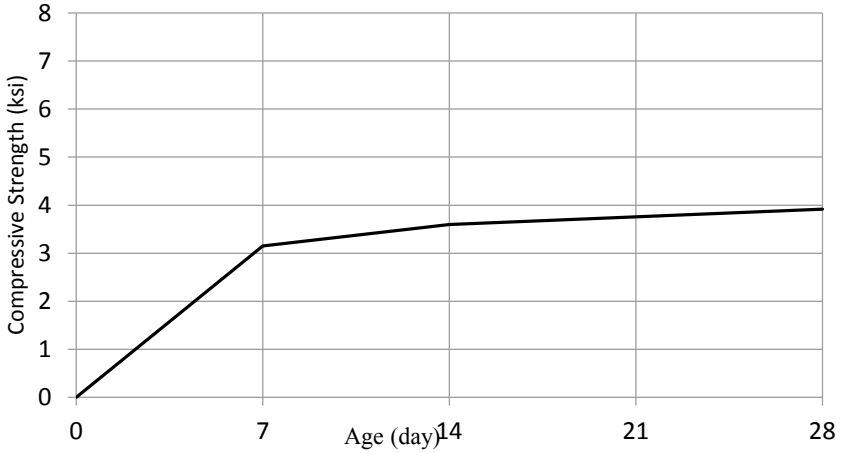

(23) LS222FLP

(Cont.) Figure E-1. Relationship between compressive strength of hardened concrete and age after casting

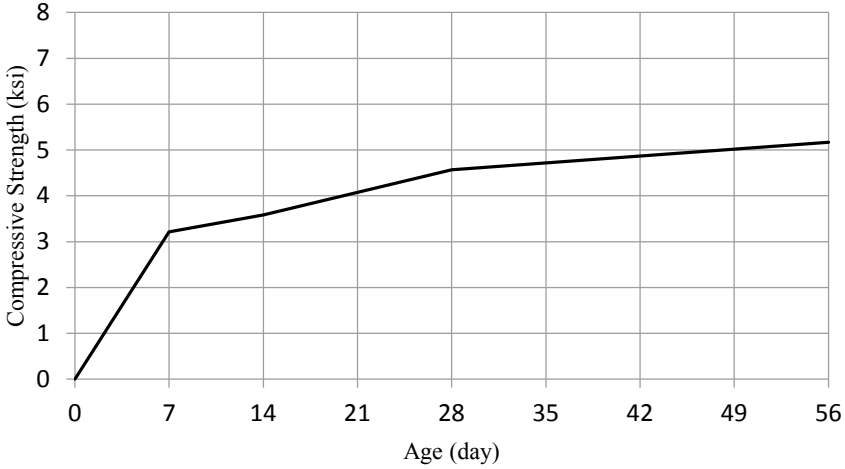

(24) G0.75 CVC

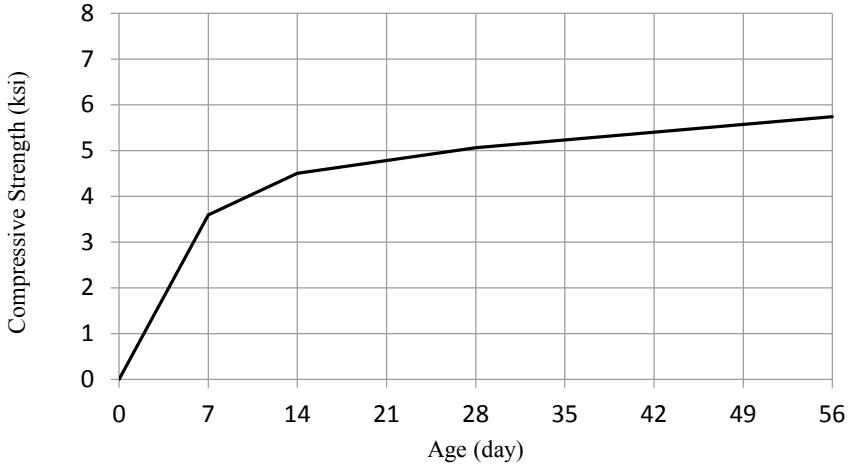

(25) G111C

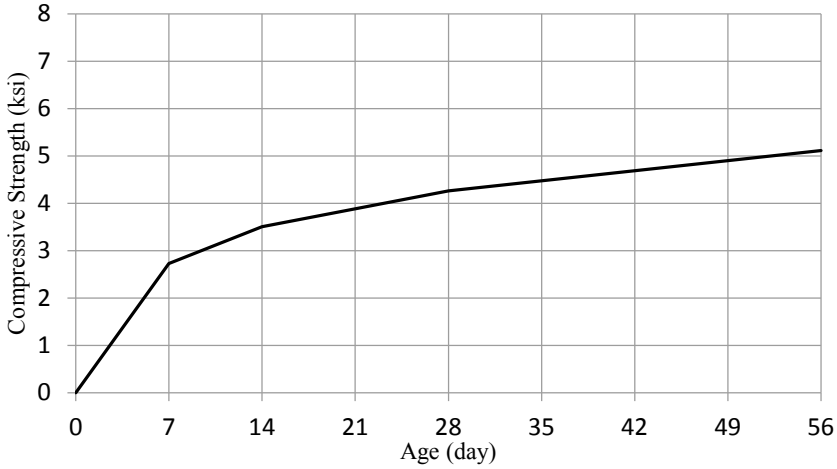

(26) G111F

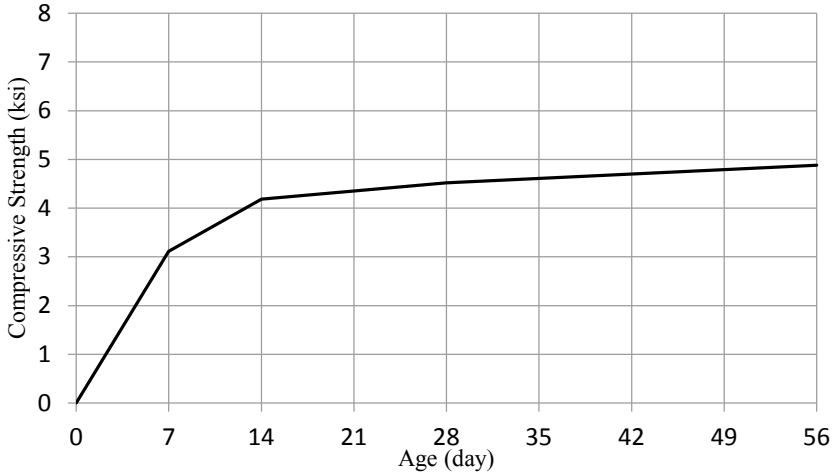

(27) G111S

(Cont.) Figure E-1. Relationship between compressive strength of hardened concrete and age after casting

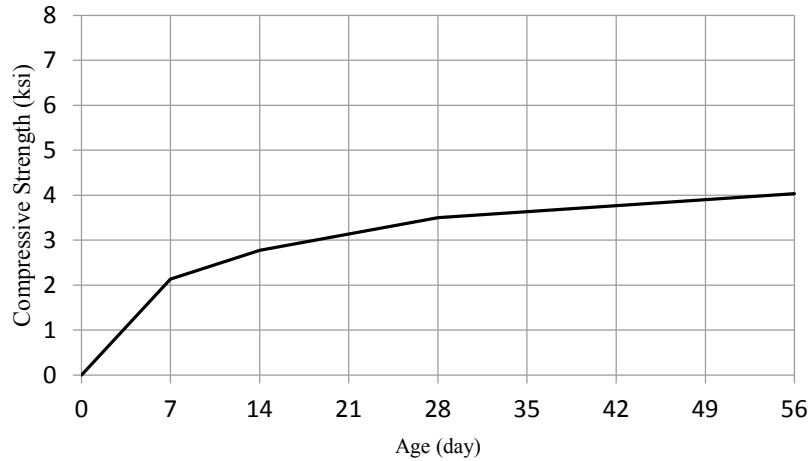

(28) G111FLP

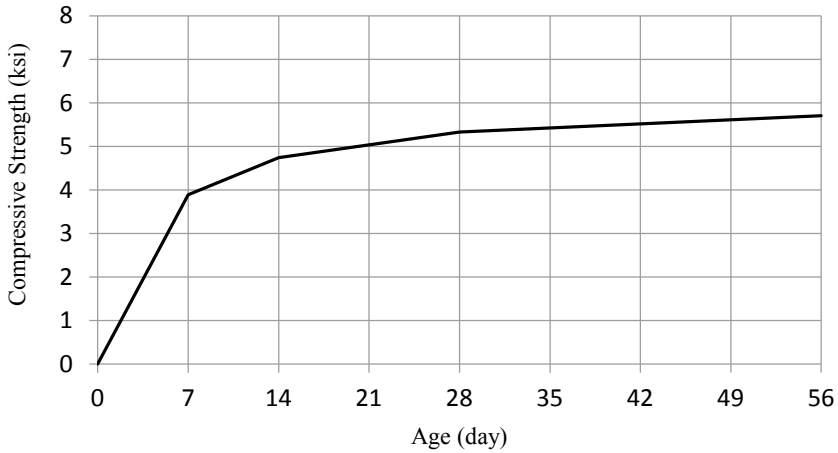

(29) G211C

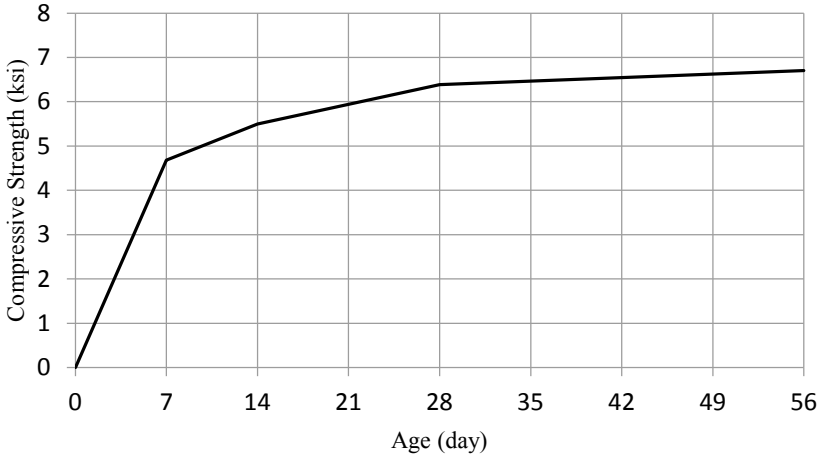

(30) G211F

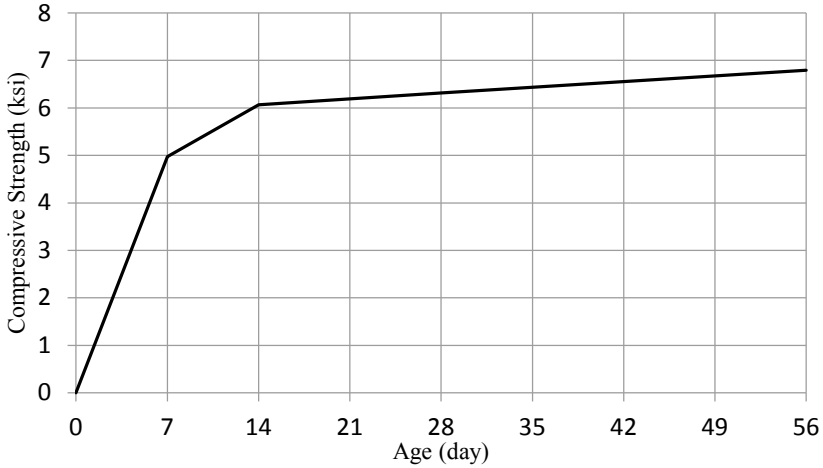

(31) G211S

(Cont.) Figure E-1. Relationship between compressive strength of hardened concrete and age after casting

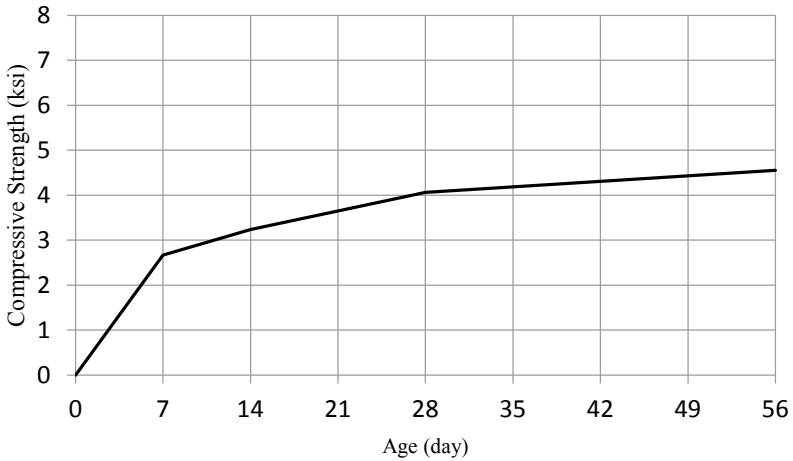

(32) G211FLP

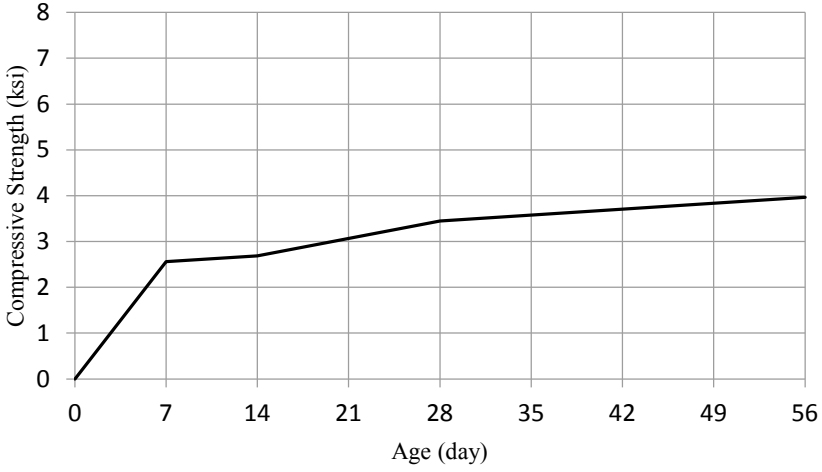

(33) G0.50 CVC

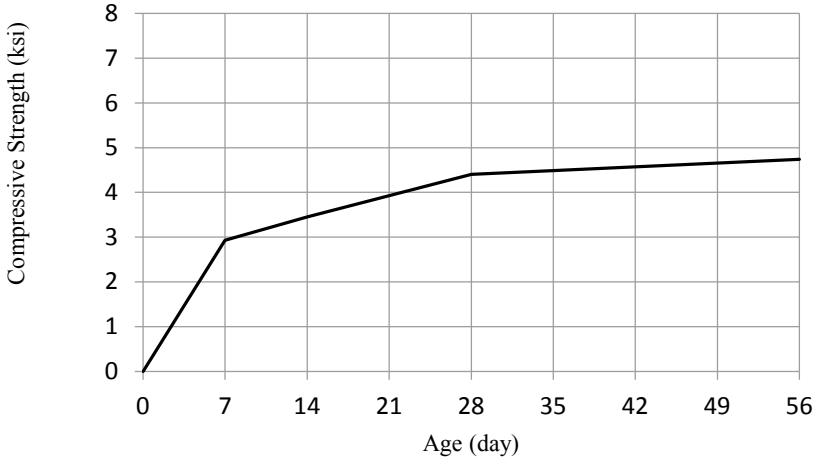

(34) G121C

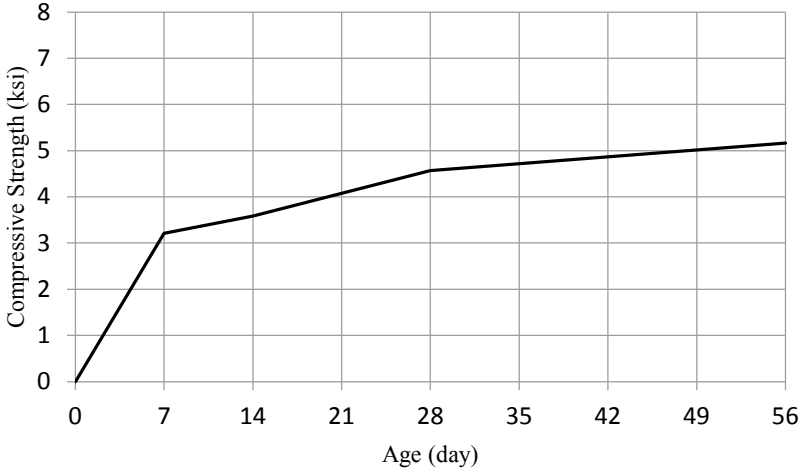

(35) G121F

(Cont.) Figure E-1. Relationship between compressive strength of hardened concrete and age after casting

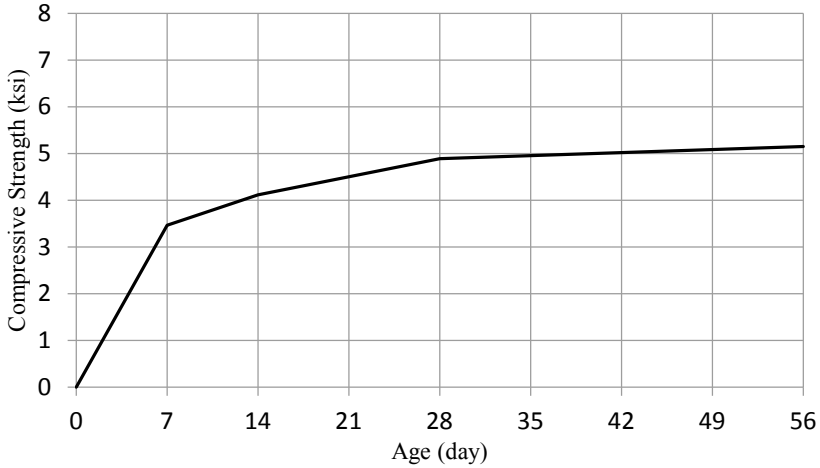

(36) G121S

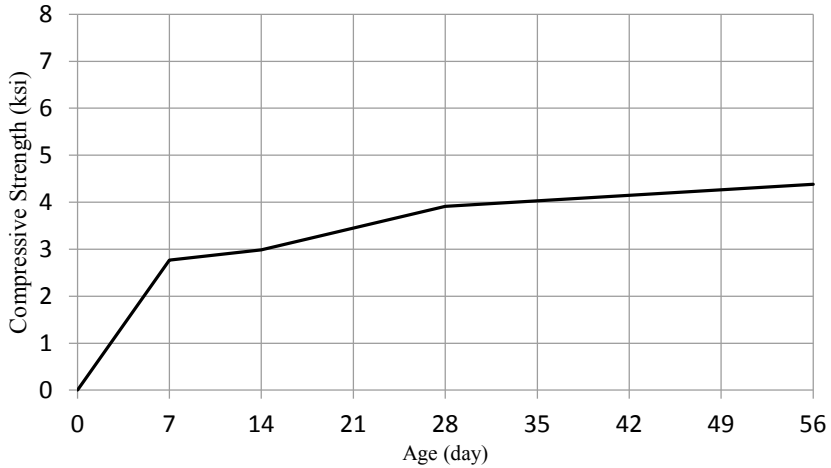

(37) G121FLP

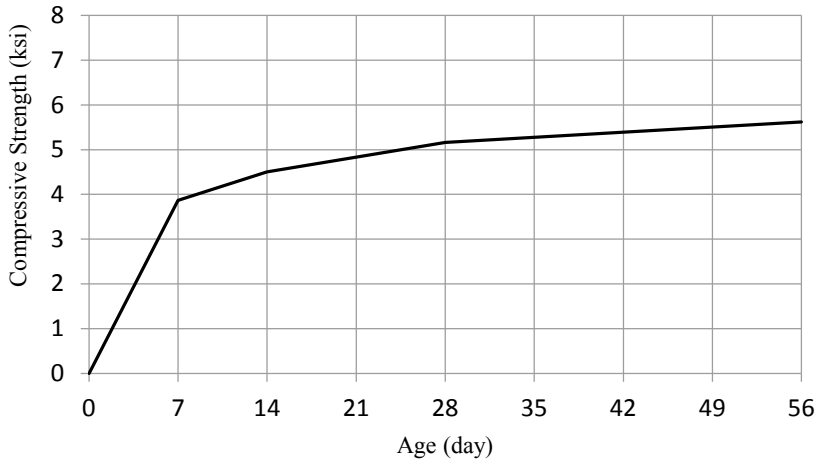

(38) G221C

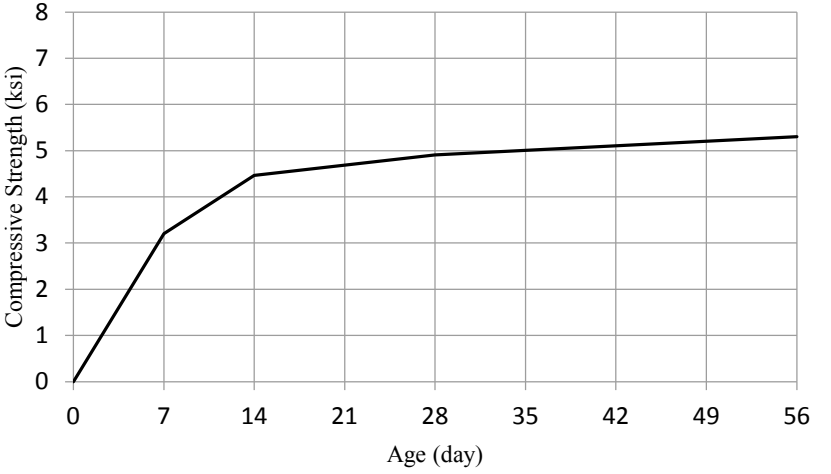

(39) G221F

(Cont.) Figure E-1. Relationship between compressive strength of hardened concrete and age after casting

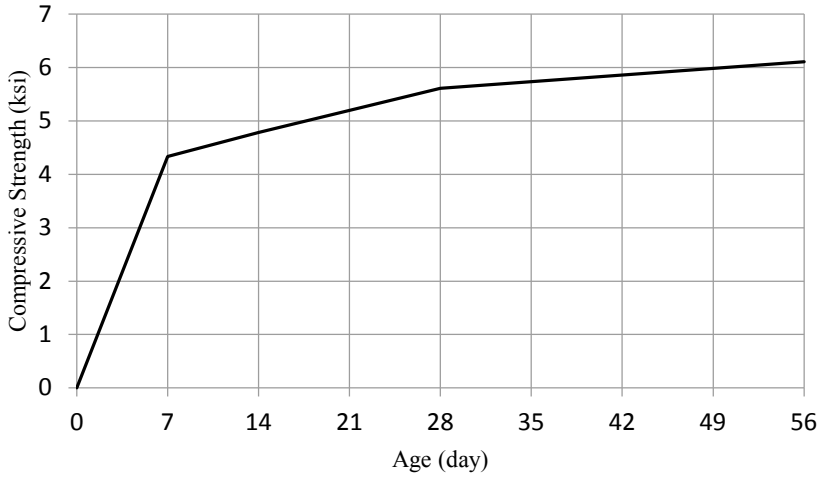

(40) G221S

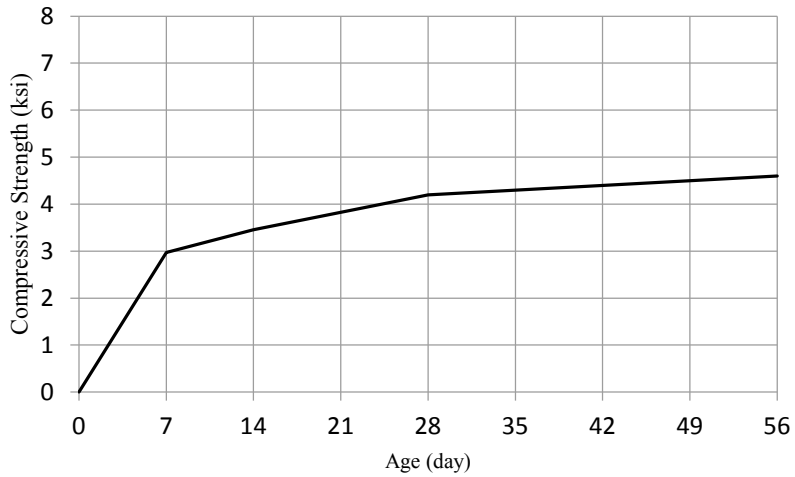

(41) G221FLP

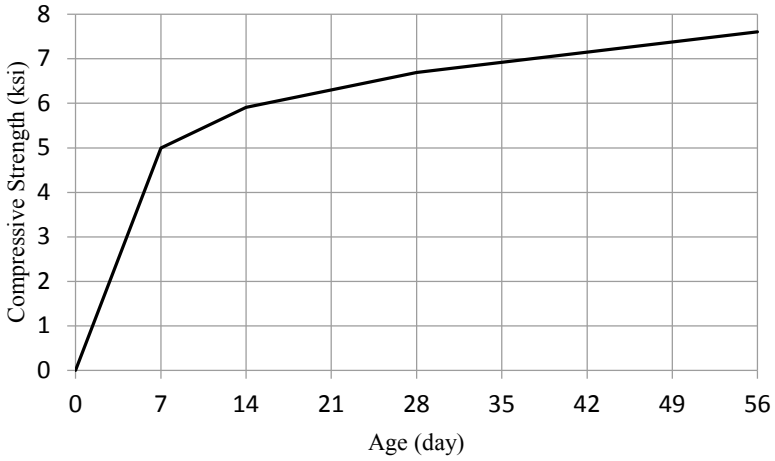

(42) G0.375 CVC

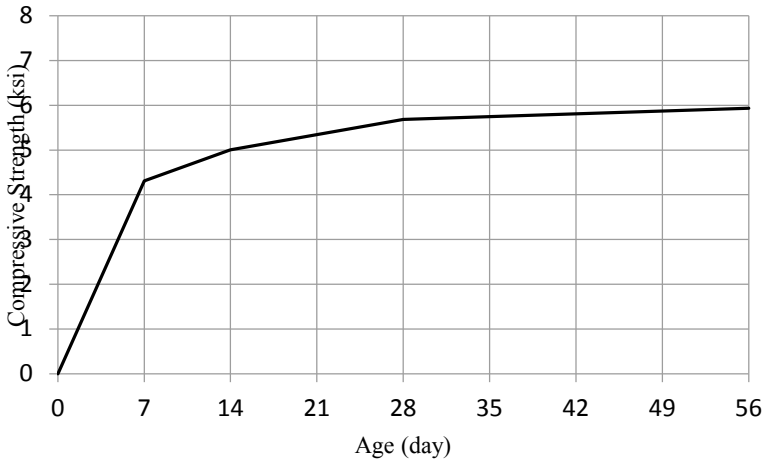

(43) G222C

(Cont.) Figure E-1. Relationship between compressive strength of hardened concrete and age after casting

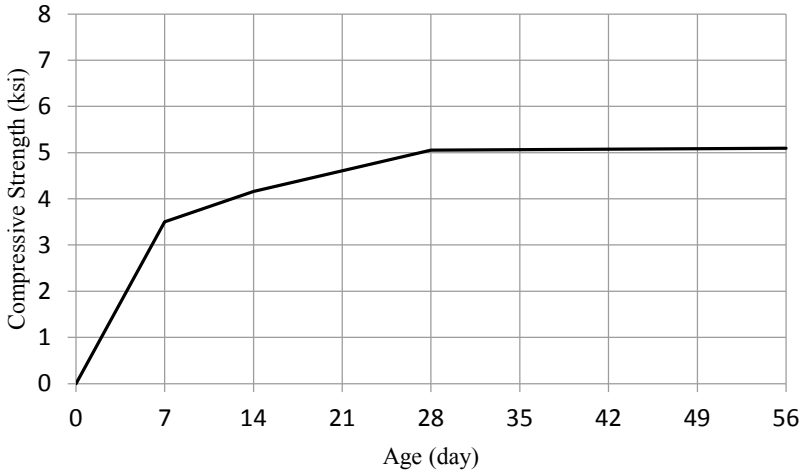

(44) G222F

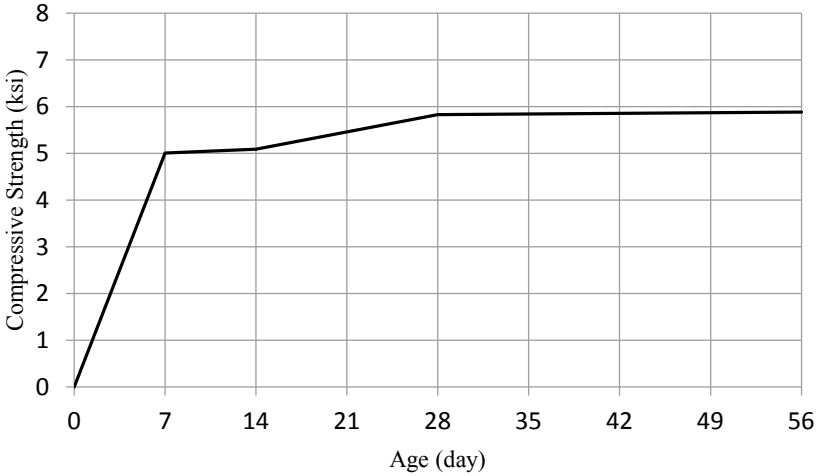

(45) G222S

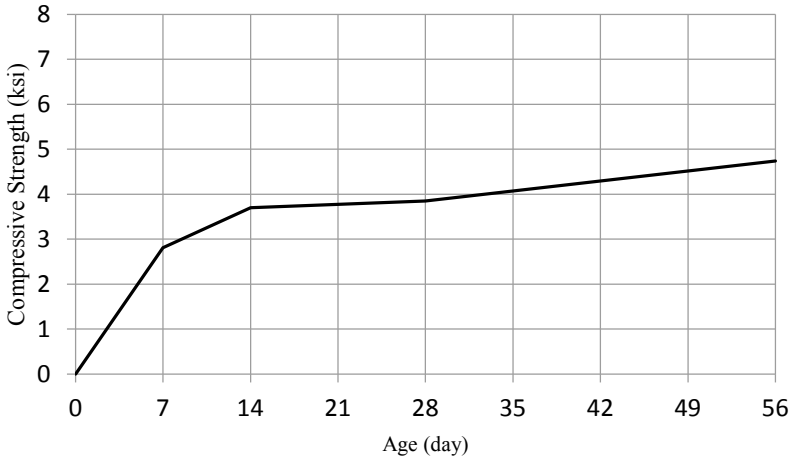

(46) G222FLP

(Cont.) Figure E-1. Relationship between compressive strength of hardened concrete and age after casting

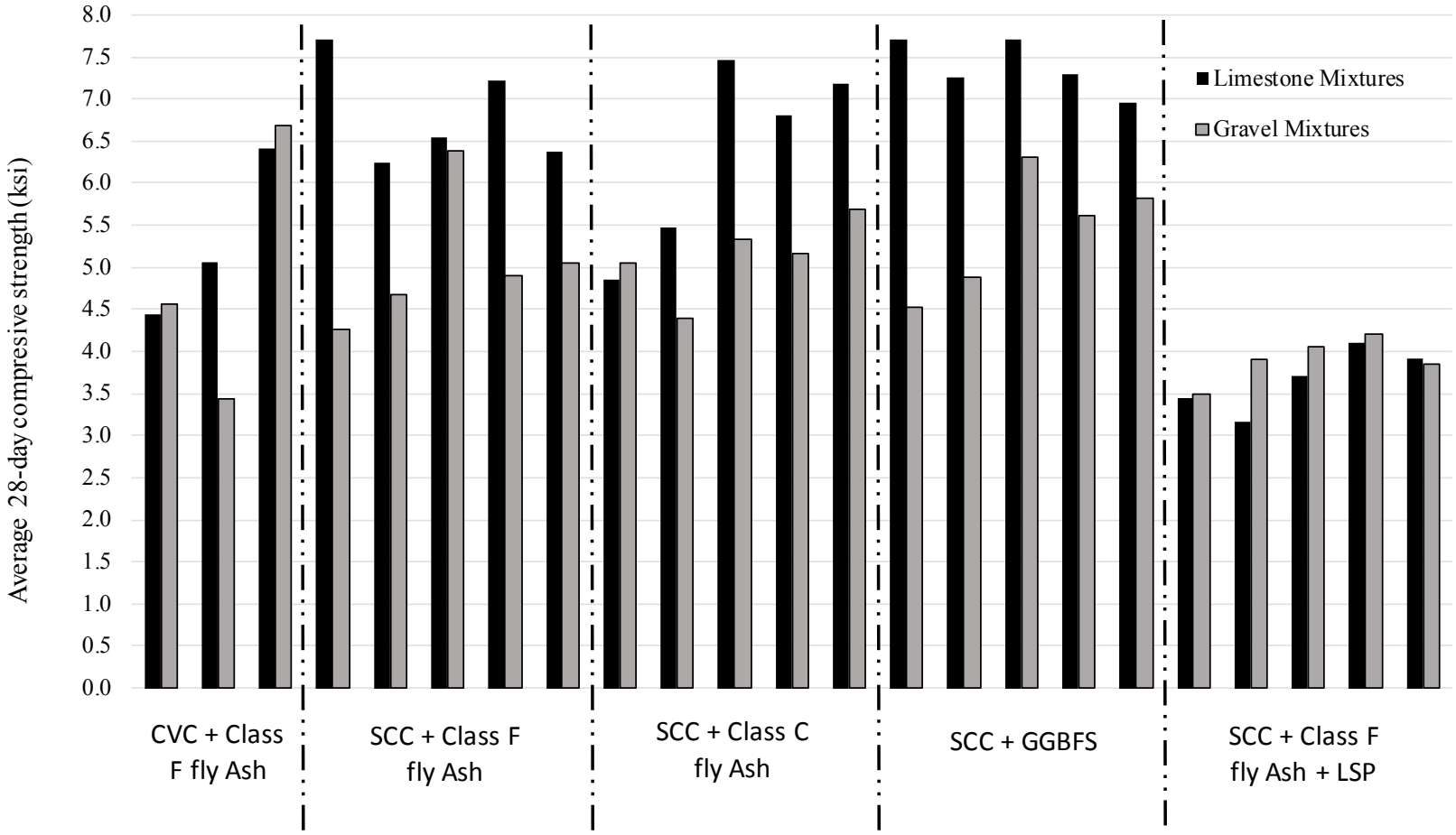

Figure E-2. Average 28-day compressive strength for all SCC and CVC mixtures containing limestone and gravel aggregates

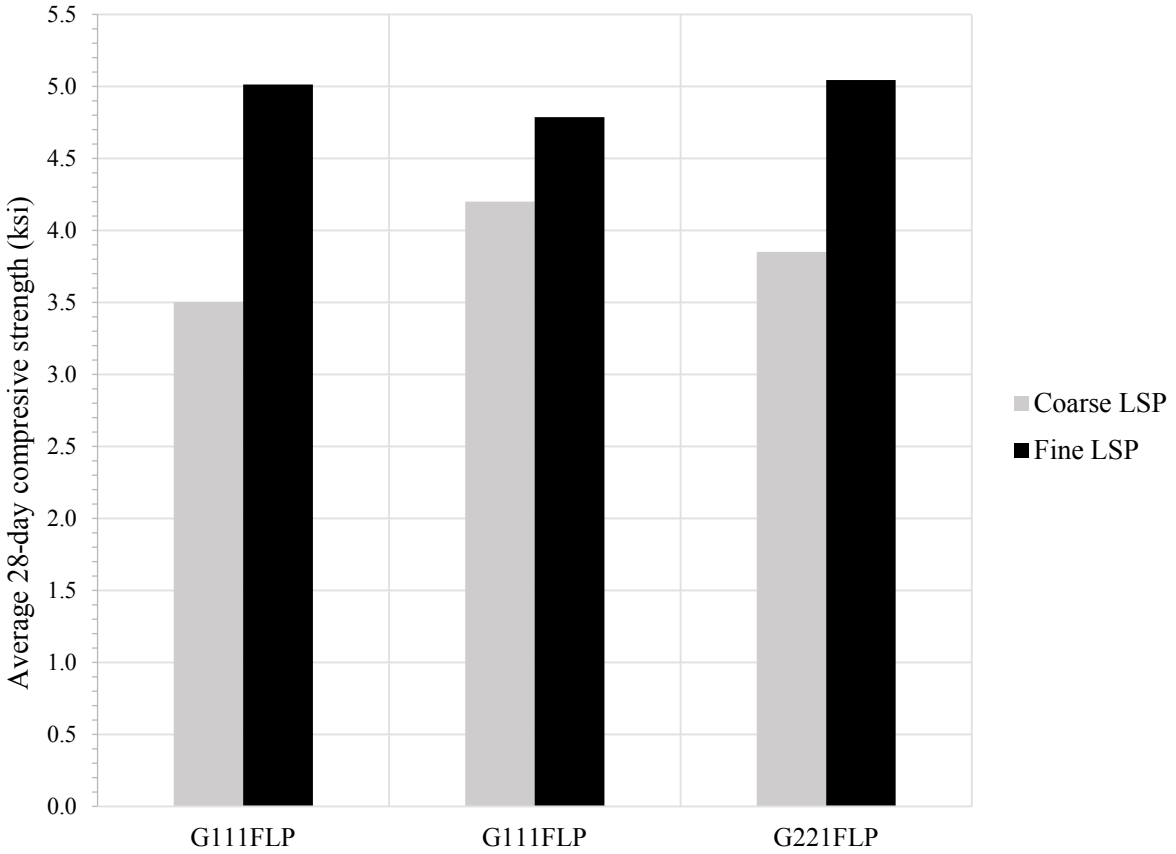

Figure E-3. Average 28-day compressive strength of SCC mixtures containing fine and coarse limestone powder

2. Modulus of Elasticity

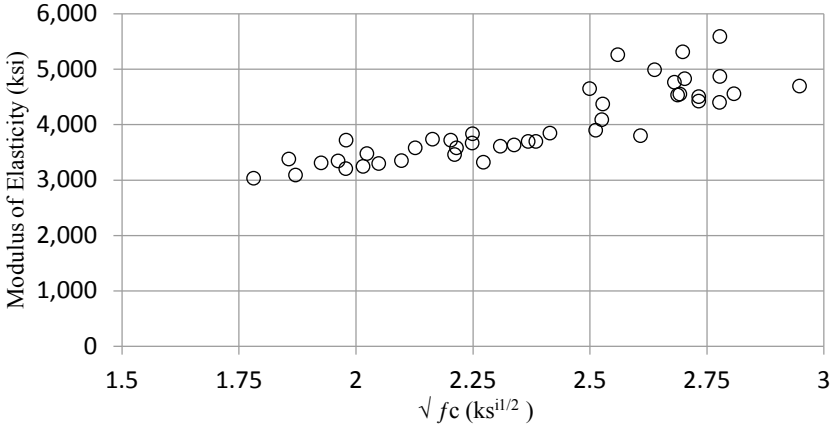

Figure E-4. CorRelationship between average measured modulus of elasticity and square root of average 28-day compressive strength for all SCC mixtures

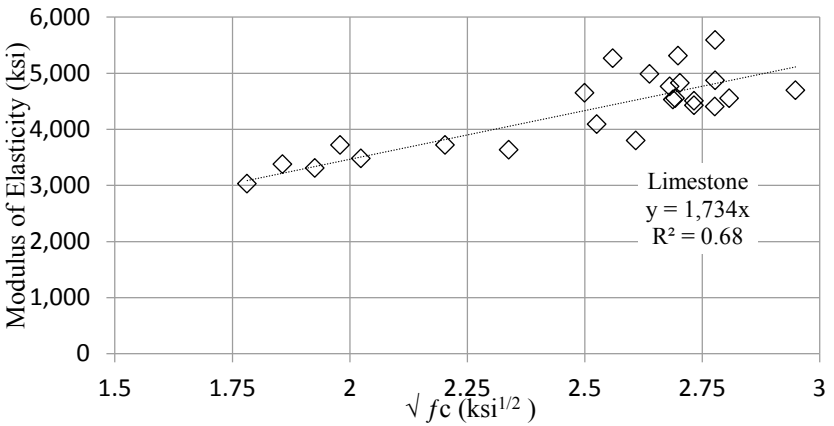

Figure E-5. CorRelationship between average measured modulus of elasticity and square root of average 28-day compressive strength for SCC mixtures with limestone aggregates

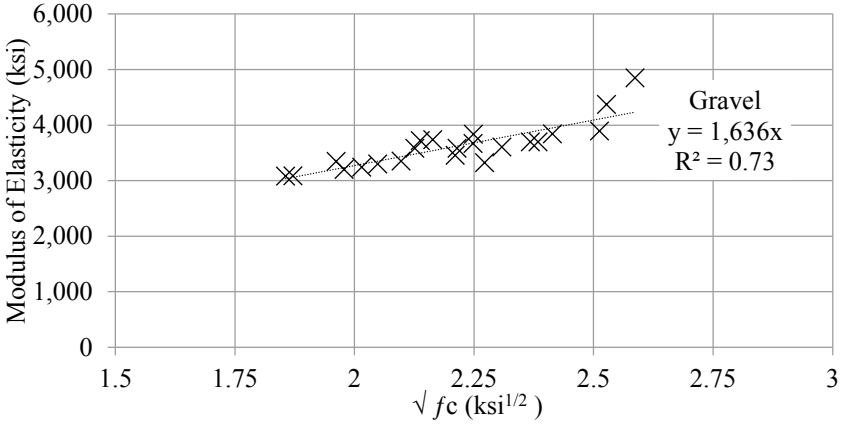

Figure E-6. CorRelationship between average measured modulus of elasticity and square root of average 28-day compressive strength for SCC mixtures with gravel aggregates

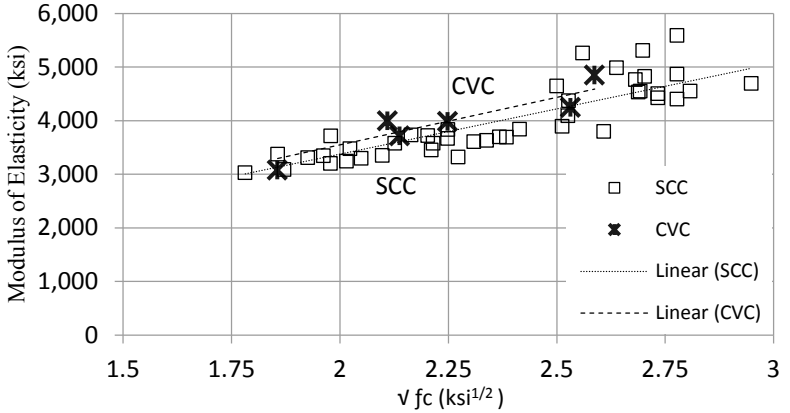

Figure E-7. Comparison of measured modulus of elasticity between SCC and CVC mixtures

3. Tensile Strength

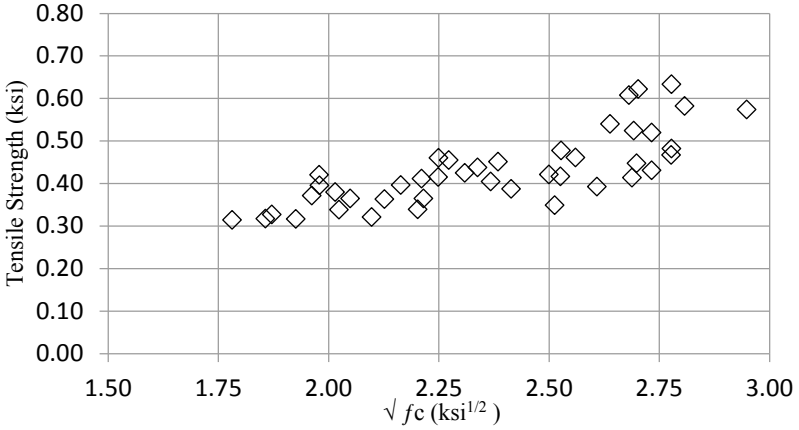

Figure E-8. CorRelationship between average measured tensile strength and square root of average 28-day compressive strength for all SCC mixtures

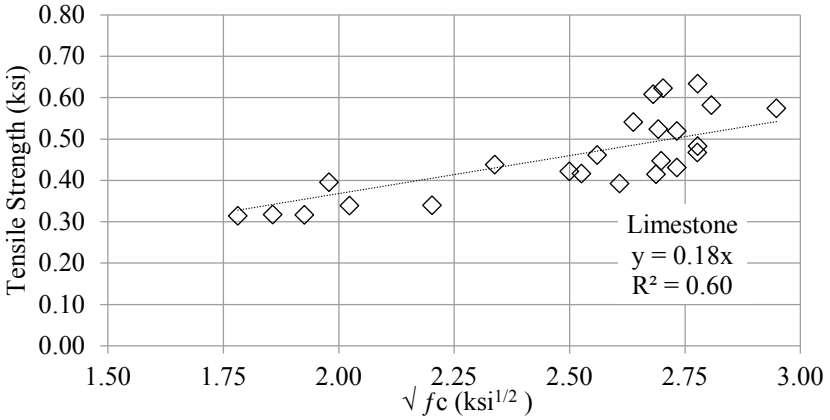

Figure E-9. CorRelationship between average measured tensile strength and square root of average 28-day compressive strength for SCC mixtures with limestone aggregates

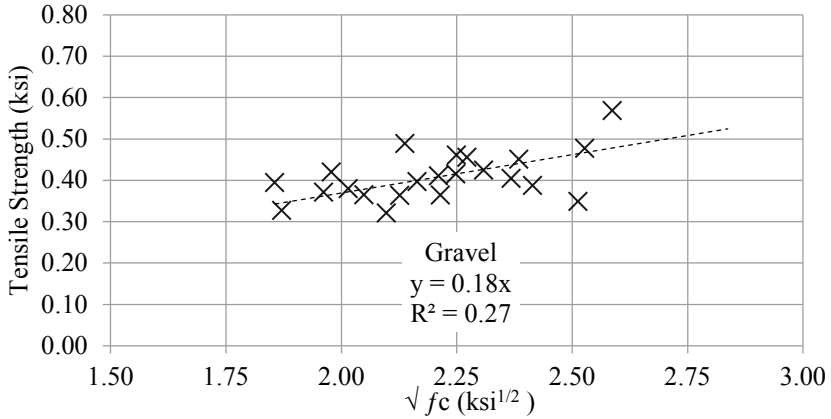

Figure E-10. CorRelationship between average measured tensile strength and square root of average 28-day compressive strength for SCC mixtures with gravel aggregates

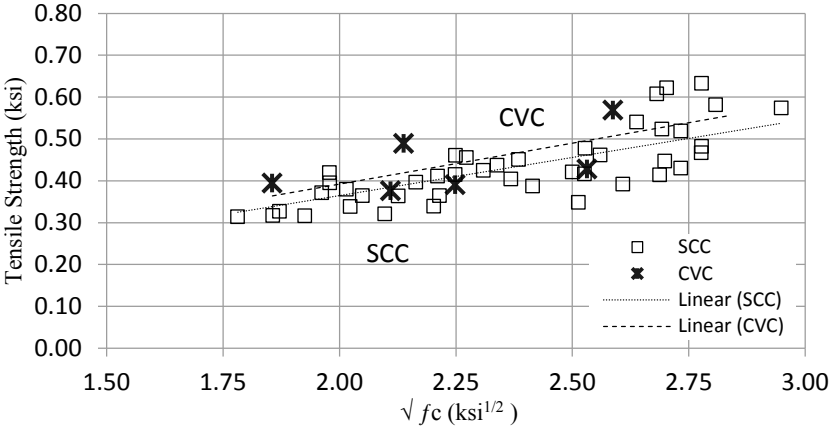

Figure E-11. Comparison of measured tensile strength between SCC and CVC mixtures

4. Modulus of Rupture

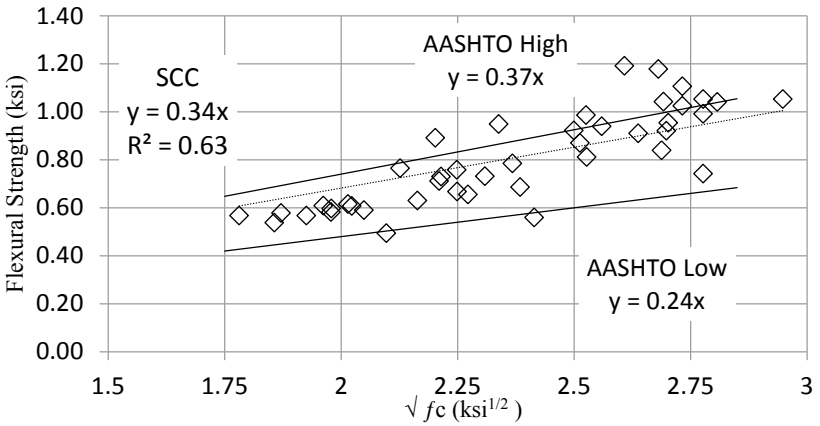

Figure E-12. CorRelationship between average measured modulus of rupture and square root of average 28-day compressive strength for all SCC mixtures

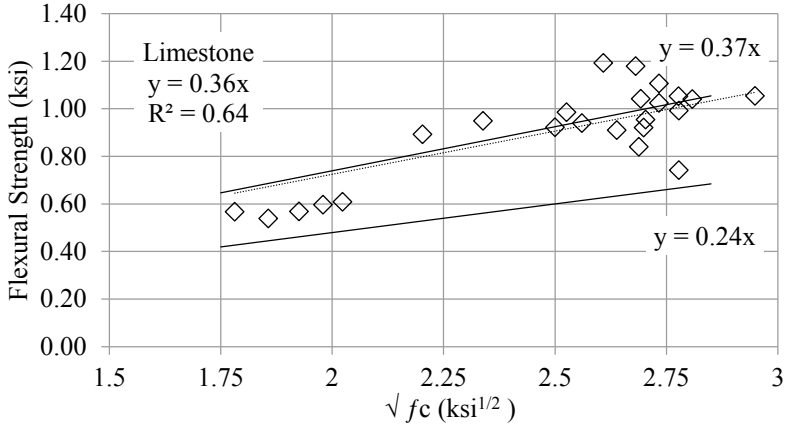

Figure E-13. CorRelationship between average measured modulus of rupture and square root of average 28-day compressive strength for SCC mixtures with limestone aggregates

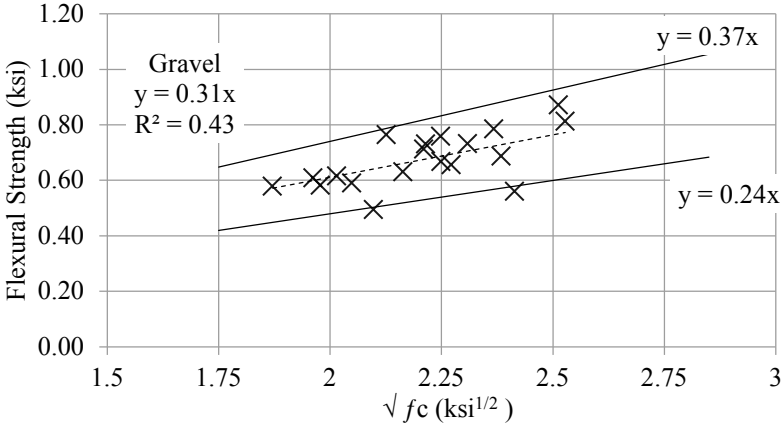

Figure E-14.CorRelationship between average measured modulus of rupture and square root of average 28-day compressive strength for SCC mixtures with gravel aggregates

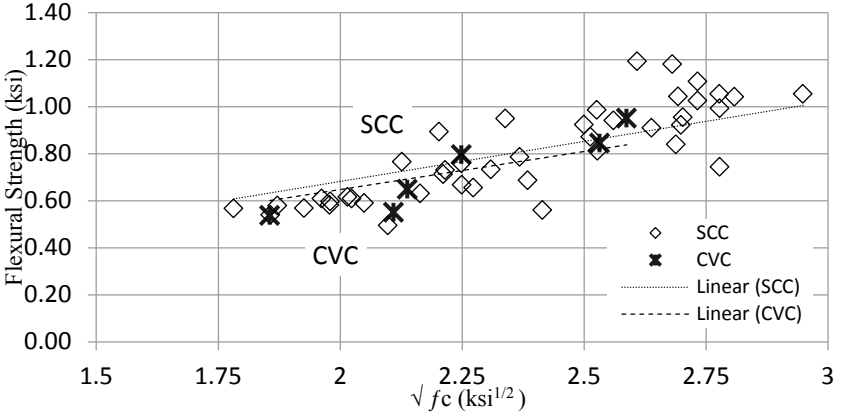

Figure E-15. Comparison of measured modulus of rupture between SCC and CVC mixtures

5. Bond Strength

Table E.1 Pull-out test results of vertical bars

Coarse Aggregate		Mixture Type	f_c (ksi)	Parameter	Specimen			Average	COV	Bond Strength/ $\sqrt{f_c}$ (ksi/ksi$^{1/2}$)
Type	NMSA (in.)				#1	#2	#3			
Gravel	3/4	SCC No. 67 (211)	4.32	Ultimate Load (lb)	21,500	19,100	18,160	19,587	8.8%	1.07
				Bond Strength (ksi)	2.43	2.16	2.06	2.22	8.8%	
				Load at Slip 0.01 in. (lb)	14,780	16,730	17,174	16,228	7.8%	
				Failure Mode	Slippage	Slippage	Slippage	N/A	N/A	
		CVC No. 67	4.57	Ultimate Load (lb)	25,000	25,300	26,100	25,467	2.2%	1.35
				Bond Strength (ksi)	2.83	2.86	2.95	2.88	2.2%	
				Load at Slip 0.01 in. (lb)	23,190	22,800	23,976	23,322	2.6%	
				Failure Mode	Slippage	Slippage	Slippage	N/A	N/A	
	1/2	SCC No. 78 (221)	3.96	Ultimate Load (lb)	17,020	14,670	16,080	15,923	7.4%	0.91
				Bond Strength (ksi)	1.93	1.66	1.82	1.80	7.4%	
				Load at Slip 0.01 in. (lb)	15,095	14,042	13,633	14,257	5.3%	
				Failure Mode	Slippage	Slippage	Slippage	N/A	N/A	
		CVC No. 78	4.63	Ultimate Load (lb)	21,400	20,700	20,700	20,933	1.9%	1.10
				Bond Strength (ksi)	2.42	2.34	2.34	2.37	1.9%	
				Load at Slip 0.01 in. (lb)	15,631	16,846	18,365	16,947	8.1%	
				Failure Mode	Slippage	Slippage	Slippage	N/A	N/A	
	3/8	SCC No. 8 (222)	4.91	Ultimate Load (lb)	20,000	19,300	16,730	18,677	9.2%	0.95
				Bond Strength (ksi)	2.26	2.18	1.89	2.11	9.2%	
				Load at Slip 0.01 in. (lb)	18,444	17,555	16,730	17,576	4.9%	
				Failure Mode	Slippage	Slippage	Splitting	N/A	N/A	
		CVC No. 8	4.74	Ultimate Load (lb)	26,700	27,300	26,300	26,767	1.9%	1.39
				Bond Strength (ksi)	3.02	3.09	2.98	3.03	1.9%	
				Load at Slip 0.01 in. (lb)	24,850	25,350	23,630	24,610	3.6%	
				Failure Mode	Slippage	Splitting	Slippage	N/A	N/A	
Limestone	3/4	SCC No. 67 (211)	7.09	Ultimate Load (lb)	29,900	30,100	35,400	31,800	9.8%	1.35
				Bond Strength (ksi)	3.38	3.41	4.01	3.60	9.8%	
				Load at Slip 0.01 in. (lb)	28,955	27,450	30,370	28,925	5.0%	
				Failure Mode	Slippage	Slippage	Slippage	N/A	N/A	
		CVC No. 67	4.27	Ultimate Load (lb)	23,600	25,600	26,900	25,367	6.6%	1.39
				Bond Strength (ksi)	2.67	2.90	3.04	2.87	6.6%	
				Load at Slip 0.01 in. (lb)	22,241	21,388	16,766	20,132	14.6%	
				Failure Mode	Slippage	Slippage	Splitting	N/A	N/A	
	1/2	SCC No. 78 (221)	8.18	Ultimate Load (lb)	30,600	32,200	31,800	31,533	2.6%	1.25
				Bond Strength (ksi)	3.46	3.64	3.60	3.57	2.6%	
				Load at Slip 0.01 in. (lb)	11,100	28,640	29,500	23,080	45.0%	
				Failure Mode	Slippage	Slippage	Slippage	N/A	N/A	
		CVC No. 78	5.78	Ultimate Load (lb)	30,100	33,100	33,700	32,300	6.0%	1.52
				Bond Strength (ksi)	3.41	3.75	3.81	3.66	6.0%	
				Load at Slip 0.01 in. (lb)	25,930	30,300	29,520	28,583	8.2%	
				Failure Mode	Splitting	Splitting	Splitting	N/A	N/A	
	3/8	SCC No. 8 (222)	6.04	Ultimate Load (lb)	26,900	26,200	27,000	26,700	1.6%	1.23
				Bond Strength (ksi)	3.04	2.97	3.06	3.02	1.6%	
				Load at Slip 0.01 in. (lb)	24,347	21,299	25,071	23,572	8.5%	
				Failure Mode	Splitting	Slippage	Splitting	N/A	N/A	
		CVC No. 8	6.59	Ultimate Load (lb)	33,400	30,900	34,700	33,000	5.9%	1.45
				Bond Strength (ksi)	3.78	3.50	3.93	3.73	5.9%	
				Load at Slip 0.01 in. (lb)	32,900	28,100	34,000	31,667	9.9%	
				Failure Mode	Splitting	Splitting	Splitting	N/A	N/A	

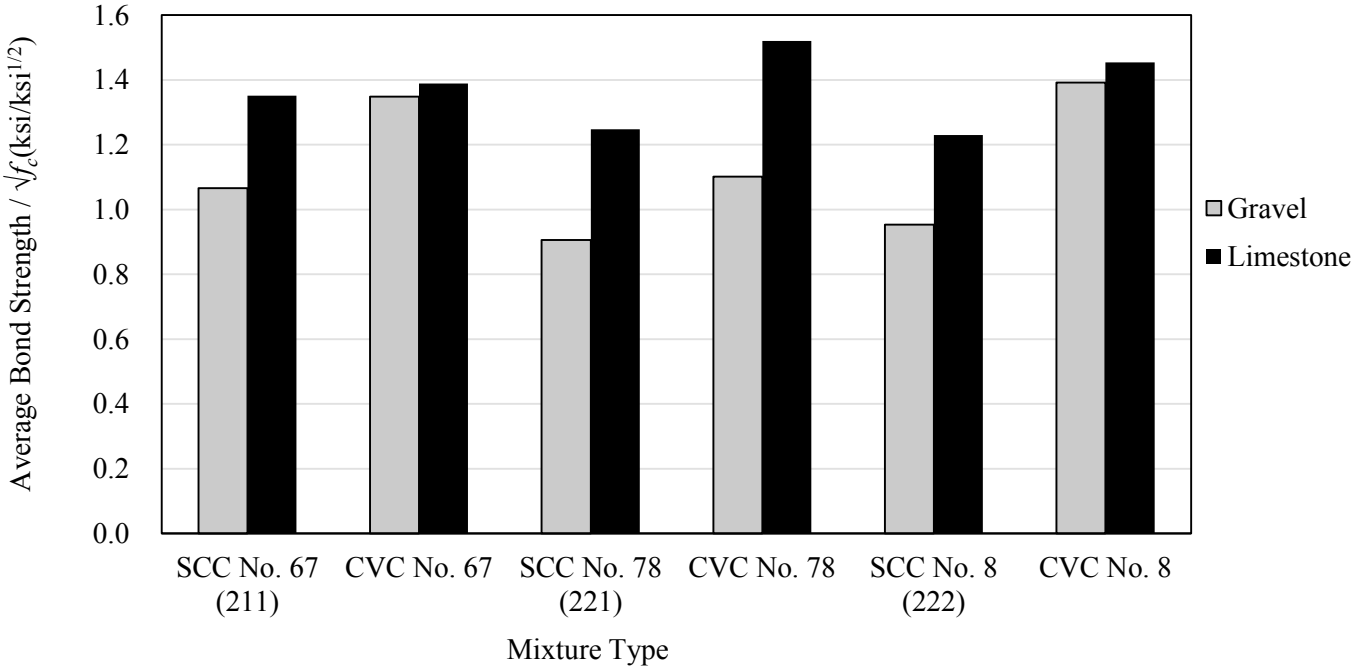

Figure E-16.Ratio of average bond strength to square root of 28-day compressive strength for SCC and CVC mixtures containing different aggregate types and sizes

Table E-2. Summary of statistical data for ratio of bond strength of vertical bars to $\sqrt{f'_c}$ of CVC and SCC mixtures

Groups	*Count*	*Sum*	*Average*	*Variance*
SCC	18	20.267	1.126	0.033
CVC	18	24.617	1.368	0.021

Table E-3. Summary of ANOVA data for ratio of bond strength of vertical bars to $\sqrt{f'_c}$ of CVC and SCC mixtures

Source of Variation	*SS*	*df*	*MS*	*F*	*P-value*	*F crit*
Between Groups	0.526	1	0.526	19.516	9.64E-05	4.130
Within Groups	0.916	34	0.027			
Total	1.441	35				

Table E-4. Pull-out test results of horizontal bars in low slump flow SCC

Maximum Load (lb)

Bar Location	Wall Specimen #1			Wall Specimen #2			Average	Std. Dev.	COV
	Bar #1	Bar #2	Bar #3	Bar #1	Bar #2	Bar #3			
Top	41,385	35,854	34,186	40,002	32,898	34,376	36,450	3,446	9.5%
Center	38,429	35,425	38,095	36,521	38,429	39,764	37,777	1,550	4.1%
Bottom	41,766	41,814	38,191	38,810	37,285	44,103	40,328	2,633	6.5%
						Top Bar Effect	**1.11**		

Ratio of Bond Strength to $\sqrt{f_c}$ (ksi/ksi$^{1/2}$)

Bar Location	Wall Specimen #1			Wall Specimen #2			Average	Std. Dev.	COV
	Bar #1	Bar #2	Bar #3	Bar #1	Bar #2	Bar #3			
Top	1.62	1.41	1.34	1.57	1.29	1.35	1.43	0.14	9.5%
Center	1.51	1.39	1.50	1.43	1.51	1.56	1.48	0.06	4.1%
Bottom	1.64	1.64	1.50	1.52	1.46	1.73	1.58	0.10	6.5%

Slip at Maximum Load (in.)

Bar Location	Wall Specimen #1			Wall Specimen #2			Average	Std. Dev.	COV
	Bar #1	Bar #2	Bar #3	Bar #1	Bar #2	Bar #3			
Top	0.031	0.023	0.031	0.006	0.030	0.029	0.025	0.010	39.1%
Center	0.036	0.019	0.023	0.026	0.026	0.037	0.028	0.007	25.8%
Bottom	0.042	0.033	0.042	0.029	0.012	0.050	0.035	0.013	38.5%

Load at 0.01 in. Slip (lb)

Bar Location	Wall Specimen #1			Wall Specimen #2			Average	Std. Dev.	COV
	Bar #1	Bar #2	Bar #3	Bar #1	Bar #2	Bar #3			
Top	36,570	32,851	28,321	37,475	29,656	30,276	32,525	3,793	11.7%
Center	37,905	32,135	35,807	34,472	34,758	37,142	35,370	2,069	5.8%
Bottom	32,217	41,528	28,130	35,235	36,570	32,898	34,430	4,529	13.2%

Compressive Strength (ksi)	8.3
Bonded Area (in^2)	8.84
Slump Flow (in.)	22

Table E-5. Pull-out test results of horizontal bars in high slump flow SCC

Maximum Load (lb)

Bar Location	Wall Specimen #1			Wall Specimen #2			Average	Std. Dev.	COV
	Bar #1	Bar #2	Bar #3	Bar #1	Bar #2	Bar #3			
Top	34,948	36,999	38,763	36,856	42,672	43,054	38,882	3,314	8.5%
Center	36,236	34,948	35,592	40,861	43,101	42,291	38,838	3,650	9.4%
Bottom	41,671	38,095	37,952	40,575	37,666	40,956	39,486	1,773	4.5%
						Top Bar Effect	**1.02**		

Ratio of Bond Strength to $\sqrt{f_c}$ (ksi/ksi$^{1/2}$)

Bar Location	Wall Specimen #1			Wall Specimen #2			Average	Std. Dev.	COV
	Bar #1	Bar #2	Bar #3	Bar #1	Bar #2	Bar #3			
Top	1.48	1.57	1.65	1.56	1.81	1.83	1.65	0.14	8.5%
Center	1.54	1.48	1.51	1.73	1.83	1.80	1.65	0.15	9.4%
Bottom	1.77	1.62	1.61	1.72	1.60	1.74	1.68	0.08	4.5%

Slip at Maximum Load (in.)

Bar Location	Wall Specimen #1			Wall Specimen #2			Average	Std. Dev.	COV
	Bar #1	Bar #2	Bar #3	Bar #1	Bar #2	Bar #3			
Top	0.033	0.098	0.059	0.022	0.043	0.034	0.048	0.027	56.8%
Center	0.034	0.033	0.033	0.024	0.044	0.076	0.041	0.018	45.3%
Bottom	0.047	0.036	0.159	0.034	0.039	0.058	0.062	0.048	77.6%

Load at 0.01 in. Slip (lb)

Bar Location	Wall Specimen #1			Wall Specimen #2			Average	Std. Dev.	COV
	Bar #1	Bar #2	Bar #3	Bar #1	Bar #2	Bar #3			
Top	31,277	27,511	31,802	32,708	39,907	39,716	33,820	4,968	14.7%
Center	32,231	31,659	31,945	39,478	38,858	35,807	34,996	3,571	10.2%
Bottom	32,326	33,184	25,746	36,808	32,326	37,046	32,906	4,108	12.5%

Compressive Strength (ksi)	7.1
Bonded Area (in^2)	8.84
Slump Flow (in.)	28

Table E-6. Pull-out test results of horizontal bars in CVC

Maximum Load (lb)

Bar Location	Wall Specimen #1			Wall Specimen #2			Average	Std. Dev.	COV
	Bar #1	Bar #2	Bar #3	Bar #1	Bar #2	Bar #3			
Top	34,758	35,330	40,765	30,991	35,664	34,853	35,394	3,131	8.8%
Center	35,044	44,532	38,906	39,907	34,281	42,196	39,144	3,986	10.2%
Bottom	40,336	40,431	42,148	39,716	38,810	36,236	39,613	1,984	5.0%
						Top Bar Effect	**1.12**		

Ratio of Bond Strength to $\sqrt{f_c}$ (ksi/ksi$^{1/2}$)

Bar Location	Wall Specimen #1			Wall Specimen #2			Average	Std. Dev.	COV
	Bar #1	Bar #2	Bar #3	Bar #1	Bar #2	Bar #3			
Top	1.43	1.45	1.67	1.27	1.46	1.43	1.45	0.13	8.8%
Center	1.44	1.83	1.60	1.64	1.41	1.73	1.61	0.16	10.2%
Bottom	1.66	1.66	1.73	1.63	1.59	1.49	1.63	0.08	5.0%

Slip at Maximum Load (in.)

Bar Location	Wall Specimen #1			Wall Specimen #2			Average	Std. Dev.	COV
	Bar #1	Bar #2	Bar #3	Bar #1	Bar #2	Bar #3			
Top	0.021	0.040	0.023	0.019	0.024	0.028	0.026	0.008	29.3%
Center	0.039	0.057	0.042	0.019	0.021	0.028	0.034	0.014	42.2%
Bottom	0.036	0.075	0.069	0.068	0.028	0.034	0.052	0.021	40.9%

Load at 0.01 in. Slip (lb)

Bar Location	Wall Specimen #1			Wall Specimen #2			Average	Std. Dev.	COV
	Bar #1	Bar #2	Bar #3	Bar #1	Bar #2	Bar #3			
Top	31,420	30,228	37,571	28,750	33,041	29,847	31,810	3,180	10.0%
Center	32,469	39,144	35,711	37,523	32,708	37,666	35,870	2,766	7.7%
Bottom	36,283	36,379	37,189	35,378	35,091	32,088	35,401	1,789	5.1%

Compressive Strength (ksi)	7.6
Bonded Area (in^2)	8.84
Slump (in.)	2

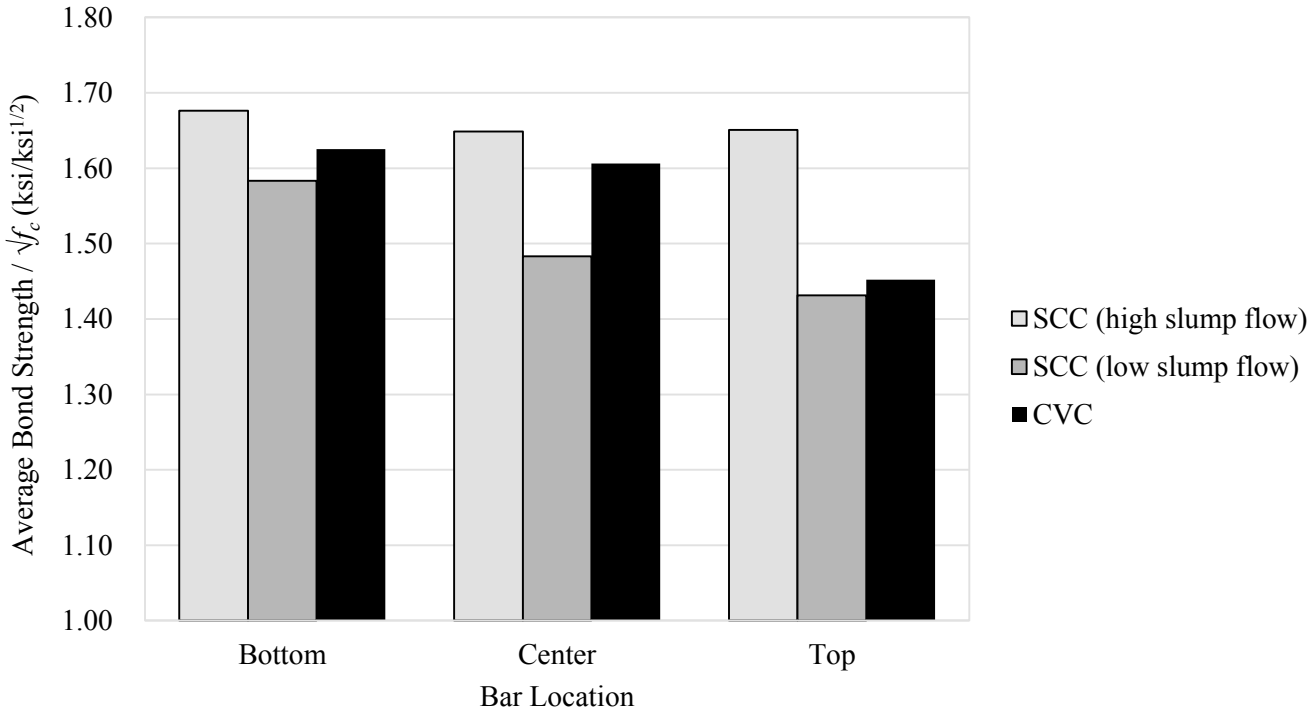

Figure E-17. Average bond strength / $\sqrt{f'_c}$ of horizontal bars at different locations in wall specimens

Table E-7. Summary of statistical data for ratio of bond strength of horizontal bars to $\sqrt{f'_c}$ of CVC and SCC mixtures

Groups	*Count*	*Sum*	*Average*	*Variance*
SCC (low slump flow)	18	26.99	1.50	0.0138
CVC	18	28.10	1.56	0.0210
SCC (high slump flow)	18	29.86	1.66	0.0147

Table E-8. Summary of ANOVA data for ratio of bond strength of horizontal bars to $\sqrt{f'_c}$ of CVC and SCC mixtures

Source of Variation	*SS*	*df*	*MS*	*F*	*P-value*	*F crit*
Between Groups	0.232	2	0.116	7.018	0.002	3.179
Within Groups	0.843	51	0.017			
Total	1.075	53				

6. Interface Shear Resistance

Table E-9. Interface shear resistance of push-off specimens containing gravel aggregate

Coarse Aggregate		Mixture Type and ID	f_c (ksi)	Parameter	Specimen		Average	Shear Resistance / $\sqrt{f_c}$ (ksi/ksi$^{1/2}$)
Type	NMSA (in.)				#1	#2		
Gravel	3/4	SCC No. 67 (211)	4.32	Depth of Shear Section (in.)	8.75	8.5	8.63	0.33
				AASHTO Prediction (ksi)	0.82	0.83	0.83	
				Ultimate Push-off Load (lb)	31.60	28.30	29.95	
				Interface Shear Resistance (ksi)	0.72	0.67	0.69	
				Ver. Displacement (in.)	0.028	0.012	0.0200	
				Horz. Displacement (in.)	0.014	0.01	0.012	
				Failure Mode	Shear	Shear	N/A	
		CVC No. 67	4.57	Depth of Shear Section (in.)	8.375	8.5	8.44	0.37
				AASHTO Prediction (ksi)	0.84	0.83	0.84	
				Ultimate Push-off Load (lb)	34.20	33.10	33.65	
				Interface Shear Resistance (ksi)	0.82	0.78	0.80	
				Ver. Displacement (in.)	0.016	0.0111	0.01355	
				Horz. Displacement (in.)	0.008	0.0063	0.0072	
				Failure Mode	Shear	Shear	N/A	
	1/2	SCC No. 78 (221)	3.96	Depth of Shear Section (in.)	9	8.75	8.875	0.29
				AASHTO Prediction (ksi)	0.81	0.82	0.82	
				Ultimate Push-off Load (lb)	23.00	28.50	25.75	
				Interface Shear Resistance (ksi)	0.51	0.65	0.58	
				Ver. Displacement (in.)	0.005	0.015	0.0100	
				Horz. Displacement (in.)	0.003	0.01	0.0065	
				Failure Mode	Shear	Shear	N/A	
		CVC No. 78	4.63	Depth of Shear Section (in.)	8.75	8.5	8.625	0.30
				AASHTO Prediction (ksi)	0.82	0.83	0.83	
				Ultimate Push-off Load (lb)	23.50	31.70	27.60	
				Interface Shear Resistance (ksi)	0.54	0.75	0.64	
				Ver. Displacement (in.)	0.007	0.013	0.01	
				Horz. Displacement (in.)	0.0003	0.007	0.0065	
				Failure Mode	Shear	Shear	N/A	
	3/8	SCC No. 8 (222)	4.91	Depth of Shear Section (in.)	8.75	9	8.88	0.32
				AASHTO Prediction (ksi)	0.82	0.81	0.82	
				Ultimate Push-off Load (lb)	30.50	33.10	31.80	
				Interface Shear Resistance (ksi)	0.70	0.74	0.72	
				Ver. Displacement (in.)	0.0077	0.0116	0.0097	
				Horz. Displacement (in.)	0.0094	0.0053	0.0074	
				Failure Mode	Shear	Shear	N/A	
		CVC No. 8	4.74	Depth of Shear Section (in.)	8.5	8.875	8.69	0.31
				AASHTO Prediction (ksi)	0.83	0.82	0.83	
				Ultimate Push-off Load (lb)	27.70	30.30	29.00	
				Interface Shear Resistance (ksi)	0.65	0.68	0.67	
				Ver. Displacement (in.)	0.008	0.028	0.0180	
				Horz. Displacement (in.)	0.005	0.009	0.0070	
				Failure Mode	Shear	Shear	N/A	

Table E-10. Interface shear resistance of push-off specimens containing limestone aggregate

Coarse Aggregate		Mixture Type and ID	f_c (ksi)	Parameter	Specimen		Average	Shear Resistance / $\sqrt{f_c}$ (ksi/ksi$^{1/2}$)
Type	NMSA (in.)				#1	#2		
Limestone	3/4	SCC No. 67 (211)	7.09	Depth of Shear Section (in.)	8.5	8.75	8.63	0.38
				AASHTO Prediction (ksi)	0.83	0.82	0.83	
				Ultimate Push-off Load (lb)	45.00	42.70	43.85	
				Interface Shear Resistance (ksi)	1.06	0.98	1.02	
				Ver. Displacement (in.)	0.0156	0.0189	0.0173	
				Horz. Displacement (in.)	0.0174	0.0094	0.0134	
				Failure Mode	Shear	Shear	N/A	
		CVC No. 67	4.27	Depth of Shear Section (in.)	8.5	9	8.75	0.40
				AASHTO Prediction (ksi)	0.83	0.81	0.82	
				Ultimate Push-off Load (lb)	35.30	37.30	36.30	
				Interface Shear Resistance (ksi)	0.83	0.83	0.83	
				Ver. Displacement (in.)	0.0143	0.0166	0.01545	
				Horz. Displacement (in.)	0.0075	0.0101	0.0088	
				Failure Mode	Shear	Shear	N/A	
	1/2	SCC No. 78 (221)	8.18	Depth of Shear Section (in.)	8.625	8.5	8.5625	0.34
				AASHTO Prediction (ksi)	0.83	0.83	0.83	
				Ultimate Push-off Load (lb)	42.60	40.50	41.55	
				Interface Shear Resistance (ksi)	0.99	0.95	0.97	
				Ver. Displacement (in.)	0.0065	0.0121	0.0093	
				Horz. Displacement (in.)	0.0015	0.0095	0.0055	
				Failure Mode	Shear	Shear	N/A	
		CVC No. 78	5.78	Depth of Shear Section (in.)	8.75	9.125	8.9375	0.34
				AASHTO Prediction (ksi)	0.82	0.81	0.81	
				Ultimate Push-off Load (lb)	34.40	38.80	36.60	
				Interface Shear Resistance (ksi)	0.79	0.85	0.82	
				Ver. Displacement (in.)	0.0174	0.0072	0.0093	
				Horz. Displacement (in.)	0.0011	0.00103	0.0055	
				Failure Mode	Shear	Shear	N/A	
	3/8	SCC No. 8 (222)	6.04	Depth of Shear Section (in.)	8.5	8.75	8.63	0.33
				AASHTO Prediction (ksi)	0.83	0.82	0.83	
				Ultimate Push-off Load (lb)	38.70	31.90	35.30	
				Interface Shear Resistance (ksi)	0.91	0.73	0.82	
				Ver. Displacement (in.)	0.0265	0.0091	0.0178	
				Horz. Displacement (in.)	0.0081	0.0042	0.0062	
				Failure Mode	Shear	Shear	N/A	
		CVC No. 8	6.59	Depth of Shear Section (in.)	8.75	8.625	8.69	0.43
				AASHTO Prediction (ksi)	0.82	0.83	0.83	
				Ultimate Push-off Load (lb)	45.40	49.60	47.50	
				Interface Shear Resistance (ksi)	1.04	1.15	1.09	
				Ver. Displacement (in.)	0.013	0.0177	0.0154	
				Horz. Displacement (in.)	0.0014	0.0083	0.0049	
				Failure Mode	Shear	Shear	N/A	

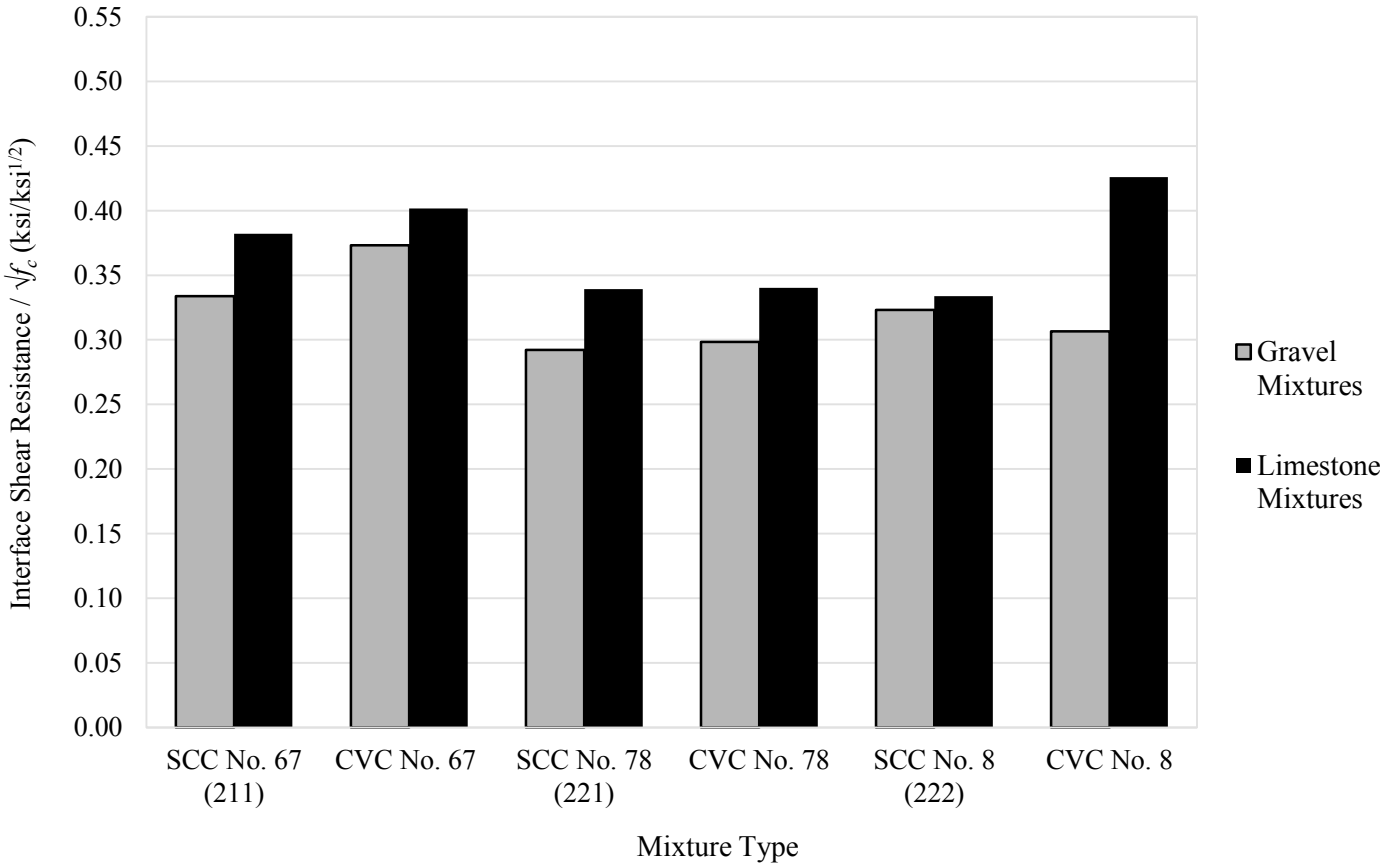

Figure E-18. Ratio of average interface shear resistance to square root of average 28-day compressive strength of SCC and CVC push-off specimens containing different aggregate types and sizes (lab-mixtures)

Table E-11. Summary of statistical data of interface shear resistance of CVC and SCC push-off specimens

Groups	*Count*	*Sum*	*Average*	*Variance*
SCC	12	4.009	0.334	0.00134
CVC	12	4.292	0.358	0.0030

Table E-12. Summary of ANOVA data of interface shear resistance of CVC and SCC push-off specimens

Source of Variation	*SS*	*df*	*MS*	*F*	*P-value*	*F crit*
Between Groups	0.003	1	0.003	1.543	0.227	4.300
Within Groups	0.048	22	0.002			
Total	0.051	23				

Table E-13. Interface shear resistance of ready-mixed SCC push-off specimens

Mixture	Average 28-day compressive strength (ksi)	Parameter	Specimens without Reinforcement			Specimens with 2#3 Reinforcement		
			#1	#2	Average	#1	#2	Average
Footing (SCC 111)	8.694	Ultimate Push-off Load (lbs)	44,600	45,800	**45,200**	59,100	54,300	**56,700**
		Section Depth (in.)	8.875	8.25	**8.56**	8.50	8.50	**8.50**
		AASHTO Prediction (ksi)	0.40	0.40	**0.40**	0.83	0.83	**0.83**
		Interface Shear Resistance (ksi)	1.01	1.11	**1.06**	1.39	1.28	**1.33**
Column (SCC 121)	8.015	Ultimate Push-off Load (lbs)	32,800	35,900	**34,350**	48,400	43,800	**46,100**
		Section Depth (in.)	8.50	8.50	**8.50**	8.50	8.50	**8.50**
		AASHTO Prediction (ksi)	0.40	0.40	**0.40**	0.83	0.83	**0.83**
		Interface Shear Resistance (ksi)	0.77	0.84	**0.81**	1.14	1.03	**1.08**
Pier Cap (SCC 221)	7.733	Ultimate Push-off Load (lbs)	35,500	49,300	**42,400**	49,900	55,900	**52,900**
		Section Depth (in.)	8.75	8.75	**8.75**	8.75	8.75	**8.75**
		AASHTO Prediction (ksi)	0.40	0.40	**0.40**	0.82	0.82	**0.82**
		Interface Shear Resistance (ksi)	0.81	1.13	**0.97**	1.14	1.28	**1.21**
Box Girder (SCC 222)	7.884	Ultimate Push-off Load (lbs)	54,300	51,800	**53,050**	63,200	61,700	**62,450**
		Section Depth (in.)	8.38	8.25	**8.31**	8.13	8.50	**8.31**
		AASHTO Prediction (ksi)	0.40	0.40	**0.40**	0.85	0.83	**0.84**
		Interface Shear Resistance (ksi)	1.30	1.26	**1.28**	1.56	1.45	**1.50**

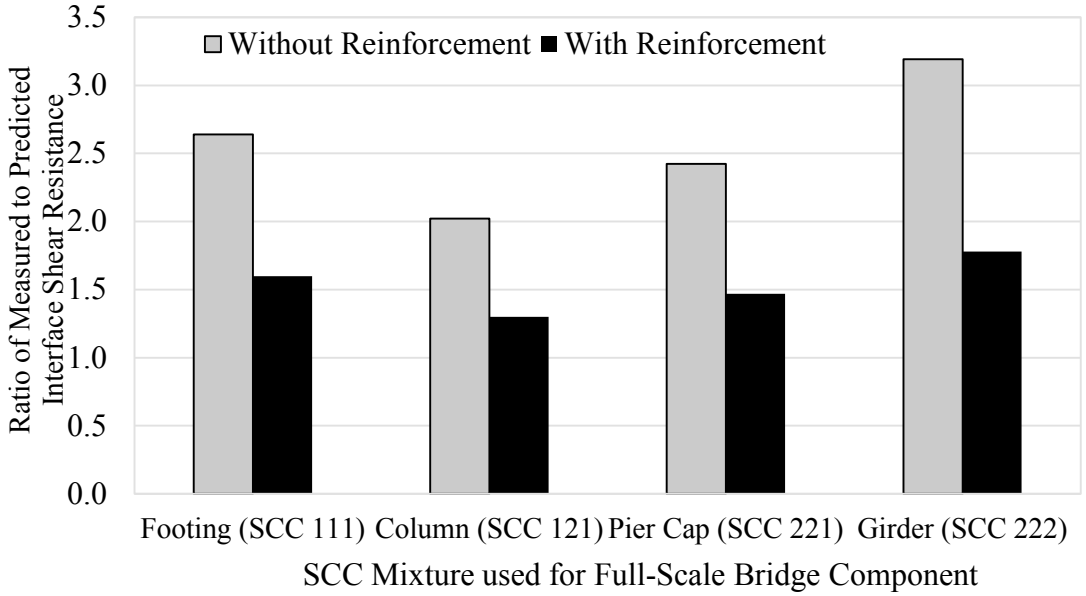

Figure E-19. Ratio of measured to predicted interface shear resistance of SCC mixtures used for full-scale bridge components

Table E-14. Shear resistance of SCC beams with low slump flow

Shear Reinforcement		SCC (low slump flow)				
		Max. Load (kip)	Shear Strength / √fc (ksi/ksi$^{1/2}$)	Corresponding Deflection (in.)	Failure Mode	Corresponding Slippage (in.)
None	#1	56.6	0.13	0.42	Shear	0.0004
	#2	34.3	0.08	0.25	Shear	0.0001
	Ave.	45.45	0.11	0.335	Shear	0.00025
	Predicted	**26.9**				
#3@8"	#1	68.6	0.16	0.62	Shear	0.0001
	#2	70.9	0.17	0.58	Shear	0.0001
	Ave.	69.75	0.16	0.6	Shear	0.0001
	Predicted	**57.5**				
#3@4"	#1	77.8	0.18	2.6	Flexure	0.0001
	#2	84.3	0.20	2.8	Flexure	0.0003
	Ave.	81.05	0.19	2.7	Flexure	0.0002
	Predicted	**88.0**				

Table E-15. Shear resistance of SCC beams with high slump flow

Shear Reinforcement		SCC (high slump flow)				
		Max. Load (kip)	Shear Strength / √fc (ksi/ksi$^{1/2}$)	Corresponding Deflection (in.)	Failure Mode	Corresponding Slippage (in.)
None	#1	28.3	0.07	0.09	Shear	0.0001
	#2	60.2	0.15	0.46	Shear	0.007
	Ave.	44.25	0.11	0.275	Shear	0.00355
	Predicted	**24.9**				
#3@8"	#1	68.4	0.17	0.47	Shear	0.0003
	#2	72.8	0.18	0.82	Shear	0.0003
	Ave.	70.60	0.18	0.645	Shear	0.0003
	Predicted	**55.4**				
#3@4"	#1	84.7	0.21	2.97	Flexure	0.0008
	#2	85.5	0.22	2.7	Flexure	0.0013
	Ave.	85.10	0.22	2.835	Flexure	0.00105
	Predicted	**86.0**				

Table E-16. Shear resistance of CVC beams

Shear Reinforcement		CVC				
		Max. Load (kip)	**Shear Strength / √fc (ksi/ksi$^{1/2}$)**	**Corresponding Deflection (in.)**	**Failure Mode**	**Corresponding Slippage (in.)**
None	**#1**	60.7	0.15	0.37	Shear	0.0034
	#2	44	0.11	0.25	Shear	0.0003
	Ave.	52.35	0.13	0.31	Shear	0.00185
	Predicted	**25.8**				
#3@8"	**#1**	70.1	0.17	0.35	Shear	0.0016
	#2	65.3	0.16	0.67	Shear	0.0003
	Ave.	67.70	0.17	0.51	Shear	0.00095
	Predicted	**56.3**				
#3@4"	**#1**	80.2	0.20	2.05	Flexure	0.038
	#2	78.5	0.19	2.8	Flexure	0.0016
	Ave.	79.35	0.19	2.425	Flexure	0.0198
	Predicted	**86.8**				

Table E-17. Summary of statistical data of shear resistance of CVC and SCC beams

Groups	*Count*	*Sum*	*Average*	*Variance*
SCC (low slump)	6	7.541	1.257	0.197
SCC (high slump)	6	8.185	1.364	0.282
CVC	6	8.303	1.384	0.310

Table E-18. Summary of ANOVA data of shear resistance of CVC and SCC beams

Source of Variation	*SS*	*df*	*MS*	*F*	*P-value*	*F crit*
Between Groups	0.056	2	0.028	0.107	0.899	3.682
Within Groups	3.945	15	0.263			
Total	4.001	17				

7. Free (Dry) Shrinkage

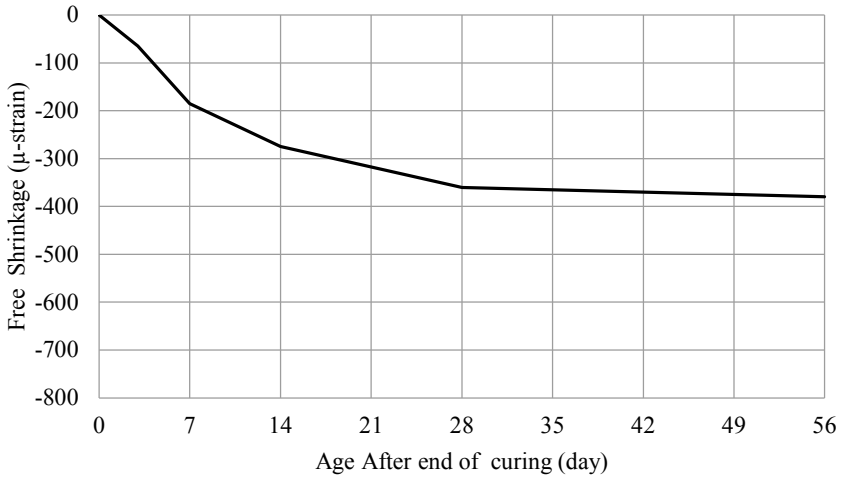

(1) LS0.75 CVC

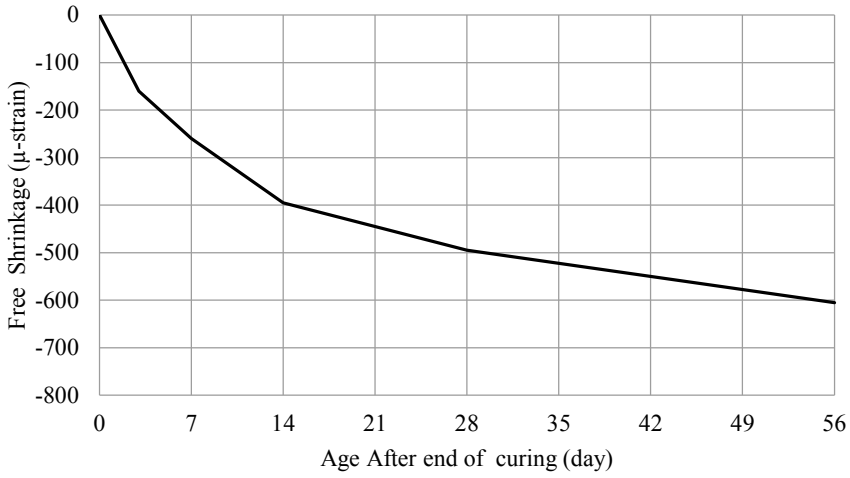

(2) LS111C

(3) LS111F

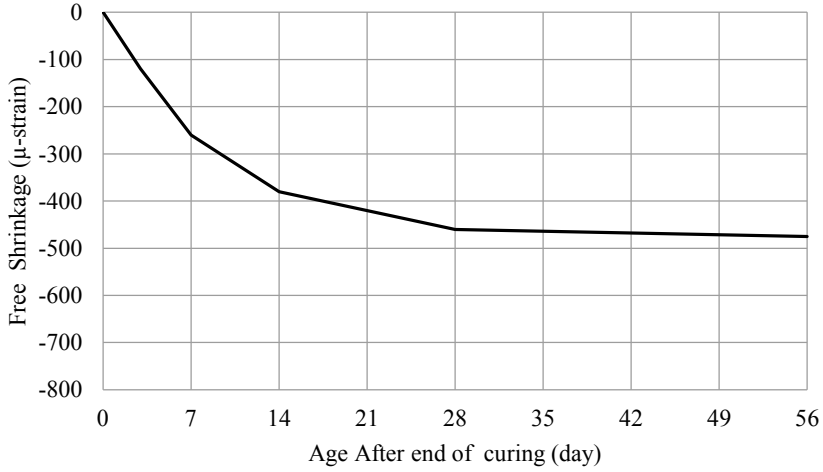

(4) LS111S

Figure E-20. Relationship between free shrinkage and age after end of curing of SCC and CVC mixtures

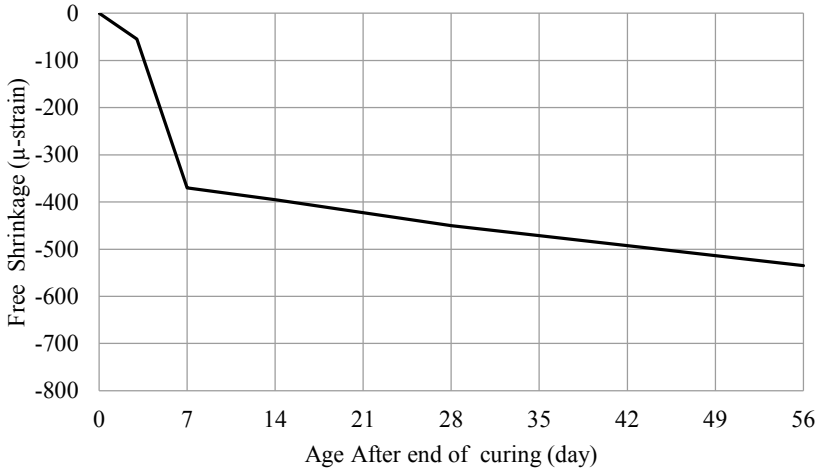

(5) LS111FLP

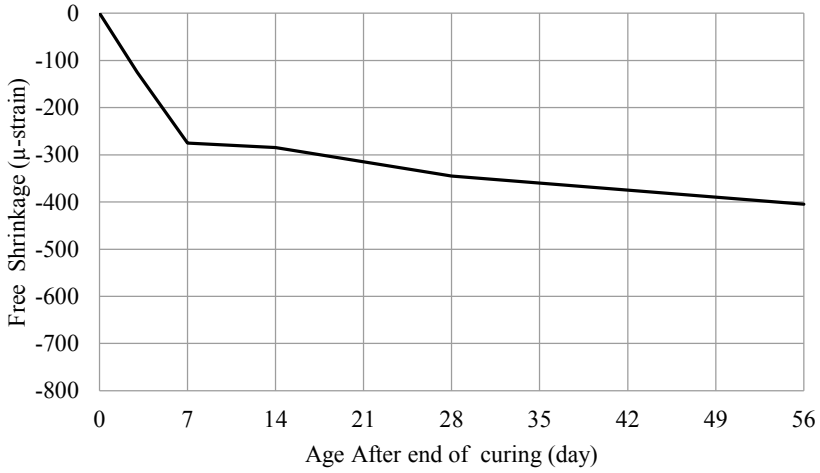

(6) LS211C

(7) LS211F

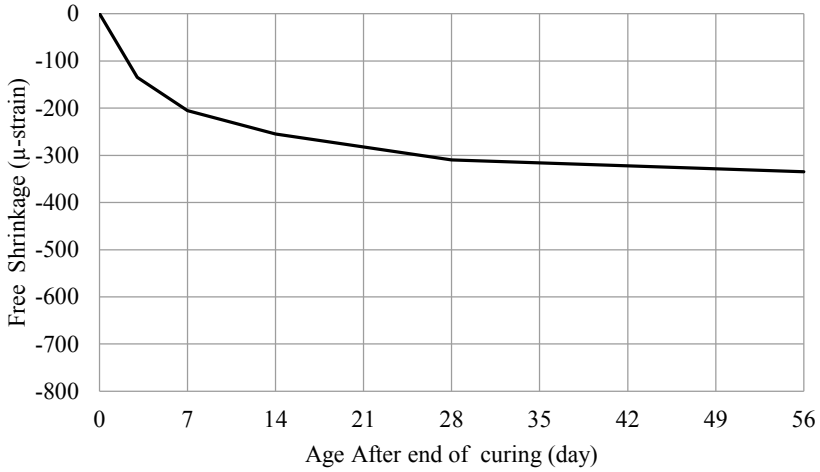

(8) LS211S

(Cont.) Figure E-20. Relationship between free shrinkage and age after end of curing of SCC and CVC mixtures

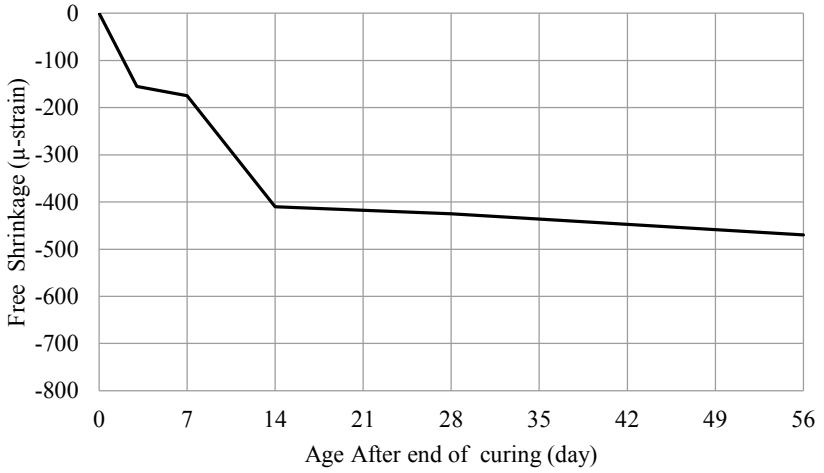

(9) LS211FLP

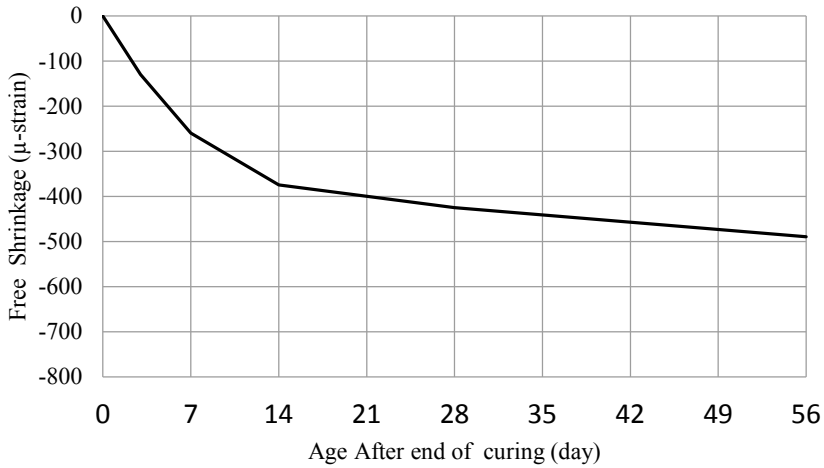

(10) LS0.50 CVC

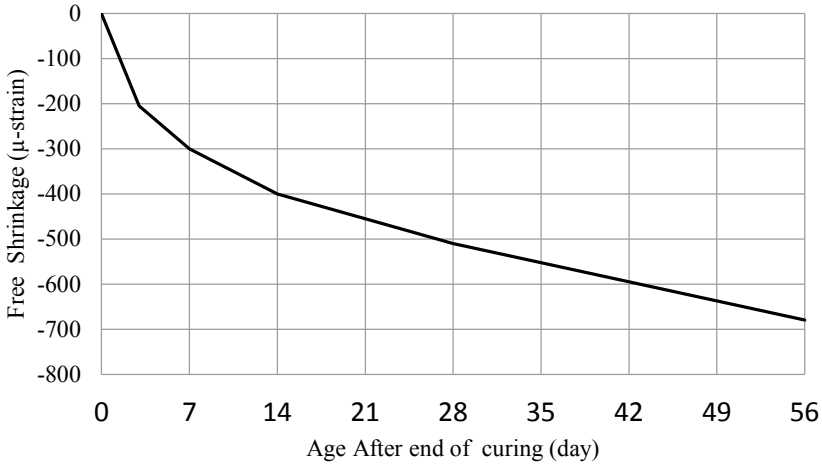

(11) LS121C

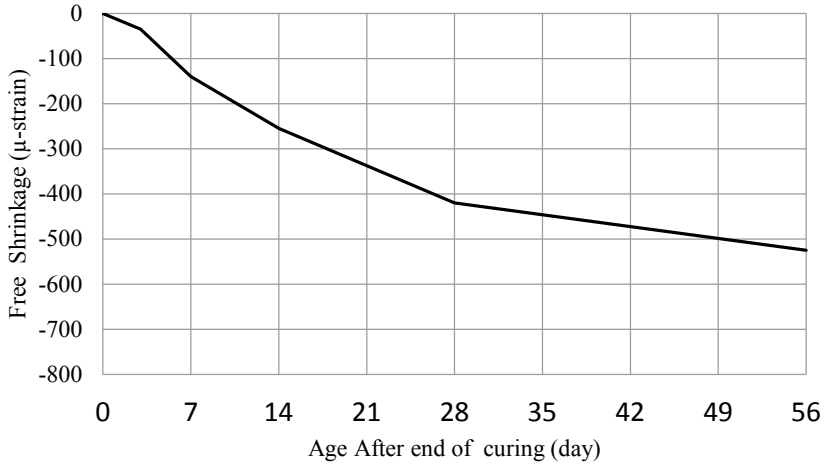

(12) LS121F

(Cont.) Figure E-20. Relationship between free shrinkage and age after end of curing of SCC and CVC mixtures

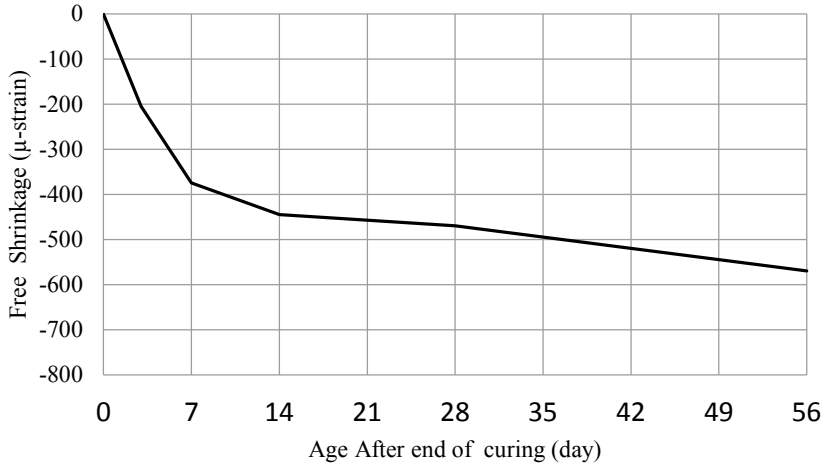

(13) LS121S

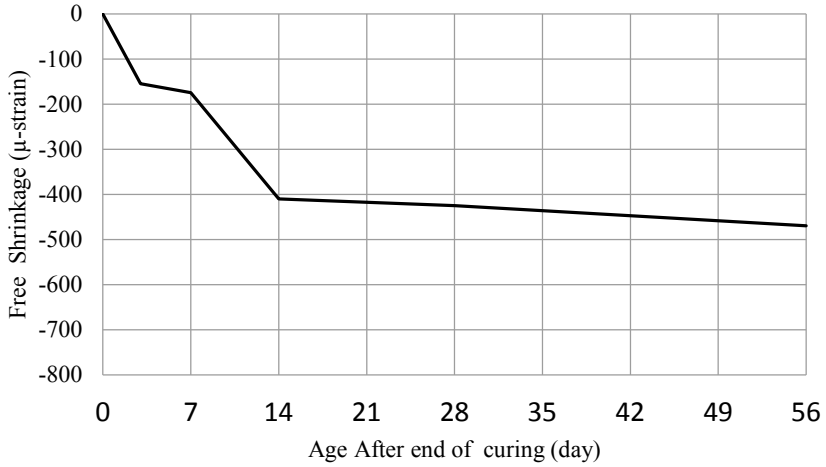

(14) LS121FLP

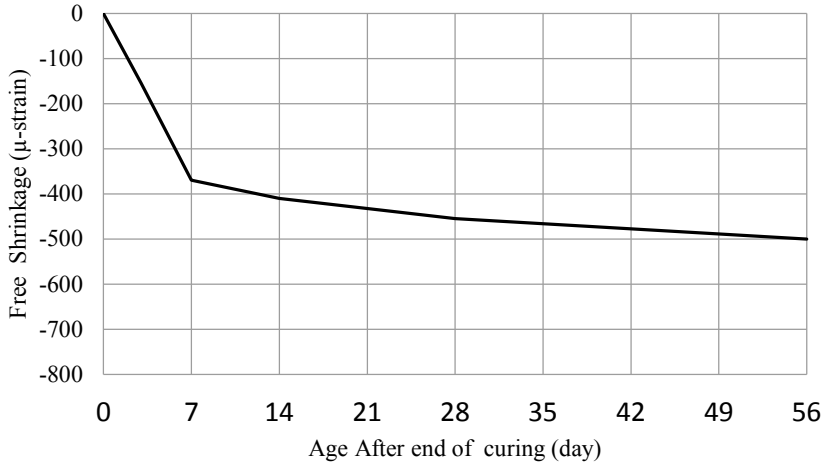

(15) LS221C

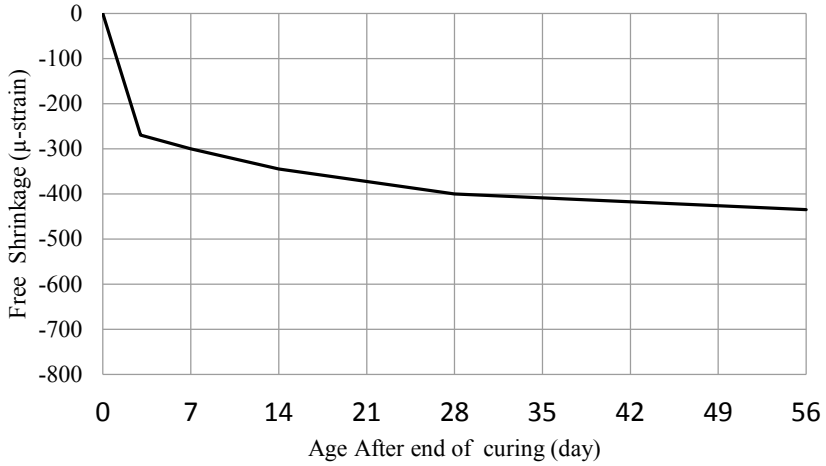

(16) LS221F

(Cont.) Figure E-20. Relationship between free shrinkage and age after end of curing of SCC and CVC mixtures

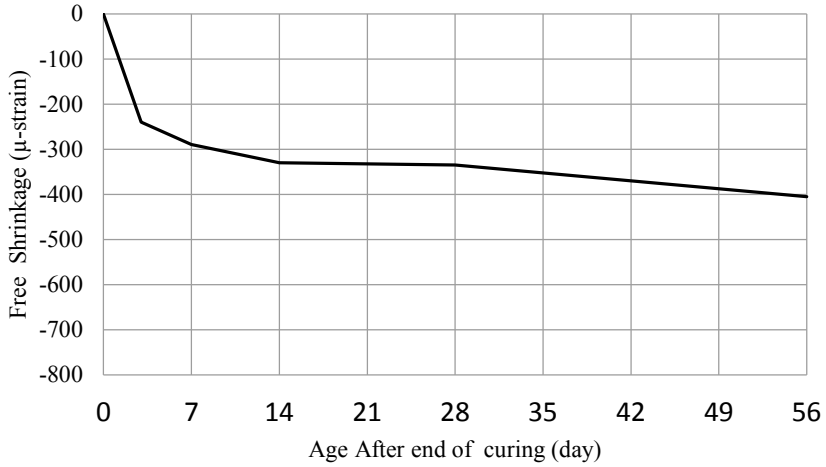

(17) LS221S

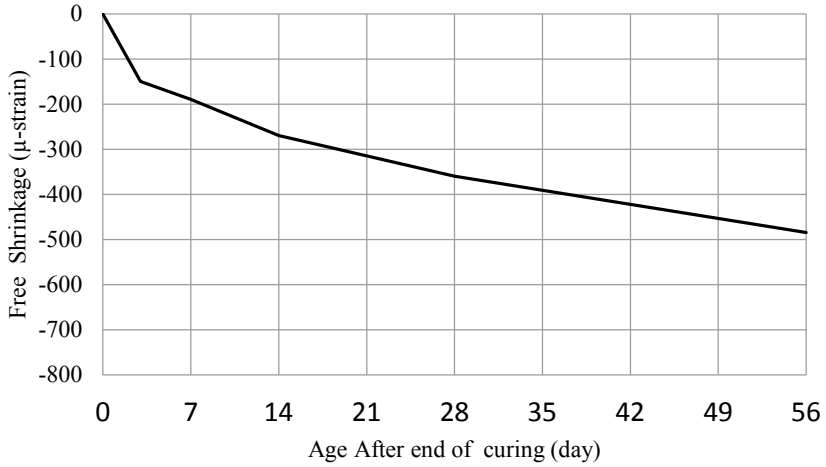

(18) LS221FLP

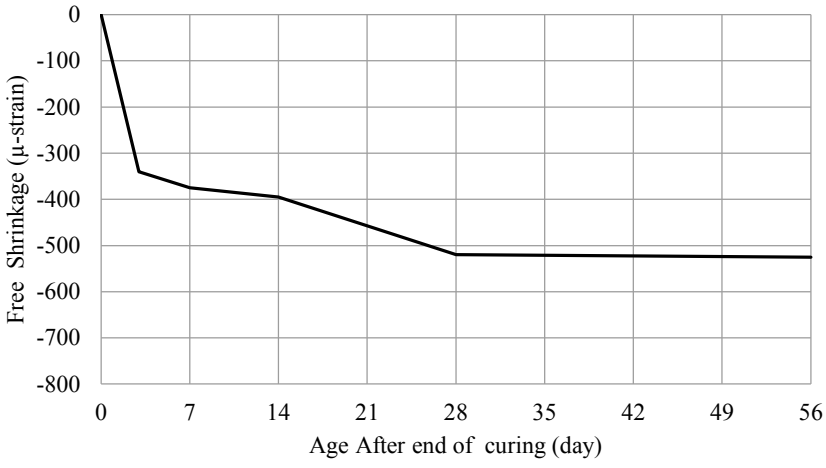

(19) LS0.375 CVC

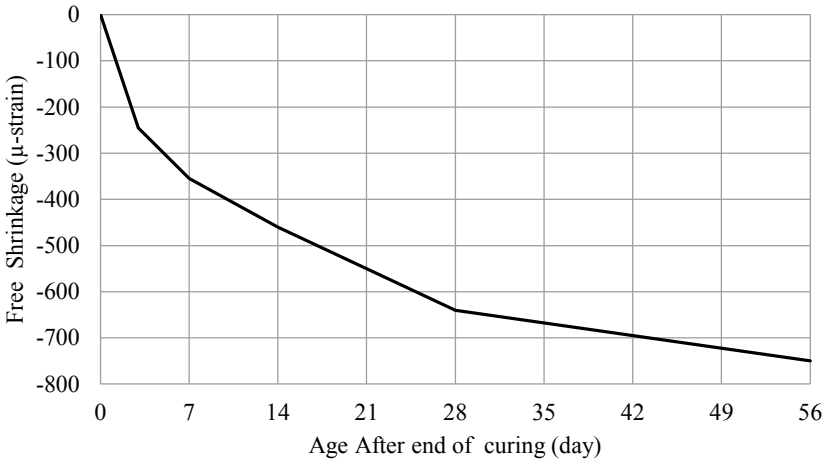

(20) LS222C

(Cont.) Figure E-20. Relationship between free shrinkage and age after end of curing of SCC and CVC mixtures

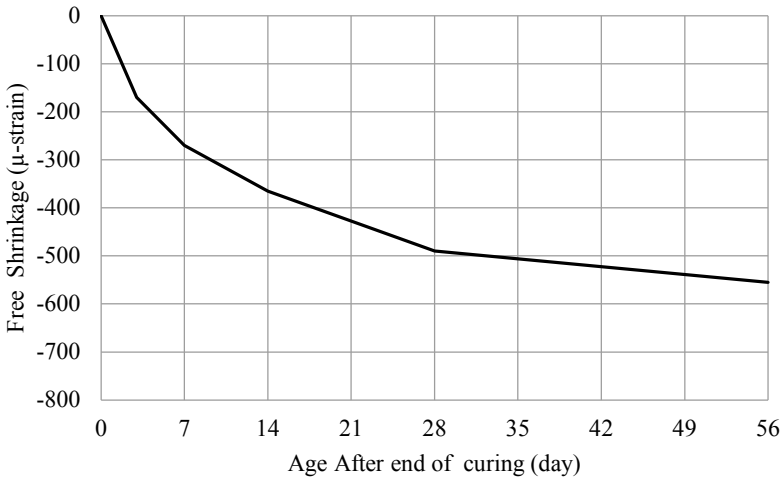

(21) LS222F

(22) LS222S

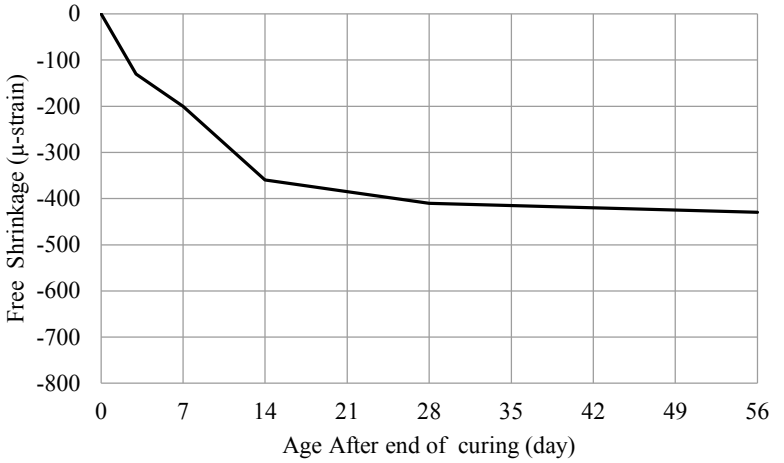

(23) LS222FLP

(Cont.) Figure E-20. Relationship between free shrinkage and age after end of curing of SCC and CVC mixtures

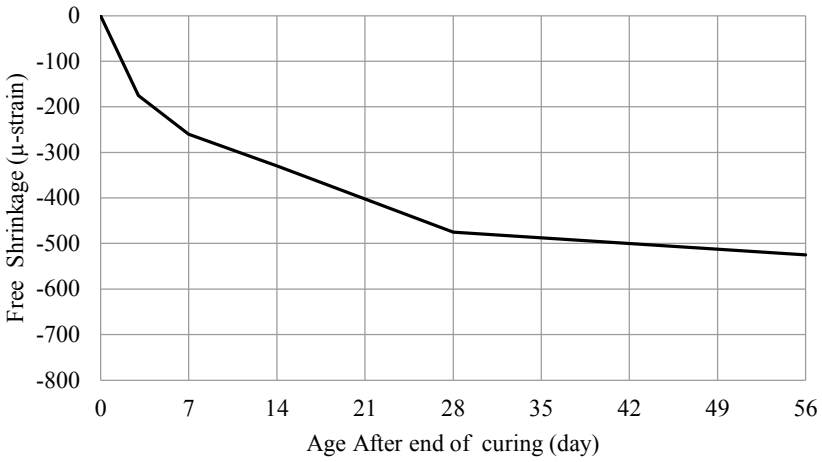

(24) G0.75 CVC

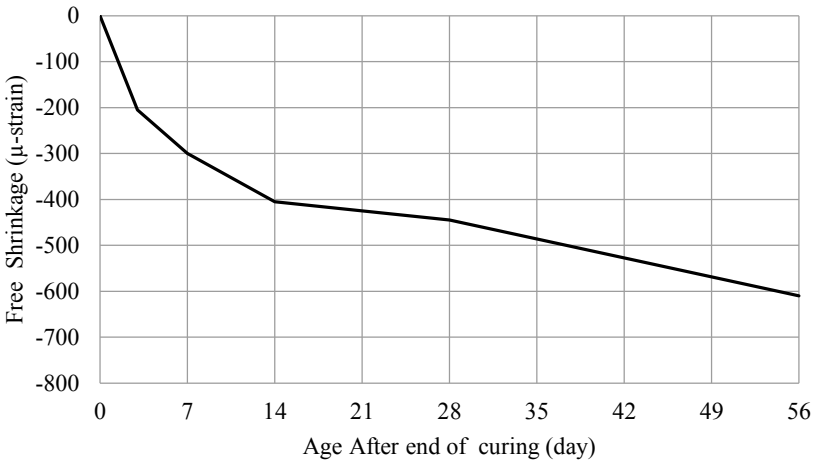

(25) G111C

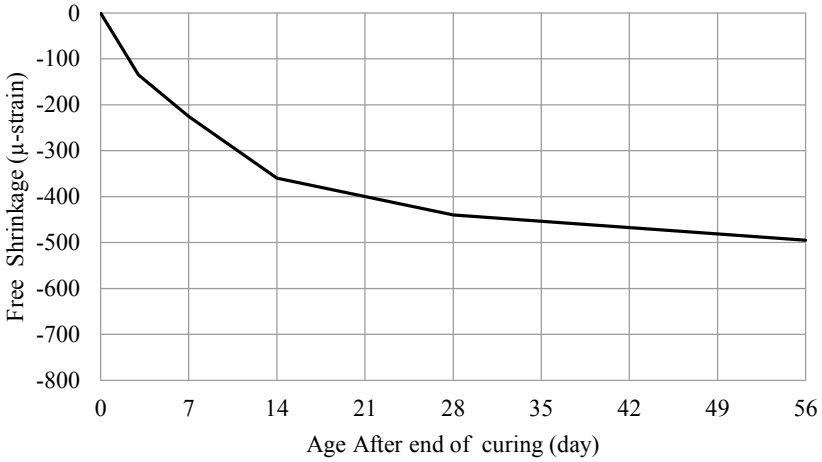

(26) G111F

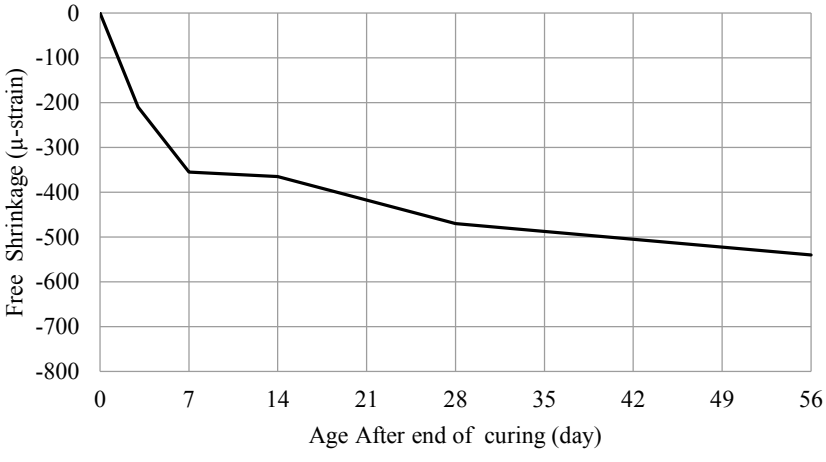

(27) G111S

(Cont.) Figure E-20. Relationship between free shrinkage and age after end of curing of SCC and CVC mixtures

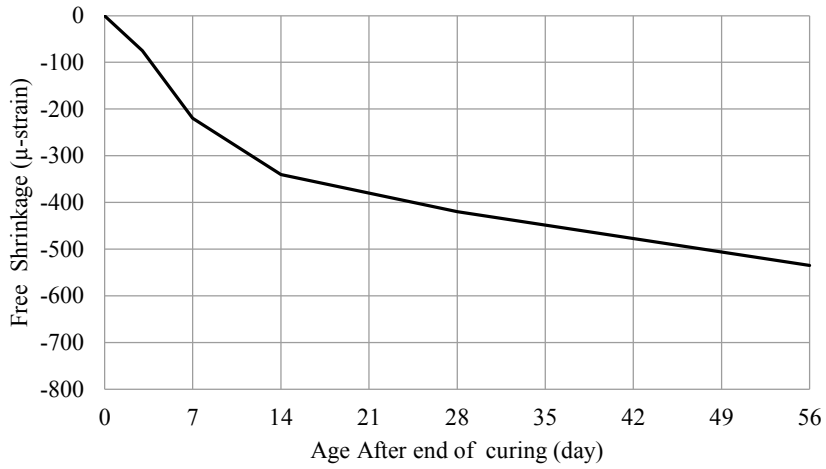

(28) G111FLP

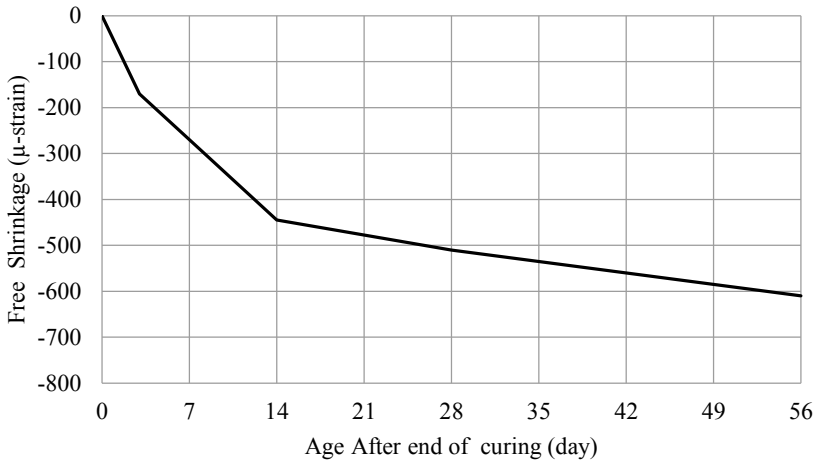

(29) G211C

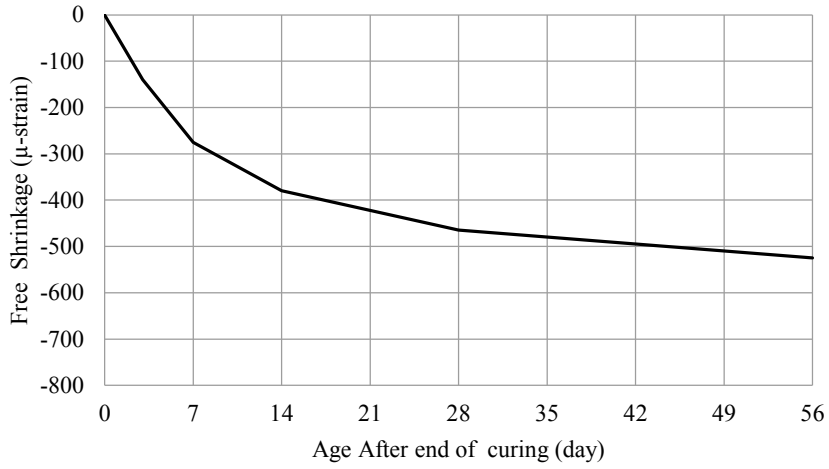

(30) G211F

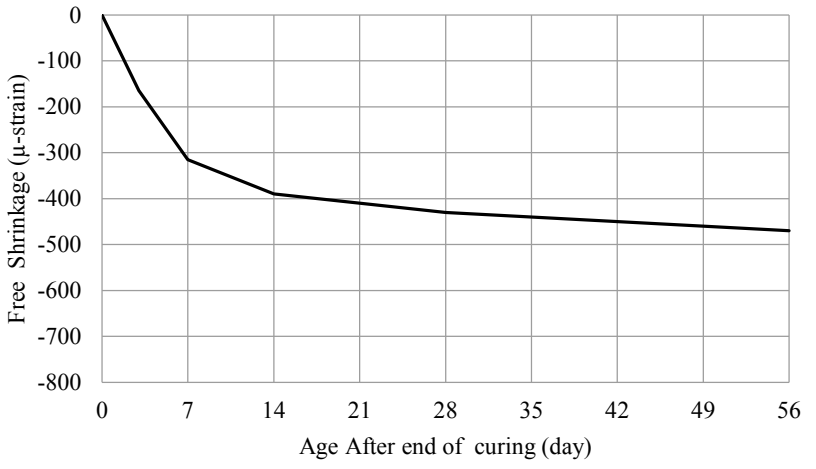

(31) G211S

(Cont.) Figure E-20. Relationship between free shrinkage and age after end of curing of SCC and CVC mixtures

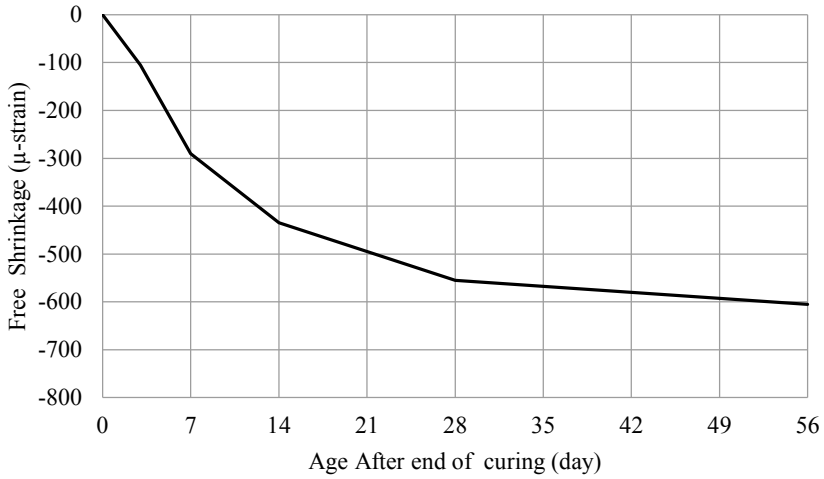

(32) G211FLP

(33) G0.50 CVC

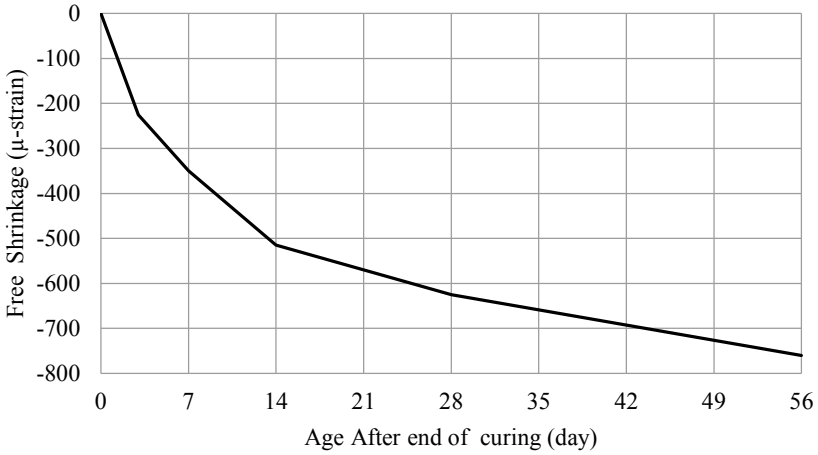

(34) G121C

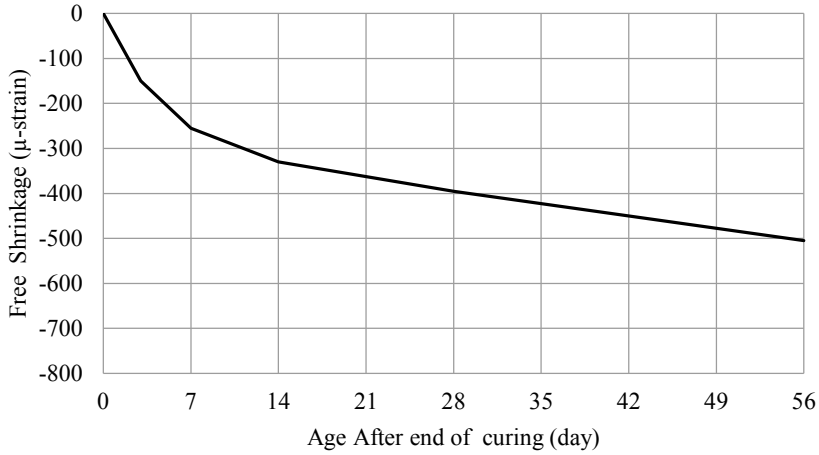

(35) G121F

(Cont.) Figure E-20. Relationship between free shrinkage and age after end of curing of SCC and CVC mixtures

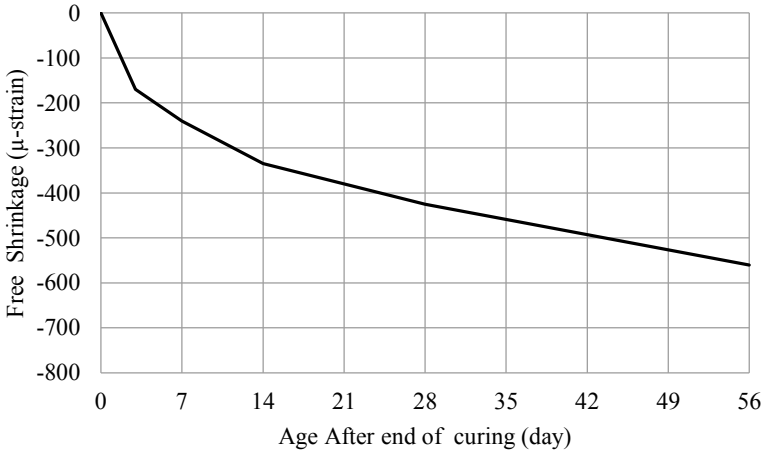

(36) G121S

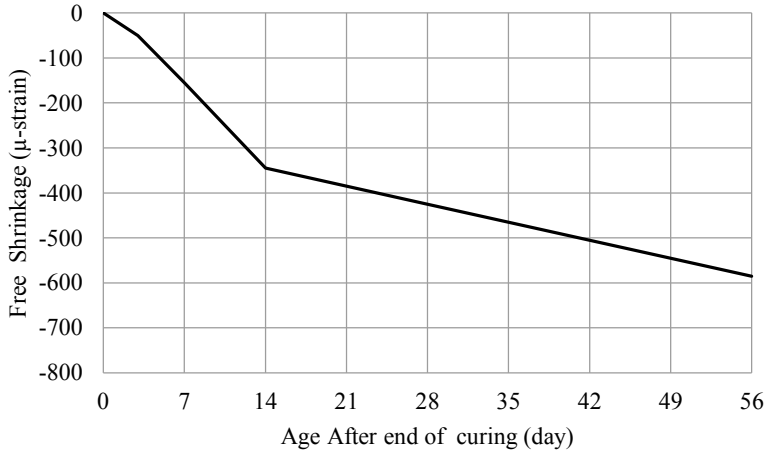

(37) G121FLP

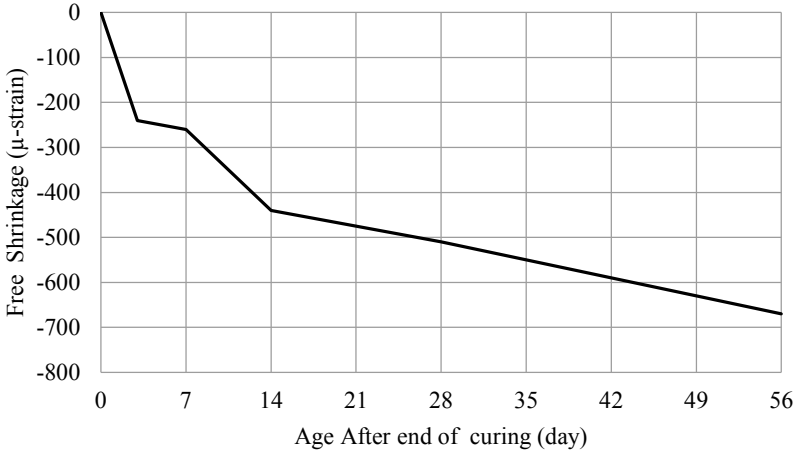

(38) G221C

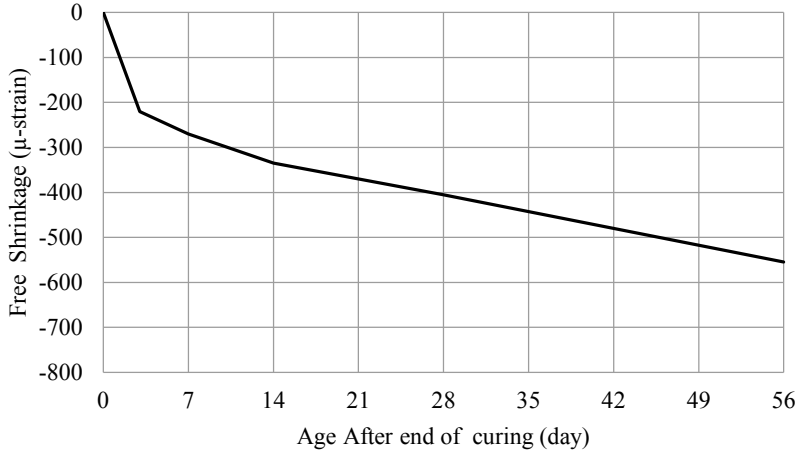

(39) G221F

(Cont.) Figure E-20. Relationship between free shrinkage and age after end of curing of SCC and CVC mixtures

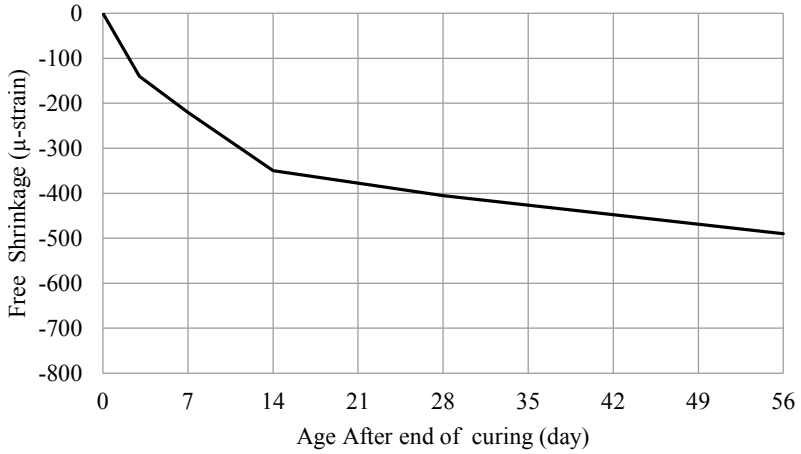

(40) G221S

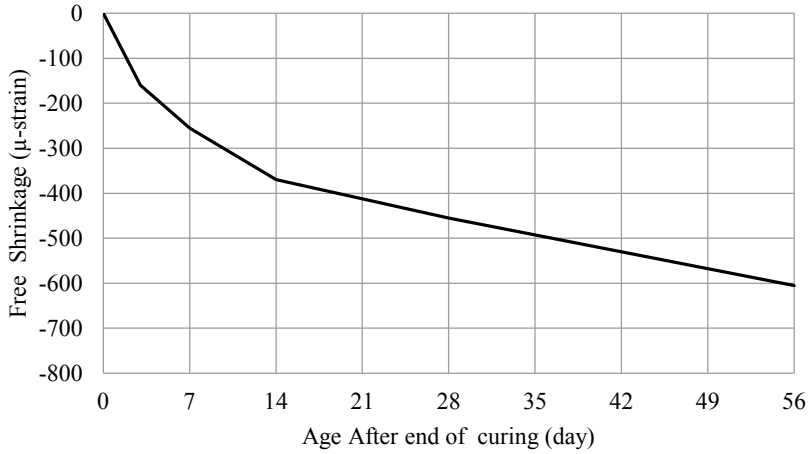

(41) G221FLP

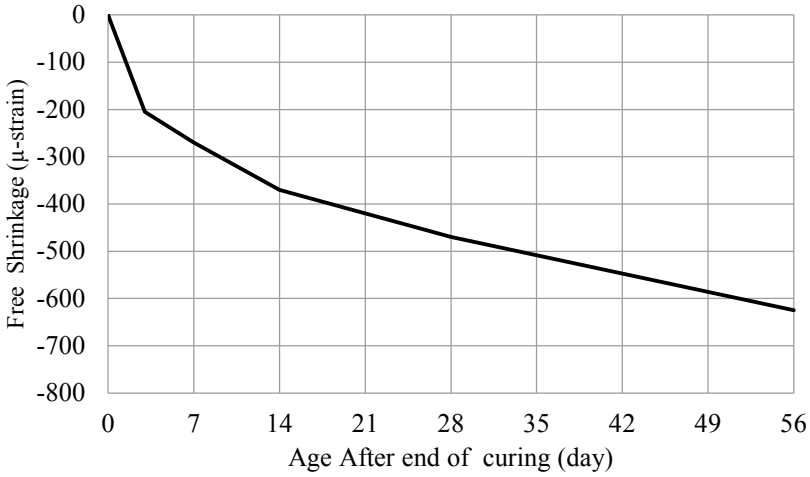

(42) G0.375 CVC

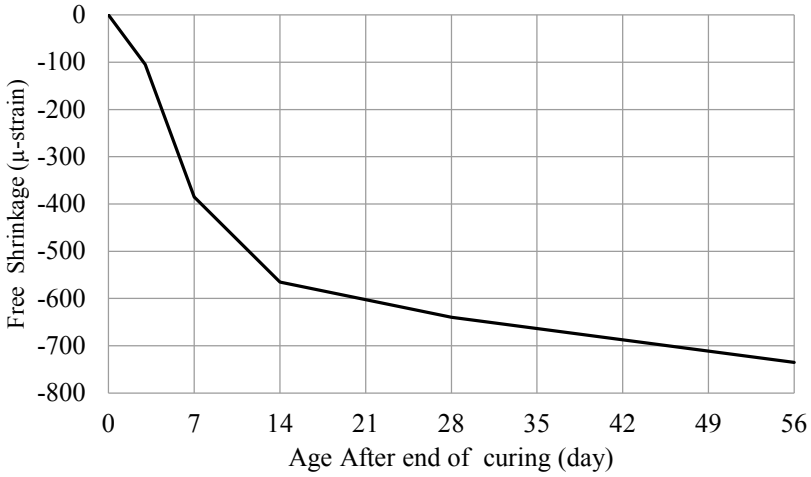

(43) G222C

(Cont.) Figure E-20. Relationship between free shrinkage and age after end of curing of SCC and CVC mixtures

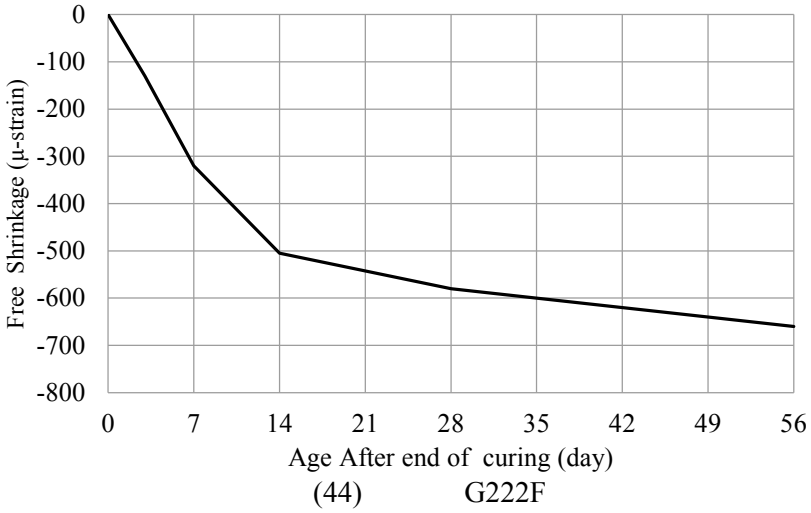

(44) G222F

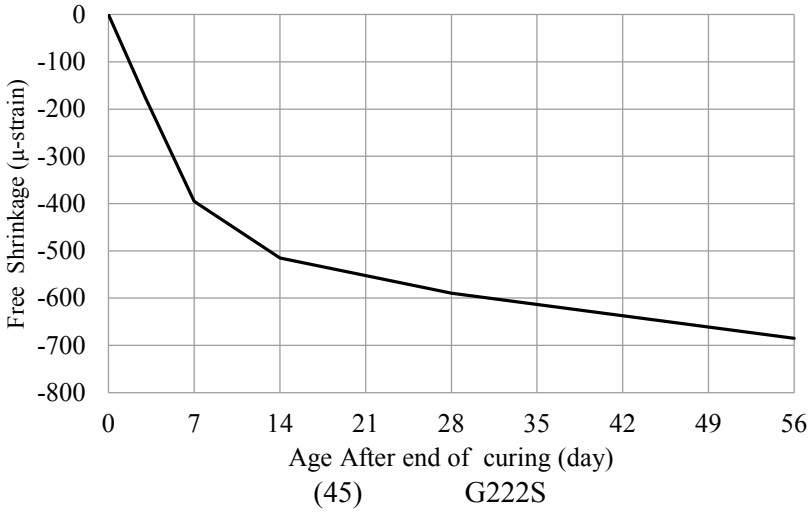

(45) G222S

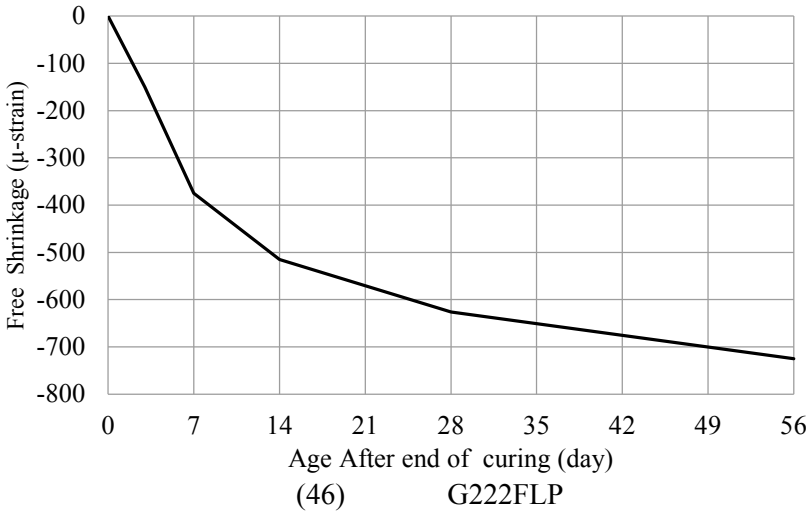

(46) G222FLP

(Cont.) Figure E-20. Relationship between free shrinkage and age after end of curing of SCC and CVC mixtures

8. Restrained Shrinkage

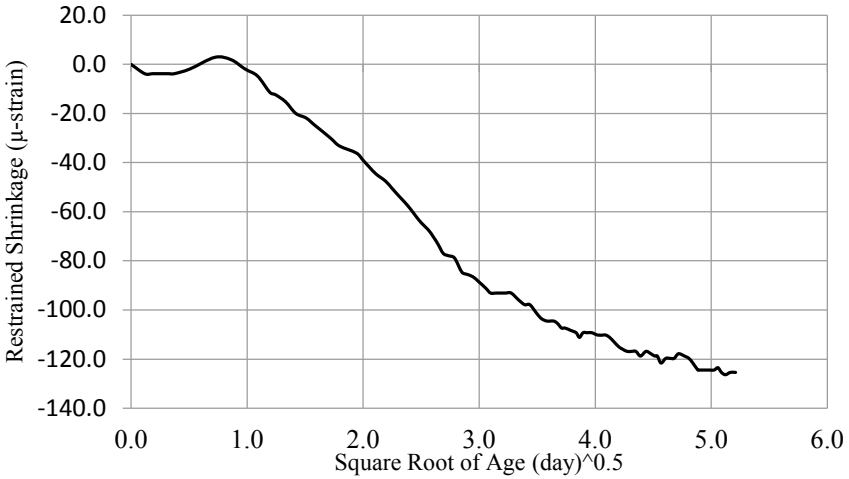

(1) LS0.75 CVC

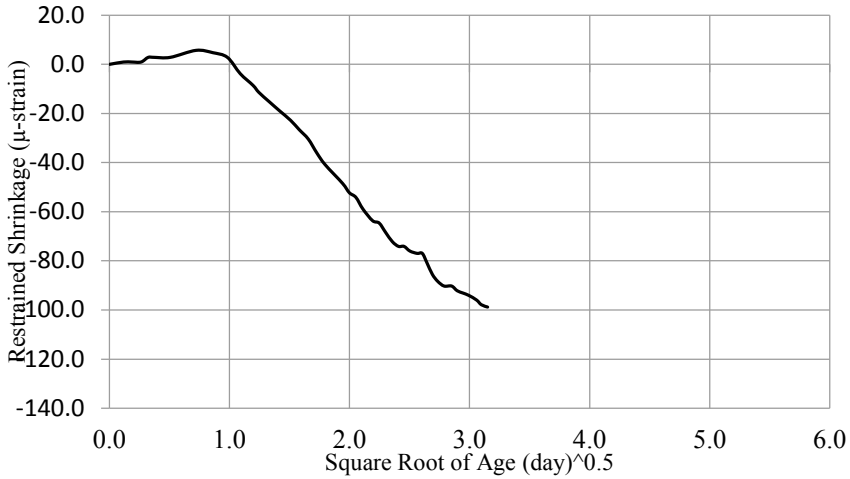

(2) LS111C

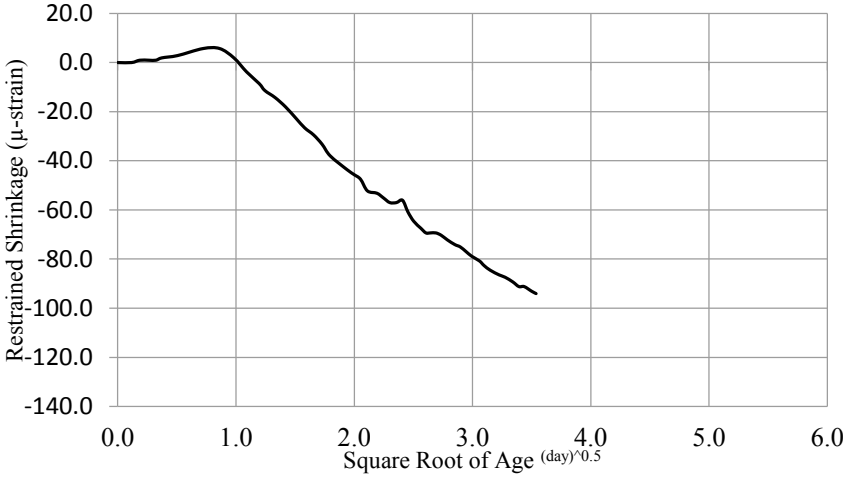

(3) LS111F

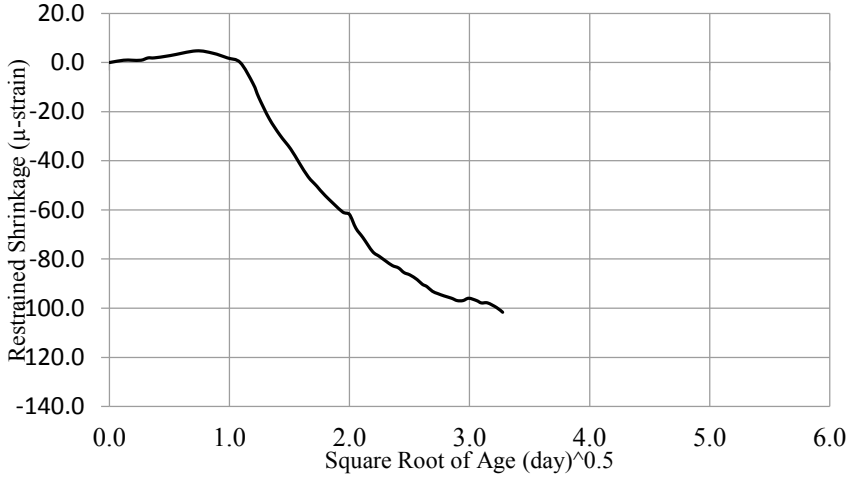

(4) LS111S

Figure E-20. Relationship between restrained shrinkage and square root of age of SCC and CVC mixtures

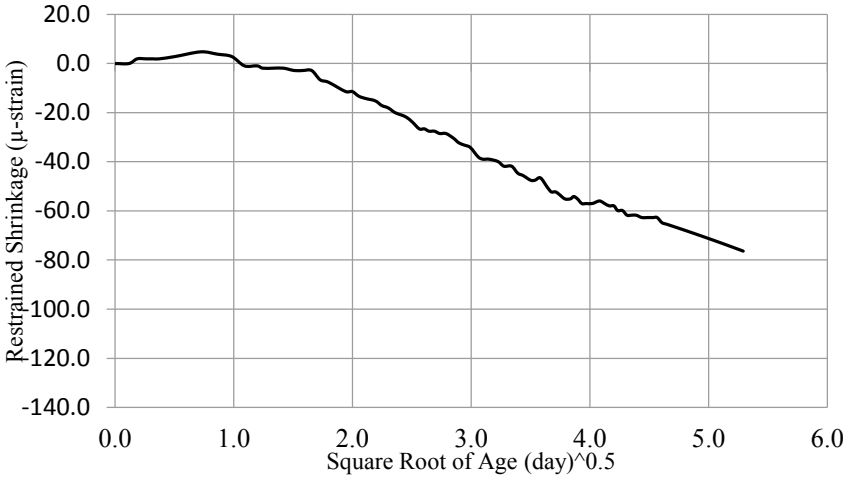

(5) LS111FLP

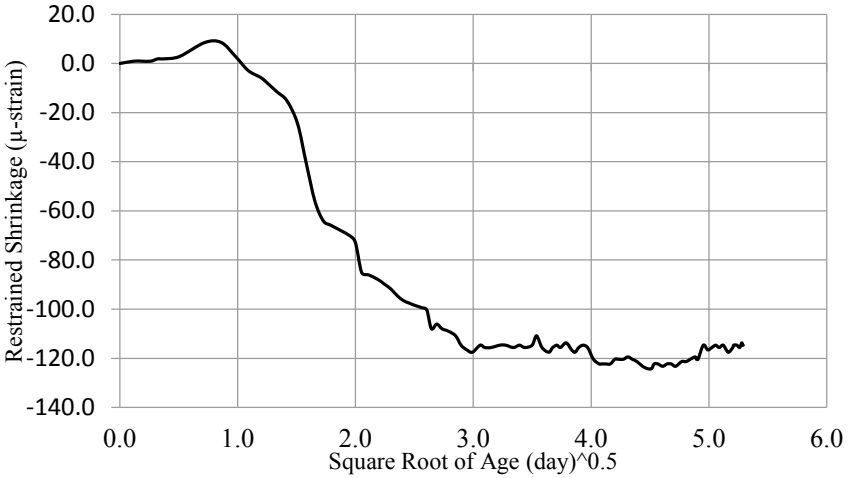

(6) LS211C

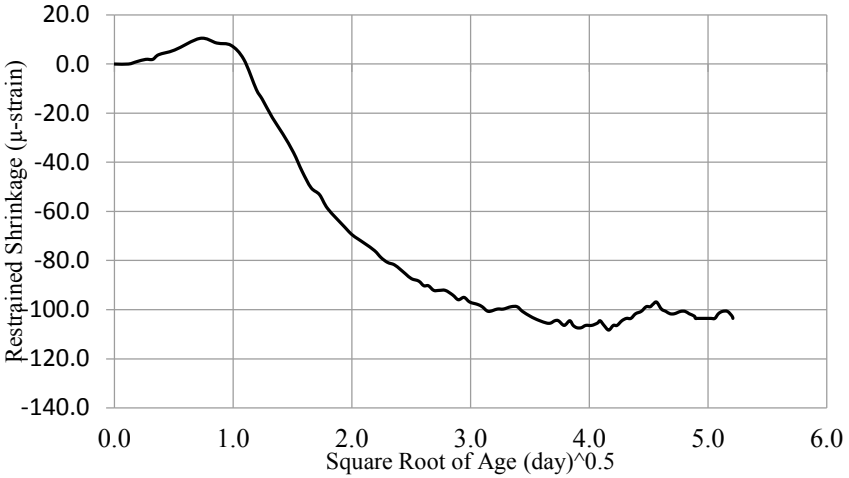

(7) LS211S

(Cont.) Figure E-20. Relationship between restrained shrinkage and square root of age of SCC and CVC mixtures

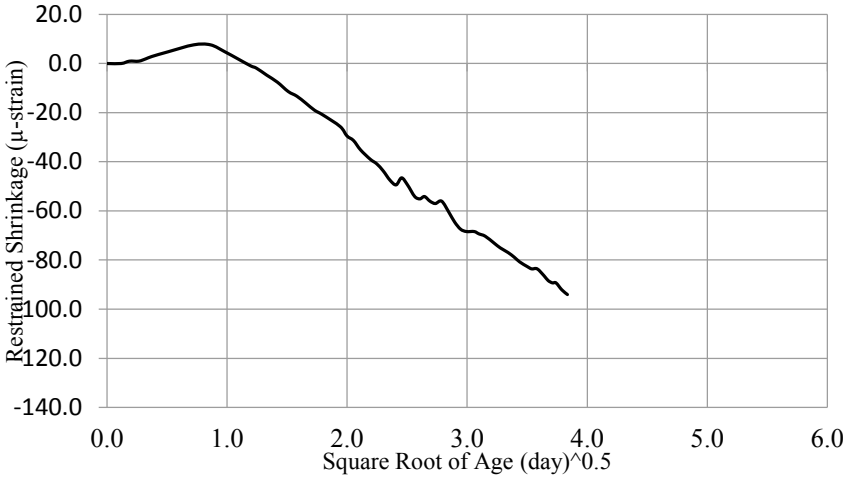

(8) LS211FLP

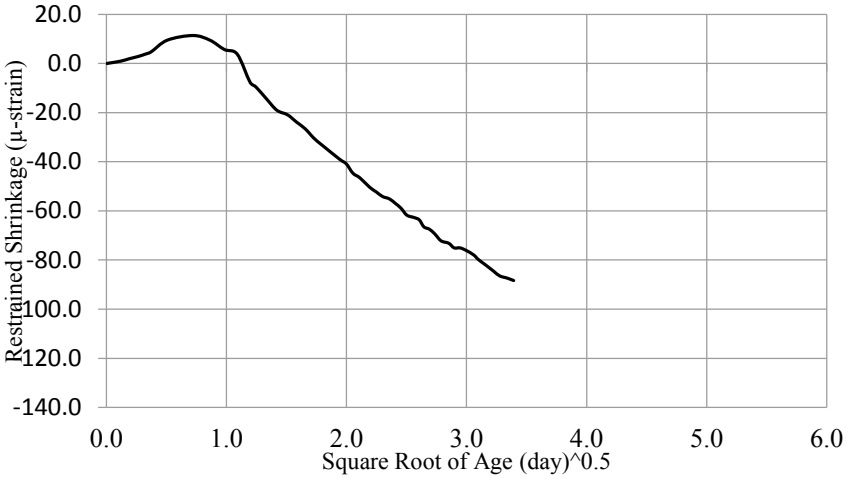

(9) LS0.50 CVC

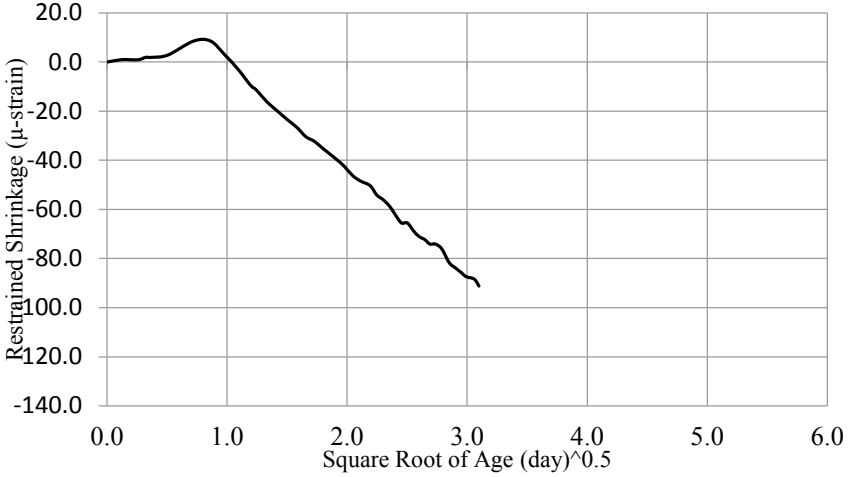

(10) LS121C

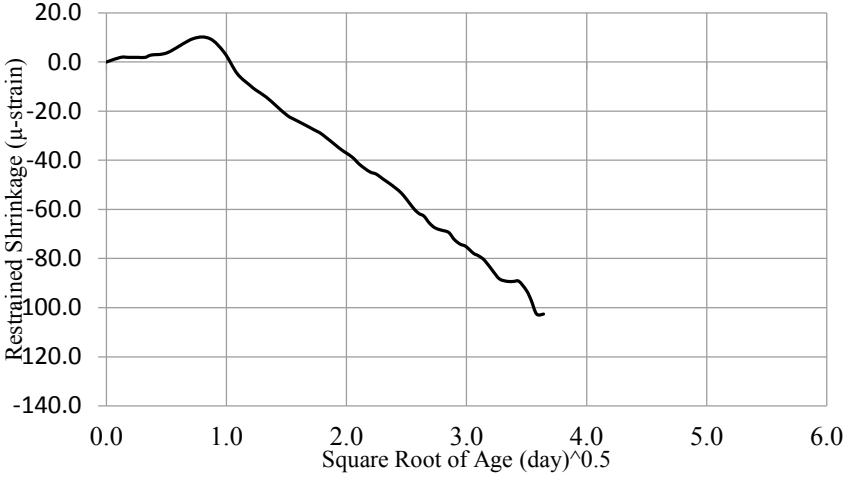

(11) LS121F

(Cont.) Figure E-20. Relationship between restrained shrinkage and square root of age of SCC and CVC mixtures

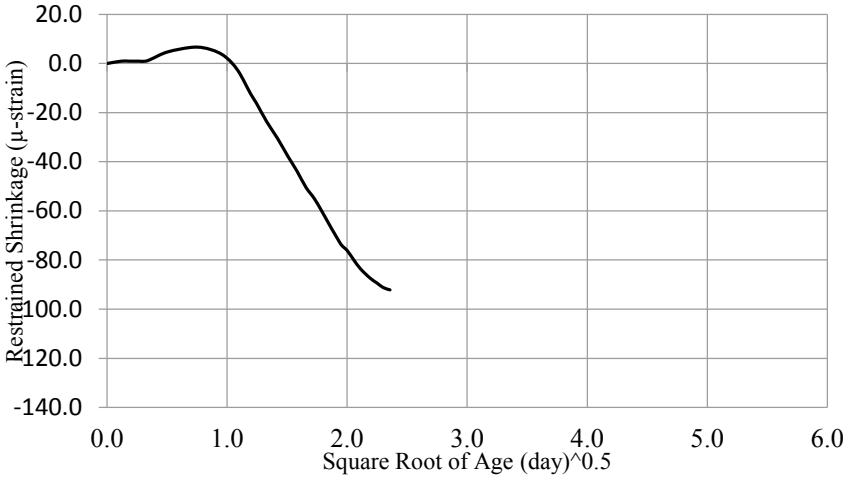

(12) LS121S

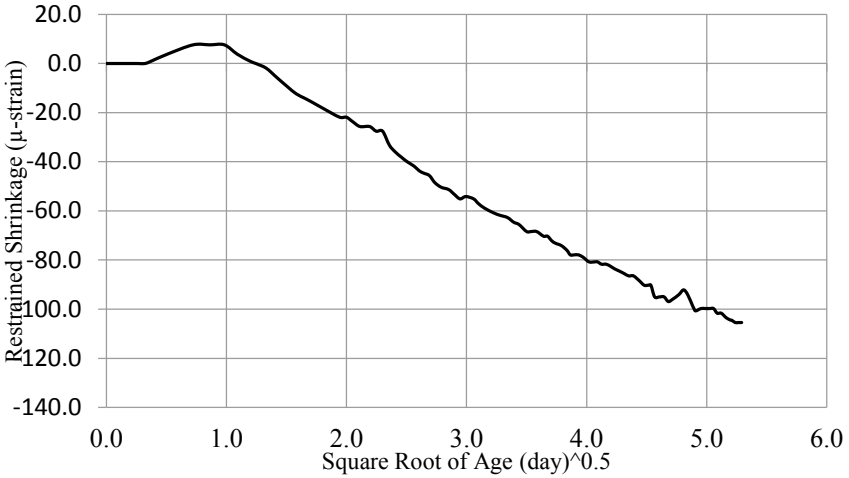

(13) LS121FLP

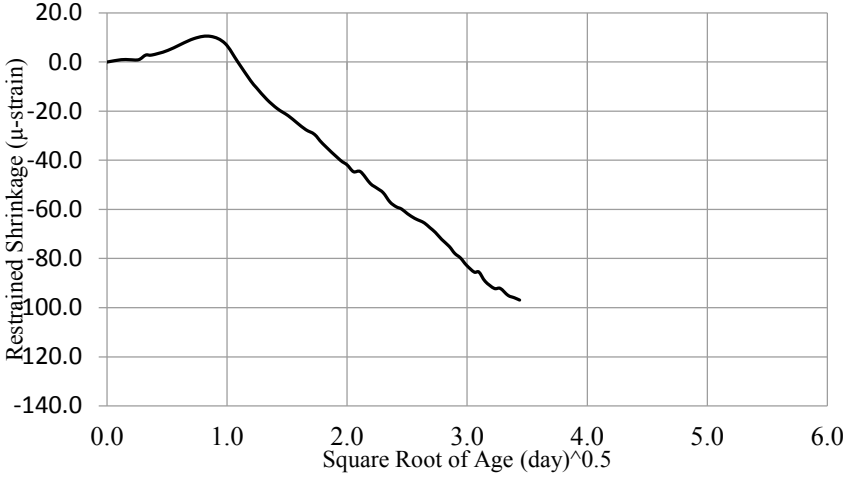

(14) LS221C

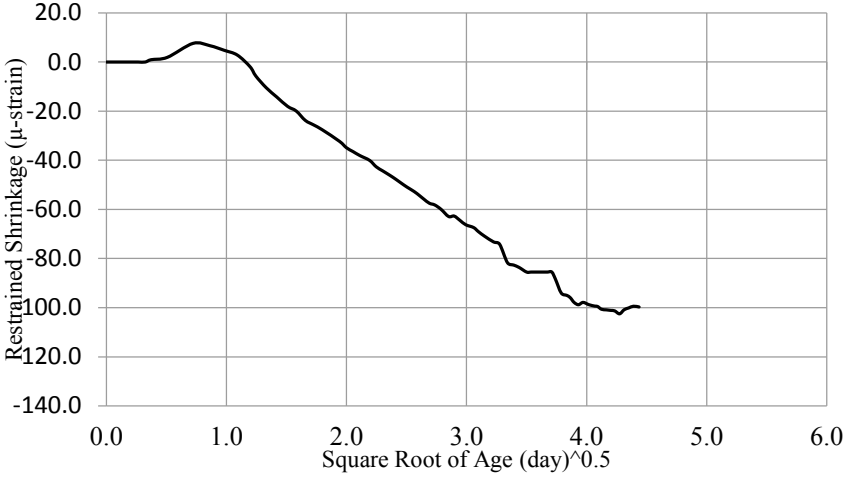

(15) LS221F

(Cont.) Figure E-20. Relationship between restrained shrinkage and square root of age of SCC and CVC mixtures

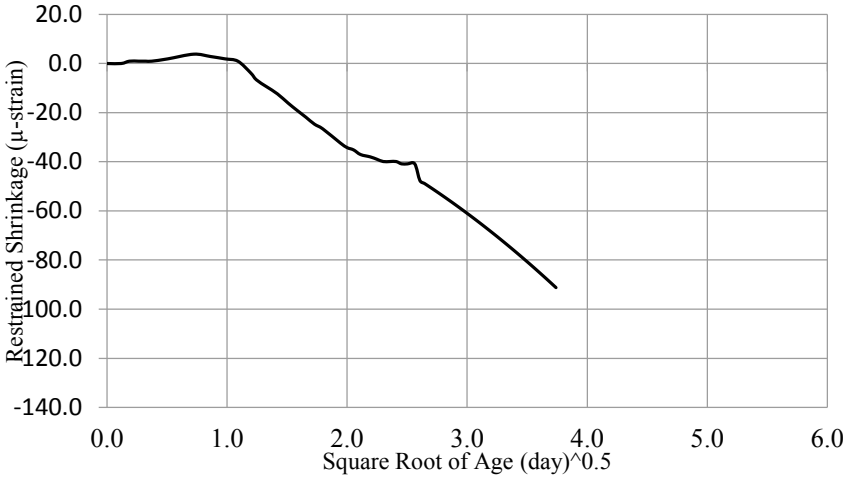

(16) LS221S

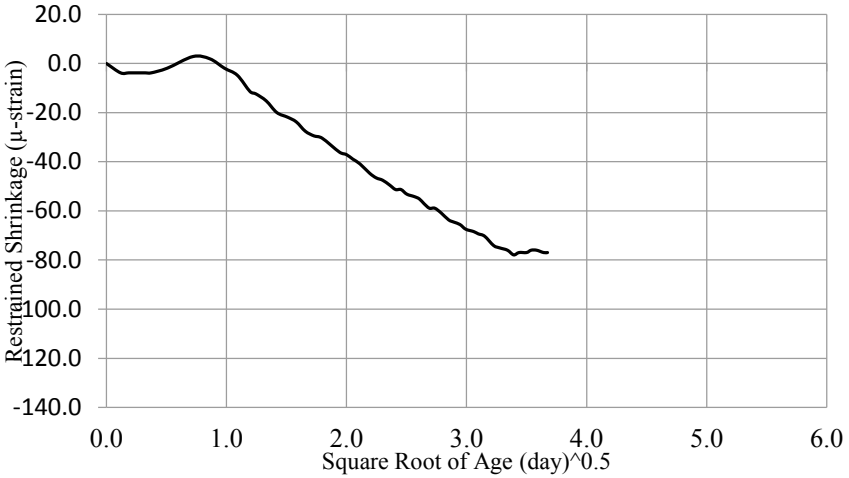

(17) LS221FLP

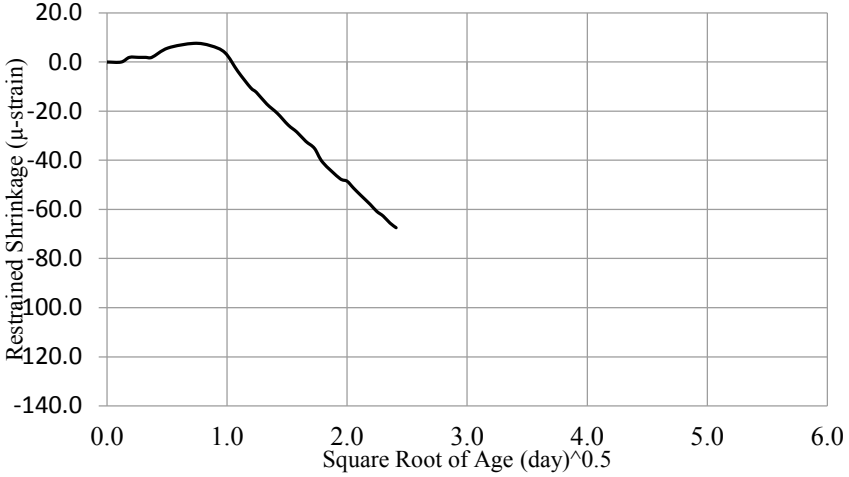

(18) LS0.375 CVC

(19) LS222C

(Cont.) Figure E-21. Relationship between restrained shrinkage and square root of age of SCC and CVC mixtures

(20) LS222F

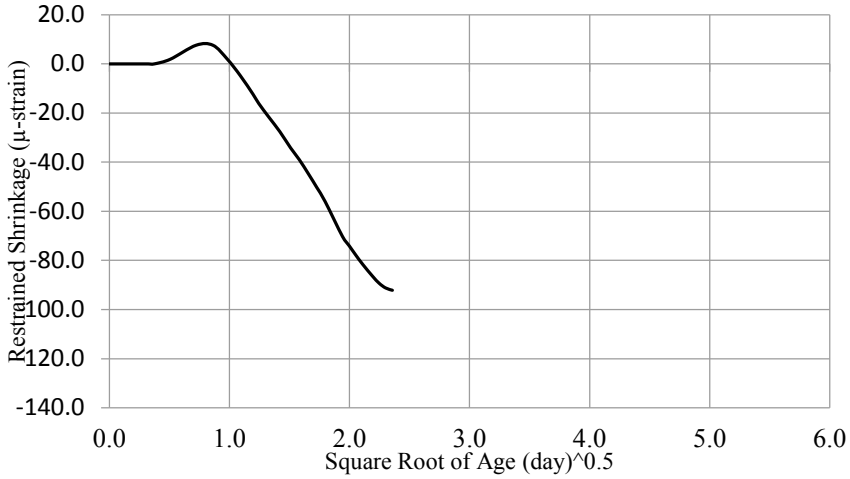

(21) LS222S

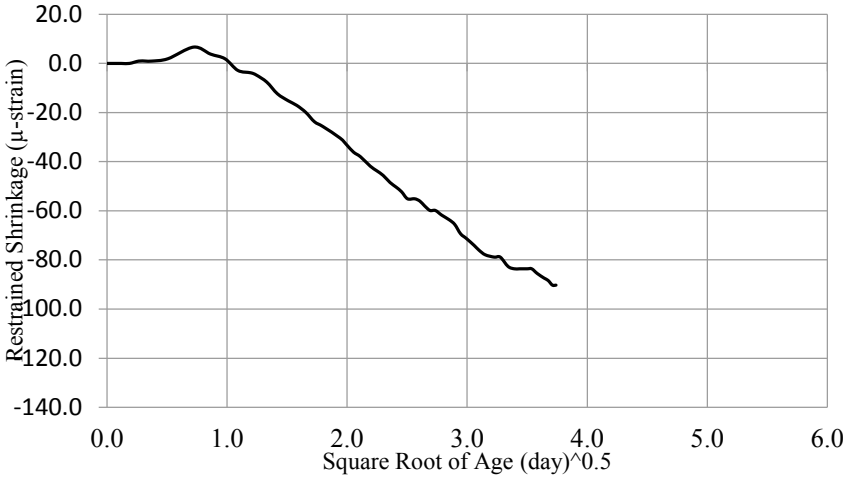

(22) LS222FLP

(Cont.) Figure E-21. Relationship between restrained shrinkage and square root of age of SCC and CVC mixtures

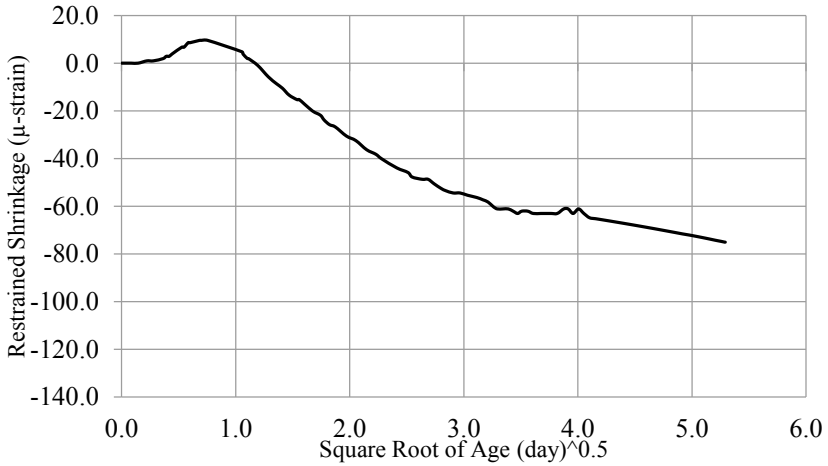

(23) G0.75 CVC

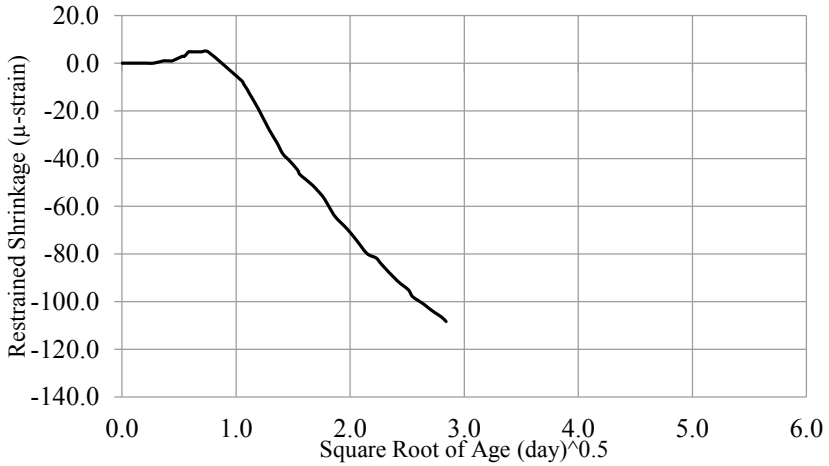

(24) G111C

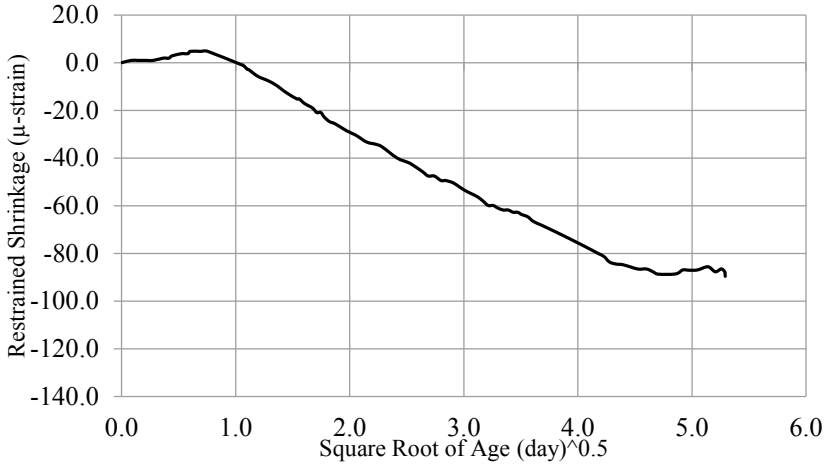

(25) G111F

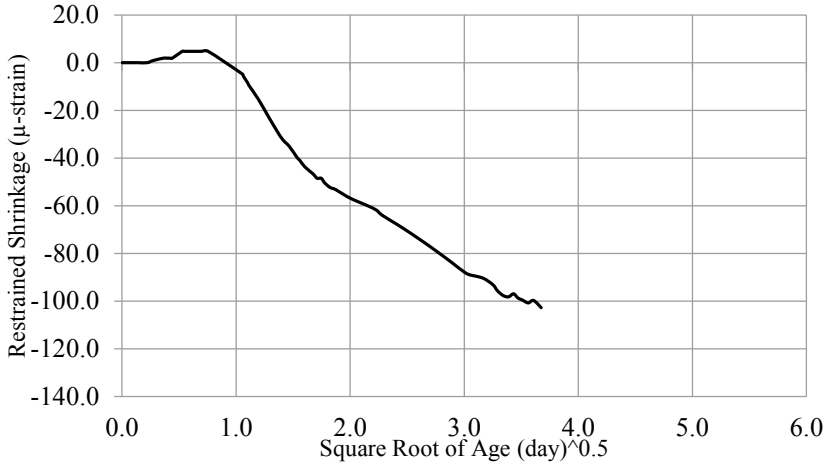

(26) G111S

(Cont.) Figure E-21. Relationship between restrained shrinkage and square root of age of SCC and CVC mixtures

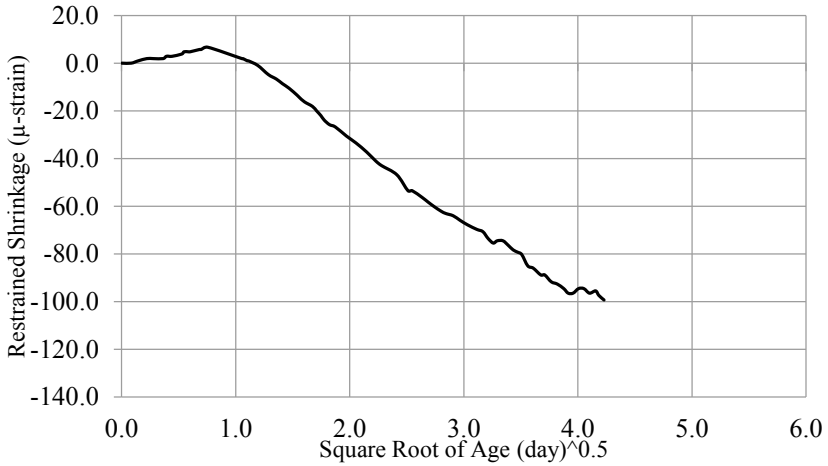

(27) G111FLP

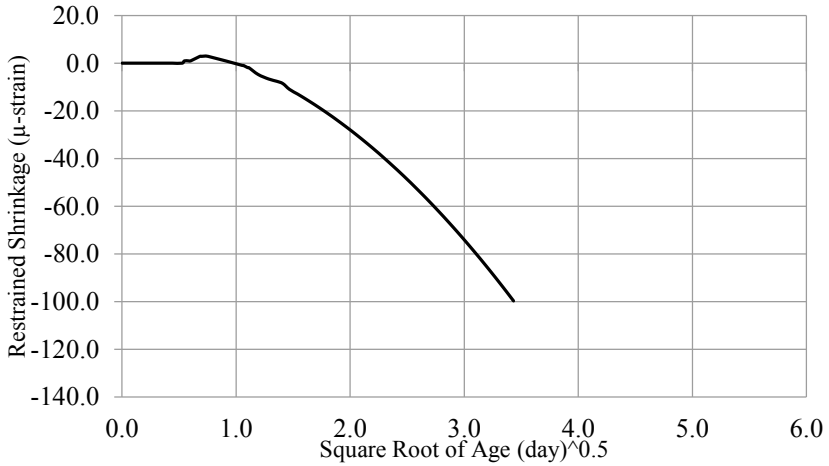

(28) G211C

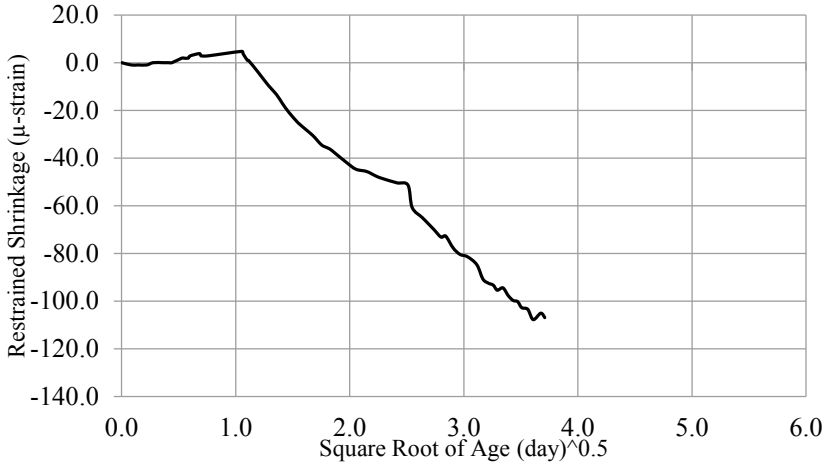

(29) G211F

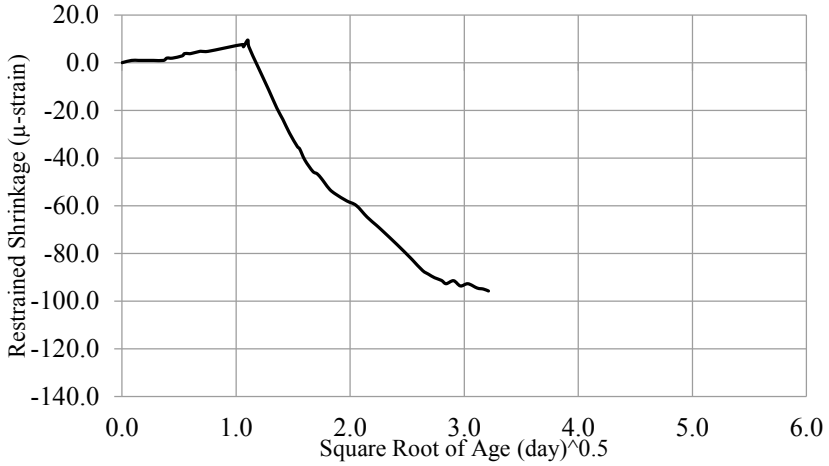

(30) G211S

(Cont.) Figure E-21. Relationship between restrained shrinkage and square root of age of SCC and CVC mixtures

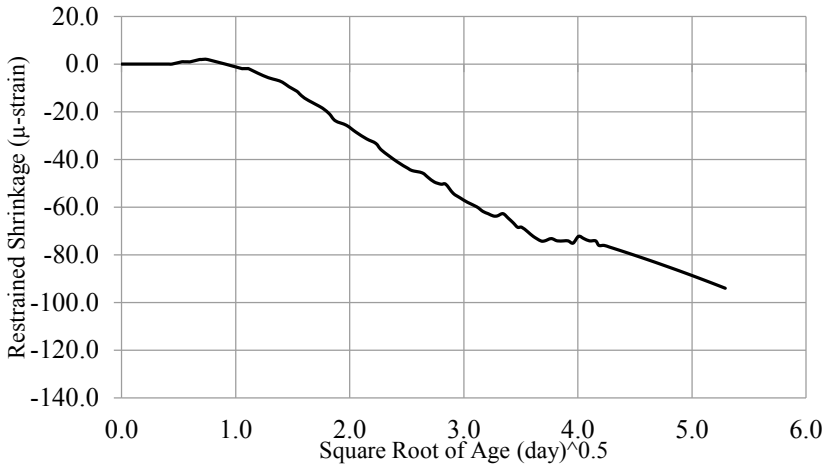

(31) G211FLP

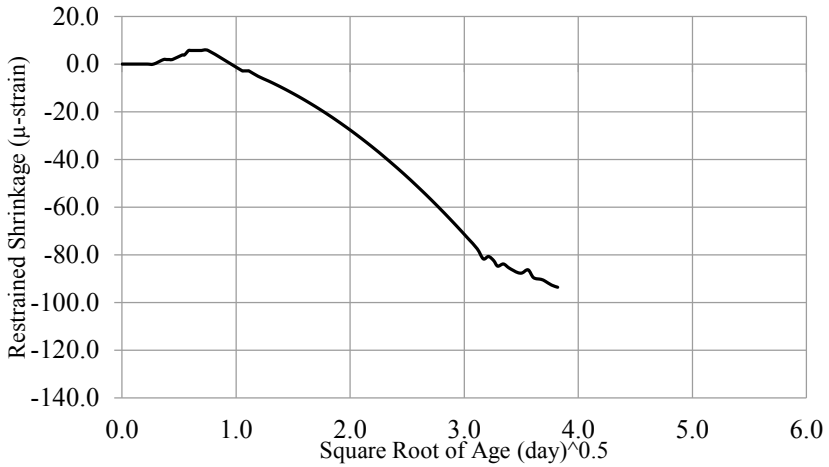

(32) G0.50 CVC

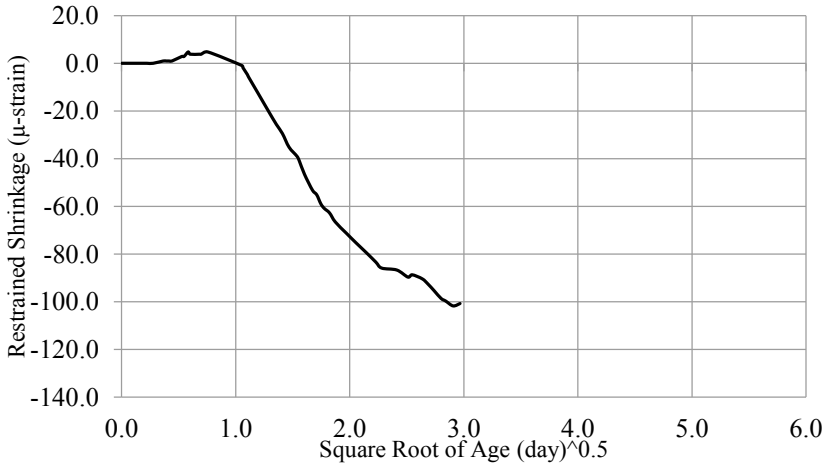

(33) G121C

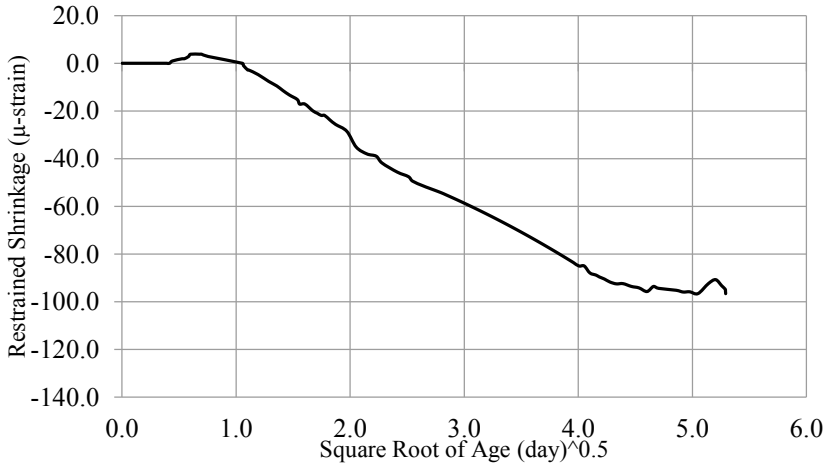

(34) G121F

(Cont.) Figure E-21. Relationship between restrained shrinkage and square root of age of SCC and CVC mixtures

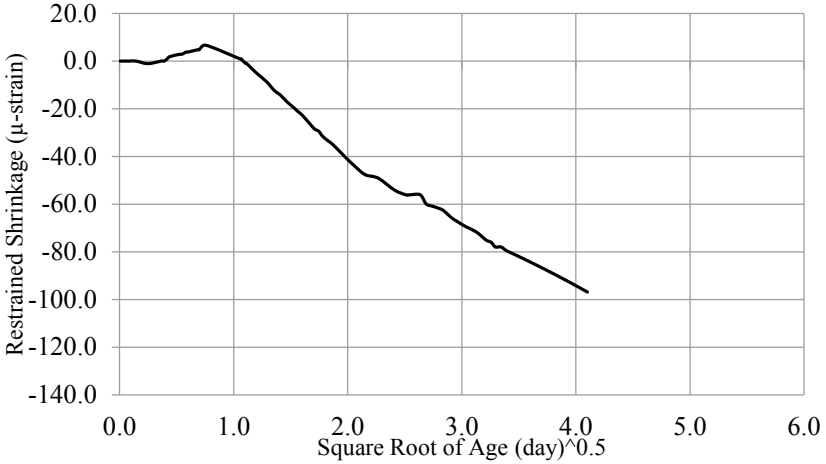

(35) G121S

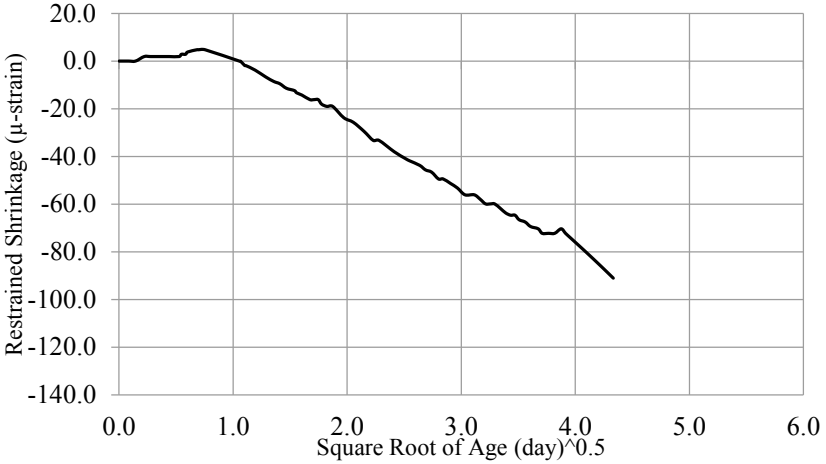

(36) G121FLP

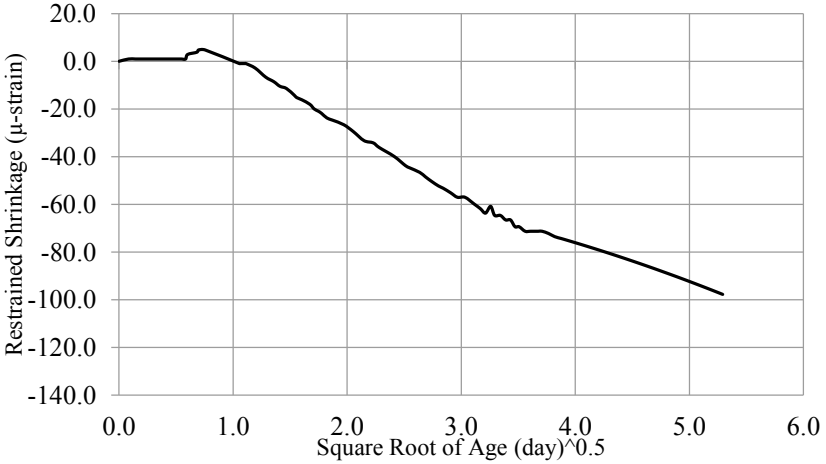

(37) G221F

(Cont.) Figure E-21. Relationship between restrained shrinkage and square root of age of SCC and CVC mixtures

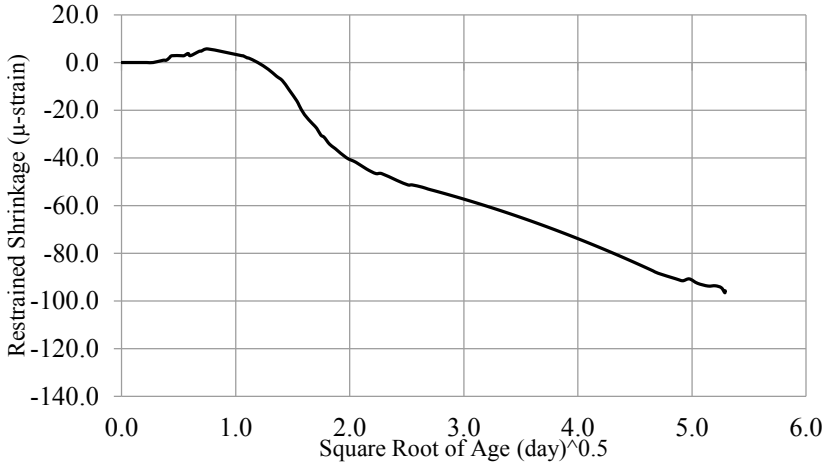

(38) G221S

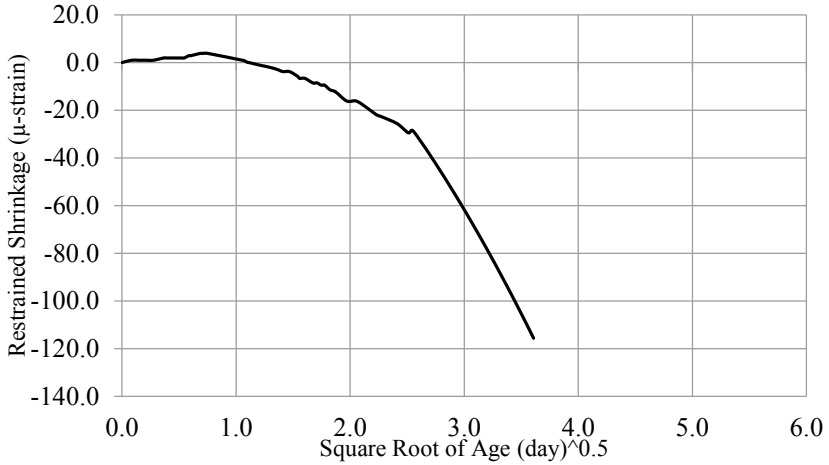

(39) G221FLP

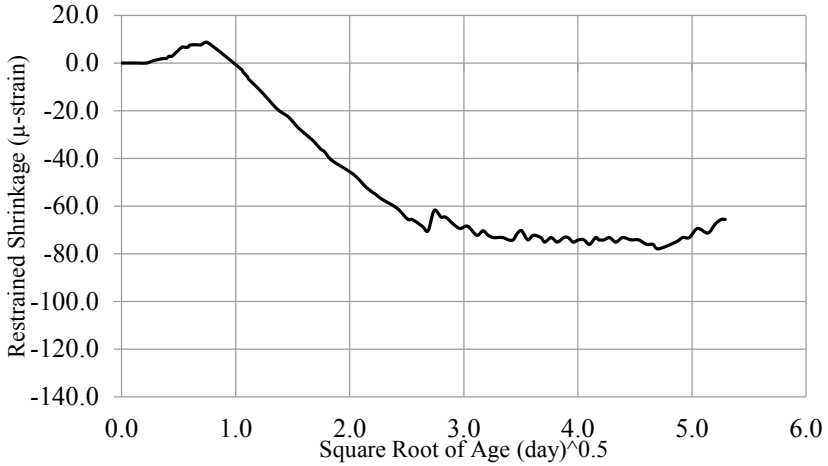

(40) G0.375 CVC

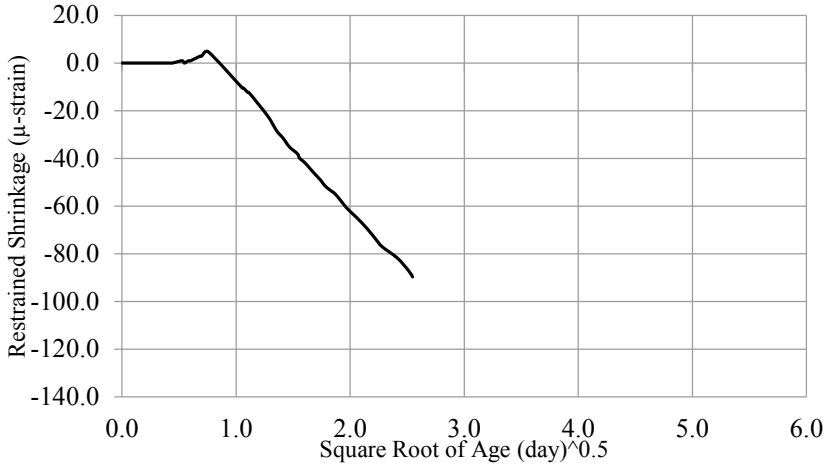

(41) G222C

(Cont.) Figure E-21. Relationship between restrained shrinkage and square root of age of SCC and CVC mixtures

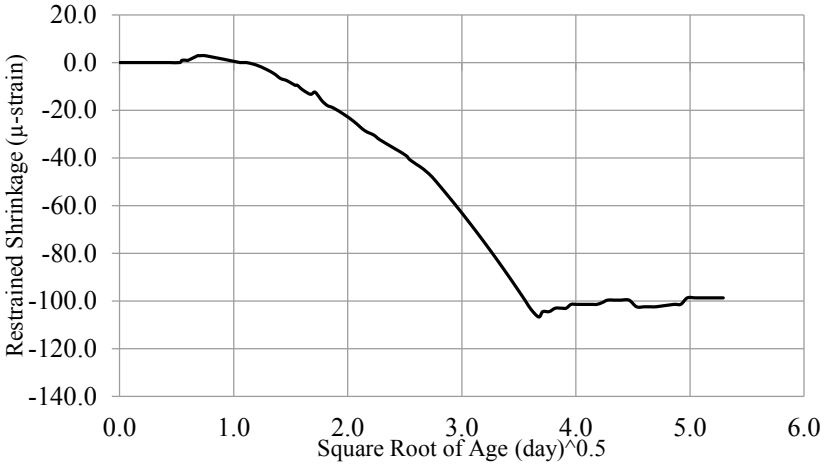

(42) G222F

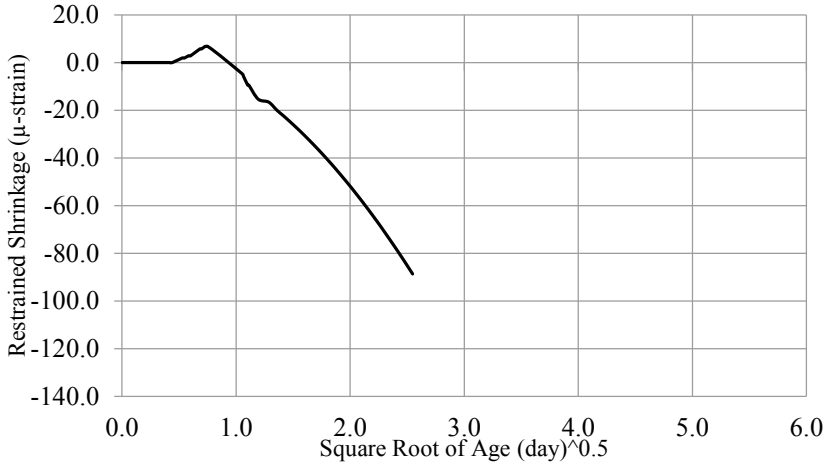

(43) G222S

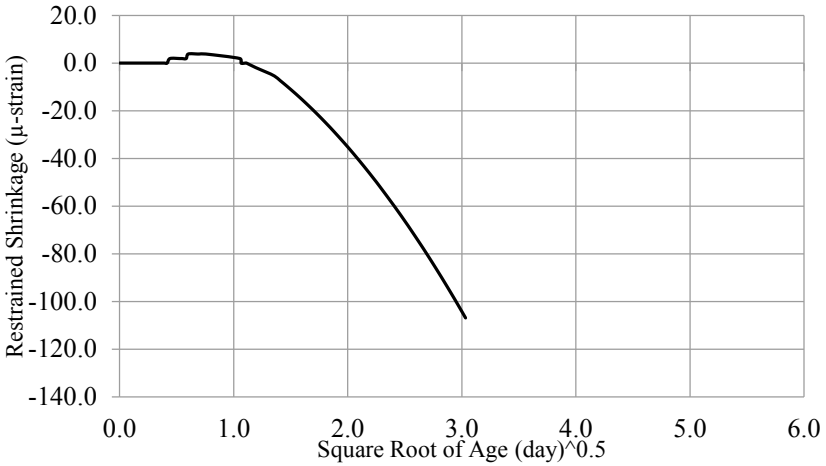

(44) G222FLP

(Cont.) Figure E-21. Relationship between restrained shrinkage and square root of age of SCC and CVC mixtures

9. Creep Strain

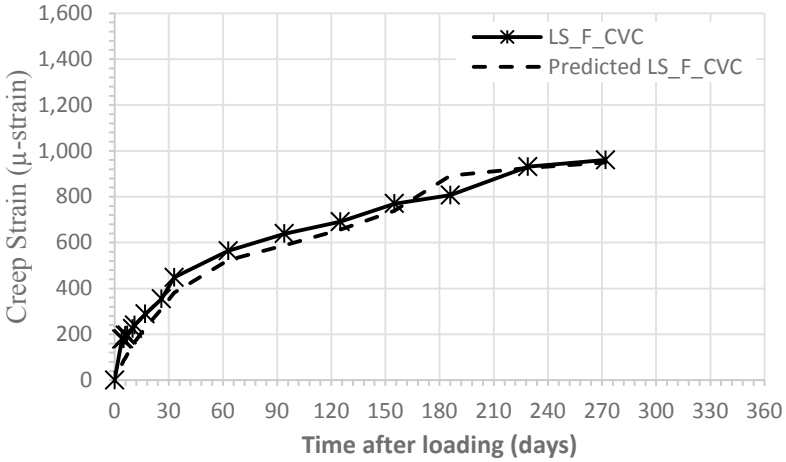

(1) LS0.375 CVC

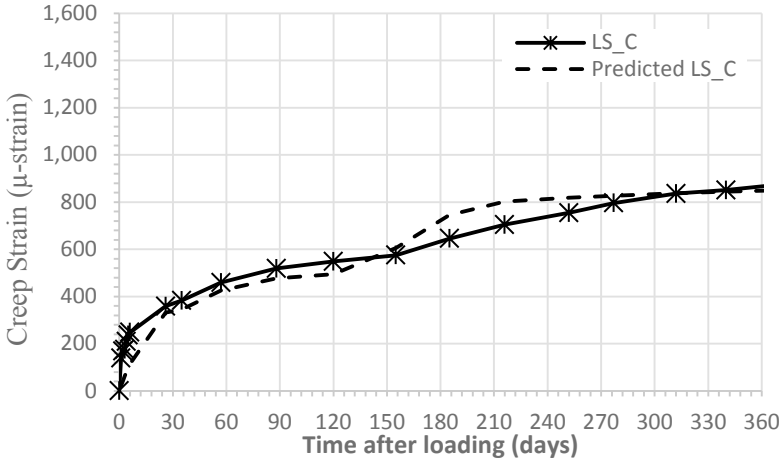

(2) LS222C

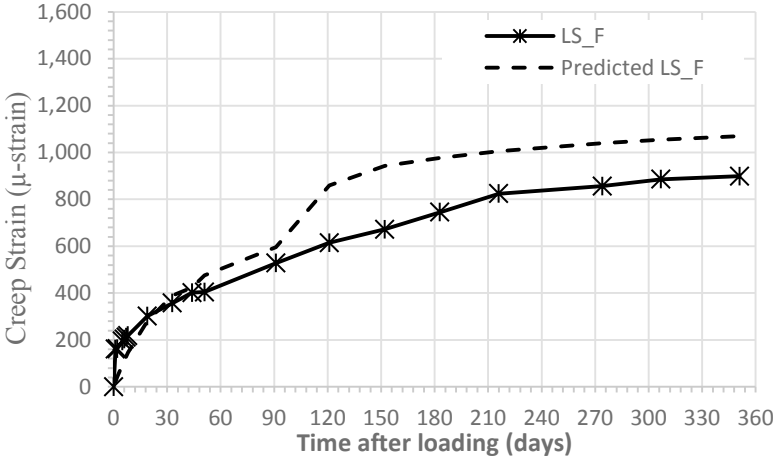

(3) LS222F

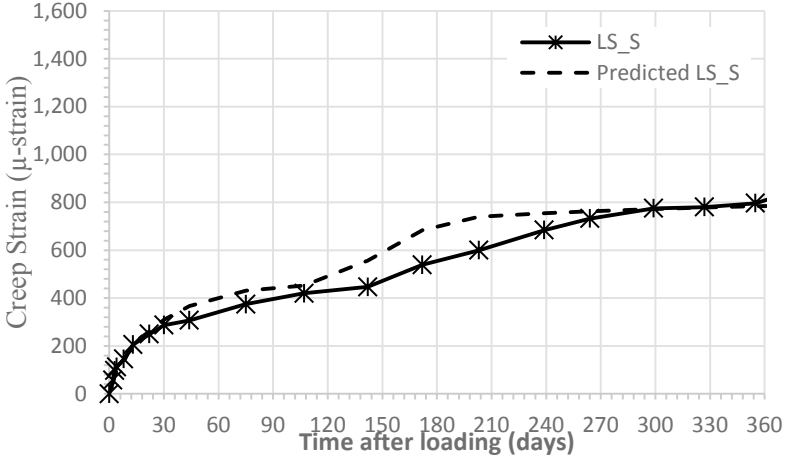

(4) LS222S

Figure E-21. Relationship between creep and time after loading of SCC and CVC mixtures

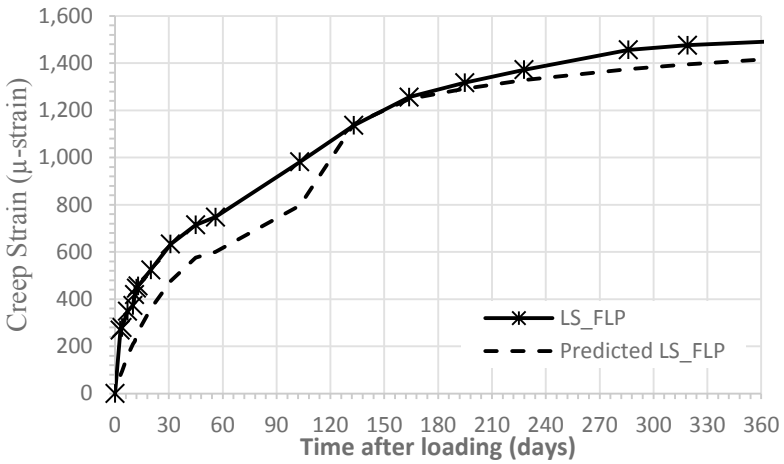

(5) LS222FLP

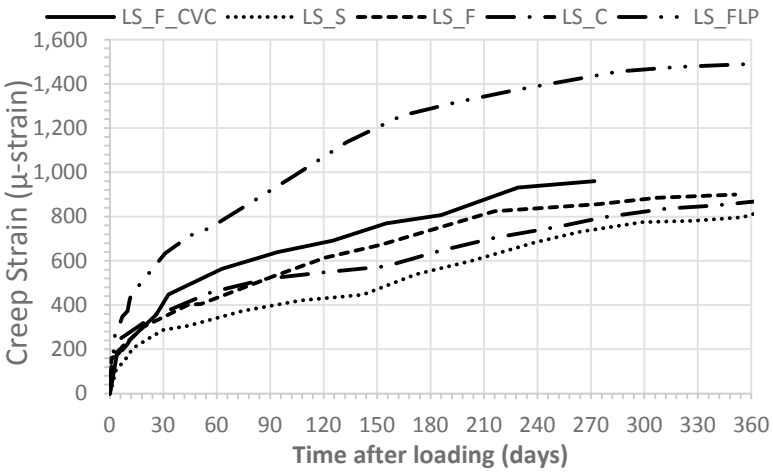

(6) All limestone mixtures

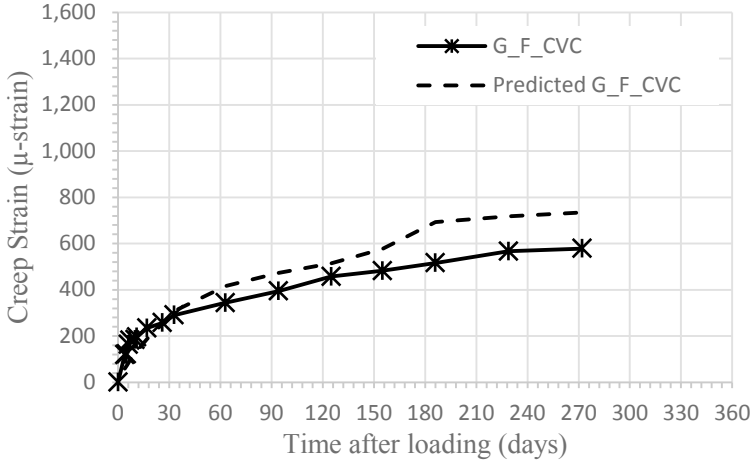

(7) G0.375 CVC

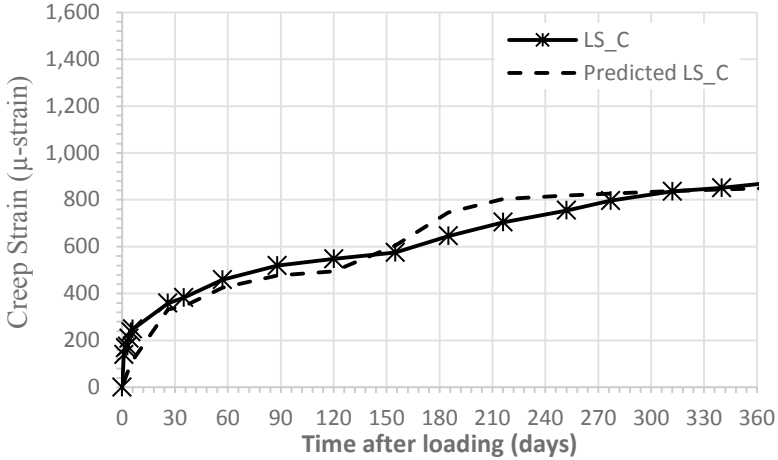

(8) G222C

(Cont.) Figure E-21. Relationship between creep and time after loading of SCC and CVC mixtures

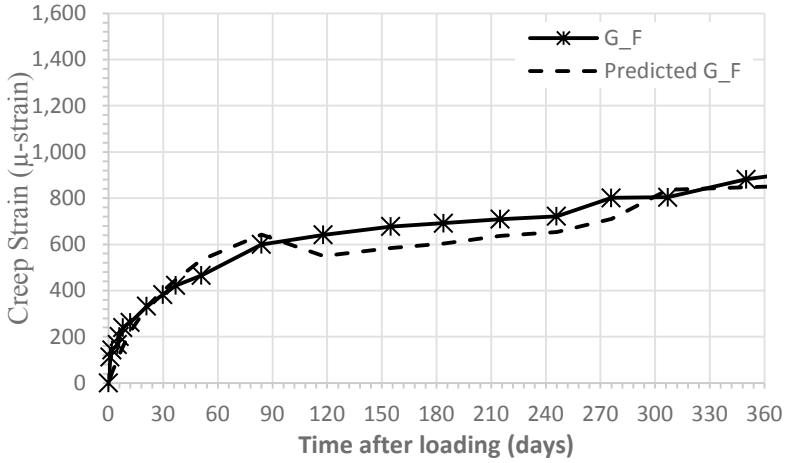

(9) G222F

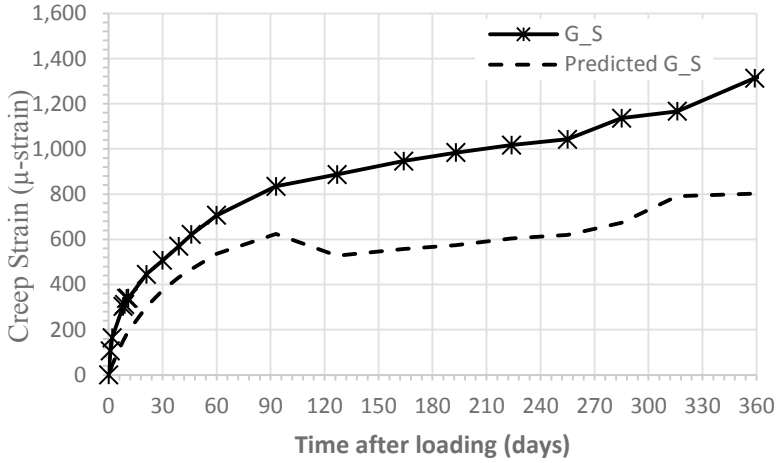

(10) G222S

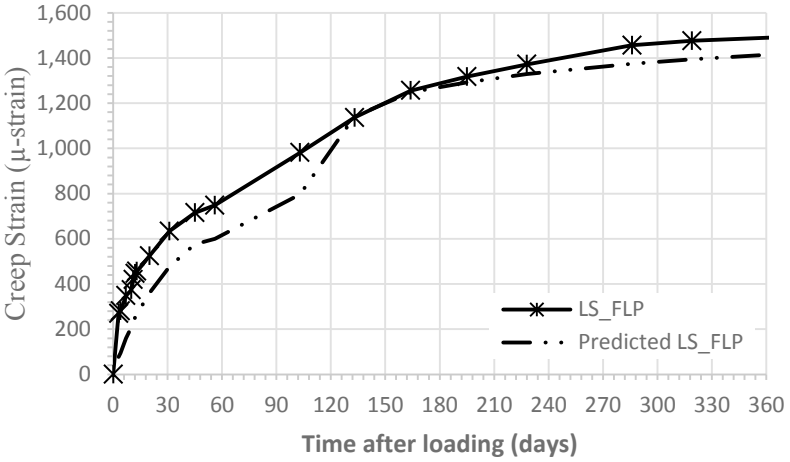

(11) G222FLP

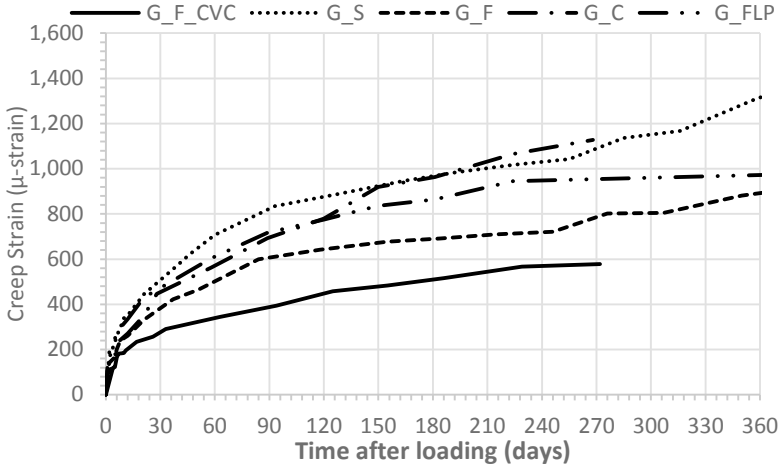

(12) All gravel mixtures

(Cont.) Figure E-21. Relationship between creep and time after loading of SCC and CVC mixtures

10. Air Void System

Table E-19. Rapid air results for limestone mixtures

Mixture Identification		Fresh Concrete Air Content	Hardened Concrete									Compressive Strength for 4 in. cylinders At 56 day, psi		
ID	NMSA (in.)		Air Content (%)			Spacing Factor (mm)			Specific Surface (mm^2/mm^3)					
		%	Top	Bottom	Ave	Top	Bottom	Ave	Top	Bottom	Ave	1	2	Ave.
LS111C	¾	6.2	6.0	5.0	5.5	0.14	0.12	0.13	39.6	36.0	37.8	6,460	6,632	6,546
LS111F	¾	6.0	4.9	5.9	5.4	0.11	0.13	0.12	41.0	44.3	42.7	6,675	6,421	6,548
LS111S	¾	8.0	6.6	7.1	6.8	0.15	0.14	0.15	32.6	36.3	34.5	6,319	6,812	6,566
LS111FLP	¾	5.5	4.2	5.7	5.0	0.15	0.13	0.14	36.0	31.0	33.5	5,716	5,860	5,788
LS211C	¾	5.2	3.0	3.4	3.2	0.14	0.18	0.16	40.6	30.8	35.7	8,902	8,743	8,823
LS211F	¾	3.5	3.0	4.3	3.7	0.15	0.14	0.15	39.2	34.1	36.7	7,241	7,738	7,490
LS211S	¾	6.5	5.9	4.5	5.2	0.10	0.18	0.14	41.1	27.6	34.4	7,950	7,639	7,795
LS211FLP	¾	6.0	5. 6	5.8	5.7	0.12	0.13	0.13	33.7	30.6	32.1	6,100	5,824	5,962
LS121C	½	4.0	3. 1	2. 8	2.9	0.15	0.14	0.15	38.2	43.2	40.7	8,009	8,040	8,025
LS121F	½	5.0	5.0	4.3	4.6	0.15	0.13	0.14	37.2	39.6	38.4	6,434	6,739	6,587
LS121S	½	6.8	5.9	6.5	6.2	0.10	0.12	0.11	44.2	40.4	42.3	6,257	6,375	6,316
LS121FLP	½	5.0	5.4	4.1	4.8	0.11	0.10	0.11	48.7	40.7	44.7	5,594	5,760	5,677
LS221C	½	3.0	3.6	3.1	3.4	0.11	0.14	0.13	47.4	40.3	43.9	8,460	7,931	8,196
LS221F	½	6.5	3.4	3.1	3.3	0.12	0.12	0.12	47.0	46.3	46.6	7,039	7,219	7,129
LS221S	½	7.5	6.3	6.9	6.6	0.12	0.11	0.11	33.6	34.4	34.0	8,013	7,955	7,984
LS221FLP	½	4.5	4.6	3.9	4.2	0.10	0.11	0.10	48.4	48.8	48.6	6,670	6,487	6,579
LS222C	$^3/_8$	5.0	4.1	3.7	3.9	0.13	0.14	0.13	40.2	37.2	38.7	7,747	7,998	7,873
LS222F	$^3/_8$	6.5	5.3	6.5	5.9	0.12	0.09	0.11	36.9	40.6	38.8	6,868	7,168	7,018
LS222S	$^{3/}_8$	7.0	6.8	6.7	6.7	0.14	0.25	0.19	25.5	15.2	20.4	7,403	7,880	7,642
LS222FLP	$^{3/}_8$	6.5	5.2	4.6	4. 9	0.16	0.12	0.14	29.4	38.5	34.0	6,402	6,050	6,226
Min.		3.0	3.0	2. 8	3.0	0.10	0.09	0.10	25.5	15.2	20.4	5,594	5,760	5,677
Max		8.0	6.8	7.0	6.8	0.16	0.25	0.19	48.7	48.8	48.6	8,802	8,743	8,823
Average		5.7	4.9	4.9	4.9	0.13	0.14	0.13	39.0	36.8	37.9	7,013	7,064	7,039
Standard Deviation		1.3	1.2	1.4	1.2	0.02	0.03	0.02	6.3	7.5	6.3	921	888	892

Table E-20. Rapid air results for gravel mixtures

Mixture Identification		Fresh Concrete Air Content %	Hardened Concrete									Compressive Strength for 4x8 in. cylinders at 56 day, psi		
ID	NMSA (in.)		Air Content (%)			Spacing Factor (mm)			Specific Surface (mm^2/mm^3)					
			Top	Bottom	Ave	Top	Bottom	Ave	Top	Bottom	Ave	1	2	Ave.
G111C	¾	8.0	6.6	7.3	6.9	0.11	0.13	0.12	34.1	35.6	34.9	5,616	5,730	5,673
G111F	¾	7.4	6.9	7.2	7.7	0.11	0.11	0.11	33.2	32.0	32.6	5,248	5,178	5,213
G111S	¾	7.8	7.2	7.3	7.3	0.10	0.09	0.09	31.0	35.3	33.1	5,088	5,486	5,287
G111FLP	¾	6.6	7.7	7.0	7.3	0.10	0.10	0.10	30.1	35.0	32.6	4,769	4,890	4,830
G211C	¾	5.7	6.8	5.2	6.0	0.11	0.10	0.11	32.4	38.6	35.5	5,758	5,808	5,783
G211F	¾	5.5	5.0	6.2	5.6	0.13	0.11	0.12	37.0	40.3	38.7	4,571	4,728	4,650
G211S	¾	5.7	6.2	5.6	5.9	0.12	0.10	0.11	37.6	35.9	36.8	5,362	5,248	5,305
G211FLP	¾	4.6	5.3	4.9	5.1	0.06	0.06	0.06	45.6	40.9	43.2	5,800	5,760	5,780
G121C	½	5.6	5.9	7.6	6.8	0.06	0.08	0.07	42.6	37.2	39.9	4,544	4,758	4,651
G121F	½	6.0	5.9	7.0	6.4	0.10	0.11	0.10	38.9	39.8	39.3	4,354	4,388	4,371
G121S	½	6.5	8.3	8.1	8.2	0.09	0.07	0.08	36.5	35.9	36.2	5,043	4,768	4,906
G121FLP	½	5.6	6.6	5.3	5.9	0.13	0.13	0.13	32.1	33.7	32.9	4,851	4,832	4,842
G221C	½	6.0	6.4	7.0	6.7	0.09	0.10	0.09	41.3	42.7	42.0	6,888	6,667	6,778
G221F	½	6.0	5.2	6.0	5.6	0.17	0.17	0.17	28.9	28.0	28.4	7,072	6,700	6,886
G221S	½	7.8	8.2	7.8	8.0	0.08	0.08	0.08	40.3	43.0	41.6	7,772	7,475	7,624
G221FLP	½	7.6	7.0	6.3	6.6	0.13	0.12	0.12	33.2	36.8	35.0	5,749	5,874	5,812
G222C	3/8	6.6	6.6	6.9	6.8	0.11	0.10	0.11	36.4	34.2	35.3	6,246	6,319	6,283
G222S	3/8	5.4	5.9	4.2	5.1	0.15	0.15	0.15	33.3	32.7	33.0	5,534	5,862	5,698
G222F	3/8	6.0	5.2	7.0	6.1	0.11	0.11	0.11	36.5	33.2	34.8	5,690	5,430	5,560
G222FLP	3/8	6.2	7.2	6.3	6.7	0.13	0.12	0.12	36.0	39. 6	37.8	4,539	4,752	4,646
Min.		4.6	5.0	4.2	5.1	0.06	0.06	0.06	28.9	28.0	28.4	4,354	4,388	4,371
Max		8.0	8.3	8.1	8.2	0.17	0.17	0.17	45.6	43.0	43.2	7,772	7,475	7,624
Average		6.3	6.5	6.5	6.5	0.11	0.11	0.11	35.8	36.5	36.2	5,525	5,533	5,529
Standard Deviation		0.9	1.0	1.0	0.9	0.03	0.03	0.03	4.3	3.8	3.78	912	805	853

11. Surface Resistivity

Table E-21. Surface resistivity results for limestone mixtures

Mixture Identification		Surface Resistance (kΩcm)				
ID	NMSA (in.)	1 day	3 day	7 day	28 day	56 day
LS0.75 CVC	¾	4.70	7.00	8.10	15.60	23.80
LS111C	¾	2.50	5.00	6.20	12.50	21.10
LS111F	¾	4.50	7.60	11.20	16.80	28.30
LS111S	¾	6.00	10.70	14.80	23.20	27.80
LS111FLP	¾	3.50	5.50	6.40	13.30	20.70
LS211C	¾	4.20	6.90	8.65	15.20	23.40
LS211F	¾	5.40	8.05	8.60	17.90	29.10
LS211S	¾	4.60	10.00	15.30	26.10	32.50
LS211FLP	¾	3.20	5.80	7.10	15.30	25.60
LS0.5 CVC	½	4.40	7.00	7.80	14.70	22.40
LS121C	½	3.85	5.20	6.30	11.50	17.80
LS121F	½	4.30	8.50	12.50	16.05	26.00
LS121S	½	4.90	8.80	12.90	23.40	24.80
LS121FLP	½	3.60	5.80	7.50	14.90	20.00
LS221C	½	3.50	5.75	7.40	13.20	19.80
LS221F	½	4.90	6.60	7.90	16.80	26.10
LS221S	½	5.70	10.50	16.20	27.10	32.80
LS221FLP	½	3.20	5.80	7.40	14.70	18.20
LS0.375 CVC	3/8	3.60	5.40	6.70	13.80	24.70
LS222C	3/8	4.20	5.30	7.10	14.40	20.25
LS222F	3/8	4.50	6.40	7.90	16.50	24.85
LS222S	3/8	3.10	8.90	15.50	24.00	25.90
LS222FLP	3/8	3.80	5.80	6.40	13.00	19.05

Table E-22. Surface resistivity results for gravel mixtures.

Mixture Identification		Surface Resistance (kΩcm)				
ID	NMSA (in.)	1 day	3 day	7 day	28 day	56 day
G0.75 CVC	¾	5.40	7.60	8.30	15.00	23.10
G111C	¾	6.00	7.10	7.80	9.90	15.10
G111F	¾	5.80	8.00	8.90	14.00	24.10
G111S	¾	6.00	10.50	14.80	22.90	25.20
G111FLP	¾	5.10	8.80	9.90	18.60	28.10
G211C	¾	4.30	7.50	8.50	12.40	15.30
G211F	¾	5.40	9.00	10.20	18.20	27.90
G211S	¾	6.50	13.00	15.30	25.40	24.00
G211FLP	¾	4.60	7.40	8.70	17.80	27.90
G0.50 CVC	½	4.70	7.10	7.80	12.50	19.90
G121C	½	3.80	6.30	6.50	8.80	16.10
G121F	½	5.90	7.50	8.30	12.80	24.50
G121S	½	6.80	9.50	13.50	20.40	24.40
G121FLP	½	4.60	7.00	7.80	14.40	26.60
G221C	½	2.80	3.90	5.80	8.00	13.40
G221F	½	4.20	6.30	6.80	11.50	21.60
G221S	½	5.40	10.00	12.50	19.20	28.30
G221FLP	½	4.10	6.00	7.10	14.50	24.20
G0.375 CVC	3/8	5.20	7.20	7.80	15.10	21.50
G222C	3/8	2.40	5.30	6.20	12.10	17.90
G222S	3/8	4.20	7.00	10.30	20.20	24.80
G222F	3/8	4.10	6.70	7.80	19.80	31.70
G222FLP	3/8	3.60	5.60	6.90	16.40	25.20

APPENDIX F: Full-Scale Bridge Components

Contents

A. Bridge Pier Specimen

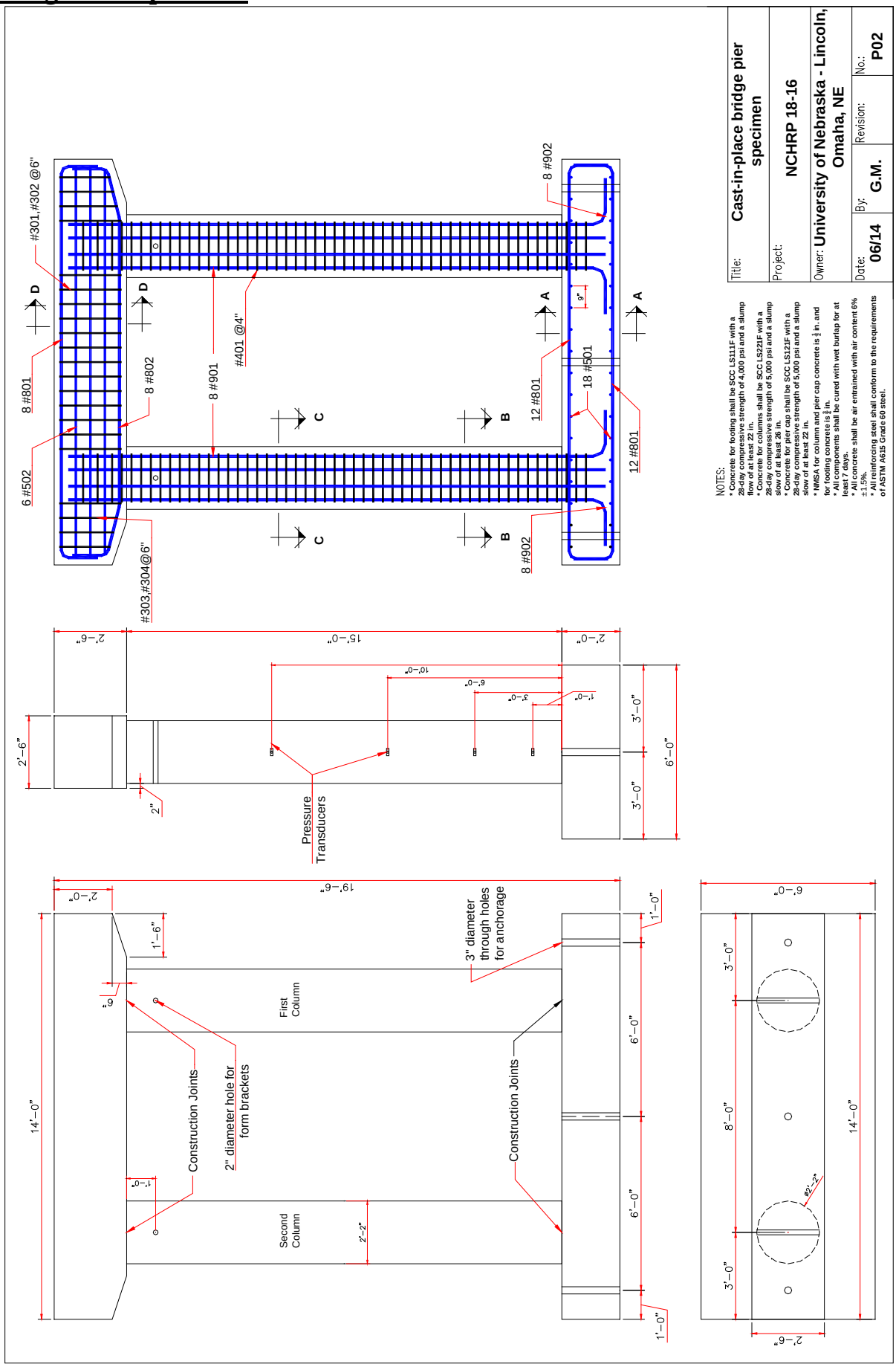

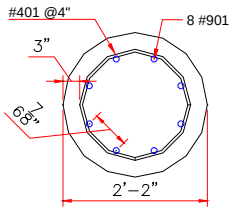

Section C-C

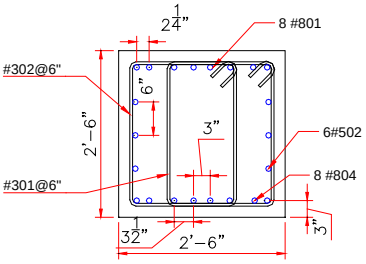

Section D-D

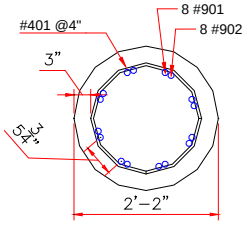

Section B-B

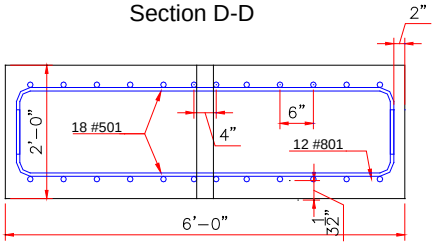

Section A-A

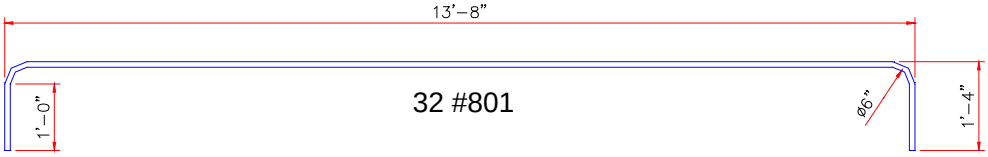

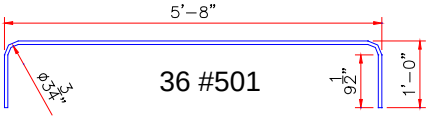

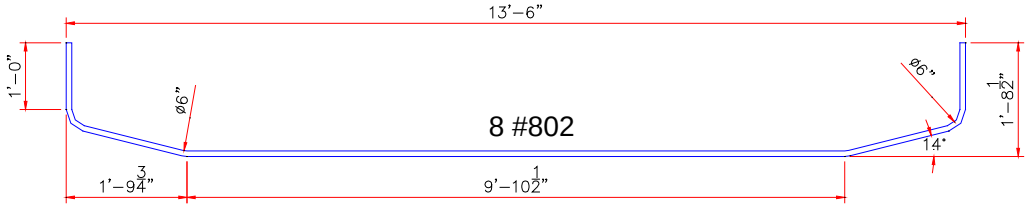

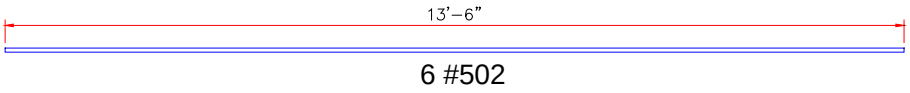

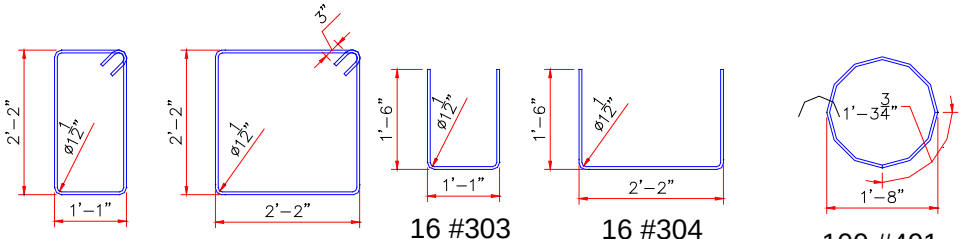

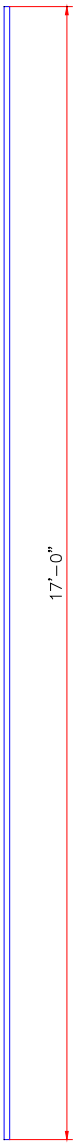

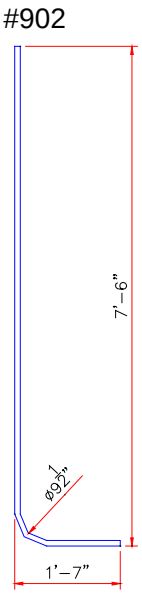

1. Fabrication (Forming, Reinforcing and SCC Placement)

(a)

(b)

Figure F-1. Forming and reinforcing of the footing

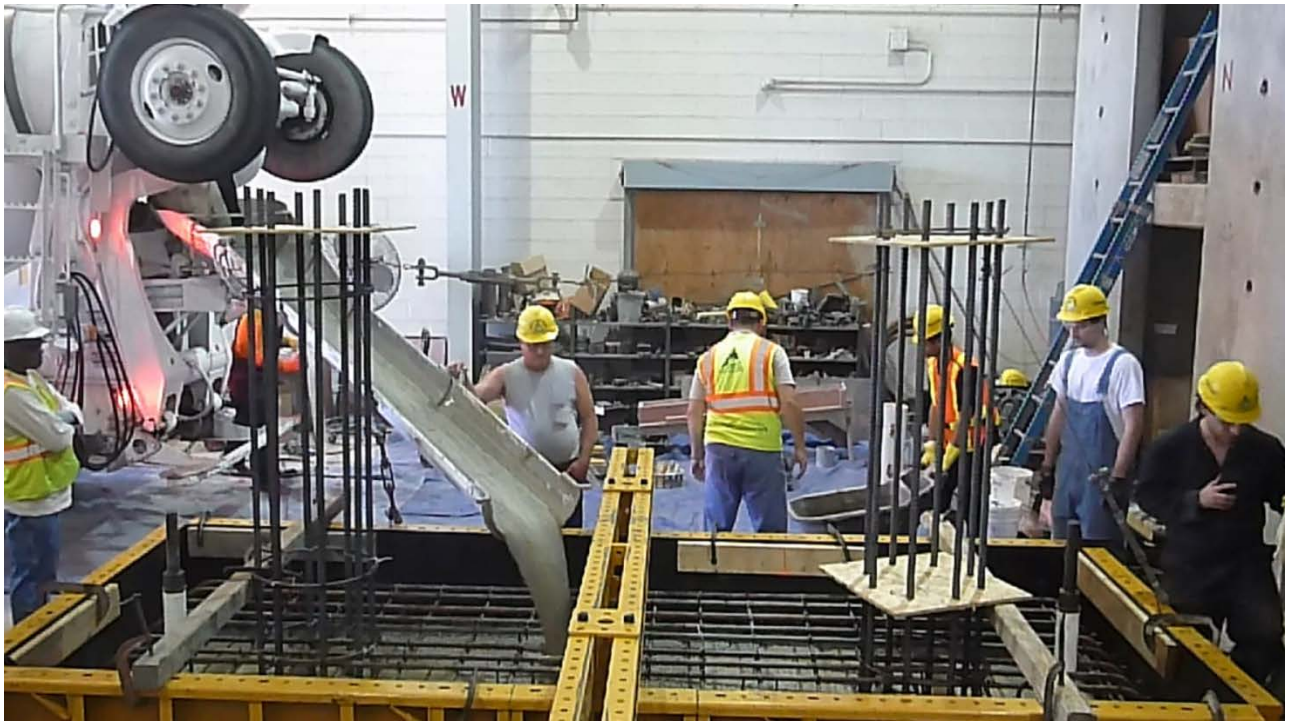

Figure F-2. Placing footing SCC using truck chute

Figure F-3. Reinforcement of the pier column

Figure F-4. Splicing footing and column reinforcement

Figure F-5. Longitudinal and transverse reinforcement of the pier column

Figure F-5. Pressure transducers (Kulite IPT-750) installed to the pier column form

Figure F-6. The funnel and tremie pipe used in placing column concrete

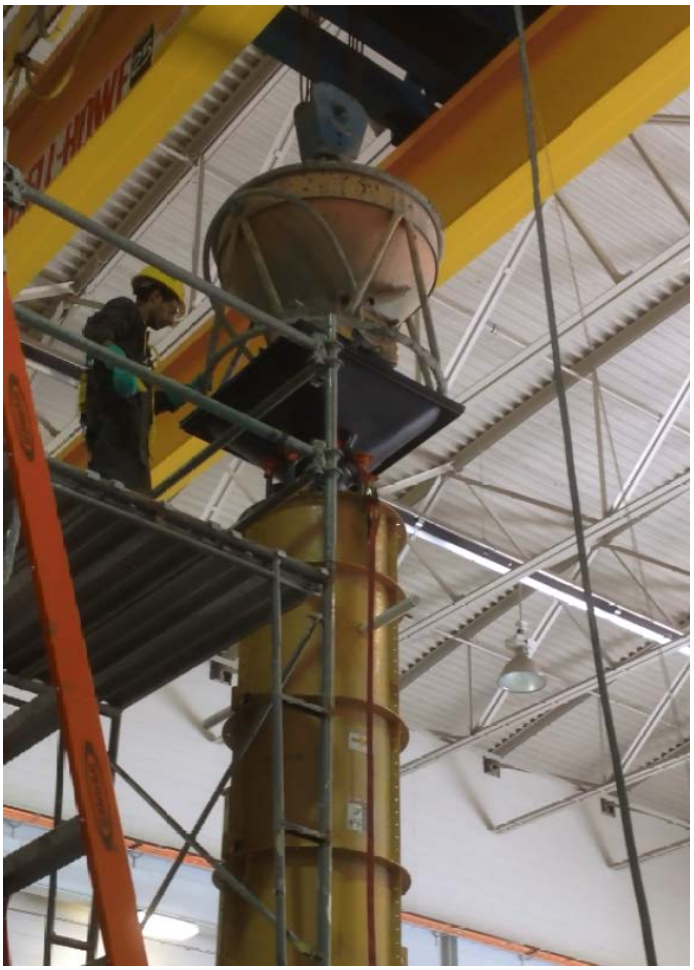

Figure F-7. Placing SCC using bucket and tremie pipe

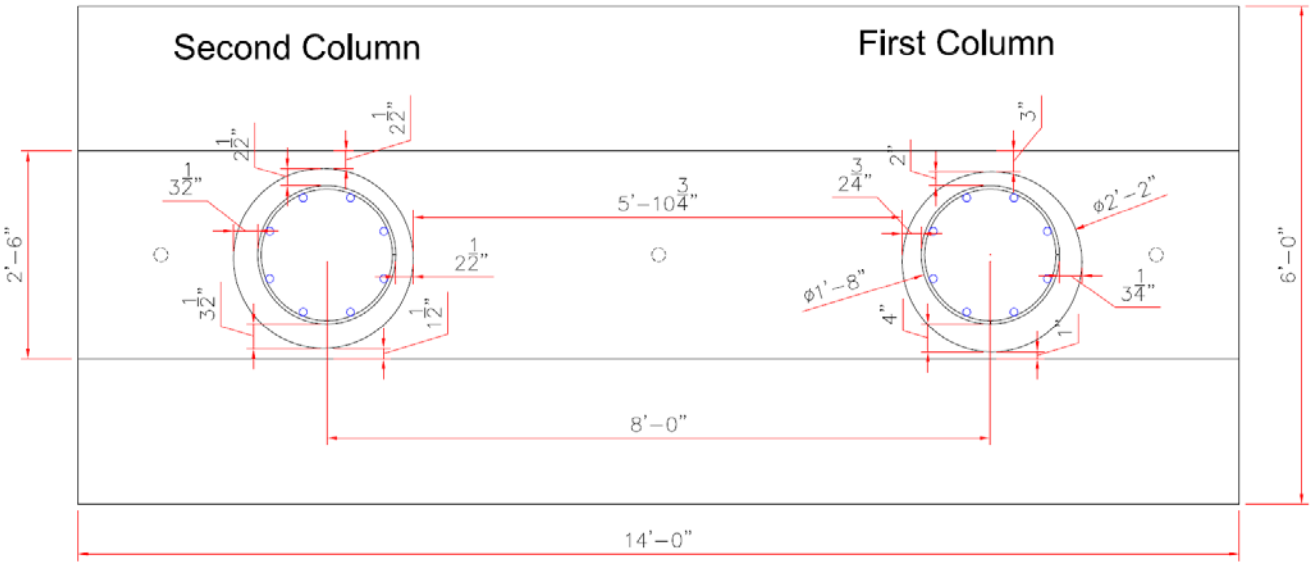

Figure F-8. As-built dimensions of both columns

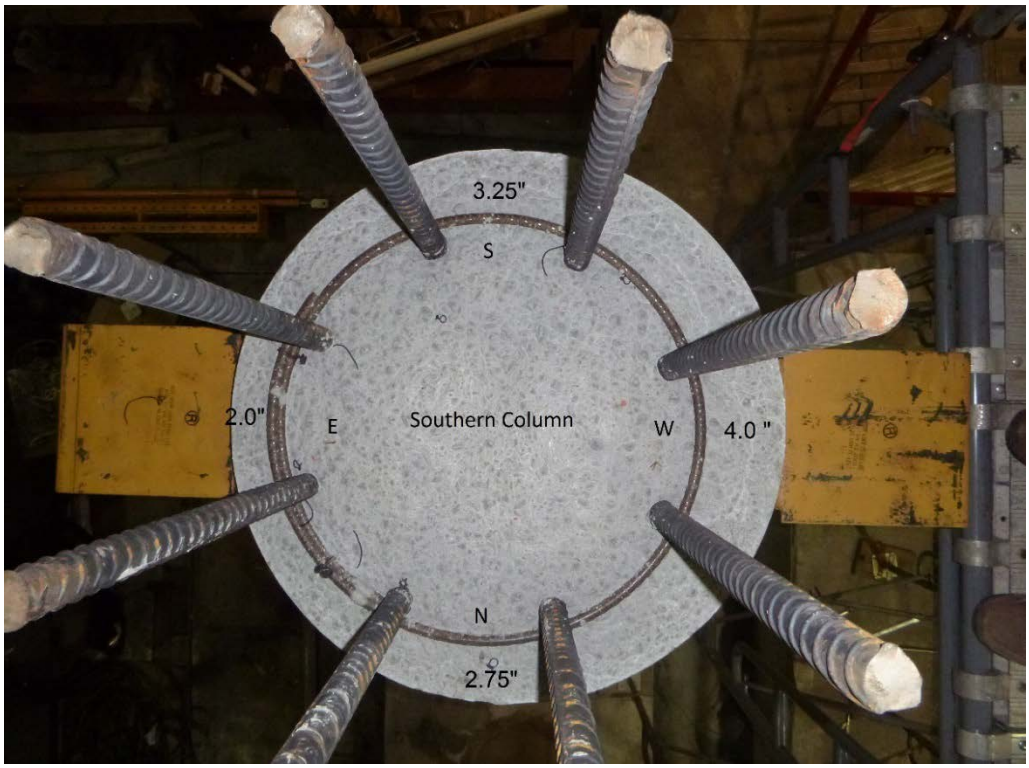

Figure F-9. As-built dimensions of the first column

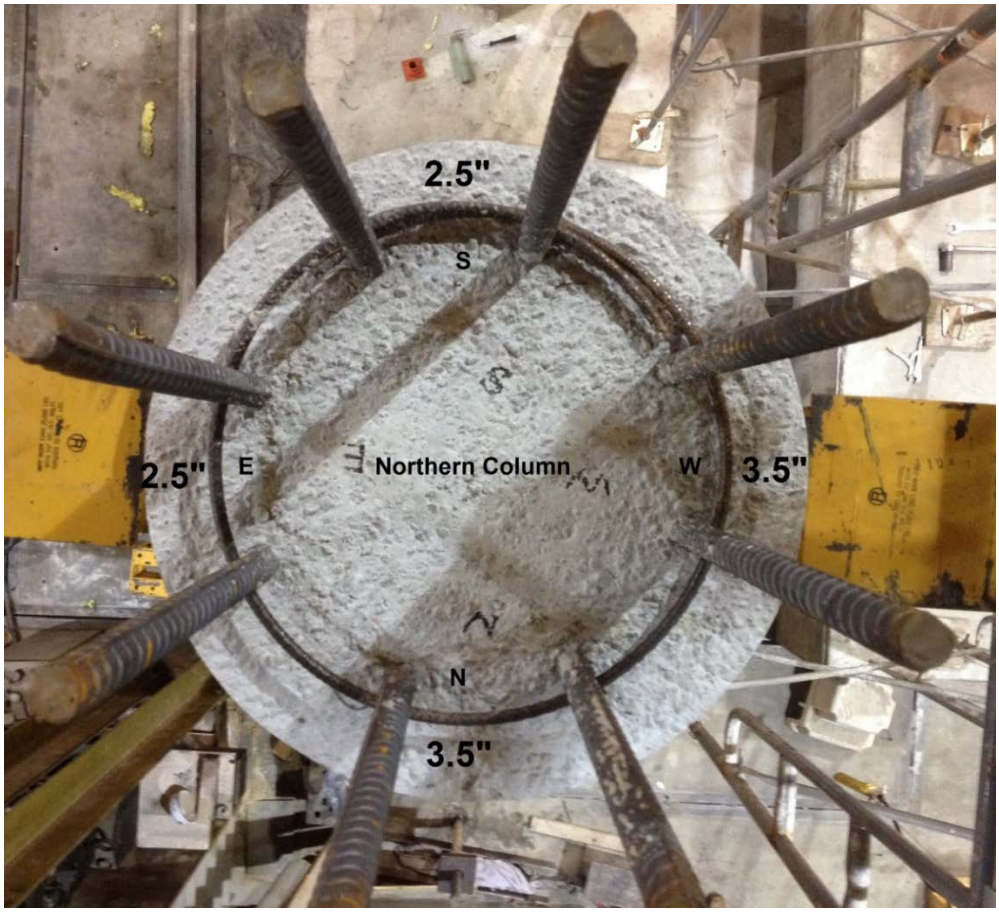

Figure F-10. As-built dimensions of the second column


Figure F-11. Brackets used to support pier cap form

Figure F-12. Oiling the pier cap form

Figure F-13. Reinforcement of the pier cap

Figure F-14. Placing pier cap SCC using a bucket

2. Formed Surface Quality

(a)

(b)

Figure F-15. Formed surface of the footing

Figure F-16. Formed surface of pier first column

Figure F-17. Formed surface of pier second column

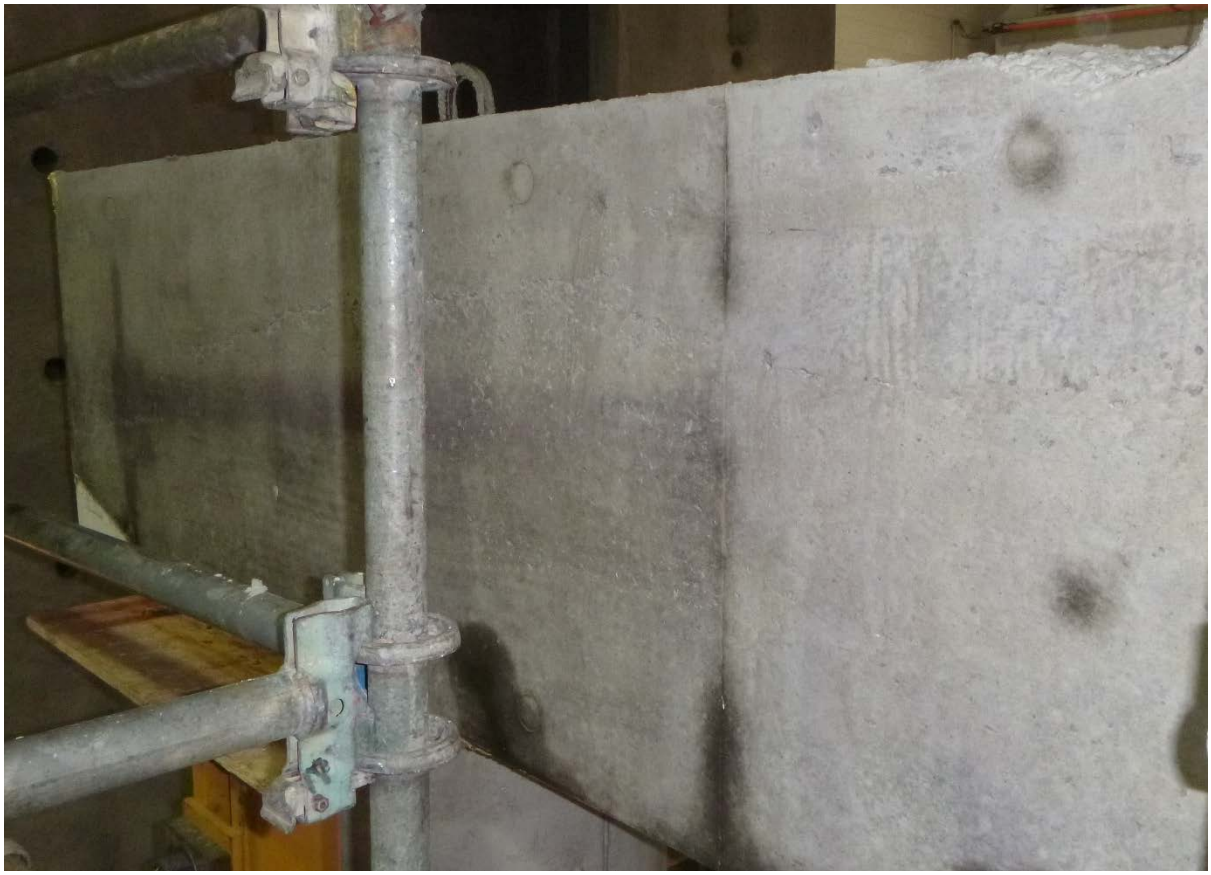

Figure F-18. Formed surface of the pier cap

Figure F-19. Side view of the pier cap showing the pour line

Table F-1. Measurements of formed surface air voids and their ratio for the pier specimen

Component	Void Size (in.)		Area of Each Void (in^2)	No. of Voids	Total Area of Surface Void (in^2)	Sum of Surface Void Area (in^2)	D_{max}	% of D_{max}	Surface Void Ratio (%)	Surface Void Ratio Class
	w	l								
Footing (Short Side)	1/8	1/8	0.02	5	0.08	0.91	3/8	27.6%	0.16%	SVR3
	1/8	1/4	0.03	2	0.06					
	1/8	3/8	0.05	1	0.05					
	1/4	1/4	0.06	3	0.19					
	1/4	1/2	0.13	2	0.25					
	3/8	3/8	0.14	2	0.28					
Footing (Long Side)	1/8	1/8	0.02	22	0.34	1.78	3/8	14.0%	0.31%	SVR3
	1/8	1/4	0.03	7	0.22					
	1/4	1/4	0.06	14	0.88					
	1/4	3/8	0.09	1	0.09					
	1/4	1/2	0.13	2	0.25					
First Coulmn (1.5 ft from the Footing)	1/4	1/2	0.13	1	0.13	0.80	3/8	35.3%	0.14%	SVR3
	1/4	5/8	0.16	1	0.16					
	3/8	5/8	0.23	1	0.23					
	3/8	3/4	0.28	1	0.28					
First Coulmn (11.33 ft from the Footing)	1/8	1/8	0.02	30	0.47	1.44	3/8	8.7%	0.25%	SVR3
	1/8	1/4	0.03	14	0.44					
	1/4	1/4	0.06	2	0.13					
	1/4	3/8	0.09	3	0.28					
	1/4	1/2	0.13	1	0.13					
Second Column (8.5 ft from the Footing)	1/8	1/8	0.02	5	0.08	1.08	5/8	78.3%	0.19%	SVR2
	1/4	1/4	0.06	1	0.06					
	1/4	3/8	0.09	1	0.09					
	3/8	3/4	0.28	3	0.84					
Second Column (10 ft from the Footing)	1/8	1/8	0.02	10	0.16	1.78	5/8	14.0%	0.31%	SVR2
	1/8	1/4	0.03	1	0.03					
	1/4	3/8	0.09	2	0.19					
	1/4	1	0.25	1	0.25					
	3/8	3/8	0.14	2	0.28					
	3/8	1/2	0.19	1	0.19					
	1/2	5/8	0.31	1	0.31					
	1/2	3/4	0.38	1	0.38					
Pier Cap (at the Pour Line)	1/8	1/8	0.02	8	0.13	3.89	5/8	12.0%	0.68%	SVR2
	1/8	1/4	0.03	16	0.50					
	1/8	3/8	0.05	1	0.05					
	1/8	1/2	0.06	4	0.25					
	1/8	5/8	0.08	8	0.63					
	1/4	1/4	0.06	8	0.50					
	1/4	3/8	0.09	5	0.47					
	1/4	1/2	0.13	6	0.75					
	1/4	5/8	0.16	1	0.16					
	1/4	3/4	0.19	1	0.19					
	3/8	3/4	0.28	1	0.28					
Pier Cap (away from the Pour Line)	1/8	1/8	0.02	24	0.38	3.09	5/8	8.1%	0.54%	SVR2
	1/8	1/4	0.03	10	0.31					
	1/8	1/2	0.06	5	0.31					
	1/4	1/4	0.06	8	0.50					
	1/4	3/8	0.09	5	0.47					
	1/4	1/2	0.13	1	0.13					
	1/4	3/4	0.19	3	0.56					
	1/4	1	0.25	1	0.25					
	3/8	1/2	0.19	1	0.19					

3. Pier Cap Structural Testing

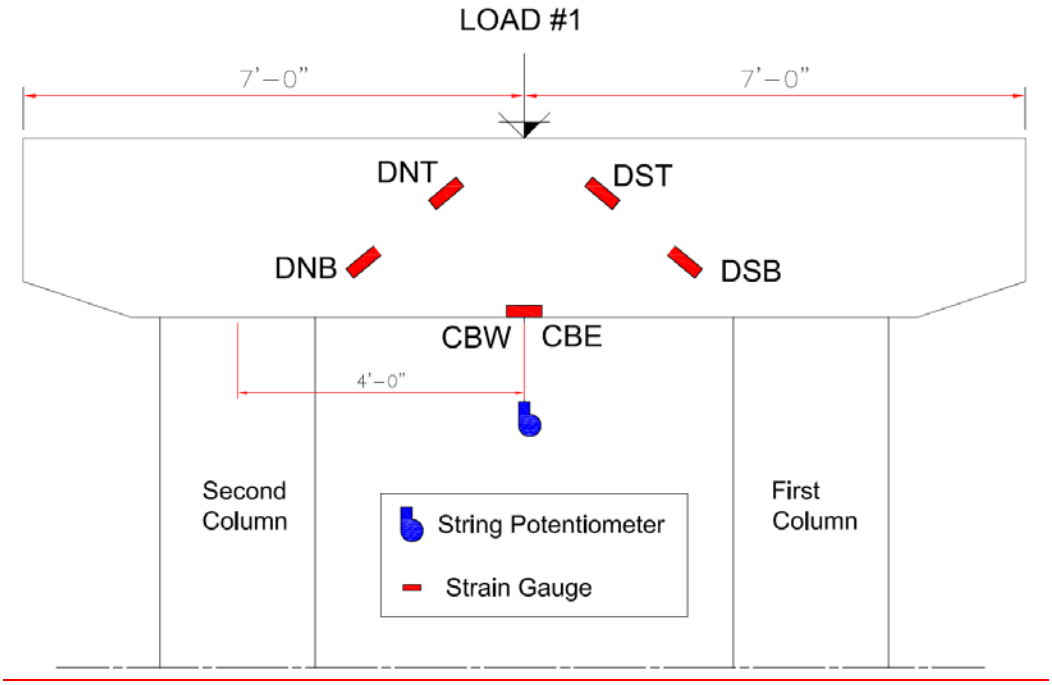

Figure F-20. Test setup of first test of the bridge pier

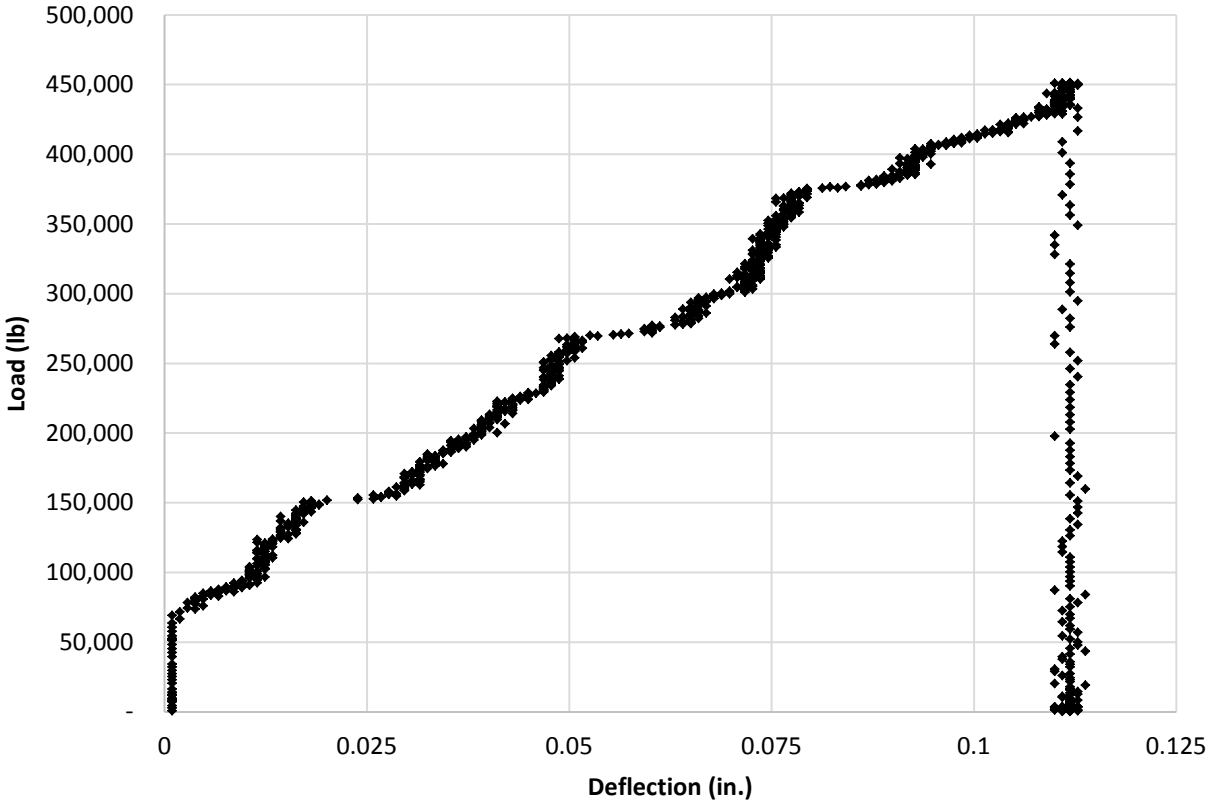

Figure F-21. Load-deflection plot of pier cap testing

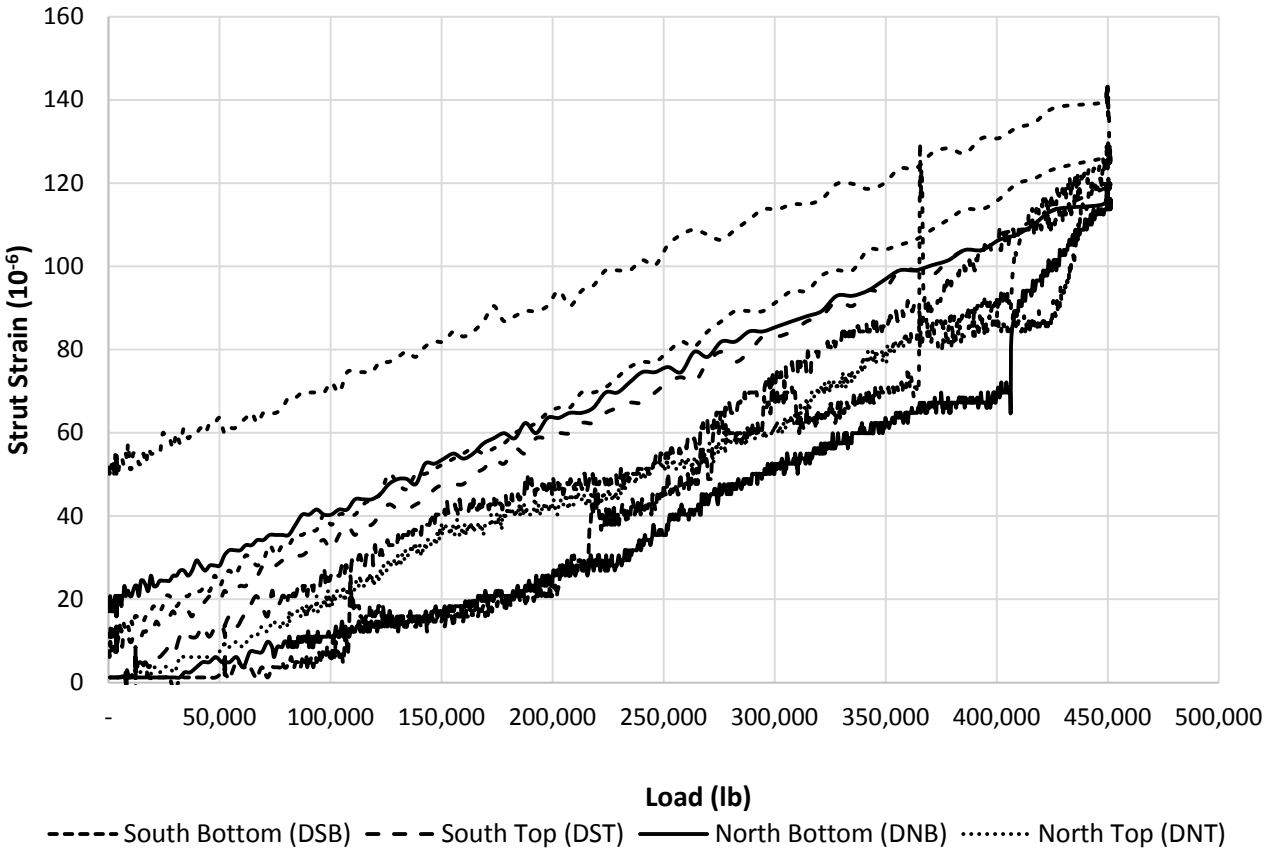

Figure F-22. Load-strain relationships for the pier cap struts

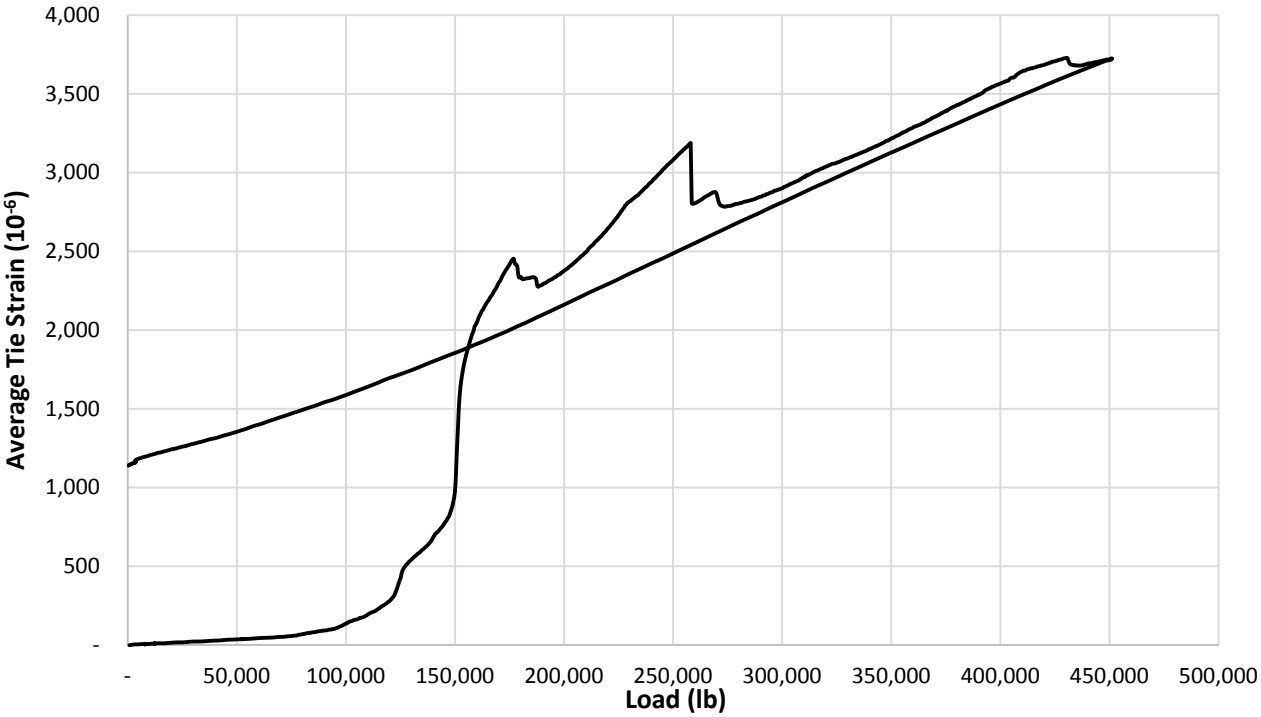

Figure F-23. Load-strain relationship for pier cap tie

Figure F-24. Pier cap instrumentation and condition after testing

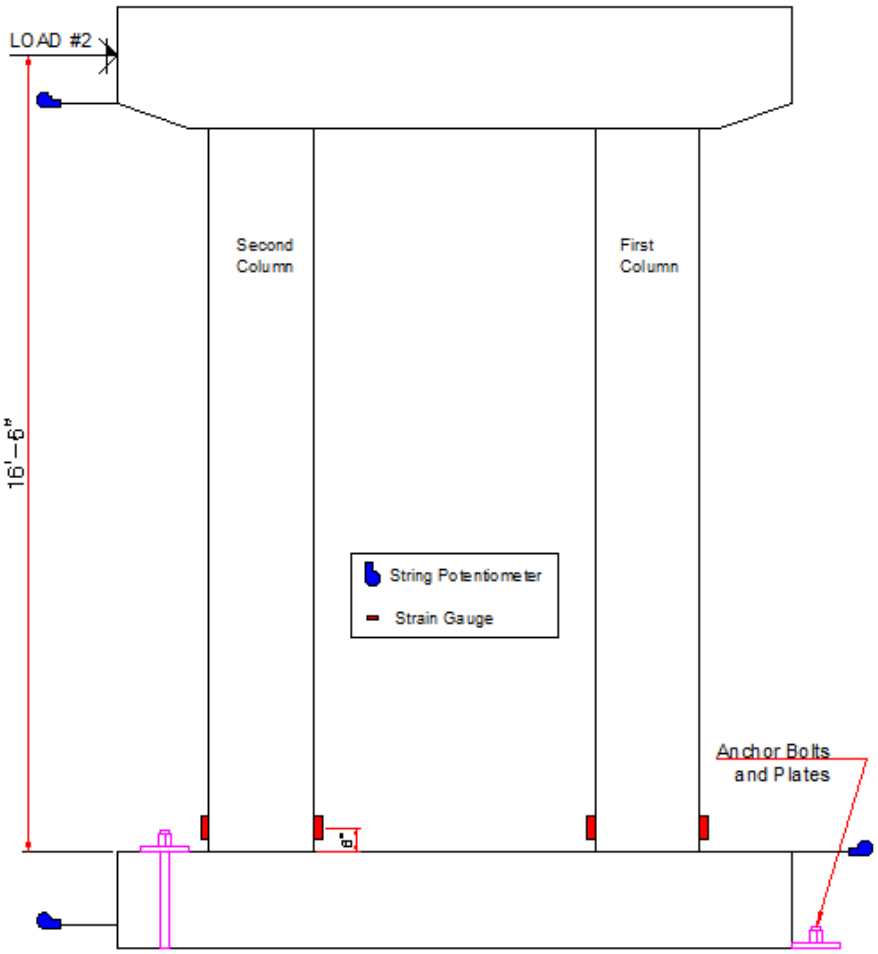

Figure F-25. Test setup of the second test of the bridge pier

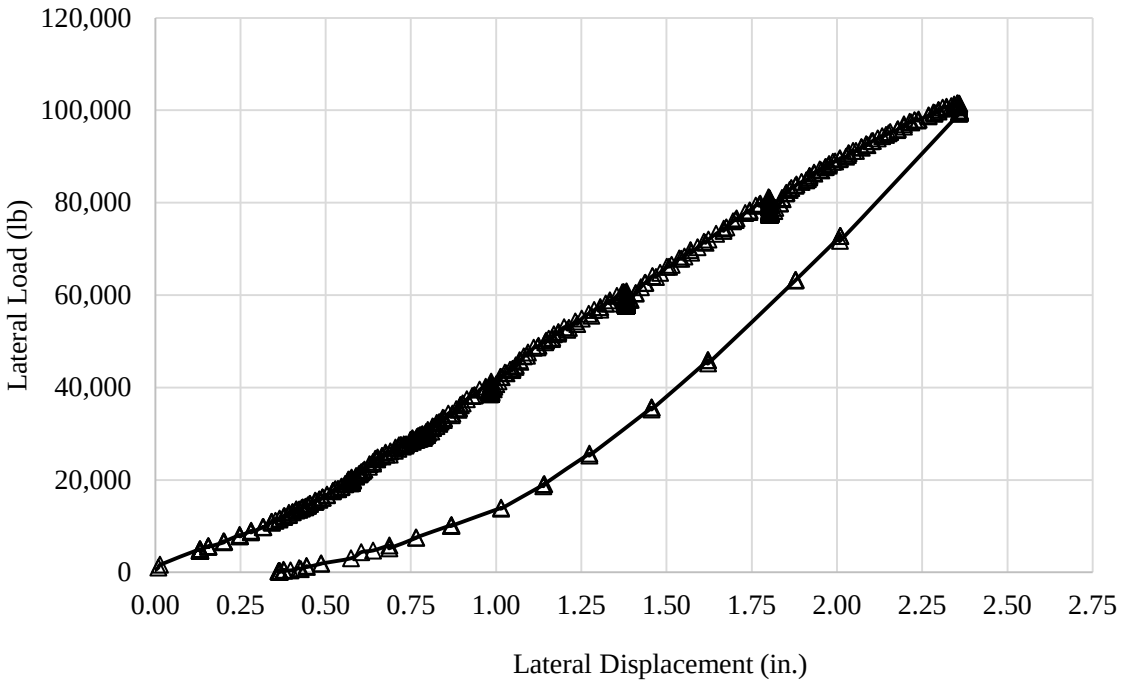

Figure F-26. Load-deflection plot of column testing

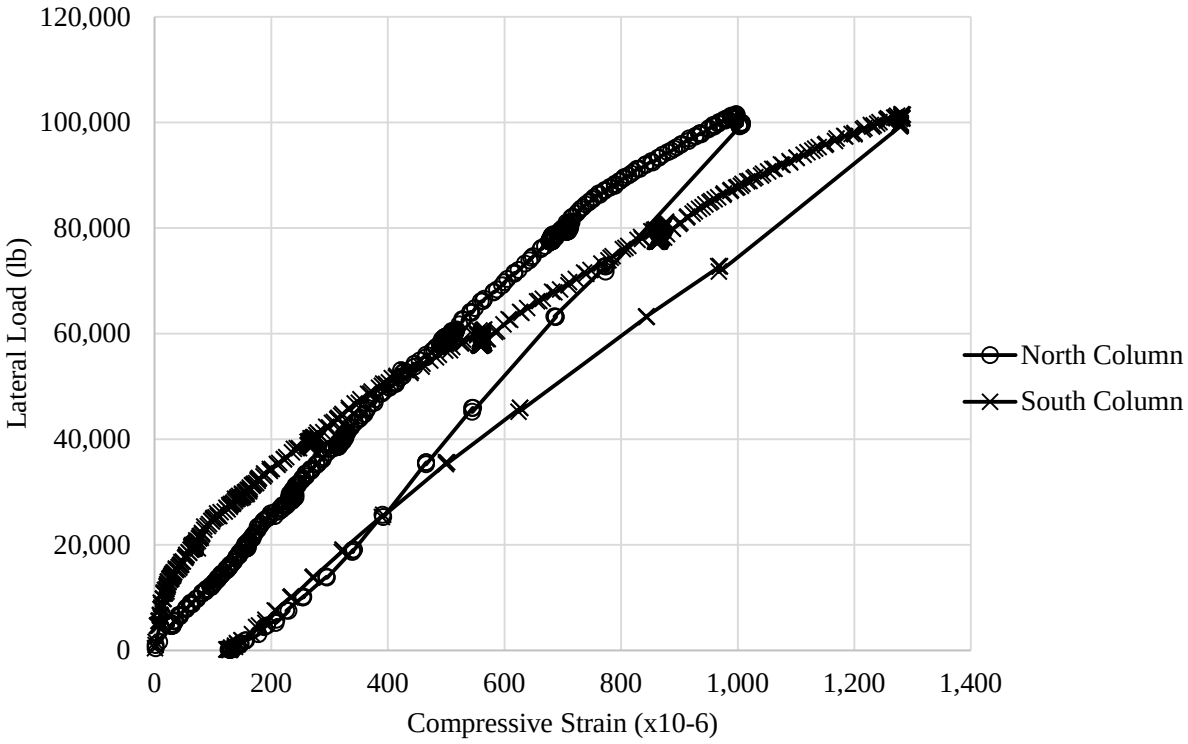

Figure F-27. Load-strain relationships for south and north columns

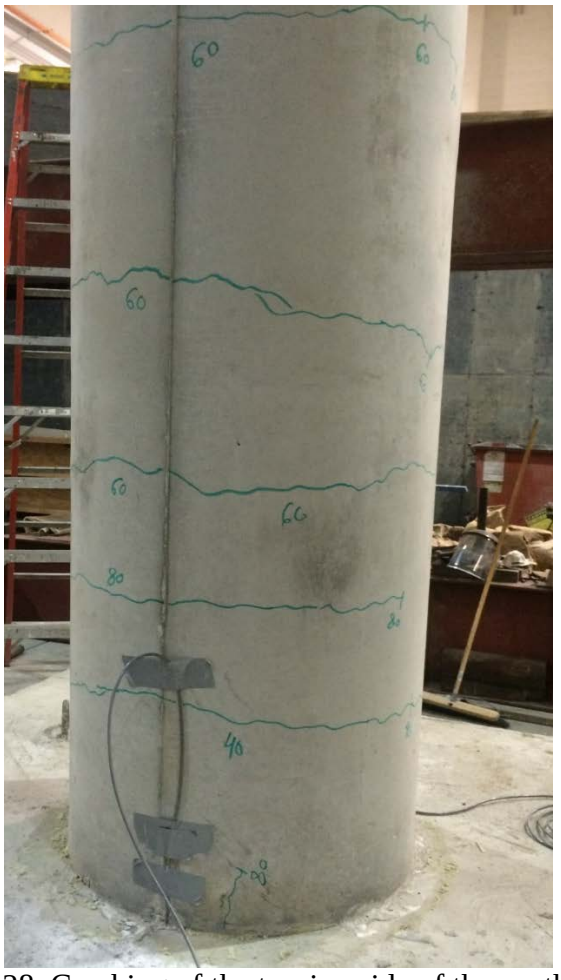

Figure F-28. Cracking of the tension side of the south column

Figure F-29. Cracking of the tension side of both columns

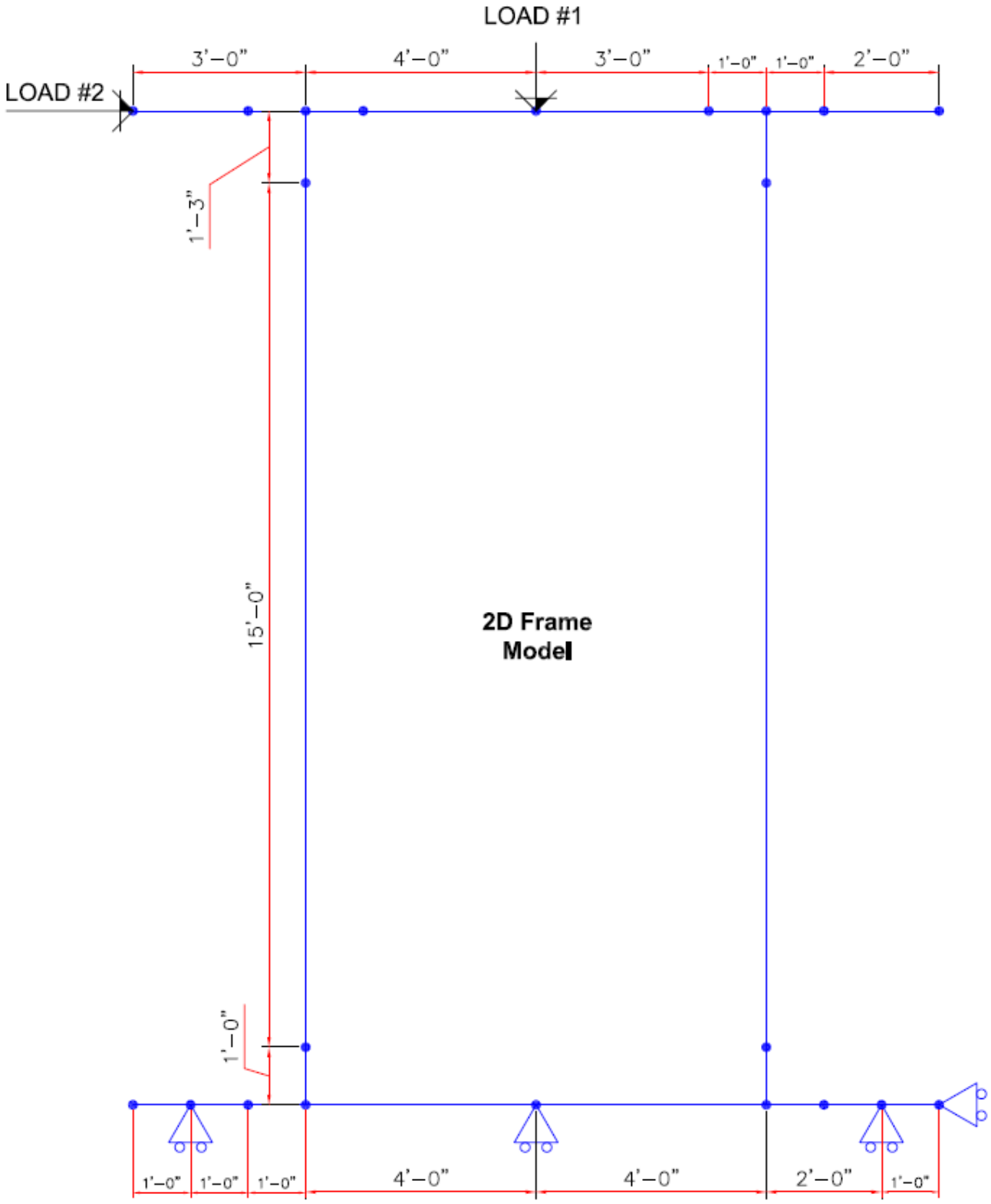

Figure F-30. 2D Frame model for the bridge pier

5. Fresh and Hardened Properties

Table F-2. Fresh properties of SCC mixtures used in bridge pier specimen

Property		**Footing**	**South Column**	**North Column**	**Pier Cap**
Air Content		2.5%	4.0%	4.0%	4.0%
Slump Flow		22.0 in.	27.0 in.	24.75 in.	22.0 in.
Visual Stability Index		0	1	0	0
J-Ring ΔD		4 in.	3 in.	3 in.	1.5 in.
Penetration		1/8 in.	3/8 in.	1/8 in.	1/8 in.
Filling Capacity		60%	85%	89%	78%
Static Segregation		7.1%	2.7%	2.5%	0.5%
Dynamic Segregation		16.2%	9.5%	8.9%	21.7%
Rheological Properties(ICAR Rheometer)	Static Yield Stress (pa)	364.8	256.4	N/A	899.7
	Dynamic Yield Stress (pa)	239	148.7	N/A	540.7
	Plastic Viscosity (pa.s)	5.1	5.1	N/A	2.6

Table F-3. Hardened properties of SCC mixtures used in bridge pier specimen

Component	**Casting Date**	**NMSA**	**Compressive Strength f_c (ksi)**				**MOR (ksi)**	**Splitting Strength (ksi)**	**MOE (ksi)**
			7 days	**14 days**	**28 days**	**56 days**			
Footing	3-Jul-14	¾ in.	7.3	8.0	8.7	9.5	1.05	0.57	4,694
Column	25-Jul-14	½ in.	5.4	6.2	7.3	8.5	0.92	0.45	5,309
Pier Cap	22-Aug-14	½ in.	5.7	6.7	7.5	8.7	1.02	0.43	4,504

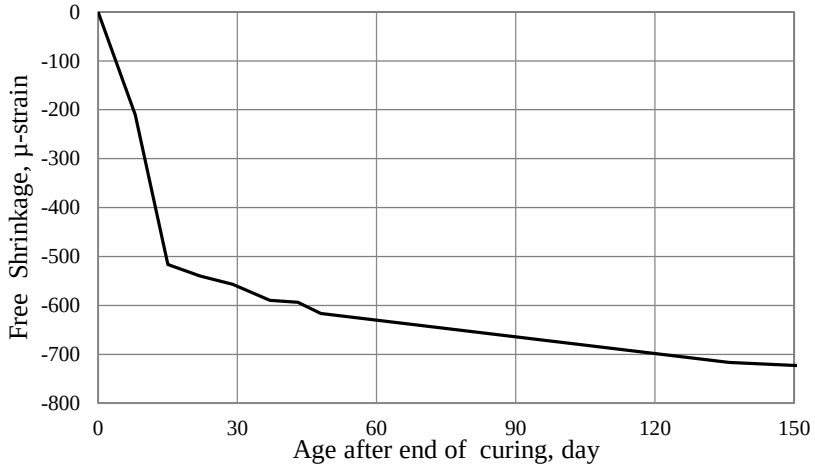

Figure F-31. Relation between free shrinkage and age of footing mixture after 7 day curing

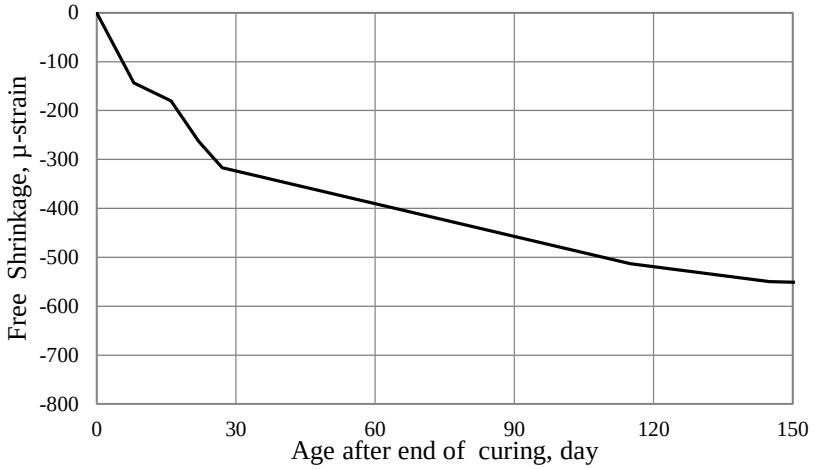

Figure F-32. Relation between free shrinkage and age of footing mixture after 28 day curing

Figure F-33. Relation between free shrinkage and age of column mixture after 7 day curing

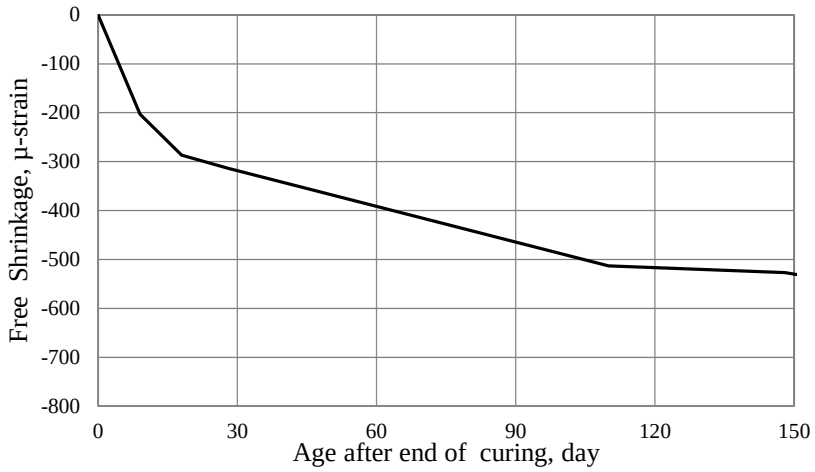

Figure F-34. Relation between free shrinkage and age of column mixture after 28 day curing

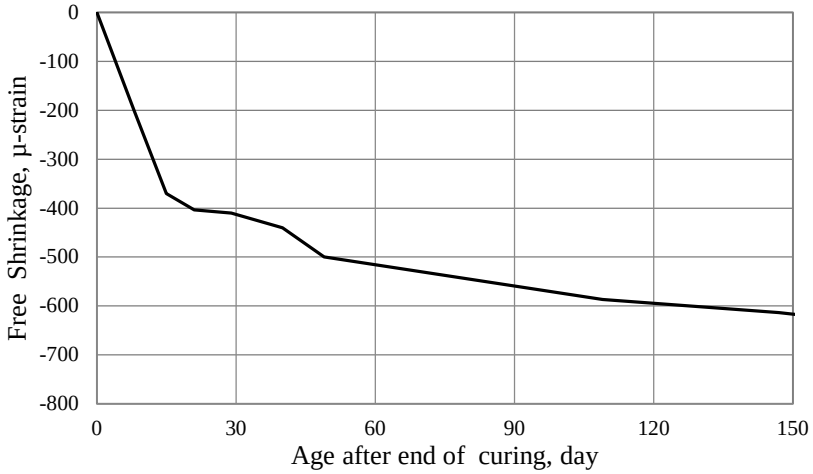

Figure F-35. Relation between free shrinkage and age of pier cap mixture after 7 day curing

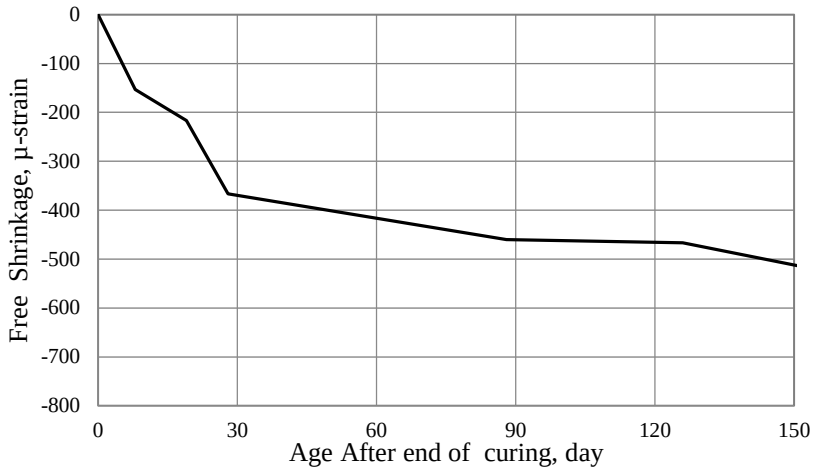

Figure F-36. Relation between free shrinkage and age of pier cap mixture after 28 day curing

B. Box Girder Specimen

1. Fabrication (Forming, Reinforcing and SCC Placement)

Figure F-37. Form used for fabricating the tub section

Figure F-38. Bearing plate and bottom layer of reinforcement in the bottom flange

Figure F-39. Two layers of web reinforcement of the box girder specimen

Figure F-40. Corrugated metal duct placed in the web of the box girder specimen

Figure F-41. Installing post-tensioning ducts in the bottom flange and placing foam block-outs

Figure F-42. Reinforcement of post-tensioning anchorage zone

Figure F-43. Forming the post-tensioning anchorage zone

Figure F-44. Reinforcement of the end diaphragm

Figure F-45. Securing the form sides and foam block-outs

Figure F-46. Slump flow measurements of the pumped SCC

Figure F-47. Pumping SCC at one location using 2 in. diameter hose

Figure F-48. Flow of SCC inside the box-girder form

Figure F-49. The complete end of the box girder specimen after the first batch

Figure F-50. Incomplete end of the box girder specimen after the first batch

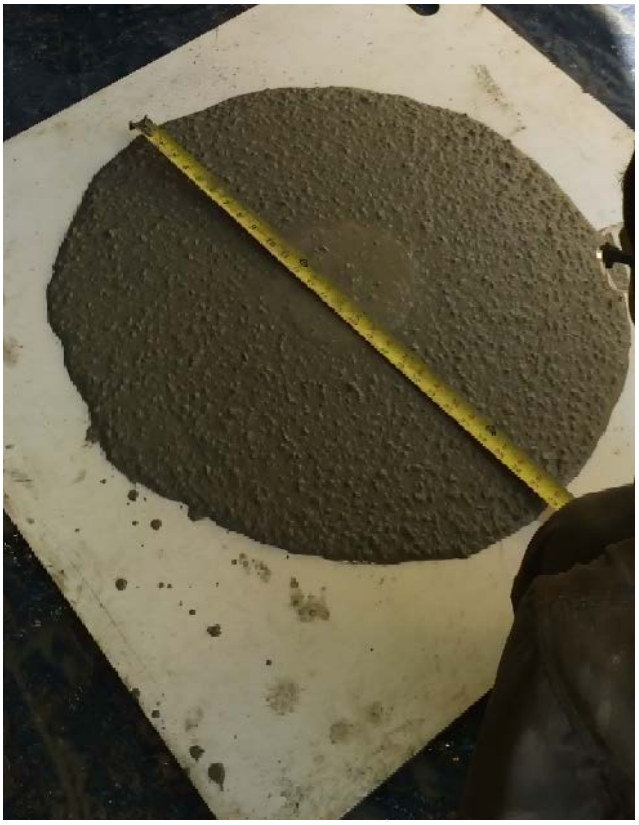

Figure F-51. Slump flow of the SCC used in the second batch for the box girder specimen

Figure F-52. Placing SCC for the top flange and incomplete tub section by pumping

Figure F-53. Finishing the top surface of the box girder specimen

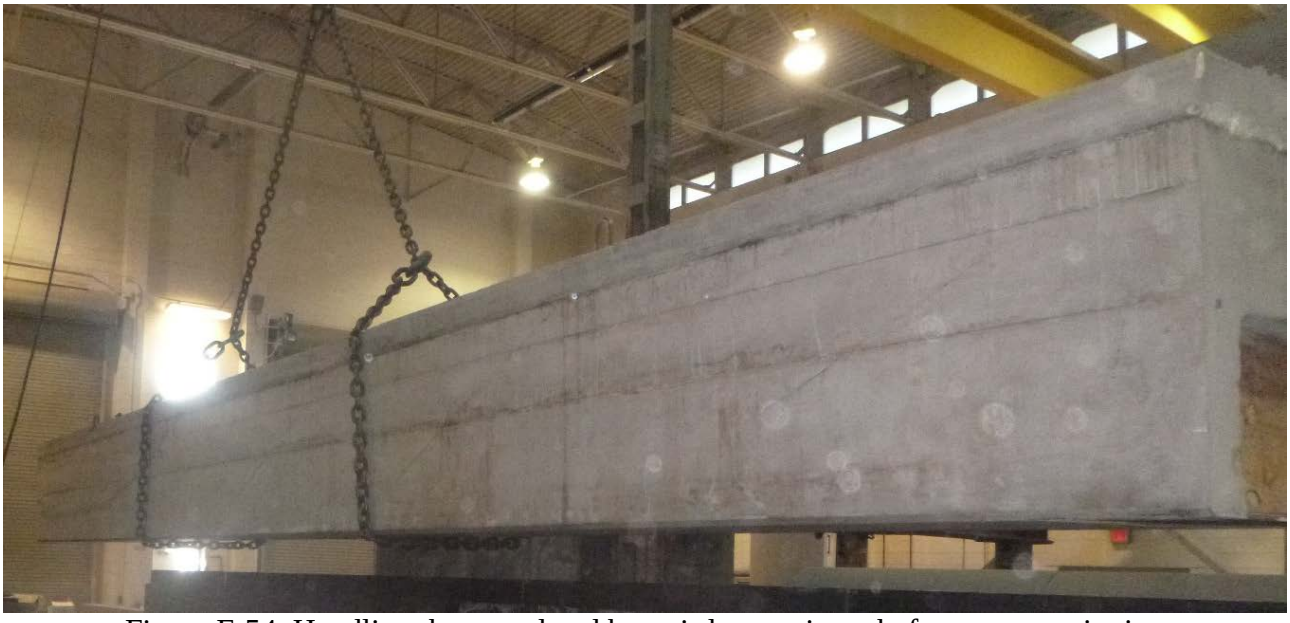

Figure F-54. Handling the completed box girder specimen before post-tensioning

Figure F-55. Post-tensioning 9-0.6 in. diameter strands in each duct

Figure F-56. Grouting post-tensioning ducts

2. Formed Surface Quality

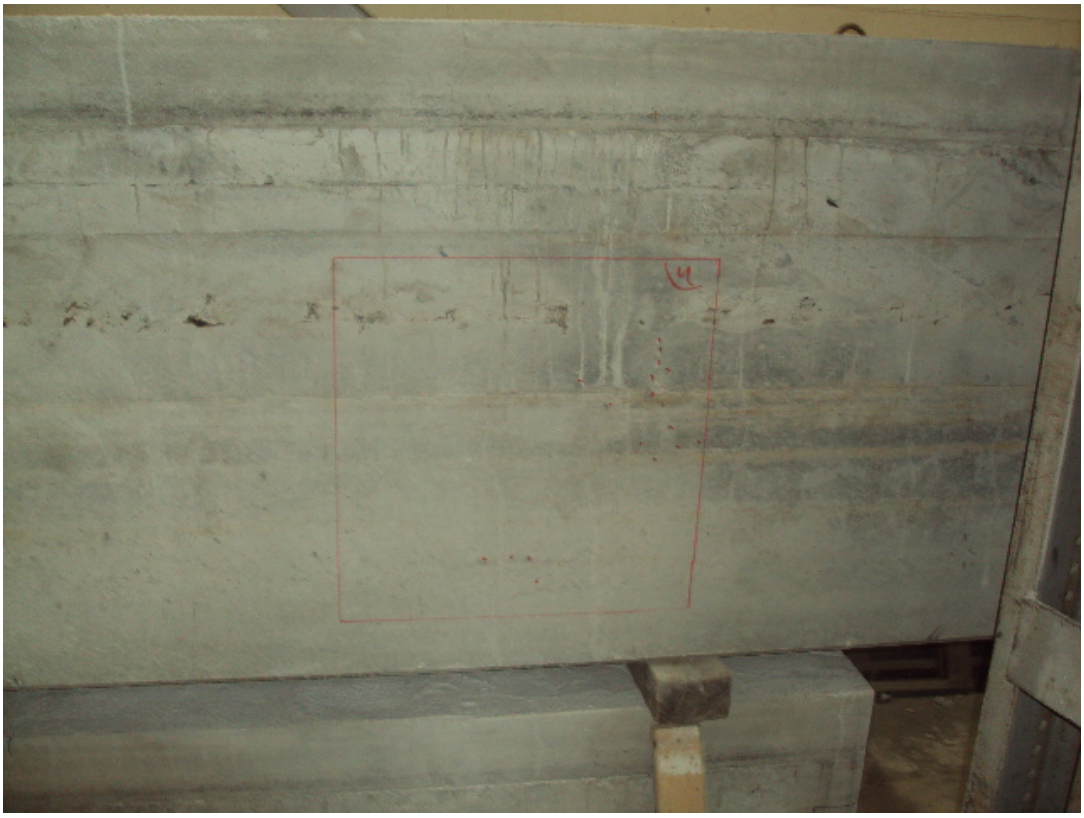

Figure F-57. Formed surface of the web close to the box girder end

Figure F-58. Formed surface at the post-tensioning anchorage zone

Figure F-59. Formed surface of the web at the construction joint location

Figure F-60. Formed surface at the bottom flange of the box girder specimen

Figure F-61. Formed surface at the middle of the box girder specimen

Table F-4. Measurements of formed surface air voids and their ratio for the box girder specimen

Component	Void Size (in.)		Void Area (in ^{2})	No. of voids	Total area of a void size (in^2)	Total area of voids (in^2)	D_{max}	% of D_{max}	Total % of void area	Surface Void Ratio
	w	l								
Top of the Girder (Pouring Side)	1/8	1/8	0.02	31	0.48	2.33	1/2	16.1%	0.40%	SVR3
	1/8	1/4	0.03	10	0.31					
	1/4	1/4	0.06	3	0.19					
	1/4	3/8	0.09	1	0.09					
	1/4	5/8	0.16	1	0.16					
	1/4	3/4	0.19	2	0.38					
	3/8	3/8	0.14	2	0.28					
	3/8	1/2	0.19	1	0.19					
	1/2	1/2	0.25	1	0.25					
Bottom of the Girder (Pouring Side)	1/8	1/8	0.02	20	0.31	2.94	1/2	37.2%	0.51%	SVR3
	1/8	1/4	0.03	9	0.28					
	1/8	1/2	0.06	1	0.06					
	1/4	1/4	0.06	8	0.50					
	1/4	3/8	0.09	2	0.19					
	1/4	1/2	0.13	2	0.25					
	1/4	5/8	0.16	5	0.78					
	1/2	1/2	0.25	1	0.25					
	1/2	5/8	0.31	1	0.31					
Bottom of the Girder (Opposite Side)	1/8	1/8	0.02	22	0.34	1.16	1/4	10.8%	0.20%	SVR4
	1/8	1/4	0.03	2	0.06					
	1/8	1/2	0.06	2	0.13					
	1/4	1/4	0.06	10	0.63					
Girder End (at the construction joint)	1/8	1/8	0.02	6	0.09	0.13	1/4	25.0%	0.02%	SVR4
	1/8	1/4	0.03	1	0.03					

3. Flexure Testing

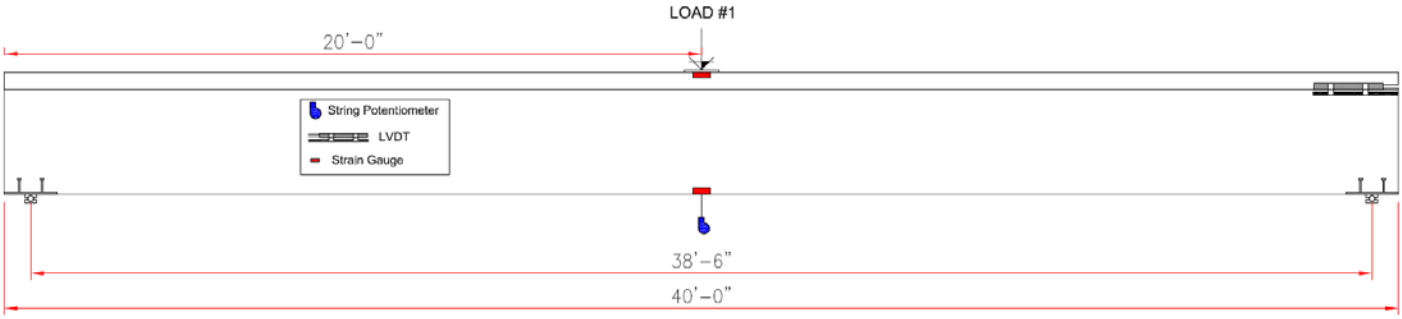

Figure F-62. Test setup for the first test of the post-tensioned girder

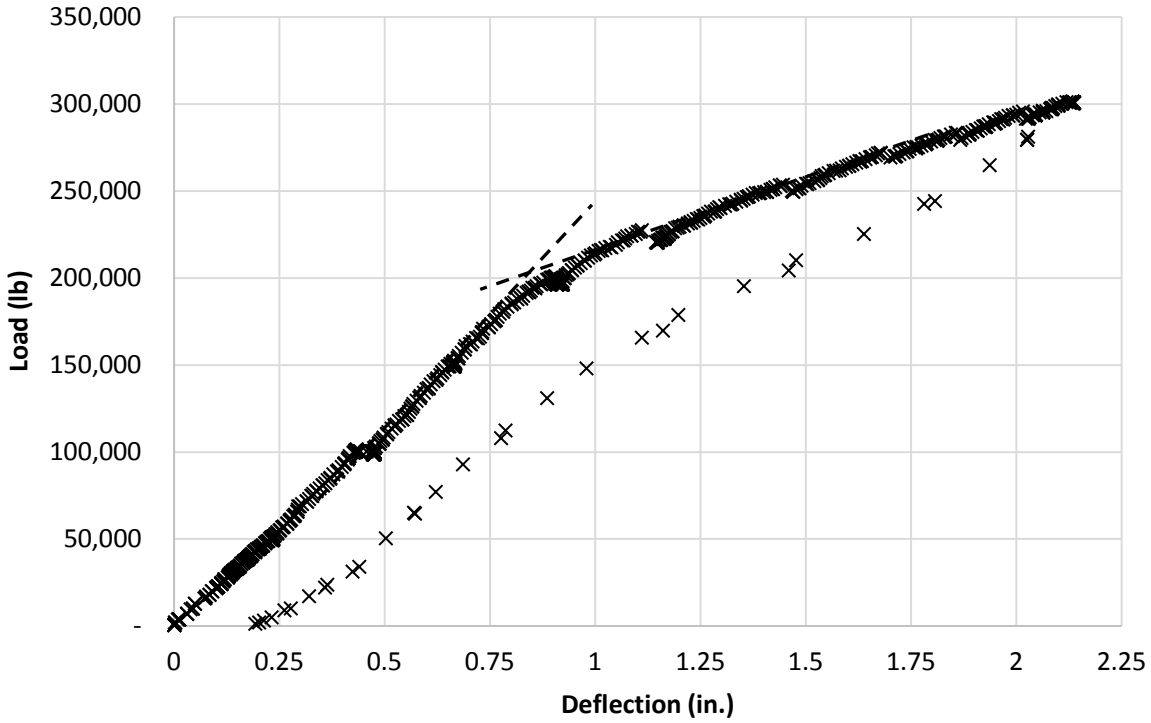

Figure F-63. Load-deflection plot of flexure testing of box girder specimen

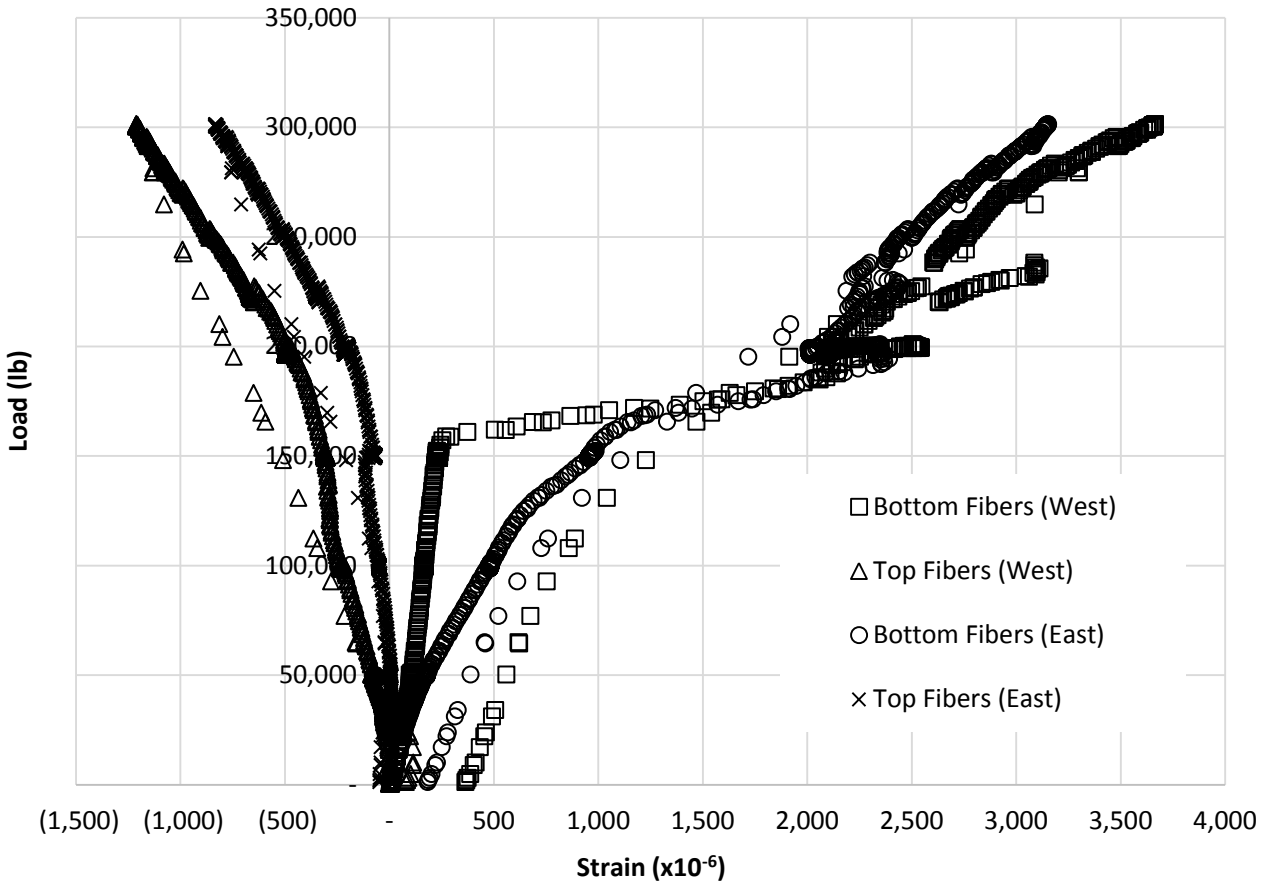

Figure F-64. Load-strain relationships at top and bottom fibers of box girder specimen in flexure testing

Figure F-65. Marked cracks during the flexure test of the box girder specimen (west side web)

Figure F-66. Marked cracks during the flexure test of the box girder specimen (bottom flange)


Figure F-67. Measuring relative displacement of top flange during flexure testing

4. Shear Testing

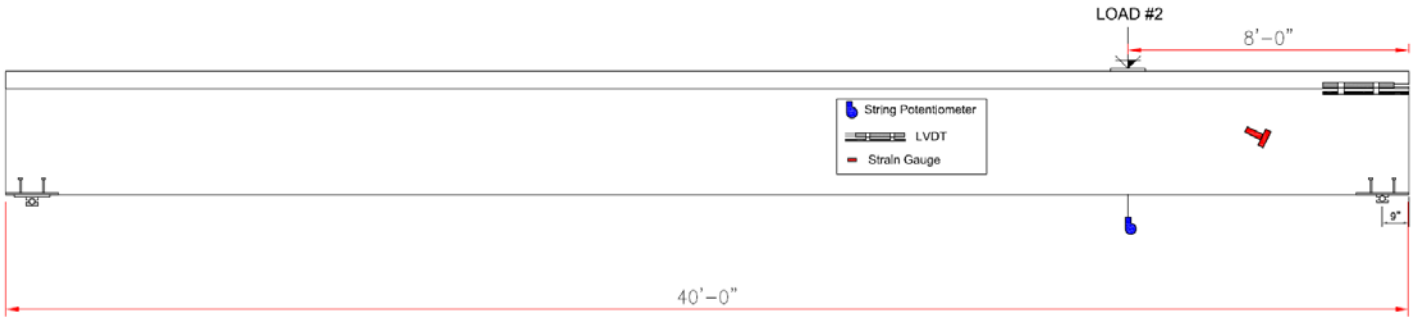

Figure F-68. Test setup for the second test of the post-tensioned girder

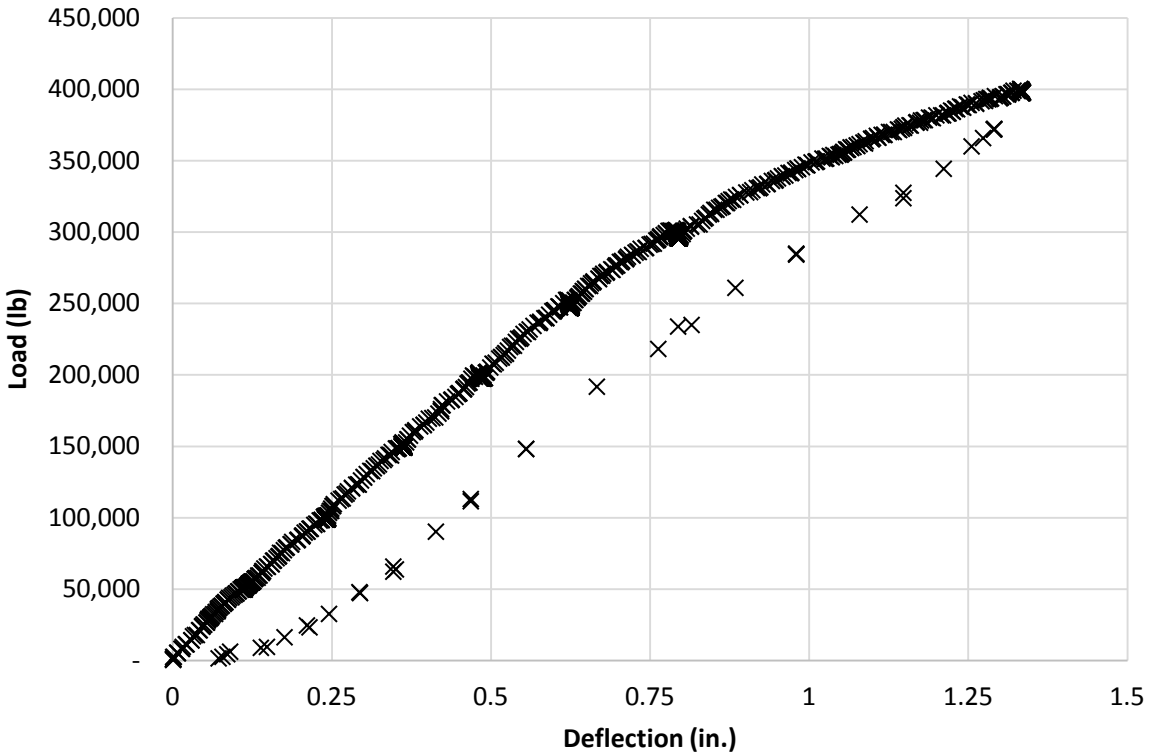

Figure F-69. Load-deflection plot of shear testing of box girder specimen

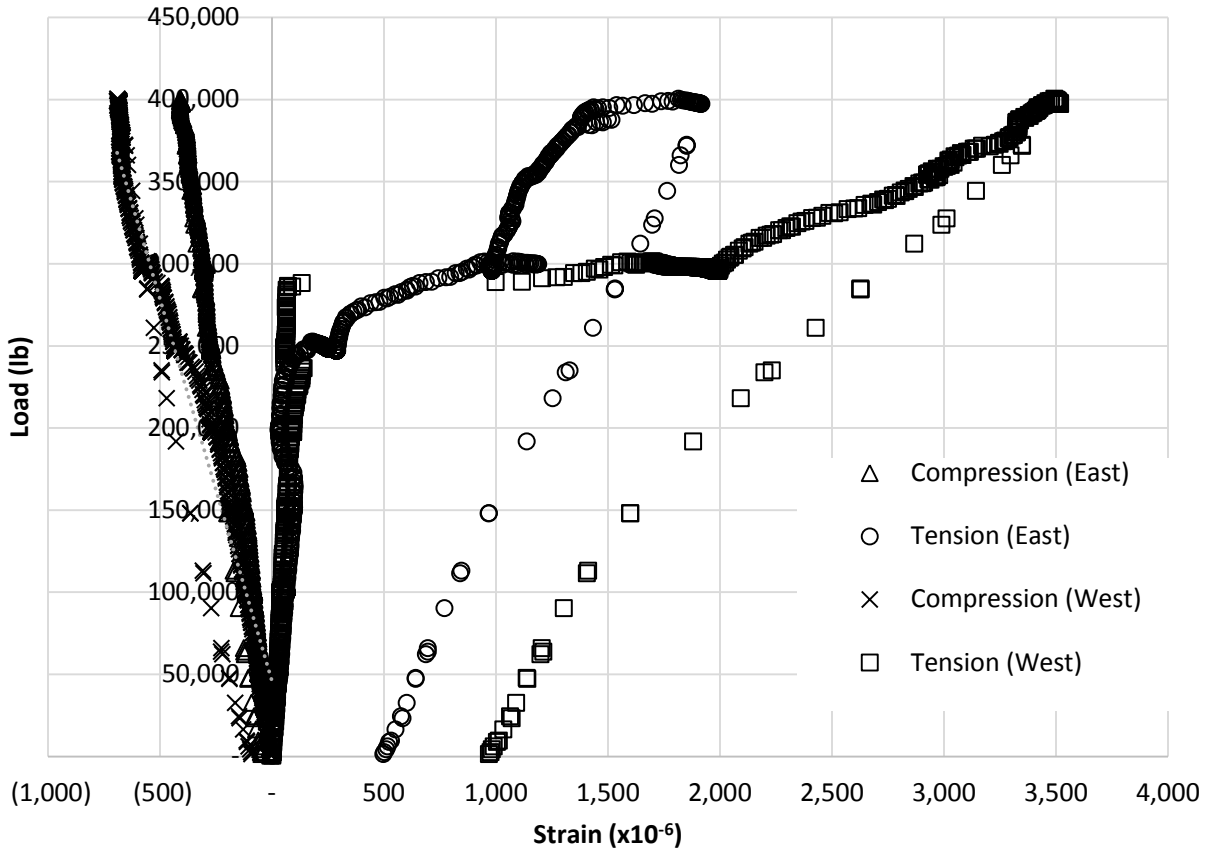

Figure F-70. Load-strain relationships at diagonal directions of box girder specimen in shear testing

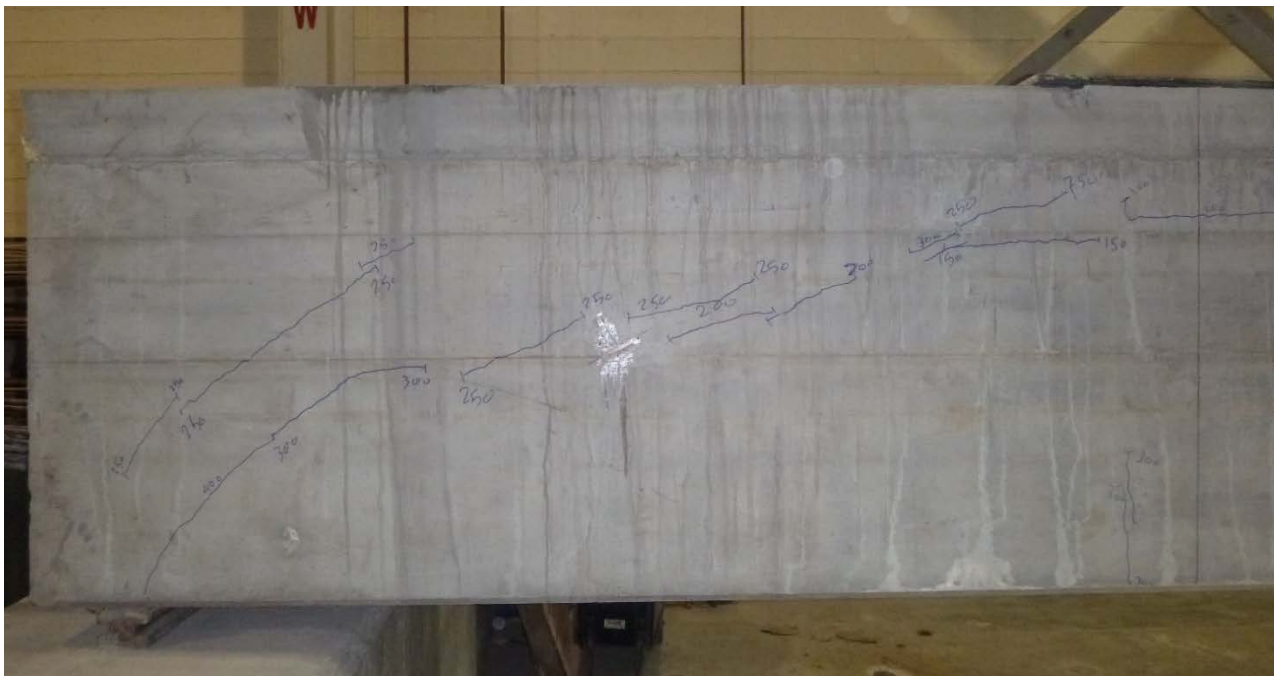

Figure F-71. Marked cracks during the shear test of the box girder (east side)

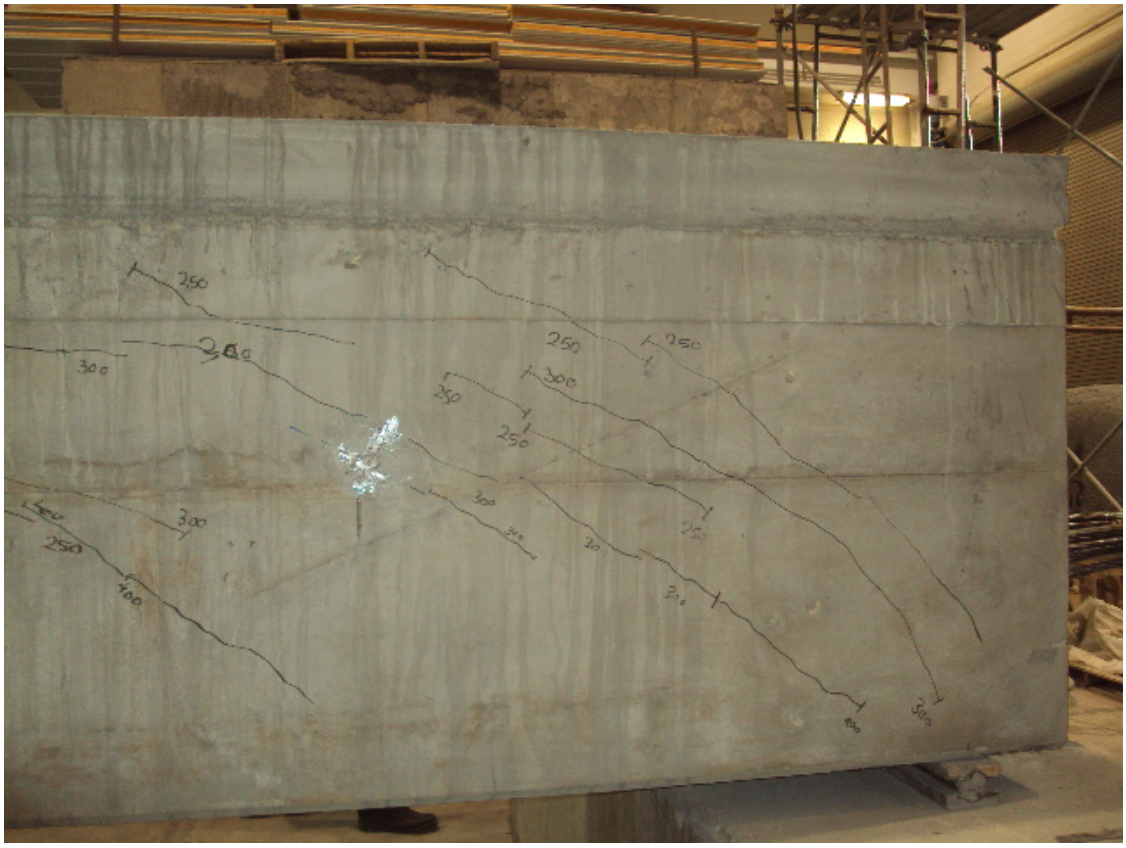

Figure F-72. Marked cracks during the shear test of the box girder (west side)

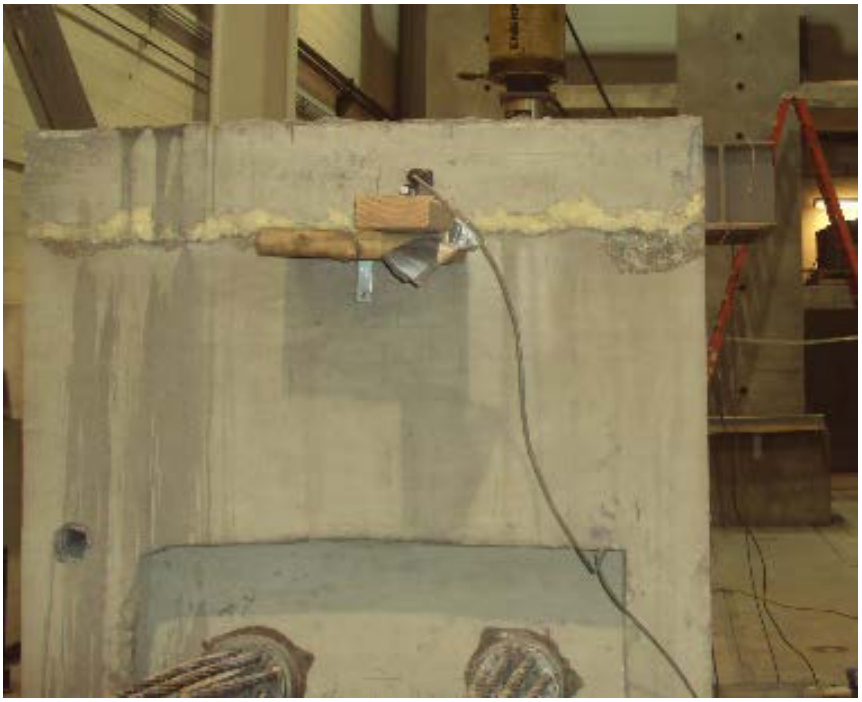
Figure F-73. Measuring relative displacement of top flange during flexure testing

5. Fresh and Hardened Properties

Table F-5. Fresh properties of SCC mixtures used in box girder specimen

Property		First Batch	Second Batch
Air Content		4.5%	3.5%
Slump Flow		26.25 in.	27.0 in.
Visual Stability Index		0	0
J-Ring ΔD		3/4 in.	0.0 in.
Penetration		1/4 in.	1/2 in.
Filling Capacity		90%	96%
Static Segregation		7.2%	5%
Dynamic Segregation		11.9%	15.3%
Rheological Properties(ICAR Rheometer)	Static Yield Stress (pa)	578.8	561.5
	Dynamic Yield Stress (pa)	528.8	523.3
	Plastic Viscosity (pa.s)	2.1	1.6

Table F-6. Hardened properties of SCC mixtures used in box girder specimen

Component	**Casting Date**	**NMSA**	**Compressive Strength f_c (ksi)**				**MOR (ksi)**	**Splitting Strength (ksi)**	**MOE (ksi)**
			7 days	**14 days**	**28 days**	**56 days**			
Tub Section (First batch)	14-Oct. 2014	3/8 in.	5.62	6.73	7.88	8.78	1.04	0.58	4,552
Top Flange (Second Batch)	24-Oct. 2014	3/8 in.	6.5	7.2	7.4	8.1	1.03	0.54	4,183

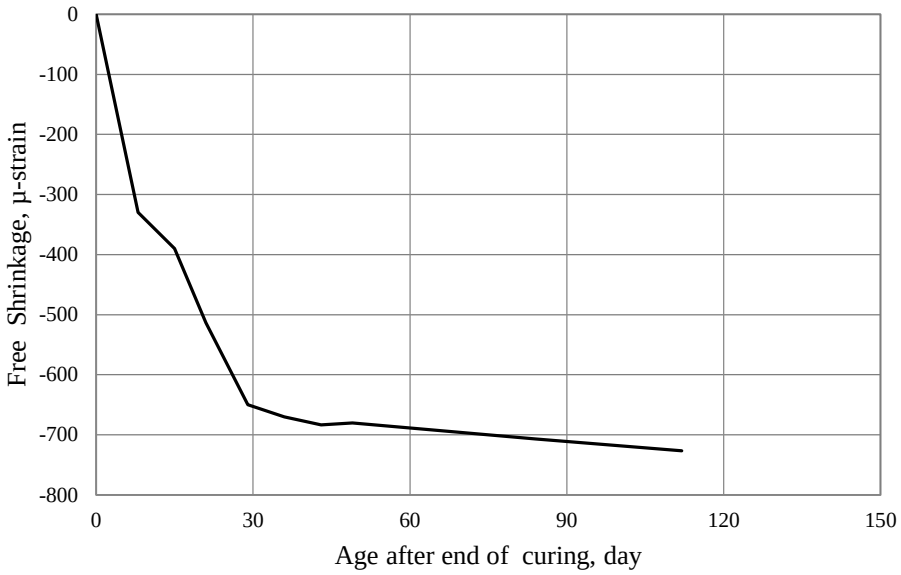

Figure F-74. Relation between free shrinkage and age of Box Girder mixture after 7 day curing

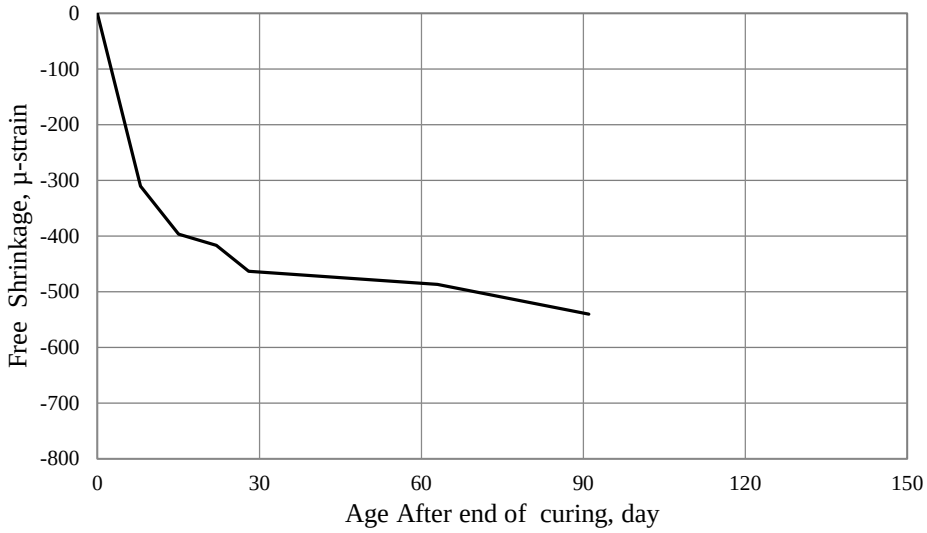

Figure F-75. Relation between free shrinkage and age of Box Girder mixture after 28day curing